Sigma-Hole Donor Host Systems for Anion and Ion-Pair Recognition

Thanthapatra Bunchuay

Wadham College, University of Oxford

A thesis submitted for the degree of Doctor of Philosophy

Inorganic Chemistry Laboratory

University of Oxford

Trinity Term 2018

Sigma-Hole Donor Host Systems for Anion and Ion-Pair Recognition

Thanthapatra Bunchuay, Wadham College, University of Oxford

Abstract of thesis submitted for the degree of D.Phil., Trinity Term 2018

This thesis describes the synthesis of acyclic, macrocyclic, and mechanically interlocked host molecules (MIMs) incorporating sigma-hole interactions including halogen and chalcogen bonding for anion and ion-pair recognition.

Chapter 1 introduces the general aspects in the field of supramolecular host-guest chemistry with particular emphasis on themes relevant to the topic of this DPhil research project, specifically anion and ion-pair recognition followed by a review of the construction of mechanically interlocked architectures and their applications.

Chapter 2 discusses rare examples of sigma-hole interactions mediated ion-pair recognition.The preparation of novel XB and unprecedented ChB heteroditopic host systems containing benzo[15]crown-5 are described, followed by investigation into ion-pair binding properties. The novel use of an ammonium[2]catenane integrated into the XB anion receptor capable of anion recognition in aqueous media is reported.

Chapter 3 focuses on the exploitation of XB interactions for anion recognition and sensing in highly competitive aqueous media. An unprecedented relationship between anion template affinity and the yield of permethylated *β*-cyclodextrin-stoppered XB [2]rotaxane is demonstrated. Anion recognition properties of these rotaxane hosts in solvent media containing up to 50% water are subsequently investigated. Moreover, the novel cationic and neutral water soluble XB anion receptors based on 3,5-bis-(iodotriazole)pyridine, pyridine-*N*-oxide, and pyridinium motifs are synthesised to elucidate thermodynamic parameters of XB anion recognition in water using isothermal calorimetric analysis. Finally, the preparation of novel osmium(II)bipyridyl functionalised water soluble hosts are reported, and investigations in their anion recognition and sensing using electrochemical and fluorescence are detailed.

Chapter 4 describes the effects of chelating XB receptors with a small bite angle on their anion recognition behaviour. A bidentate ortho-substituted iodotriazolium benzene motif is incorporated into acyclic, macrocyclic, and interlocked anion host molecules for their anion binding studies in solution phase, supported by solid-state structures of various anion complexed acyclic structural frameworks.

Chapter 5 details the experimental procedures used in this work, including synthetic protocols and characterisation data for novel compounds.

Acknowledgement

Firstly, I would like to express my deepest gratitude to my research supervisor Professor Paul Beer for seeing the potential in me and providing me the opportunity to work and develop my research and social skills in his group. If Marvel heroes had many sources of power to fight with enemies, this real "*Suprahero*" always has *"crazy ideas"* to challenge and push my limits beyond who I was before. Again, I have been incredibly lucky to have worked with such a trusting, supportive and friendly supervisor. P.S. Don't forget to support me in winning a Nobel Prize in Chemistry 2045 :)

During four years of my D.Phil, the Beer group has been my second family, and I would like to thank members, present and past, who have supported and made this journey an enjoyable and loving place to work in. The first person I must thank is Dr. Sean Robinson for his help and useful suggestions throughout my first year. I know you were very patient in supervising me in the beginning due to my poor ability to communicate in English, however you made it possible. I would also like to thank Dr. Vicente Marti-Centelles for his genius synthetic guidance, Dr. Robert Edkins for his kind and endless suggestions and Dr. Lydia Gilday for being a big sister of our group and S8 particularly. I must also offer my gratitude to the Beer group members I have worked with in my time; Tim Barendt (don't need to talk so much, you know how much I care about you, thanks), Stuart Cornes (you are one of my favourite chemist), Tom Mole (thank you for your kind support in my insane synthetic chemistry and English), Alex Hess (Cheers), Sam Sutton and Hena Bagha (my unforgettable lab partner, really glad to be in the same class with you guys and to have spent all those wonderful moment of our lives together), Grace Turner (thanks so much for making S8 such a nice place to work and always being my mentor inside and outside the lab), Jane Liew (I really like you actually, again I wished you have a nice husband), Jess Pancholi (you are a wonderful postdoc that always fights for us), Harry Klein (thanks for sharing the same fate in thesis writing and please check your flow…), George Li (I wish you best in your future postdoc endeavours.), Luiza (thanks so much for your organising skills in keeping the lab inventories in check), Arseni Borissov (you are the most insane and excellent chemist I've ever met), TJ Mitchell (Cheers mate). In addition, the lab without part II students is not a right place to carry out enjoyable research, big thanks to Will Arthur, Dan Lucy, Ewan McAulley, Anna Spearing-Ewan, Andrew Docker, Tom Trehern, Amy Ford, Dan McNaugton (alright mate), Tim Kench, Peter Greenman, Michael Ahrens, Niles Beadsman, Benji Gibber, Adam Beecroft, Olivia Knapp and especially Caspar Whitehead (- -) for making this group a colourful place.

I was fortunate to supervise a summer project student from my hometown, Hi Araya who worked really hard and managed to achieve nice results at the very end. I was also very lucky to have an opportunity to suggest and work alongside Richard, a Hong Kong scholar D.Phil student. It was a great whole year that we've learnt and gained a lot of experiences in porphyrin chemistry. I guaranteed they were real pleasure (not pressure) to work with in those times.

"*Teamwork makes the dream work*". It was always a pleasure having a chance to collaborate with lovely and engaging people. I would like to show my appreciation to Dr. Jason Lim for his help and supportin many aspects during my D.Phil. I look forward to more future collaborations with you! Special thanks to genius chemist Dr. Asha Brown who have given me an opportunity to be a part of the "Beer Can" project. She has been a chemistry encyclopedia of our group and have been generous in sharing her knowledge and neverending guidance throughout my time. A chemist who has showed me the electrochemistry world is Robert Hein . I appreciate his efforts on all things electrochemical in my thesis and in our (to be published) papers. Despite being in the different lab, Dr. Antonio Martinez Martinez has been very helpful in sorting out my crystallographic work. I hope this is just a beginning of our collaborations in the future. I am also appreciative to Dr. Nick Rees, Dr. Nader Amin, and Dr. Victor Mikhailov for their guidance to carry out any special NMR and mass spectrometry experiments required in my thesis.

Everyone knows my English is not my mother tongue language; however this thesis has been proofread and corrected by Grace Turner, Jessica Pancholi, Jane Liew, Andrew Docker, Dr. Jason Lim, and of-course Paul Beer. I thank you all for your formidable work that requires your time and patience, Thanks.

This paragraph is for my very special one, Andrew Docker, I would never have made it this far without you. You started as my Part II student who worked really hard and have put in so much effort into our research and you become as a part of my life. I am very happy in all the time we have spent together for almost three years and hopefully for more to come.

Outside of the lab I would like to thank all of my friends from Oxford Thai Society, AAICP, and Mahidol University in particular Korbua, Kate, Natta and Pop. For financially supporting my studies, I am indebted to the generosity of Development and Promotion of Science and Technology Talents Project (DPST) in Thailand who have provided me with funding for over 14 years.

And finally, a huge thanks to my family and my parents for your unconditional support and encouragement. (Thanks for the good genes Mom and Dad)

This thesis is dedicated to H.M. King Bhumibhol Adulyadej (1950 -2016)

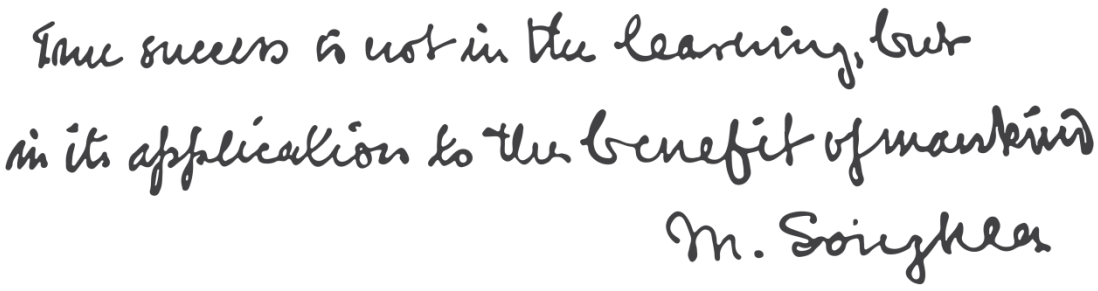

Mahidol Adulyadej the Prince Father (1892-1929)

Abbreviations

δ	chemical shift
λ	wavelength
μ	micro, dipole moment
v	frequency
°	degree
°C	degrees Celsius
Å	Ångstrom
A	acceptor
A^-	anion
abs	absorption
aq.	aqueous
Ar	aromatic
Arg	arginine
Asp	aspartate
ATP	adenosine triphosphate
a.u.	arbitrary units
bipy	2,2'-bipyridine
Boc	di-*tert*-butyl dicarbonate
BODIPY	Boron-dipyrromethene
br	broad
Bu	butyl
cat.	catalytic
conc.	concentrated
COSY	homonuclear correlation spectroscopy
CPS.	counts per second
CuAAC	copper(I)-catalysed azide–alkyne cycloaddition
D	donor
d	doublet
dd	doublet of doublets
DIPEA	*N*,*N*-di-*iso*-propylethylamine
DMF	*N*,*N*-dimethylformamide
DMSO	dimethyl sulfoxide
DNA	deoxyribonucleic acid
e.*g*.	*exempli gratia*
eq., equiv.	equivalent
ESI	electrospray ionisation
Et	ethyl
g	gram
G	Gibbs free energy
Grubbs' I/II	Grubbs' first/second generation catalyst

HB	hydrogen bonding
HOMO	highest occupied molecular orbital
hr.	hour
HSQC	heteronuclear single quantum coherence
Hz	hertz
I	intensity
int.	internal
i.e.	*id est*
J	Joule
J	coupling constant
k	kilo
K	Kelvin
K_{Ass}	association constant
L	litre
LUMO	lowest occupied molecular orbital
M	molar
M	mega, molecular ion
m	milli, multiplet,
m	*meta*
m/z	mass-to-charge ratio
Me	methyl
Mes	1,3,5-trimethylbenzene
MIM	mechanically interlocked molecule
min	minute
MLCT	metal-to-ligand charge transfer
mol	mole
MS	mass spectrometry
Ms, mesyl	methanesulfonyl chloride
n	nano
NMR	nuclear magnetic resonance
OAc	acetate
o/n	overnight
p	*para*
PET	photoinduced electron transfer
pH	$-\log_{10}[H^+]$
Ph	phenyl
pK_a	$-\log_{10}K_a$
ppm	parts per million
Pr	propyl
Py	pyridinium
q	quartet
quin.	quintet
R	chemical substituent

RCM	ring closing metathesis
ROESY	rotating-frame nuclear Overhauser effect correlation spectroscopy
rt	room temperature
s	second, singlet
sat.	saturated
sept.	septet
St	stopper
t	triplet
t, tert	tertiary
TBA	tetrabutyl ammonium
TBDMSCl	tert-butyldimethylsilyl chloride
TBTA	tris[(1-benzyl-1*H*-1,2,3-triazol-4-yl)methyl]amine
TLC	thin layer chromatography
Ts, tosyl	*para*-toluenesulfuonyl chloride
UV	ultra-violet
V	volt
vis.	visible
vs.	*versus*
VT	variable temperature
v/v %	volume/volume percent
wt.	weight
X	halogen atom
XB	halogen bonding

TABLE OF CONTENTS

Chapter 1
Introduction

Chapter 1: Introduction

1.1 Supramolecular Chemistry: Where from?

Nature has developed a number of hierarchical systems that function in highly specific and dynamic environments including enzyme—substrate interactions, selective transport of metal ions or molecules, and encoding of genetic information by DNA.[1] The foundation of such processes is the reversible molecular recognition of chemical species by the assistance of concerted weak non-covalent intermolecular interactions. Taking inspiration from the natural world, the interdisciplinary field of supramolecular chemistry, defined as the chemistry of molecular assemblies and of the intermolecular bond, has emerged from fundamental investigations of host—guest interactions to the discipline of complex self-assembly. Recent progress in the field has culminated in the application of supramolecular architectures for real world applications in medicine, industry, biology, and nanotechnology.

More than half a century after Fischer proposed the concept of host—guest association in terms of a "lock and key" analogy to explain the behaviour of substrate recognition by enzymes,[2-4] Pedersen reported his seminal work on the alkali metal cation binding properties of crown ether hosts.[5] This serendipitous discovery stimulated research into the field of molecular recognition through the design and synthesis of molecular host architectures with tailored cavity coordination environments to afford selectivity for target guest species. Further progress in the field of Group I metal cation recognition was achieved by Lehn's three dimensional cryptands, and Cram's rigid spherands, resulting in the 1987 Nobel Prize in Chemistry being awarded to Pedersen, Lehn, and Cram *"for their development and use of molecules with structure-specific interactions of high selectivity"* Less than a year after the publication of Pedersen's crown ethers, Park and Simmons reported the first example of an anion host system, a macrobicyclic protonated cage coined a 'katapinand', capable of binding halides in acidic aqueous solution.[6]

In 2016, the advancements of the supramolecular chemistry field were again acknowledged when the Nobel Prize in Chemistry was awarded to Jean-Pierre Sauvage,[7] Fraser Stoddart,[8] and Ben Feringa[9] for being pioneers in "the design and synthesis of molecular machines". The prototypes of molecular nano-machines by Sauvage and Stoddart were based on interlocked molecules in which the components are held together by "the mechanical bond" (Figure 1.1).

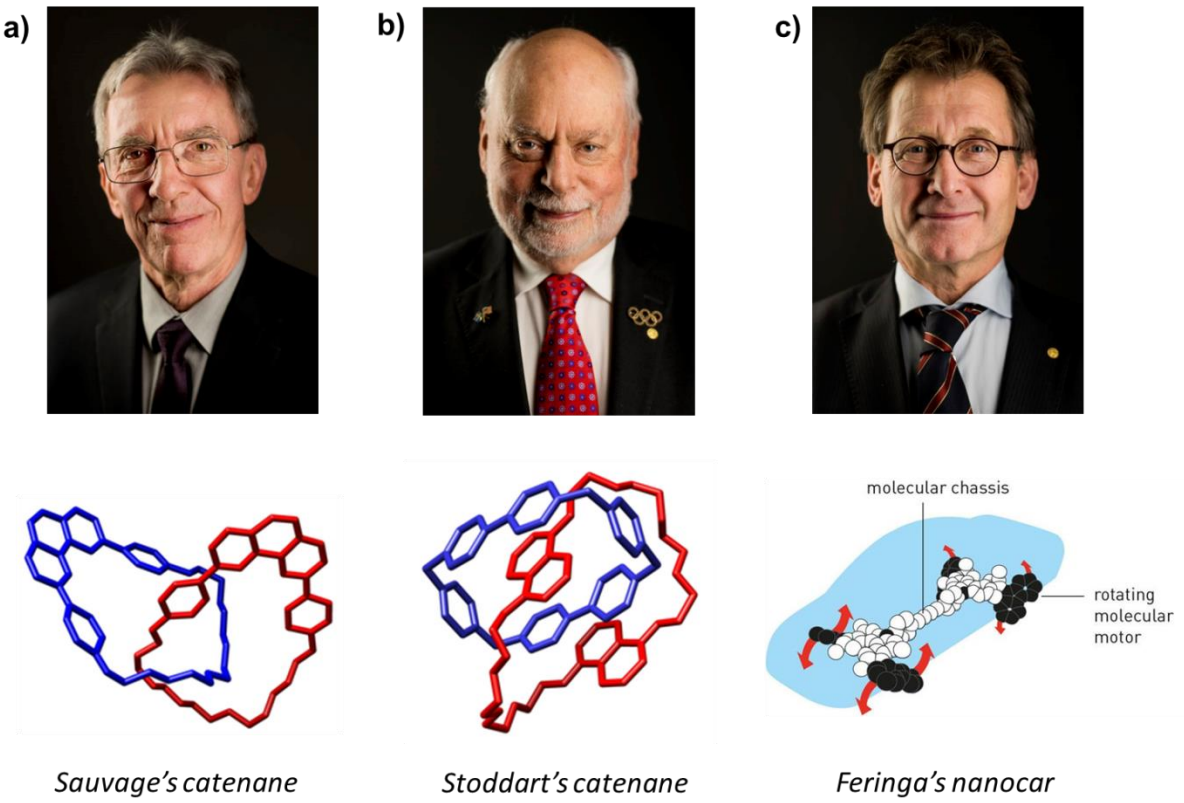

Figure 1.1 Nobel Laureates in Chemistry 2016 a) Jean-Pierre Sauvage b) Fraser Stoddart and c) Bernard Lucas Feringa for the design and synthesis of molecular machines.

This introductory chapter focuses initially on the general aspects of supramolecular host-guest chemistry with particular emphasis on themes relevant to the topic of this DPhil research project, anion and ion-pair recognition followed by a review of the construction of mechanically interlocked architectures and their applications.

1.2 Non-covalent interactions

Non-covalent interactions are the intermolecular forces which are responsible for the association of two or more molecular entities. These forces span a wide range of interaction energies, which in combination are commonly exploited to achieve thermodynamically stable host-guest complex assemblies.

1.2.1 Electrostatic interactions[10]

These interactions can be divided into three main categories: i) ion—ion ii) ion—dipole and iii) dipole—dipole. Ion—ion pairing interactions occur *via* Coulombic attraction between opposite charges which are of comparable strength to covalent bond energies, but non-directional in nature. In solution the interaction energy between two

charged species inversely depends on the dielectric constant (ε) of the solvent medium. The ion pairing effect is substantially attenuated on moving from the gas phase (ε = 1) to high polarity media such as water (ε = 78). In the case of ion—dipole interactions which demonstrate greater distance dependence, the orientation of the dipole with respect to the ion is important as in the archetypal example, hydrogen bonding discussed below.

1.2.2 Hydrogen bonding[11, 12]

The hydrogen bond is a pivotal attractive force and arguably the most utilized in the design of artificial supramolecules. A hydrogen bond is described as a Coulombic interaction between a polarised hydrogen bond donor and Lewis base. When an electronegative atom (*e.g.* N, O, F) is attached to a hydrogen atom, a permanent dipole is formed with a small positive charge on the hydrogen atom. The strength and high directionality has made hydrogen bonding (HB) the most universal interaction that controls functions in biotic systems, as illustrated by nucleotide base pair formation between guanine and cytosine in DNA strands (Figure 1.2).

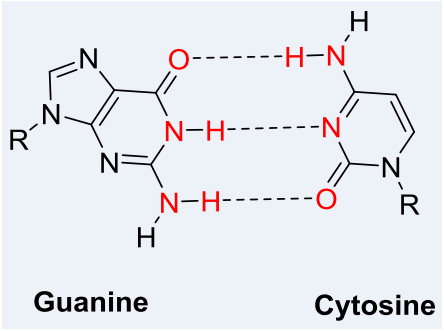

Figure 1.2 Nucleotide guanine and cytosine base pair hydrogen bond formation.

1.2.3 Halogen bonding

Halogen bonding (XB) is defined by IUPAC as *"evidence of a net attractive interaction between an electrophilic region associated with a halogen atom in a molecular entity and a nucleophilic region in another, or the same, molecular entity".*[13] XB can be represented as R—X···B (Figure 1.3a) which is the non-covalent interaction between an electrophilic halogen atom (X, XB donor) bonded to an electron-withdrawing group (R) and a Lewis base (B, XB acceptor); for example the XB association between ICl and NMe_3 (Figure 1.3b).

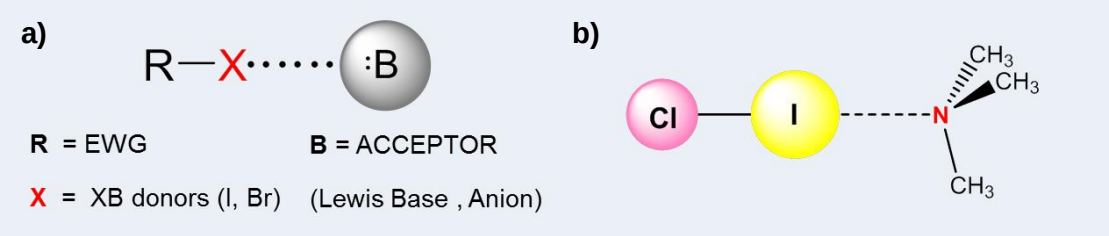

Figure 1.3 (a) XB formation between XB donor and acceptor and (b) XB interaction between ICl and NMe_3.

Theoretical predictions and experimental evidence support an anisotropic distribution of electron density on the halogen atom as shown in Figure 1.4. The region of positive potential (red) at the terminus of the C—X bond is called the σ-hole, surrounded by an equatorial ring of negative potential. The pole position of the σ-hole on the halogen atom results in a highly directional near linear interaction with a Lewis base.[14] The strength of XB is comparable to HB (10-200 kJ/mol) and can be tuned by the nature of the halogen atom itself and/or by the electron-withdrawing capability of the covalently attached group R. The magnitude of the σ-hole (and thus XB donor ability) increases as the polarizability of the halogen atom increases, moving from F<Cl<Br<I (Figure 1.4). The hybridization state of the substituent R has also been demonstrated to affect XB donor strength, where halogen bond donor ability increases in the order of $sp > sp^2 > sp^3$.[14, 15]

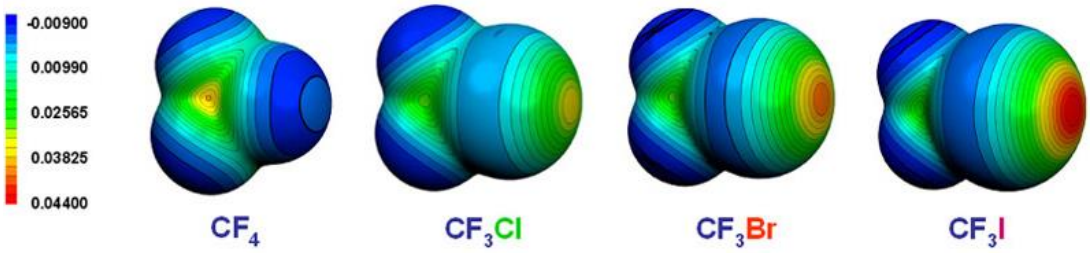

Figure 1.4 Calculated molecular electrostatic surface potential of halotrifluoromethanes.[16]

Sigma (σ) holes are also found in the atoms of p-block main group elements when covalently linked to more electronegative substituents. Similar to XB, these electrophilic regions are available to form attractive interactions with Lewis bases such as anions and are named after the groups the donor atoms are a member of: chalcogen bonding (ChB) for group 16 elements, pnictogen bonding (PnB) for group 15 elements, and tetrel bonding (TrB) for group 14 elements. [17, 18]

1.2.4 π effects

Non-covalent interactions arising from π effects include: aromatic—aromatic interactions, cation—π and more recently anion—π.

Aromatic—aromatic interactions can be categorised into two main types: displaced or slipped stack (Figure 1.5a) and edge-to-face or T-shaped (Figure 1.5b). Theoretical and experimental investigations have elucidated the origins of these interactions to be a combination of dispersion forces, electrostatics and solvent effects. Such π – π effects are frequently encountered in nature, for example between base-pairs along the length of the double helix structure of DNA. [19-22]

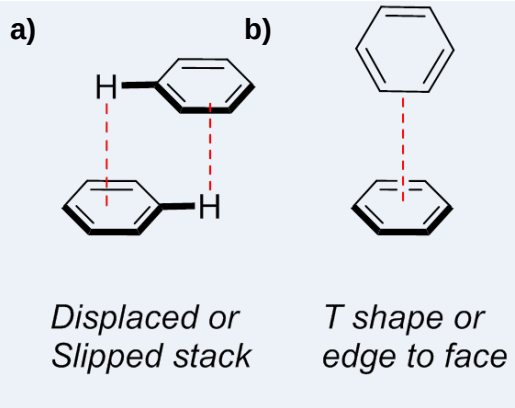

Figure 1.5 Aromatic—aromatic interactions.

The cation—π interaction originates from a favourable Coulombic contribution between a cationic species and the electron-rich region from an aromatic system (Figure 1.6a).[23, 24] In the gas phase examples have been shown to possess considerable enthalpies of association, such as between K^+ and benzene with ΔH = -19 kJ/mol which is commensurate with the ion—dipole interaction between K^+ and water (ΔH = -18 kJ/mol). Additionally, this interaction plays significant roles in biological molecular recognition in protein structures with electron rich aromatics of amino acid residues; for example between the quaternary ammonium group of acetyl choline and tryptophan residues in nicotinamide acetylcholine receptors (Figure 1.6b).[25] The anion—π interaction is the result of electrostatics and anion-induced polarisation of the π -delocalised electron density of an aromatic system functionalised with highly electron-withdrawing substituents (Figure 1.6c). Due to their intrinsically weak nature, they are only observed in combination with additional non-covalent interactions.[26 27]

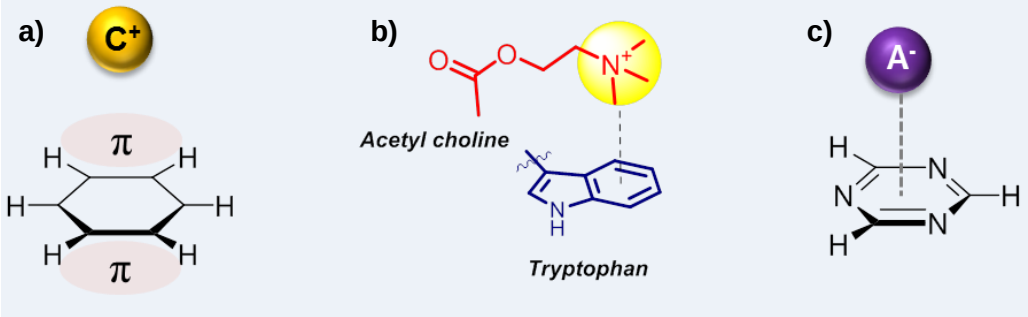

Figure 1.6 a) Cation—π interaction b) cationic acetylcholine binding to a tryptophan residue of the nicotinamide acetylcholine receptors and c) anion—π interaction.

1.2.5 Hydrophobic interactions[28-31]

The hydrophobic effect is of importance in biological recognition processes and acts as the main contributor in protein folding, and maintenance of phospholipid bilayer membranes. Such effects also assist the binding of organic guests in the host cavities of water soluble macrocycles such as cyclodextrins and cyclophanes. The classical hydrophobic effect was attributed to a favourable entropic contribution that results from the host exclusion of water molecules upon binding hydrophobic guest species. However, a dominant enthalpic contribution has been demonstrated to be a strong driving force in many recent examples, termed the non-classical hydrophobic effect.[32]

1.2.6 Coordinate bond

Lewis acid—Lewis base association contains significant orbital overlap, and thus is not strictly considered as a non-covalent interaction. Common Lewis acidic sites include main group elements such as boron,[33, 34] and antimony,[35] and transition metal cations such as zinc,[36] nickel, copper.[37] Moreover, the lability of coordinate bond formation has frequently been exploited in molecular recognition, self-assembly, and in the construction of higher order supramolecular architectures.

1.3 Anion Supramolecular Chemistry

1.3.1 Importance and challenges of anion recognition

Anions are ubiquitous and play fundamental roles in biological, medical, environmental, and industrial processes. In biotic systems, the majority of biomolecules are negatively charged in the form of large polyanions under physiological conditions. These include nucleic acids such as DNA, RNA which control the genetic information required for the development and function of organisms, while adenosine triphosphate ATP serves as the energy source for intercellular energy transfer. Furthermore, simple inorganic anion dysregulation is linked to physiological diseases; for example the malfunction of the chloride membrane transport protein causes cystic fibrosis and is also associated with Alzheimer's disease, while iodide is key for the biosynthesis of tyrosine based hormones by the thyroid gland.[38] In the environment overuse of phosphate and nitrate fertilisers in agriculture has led to eutrophication of natural water sources and disruption of the ecosystem.[39, 40] Increasing levels of nitrate in food and drinking water, arising from human activity, is associated with a range of health problems (*i.e.* formation of carcinogenic nitrosamine).[41, 42] Nitrate and sulfate in acid rain causes the corrosion of buildings[43] and highly toxic anionic pollutants from industrial processes including cyanide, azide, perchlorate, and nuclear waste by-product radioactive pertechnetate ($^{99}TcO_4^-$) are of ever increasing concern to humankind. Hence, the case for the design and synthesis of artificial anion receptors, sensors, and sequestering agents, especially those that function in aqueous media is currently an intensely investigated research topic in supramolecular chemistry.

1.3.2 Intrinsic properties of anions

In anion host design, overcoming the intrinsic properties of anions is comparatively more challenging than that of cation binding, especially in water. This section summarises these issues.[44]

Size and Shape

Anions are generally larger in size than their isoelectronic cations, and thus display a lower charge to radius ratio (Table 1.1). This results in significantly weakened electrostatic interactions between an anionic guest species and host system.[44] Even simple inorganic anions adopt a broad range of geometries (Figure 1.7) including spherical (halides), linear (thiocyanate, azide), bent (nitrite), trigonal planar (nitrate, carbonate), square planar (tetrachloroaurate), tetrahedral (sulphate, phosphate, perrhenate), octahedral (hexafluorophosphate) and icosahedral (dodecaborate). Biological anions such as nucleotides have more complex structures in the form of polyanions such as double helical DNA. The diversity of their size and shape is an attractive feature to exploit in complementary anion host cavity design although this can prove to be a synthetic challenge.

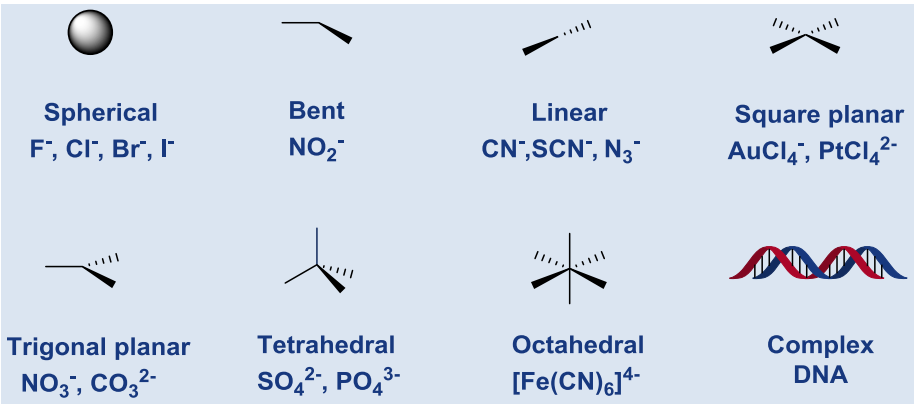

Figure 1.7 Anions with different geometries.

Table 1.1 Comparison of the radii and hydration enthapies of halide anions with their isoelectronic alkali metal cation counterparts.

Anion	Radius (Å)	$\Delta G_{hydration}$ ($kJmol^{-1}$)	Cation	Radius (Å)	$\Delta G_{hydration}$ ($kJmol^{-1}$)
F^-	1.19	-465	Na^+	1.16	-365
Cl^-	1.67	-340	K^+	1.52	-295
Br^-	1.82	-315	Rb^+	1.66	-
I^-	2.06	-275	Cs^+	1.81	-250

pH dependence

Many anions exist in a relatively narrow pH window and are subject to speciation due to their multiple protonation equilibria. This issue can be problematic for certain classes of anion receptor containing polyammonium motifs which are also pH sensitive. Consequently, anion recognition by these hosts can only occur in the pH window wherein the target anion species maintains its negative charge and the receptor remains protonated.

Solvation energy

The nature of the solvent plays a crucial role in the recognition of anionic guest species in terms of governing the binding strength as well as influencing selectivity. In comparison to a cation of similar charge and size, an anion displays a higher free energy of solvation; for example the standard free energy of hydration (ΔG_{hyd}^{0}) for K^+ and F^- are -295 kJ mol^{-1} and -465 kJ mol^{-1}, respectively (Table 1.1). Therefore an anion receptor has to overcome the larger enthalpic penalty of anion desolvation to effect binding relative to a host for cations. Weakly solvating media such as acetone or chloroform allows neutral receptors to recognize anionic guests. Polar protic solvents such as methanol and water strongly solvate species by the formation of hydrogen bonds to both host and anion guest molecules. Hence synthetic anion receptors capable of functioning in aqueous media commonly require multiple positively charged binding sites for anion recognition to occur.

1.3.3 Biotic anion receptors

Biotic anion receptors often participate in key biological activities such as anion transport and biosynthesis. This requires these natural anion receptors (*e.g.* phosphate binding protein (PBP) and sulphate binding protein (SBP)) to display strong and selective binding to a specific anionic guest under physiological conditions.[45, 46] The high selectivity arises from the complementary arrangement of convergent hydrogen bonding motifs at the protein recognition site. The X-ray diffraction crystal structure of PBP with HPO_4^{2-} reveals 12 hydrogen bonding interactions; seven NH donors from the protein main chain and arginine side chain, four OH donors from serine and threonine, and an additional hydrogen bonding acceptor from a carboxylate side chain (Asp56) are exploited for the selective recognition of the phosphate species (Figure 1.8a). While the SBP stabilises the sulfate anion by the assistance of seven hydrogen bonds from the peptide backbone NH groups, serine OH, and NH of tryptophan (Figure 1.8b).

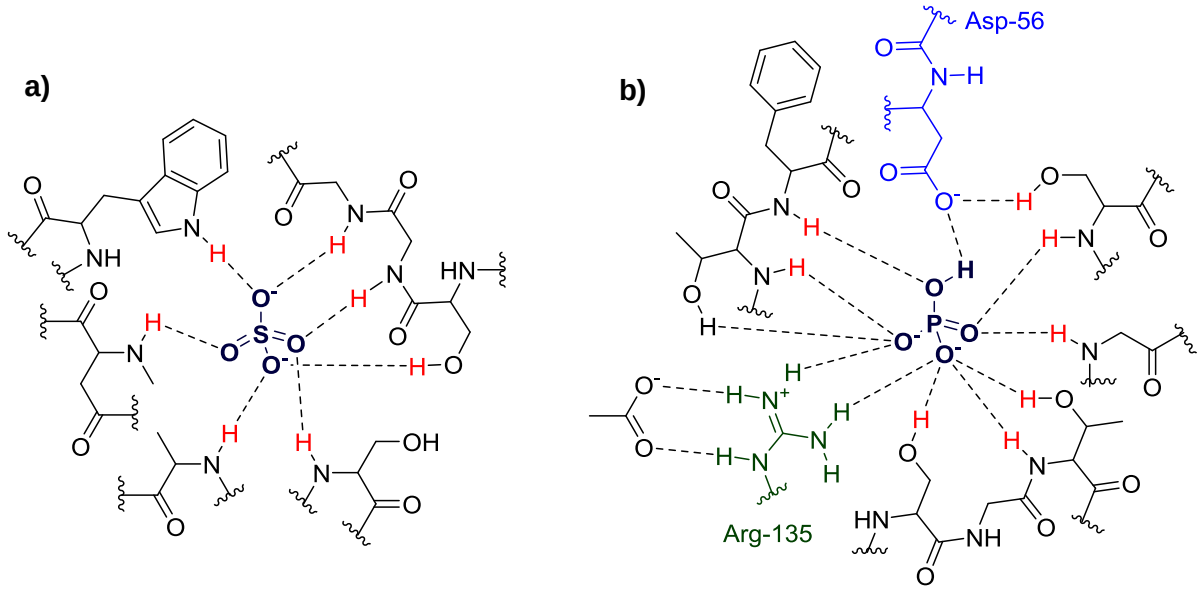

Figure 1.8 Complementary convergent hydrogen bonding interactions in the anion binding pocket of (a) phosphate and (b) sulfate binding proteins.

1.3.4 Synthetic anion receptors for anion recognition

This section gives an overview of synthetic anion receptors, classified by the type of non-covalent interaction used to mediate anion recognition.

1.3.4.1 Hydrogen bonding receptors

Hydrogen bonding (HB) donor motifs have been integrated into a broad range of anion receptors that function in highly competitive solvent media. Versatile NH bond donors in particular are represented in contemporary anion receptors in various forms including ammonium, guanidinium, amide, urea, and thiourea. In more recent years anion binding has been achieved utilising preorganised C—H donors especially as an alternative motif for the binding of more hydrophobic anions. This section will highlight key examples of both cationic and neutral hydrogen bonding anion receptors.[47]

a) Cationic hydrogen bonding receptors

Positively charged hosts have been exploited as the main class of anion receptors for recognition in highly competitive polar protic solvents such as methanol and water. Strong electrostatic contributions empower host association to anions, yet the non-directional nature of Coulombic forces alone can result in poor selectivity. Therefore directional hydrogen bonding is frequently additionally employed to enhance anion association as well as selectivity.[48]

Positively charged NH containing receptors are arguably the most established hosts to bind anions in aqueous solution. Early examples of receptors in this class include a macrobicyclic “katapinand” described by Park and Simmons (Figure 1.9a),[6] and a polyammonium cryptand from Lehn (Figure 1.9b),[49] that bind anions in acidic media through protonated ammonium groups. Guanidinium motifs have been used for anion recognition in a much wider pH range than the ammonium group.[50] As described by Kuchelmeister and Schmuck, a guanidinium containing tweezer-like anion receptor shows strong affinity for nucleotide based anions in water under physiological conditions with notable selectivity for monoanionic AMP over trianionic ATP (Figure 1.9c).[51]

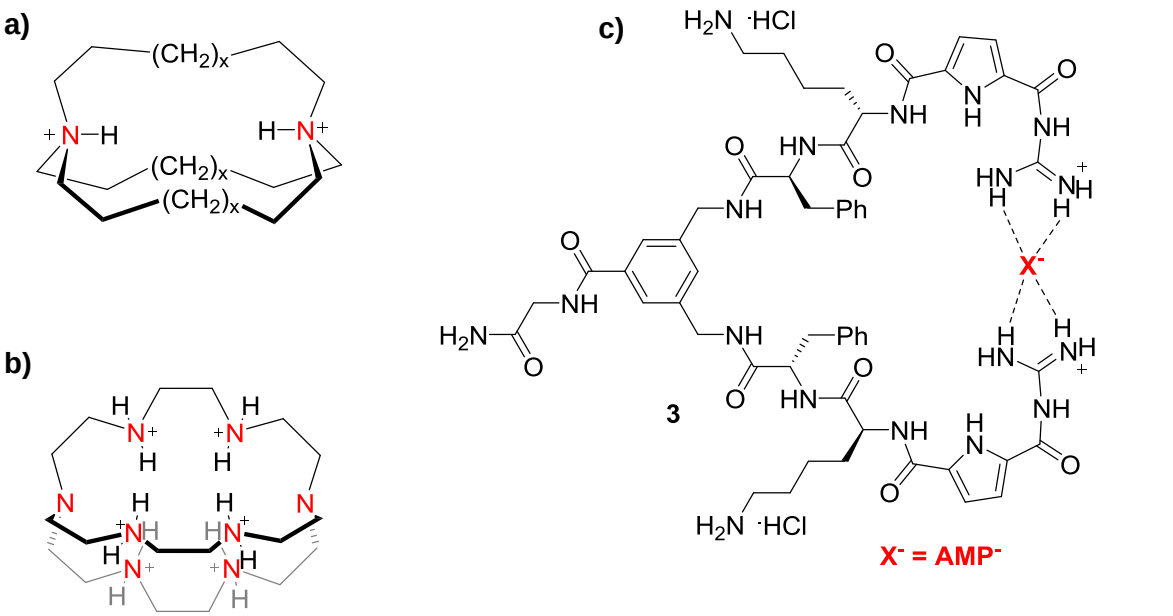

Figure 1.9 Cationic NH hydrogen bonding anion receptors: a) katapinand;[6] b) polyammonium cage[49] and c) guanidinium tweezer host.[51]

Anion receptors utilising charge assisted C—H donors commonly rely on imidazolium and triazolium motifs. [52, 53] A recent example of an imidazolium receptor capable of anion recognition in aqueous media was reported by You and co-workers.[54] The macrocyclic tetrakis(imidazolium) receptor exhibited 2:1 host-guest stoichiometry for sulfate recognition in water and in the solid state X-ray crystal structure (Figure 1.10)

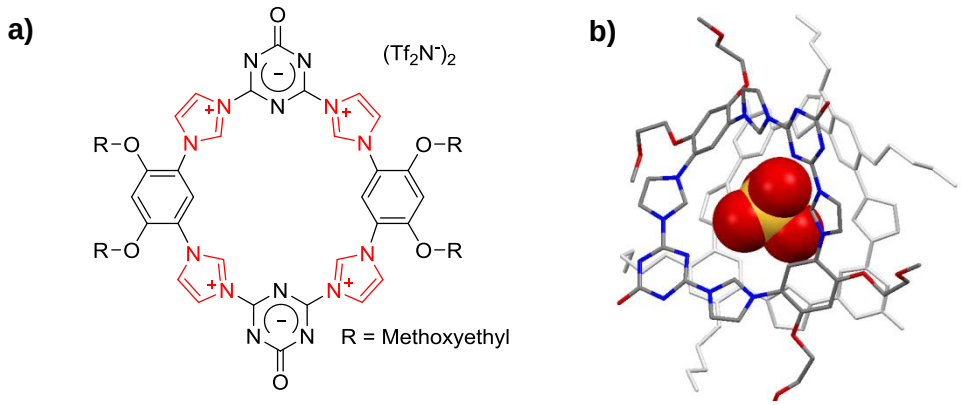

Figure 1.10 a) Structure of cationic imidazolium macrocycle reported by You; b) X-ray crystal structure with sulfate anion.[54]

Due to the synthetic accessibility of 1,2,3-triazole heterocycles *via* the copper(I) catalysed azide - alkyne cycloaddition (CuAAC) reaction, cationic triazolium C—H donors have gained more attention and been widely incorporated into a broad range of anion receptors including acyclic, macrocyclic, and interlocked hosts.[55] Hay, Sessler and co-

workers reported a pyrrole-triazolium containing cyclophane (Figure 1.11) which exhibits strong and selective binding of oxoanions in competitive organic-aqueous solvent mixtures containing up to 60% water.[56]

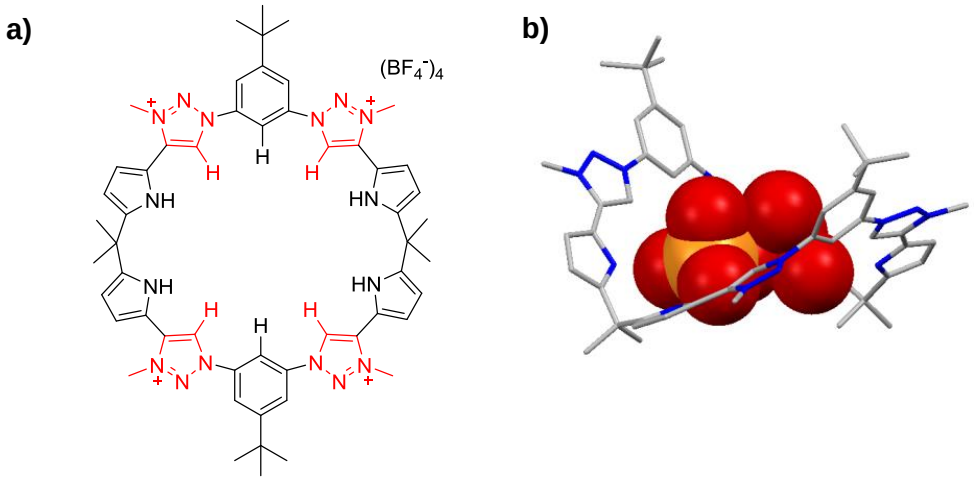

Figure 1.11 a) Structure of cationic CH triazolium macrocycle reported by Hay and Sessler b) X-ray crystal structure with pyrophosphate anion.[56]

b) Neutral and anionic hydrogen bonding receptors

Electroneutral hosts have primarily been designed to function in relatively non-polar organic solvent media. The seminal example of an amide based receptor was reported by Pascal and co-workers in 1986 (Figure 1.12a).[57] Over a decade later, Crabtree described a neutral acyclic isophthalamide receptor capable of strong halide binding in dichloromethane (Figure 1.12b).[58, 59] Due mainly to its facile synthetic accessibility, the isophthalamide motif has been subsequently integrated into a variety of host architectures. In 1996, Sessler reported the calixpyrrole class of anion receptor (Figure 1.12c).[60] The macrocyclic calix[4]pyrrole was demonstrated to strongly bind anions, in particular fluoride and dihydrogenphosphate in polar organic solvents.[61, 62]

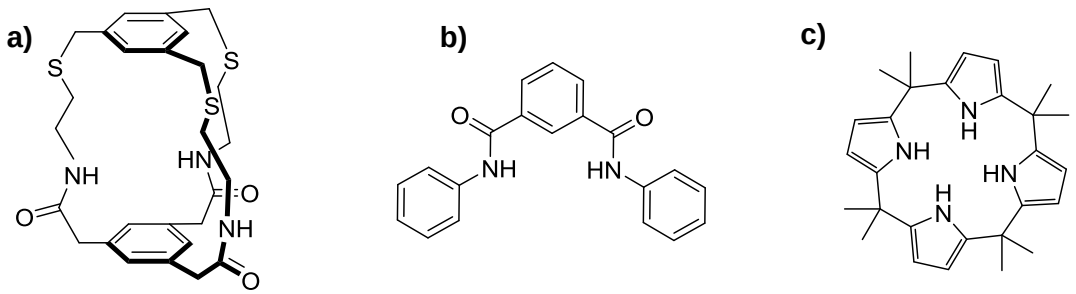

Figure 1.12 Neutral anion receptors

Highly preorganised neutral hosts in combination with hydrophobic effects have been demonstrated to bind anions in competitive aqueous media.[63, 64] A neutral macrocyclic cyclopeptide capable of recognising both hydrophilic sulfate and hydrophobic iodide anions in 4:1 water-methanol solution was reported by Kubik *et. al*.[65, 66] A 2:1 stoichiometric host-guest sandwich complex was formed with both anions stabilised by NH hydrogen bonds and hydrophobic effects (Figure 1.13a and b). Flood and co-workers exploited a preorganised foldamer that forms a 2:1 stoichiometric complex with chloride anion in a mixture of 1:1 acetonitrile/water by virtue of 'hydrophobic collapse'. Eleven concerted C—H triazole HB interactions in the hydrophobic binding site results in the encapsulation of the chloride anion (Figure 1.13c and d).[67] More recently, Sindelar and co-workers reported a novel water soluble glycouril macrocyclic host appended with negatively charged carboxylate solubilising groups, coined Bambusuril. The host displayed a remarkable affinity for hydrophobic anions stabilised by convergent C—H donor (K_a for iodide in D_2O = 1×10^7 M^{-1}) (Figure 1.13e and f).[68]

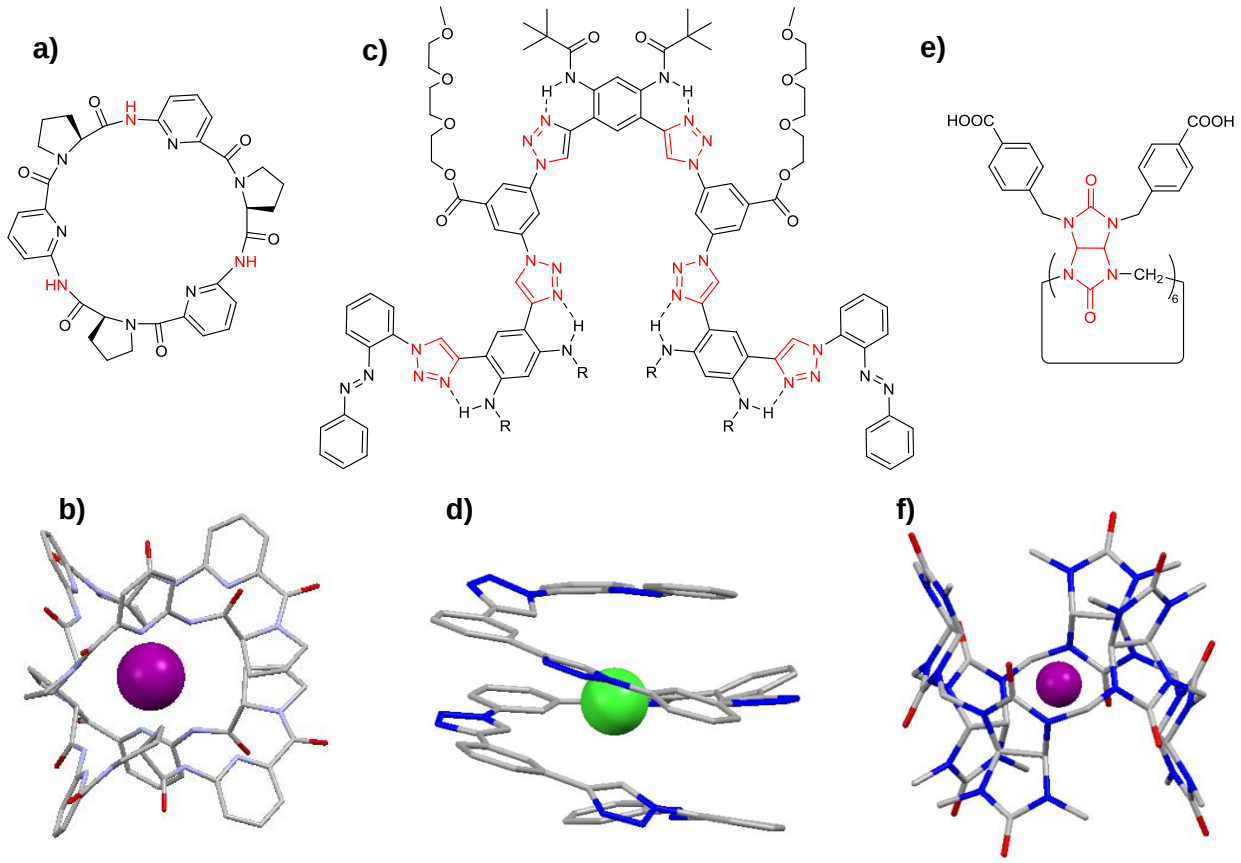

Figure 1.13 Neutral NH and CH hydrogen bonding hosts for recognising anion in aqueous media.

1.3.4.2 Metal and Lewis acid containing anion receptors

Metal and Lewis acid containing anion receptors offer alternative approaches for anion binding particularly in water where the role of metal can be as: [69, 70]

i) a Lewis acid site for direct anion coordination;

ii) a charged motif assisting anion binding *via* electrostatic interactions and/or for polarising hydrogen bond donor motifs;

iii) an electrochemical or spectrochemical reporter group;

iv) a water solubilising agent.

Since the early examples of dinuclear copper (II) cryptate complexes described by Lehn,[71] numerous examples of transition metal anion receptors have been reported including a Cu(II) calix[6]arene by Reinaud which binds fluoride anions strongly in acidic aqueous solution (log K_a = 4.9) (Figure 1.14a).[72] The Zn(II) dipicolylamine based hosts are the most prevalent class of anion receptor used for the selective recognition of biologically relevant polyoxoanions in water,[36] as illustrated by Jolliffe's bis-zinc(II)dipicolylamino-peptide which displays high affinity for pyrophosphate in buffered media (log K_a > 9) (Figure 1.14b).[73]

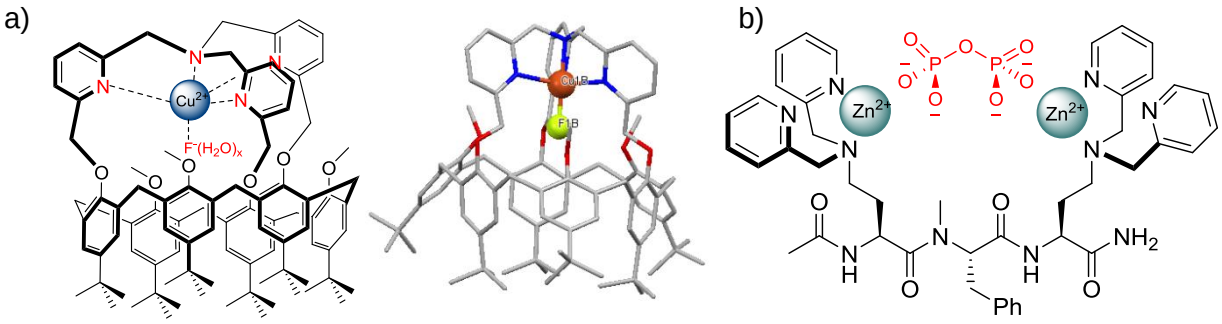

Figure 1.14 Metal based receptors for anion recognition.

A series of Lewis acidic main group element containing receptors have also been reported incorporating boron,[34] silicon, tin,[74] germanium, tellurium, and antimony.[35] Hirai and Gabbai demonstrated the first example of a neutral bidentate antimony(V) receptor capable of fluoride binding in water by means of chelation between two coordinatively unsaturated Sb(V) sites (Figure 1.15a).[75] The use of lanthanide based receptors has been established for anion sensing purposes.[76] For example, a triazacyclononane-Eu^{III} complex reported by Parker and co-worker demonstrates high affinity towards oxoanions by displacement of ligating water at the metal centre (Figure 1.15b). This complex was demonstrated to be capable of quantifying the concentration of bicarbonate anion in human serum by luminescence ratiometric analysis.[77]

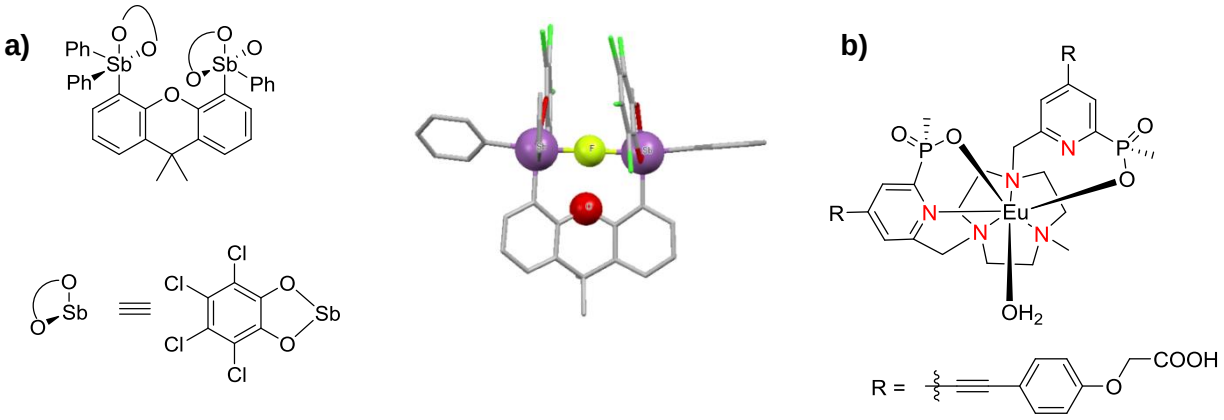

Figure 1.15 Lewis acidic anion receptors a) antimony(V) anion receptors and its X-ray crystal structure with fluoride[75] and b) triazacyclononane-Eu^{III} complex.[77]

1.3.4.3 Hydrophobic effect

In addition to exploiting electrostatics and HB interactions for anion recognition, the hydrophobic effect has been employed to achieve strong and selective binding of anionic guests in aqueous solution. Gibb and co-workers have extensively investigated this phenomenon and correlated selectivity to the Hofmeister series through anion binding experiments using deep cavity hosts called cavitands. In the original host design the water soluble cavitand possesses a neutral hydrophobic cavity built from an aromatic-walled interior with peripheral carboxylates as water solubilising groups (Figure 1.16). The authors observed an enhancement in adamantane carboxylate (hydrophobic anion guest) binding in the presence of highly hydrated anions such as fluoride, acetate, and sulfate, whilst less hydrated anions like perchlorate decreased the affinity of this organic anion.[78] These observations were attributed to competitive binding between the targeted hydrophobic guest and weakly hydrated anions, particularly perchlorate within the cavitand hydrophobic binding pocket.[79] Subsequent studies indicated the cavitand's preferential binding of hydrophobic anions was driven exclusively by favourable enthalpy, the thermodynamic fingerprint of the non-classical hydrophobic effect.[80]

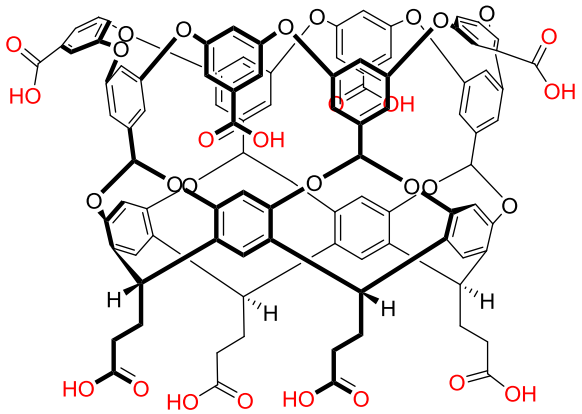

Figure 1.16 Gibb's water soluble cavitand.

1.3.4.4 Halogen bonding

The halogen bond has only relatively recently emerged as a potent non-covalent interaction to utilise in the field of anion recognition. To date halogen bonding (XB) has focused on five versatile motifs; neutral haloperfluoroarene, halotriazole, haloimidazole, and the charge assisted analogues halotriazolium and haloimidazolium (Figure 1.17). [81]

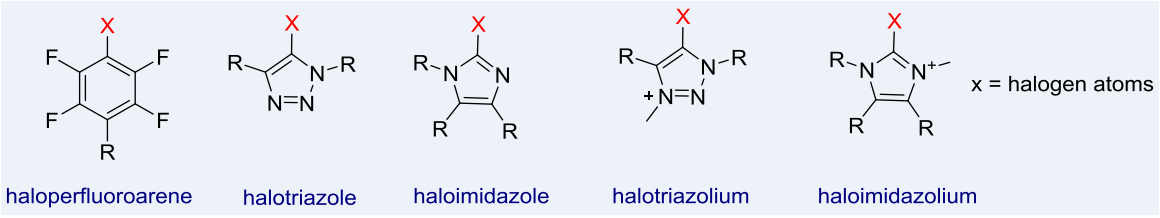

Figure 1.17 Halogen bonding (XB) motifs for anion recognition.

A seminal work in solution phase XB anion recognition was reported by Metrangolo, Resnati, and co-workers in 2005 using a tripodal iodoperfluoroarene polyether host capable of sodium cation-iodide anion ion-pair recognition (further details are discussed in Chapter 2).[82] Five years later in 2010 Taylor and co-workers designed a tridentate iodoperfluorobenzene based receptor which displayed a strong Cl^- binding affinity (K_a= 1.9 $\times 10^4$ M^{-1}) in d_6-acetone (Figure 1.18). Replacing iodine atoms by bromine, fluorine, or hydrogen resulted in substantially reducing Cl^- binding strength.[83-85]

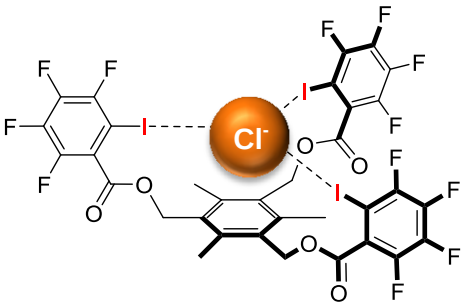

Figure 1.18 Taylor's tripodal iodoperfluoroarene XB anion receptor.

Metrangolo, Resnati, and co-workers observed a rare example of XB selective oxoanion binding using the 2-iodoimidazolium motif.[86] In polar aprotic DMSO, the anthracene functionalised XB iodoimidazolium receptor exhibited selective $H_2PO_4^-$ binding over AcO^- and halides, with superior affinity in comparison to the analogous HB receptor (Figure 1.19a). Subsequently Beer and co-workers developed a series of macrocyclic haloimidazolium receptors which are capable of halide recognition in a competitive water-methanol solvent mixture. The *syn* atropisomer of the bromoimidazolium bis-naphthyl macrocycle displayed

notable selectivity for Br^- among the halides, while the HB analogue showed modest affinity to all the halides (Figure 1.19b).[87-89]

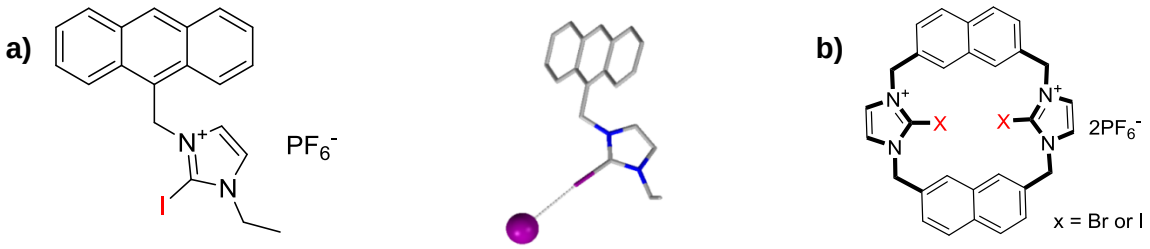

Figure 1.19 Haloimidazolium anion binding receptors (a) acyclic iodoimidazolium and its crystal structure with iodide and (b) iodoimidazolium macrocycle.

The synthetic accessibility of the 5-halotriazole motif has enabled preorganised halotriazole receptors as well as charge assisted halotriazolium receptor analogues to be constructed. Schubert *et al.* prepared a neutral bidentate bis-iodotriazole carbazole anion receptor where intramolecular hydroxyl—triazole nitrogen interactions preorganise the receptor in the *syn-syn* conformation to facilitate cooperative anion binding in a bidentate fashion (Figure 1.20a).[90] Rhenium(I) complexation preorganises a bis-iodotriazole pyrimidine receptor to achieve the recognition of halides in competitive $CDCl_3/CD_3OD$ (1:1) media (Figure 1.20b). The two metal centres also act as chromophoric probes for anion sensing, exhibiting significant perturbations of the MLCT absorption band upon addition of anions in acetonitrile. [91]

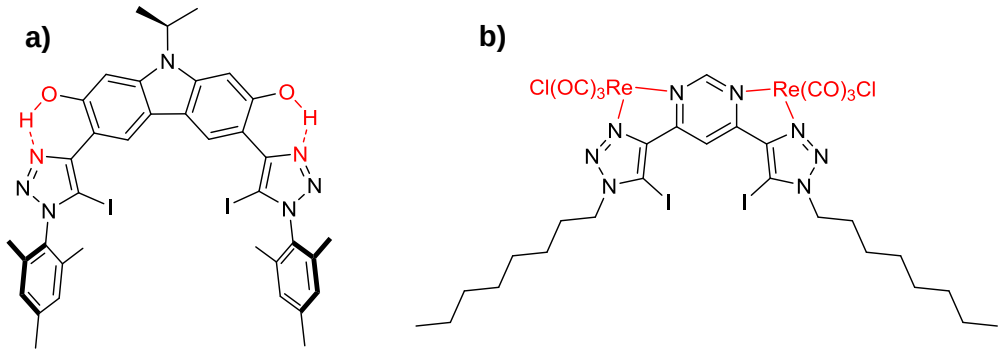

Figure 1.20 Preorganised bidentate XB anion receptors

Alkylation of iodotriazole motifs produces potent cationic iodotriazolium XB donors which have been integrated into various acyclic receptor frameworks. The water soluble bis-iodotriazolium XB receptor displays selective ReO_4^- binding in pure water *via* bidentate anion coordination (Figure 1.21a),[92] while the pyrene functionalised bis-iodotriazolium compound reported by Molina, demonstrates pyrophosphate fluorescence sensing in acetone (Figure 1.21b).[93]

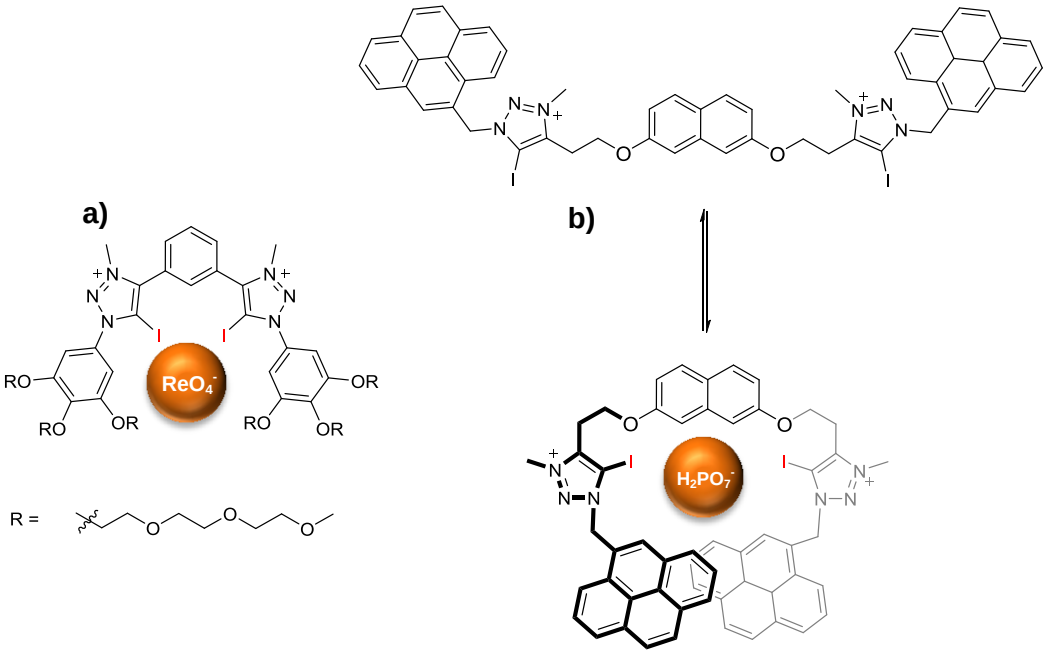

Figure 1.21 Cationic triazolium anion receptors

1.3.4.5 Chalcogen bonding

Chalcogen bonding (ChB) can be considered as a sister non-covalent interaction to XB, where the electron deficient chalcogen atom acts as a Lewis acidic group. Compared to XB, the application of ChB in anion recognition is much less developed. The first example of solution phase anion recognition behaviour of such an interaction was reported by Zibarev et. al. on a series of 4,5-dicyano-1,2,5-chalcogendiazole anion receptors (Figure 1.22a). The tellurium heterocycle displayed impressive iodide binding in polar aprotic organic solvents including THF (K_a= 6.8 $\times 10^5$ M^{-1}), acetonitrile (K_a= 1.5 $\times 10^3$ M^{-1}) relative to the selenium analogue. Taylor and co-workers subsequently prepared a series of related benzochalcogenodiazoles appended with various electron withdrawing substituents on the benzene ring. These receptors displayed neutral and anionic Lewis base binding with selectivity towards highly charged dense anions in THF solution. The ChB donor ability was demonstrated to be tunable by increasing the number of electron withdrawing substituents attached to the benzene ring (Figure 1.22b). For example, the highly electron deficient perfluoro-substituted analogue exhibited a stronger chloride binding affinity (K_a = 130000 M^{-1}) in comparison to the cyano- (K_a = 38000 M^{-1}), bis-bromo- (K_a = 12200 M^{-1}), and the benzene derivatives (K_a = 970 M^{-1}).[94]

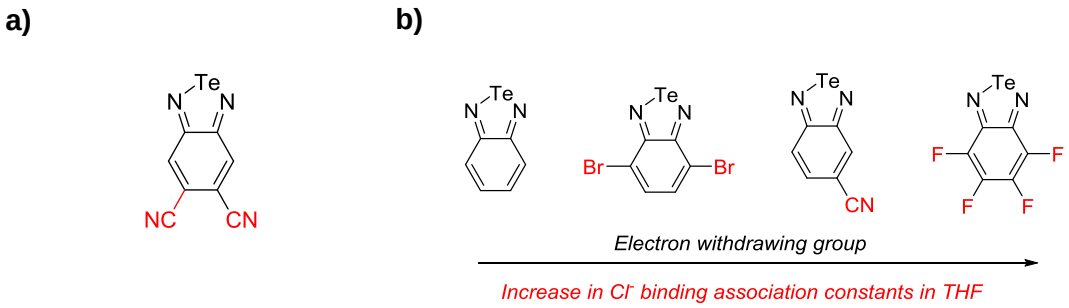

Figure 1.22 Chalcogen bonding anion receptors.

Recently Beer and co-workers used the agonistic properties of a selenium containing macrocycle as a donor ligand for Cu(I) to prepare a series of ChB [2]rotaxanes *via* an active metal template approach, and as a ChB donor for anion binding. The resulting rotaxane host exhibited stronger anion binding affinities to halides and oxoanions in comparison to its HB analogue in water-acetone mixtures.[95]

1.3.5 Anion sensing

Molecular anion sensors are designed to produce a macroscopic detectable signal upon the selective binding of a target anion guest species. Typically such systems contain an optical or electrochemical reporter group covalently linked to an anion recognition site.

1.3.5.1 Optical anion sensing

Optical anion sensors can be divided into two major classes based on their mode of signalling: colorimetric and fluorescent anion sensors. Anion sensing by colorimetric analysis exploits the anion binding induced perturbation of the chromophore's electronic visible spectrum, which results in naked-eye detection. With highly basic anions, deprotonation of a receptor's acidic protons in aprotic organic solvents often results in naked-eye colour changes. For example, Fabrizzi and co-workers demonstrated a bis-naphthalimide urea receptor (Figure 1.23a) that undergoes double-deprotonation upon addition of two equivalents of fluoride anion in DMSO producing a blue solution, whilst acetate forms a red solution as a result of monodeprotonation. Similarly, Sessler designed a series of chromophore appended calix[4]pyrrole hosts capable of sensing basic anions in dichoromethane (Figure 1.23b).[96] Fluorescent anion sensors rely on anion binding induced changes of the excited-state emission profile *via* photoinduced electron transfer (PET), excimer formation, and non-radiative decay pathways. A boron-dipyrromethane (BODIPY) appended amidothiourea anion receptor undergoes quenching of fluorescence *via* PET upon addition of fluoride in 1:1 DMSO/H_2O (Figure 1.23c).[97]

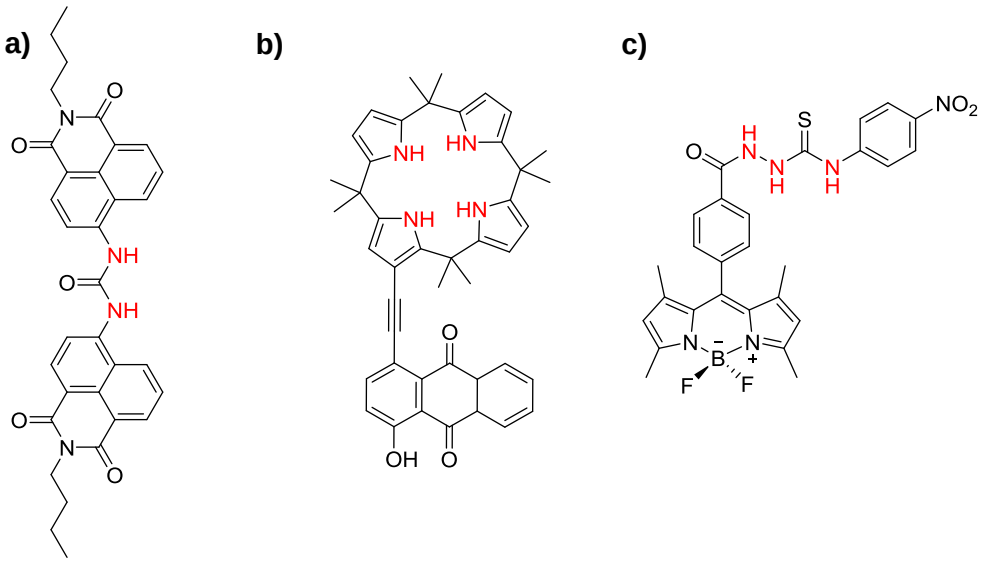

Figure 1.23 Optical anion sensors.

1.3.5.2 Electrochemical sensing

Voltammetric electrochemical sensors typically contain redox responsive motifs, such as metallocenes, covalently linked to an anion binding site. In the late 1980s early 1990s Beer and co-workers reported the first cobaltocenium and ferrocene redox responsive anion sensors. Since then ferrocene in particular has been integrated into a wide range of anion host systems. Tucker and co-workers have reported a series of urea receptors containing ferrocene redox active groups capable of chiral carboxylate recognition. The addition of the (S)-enantiomer of benzenesulfonyl proline guest caused a larger cathodic shift in the ferrocene/ferrocenium redox couple (ΔE = 80 mV) relative to the (R)-stereoisomer (ΔE = 70 mV) in acetonitrile solution (Figure 1.24a). A calix[4]pyrrole receptor functionalised with the organic redox-active tetrathiafulvalene (TTF) group which demonstrated electrochemical sensing behaviour in MeCN by a significant cathodic shift of the first TTF oxidation potential upon the addition of chloride and bromide (Figure 1.24b).[98]

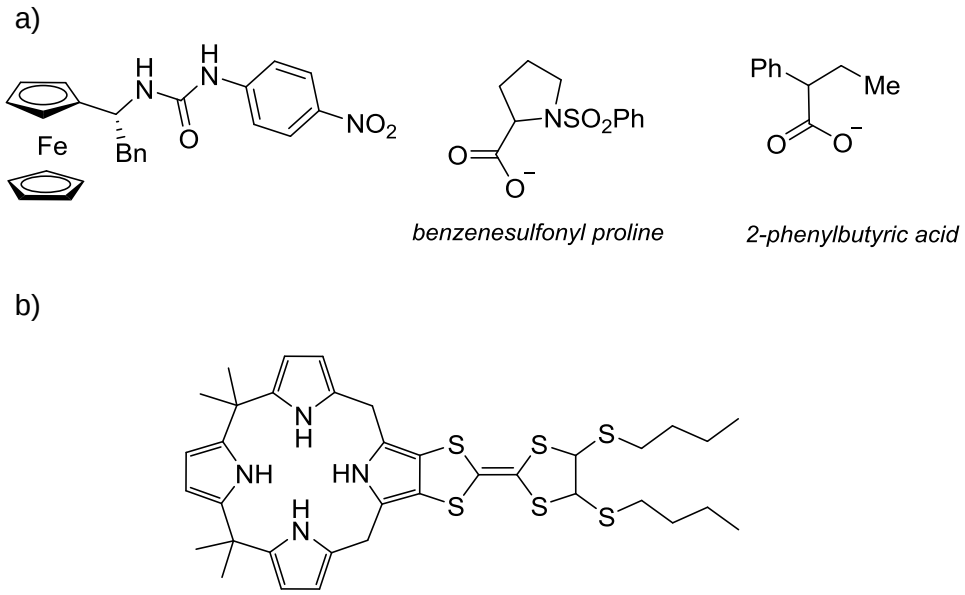

Figure 1.24 Electrochemical anion sensors.

1.4 Recognition of Ion-Pairs

Charged species are ubiquitous in playing crucial roles in chemical, biological, medical, environmental, and industrial processes. The cation and anion binding affinities of monotopic receptor systems are critically influenced by the nature of the respective counterions. This has stimulated an ever increasing interest in the construction of heteroditopic receptors for ion-pair recognition where favourable proximal cation—anion electrostatic interactions enhance the strength of binding the charged guest species. Such systems have been demonstrated to facilitate the solubilisation of inorganic salts into organic media, to function as efficient extraction and membrane transport agents, and to be capable of recognising biologically relevant zwitterionic species.[99, 100] Despite their plethora of potential applications, progress in the field remains relatively limited, in part attributed to the sometimes challenging synthesis of heteroditopic host structural frameworks.

Ion-pair recognition is associated with multiple complex equilibria (Figure 1.25). In solution charged species do not completely dissociate, particularly in low polarity solvent, due to strong ion-pairing effects. In the presence of a heteroditopic receptor, the anion or cation may bind to the receptor separately *via* their monotopic sites (K_1 and K_3). They can also bind to the ditopic receptor simultaneously (K_2), or may form ion-paired species external of the receptor (K_{ip}). For cooperative binding, K_2 is larger than the sum of K_1 and K_3 (see Chapter 2, section 2.1 for further discussions).

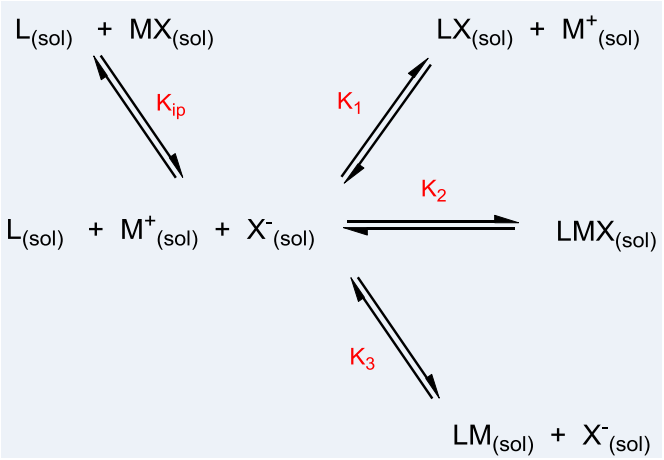

Figure 1.25 Diagram illustrating the various equilibria that need to be considered in an ion-pair binding system.

Common designs of heteroditopic receptors can be summarised into three different types which are shown in Figure 1.26. Cascade complexes occur where anionic species bridge between two bound cations in the host (Figure 1.26a). In the case where cation and

anion recognition sites are far apart, separated ion-pair binding is observed (Figure 1.26b). With the binding sites for the cation and anion in close proximity, contact ion-pair complexation is favoured (Figure 1.26c).

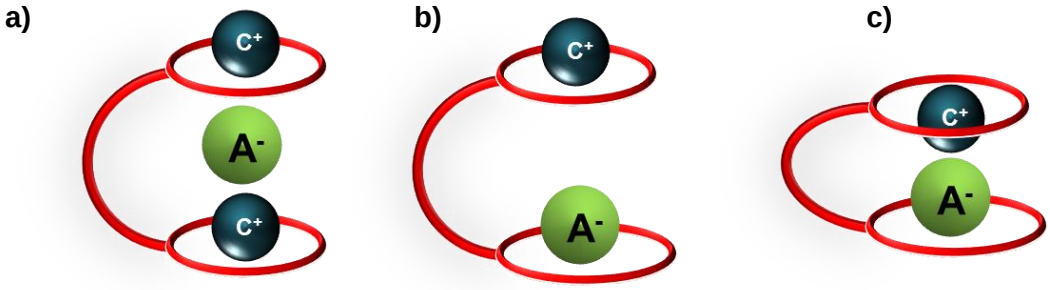

Figure 1.26 Cartoon representations of general types of heteroditopic ion-pair receptors: a) cascade complex, b) separated ion-pair host, and c) contact ion-pair receptor.

1.4.1 Heteroditopic receptors for cascade ion-pairs

In nature, an important example of a cascade receptor is haemocyanin, a dinuclear copper respiratory protein found in most molluscs and some athropods. The two histidine coordinated copper (I) binding sites in the deoxy-haemocyanin protein are available for the binding of O_2, resulting in the formation of the dicopper(II)-O_2^{2-} ligand bridged cascade assembly. Abiotic examples include the [24]ane-N_2S_4 macrocycle (Figure 1.27a) which contains two tridentate SNS copper (II) binding sites, and bridging azide counter anions.[101] Another example is a series of bis-tren incorporated macrobicyclic cryptands with various spacer units (Figure 1.27b). These receptors form nickel(II) and copper(II) complexes in each tren unit to facilitate cascade complex formation with azide and bromide anions.[102, 103]

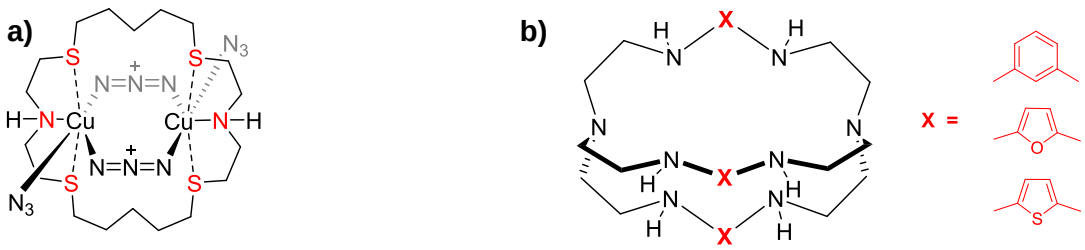

Figure 1.27 Cascade ion-pair receptors: a) the [24]ane-N_2S_4 macrocycle and b) a series of bis(tren) cryptands**.**

1.4.2 Heteroditopic receptors for separated ion-pairs

Separated ion-pair host structures typically employ allosteric and solvent effects to facilitate coordination. Reinhoudt and co-workers reported a urea functionalised tetraester calix[4]arene heteroditopic receptor capable of solubilizing inorganic sodium halide salts such as NaCl into chloroform (Figure 1.28a).[104] Recently, Ghosh and co-workers designed a simple ion-pair host by combining dibenzo-18-crown-6 with an electron deficient pentafluorophenyl-urea anion binding motif. This receptor exhibited enhanced nitrate and bromide strength of binding in the presence of a crown ether complexed potassium cation in acetonitrile, and demonstrated selectivity for KBr in solid-liquid extraction experiments (Figure 1.28b).[105]

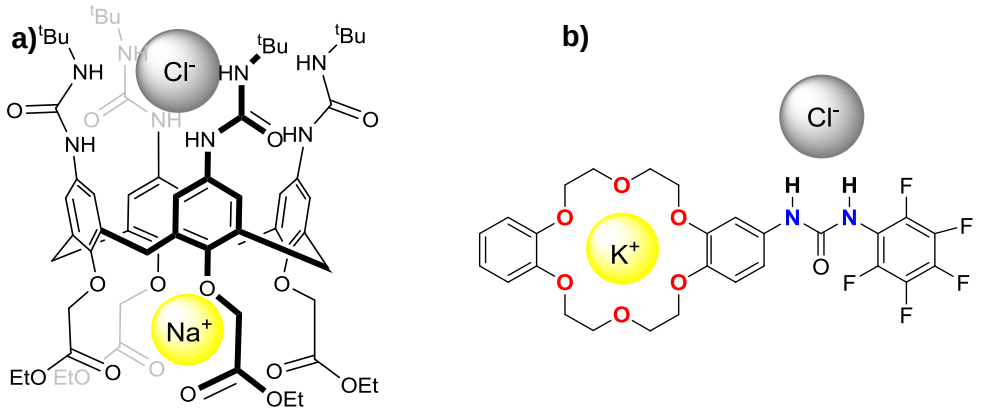

Figure 1.28 Separated ion-pair receptors having an alkali metal cation binding site.

Saha has integrated naphthalenediimide (NDI) moieties into a tridentate bis-imine-pyridine metal cation binding group which upon addition of transition metal cations (Zn^{2+}or Cd^{2}) resulted in the formation of a U-shape 2:1 stoichiometric host-guest assembly with two intercalated perchlorate (ClO_4^-) counteranions between the bis-NDI units. The transition metal ion-pair complexation process was demonstrated to be reversible by the addition of a competitive macrocyclic ligand, cyclam (Figure 1.29).[106]

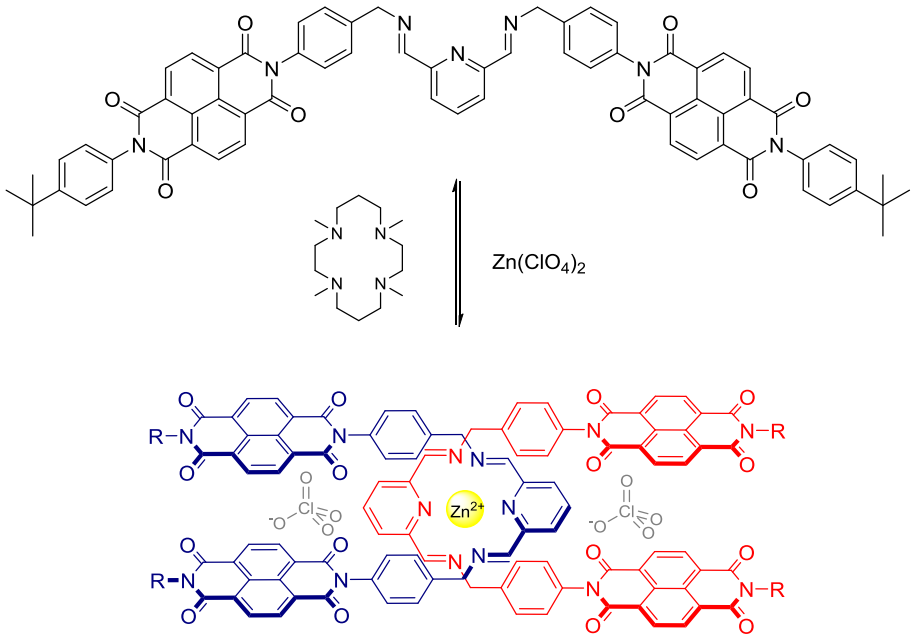

Figure 1.29 Separated ion-pair receptor having a transition metal cation binding site.

In addition to inorganic ion-pair binding, Arduini and co-workers described a calix[4]arene based receptor capable of binding organic ion-pairs. Hydrogen bonding interactions between anionic guest species (sulfonate, tosylate, and chloride) and terminal phenolic groups within the host provided a preorganised cavity for binding of a tetramethylammonium (TMA) cation *via* cation—π interactions (Figure 1.30).[107, 108]

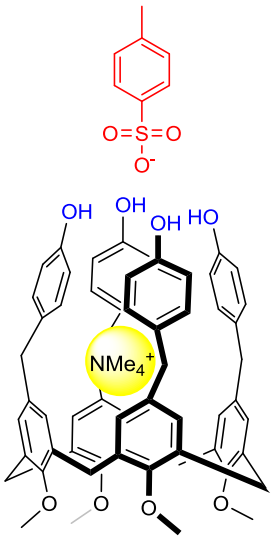

Figure 1.30 Phenol containing separated ion-pair receptor for organic ion-pair binding.

In 2017, a cavatind class of heteroditopic receptor was reported by Lledo and co-workers. The novel preorganised cavitand receptor contained complementary binding sites where an electron-rich aromatic pocket was designed for quaternary ammonium cation binding, covalently linked with an appended thiourea anion recognition site (Figure 1.31). Remarkably strong binding affinities were observed with tetramethylammonium (Me_4N^+) ion-pair salts, while a series of more sterically hindered ammonium salts exhibited modest binding strength in $CDCl_3$.[109]

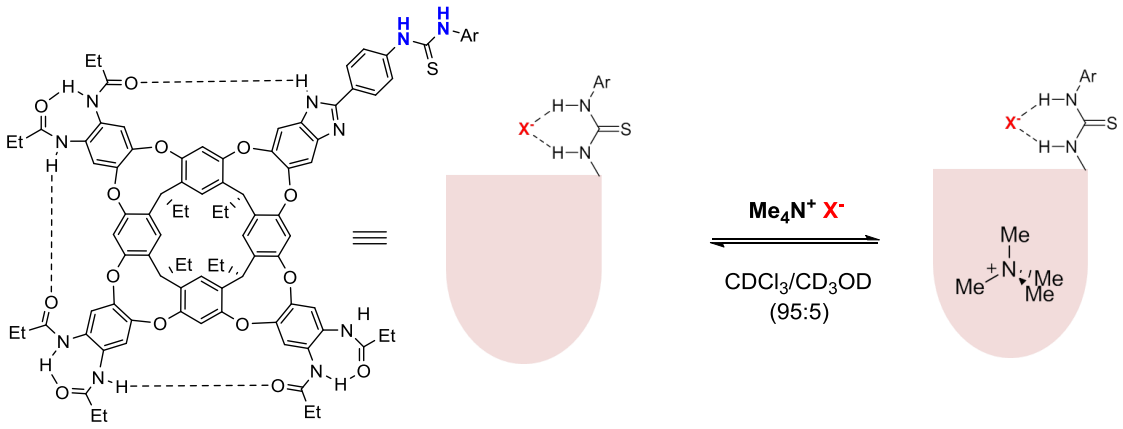

Figure 1.31 Urea appended separated ion-pair receptor for organic ion-pair binding

1.4.3 Heteroditopic receptors for Contact Ion-Pairs

Contact ion-pair receptors are designed to minimize energetically unfavourable cation—anion charge separation. In 2001, Smith and his group combined diaza[18]crown-6 with an isophthalamide anion binding motif to produce the ion-pair macrobicyclic host shown in Figure 1.32a.[110, 111] The receptor exhibits an impressive enhancement of chloride binding in the presence of sodium and potassium cations in d_6-DMSO. Single crystal X-ray diffraction structures of the NaCl and KCl complexes revealed the formation of favourable contact ion-pairs between the crown ether complexed alkali metal cation and the diamide chelated chloride anion. With the same cation binding motif, an analogous ferrocene bis-amide heteroditopic host system was shown to selectively bind NaBr in 95:5 $CD_3CN/CDCl_3$ (Figure 1.32b).[112] The redox-active receptor was also capable of electrochemically sensing anions *via* cathodic shifts of the ferrocene electrochemical transducer. Importantly the magnitudes of these cathodic shifts were enhanced in the presence of co-bound sodium cations. The first example of a contact ion-pair complex that required the simultaneous binding of cation and anion for cooperative ion pair recognition was reported by Beer and coworkers. The

isophthalamide strapped calix[4]diquinone receptor (Figure 1.32c), complementary bound NaCl and NH_4Cl ion-pairs in 98:2 CD_3CN/D_2O.[113-116]

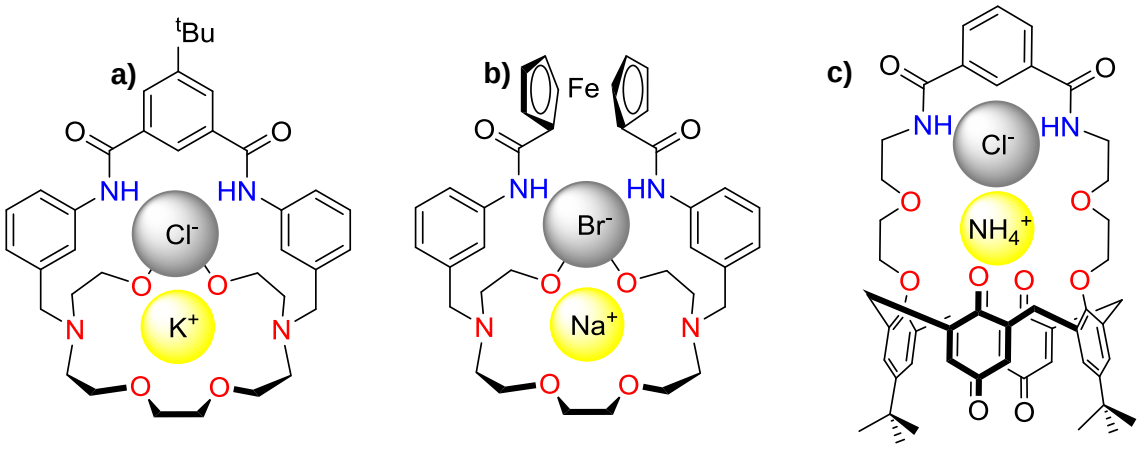

Figure 1.32 Contact ion-pair receptors

Typically heteroditopic receptors capable of contact ion-pair recognition have been restricted to alkali metal halide binding. Recently, Lacour and co-workers prepared a series of polyamide cryptands synthesised *via* three steps from 1,4-dioxane. The receptors exhibited selective binding of linear triatomic anions such as azide, cyanate, thiocyanate, over halides in the presence of co-bound alkali metal cations (Figure 1.33), in contrast to analogous bis-amide macrobicyclic host structures reported by Smith and Tantulani.[117]

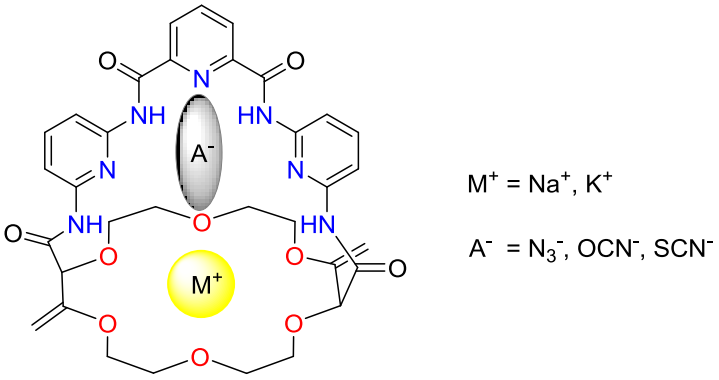

Figure 1.33 Contact ion-pair receptors for alkali metal salts binding.

Yuan and co-workers reported a novel class of shape-persistent cyclic host coined cyclo[6]aramides. Intramolecular HB interactions preorganise a complementary arrangement

between the bis-amide units and carbonyl groups allowing recognition of organic ion-pair species such as dialkylammonium,[118] and amidinium salts.[119] An X-ray crystallographic structure revealed dibutylammonium chloride binding within the host cavity as a contact ion-pair complex in a pseudorotaxane assembly fashion (Figure 1.34).

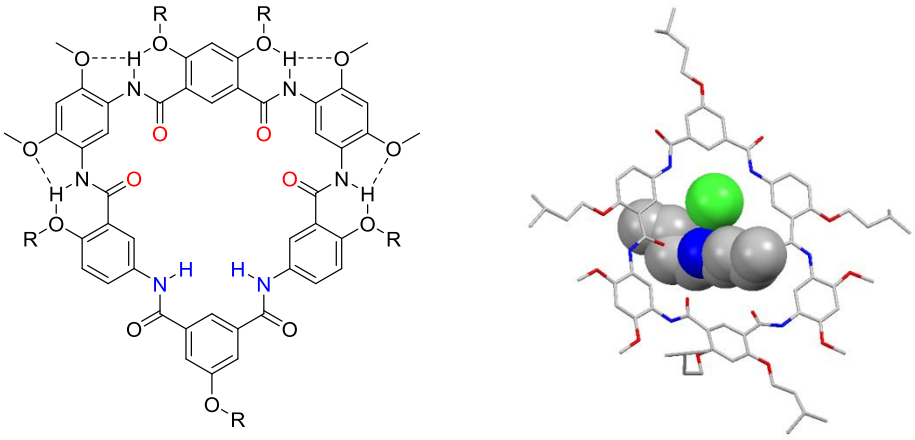

Figure 1.34 Cyclo[6]aramides macrocycle for ion-pair recognition and its X-ray crystal structure with diethylammonium chloride.

1.4.4 Applications of Ion-Pair Receptors

1.4.4.1 Receptors for Zwitterions

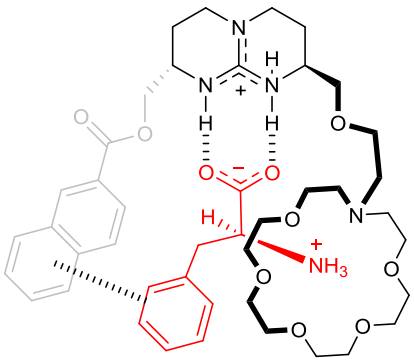

Figure 1.35 Zwitterionic amino acid recognition.

Zwitterions are neutral ion-pair species wherein the cationic and anionic residues are covalently linked in the same molecule; for example, amino acids are zwitterions at physiological pH. Hence, heteroditopic receptors have been designed to recognise such species. The receptor in Figure 1.35 is capable of extracting amino acids from aqueous solution into dichloromethane, with a particular high efficacy for aromatic side chain containing amino acids such as L-tryptophan. The ditopic receptor binds L-tryptophan *via* multiple complementary non-covalent interactions, including carboxylate hydrogen bonds to the receptor's cationic guanidinium motif, ammonium–crown ether complexation, and additional aromatic–π stacking between the receptor's naphthalene moiety and the aromatic side chain of the amino acid guest species.[120] Phospholipids are a major class of zwitterionic lipids found in cell membranes. In 2015, Jabin and co-workers reported a heteroditopic calix[6]tube receptor capable of the selective recognition of phosphatidylcholine (PC) zwitterionic phospholipids in non-polar organic media. This ditopic host utilised a combination of anion—urea HB interactions as well as ammonium cation—π

and CH—π interactions for phospholipid binding (Figure 1.36a).[121] Recently, the same group integrated pyrene reporter units into the calix[6]arene ditopic host to obtain a fluorescent chemosensor , exhibiting PC sensing in biphasic $CDCl_3$/water mixtures (Figure 1.36b).[122]

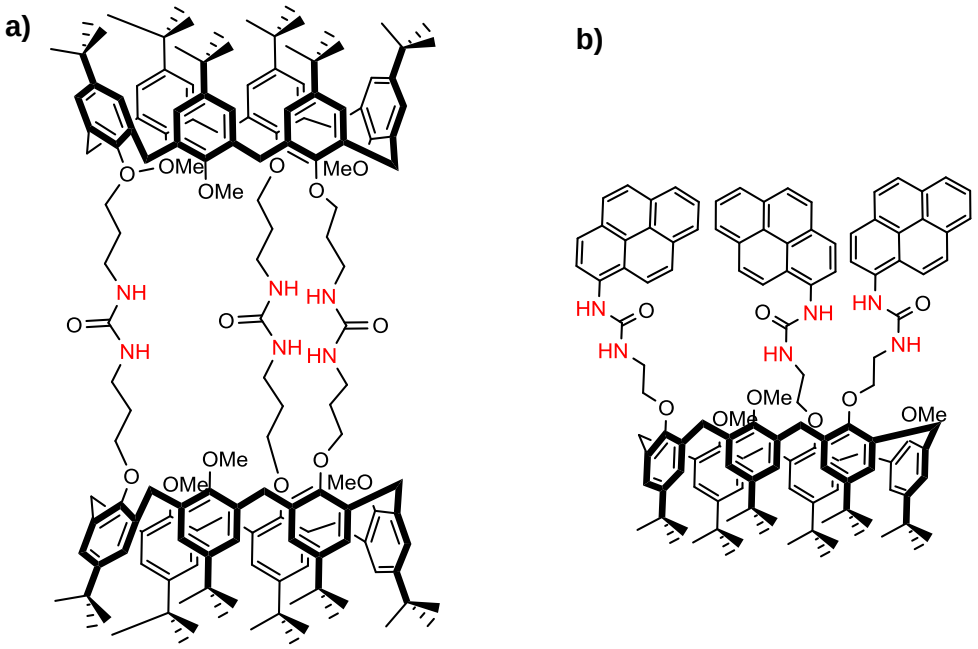

Figure 1.36 Calix[6]arene based ion-pair receptors for zwitterionic species binding.

1.4.4.2 Salt Extraction

Ion-pair receptors offer potential solutions to industrial and environmental issues. In the conventional extraction of precious and valuable transition metals from industrial waste, cation exchange materials as well as solvating reagents are exploited to extract and pre-concentrate metal ions from acidic aqueous solutions into organic media.[1] In a seminal publication, Tasker and co-workers reported the solvent extraction of $CuSO_4$ using salen based heteroditopic receptors. By virtue of the cooperative ion-pair binding sites, the salen extracting agents performed near quantitative recovery of $CuSO_4$ from acidic aqueous media into chloroform (Figure 1.37a).[123] More recently, the same group investigated the solvent extraction behaviour of a ditopic urea ligand containing a cyclen unit (Figure 1.37b). This ligand displayed a moderate recovery of $CuSO_4$ from acidic aqueous solutions, with high extracting selectivity for Cu(II) salts over other divalent transition metal cations such as Ni(II), Co(II), and Zn(II) present in the aqueous phase.[124]

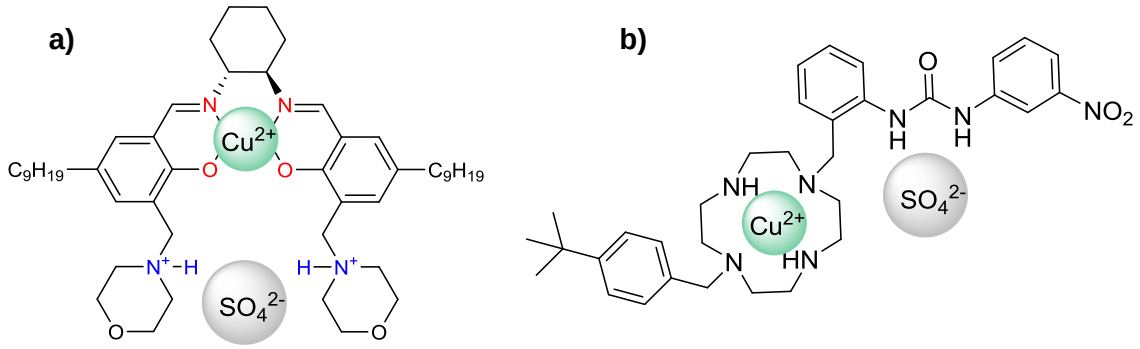

Figure 1.37 Heteroditopic receptors for copper(II) sulfate extraction.

Piątek and co-workers have been investigating the use of simple molecular scaffolds such as propionic acid and amino acid derivatives in the synthesis of ion-pair receptors specifically for salt extraction applications. The L-orthinine amino acid was exploited to prepare heteroditopic receptors containing a bis-urea anion binding motif covalently attached to aza[18]crown-6 (Figure 1.38a). The nature of the spacer group between cation and anion binding sites played a key role to regulate alkali metal cation binding affinity and, as a consequence, strongly influenced ion-pair binding. This behaviour was highlighted by an N-alkyl linked receptor demonstrating superior binding of KCl to the more electron deficient N-acyl derivative. Moreover, the N-alkyl host performed effective liquid-liquid extraction of KCl and NH_4Cl from the aqueous phase into $CHCl_3$ solution, while the N-acyl host was inactive. Recently, the same group reported a related ditopic receptor that was capable of extracting the hydrophilic potassium acetate salt (Figure 1.38b).

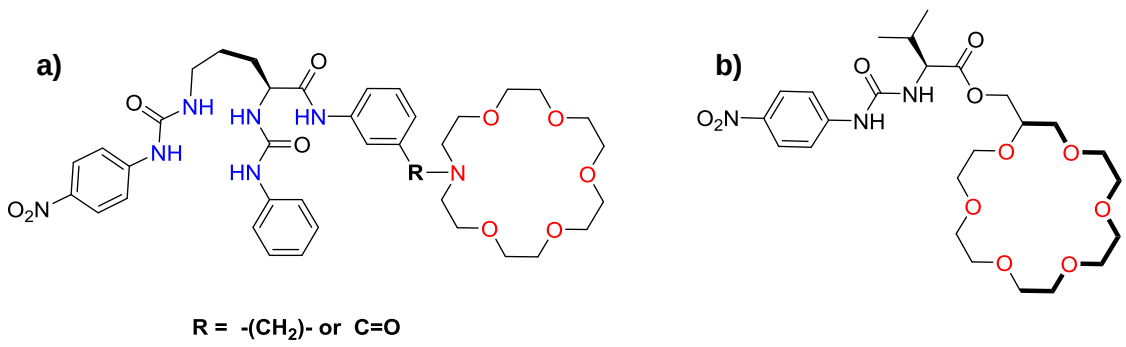

Figure 1.38 Heteroditopic receptors for salt extractions.

Romański and co-workers immobilised a series of thiourea receptors appended with aza[18]crown-6 onto a polymeric resin to function as efficient sodium nitrite extracting agent materials (Figure 1.39).

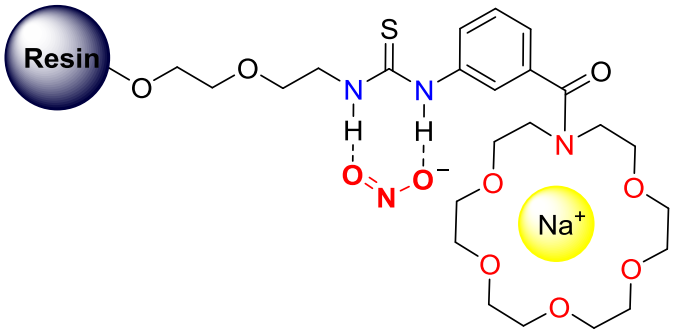

Figure 1.39 Heteroditopic receptor functionalised polymeric resin.

Sessler and co-workers used a multitopic hemispherand calix[4]pyrrole host for extraction of CsOH and Cs_2CO_3. The basic nature of the counter anions resulted in the pH value of the aqueous phase to be lowered without the addition of any acid (Figure 1.40a).[125] The same group constructed a phenanthroline strapped calix[4]pyrrole host which displayed the selective recognition and extraction of LiCl salts (Figure 1.40b).[126]

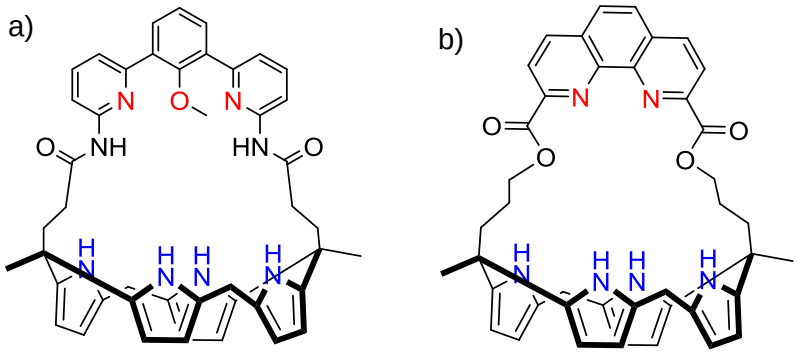

Figure 1.40 Sessler's (a) hemispherand strapped calix[4]pyrroles and (b) phenanthroline strapped calix[4]pyrrole for ion-pair extraction.

1.4.4.3 Membrane transporting agents

The cellular membrane transport of ionic species is a key biological mechanism required to maintain the local charge neutrality of living cells. Over many years, a range of abiotic monotopic carrier hosts have been studied, however, examples of heteroditopic transporters are rare. In 2003, Smith and his group reported a ditopic macrobicycle capable of transporting alkali metal halide contact ion-pair species (Figure 1.32a). Importantly, this receptor enhanced the rate of ion-pair transport in comparison to using a monotopic host.[127] Gale and co-workers demonstrated the use of an octamethylcalix[4]pyrrole macrocycle to facilitate the selective transport of CsCl as a separated ion-pair complex through phospholipid bilayers (Figure 1.41a). A year later the same group designed a triazole strapped calix[4]pyrrole macrobicycle (Figure 1.41b). As a result of more efficient anion binding, this ion-pair host exhibited contrasting behaviour by transporting more hydrophilic alkali metal chloride salts in comparison to the parent calix[4]pyrrole.[128]

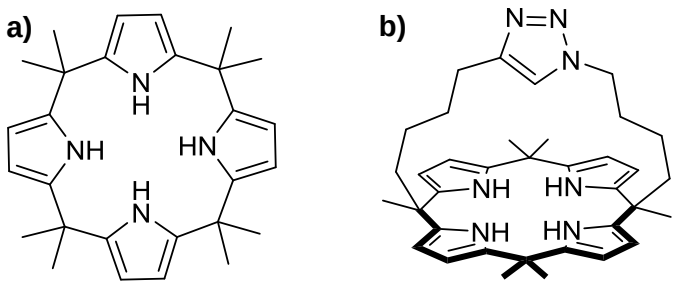

Figure 1.41 Heteroditopic receptors for membrane transport.

Jeong and co-workers used a series of urea appended aza-crown ether derivatives also for the application of alkali metal chloride salt transport. The nature of the cation binding motif strongly influenced the selectivity of transported ion-pairs. For example, the host containing the aza[15]crown-5 motif (Figure 1.42) demonstrated selective NaCl transport, whilst the aza[18]crown-6 analogue altered the selectivity to KCl.[129]

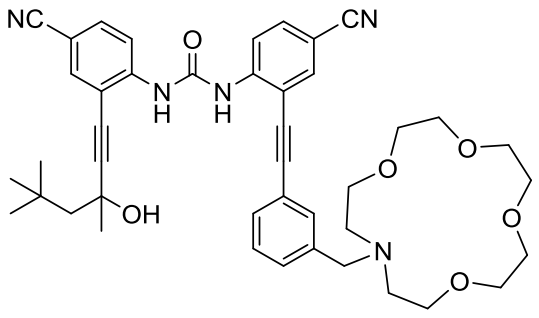

Figure 1.42 Heteroditopic receptor for NaCl membrane transport.

1.5 Mechanically Interlocked Molecules

A mechanical bond has been defined as an entanglement in space of at least two components which cannot be separated from each other without breaking of one counterpart. Impressively, nature has created a variety of biological molecular architectures containing mechanical bonds from the macroscopic to microscopic level. On the molecular scale, a category of structures containing at least two molecular components held together with a mechanical bond is referred to as a mechanically interlocked molecule (MIM).[130]

The two fundamental structures of MIMs are catenanes and rotaxanes (Figure 1.45). Catenane (from catena in Latin meaning chain) is a class of MIMs which consists of two interlocking rings, while a rotaxane (from the Latin for wheel and axle) is made up of a macrocycle (or 'wheel' component) threaded by a dumbbell shaped axle where the bulky terminal groups prevent components from dissociation. A related structure in this class is the pseudorotaxane which lacks the bulky stopper groups. In addition to these structures, the interlocked molecular topologies also belonging to MIMs include elegant complex architectures including trefoil knots,[131] Boromean rings,[132, 133] and Solomon links.[134]

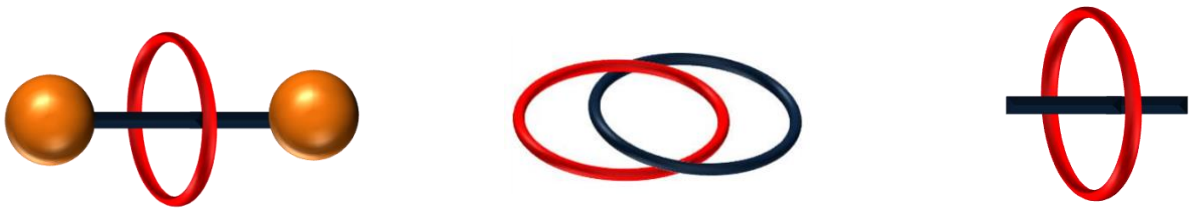

[2]Rotaxane *[2]Catenane* *pseudorotaxane*

Figure 1.45 Schematic representation of interpenetrated and interlocked molecules

1.5.1 Synthesis of Mechanically Interlocked Molecules

Rotaxanes can be synthesised by a wide set of strategies either with or without the formation of a pseudorotaxane (Figure 1.46 and Table 1.2). The former methodology involves pseudorotaxane assembly between a macrocyclic component and a molecular thread, followed by appending with bulky stopper groups (stoppering),[135] or increasing in size of a chemical functionality within the thread to prevent deslipping (swelling),[136, 137] or reducing an effective size of macrocyclic cavity (shrinking)[138] to form the rotaxane axle as well as the mechanical bond.

The routes that do not proceed *via* a formation of pseudorotaxane are clipping and slippage methodology. Clipping exploits a macrocyclisation of an acyclic component around a dumbbell shaped-axle, while slippage is an approach that a macrocycle can bypass the stopper in the presence of external energy (i.e. heat, pressure) to form a kinetically stable rotaxane under ambient conditions.[139] On the other hand, the synthesis of catenanes is more restricted to a single clipping of an acyclic precursor around a macrocyclic component, or a double clipping macrocyclisation to form the catenane. Importantly, essential templating methods are exploited to assemble pseudorotaxane for MIM formation which is discussed in the next section.

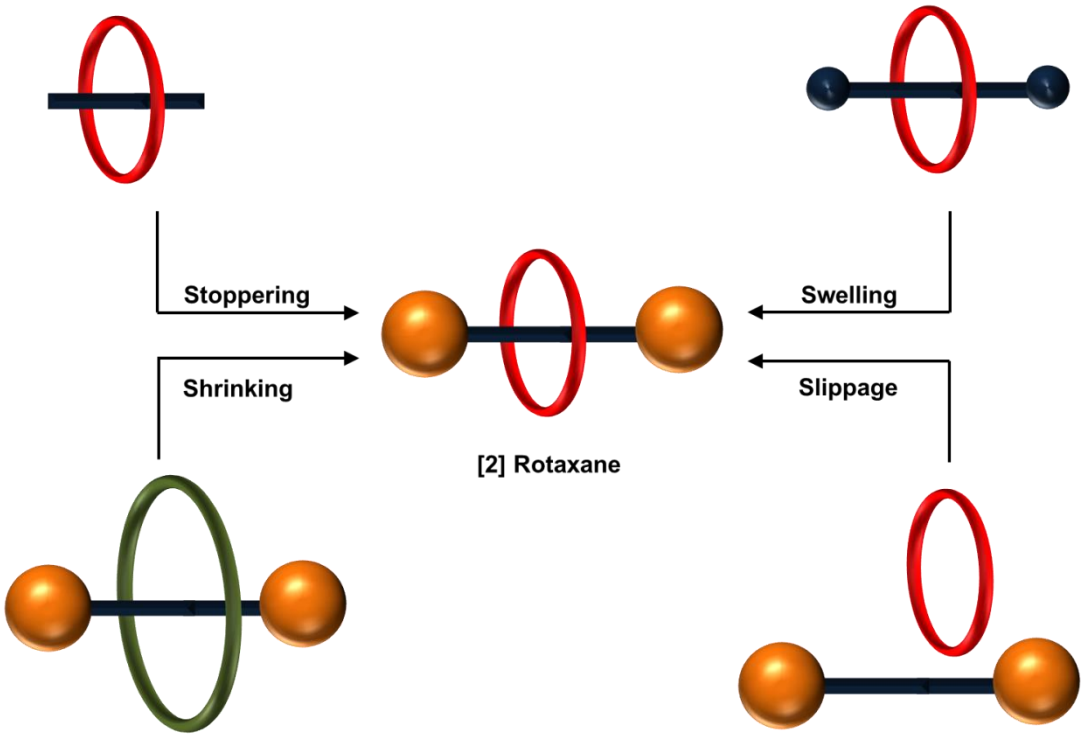

Figure 1.46 Synthetic routes for rotaxane synthesis.

Table 1.2 Examples of MIMs synthesis.

Examples of rotaxane synthesis *via* different routes
Stoppering[140]
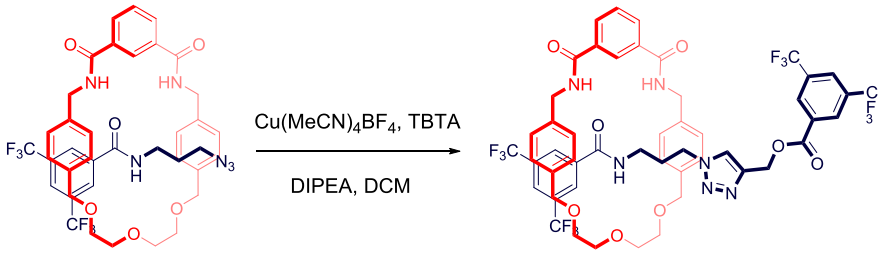
Swelling[136, 137]
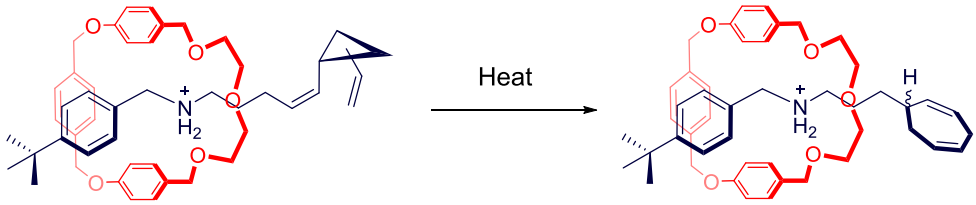
Shrinking[138]
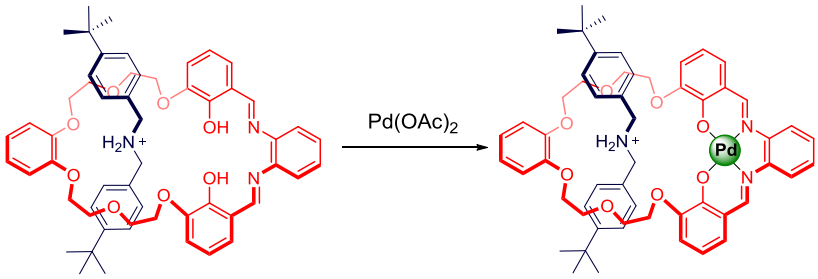
Slippage[139]
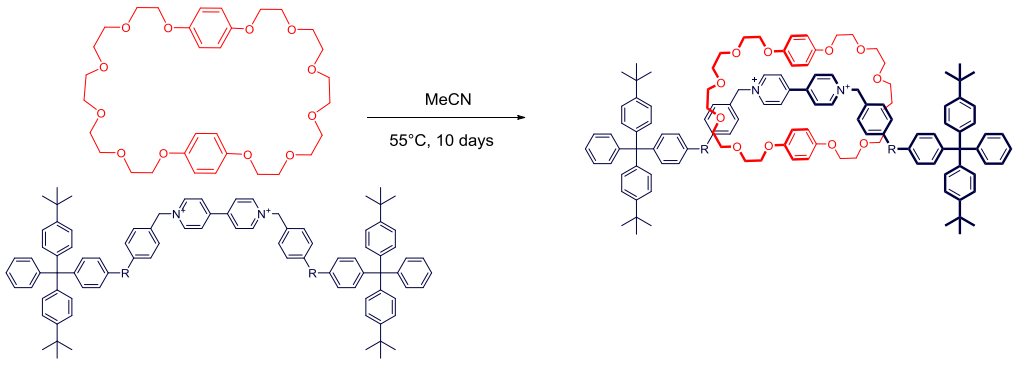

1.5.2 Template Directed Synthesis

The seminal synthesis of MIMs was described by Wasserman relying on a statistical acyloin reaction around a 34-membered cycloalkane with 0.0001% yield of the isolated MIM that he coined a catenane in 1960.[141] Subsequently, Harrison used an immobilised acyloin macrocycle on a solid support to prepare the structure called “hooplane” (later named rotaxane) by a stoppering reaction between 1,10-dodecanediol and trityl chloride isolated in a 6% yield.[135] Vital templating directed synthetic methodologies have since been developed to prepare MIMs in much improved yields. This section will cover the invention of template directed synthesis of MIMs *via* cationic, neutral, and anionic templates.

1.5.2.1 Cation Templated Synthesis of Mechanical Bonds

Exploiting the coordination stereochemical preference of transition metals to control the assembly and arrangement of precursors for the synthesis of mechanical bonds has become a powerful strategy since Sauvage introduced the first metallo-catenane templated by a copper(I) tetrahedral complex in 1983. This approach utilised the favourable tetrahedral coordination geometry of the d^{10} transition metal ion to organise the formation of a homoleptic copper(I) bis-phenanthroline complex in an orthogonal orientation, with a subsequent Williamson ether double macrocyclisation affording the interlocked [2]catenane product in 27% yield. On the other hand, a threading approach that required formation of a heteroleptic pseudorotaxane intermediate produced the same [2]catenane in an improved yield of 42% (Scheme 1.1).[142]

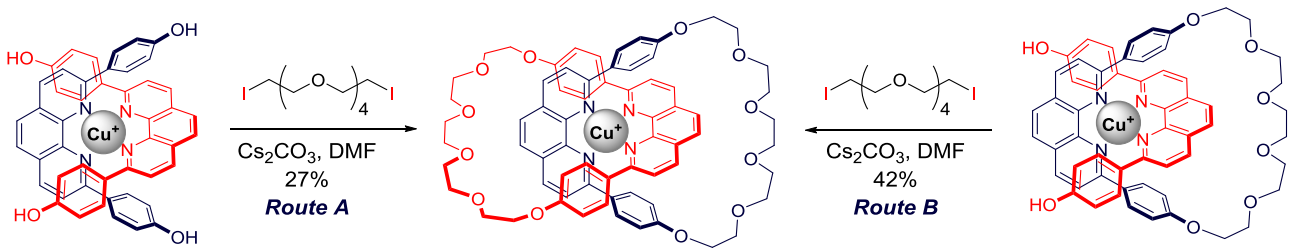

Scheme 1.1 Sauvage’s seminal Cu(I) templated synthesis of [2]catenane**.**

Since this seminal work, a plethora of examples of the metal template directed synthesis of mechanically interlocked structures has been reported with a wide range of transition metal templates exploiting different coordination geometries including octahedral (Ru^{2+}),[143] linear (Au^{+}),[144] square plana (Pd^{2+}, Pt^{2+})[145, 146] and trigonal bipyramidal (Zn^{2+}).[147]

The complementary ion-dipole interactions between hard donor atoms such as polyether oxygens in chelating ligands and hard alkali metal ions have been successively applied in the construction of interlocked molecules. Recently, Chiu and co-workers described the Schiff base condensation preparation of a [2]catenane by virtue of two diamine polyether precursors coordinating to sodium metal cation template reacting with a dialdehyde (Scheme 1.2a).[148] The same group used a sodium cation templating approach to prepare [2]rotaxane derivatives where the urea carbonyl group of an axle precursor coordinates with the alkali metal cation template (Scheme 1.2b). [149]

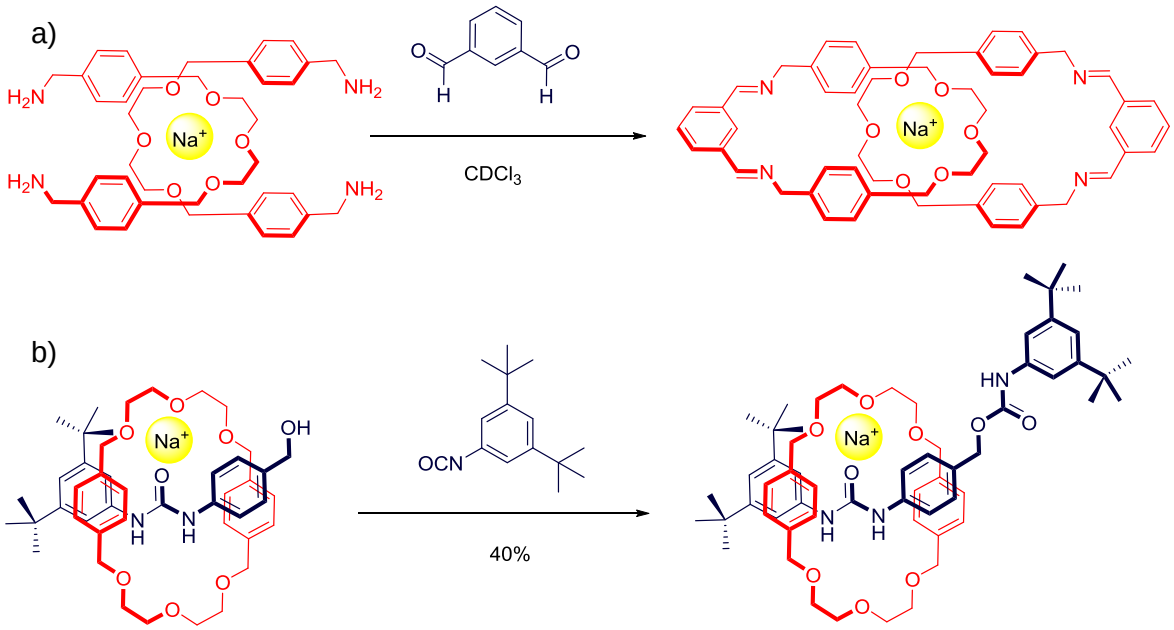

Scheme 1.2 Chiu's sodium metal cation template synthesis of a) [2]rotaxane[148] and b) [2]catenane.[149]

The first example of MIM construction using a lanthanide templates was reported by Beer and co-workers. This strategy employed the replacement of the inner sphere coordinating solvent of a lanthanide containing macrocycle with a pyridine *N*-oxide axle precursor to form a pseudorotaxane; a subsequent CuAAC stoppering reaction gave the [2]rotaxane in 20% yield (Scheme 1.3).[150]

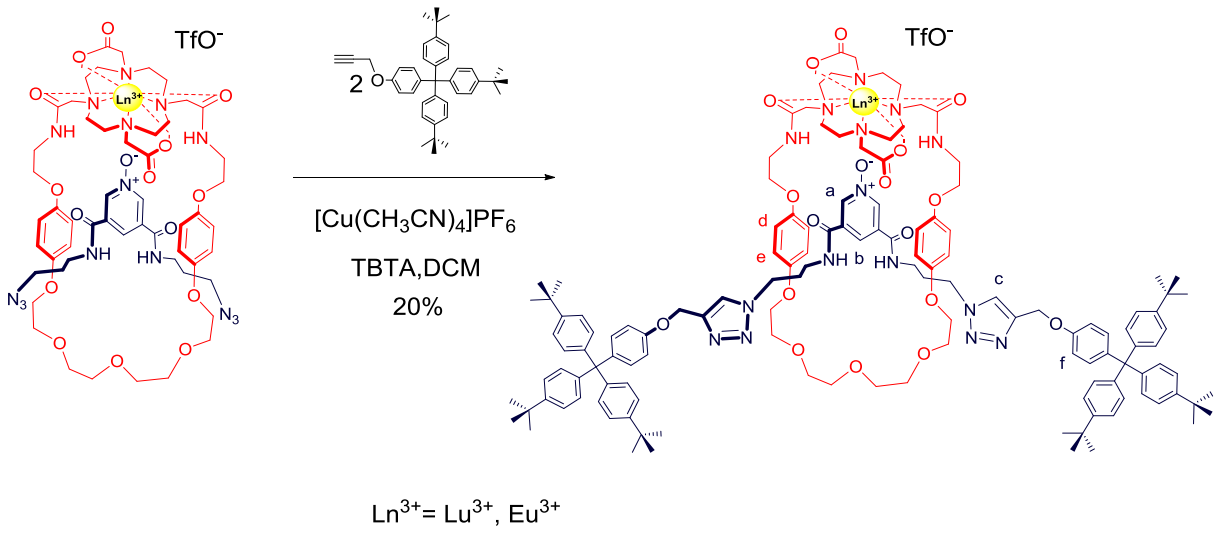

Scheme 1.3 Beer's lanthanide metal template synthesis of [2]rotaxane by CuAAC stoppering reaction.[150]

In the previous examples, the metal ions are considerable to act as a *passive templates* for organising the sub-components for MIM assembly. In 2006, Leigh and co-workers introduced the active metal template concept, in which a transition metal centre acts as a catalyst for forming the mechanical bond. The first example of an active metal template approach employed the versatile copper(I) catalysed azide-alkyne cycloaddition (CuAAC) reaction to prepare a series of interlocked molecules (Scheme 1.4**)**. [151] In this example, the Cu(I) cation template endotopically coordinates within the cavity of the 2,6-pyridine macrocyclic ligand, resulting in the azide and alkyne axle precursors binding to the metal centre on opposite faces of the macrocycle to produce the favoured tetrahedral coordination geometry. This interpenetrated assembly, held together by the catalytically active Cu(I) site, is mechanically locked by a subsequent cycloaddition reaction to form a triazole linkage. The rotaxane yield was found to depend on a number of factors including macrocycle rigidity, nature and orientation of donor atoms and steric hindrance near the binding site.The key factor however to achieve the interlocked product is the ability of the macrocycle to form either a mono or bidentate endotopic Cu(I) catalytically active intermediate. More recently, Goldup and co-workers also found rotaxane yield depended on macrocyclic ring size; the smallest investigated macrocycle gave a quantitative yield of rotaxane product (Scheme1.5).[152]

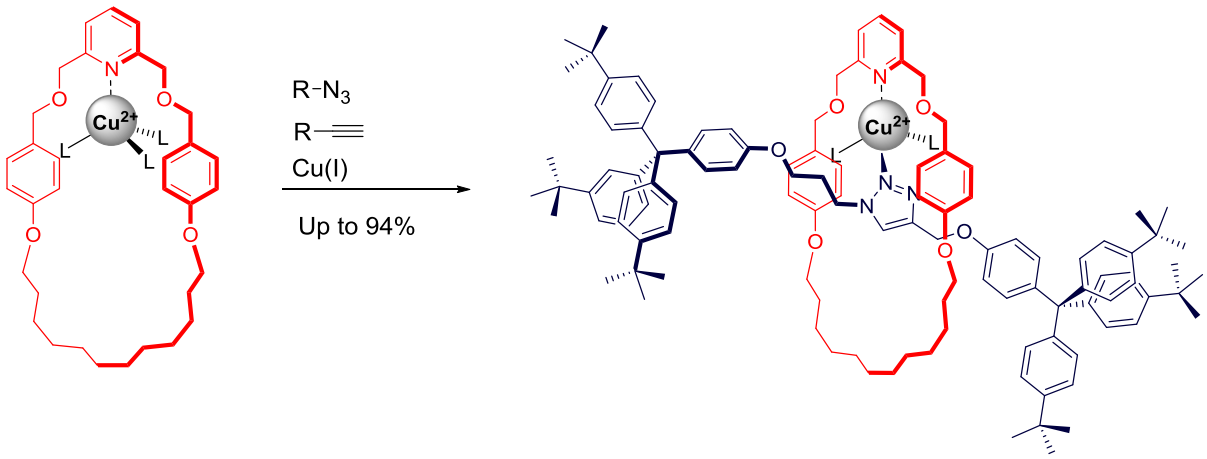

Scheme 1.4 Leigh's seminal active metal template synthesis of [2]rotaxane by CuAAC.[151]

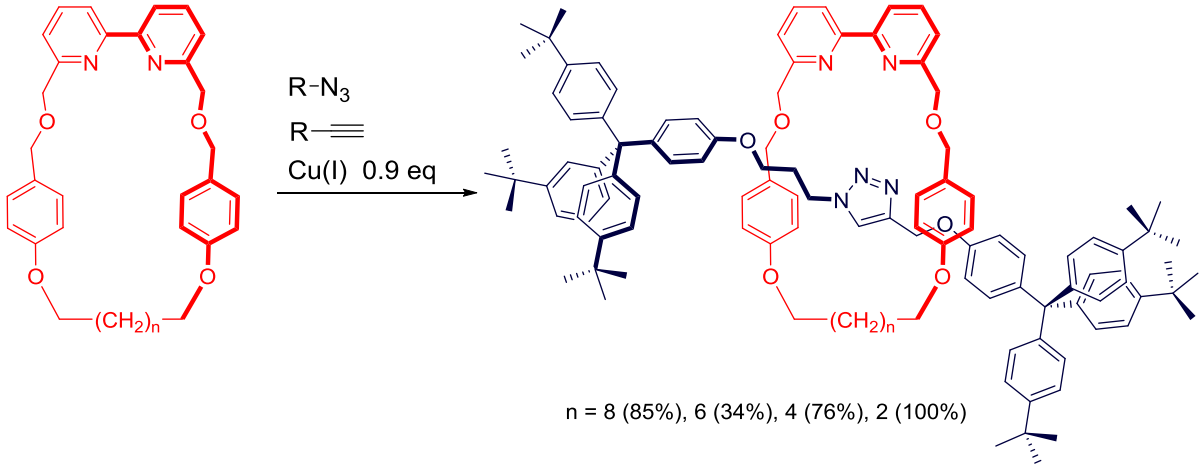

Scheme 1.5 Goldup's study on the effect of different macrocycle ring sizes for active metal template synthesis of [2]rotaxane.[152]

Organic cation templates have been vastly exploited in the preparation of interlocked molecules. In particular, secondary ammonium cations complexed by crown ether macrocycles have become a ubiquitous and powerful building block in broad ranges of architectures such as the preparation of a [4]heterorotaxane reported by Qu The synthesis of the [4]rotaxane employed a self-sorting principle in which the size complementary control results in the selective formation of two cationic pseudorotaxane intermediates; the dibenzo[24]crown-8 with dibenzylammonium cation, and the benzo[21]crown-7 with dialkylammonium cation (Figure 1.47). [153] Loeb investigated the use of 1,2-bis(4,4'-bipyridinium)ethane and imidazolium cationic motifs to construct a variety of rotaxanes with dibenzo[24]crown-8 macrocycles (Figure 1.48). [154-157] Stoddart utilised the 4,4'-bipyridinium dication and aromatic donor—acceptor charge transfer interactions to prepare the elegant supramolecular architecture called Stoddart's [5]catenane or "Olympiadane" (Figure 1.49). [158]

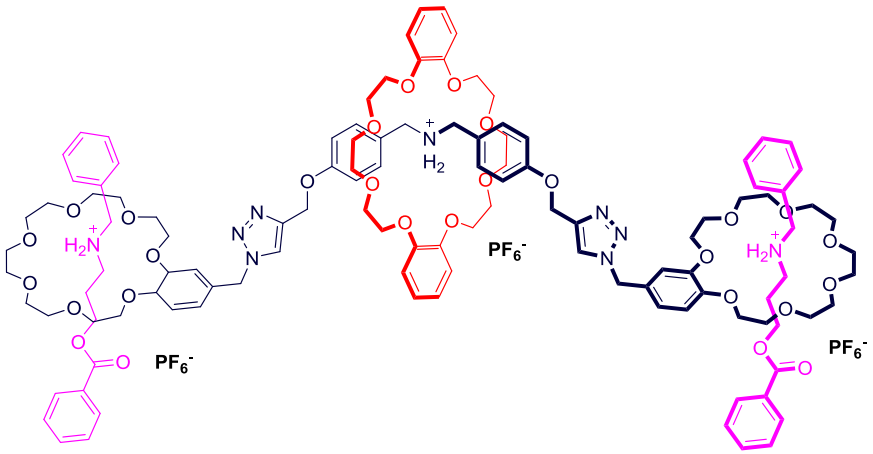

Figure 1.47 Ammonium cation templated synthesis of [4]rotaxane by self-sorting principle.[153]

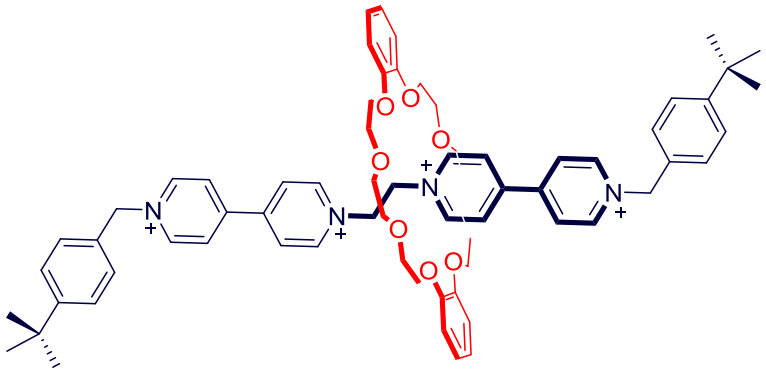

Figure 1.48 Loeb's 1,2-Bis(4,4'-bipyridinium)ethane motif for synthesis of [2]rotaxane.[154-157]

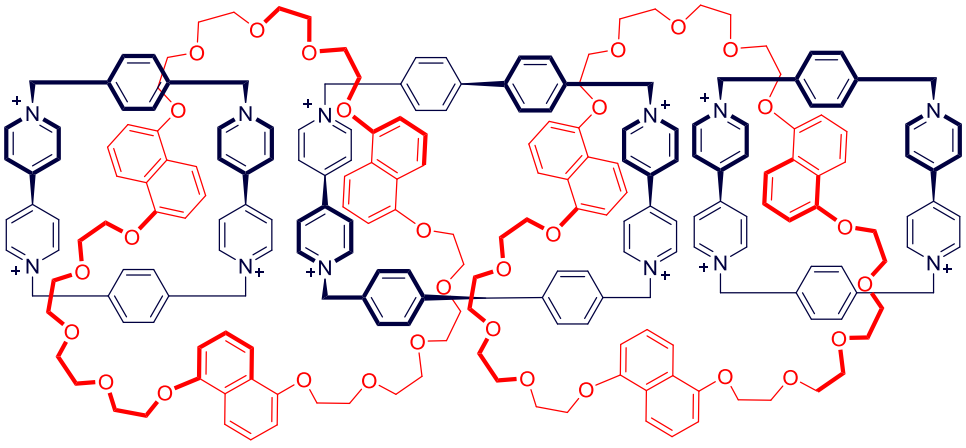

Figure 1.49 Stoddart's [5]catenane or "Olympiadane".[158]

1.5.2.2 Neutral Templates for MIM Construction

The first examples of using neutral binding motifs to template the synthesis of interlocked molecules using hydrogen bonding interactions were reported independently by Vogtle and Hunter in 1992. [159] The unexpected discoveries of [2]catenane formation was observed during the synthesis of a tetralactam macrocycle *via* an acid chloride and amine condensation reaction (Scheme 1.6). [160] Leigh's group have since used this neutral amide hydrogen bonding template introduced in the synthesis of rotaxanes using inter-component hydrogen bonding interactions between derivatives of this macrocycle with various axles, for example, the nitrone and amide. [161-163] Smith and co-workers have also exploited this approach in the preparation of squaraine based rotaxanes boasting many biological applications. [164-166]

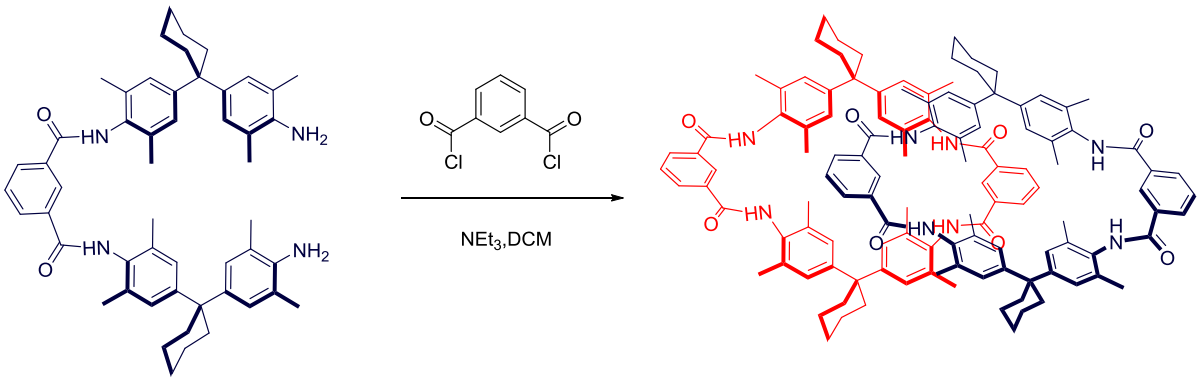

Scheme 1.6 Vogtle and Hunter's hydrogen bond-templated [2]catenane.

Sanders pioneered the use of neutral aromatic donor—acceptor interactions between an electron rich 1,5-dioxynaphthalene (DNP) donor polyether containing macrocycle and an electron deficient acceptor such as pyromellitic dimiide to produce a [2]rotaxane in a satisfactory 52% yield by oxidative alkyne coupling (Scheme 1.7).[167]

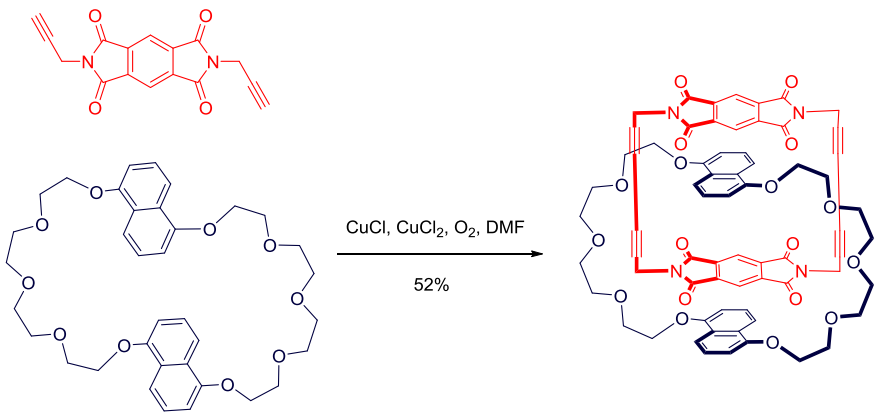

Scheme1.7 Sander's aromatic donor-acceptor catenane.[167]

By employing the hydrophobic effect to template the formation of a psuedorotaxane, Ogino formed an inclusion complex of 1,12-diaminododecane thread within the hydrophobic cavity of α-cyclodextrin to prepare a [2]rotaxane *via* a metal complexation stoppering reaction, [168] whilst Anderson has also used this strategy to prepare insulated molecular wires (Figure 1.50). [169]

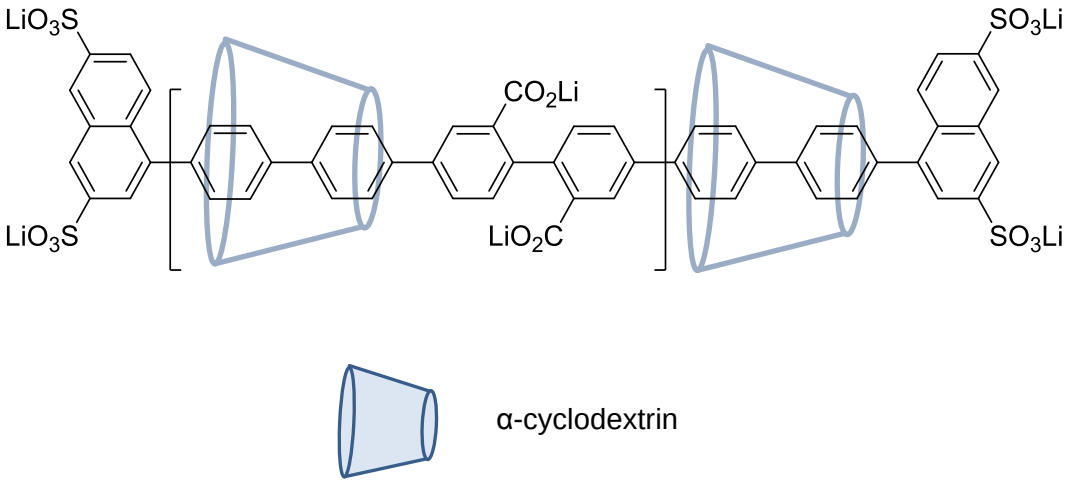

Figure 1.50 Anderson's molecular wires.

1.5.2.3 Anion Templates

Vogtle introduced the first synthesis of anion templated MIMs manipulating the capability of the tetralactam macrocycle to capture an anionic nucleophile within its cavity *via* convergent N—H amide hydrogen bond donors. The macrocycle bound phenoxide-functionalised axle precursor reacts with an electrophilic moiety appended with a stopper group to form the axle component of the rotaxane interlocked structure (Scheme 1.8). [170]

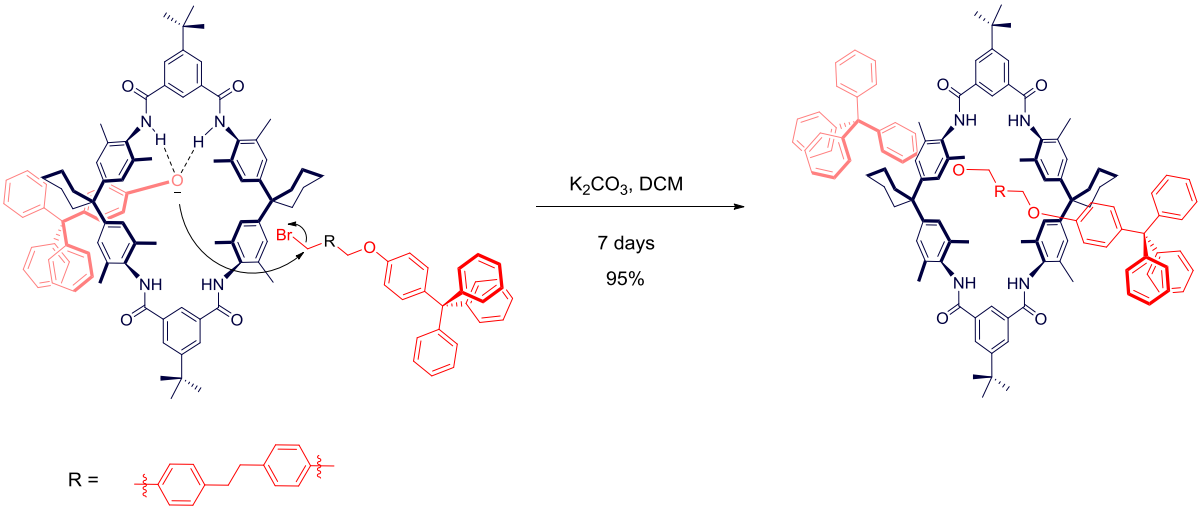

Scheme 1.8 Vogtle's phenoxide anion template synthesis of [2]rotaxane.[170]

Flood's group have recently exploited the anion—C-H hydrogen bonding interaction between the dipropargylphosphate anion template and the cyanostar macrocycle to form a 2:1 stoichiometric host-guest sandwich complex [3] pseudorotaxane. The threaded bis-alkyne groups were subsequently reacted with an azide funcationalised stopper component using the CuAAC reaction to afford the bis-triazole linked [3]rotaxane (Scheme 1.9). [171]

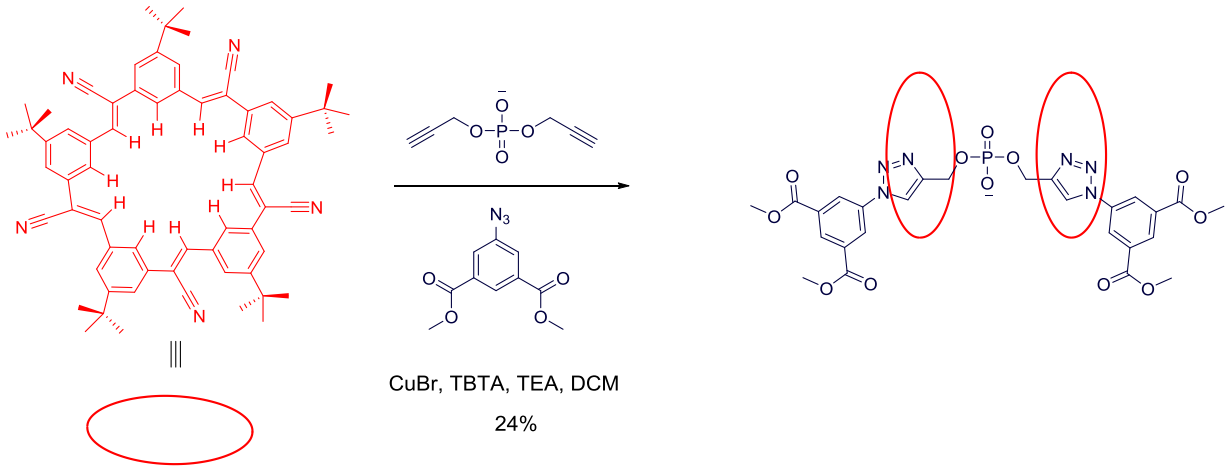

Scheme 1.9 Phosphate-cyanostar macrocycle [3]rotaxane.[171]

In the previous examples, the anionic template was consumed upon the formation of the interlocked product as demonstrated by Vogtle's rotaxane, whilst Flood's rotaxane integrated the anionic part as the axle component of the rotaxane structure. However, the use of a discrete anion acting as passive anion template, in an analogous fashion to the copper(I) cation template introduced by Sauvage, has been developed by Beer and co-workers. This seminal work was established after the discovery of the encapsulation of a chloride anion by an orthogonal complex assembly between a cationic bis-amide 3,5-pyridinium and a neutral isophthalamide motif. The chloride anion is stabilised by formation of four amide NH···Cl^- hydrogen bonds and two CH···Cl^- interactions from both central pyridinium and phenyl rings (Figure 1.51).[172]

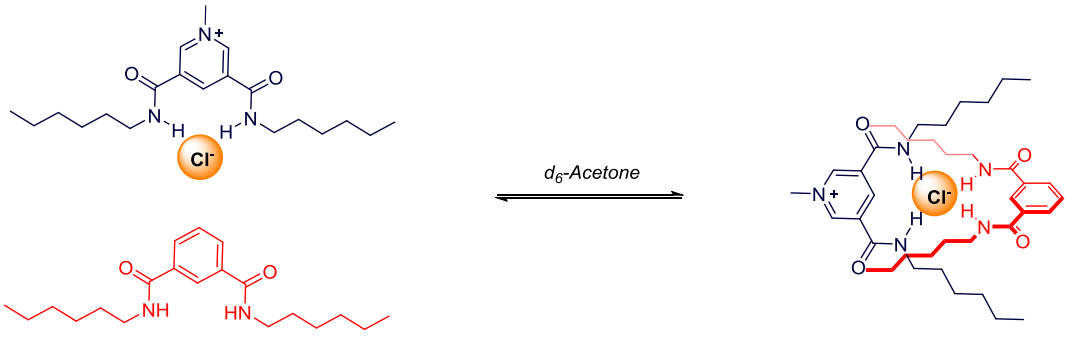

Figure 1.51 Orthogonal association of hydrogen bonding acyclic motifs around a chloride anion template.

Applying this approach, a chloride anion template was initially used to prepare a pseudorotaxane by integrating the anion binding isophthalamide motif into a hydroquinone containing macrocycle. The strong association of the interpenetrated species was further stabilised by aromatic donor—acceptor interactions between the electron deficient pyridinium guest and macrocyclic host electron rich hydroquinone groups (Figure 1.52).[172, 173]

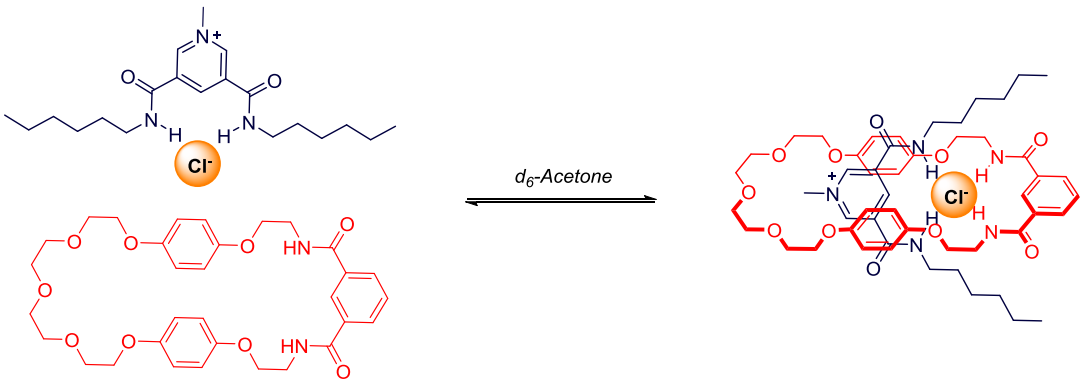

Figure 1.52 Chloride anion-templated pseudorotaxane assembly.

In 2002, this strategic anion template methodology was successfully exploited in the synthesis of a [2]rotaxane.[174] A terphenyl-stoppered pyridinium axle containing a chloride template formed an orthogonal intermediate with an acyclic isophthalamide bis-vinyl macrocycle precursor, subsequent macrocyclisation by ring closing metathesis afforded target [2]rotaxane in 47% (Scheme 1.10).[174] The chloride anion template was removed from the interlocked host cavity by exchanging with a non-coordinating anion, in this case using salt metathesis with $AgPF_6$, to produce a rotaxane with a unique interlocked cavity vacant anion coordination site. Impotantly, the rotaxane host demonstrated enhanced anion binding affinity and selectivity over non-interlocked axle and macrocycle components in competitive media. The [2]rotaxane displayed selectivity for Cl^- the templating anion, over more basic anions such as $H_2PO_4^-$ and AcO^- which cannot penetrate to the binding site.

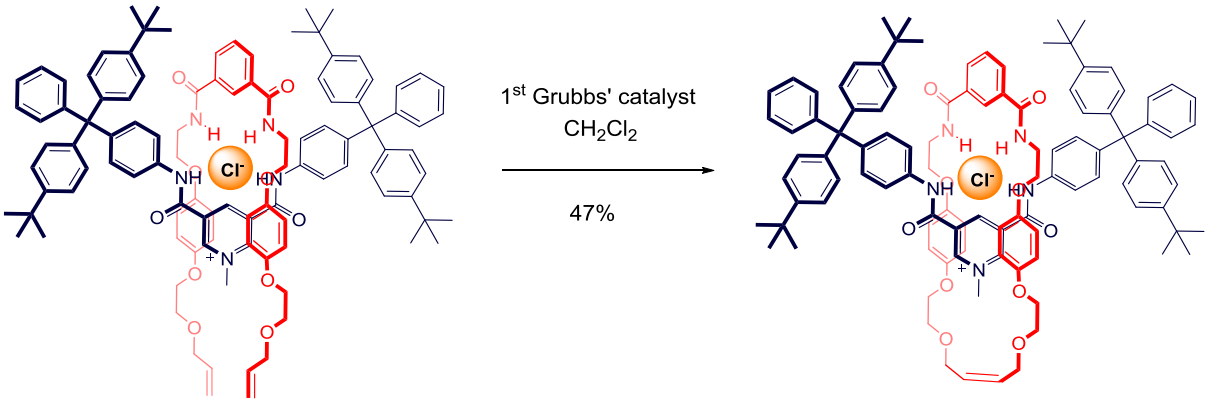

Scheme 1.10 Chloride anion-templated [2]rotaxane synthesis *via* ring closing metathesis.[174]

The discrete anion template methodology has since progressed to the construction of a range of MIMs (hand-cuff catenane, Janus[2]rotaxane, and [3]rotaxane molecular shuttle)[175-177] using in particular amide condensation (Scheme 1.11) and CuAAC reactions[178, 179] with a wide scope of anion templates including sulfate, nitrate, and nitrire.[180-182]

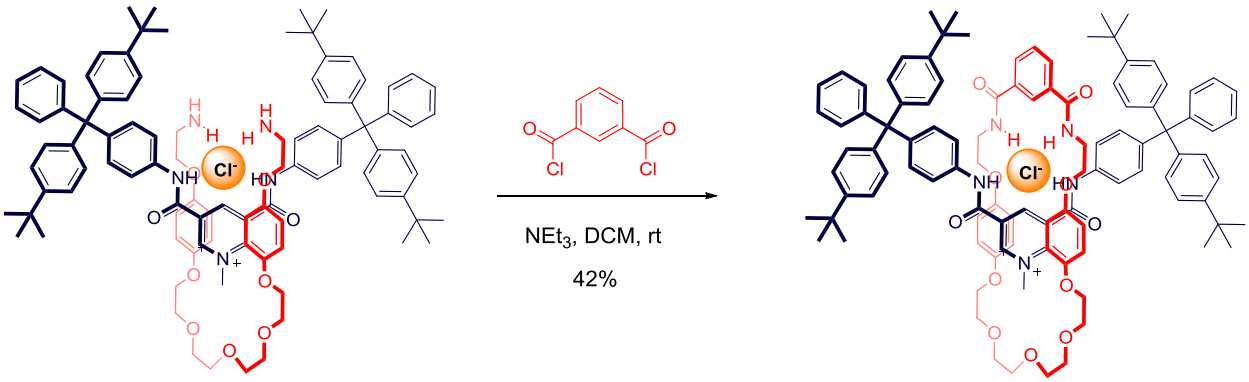

Scheme 1.11 Chloride anion-templated [2]rotaxane synthesis *via* amide macrocyclisation.[178]

1.5.3 Applications of mechanically interlocked ligands

Rotaxanes and catenanes have been of central interest as prototypical nanomachines due to their capability of certain kinds of molecular translational motion. Electrochemical switching between Cu(I) and Cu(II) oxidation states has been elegantly utilised by Sauvage in [2]catenane and [2]rotaxane systems to induce pirouetting-like motion by the macrocyclic component (Figure 1.53).[183] Whilst a translocation motion along the axle component in Stoddart's molecular elevator demonstrated a pH responsive shuttling (Figure 1.54).[184]

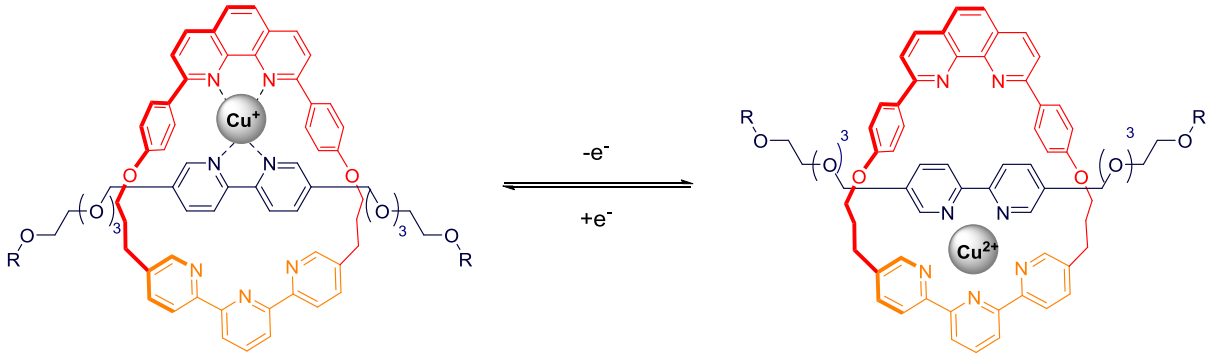

Figure 1.53 Electrochemical induced pirouetting motion in a [2]rotaxane.[183]

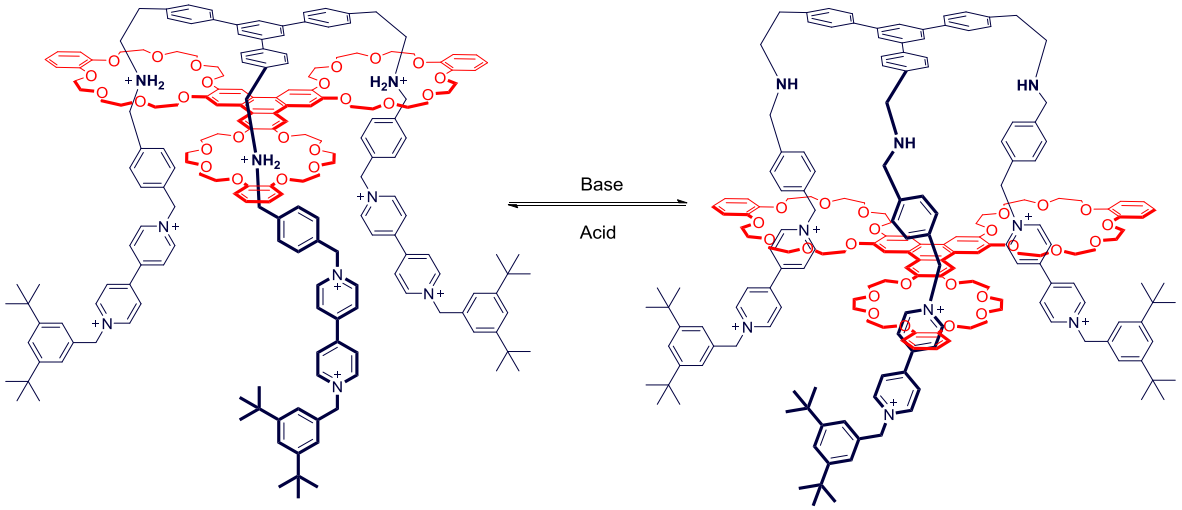

Figure 1.54 Acid-base induced molecular motion in Stoddart's nanoelevator.[184]

Rotaxanes and catenanes have demonstrated potential in selective recognition and sensing of neutral or charged guest species by virtue of their elaborate three dimensional interlocked binding cavities. For example, Swager and co-workers demonstrated the metal sensing properties of Sauvage's Cu(I)-phenanthroline rotaxane derivative (Figure 1.55).[185, 186] The metal free rotaxane displays strong fluorescent emission due to an exciplex formation between interlocked components. Addition of Zn(II) to a solution of the rotaxane quenches the emission signal attributed to a destabilisation of the exciplex formation due to strong coordination of Zn(II) within the interlocked phenanthroline binding cavity.

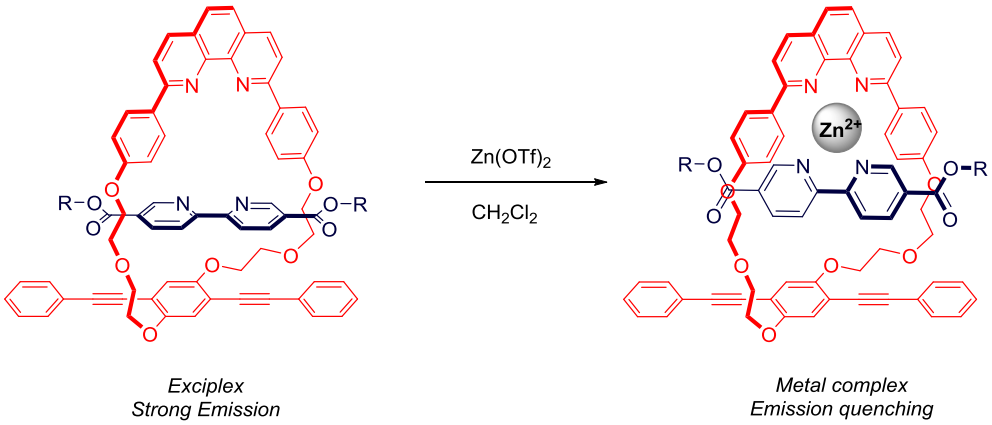

Figure 1.55 Metal ion responsive rotaxane by Swager et. al.[185, 186]

Li and co-workers applied the concept of metal ion induced molecular motion to display optical responses with different coordination states. In the metal free-state, PET from the amine groups of both axle and macrocycle quenches the anthracene stopper emission. The addition of Li^+ cation induces a conformational change in the macrocyclic component which attenuates the PET quenching process. Whilst Zn^{2+} coordination led to translocation of the macrocycle to form a tetra-aza Zn^{2+} interlocked complex, leading to dramatically enhanced emission intensities (Figure 1.56). [187]

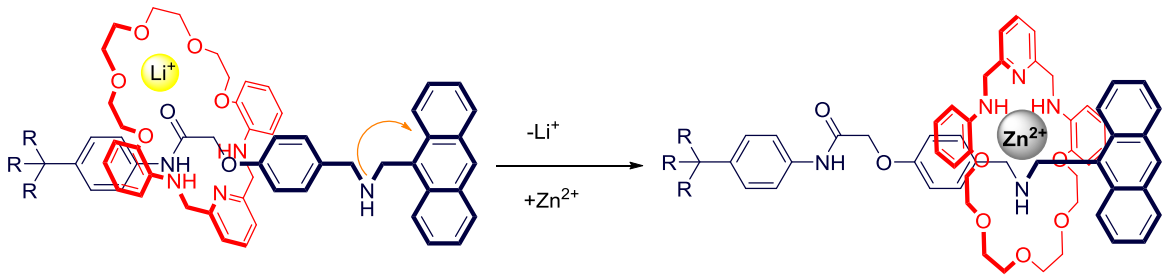

Figure 1.56 Metal responsive rotaxane by Li and co-workers.[187]

Beer and co-workers have integrated transition metal probes into anion binding interlocked structures for anion sensing applications. For example, a gold surface functionalised Os(II) containing rotaxane is capable of selective chloride sensing using electrochemical methods (Figure 1.57).[188]

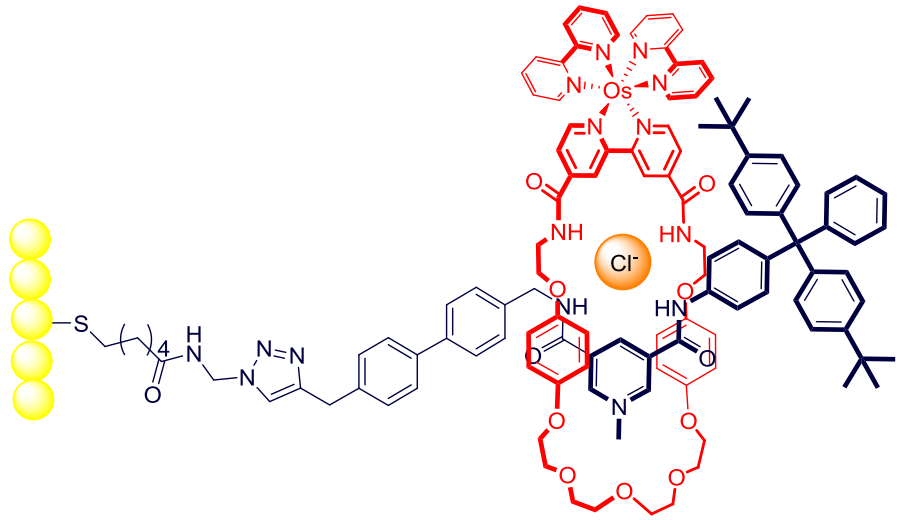

Figure 1.57 Surface functionalised electrochemical anion sensing by Os(II)hydrogen bonding [2]rotaxane.[188]

The more recent years MIMs are beginning to emerge as potential catalysts. Leigh's group applied the dynamic molecular shuttling behavior of a rotaxane as a switchable organocatalyst for an asymmetric Michael addition reaction.[189] Under acidic conditions, dibenzo[24]crown-8 occupied the protonated ammonium axle station which sterically blocks the catalytically active site, while addition of base translocates the crown ether macrocycle to sit over the triazolium station, switching on the catalytic activity (Figure 1.58a). Goldup reported the first example of a rotaxane based metal complex with stimuli responsive behaviour in catalytic activity. Binding of a zinc(II) cation guest displaces gold(I) from the rotaxane's cavity switching on the noble metal's catalytic capability and also alters the rotaxane's conformation that controls selectivity (Figure 1.58b).[190]

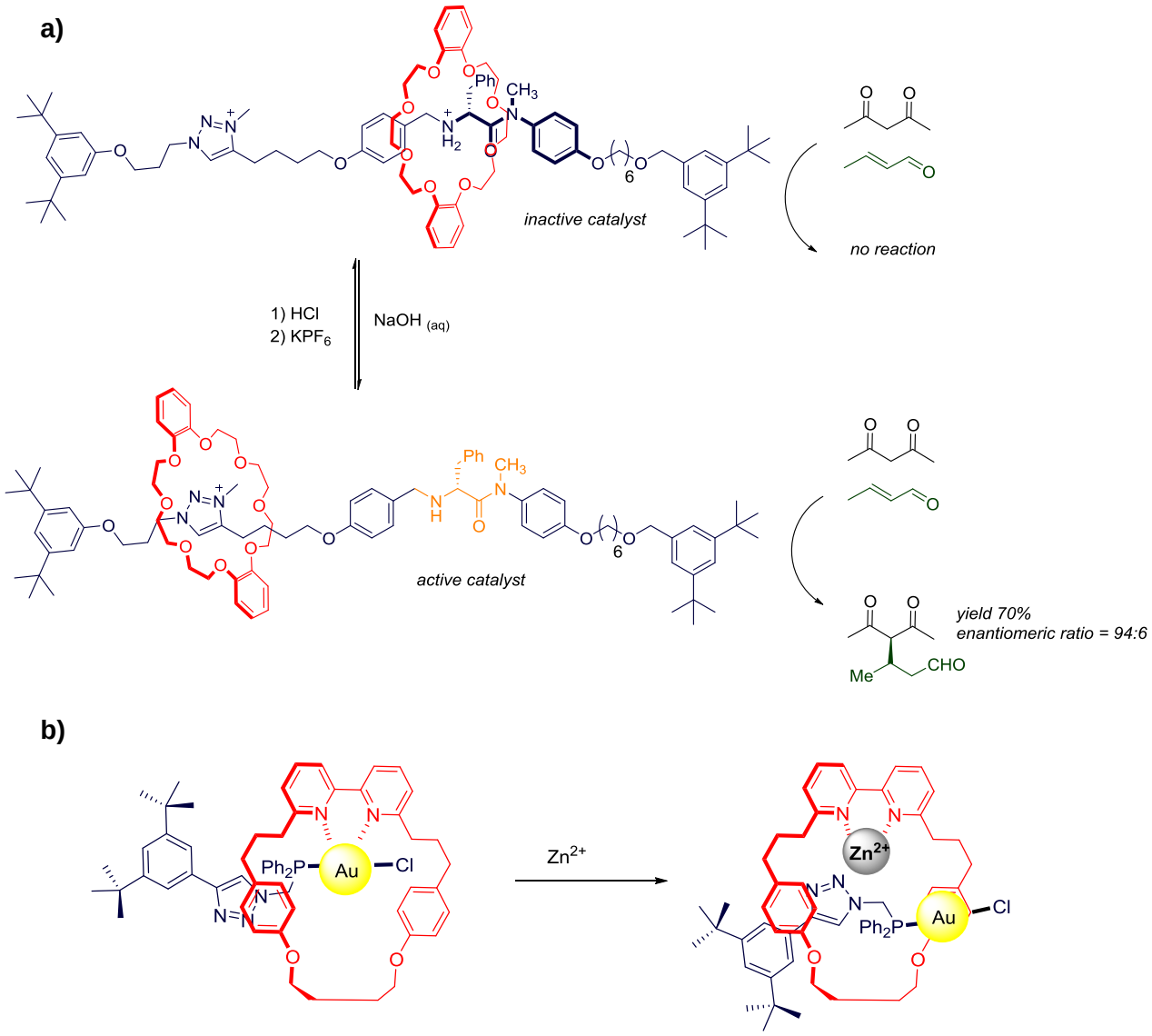

Figure 1.58 Rotaxane for catalysis applications: a) Leigh's switchable [2]rotaxane organocatalyst[189] and b) Goldup's swithchable gold(I) rotaxane catalyst.[190]

For medical applications, Smithrud investigated the calcium cation coordination behaviour of a crown ether stoppered [2]rotaxane in the transport of calcium ions across cell membranes, resulting in inhibition in the growth of ovarian cancer cells (Figure 1.59a).[191, 192] The application of mechanical bonding to provide stabilisation of bioactive peptide Met-encephalin in comparison to the parent peptide and its non-interlocked compund was demonstrated by Leigh's group. The peptide moiety was released by β-galactosidase mediated enzymatic hydrolysis of monosaccharide stopper, allowing the free peptide to be released by de-threading (Figure 1.59b).[193, 194]

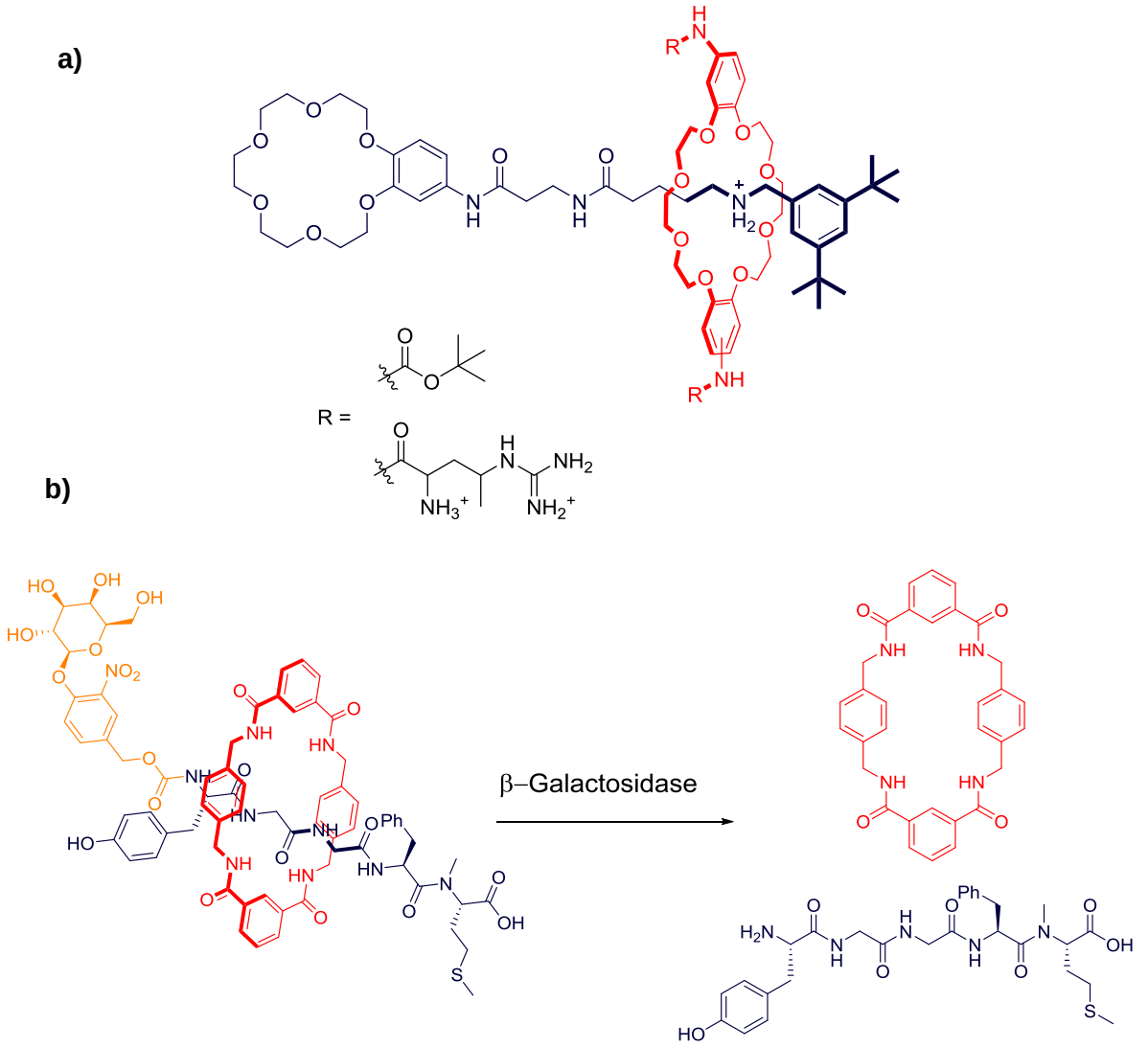

Figure 1.59 Rotaxane for Biomedical applications: a) Smithrud's Ca^{2+} transport [2]rotaxane[191, 192] and b) Leigh's rotaxane protected peptide.[193, 194]

1.6 Project outlines

The main objective of the various research projects discussed in this thesis is to develop novel sigma-hole donor host molecules for anion and ion-pair recognition that are capable of functioning in competitive organic and aqueous solvent media including pure water.

Chapter two discusses rare examples of sigma-hole interaction mediated ion-pair recognition. The preparation of novel XB and unprecedented ChB heteroditopic receptors appended with benzo[15]crown-5 are described initially, and investigation into their ion-pair binding properties in comparison to a HB analogue are detailed. Replacing the XB design with an ammonium[2]catenane affords a novel host system that is capable of aqueous anion

Chapter three focuses on the exploitation of a bidentate 3,5-bis-iodotriazole-pyridinium motif for anion recognition in highly competitive aqueous solvent media. Three main avenues of the investigations are described. First, a series of novel 3,5-bis-iodotriazole-pyridinium acyclic motifs containing alkyl, aryl, and perfluoroaryl substituents are prepared and integrated into β-cyclodextrin stoppered [2]rotaxanes for halide recognition studies in solvent media containing up to 50% water. An unprecedented relationship between anion template affinity and rotaxane yield is demonstrated. The second part of this chapter discusses the preparation of water-soluble XB receptors for anion recognition in pure water. ^{1}H-NMR spectroscopic titrations of both acyclic and interlocked anion receptors with a broad range of anions are studied. Furthermore, isothermal titration calorimetric analysis is used to elucidate thermodynamic features of XB anion recognition in water. Finally, novel osmium(II)bipyridine functionalized water soluble hosts are synthesised, and investigations into their anion recognition and sensing properties by electrochemistry and fluorescence are detailed.

Chapter four describes how chelating XB receptors with a small bite angle affects their anion recognition behaviour. A bidentate *ortho*-substituted iodotriazolium benzene motif is incorporated into acyclic, macrocyclic, and interlocked anion host structures, and their anion binding properties are examined, supported by solid-state structures of various anion complexed acyclic structural frameworks.

Chapter 2

Sigma-Hole Interaction Mediated Cooperative Ion-Pair Recognition

Chapter 2: Sigma-Hole Interaction Mediated Cooperative Ion-Pair Recognition

2.1 Ion-pair recognition and cooperativity

This section seeks to elaborate on the general concepts of ion-pair recognition introduced in section 1.4. For many decades research in host-guest chemistry has primarily focused on the design of monotopic hosts for individual cation or anion binding. The nature of the associated counter-ion however was overlooked, yet their roles in regulating the binding event have become increasingly apparent. In 2000, Smith and co-workers demonstrated that anion binding strength by a neutral monotopic host was attenuated in the presence of certain alkali metal cations as a consequence of relatively strong salt ion-pairing in organic media. The octyl appended urea receptor exhibited a diminished acetate association in the presence of sodium cations (K = 90 M^{-1}) in comparison to less charge dense cesium cations (K = 340 M^{-1}) in d_6-DMSO (Figure 2.1a). By combining [15]crown-5 with the urea receptor, a 7.5 fold enhancement in acetate binding in the presence of co-bound cesium cations relative to titration with TBAOAc in acetonitrile solution was observed (Figure 2.1b).[195] The interplay between the co-bound ions and their influence on association with the host is referred to as *cooperativity*.

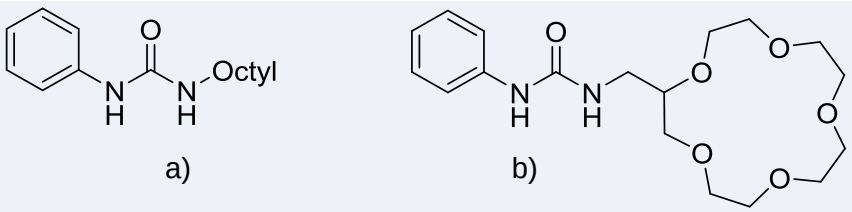

Figure 2.1 a) Urea anion receptor and b) [15]crown5 appended urea ion-pair receptor.

Cooperativity of ion-pair binding in heteroditopic receptors can be classified into three types comprising of:

i) Cooperative binding (positive cooperativity);
   - binding of one ion enhances the binding of the counter-ion.

ii) Non-cooperativity;
   - ions bind independently of each other.

iii) Anti-coopertive binding (negative cooperativity);
   - binding of one ion inhibits the binding of the counter-ion.

Cooperative ion-pair binding can result from favourable Coulombic electrostatic interactions between co-bound ions and conformational allosteric effects.[196] Flood and co-workers used experimental observations and computational methods to determine how electrostatic contributions controlled cooperative ion-pair binding in heteroditopic aryl-triazole polyether macrocycles.[197] The preorganised structure of the macrocycle allowed the formation of a contact ion-pair (Figure 2.2), and the relative sizes of the cation and anion ion-pair guest species dictated the strength of the electrostatic interaction, according to Coulomb's law. Hence for sodium salts, the magnitude of electrostatic contribution was observed to be larger for the smaller counter-anion (NaI > $NaClO_4$).

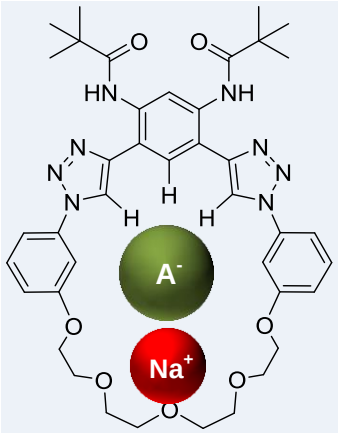

Figure 2.2 Aryl triazole macrocycle for contact ion-pair binding.

Conformational allostery utilises the binding of the first ion guest to preorganise the receptor in a more favourable conformation for the subsequent counter-ion guest binding event. For example, with a calix[4]arene based heteroditopic receptor, Beer and co-workers exploited the different coordination geometries of bis-benzo[15]crown-5 complexed alkali metal cations to regulate binding of a co-bound anion. The formation of a 1:1 stoichiometric K^+ sandwich complex (Figure 2.3a) preorganised the two amide groups to facilitate cooperative chloride anion binding in 1:1 CD_3CN/d_6-DMSO. By contrast, mutual electrostatic repulsion between the benzo[15]crown-5–sodium complexes inhibited the formation of a favourable anion binding geometry (Figure 2.3 b).[198]

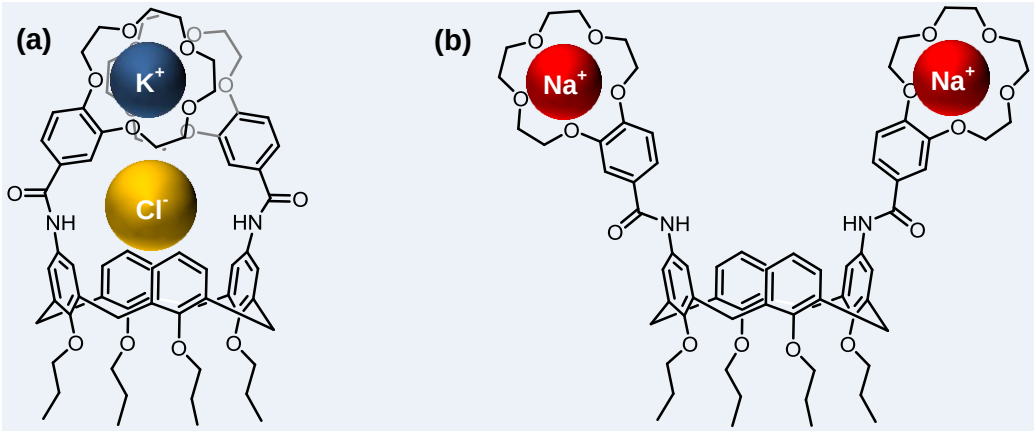

Figure 2.3 Beer's calix[4]arene heteroditopic receptor: a) cooperative binding of KCl and b) anti-cooperative binding in the presence of co-bound crown ether–sodium cations.

Recently, Thordarson and his group described cooperativity in a tetratopic macrocyclic receptor which upon complexation of calcium cations resulted in allosterically switching on the binding of chloride anions in CD_3CN (Figure 2.4).[199]

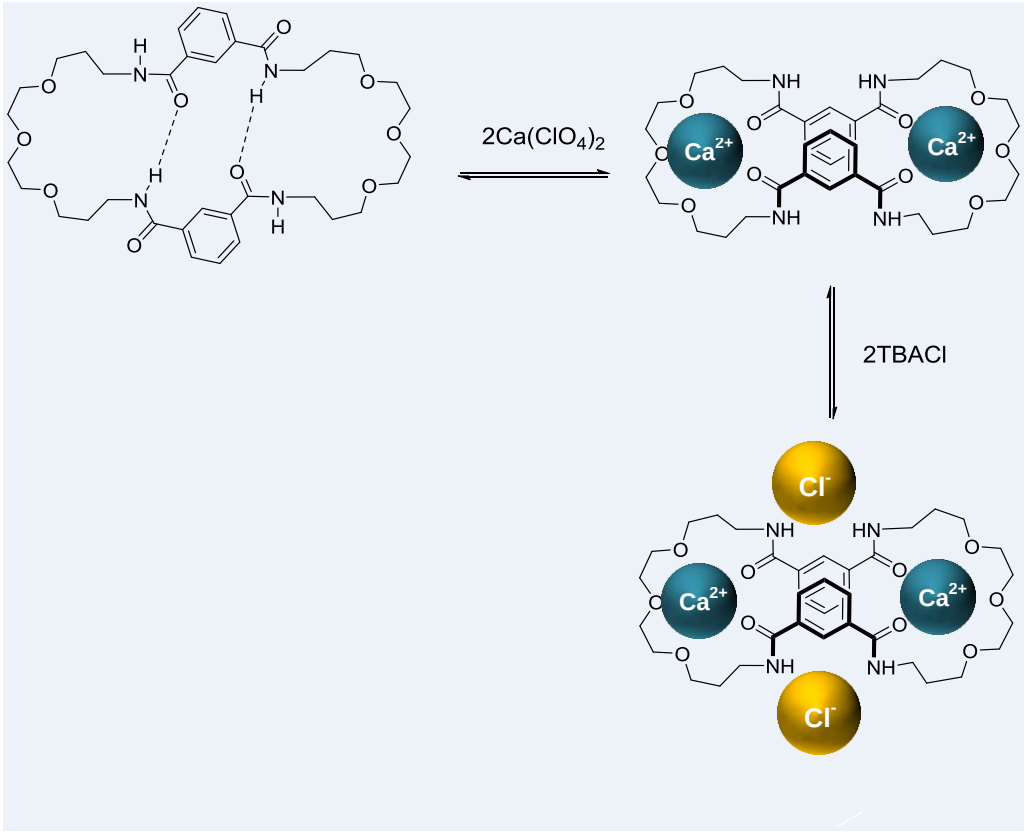

Figure 2.4 Thordarson's tetratopic macrocycle.

2.2 Sigma-hole interaction mediated ion-pair recognition

As mentioned in the previous section, heteroditopic receptors take advantage of cooperativity between both cation and anion recognition sites in a single molecular entity to affect ion-pair recognition. Commonly employed cation binding motifs are crown ethers, which exploit ion-dipole interactions between an alkali metal cation and oxygen donor atoms. To achieve anion binding, such hosts frequently integrate Lewis acidic sites from electrophilic N–H or C–H donors such as amides,[113, 200, 201] ureas,[104, 202-204] thioureas,[205, 206] pyrrole,[207, 208] and triazoles.[197] Compared to the plethora of HB heteroditopic receptors in the literature, the exploitation of sigma-hole interactions for ion-pair recognition is extremely rare. To date, only two examples of XB heteroditopic hosts have been reported by Resnati[82] and Schubert[209] whilst a ChB ion-pair receptor is unprecedented.[100]

In 2005, Resnati and co-workers reported the first prototype of an XB receptor, a C_{3v} symmetric XB tripodal host containing 4-iodoperfluoroaryl appended polyether arms, capable of anion recognition by virtue of ion-pair binding (Figure 2.5a). X-ray crystallographic evidence revealed ion-pair complexation in which Na^+ was coordinated by the oligoether podands, whilst I^- formed an XB interaction with an iodine atom of the perfluoroaryl motif (Figure 2.5b). The ditopic host displayed a 20-fold enhancement of NaI binding strength in $CDCl_3$ in comparison to an analogous host lacking XB donors.[82] More recently, Schubert and co-workers reported an iodotriazole containing macrocyclic oligoether whose conformational flexibility allowed the nitrogen donors of the iodotriazole unit to bind an alkali metal cation, concomitantly with iodide association *via* XB. In the presence of a co-bound sodium cation, ^1H and ^{13}C-NMR spectroscopic titration experiments demonstrated a 20-fold enhancement of halide binding in 3:1 CD_2Cl_2/CD_3CN in comparison to the cyclic receptor in the absence of sodium (Figure 2.5c).[209]

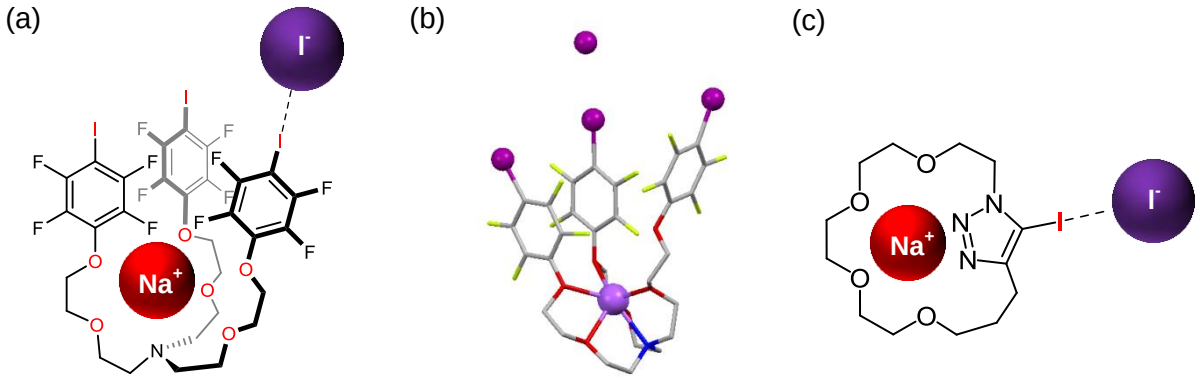

Figure 2.5 XB heteroditopic receptors.

2.3 Chapter aims

Stimulated by the few examples of sigma-hole donor based ion-pair hosts, this chapter aims to explore a series of novel XB and ChB heteroditopic receptors containing benzo-crown ether cation binding groups that are directly conjugated to the anion binding motifs (Figure 2.6). Extensive ^{1}H-NMR spectroscopic titration experiments will determine quantitative anion binding data, as well as cooperativity factors of such hosts resulting from alkali metal cation–crown ether coordination. Additionally this chapter investigates using mechanically bonded ammonium cation-crown ether complexes to achieve anion recognition in aqueous media.

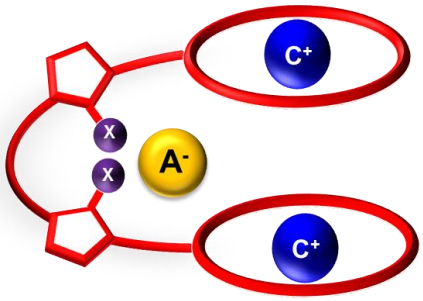

X = I, TeMe, H

C^+= alkali metal cation

A^- = anion

Figure 2.6 Cartoon represented target XB, ChB, and HB heteroditopic receptors.

2.4 XB and ChB heteroditopic receptors

2.4.1 Design and syntheses of heteroditopic receptors

Synthetic anion receptors containing a central pyridinium motif substituted at the 3,5-positions with iodotriazole groups have demonstrated their ability to coordinate halide anions in a bifurcate manner *via* convergent XB interactions.[210] The strong anion association of this motif presumably derives from a combination of electrostatic interactions and charge assisted XB. By covalently linking benzo[15]crown-5 groups to a neutral 3,5-pyridine-bis-iodotriazole motif, anion association could be enhanced as a result of alkali metal cation complexation at the crown ether binding sites. The synthetic accessibility of the 1,2,3-triazole heterocycle allows for the preparation of iodotriazole, methyltellurotriazole, and prototriazole functionalized structures **2.1·XB**, **2.1·ChB** and **2.1·HB** to be attractive scaffolds for systematic ion-pair recognition studies (**Figure 2.7**).

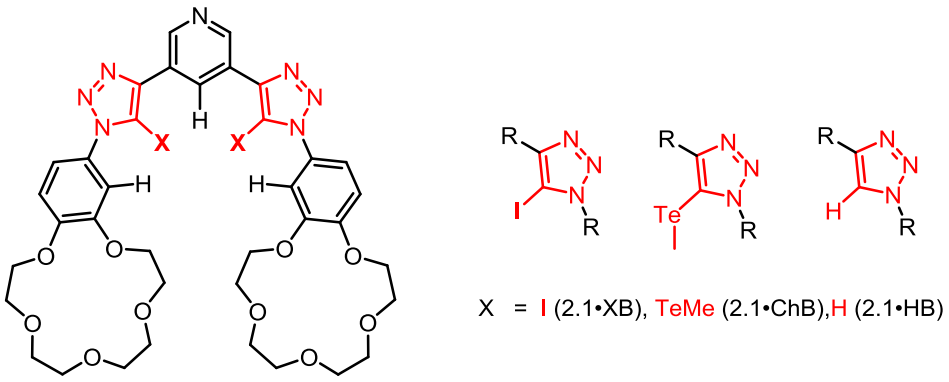

Figure 2.7 Target heteroditopic receptors **2.1·XB**, **2.1·ChB** and **2.1·HB**.

The XB and HB heteroditopic receptors were synthesised by CuAAC reaction between 4-azido-benzo[15]crown-5 and the corresponding alkynes. The initial alkyne precursor; 3,5-diethynylpyridine **2.2**, was prepared from commercially available 3,5-dibromopyridine *via* a Sonogashira cross coupling reaction with an excess of TMS-acetylene in the presence of $Pd(PPh_3)_2Cl_2$ and CuI. Subsequent cleavage of the TMS protecting group in basic solution afforded the 3,5-diethynylpyridine **2.2** in 61% yield over two steps. [53, 210] The iodination reaction of **2.2** using CuI and N-iodomorpholine provided the target 3,5-diiodoethynylpyridine **2.3** in 59% yield (Scheme 2.1).

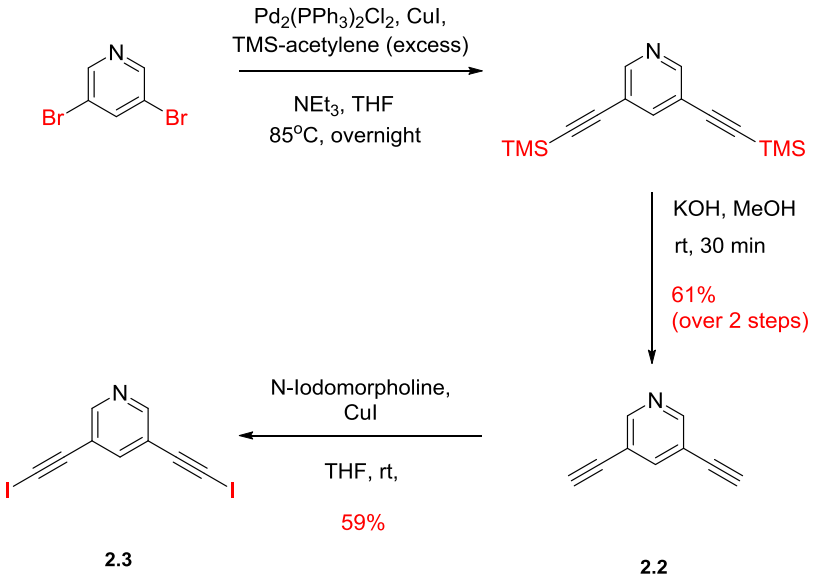

Scheme 2.1 Synthesis of 3,5-diethylnylpyridine **2.2** and 3,5-diiodoethynylpyridine **2.3**.

Azide functionalised benzo[15]crown-5 **2.7** was prepared using a modified literature procedure (Scheme 2.2).[211] Nitration of benzo[15]crown-5 **2.4** using concentrated nitric acid in a mixture of $CHCl_3$ and acetic acid gave 4-nitrobenzo[15]crown-5 **2.5** in 70% yield. Reduction using hydrazine monohydrate in the presence of catalytic Pd/C in ethanol afforded 4-amino-benzo[15]crown-5 **2.6** in quantitative yield. Diazotization of amine **2.6** using $NaNO_2$ under acidic conditions and subsequent addition of NaN_3 produced the target azide **2.7** in 90% yield without the need for further purification.

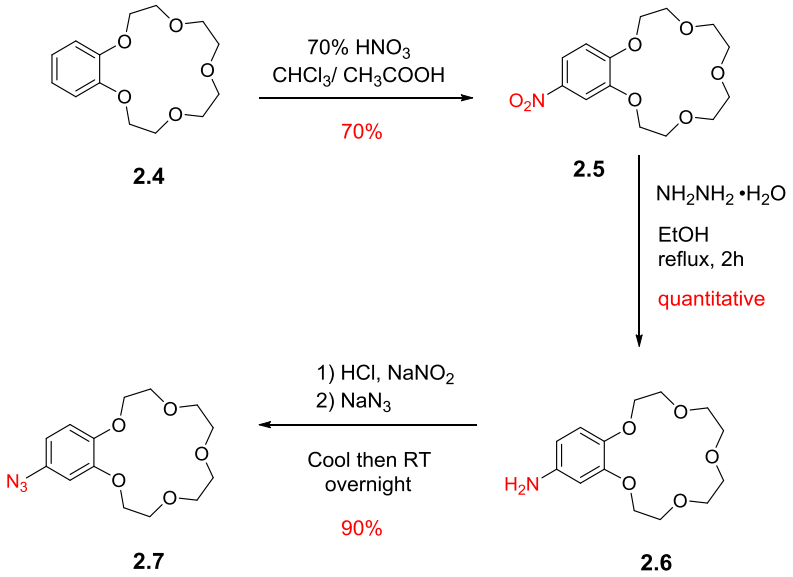

Scheme 2.2 Multistep synthesis of azido-benzo[15]crown-5 **2.7**.

Receptor **2.1·XB** was prepared *via* CuAAC reaction between two equivalents of azide **2.7** and bis-iodoalkyne **2.3** in the presence of a catalytic amount of $[Cu(MeCN)_4]PF_6$ and TBTA in a mixture of 1:1 THF/DCM at room temperature. Trituration and recrystallisation in MeOH afforded **2.1·XB** in 84% yield. The HB analogue was synthesised from 3,5-diethynylpyridine **2.3** in DCM under the same conditions and purification methods to give **2.1·HB** in 72% yield (**Scheme 2.3**). It is noteworthy that up to this point all synthetic steps were accomplished without the need for chromatographic purification.

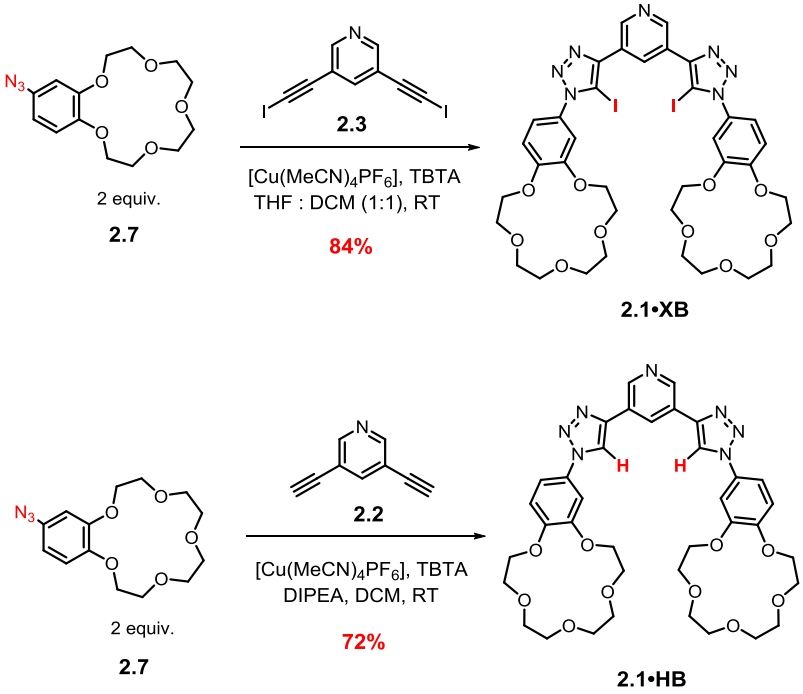

Scheme 2.3 Synthesis of **2.1·XB** and **2.1·HB** heteroditopic receptors *via* CuAAC reaction.

The preparation of ChB receptor **2.1·ChB** bearing methyltelluro triazoles proved to be much more challenging and was initially attempted by a nucleophilic substitution reaction between *in situ* generated lithium methyl telluride anion and **2.1·XB**. Under these conditions, the bis-iodotriazole (**2.1·XB**) starting material was dehalogenated to the bis-prototriazole analogue **2.1·HB** with no evidence of formation of the desired product. An alternative synthetic approach was undertaken *via* the preparation of a bis-fluorotriazole intermediate **2.8**[213] which is more reactive towards nucleophilic aromatic substitution. The XB receptor (**2.1·XB**) was reacted with an excess of KF in 1:1 MeCN/H_2O mixture under microwave irradiation,[213] and the desired product **2.8** was isolated as an orange solid in 20% yield after chromatographic purification (Scheme 2.4).

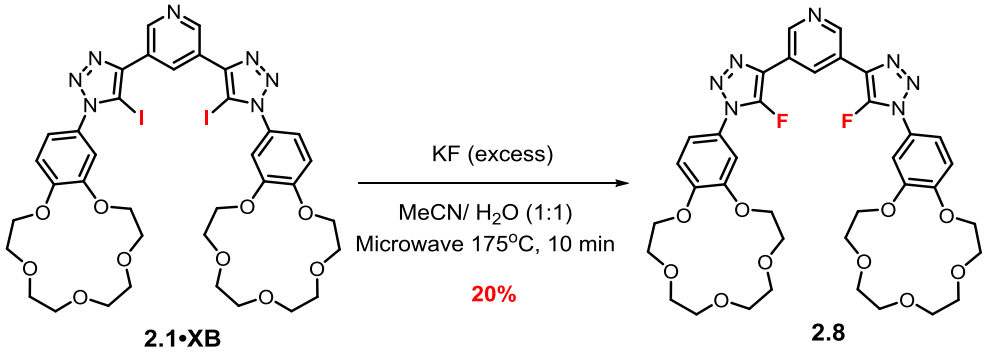

Scheme 2.4 Synthesis of the fluorotriazole analogue **2.8**.

An S_NAr reaction of lithium methyl telluride THF solution, generated *in situ* from methylithium and tellurium powder, with **2.8** gave, as evidenced from ESI-MS analysis, a mixture of products including **2.1·ChB**, **2.1·HB** and the mixed ChB/HB compound analogue. The target **2.1·ChB** was successfully isolated in 15% yield after chromatographic purification (Scheme 2.5). All three heteroditopic receptors were characterized by ^1H, ^{13}C-NMR spectroscopy and high resolution mass spectrometry (HRMS).

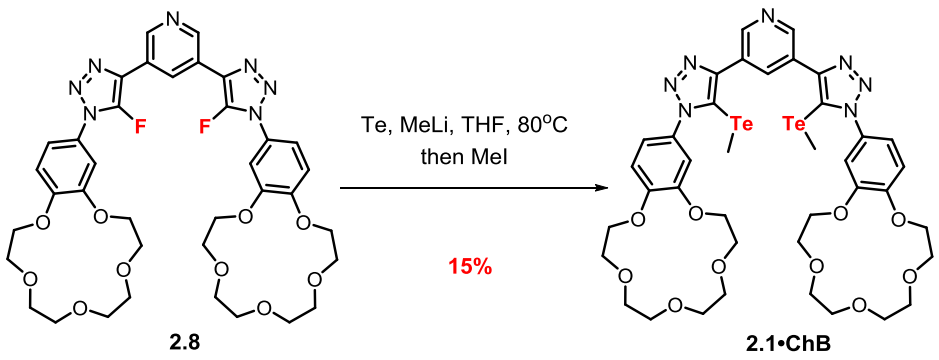

Scheme 2.5 Synthesis of **2.1·ChB**.

The ^{1}H-NMR spectra of **2.1·XB**, **2.1·ChB**, and **2.1·HB** are shown in Figure 2.8 where all receptors have three common proton resonance regions; pyridyl protons (H_a and H_b), phenyl protons from the benzo[15]crown-5 groups (H_{phenyl}), and ethylene protons from the crown ether (H_{crown}). In the case of **2.1·HB**, there is an additional resonance from the triazole protons (H_{trz}). Interestingly, the chemical shift of internal pyridyl proton (δ_{Ha}) moves downfield in the order of HB < ChB < XB which correlates with the electron withdrawing properties of the triazole substituents.

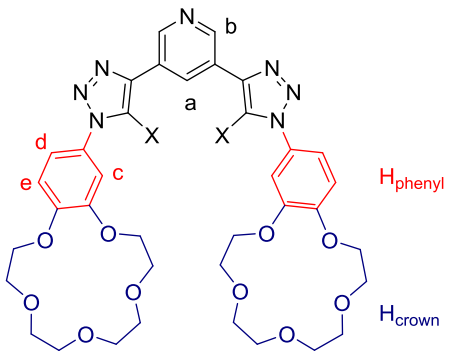

X = I (XB), TeMe (ChB), H (HB)

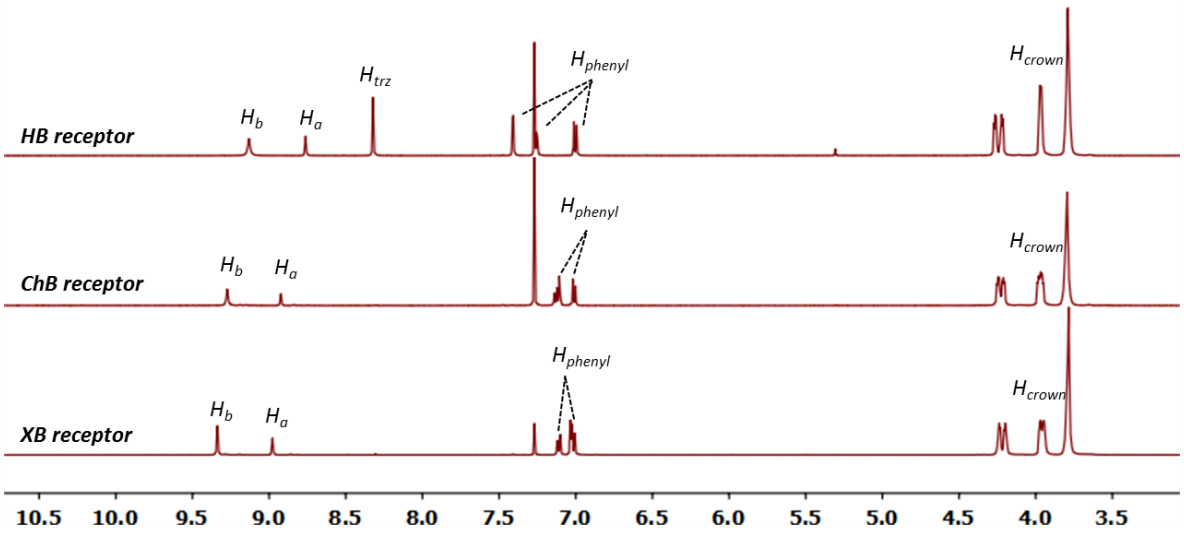

Figure 2.8 ^{1}H-NMR spectra of heteroditopic receptors HB (top), ChB (middle), XB (bottom) in $CDCl_3$ (400 MHz, 298K).

2.4.2 Ion-pair binding studies

The ion-pair binding properties of **2.1·XB**, **2.1·ChB** and **2.1·HB** were studied by ^{1}H-NMR spectroscopic titration experiments in 10% d_6-DMSO-$CDCl_3$. To evaluate quantitative analysis of ion-pair recognition, anion titrations were carried out in the presence and absence of sodium cations, the complementary sized alkali metal cation for the benzo[15]crown-5 binding motif.[198] In addition cooperativity factors were determined for comparison of XB, ChB, and HB enhancement of anion binding that results from crown ether co-bound sodium cation complexation.

A) Sodium cation complexation studies

The sodium cation binding properties were studied by addition of two equivalents of $NaPF_6$ to ^{1}H-NMR solutions (10% d_6-DMSO-$CDCl_3$) of each host. In all cases significant downfield perturbations of the phenyl resonances as well as the crown ether ethylene protons were observed indicative of sodium cations binding in each crown ether group (Figure 2.9). Also perturbations of the respective pyridyl protons (H_a and H_b) were observed. To test whether the hexafluorophosphate anion was coordinating to the respective host's anion binding site, analogous titrations with two equivalents of $TBAPF_6$ were undertaken. No changes in the proton signals associated with the anion binding cleft were seen, confirming that the hexafluorophosphate anion does not participate in anion complexation.

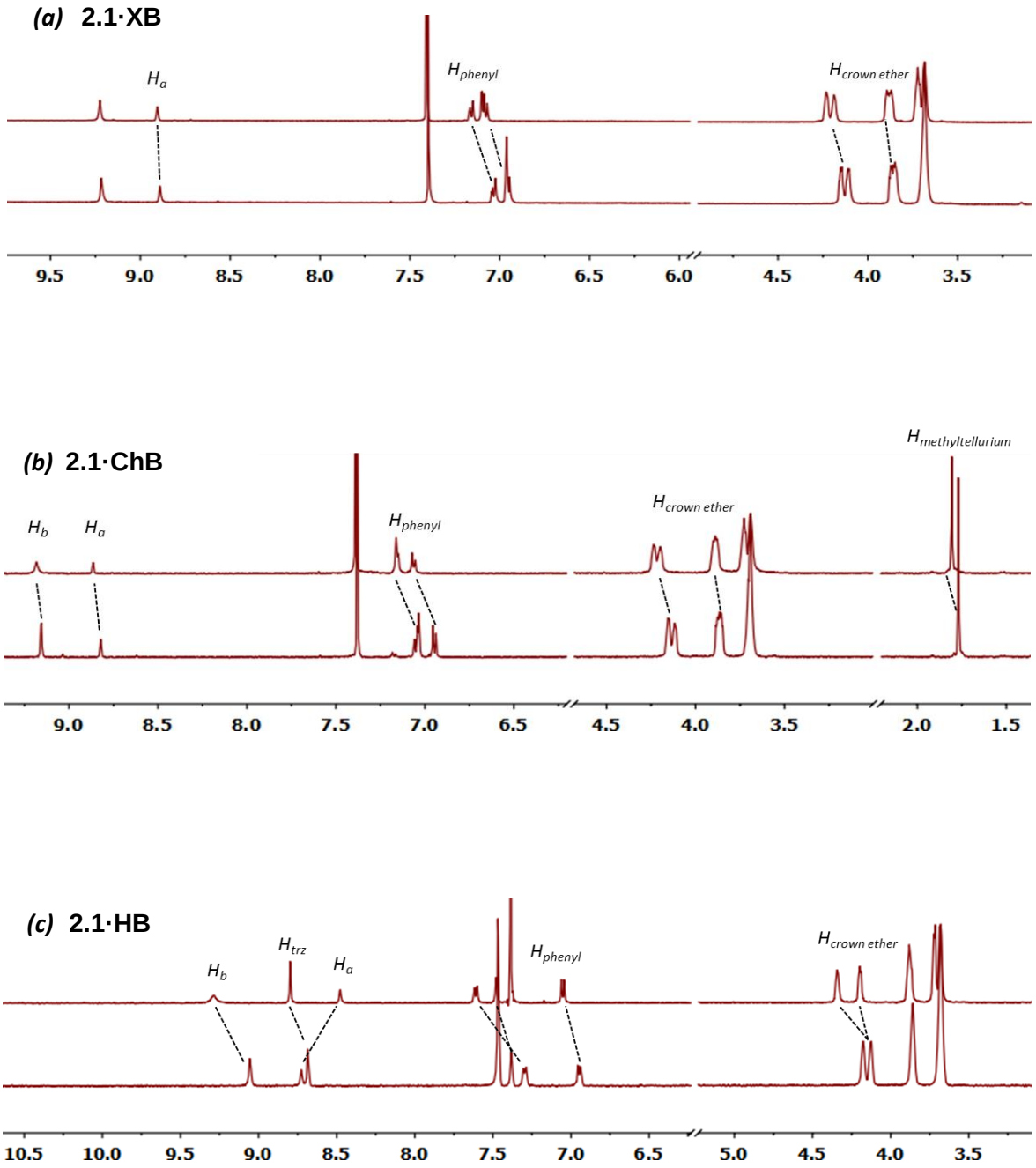

Figure 2.9 ^{1}H-NMR spectra of heteroditopic receptors (a) **2.1·XB**, (b) **2.1·ChB**, and (c) **2.1·HB** in the presence (top) and absence (bottom) of 2 equivalents of $NaPF_6$ in 10% d_6-DMSO/$CDCl_3$ (500MHz/ 298K)

B) *Anion complexation studies*

Quantitative ^{1}H-NMR titration experiments of **2.1·XB** and **2.1·HB** with TBA halide salts typically caused a downfield shift of the internal pyridyl (H_a) and phenyl proton ($H_{c,d,e}$) resonances in the ditopic receptors providing evidence for anion coordination. Additionally, the shift of the triazole proton (H_{trz}) in the **2.1·HB** receptor also indicated its participation in the anion binding event. Only small perturbations were observed in analogous halide titrations with **2.1·ChB**. Monitoring the perturbation in the chemical shift of the internal pyridyl proton (H_a) as a function of anion concentration, WinEQNMR2 analysis of the titration data determined 1:1 stoichiometric association constants shown in Table 2.1. Although the halide association constant values are modest, notably the **2.1·XB** receptor displays stronger halide binding than the **2.1·HB** and **2.1·ChB** receptors, with no selectivity preference. Interestingly, **2.1•ChB** host binds all the halides very weakly (K_a < 5 M^{-1}) compared to **2.1·XB** and **2.1·HB** analogues.

C) Anion binding investigations in the presence of sodium cations

The ^{1}H-NMR halide titrations were repeated in the presence of two equivalents of $NaPF_6$. With all three heteroditopic receptors, significant downfield shifts of the respective internal pyridyl (H_a) and phenyl proton (H_c,H_d,H_e) resonances were observed whilst the signals associated with the crown ether protons remained unchanged (Figure 2.10). This implies that halide anion binding occurs within the bis-triazole cleft of the respective heteroditopic receptor and not simply *via* direct electrostatic association with the benzo crown ether bound sodium cations. Association constants were again determined from the titration data using WinEQNMR2 (Table 2.1). For all the receptors in the presence of sodium cations, quantitative data could not be evaluated from the chloride titration experiments suggesting complex equilibria that may involve contact ion pairs with the crown ether complexed sodium cations and possible competing salt precipitation. In the case of Br^- and I^-, the sigma hole type receptors (**2.1·XB** and **2.1·ChB**) display much stronger halide binding compared to the **2.1·HB** analogue; impressively over an order of magnitude greater with **2.1·XB**. The superior anion binding strength of the **2.1·XB** receptor in comparison to the **2.1·ChB** receptor is also noteworthy and is consistent with recently reported monotopic XB and ChB host systems.[95]

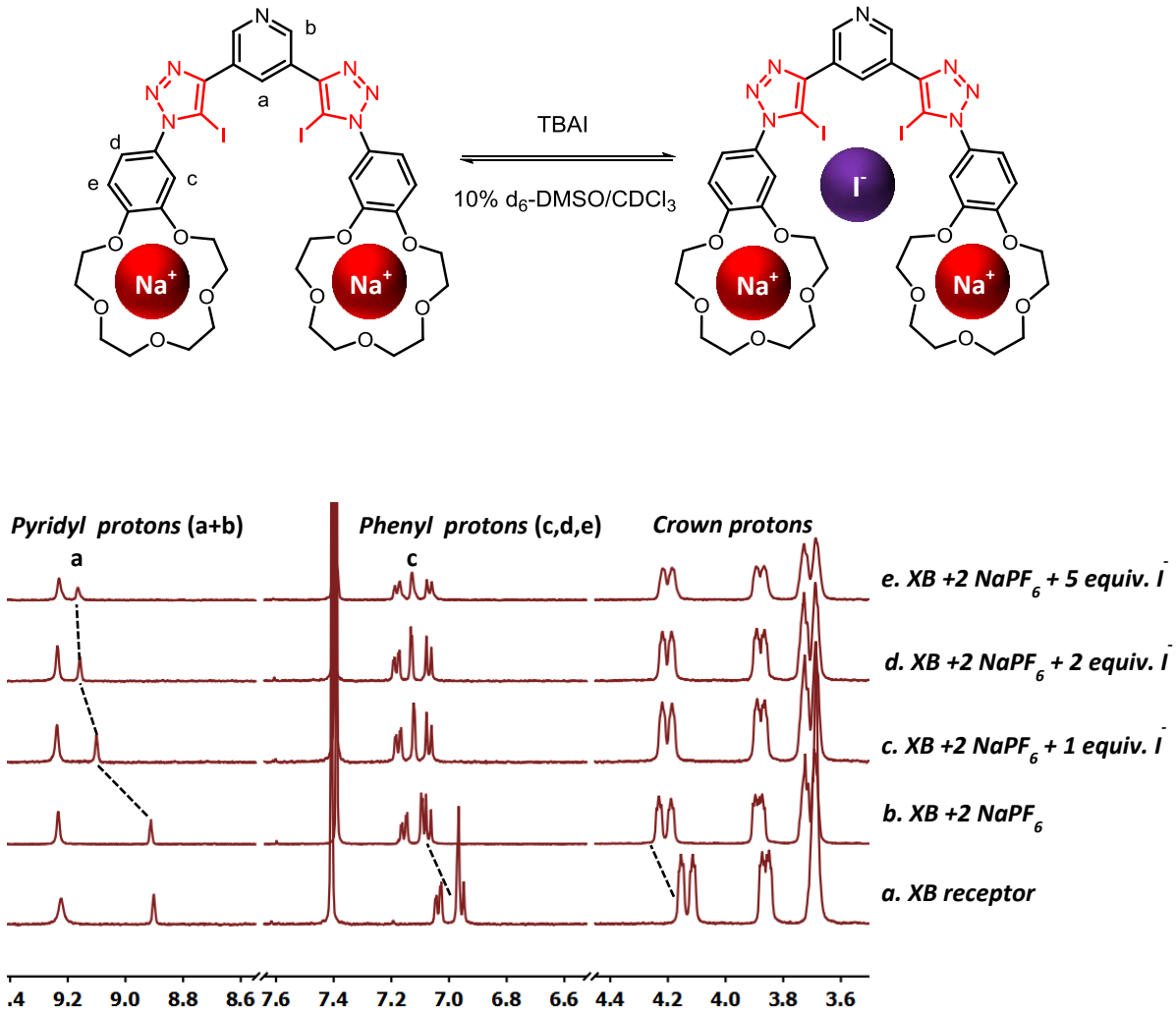

Figure 2.10 Truncated ^{1}H-NMR spectra of (a) **2.1·XB** receptor, **2.1·XB** in the presence of 2 equivalents of $NaPF_6$ with TBAI (b) 0 equiv., (c) 1 equiv., (d) 2 equiv., and (e) 5 equiv. in 10% d_6-DMSO in $CDCl_3$ (500 MHz, T = 298K).

Table 2.1 Anion association constants K_a (M^{-1}) for **2.1·XB**, **2.1·ChB**, and **2.1·HB** in the absence and presence of two equivalents of sodium cation (10% d_6-DMSO in $CDCl_3$, 298 K); sodium cations added as $NaPF_6$; Error is less than ±10%

Anions	Association constants K_a (M^{-1}) for heteroditopic acyclic receptors								
	2.1•XB			2.1•ChB			2.1•HB		
	Na^+	None	α[a]	Na^+	None	α	Na^+	None	α
Cl^-	c	35	-	c	<5	-	c	10	-
Br^-	5056	40	126	1397	<5	~279[b]	379	18	21
I^-	5660	35	162	1084	<5	~217[b]	364	16	23

[a] α is cooperativity factor (K_{Na+}/K_{none})

[b] α calculated based on K_{none} = 5 M^{-1}

[c] It was not possible to determine an association constant from the titration data suggesting complex equilibria.

Importantly, Table 2.1 demonstrates that for each heteroditopic receptor the association constant values for bromide and iodide anions are increased dramatically in the presence of co-bound sodium cations. It is noteworthy that the calculated cooperativity factors ($\alpha = K_{Na+}/K_{none}$) are the greatest for **2.1·ChB**, showing at least over a 200-fold enhancement of halide binding strength, followed by **2.1·XB** over a 100-fold, which is an order of magnitude larger than **2.1·HB** (Table 2.1). In effect, the chalcogen bonding heteroditopic receptor **2.1·ChB**, in the presence of crown ether bound sodium cations switches on its capability to recognise bromide and iodide, highlighting the unique nature of sigma hole mediated ion-pair recognition.

Further evidence for the participation of XB in the ion-pair recognition process was obtained by a comparison of ^{13}C-NMR spectra of **2.1·XB** in the presence of two equivalents of $NaPF_6$, and two equivalents of NaI (Figure 2.11). The chemical shift of the quaternary carbon of the bis-iodotriazole motif was significantly perturbed upfield with NaI (Δδ = -2.22 ppm). Iodide anion complexation was also confirmed by the upfield shift of internal pyridyl carbon (Δδ = -1.45 ppm) resulting from the halide anion being located in the bis-iodotriazole XB binding cleft of the receptor.

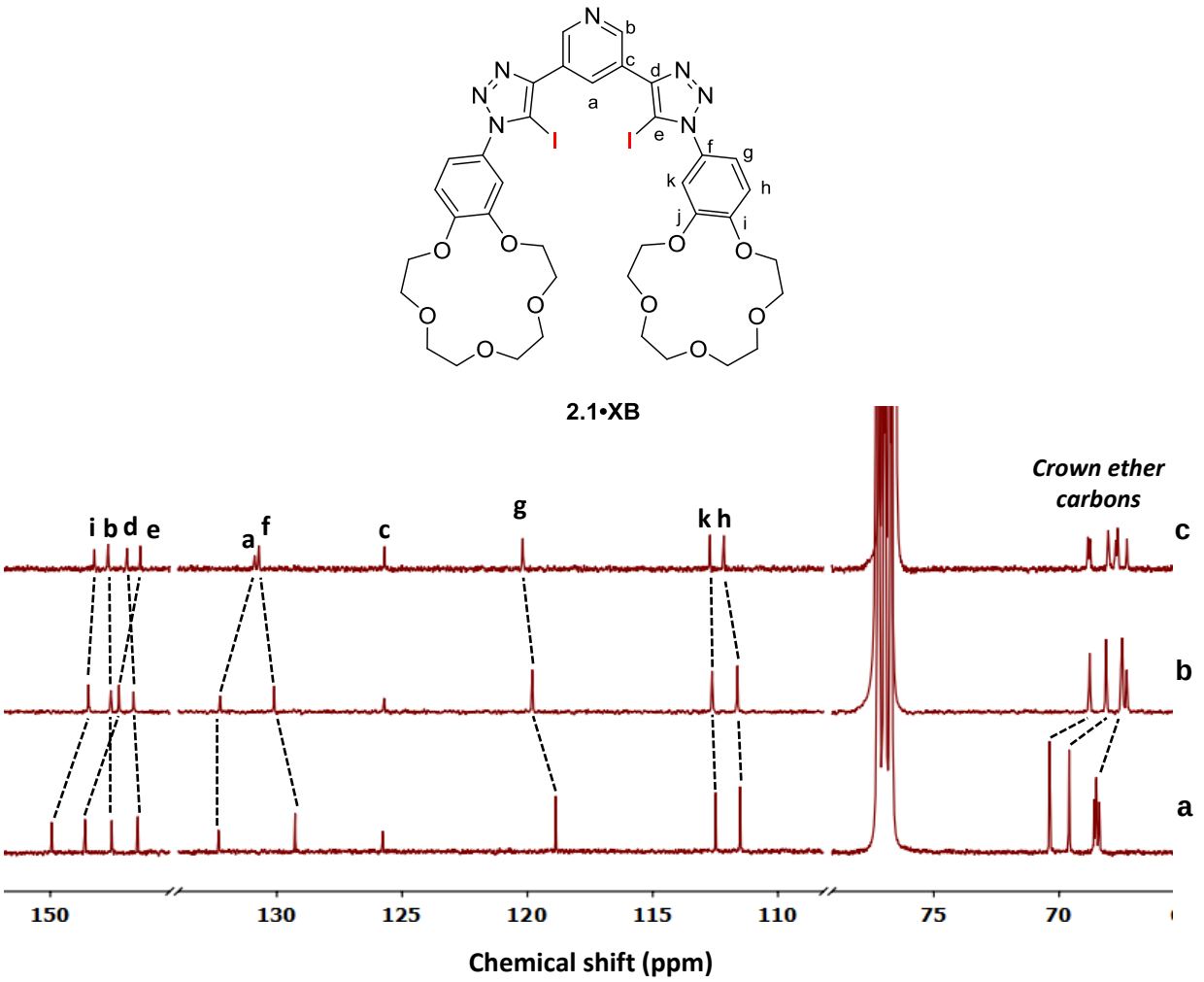

Figure 2.11 ^{13}C-NMR spectra of (a) **2.1·XB**, (b) with 2 equivalents of $NaPF_6$, and (c) with 2 equivalents of NaI in 10% d_6-DMSO in $CDCl_3$ (126 MHz, T = 298K).

Analogous ^{125}Te-NMR experiments with **2.1·ChB** were carried out to provide evidence for chalcogen bond formation between the bis-methyltelluro triazole motif and iodide. The ^{125}Te nucleus, despite its low natural abundance, is highly sensitive to changes in chemical environment as well as non-covalent interaction formation in solution.[94, 95, 214] Addition of two equivalents of $NaPF_6$ caused an upfield perturbation due to crown ether sodium cation complexation. By contrast, adding two equivalents of NaI induced a downfield shift of the ^{125}Te signal (Figure 2.12).

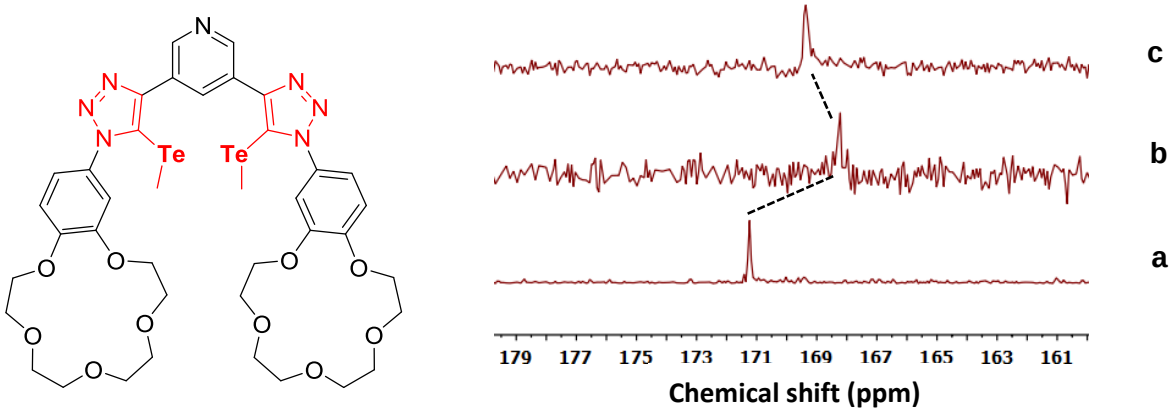

Figure 2.12 ^{125}Te-NMR spectra of (a) **2.1·ChB**, (b) with 2 equivalents of $NaPF_6$, and (c) with 2 equivalents of NaI in 10% d_6-DMSO in $CDCl_3$ (158 MHz, T = 298K).

The combination of favourable electrostatics and the crown ether bound sodium cations inductively withdrawing electron density from the respective XB, ChB and HB anion recognition site, *via* a conjugated through bond mechanism, is presumably responsible for the observed cooperativity of ion-pair binding. This provides evidence for a genuine participation of XB or ChB interactions in ion-pair recognition, as opposed to a solely electrostatic contribution, as confirmed by a series of control experiments using the 3,5-bis-fluorotriazole pyridine crown ether host **2.8**. The fluorotriazole derivative serves as a non-halogen bond donor group.[15] Qualitative ^{1}H-NMR spectroscopic experiments, revealed that the addition of 5 equivalents of TBAI to the bis-sodium cation crown ethers complexed fluorotriazole receptor **2.8** did not display any proton resonance perturbations indicating that no halide binding occurs (Figure 2.13A). Moreover, the ^{19}F-NMR spectra also showed no perturbation of the fluorine chemical environment of the fluoro-triazole groups on addition of iodide (Figure 2.13B).

These experiments confirm that the observed cooperativity behaviour of the sodium cation crown ethers complexed bis-triazole derivatives (**2.1·XB**, **2.1·ChB**, and **2.1·HB**) is not a result of simple direct electrostatic interaction between the sodium cations and halide anion. The nature of the anion binding motif is of crucial importance in dictating anion binding affinities and as a consequence the magnitude of cooperativity factors. The greatly enhanced cooperativity of ion-pair recognition by the XB and ChB receptors relative to the HB analogue may be rationalised by increased polarisation of the C—X (X = I, TeMe) bond due to sodium cation–crown ether complexation in the conjugated heteroditopic receptors. Importantly, this demonstrates an unprecedented mechanism for cooperativity in ion-pair recognition unique to sigma hole mediated interactions and expands the possibilities to affect selectivity and affinity of heteroditopic hosts.

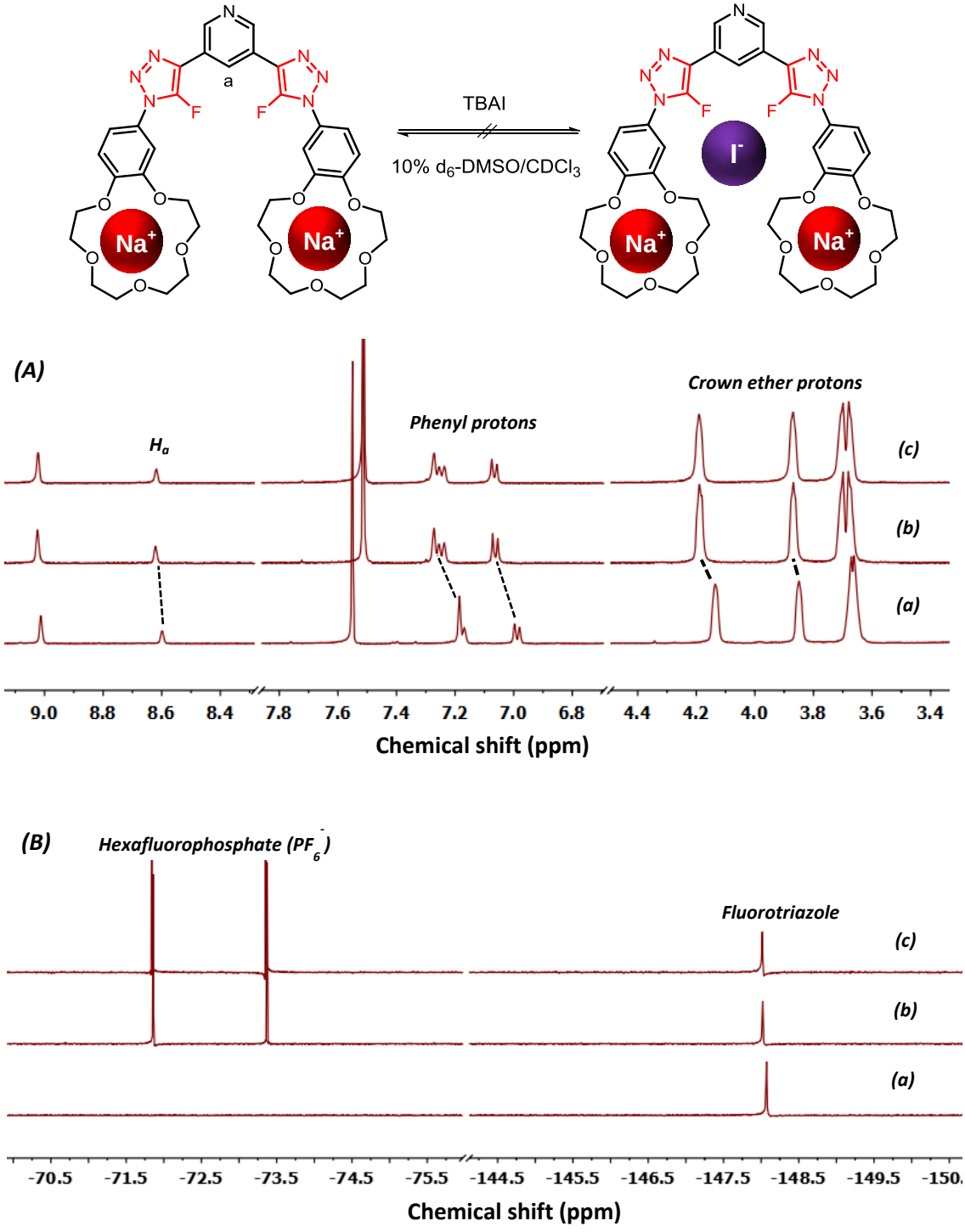

Figure 2.13 Truncated (A) ^{1}H-NMR spectra and (B) ^{19}F-NMR spectra of **2.8** in the presence of (a) 0 equivalent. (b) 2 equivalents of $NaPF_6$ and (c) with 5 equivalents of TBAI in 10% d_6-DMSO in $CDCl_3$ (500 MHz, T = 298K)**.**

D) X-ray crystallographic structures

Solid state evidence of the ion-pair binding properties of the ditopic receptors was obtained by single crystal X-ray structural analysis of the receptor's NaI complex **2.1·HB** (Figure 2.14). Crystals were grown by slow evaporation of a saturated solution of **2.1·HB** with an excess of NaI in 10%MeCN/$CHCl_3$. The X-ray crystallographic data was collected and refined by Dr. Asha Brown. The complex crystallised in the triclinic space group P-1 and the asymmetric unit contains two independent **2.1·HB·2NaI** complexes which form a dimeric assembly in the solid state. A sodium cation is bound within the cavity of each of four benzo[15]crown-5 moieties. The coordination spheres of sodium are occupied by five oxygen donor atoms from the crown ether host (Na^+—O distances ranging from 2.307(10) Å to 2.484(10) Å), together with additional interactions with water solvate molecules and iodide anions. An iodide anion is encapsulated within each of the 3, 5-bis-triazole pyridine anion-binding clefts via an array of CH—I^- hydrogen bonding interactions. Both of the cleft-bound iodide anions are also involved in ion-pair interactions with sodium cations from the adjacent molecular unit within the dimeric assembly; one forms a direct Na^+—I^- contact ion-pair, while the other forms a solvent-separated ion-pair bridged by a water molecule. The remaining two iodide counteranions are disordered over five partially occupied positions which are all in proximity to a crown-ether-bound sodium cation, and in each case the anion is observed to form either a contact or solvent-bridged ion-pair with the proximal cation. In addition, a series of CH—I^-, CH—O and CH—N short contacts involving the crown ether ethylene CH_2 groups are observed, suggesting that these groups participate in extensive intermolecular CH—X^- hydrogen bonding interactions which contribute to the overall stability of the crystalline lattice.

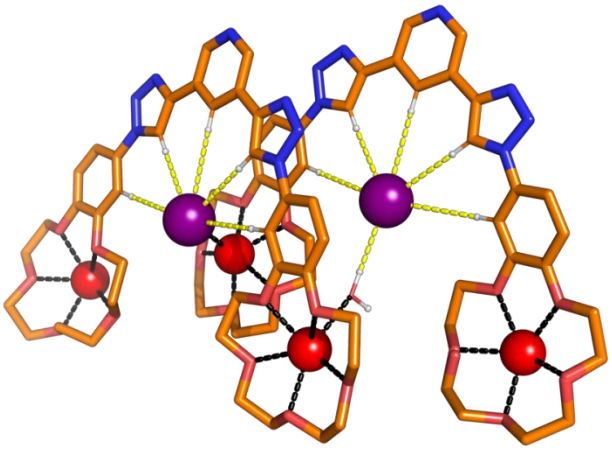

Figure 2.14 Solid state structure of the complex **2.1·HB·2NaI**.

An additional preliminary solid state structure of the iodide complex of the *N*-pyridyl-protonated halogen bonding receptor, **2.1·XB·HCl**, was also obtained. As a consequence of severe radiation damage to the crystal during data collection, the data is not of sufficient quality for discussion. However, it is possible to observe the iodide anion bound within the 3,5-bis-iodotriazole cavity *via* bidentate halogen bonding interactions (Figure 2.15).

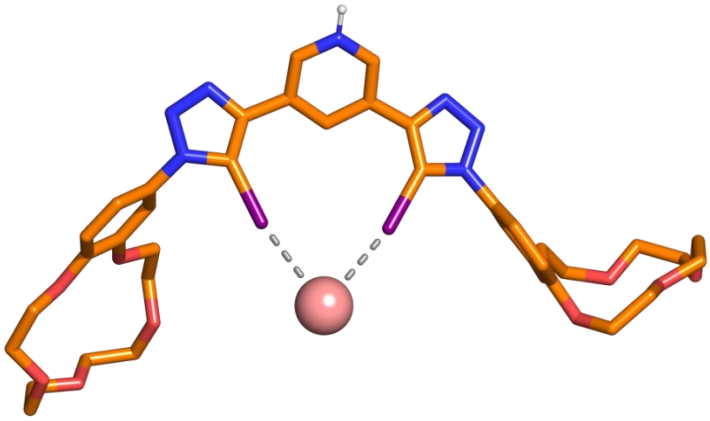

Figure 2.15 Preliminary solid state structure of the complex **2.1·XB·HCl**. For clarity, non-polar hydrogen atoms and selected counteranions and water molecules have been omitted.

E) Oxoanion binding studies

The scope of studied anionic guests was expanded to investigate the efficacy of the heteroditopic receptors to recognise oxoanions including perchlorate (ClO_4^-), periodate (IO_4^-), and perrhenate (ReO_4^-). In the absence of sodium cations, ^{1}H-NMR titration studies revealed the spectra of all three receptors remained unchanged upon addition of these TBA oxoanion salts in 10% d_6-DMSO/$CDCl_3$; presumably the receptors do not bind these anions due to their weakly coordinating nature. Analogous oxoanion titrations in the presence of two equivalents of $NaPF_6$ only perturbed the anion binding cleft protons of **2.1·HB** (Figure 2.16).

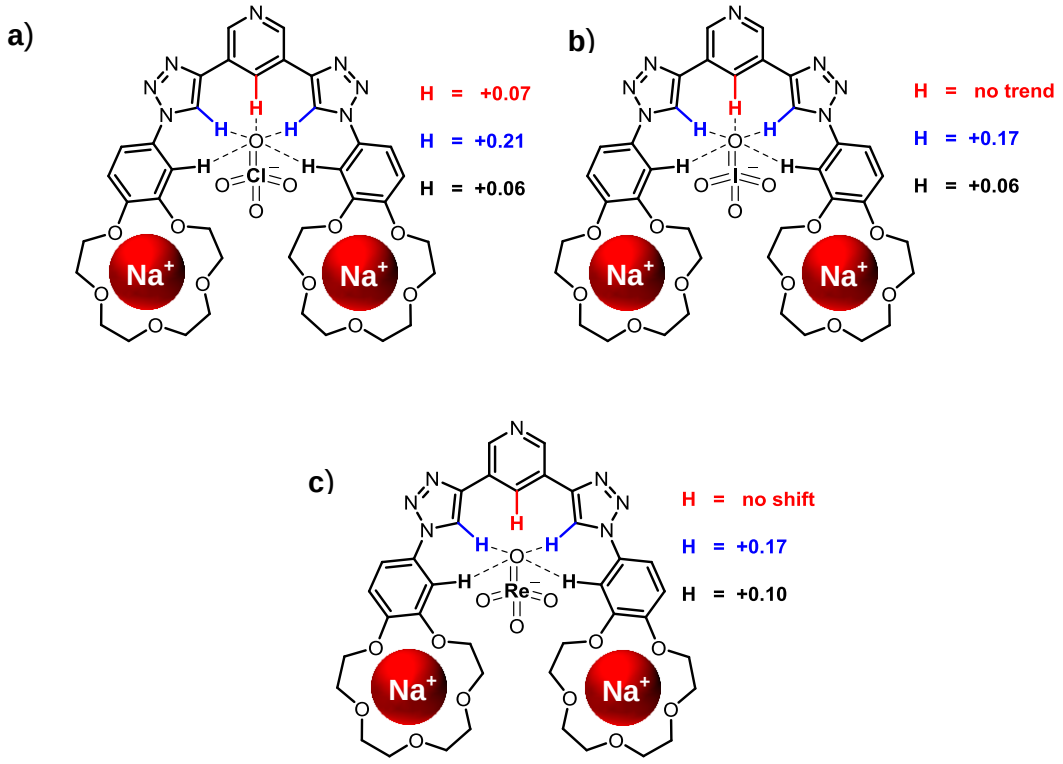

Figure 2.16 ^{1}H-NMR chemical shift change (ppm) of protons related to the binding site in crown ether sodium complexed **2.1·HB** upon the addition of 10 equivalents of (a) $TBAClO_4$, (b) $TBAIO_4$, and (c) $TBAReO_4$ in 10% d_6-DMSO in $CDCl_3$ (500 MHz, T=298 K).

Table 2.2 Anion association constants K_a (M^{-1}) of **2.1·HB** in the presence of two equivalents of sodium cation (10% d_6-DMSO in $CDCl_3$, 298 K); sodium cations added as $NaPF_6$; Errors are less than ±10%

Anions	Association constants K_a (M^{-1}) for 1•HB + 2 equivs. of $NaPF_6$
ClO_4^-	426
IO_4^-	268
ReO_4^-	224

Unlike the binding of halides, the internal pyridyl proton (H_a) resonance of sodium complexed **2.1·HB** only moved significantly upon addition of ClO_4^-. Therefore, quantitative oxoanion binding data was calculated by monitoring the downfield shift of the phenyl (H_c) and triazole (H_{trz}) proton resonances. WinEQNMR2 analysis of titration data determined 1:1 stoichiometric association constants shown in Table 2.2. The presence of sodium cations switches on the recognition of the oxoanions, as no binding is observed in the alkali metal cation's absence. Typically anion selectivity trends of synthetic hosts in organic media are influenced by the anion guest's charge density and basicity. However, **2.1·HB** demonstrates greatest affinity for the ClO_4^- anion which is the least basic among this group of oxoanions. No binding was observed for **2.1·XB** and **2.1·ChB** receptors, highlighting again the contrasting properties of HB and sigma hole mediated ion-pair recognition.

2.4.3 Solid-liquid extraction studies

The ability of ion-pair receptors to extract and solubilise salts into organic media is another interesting application of the ditopic host. While a number of alkali metal halide salt HB based systems are known.[105, 207, 215, 216] To the best of our knowledge, exploiting sigma-hole type ion pair receptors in the study of solid-liquid salt extraction is unprecedented.

Solid-liquid extraction studies were carried out by exposing a selected organic solvent solution of each ditopic receptor to an excess of microcrystalline sodium halide salts. After 1 h of sonication at ambient temperature, the solution was filtered and analysed by ^{1}H-NMR spectroscopy and electrospray mass spectrometry (ESI-MS).

^{1}H-NMR and ESI-MS studies of single salt extractions

The organic solvent mixture of 10% $CD_3CN/CDCl_3$ was found to be the most suitable for the extraction studies with NaX (X = Cl, Br, I, NO_3) salts. Significant ^{1}H-NMR chemical shift changes were observed for **2.1·XB** with $NaNO_3$, NaBr and NaI whilst the signals from the NaCl extraction remained unchanged (Figure 2.17). The downfield perturbations of the receptor's internal pyridyl proton H_a observed in NaBr and NaI extraction experiments indicated that extraction had occured. High resolution ESI-MS revealed signals corresponding to $[M+2Na+X]^+$ where X is Br^- and I^- (Figure 2.18). With **2.1·HB**, NaBr and NaI extraction solutions revealed the significant ^{1}H-NMR chemical shift changes, whilst no perturbation of proton resonances were noted with NaCl and $NaNO_3$ (Figure 2.19). The ESI-MS analysis showed signals corresponding to $[M+2Na^++X^-]^+$ where X is Br^- and I^- (Figure 2.20). Successful solid-liquid extraction of NaBr and NaI was also seen by ^{1}H-NMR spectra of **2.1·ChB** (Figure 2.21), however ESI-MS evidence displayed only signals corresponding to $[M+X]^-$ where X = Br and I (Figure 2.22).

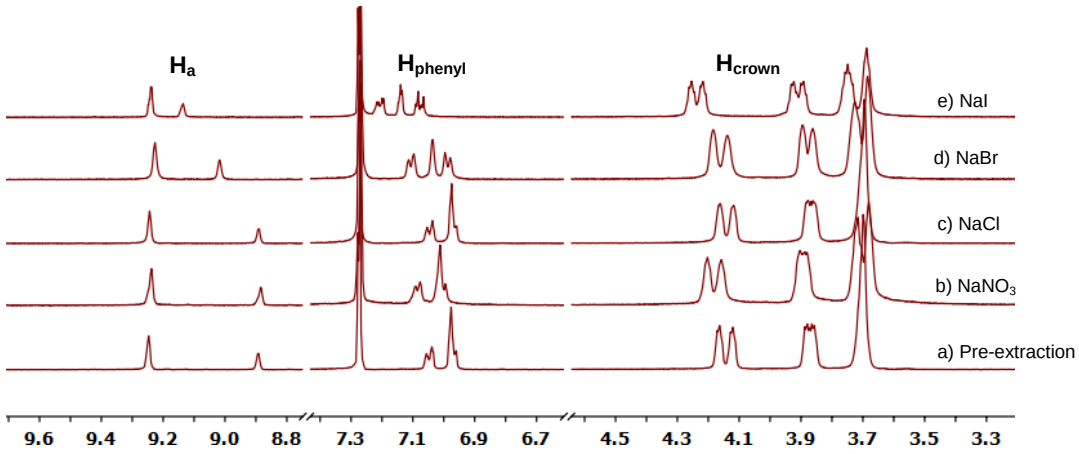

Figure 2.17 ^{1}H-NMR spectrum of (a) pre- and post- solid/liquid extraction experiments of **2.1·XB** receptor with (b) $NaNO_3$,(c) NaCl,(d) NaBr and (e) NaI in 10%$CD_3CN/CDCl_3$.

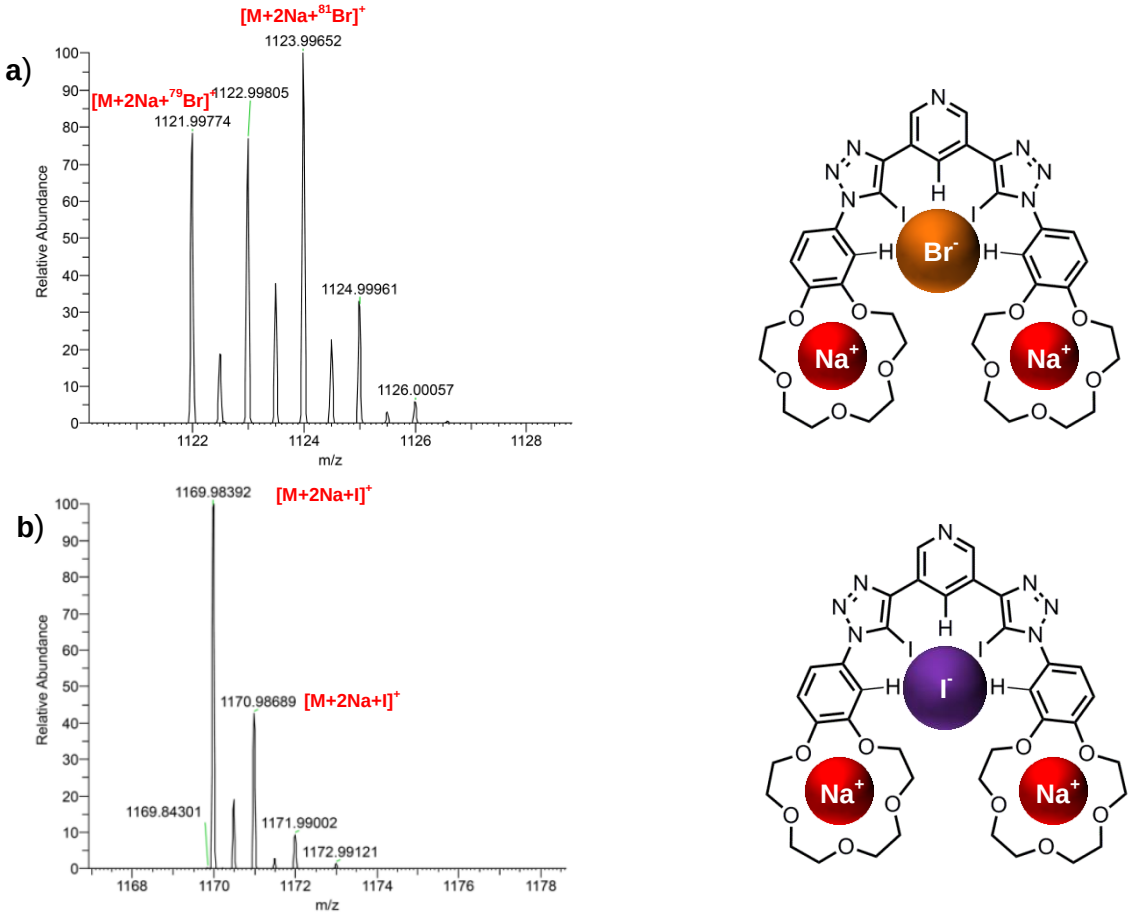

Figure 2.18 ESI-MS of post-extraction solution of sodium complexed **2.1·XB** with (a) NaBr and (b) NaI in 10%MeCN/$CHCl_3$ at 298K; where M is m/z of **2.1·XB**.

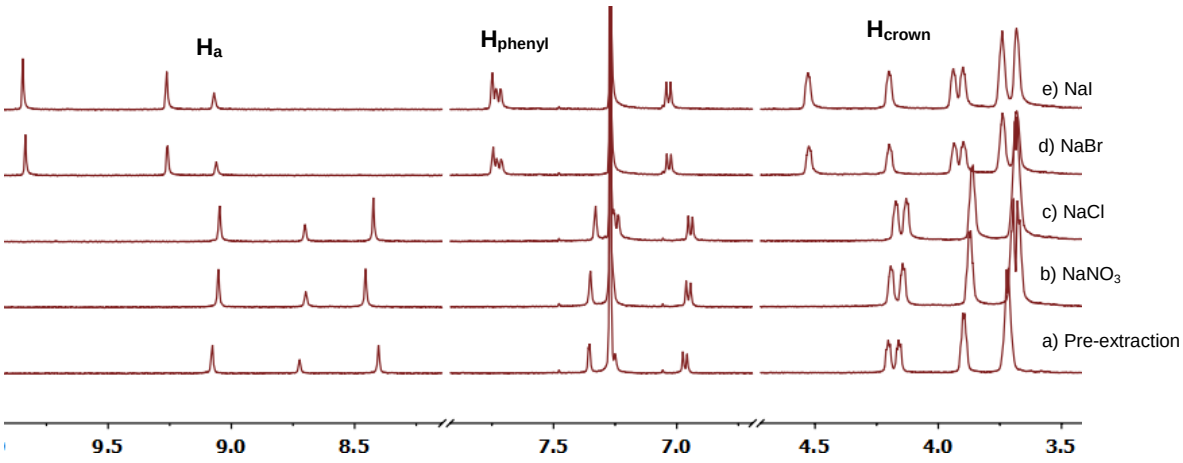

Figure 2.19 ^{1}H-NMR spectrum of (a) pre- and post- solid/liquid extraction experiments of **2.1·HB** receptor with (b) $NaNO_3$,(c) NaCl,(d) NaBr and (e) NaI in 10%$CD_3CN/CDCl_3$.

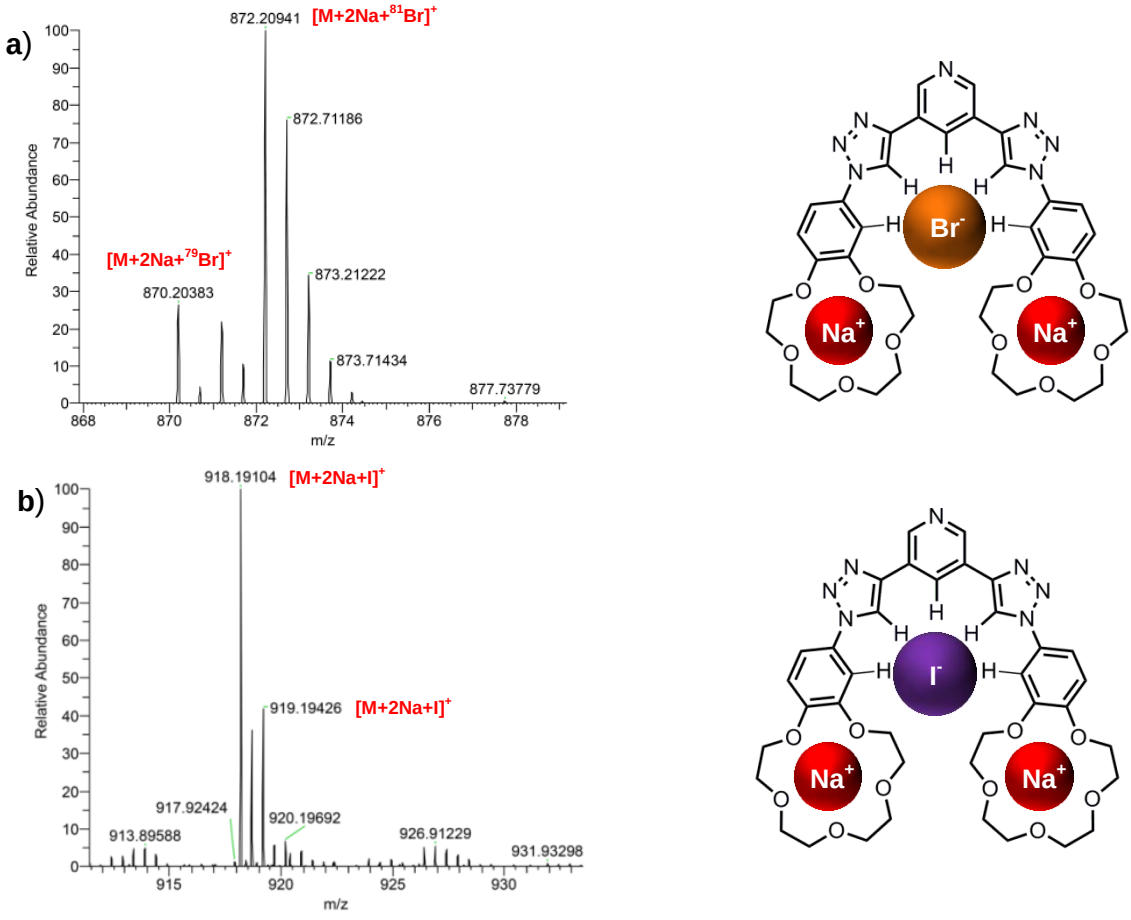

Figure 2.20 ESI-MS of post-extraction solution of sodium complexed **2.1·HB** with (a) NaBr and (b) NaI in 10%MeCN/$CHCl_3$ at 298K; where M is m/z of **2.1·HB**.

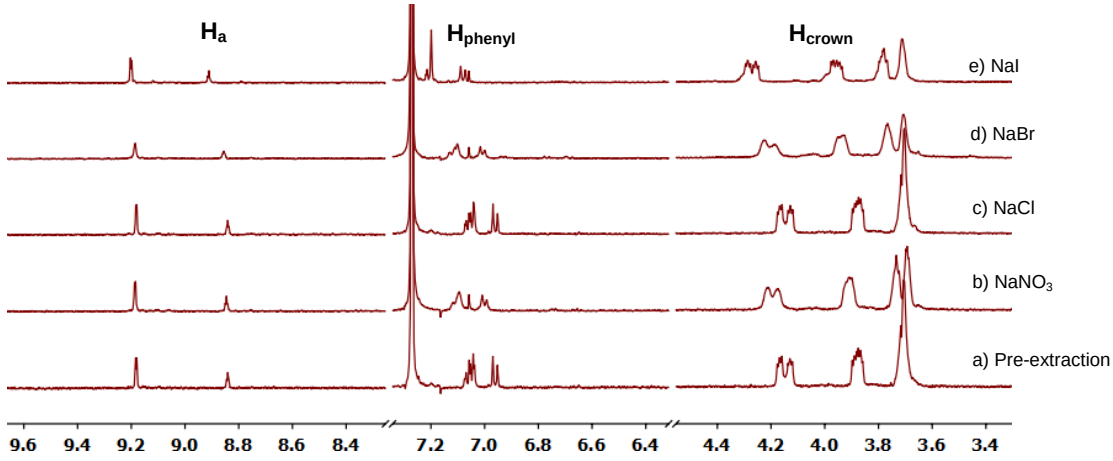

Figure 2.21 ^{1}H-NMR spectrum of (a) pre- and post- solid/liquid extraction experiments of **2.1·ChB** receptor with (b) $NaNO_3$,(c) NaCl,(d) NaBr and (e) NaI in 10%$CD_3CN/CDCl_3$.

a)

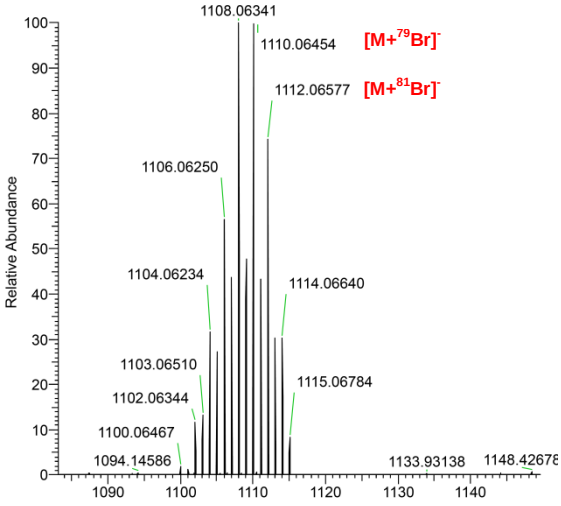

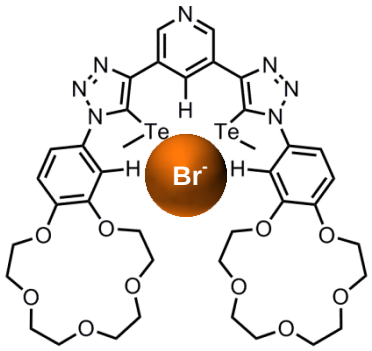

b)

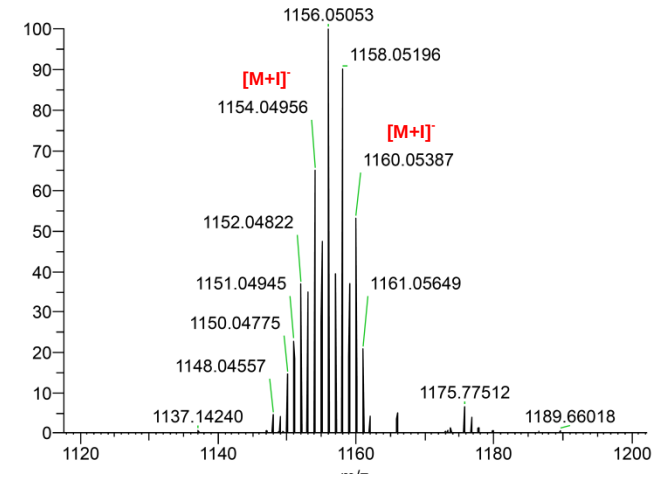

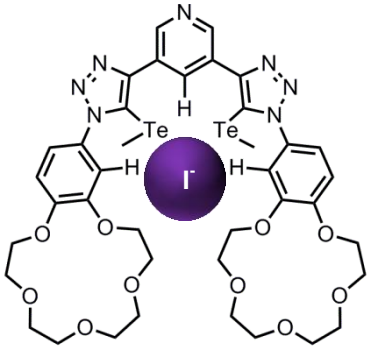

Figure 2.22 ESI-MS of post-extraction solution of sodium complexed **2.1·ChB** with (a) NaBr and (b) NaI in 10%MeCN/$CHCl_3$ at 298K; where M is m/z of **2.1·ChB**.

2.5 Secondary ammonium–crown ether [2]catenane appended XB anion receptor

2.5.1 Ammonium cation binding

In addition to alkali metal cation recognition, crown ethers are capable of binding organic cations.[5] From pioneered work by Stoddart, the secondary ammonium cation was demonstrated to form a pseudorotaxane assembly with dibenzo[24]crown-8 *via* ion—dipole HB interactions (Figure 2.24).

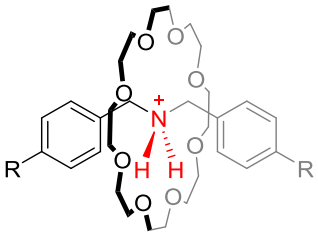

Figure 2.24 Pseudorotaxane formation between dibenzylammonium cation and [24]crown8.

The stability of secondary ammonium-crown ether pseudorotaxane complexes, has led to their extensive employment in the formation of a range of rotaxane and catenane supramolecular architectures.[217-220] In 2013, Iwamoto and co-workers developed synthetic methodologies to prepare catenanes using an ammonium—crown ether template, where pseudorotaxane formation between a dibenzo[24]crown-8 macrocycle and a bis-vinyl functionalised dibenzylammonium thread allows for an olefin metathesis ring closing macrocyclisation reaction to afford [2] and [3]catenanes(Figure 2.25).[221]

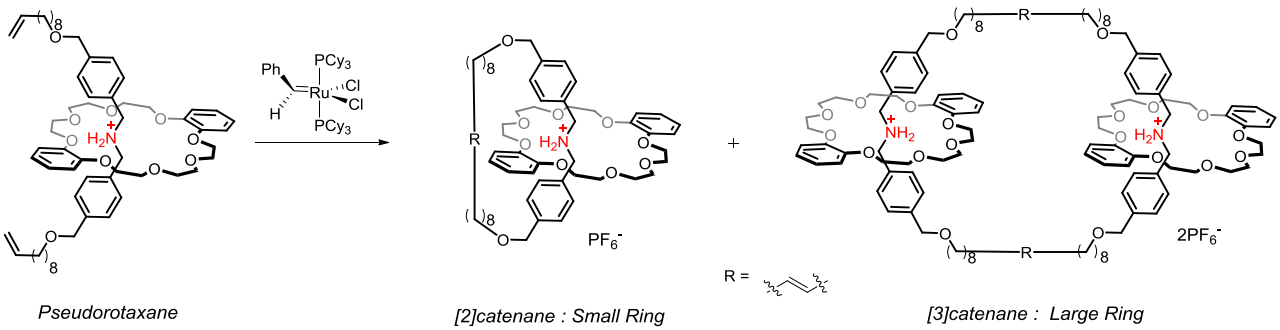

Figure 2.25 Formation of [2] and [3]catenanes by Grubbs'(I) catalysed ring closing metathesis macrocyclisation.

The same research group constructed higher order interlocked molecules including [5]catenanes, *via* dimerization of a pseudorotaxane composed of a [2]catenane and secondary ammonium salt (Figure 2.26).[222]

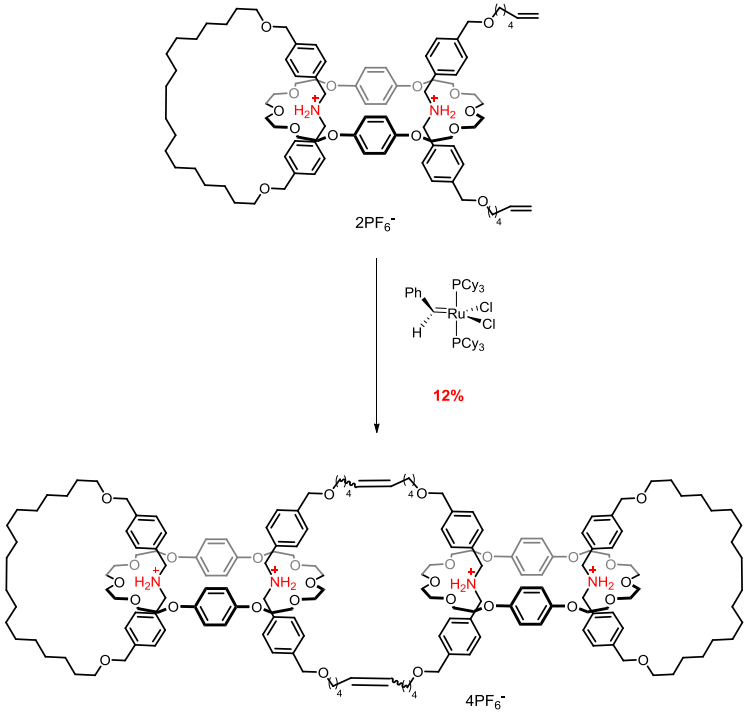

Figure 2.26 Dimerization of pseudorotaxane for the synthesis of a [5]catenane.

In the previous section the strength of anion binding by XB and ChB heteroditopic receptors was shown to be significantly augmented *via* co-bound sodium cation-benzo[15]crown-5 complexation. With the idea of replacing the sodium cation–crown ether complexed motifs with a secondary ammonium–crown ether [2]catenane group (Figure 2.27), a novel XB anion receptor was designed and constructed.

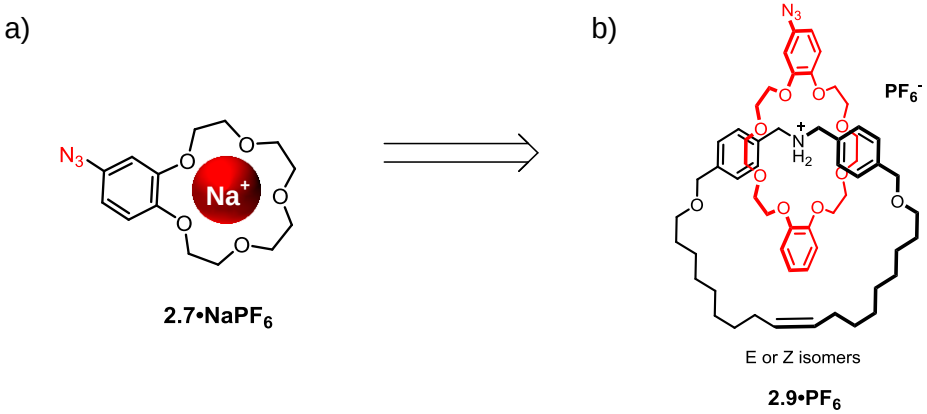

Figure 2.28 Structural comparison of (a) **2.7·NaPF$_6$** and (b) azido-ammonium [2]catenane.

2.5.2 Synthesis of ammonium bis-alkene thread

Before embarking upon the azide catenane synthesis, it was necessary to prepare the appropriate bis-alkene thread, using a modified procedure reported by Stoddart and Iwamoto (Scheme 2.6).[221, 223] Firstly, esterification of commercially available 4-aminomethyl benzoic acid **2.9** with thionyl chloride and methanol afforded the methyl 4-aminomethyl benzoate **2.10** in 88% yield. An equivalent of 4-formylmethylbenzoate was reacted with **2.10** in dry methanol overnight to form imine **2.11,** which was subsequently reduced using $NaBH_4$ to obtain the secondary amine **2.12** without further purification. The reaction of **2.12** with *tert*-di-*tert*-butyl dicarbonate in the presence of a catalytic amount DMAP gave the Boc-protected secondary amine **2.13** in 82% yield. Reduction of the methyl ester group using $LiAlH_4$ was achieved in quantitative yield to obtain the bis-alcohol **2.14**. A S_N2 reaction of **2.14** and decenyl tosylate in the presence of NaH in DMF afforded the bis-alkene **2.15** in 72% yield. Deprotection of the Boc group using acid gave the bis-alkene ammonium thread **2.16·PF$_6$** in 90% yield after anion exchange.

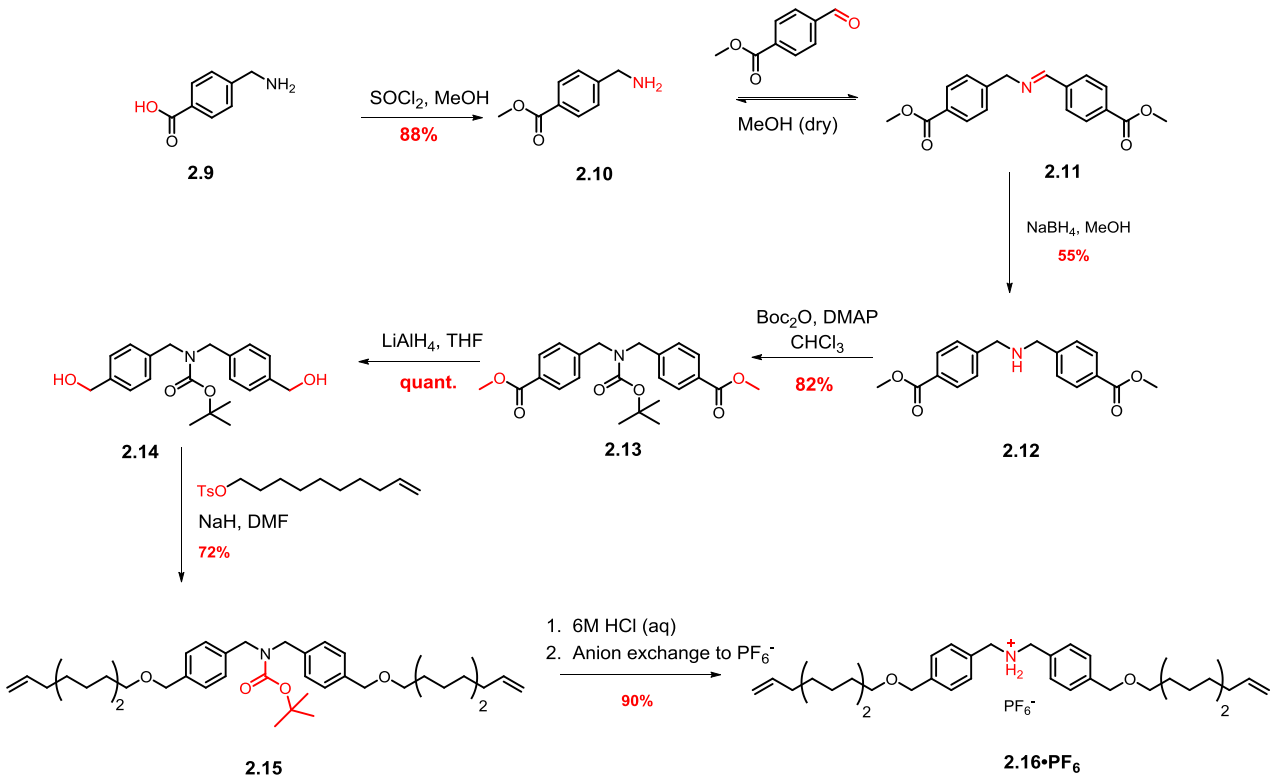

Scheme 2.6 Synthesis of bis-vinyldibenzyl ammonium thread **2.16·PF$_6$.**

2.5.3 Synthesis of the azido-dibenzo[24]crown-8 macrocycle component

The synthesis of azido-dibenzo[24]crown-8 was carried out as shown in Scheme 2.2 and 2.8. Triethylene glycol monotosylate was prepared by reacting an excess of triethylene glycol with one equivalent of *p*-toluenesulfonyl chloride (TsCl) and NaOH in DCM to obtain **2.17** in 70 % yield. An alkylation reaction of catechol **2.18** with two equivalents of the monotosylate **2.17** in the presence of K_2CO_3 in acetonitrile afforded the bis-hydroxyl intermediate **2.19**. Subsequent tosylation of **2.19** in DCM gave the bis-tosylate **2.20** in 60% yield over two synthetic steps.[187, 224] Macrocyclisation was achieved via a potassium cation templated ring closing reaction using a modified literature procedure reported by Gibson et. al..[225] An equimolar solution of the bis-tosylate **2.20** and 4-nitrocatechol in MeCN was refluxed in the presence of KPF_6 and K_2CO_3 in the absence of external light for 72 h. The crude product was washed with aqueous pyridine hydrochloride, and recrystallised from hot EtOH to give nitro-functionalised dibenzo[24]crown-8 as a yellow powder **2.21** in 87% yield.

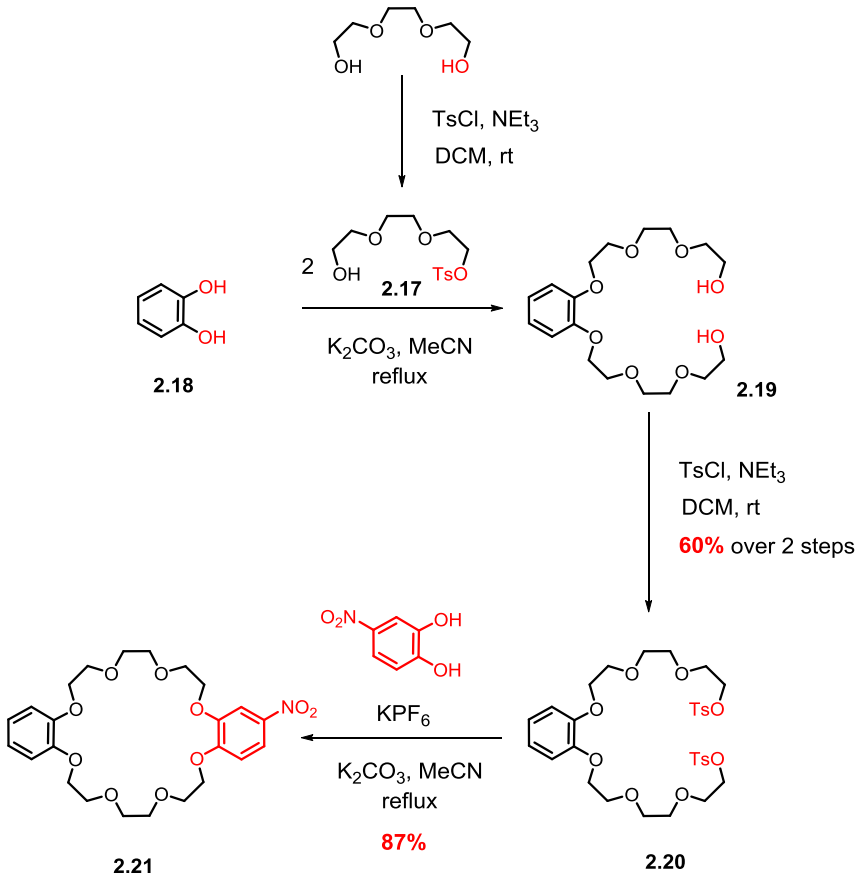

Scheme 2.7 Synthesis of the novel nitro-dibenzo[24]crown-8 **2.21**.

Reduction of **2.21** with hydrazine monohydrate in the presence of Pd/C in EtOH afforded the amino derivative **2.22** in quantitative yield without the need for chromatographic purification. Diazotization of amine **2.22** with $NaNO_2$ under acidic conditions, followed by a nucleophilic aromatic substitution reaction with NaN_3 gave azido-dibenzo[24]crown-8 **2.23** in 90% yield (Scheme 2.8). The novel crown ether was characterised by ^1H and ^{13}C-NMR spectroscopy, and HRMS.

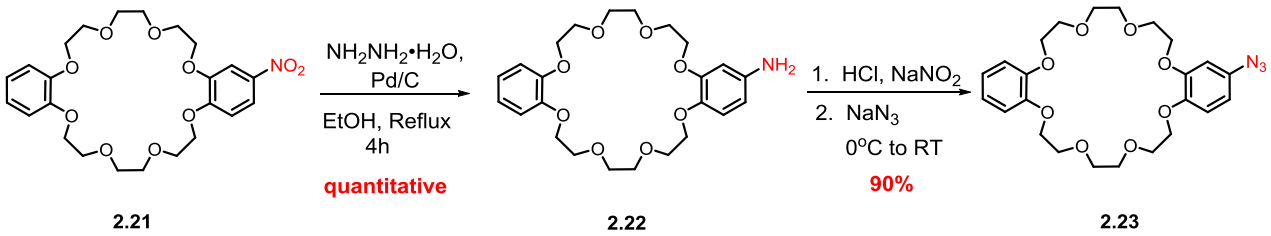

Scheme 2.8 Preparation of azido-dibenzo[24]crown-8 **2.23**.

2.5.4 Pseudorotaxane studies

Qualitative ^1H-NMR spectroscopic pseudorotaxane studies between **2.16·PF$_6$** and **2.23** were conducted by mixing an equimolar solution of each component in *d_2*-dichloromethane at room temperature, giving a homogeneous solution. The ^1H-NMR spectrum of the resulting solution shows well resolved signals of both a threaded and unthreaded state, indicating the pseudorotaxane equilibria is in slow exchange on the NMR timescale (Figure 2.29). The aromatic proton resonances from the ammonium thread component (H_c and H_b) displayed an upfield shift upon interpenetration. This is consistent with these protons being shielded by the aromatic groups of the crown ethers (H_1, H_2, H_{13} and H_{phenyl}). Additionally, the macrocycle proton resonances are split into multiple signals, in which the proton signals from the threaded state are shifted to the upfield region. Downfield perturbations were observed for the methylene protons (H_a) adjacent to the ammonium group, whereas all methylene protons from the crown ether moiety were shifted upfield. These evidences all indicate the formation of pseudorotaxane **2.24**, in which hydrogen bonding and ammonium cation—dipole NH^+—O interactions, along with π—π interactions stabilise the complexed assembly in d_2-dichloromethane.

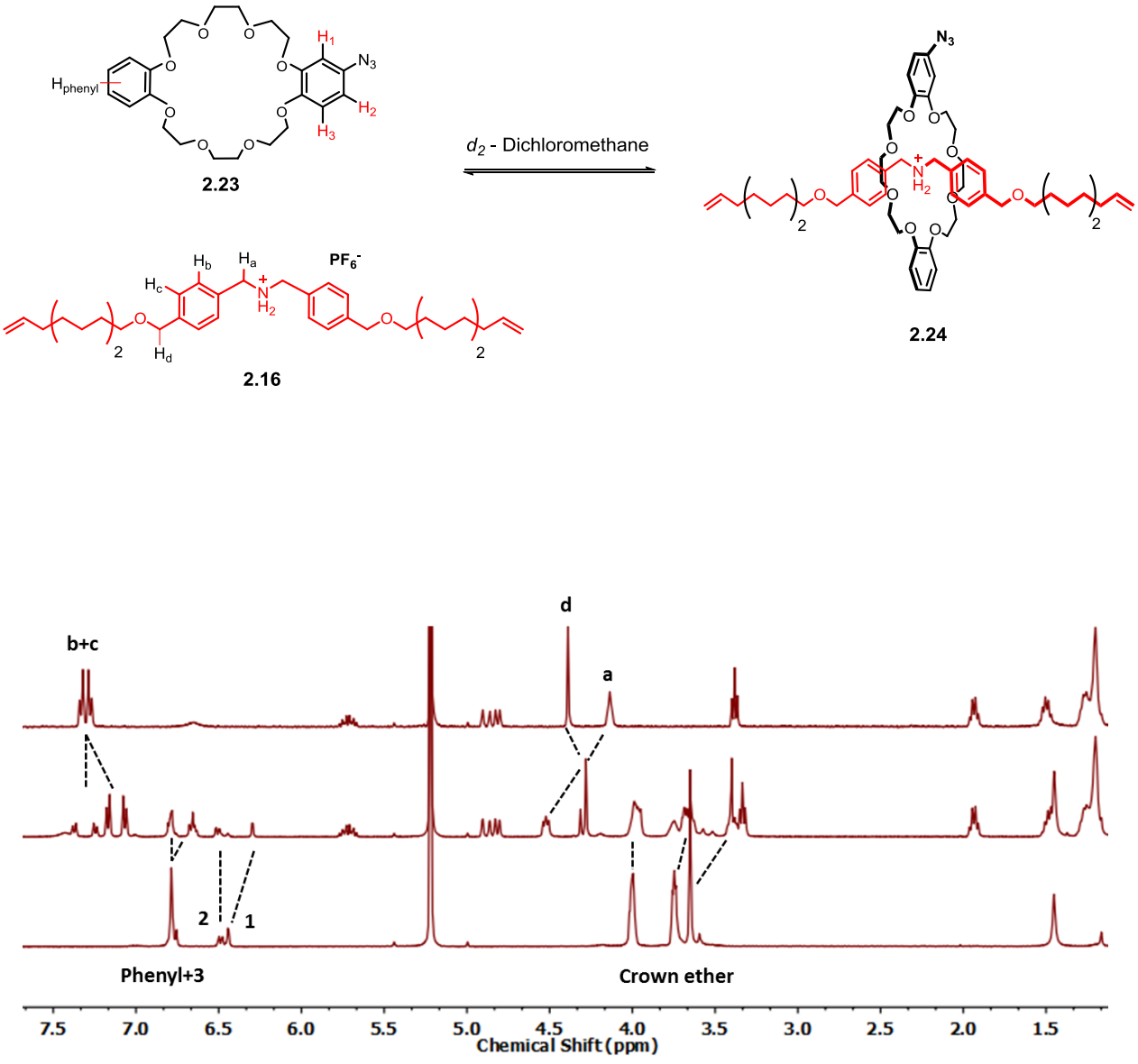

Figure 2.29 Stacked truncated ^{1}H-NMR spectra of the azido-dibenzo[24]crown-8 **2.23** (bottom), the mixture of **2.16·PF$_6$** and **2.23** (middle), and the ammonium thread **2.16·PF$_6$** (top) in d_2-dichloromethane ([host] = 2mM, T= 298K, 500 MHz).

2.5.5 Azide functionalized [2]catenane synthesis

The stability of the pseudorotaxane complex assembly was exploited to prepare the azide appended catenane **2.25·PF$_6$** *via* a ring closing metathesis reaction. This was initially attempted by the addition of Grubbs' 2nd generation catalyst to an equimolar mixture of **2.16** and **2.23** in dry and degassed DCM with 2nd generation Grubbs' catalyst.[226] Under these conditions, no evidence of either the target [2]catenane or cyclisation products was observed. Presumably, Grubbs' catalyst poisoning occurred in the presence of acidic ammonium.[227] Replacing the 2nd generation catalyst with the 1st generation Grubbs' catalyst[228] produced the [2]catenane **2.25·PF$_6$** (Scheme 2.9) as observed by ESI-MS with undefined oligomeric byproducts. The crude product was purified by stirring in a suspension of activated charcoal to remove catalyst residue, and isolated by preparative silica gel thin-layer chromatography, followed by size exclusion chromatography and anion exchange to afford the azido[2] catenane **2.25·PF$_6$** product in 30% yield. The resulting [2]catenane was characterised by ^{1}H, ^{13}C-NMR spectroscopy and HRMS.

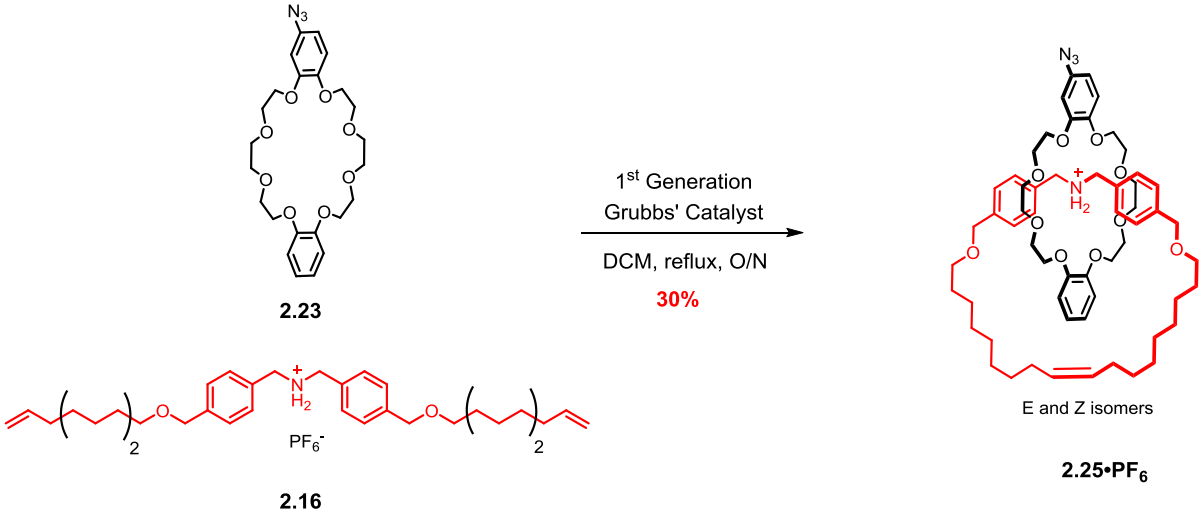

Scheme 2.9 Synthesis of the azido-[2]catenane **2.25·PF$_6$** *via* olefin ring closing metathesis.

Further evidence of the interlocked nature of **2.25·PF$_6$** was observed by ^{1}H-^{1}H ROESY NMR spectroscopy (Figure 2.30), in which through space interactions between proton resonances of the two macrocycles (H_a and H_c from the dibenzyl ammonium macrocycle with $H_{crown\ ether}$ from **2.23**) are observed. In addition, strong through space coupling between H_c and methylene protons from the crown ether group indicates that the secondary ammonium group is stabilised in the cavity of dibenzo-24-crown-8.

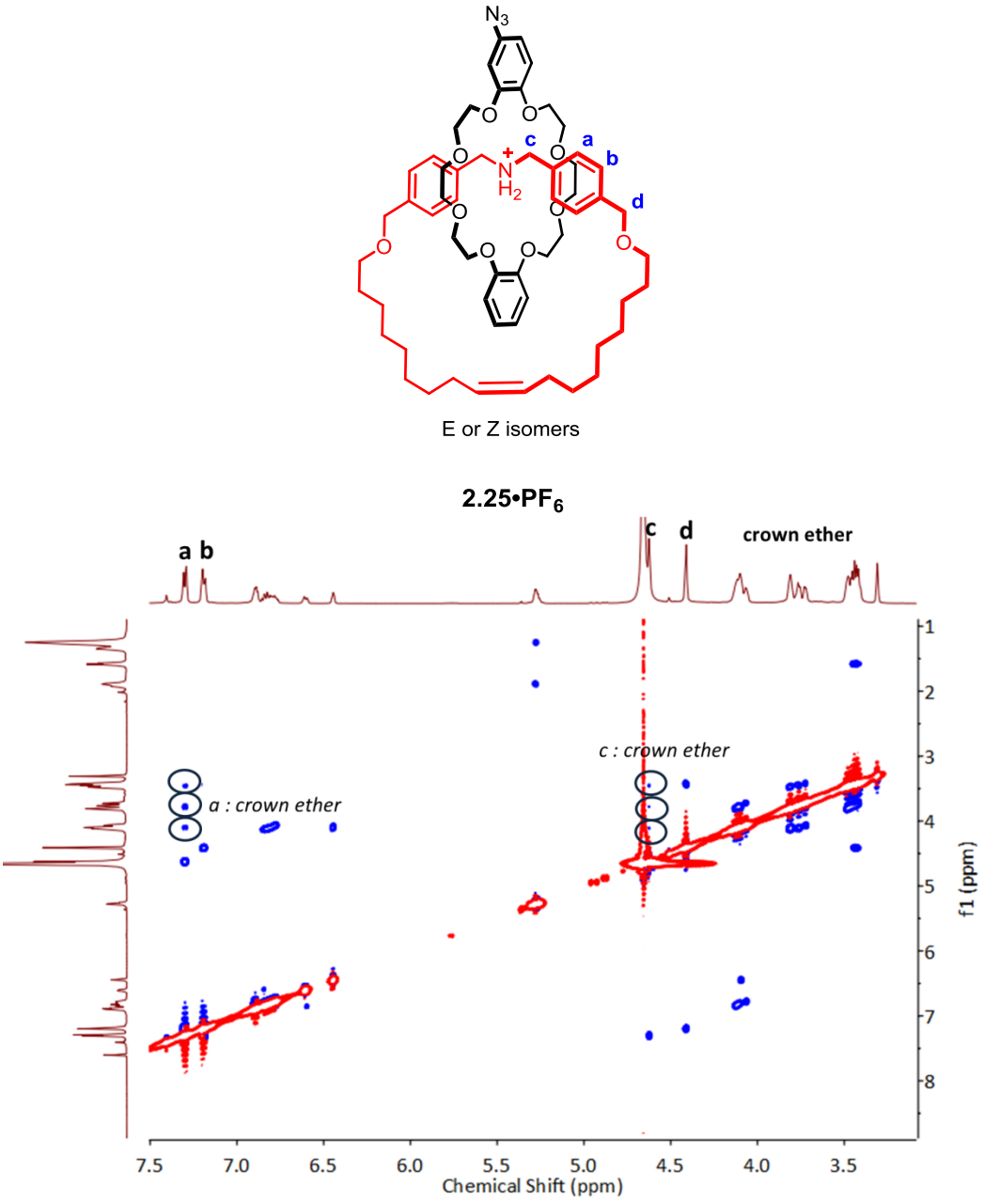

Figure 2.30 ROESY ^{1}H-NMR spectrum of the azido-[2]catenane **2.25·PF$_6$** in 1:1 $CD_3OD/CDCl_3$ (298K, 500 MHz).

2.5.6 Synthesis of XB host

To append the [2]catenane group **2.25·PF$_6$** to an XB anion binding motif, a CuAAC reaction between 3,5-diiodoethynylpyridine **2.3** and two equivalents of azido-[2]catenane **2.25·PF$_6$** was carried out using Cu(MeCN)$_4$PF$_6$ and TBTA in THF at ambient temperature for 72 hours. The crude product was purified by preparative thin layer silica gel chromatography, and anion exchange to ensure anionic purity to its PF_6^- salt, affording the novel target XB receptor **2.26·(PF$_6$)$_2$** in 85% yield. The product was characterised by ^{1}H, and ^{13}C-NMR spectroscopy and ESI-MS.

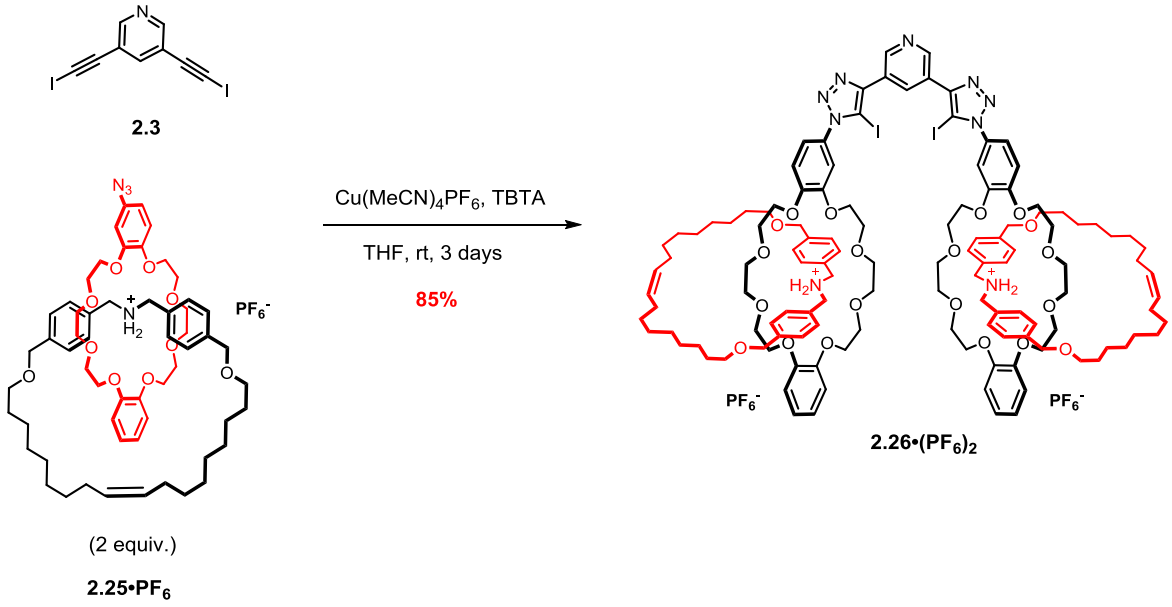

Scheme 2.11 Synthesis XB anion binding receptor **2.26·(PF$_6$)$_2$**.

A comparison of the ^{1}H-NMR spectra of **2.26·(PF$_6$)$_2$** and the azido[2]catenane **2.25·PF$_6$** is shown in Figure 2.31. The ^{1}H-NMR spectrum of **2.26·(PF$_6$)$_2$** shows broad proton signals from the pyridyl ring (H_a and H_b) with a significant downfield perturbation of aryl protons (H_c, H_d, and H_e) compared to those in the starting material. Additionally, the methylene proton resonances of **2.26·(PF$_6$)$_2$** are split into multiple signals whilst the alkyl proton resonances remain unchanged. Moreover, the HRMS of **2.26·(PF$_6$)$_2$** revealed a signal of m/z = 1185.02466, corresponding to $[M\text{-}2PF_6^-]^{2+}$, in agreement with the theoretical spectrum (Figure 2.32 a and b).

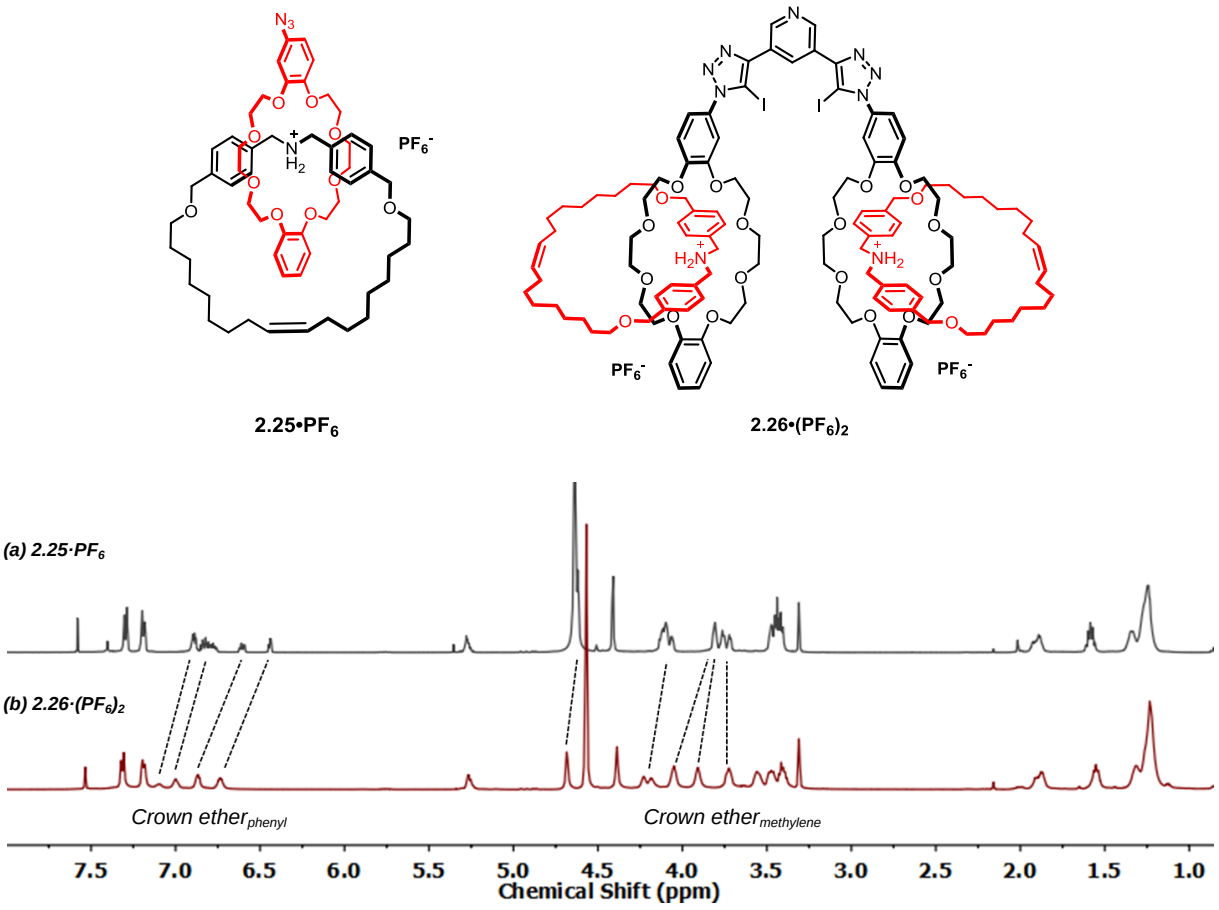

Figure 2.31 Truncated ^{1}H-NMR spectra of the azido-[2]catenane **2.25·PF$_6$** (a) and **2.26·(PF$_6$)$_2$** (b) (1:1 $CD_3OD/CDCl_3$ 298K, 500 MHz).

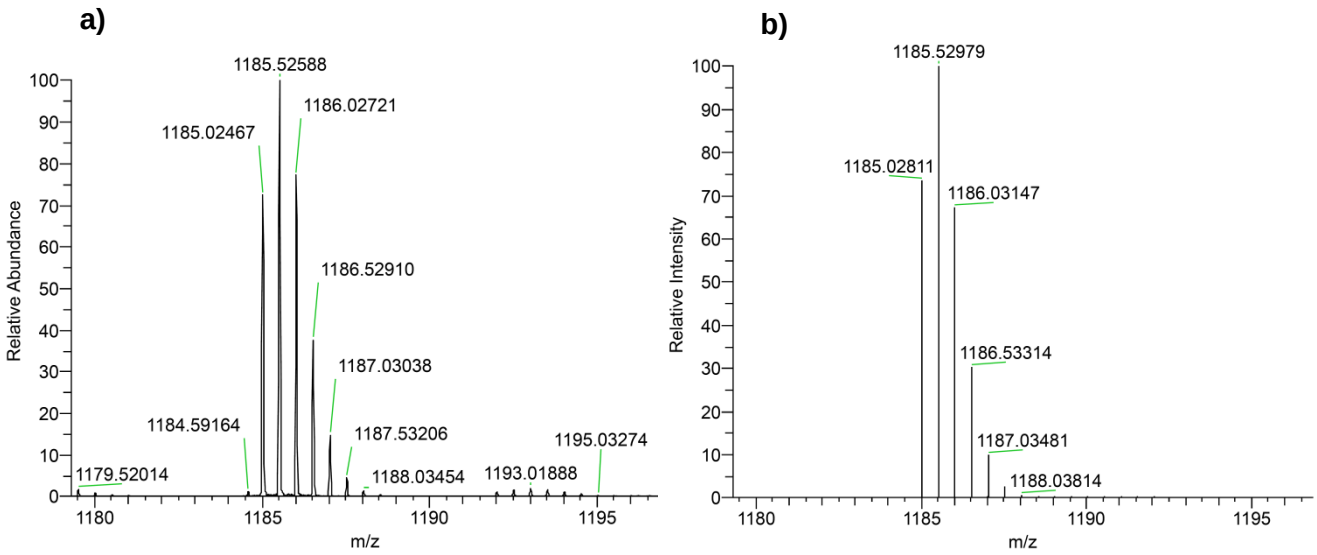

Figure 2.32 High resolution mass spectrum of **2.26·(PF$_6$)$_2$** (a) Measured spectrum and (b) theoretical spectrum.

2.5.7 ^{1}H-NMR anion binding studies

The anion recognition properties of **2.26·$(PF_6)_2$** were initially investigated by ^{1}H-NMR spectroscopic titration experiments with TBAI in the organic solvent mixture 10% d_6-DMSO/$CDCl_3$ using the protocol mentioned in the previous section. Monitoring the perturbation in the chemical shift of the internal pyridyl proton (H_a) as a function of iodide anion concentration, WinEQNMR2 analysis of the titration data determined a 1:1 host-guest stoichiometric association constant (K_a) of >10^4 M^{-1}. Hence, more competitive analogous ^{1}H-NMR anion titration experiments of **2.26·$(PF_6)_2$** were undertaken in the aqueous solvent mixture 5%D_2O/d_6-acetone. Using iodide as an example, anion addition resulted in a large downfield perturbation (Δδ = +0.2 ppm, 10 equiv. I^-) of the internal pyridyl proton signal (H_a) with a concomitant splitting of the resonances arising from the phenyl protons (H_c, H_d, H_e), linked to the iodotriazole mtifs. In contrast, the crown ethers protons (H_{phenyl}) and the methylene protons adjacent to the ammonium cation group (H_f) showed negligible perturbations, clearly indicating that the halide anion was binding in the XB cleft of the receptor and not interacting directly with the ammonium–crown ether catenane complex (Figure 2.33) .

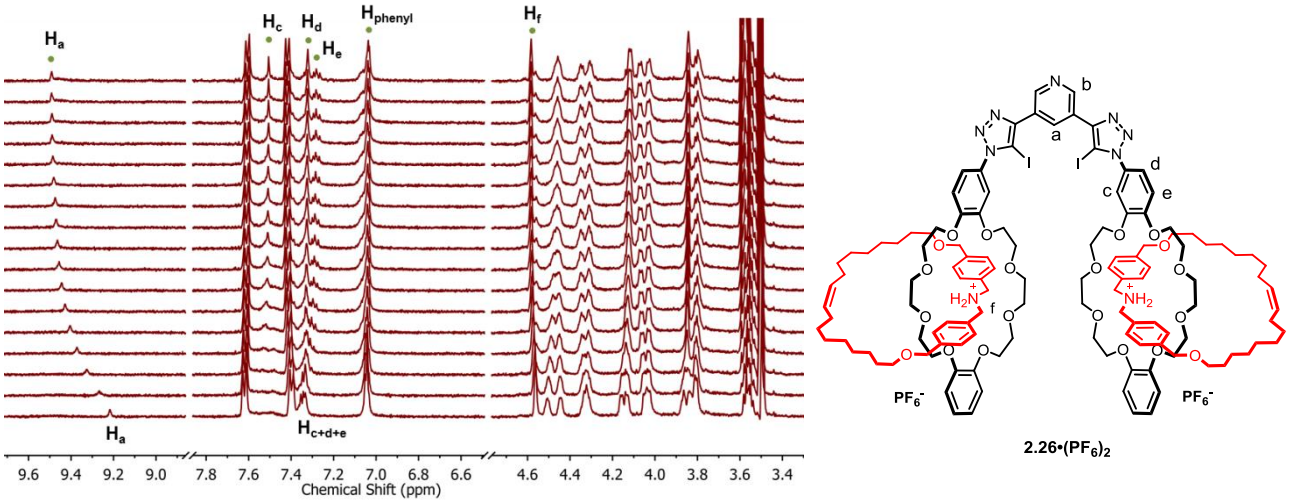

Figure 2.33 Truncated ^{1}H-NMR spectra of **2.26·$(PF_6)_2$** in 5%D_2O/d_6-acetone upon addition of TBAI (T=298K, 500 MHz).

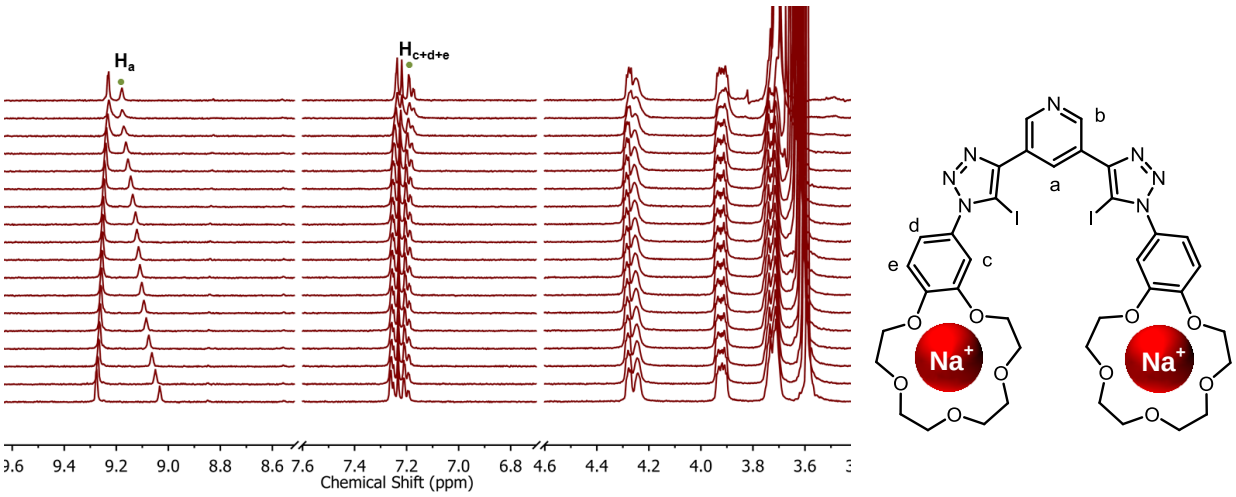

Figure 2.34 Truncated ^{1}H-NMR spectra of **2.1·XB·2NaPF$_6$** in 5%D_2O/d_6-acetone upon addition of TBAI (T=298K, 500 MHz), counter-anions in the structure are omitted for clarity.

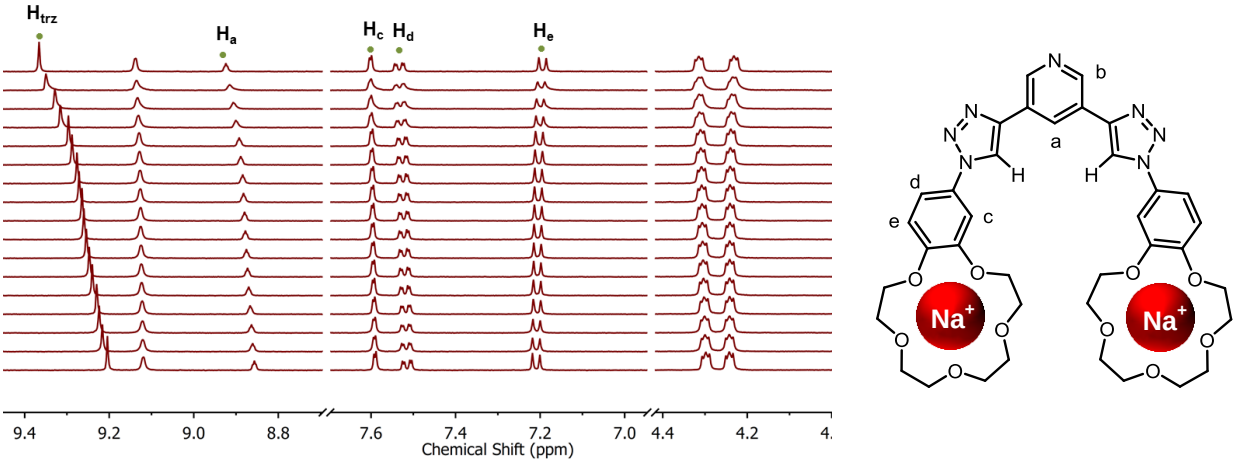

Figure 2.35 Truncated ^{1}H-NMR spectra of **2.1·HB·2NaPF$_6$** in 5%D_2O/d_6-acetone upon addition of TBAI (T=298K, 500 MHz), counter-anions in the structure are omitted for clarity.

Table 2.3 Anion association constants of **2.26·$(PF_6)_2$** and bis-sodium cations complexed heteroditopic XB(**2.1·XB**), ChB(**2.1·ChB**), and HB (**2.1·HB**) in 5%D_2O/d_6-acetone, 298 K).[a]

Anion	Association constants K_a (M^{-1})			
	2.26·$(PF_6)_2$	**2.1·XB**[b]	**2.1·HB**[b]	**2.1·ChB**[b]
Cl^-	44	precipitate	precipitate	precipitate
Br^-	5303	273	149	NB
I^-	$>10^4$, 860[c]	455	95	NB
ReO_4^-	NB[e]	NB	NB	NP
SO_4^{2-}	293[d]	precipitate	precipitate	NP[e]

[a] K_a values obtained by fitting the binding isotherm (monitored chemical shift perturbation of H_a) to a host-guest 1:1 stoichiometric binding model using WinEqNMR2; error(±) is less than 10%; anion added as tetrabutylammonium (TBA) salt.

[b] Titrations in the presence of 2 equivalents of sodium cations added as $NaPF_6$

[c] Titration in 20% D_2O/d_6-acetone

[d] Fitting with Bindfit v.05

[e] NB = no binding , NP = not performed

WinEQNMR2 and Bindfit v.05 analysis of the anion titration data monitoring the shifts of the internal pyridyl proton (H_a) determined 1:1 stoichiometric anion-host association constants shown in Table 2.3 together with quantitative data obtained from analogous titrations with **2.1·XB**, **2.1·ChB**, and **2.1·HB** in the presence of two equivalent of $NaPF_6$. In the presence of water, the XB receptor **2.26·$(PF_6)_2$** bound the heavier halides much more strongly than **2.1·XB**, displaying over a 20-fold and a 19-fold enhancement of iodide and bromide binding strength respectively. As expected, the presence of water diminished the halide binding affinities of **2.1·XB, 2.1·ChB,** and **2.1·HB** (Table 2.3) which can be attributed to the reduced stability of the sodium cation–benzo[15]crown-5 complex in the aqueous solvent mixture. The catenane XB receptor **2.26·$(PF_6)_2$** showed an impressive I^- association constant ($K_a > 10^4$ M^{-1}) followed by Br^-, SO_4^{2-}, and Cl^-, while no evidence of ReO_4^- binding was observed. In a 20% D_2O in d_6-acetone, the maximum amount of water to solubilise the host for ^{1}H-NMR spectroscopic titration, **2.26·$(PF_6)_2$** was still able to bind iodide strongly (K_a = 860 M^{-1}). This clearly demonstrates that the combination of mechanically interlocked ammonium cation containing substituents appended to a XB anion binding scaffold is as an effective methodology to achieve anion recognition in highly competitive solvent mixtures.

2.6 Conclusion

In conclusion, a series of novel heteroditopic receptors were synthesised, each containing crown ether cation binding groups covalently attached to anion binding motifs, providing HB, XB, and unprecedented ChB ion-pair receptors. These systems enabled sigma-hole interaction mediated ion-pair recognition studies to be undertaken. In organic solvent media (10% d_6-DMSO/$CDCl_3$), all hosts exhibited cooperative ion-pair binding properties in which the sodium complexed receptors could switch on halide binding in comparison to their in non-metal cation complexed forms. In the presence of sodium ions **2.1·XB** exhibited the strongest halide binding affinity followed by **2.1·ChB** and **2.1·HB**. Interestingly the sigma hole hosts displayed an unexpectedly high degree of enhancement (or cooperativity factor) in halide binding, especially in the case of the ChB analogue. These observations highlight the unique properties of sigma-hole mediated ion-pair recognition, allowing a new approach to control cooperativity *via* co-bound metal cation induced through bond polarization of the XB and ChB donor atoms

The integration of a kinetically inert secondary ammonium–crown ether[2] catenane, into the 3,5-bisiodotriazole pyridine scaffold resulted in the novel host **2.26·$(PF_6)_2$** displaying strong and selective halide binding affinity in aqueous media that was superior to the sodium cations bound XB, ChB, and HB receptors.

2.7 Future directions

Taking inspiration from these results, it would be desirable in the future to utilise the ammonium cation induced polarization of XB donors in the constructions of higher order exotic hosts for XB anion recognition in aqueous media (Figure 2.36 b).

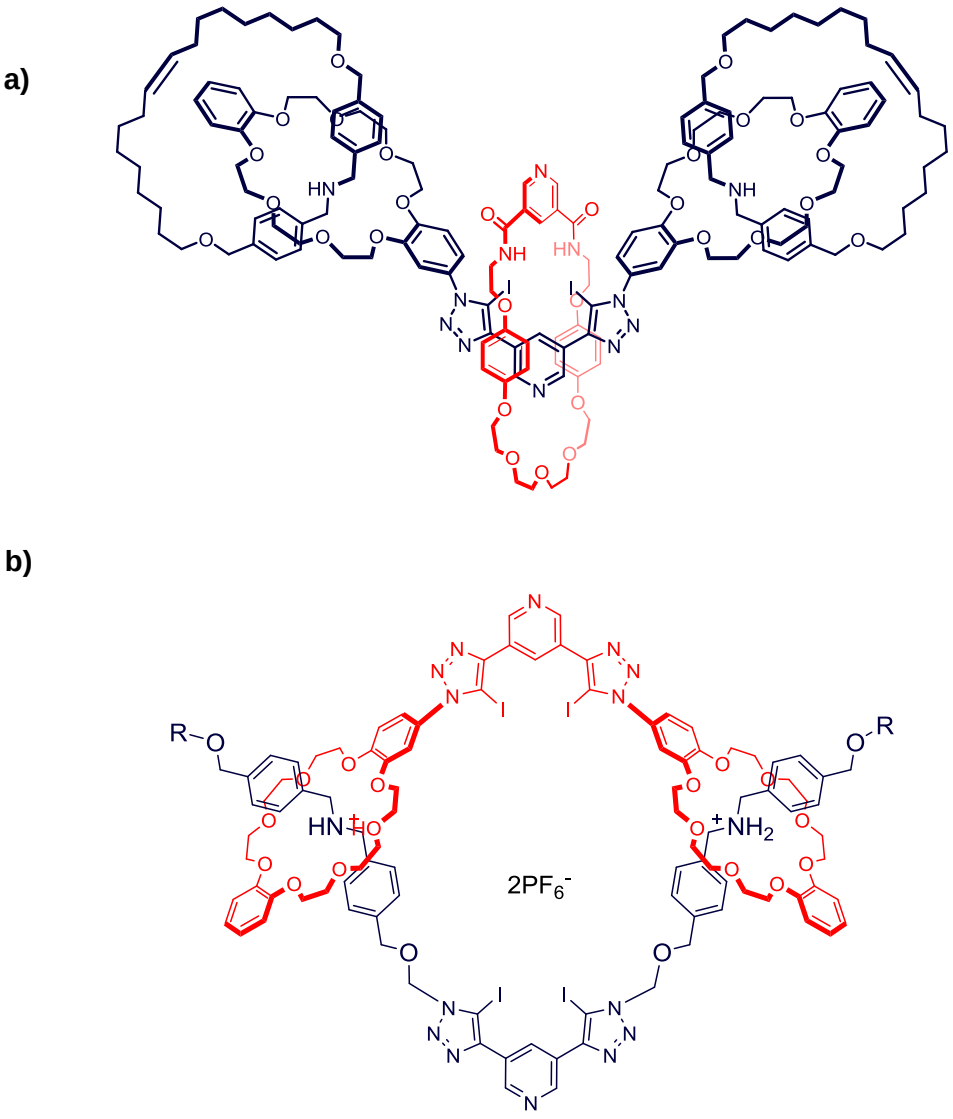

Figure 2.36 Future target higher order XB interlocked host structures.

Chapter 3

Halogen Bonding Interlocked Host Molecules for Anion Recognition and Sensing in Aqueous Media

Chapter 3: Halogen Bonding Interlocked Host Molecules for Anion Recognition and Sensing in Aqueous Media

Introduction

Mechanically interlocked molecules (MIMs) such as catenanes and rotaxanes have shown great promise in a range of potential applications including drug delivery, catalysis and functional materials.[130] Additionally, their mechanically-interlocked structure results in the formation of elaborate three-dimensional preorganised binding cavities capable of guest encapsulation and recognition, whilst their dynamic nature allows for unique molecular machine-like and switchable sensory behaviour.[229, 230] There is an ever increasing interest in the nanotechnological applications of MIMs, and it is therefore of paramount importance that new practical methods towards their synthesis continues to develop. Complementary to the pioneering metal cation templated,[142, 231, 232] π–π donor–acceptor aromatic stacking[167, 187, 233, 234] and directed-hydrogen bonding[154, 155, 159-163, 235-237] synthetic methodologies for MIMs detailed in Chapter 1, anion templated synthesis has also been developed with applications in anion recognition and sensing.[174, 238, 239] However, the search for efficient synthetic methods to achieve interlocked structure formation, in high yield is still continuing.

3.1 Near quantitative synthesis of mechanically interlocked molecules

Quantitative preparations of MIMs have been achieved by various template directed synthetic methodologies including transition metal, hydrogen bonding, and aromatic donor–acceptor interactions. Utilizing the seminal Sauvage's Cu(I) template strategy, the application of ring closing metathesis was shown to be a highly efficient method for the preparation of a [2]catenane in 92% isolated yield (Figure 3.1).[240, 241]

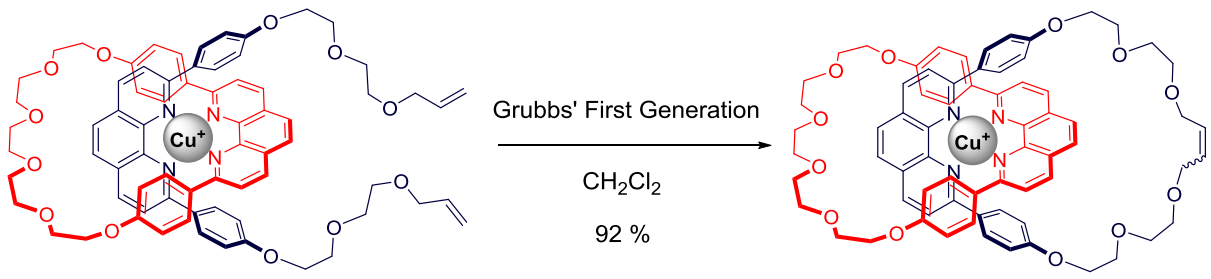

Figure 3.1 Cu(I) templated synthesis of Sauvage's [2]catenane.

The 'active' metal-template approach has been pioneered by Leigh utilising the CuAAC reaction (Section 1.5.2.1),[151] and has been further developed by Goldup and co-workers for the efficient preparation of oligo[n]rotaxanes[27] and catenanes in excellent yield

(up to 94% yield) by using a constrained bipyridine macrocyclic ligand (Figure 3.2).[242, 243] The favourable endo-coordination of the Cu(I) active species facilitated the formation of a tetrahedral intermediate allowing for CuAAC reaction inside the macrocyclic cavity.

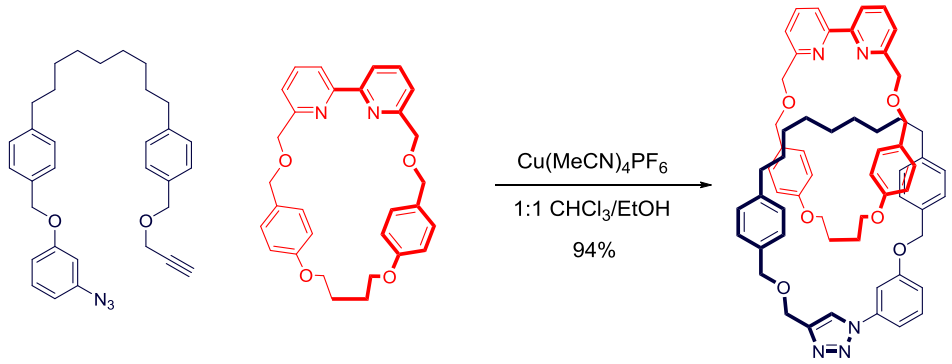

Figure 3.2 Active metal template of [2]catenane.

Organic cation templates have been successfully exploited for the preparation of MIMs in high yield *via* pseudorotaxane formation between a variety of cationic threads and crown ether macrocycles. Stoddart and co-workers demonstrated thermodynamically controlled complexation between an electron deficient tetracationic 4,4'-bipyridinium macrocycle with an electron rich dinaphtho[34]crown-10 macrocycle for the synthesis of donor–acceptor [2]catenanes. Iodide promoted ring opening of the π-acceptor macrocycle in the presence of a π-donor macrocycle afforded a hetero[2]catenane in 93% isolated yield (Figure 3.3).[244]

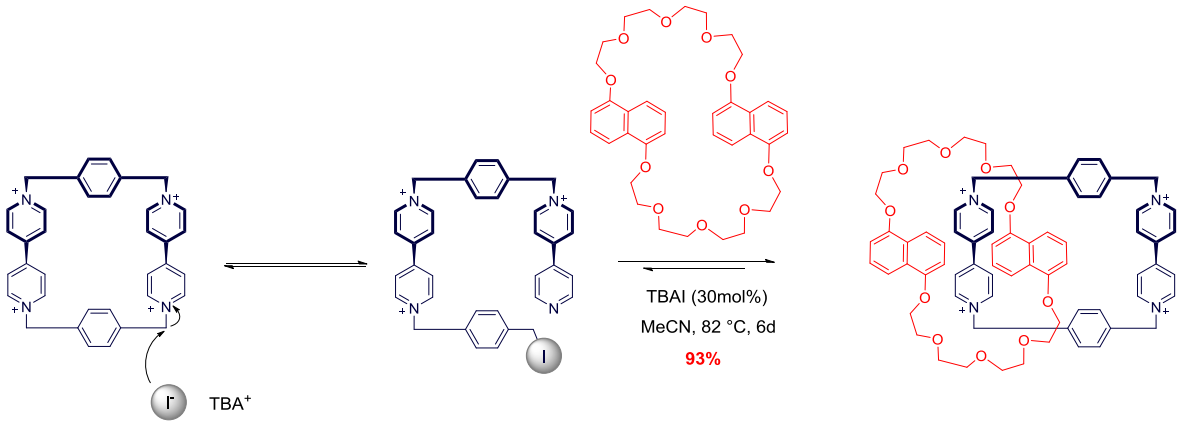

Figure 3.3 Stoddart π-donor and π-acceptor [2]catenane.

The versatility of the bis-4,4'-bipyridinium motif as an effective thread in the synthesis of MIMs was also demonstrated by Huang and co-workers. Favourable charge transfer interactions between an electron rich benzene capped cryptand and an electron deficient bis-

4,4'-bipyridinium axle precursor promoted near quantitative formation of a [2]rotaxane *via* a stoppering reaction (Figure 3.4).[245]

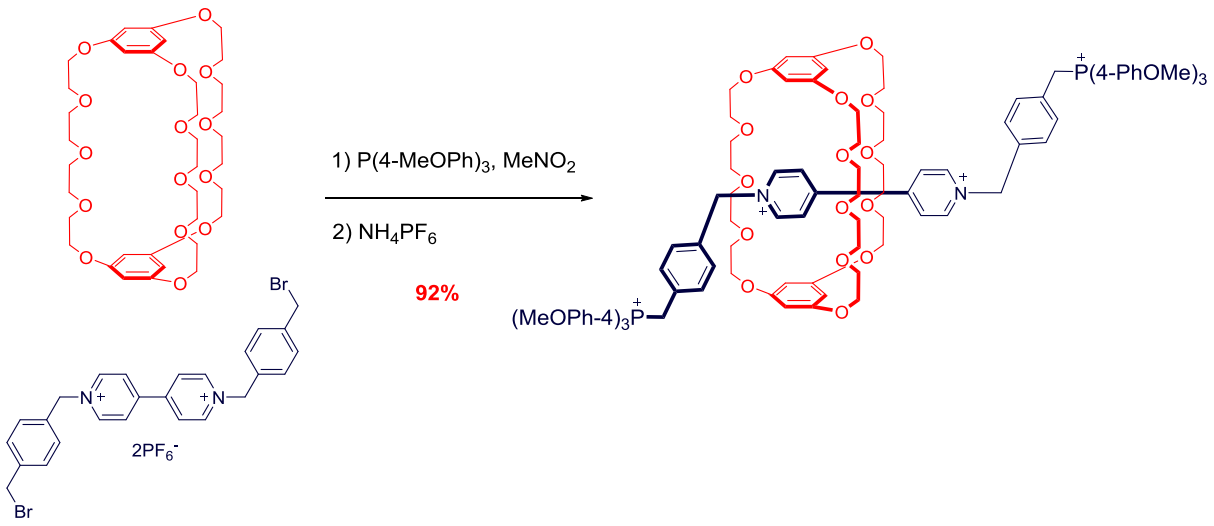

Figure 3.4 Huang's aromatic donor–acceptor [2]rotaxane.

Loeb and co-workers have developed bis-(benzimidazolium) cationic motifs capable of complexation with a wide range of crown ether macrocycles. Maximizing the non-covalent interactions between the pseudorotaxane components by controlling ring sizes and substituents on the crown ether rings resulted in near quantitative formation of a [2]rotaxane with a dinaphtho[24]crown-8 macrocycle (Figure 3.5).[157]

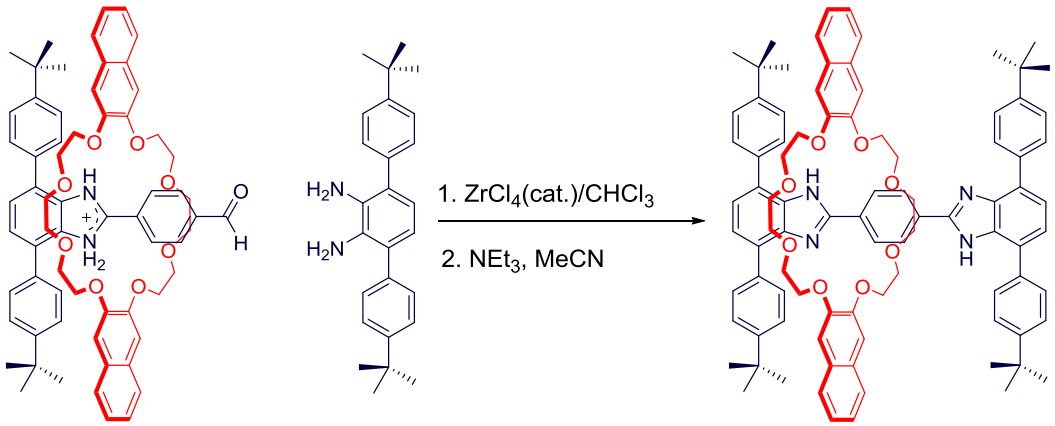

Figure 3.5 Loeb's benzimidazolium templated [2]rotaxane.

The importance of template structural complementarity for the synthesis of MIMs was highlighted by Leigh and co-workers using neutral hydrogen bond templates directed assembly of rotaxanes. The structural rigidity and preorganization of the axle component fumaramide enhanced cooperative HB interactions which facilitated [2]rotaxane formation in a "world record" at the time, yield of 97% (Figure 3.6).[246]

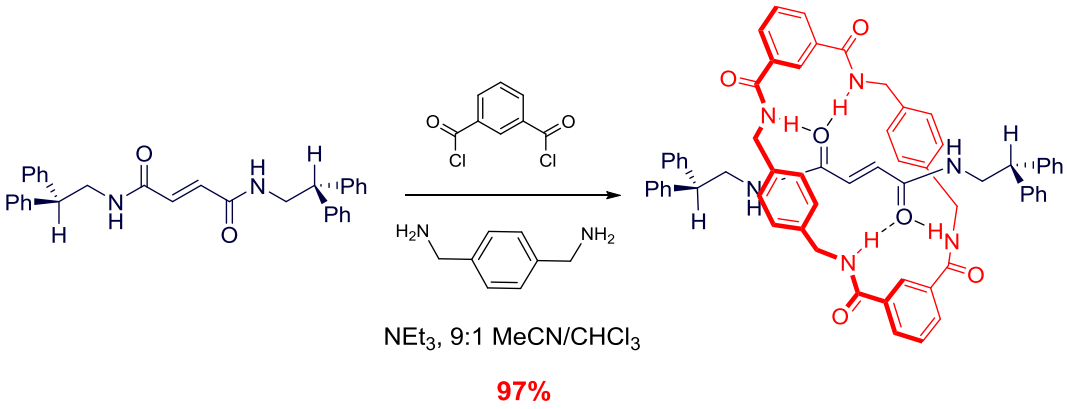

Figure 3.6 Leigh's fumaramide preorganised [2]rotaxane

3.2 Halogen bonding mediated assembly of MIMs

Halogen bonding (XB), the highly directional, attractive intermolecular non-covalent interaction between an electrophilic halogen atom and a neutral or charged Lewis base, has been demonstrated to be a powerful complement to ubiquitous hydrogen bonding (HB) interactions for anion recognition.[15, 247] Importantly, incorporation of XB donor motifs into host structural frameworks commonly enhanced anion affinities in comparison to HB host analogues. (Ref) Furthermore, XB–anion (and charge-assisted XB) interactions have been shown to successfully template MIM assemblies.[81]

In 2010, the first XB–anion templated MIM synthesis was reported by Beer and co-workers; a bromide–templated pseudorotaxane assembly between iodotriazolium XB axle and an isophthalamide macrocycle precursor formed the corresponding [2]rotaxane *via* a ring closing metathesis 'clipping' macrocyclisation reaction in a modest isolated yield of 15% (Figure 3.7). [248]

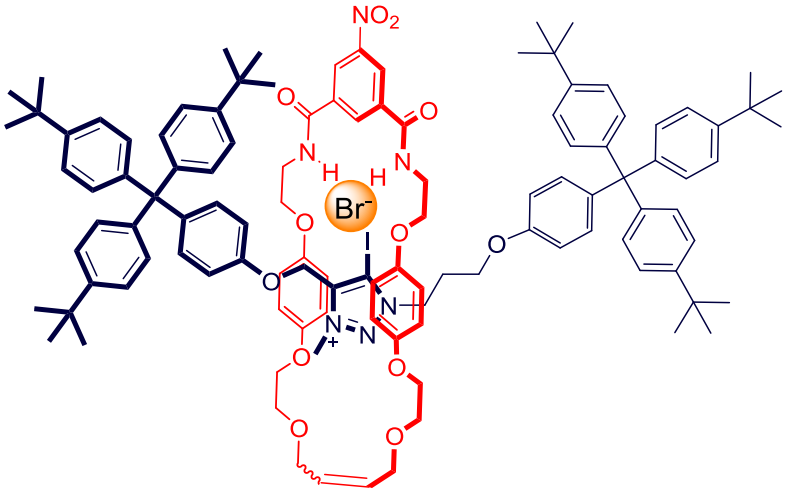

Figure 3.7 Beer's rotaxane containing iodotriazolium XB donor motif.

The bidentate 3,5-bis-(iodotriazole)pyridinium XB donor motif was first integrated into an interlocked host using a chloride anion templated ring closing metathesis 'clipping' reaction to produce the XB [2]catenane in 41% yield (Figure 3.8). The catenane host exhibited remarkably enhanced halide binding affinities in comparison to the analogous HB [2]catenane with a preference for iodide and bromide in a competitive aqueous-organic 45: 45: 10 $CDCl_3/CD_3OD/D_2O$ solvent mixture.[210]

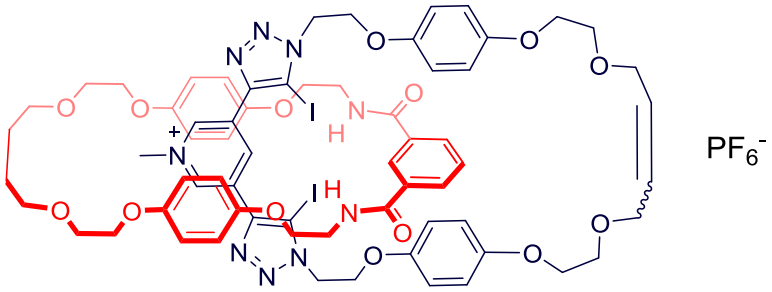

Figure 3.8 [2]catenane incorporating a bidentate bis-(iodotriazole) pyridinium motif.

3.3 Halogen bonding anion recognition in highly competitive aqueous media

Halogen bonding anion receptors which operate in water are extremely rare. In 2014, Beer and co-workers reported a seminal work on the exploitation of XB interactions for anion recognition in water. A series of permethylated β-cyclodextrin functionalised XB acyclic and [2]rotaxane host structures were demonstrated to bind halides in pure water with pronounced selectivity towards larger halides and superior affinity in comparison to their HB analogues (Figure 3.9).[249] This investigation also demonstrated that remarkable anion binding in water could be achieved by low charge acyclic XB receptors.

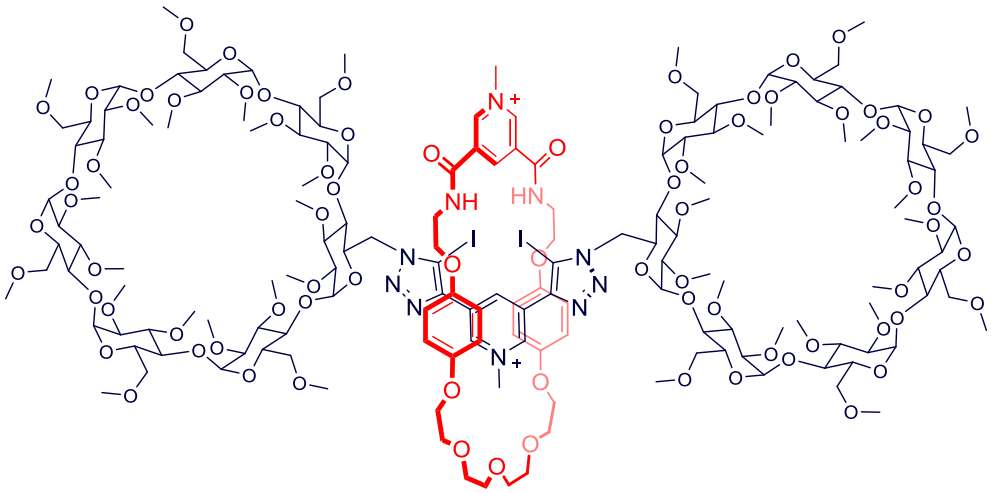

Figure 3.9 Water soluble XB [2]rotaxane anion host system.

3.4 Chapter aims

The major research aim in this chapter focuses on the preparation of novel XB acyclic and interlocked host systems for the selective recognition of anionic guests in highly competitive aqueous media. In particular, this chapter will explore three specific avenues related to this theme, as outlined below

Part I: With the objective of increasing both the efficacy of the anion template for high yielding XB MIM synthesis and the potent strength of XB–anion interactions for recognition, this section describes a correlation between the chloride anion association strength of various XB template motifs and isolated yield of rotaxane formation. By integrating electron withdrawing substituents into a permethylated β-cyclodextrin stoppered bis-iodotriazole pyridinium axle component, a chloride anion-template amide condensation clipping reaction is shown to produce a series of target XB [2]rotaxanes. Moreover, the halide binding studies of XB acyclic and [2]rotaxane hosts are elucidated by ^{1}H-NMR titration experiments in competitive 50% water containing aqueous media.

Part II: Novel water soluble XB anion host containing 3,5-bis-(iodotriazole)pyridine, pyridine-N-oxide, and pyridinium motifs are prepared, whose thermodynamic anion binding properties are elucidated via isothermal titration calorimetric (ITC) analysis. Moreover, a novel XB water soluble [2]rotaxane host molecule is also constructed.

Part III: The incorporation of the photo and redox-active tris(bipyridyl)osmium(II) motif into a water soluble XB [2]rotaxane host structural framework enabled luminescence and electrochemical anion sensing in aqueous media to be investigated

Part I: Near Quantitative Chloride Anion Template Synthesis of an XB[2]Rotaxane Capable of Selective Anion Recognition in Aqueous Media

3.5 Halogen bonding acyclic receptor synthesis and halide binding properties

In order to investigate whether XB halide anion binding potency could be tuned *via* the covalent attachment of suitable electron withdrawing substituents, the synthesis of a series of XB acyclic receptors consisting of a 3,5-bis-(iodotriazole)pyridinium motif functionalized with methylene linked benzylic and ester groups, and aryl linked benzene and perfluorinated benzene ester groups was initially undertaken (Figure 3.10). The monocationic pyridinium XB receptors were prepared *via* copper(I)-catalysed azide-alkyne cycloaddition (CuAAC) reactions between appropriate azides and 3,5-diiodoethynylpyridine. Subsequent methylation with iodomethane and anion exchange afforded receptors **3.1·PF$_6$**-**3.4·PF$_6$**

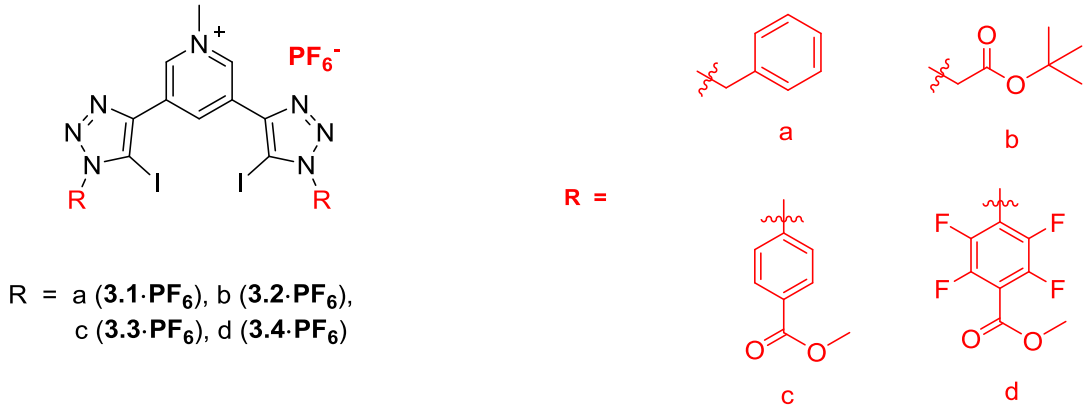

R = a (**3.1·PF$_6$**), b (**3.2·PF$_6$**), c (**3.3·PF$_6$**), d (**3.4·PF$_6$**)

Figure 3.10 A series of 3,5-bis-(iodotriazole)pyridinium XB acyclic receptors.

3.5.1 Synthesis of azide precursors

A series of selected azides were prepared following literature procedures (Scheme 3.1).[250-252] The nucleophilic substitution of parent alkyl bromide with NaN_3 in DMSO gave **3.5**. In the case of aryl azide, a diazotization reaction of 4-aminobenzoic acid and subsequent aromatic substitution with NaN_3 provided **3.6** in 90% yield. Subsequent acid catalyzed esterification gave **3.7** in 69% yield. The nucleophilic aromatic substitution of perfluorobenzene ester with NaN_3 in acetone/water mixture afforded **3.8** in 80% yield. (Scheme 3.1).

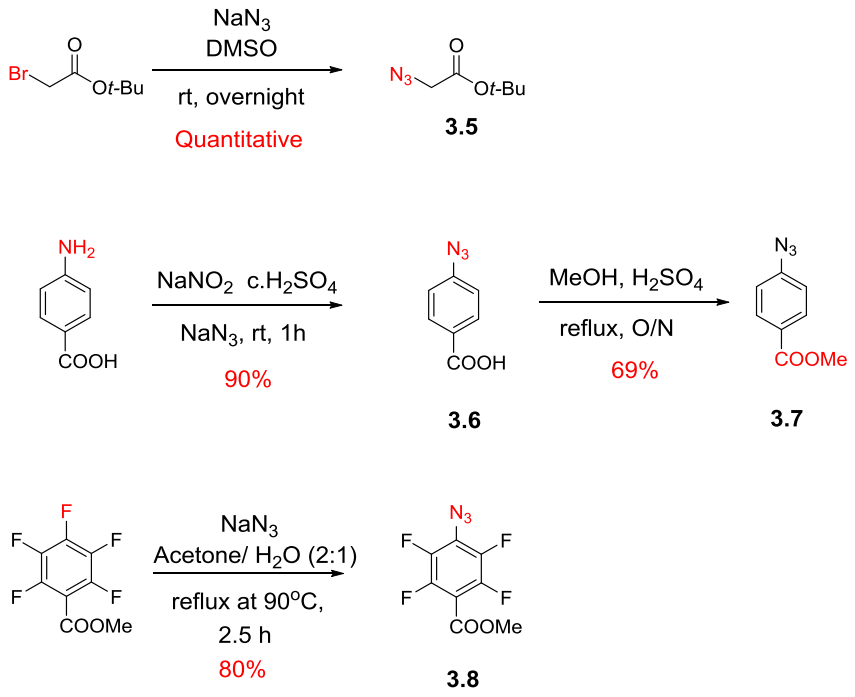

Scheme 3.1 Synthesis of alkyl and aromatic azide precursors.

3.5.2 Synthesis of monocationic XB anion receptors

Employing the CuAAC methodology, 3,5-diiodoethynylpyridine **2.3** and two equivalents of the appropriate azide precursors were reacted in the presence of a catalytic amount of CuI and TBTA in THF at room temperature to afford the 3,5-bis-iodotriazole pyridine precursors **3.9**-**3.11**, in yields ranging from 51% to 93% (Scheme 3.2).

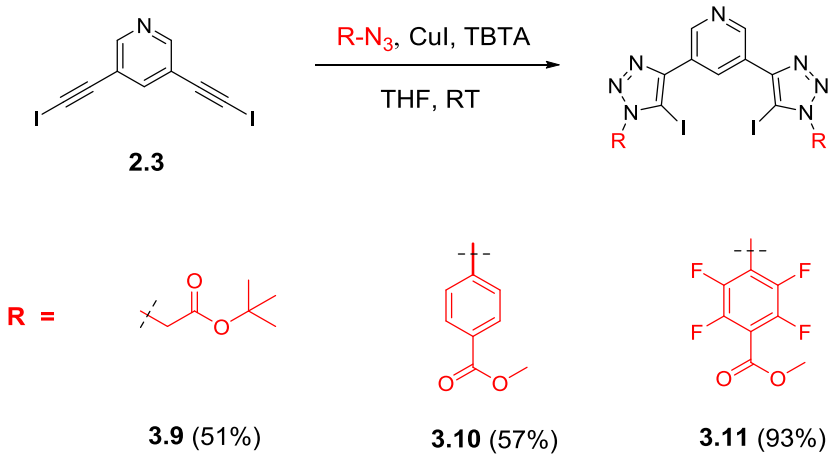

Scheme 3.2 Synthesis of XB anion receptors *via* CuAAC reaction.

The monocationic XB receptors were prepared by a methylation reaction using excess iodomethane in chloroform at 60 °C, resulting in precipitation of the pyridinium products in quantitative yield**.** Despite poor solubility of the iodide salts**,** anion exchange to hexafluorophosphate improved their solubility in organic solvent media (Scheme 3.3). The final products were characterized by ^{1}H, ^{13}C, and ^{19}F NMR spectroscopy, and high resolution electrospray mass spectrometry (HRMS).

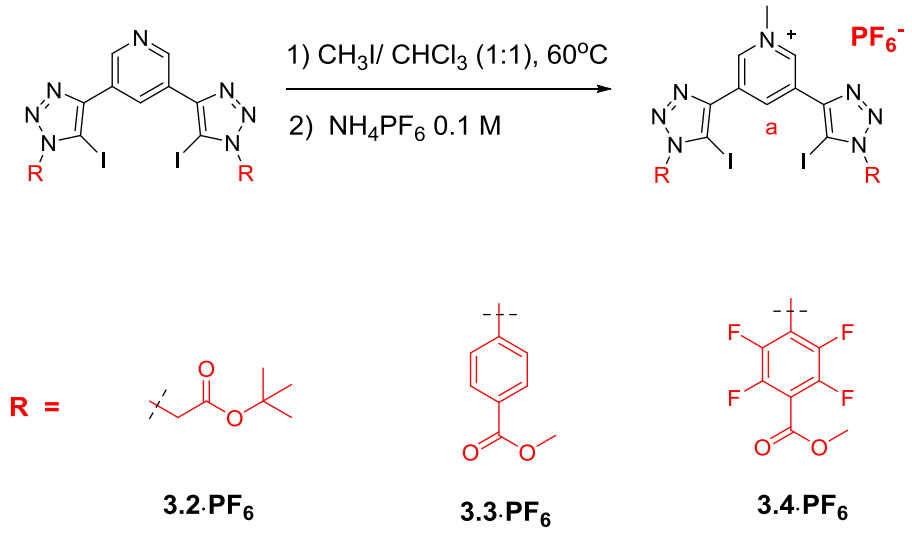

Scheme 3.3 Synthesis of monocationic 3,5-bisiodotriazole pyridinium receptors.

3.5.3 Halide Binding Studies

The halide anion binding properties of the XB acyclic receptors were studied by ^{1}H-NMR titration experiments, in which aliquots of tetrabutylammonium (TBA) halide salts were added to d_6-DMSO solutions of the receptors.Typically, with all four receptors the addition of halides resulted in a significant downfield perturbation of the internal pyridinium proton ***a*** (labeled in Scheme 3.3) indicative of halide anion binding in the vicinity of the XB bis-iodotriazole binding cleft. Amongst the halides, Cl^- binding caused the largest shifts with all receptors (Figure 3.11). Monitoring the internal pyridinium proton ***a***, WinEQNMR2[253] analysis of the titration data determined 1:1 stoichiometric host-guest anion association constants, shown in Table 3.1

Table 3.1 Anion association constant (K_a/ M^{-1}) for 3,5-bis-(iodotriazole)pyridinium receptors in d_6-DMSO.

Anion	Anion association constants (K_a, M^{-1}) in d_6-DMSO			
	3.1·PF_6[254]	**3.2·PF_6**	**3.3·PF_6**	**3.4·PF_6**
Cl^-	387	403	429	1395
Br^-	238	206	277	491
I^-	146	62	98	190

[a] Anions added as TBA salts, errors (±) less than 10%, 1:1 association constants calculated using WinEQNMR2 software,[253] monitoring the perturbation of the internal pyridinium proton H_a (500MHz, 298K)

In the polar aprotic solvent, DMSO, the anion binding affinities of each receptor correlates with halide anion charge density, with chloride forming the strongest complexes. This is clearly seen in the case of receptor **3.4·PF_6** which binds chloride much more strongly than bromide and iodide. It is noteworthy that the largest association constant magnitudes were observed with the perfluorinated arene functionalized receptor **3.4·PF_6** with all halides. The receptor displays chloride association affinity values approximately 3.5 times larger in magnitude than the other XB receptor analogues (Table 3.1). This result highlights the effect of the strongly electron withdrawing perfluoroaryl spacer motifs on anion binding, postulated to be due to polarisation of the iodine atoms of the bis-iodotriazole XB donor groups facilitating stronger XB-anion interactions. On the other hand, the benzyl (**3.1·PF_6**), methylene (**3.2·PF_6**), and aryl (**3.3·PF_6**) spacers display similar halide association constants reflecting the similarity in their electron-withdrawing nature.

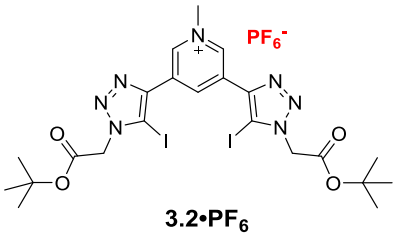

3.2•PF$_6$

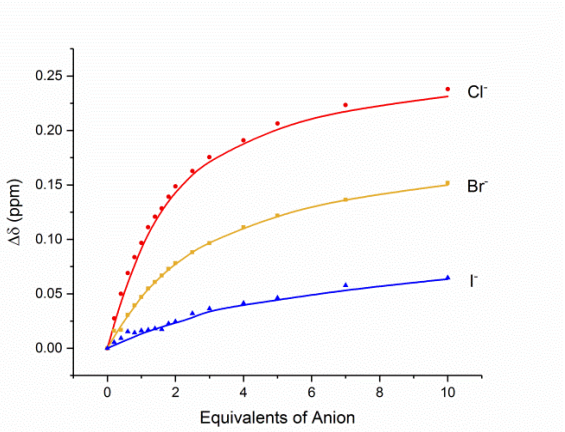

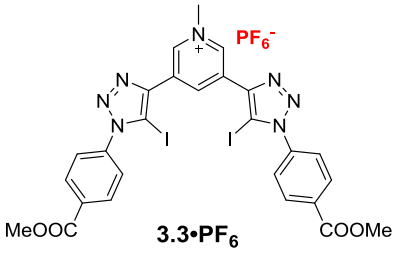

3.3•PF$_6$

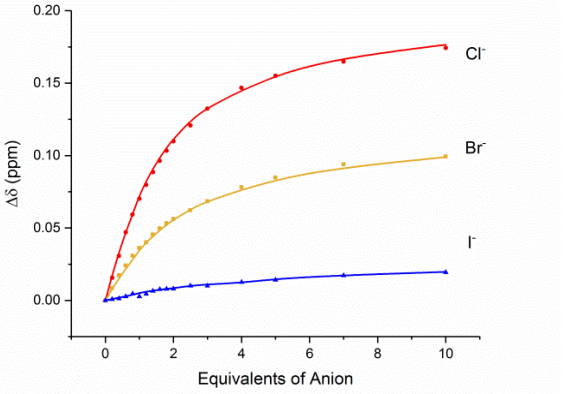

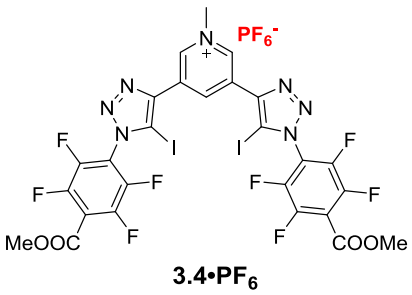

3.4•PF$_6$

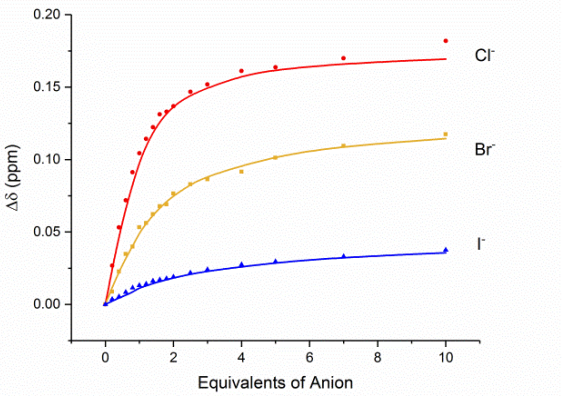

Figure 3.11 Observed data (solid points) and fitted isotherms (lines) for addition of anions as their TBA salts to **3.2·PF$_6$**, **3.3·PF$_6$**, **and 3.4·PF$_6$** (500 MHz, d_6-DMSO, 298 K).

3.5.4 X-Ray Crystallographic Structures

X-ray crystal structural data were collected and refined by Dr. Antonio Martinez, a postdoctoral research fellow of Weller group, University of Oxford. Single crystals suitable for X-ray diffraction studies were obtained for the 3,5-bis-(iodotriazole)pyridinium receptor **3.4**$^{+}$ with chloride and iodide anions as 1:1 complexes, **3.4·Cl** and **3.4·I**, respectively. **3.4·Cl** crystallises in the triclinic space group *P*-1 with two molecules of acetone, whereas **3.4·I** is in the orthorhombic space group *Pbcn*. The receptor **3.4**$^{+}$ adopts a close triazole–I conformation in both examples encapsulating the corresponding anion guest through halogen bond-halide interactions (Figure 3.12). Examining the anion-binding cavity of the 3,5-bis-(iodotriazole)pyridinium receptor, strong halogen bonds are observed indicated by triazole–I···X^{-} interatomic distances significantly shorter than the sum of the van der Waals radii (Table 3.2).[255]

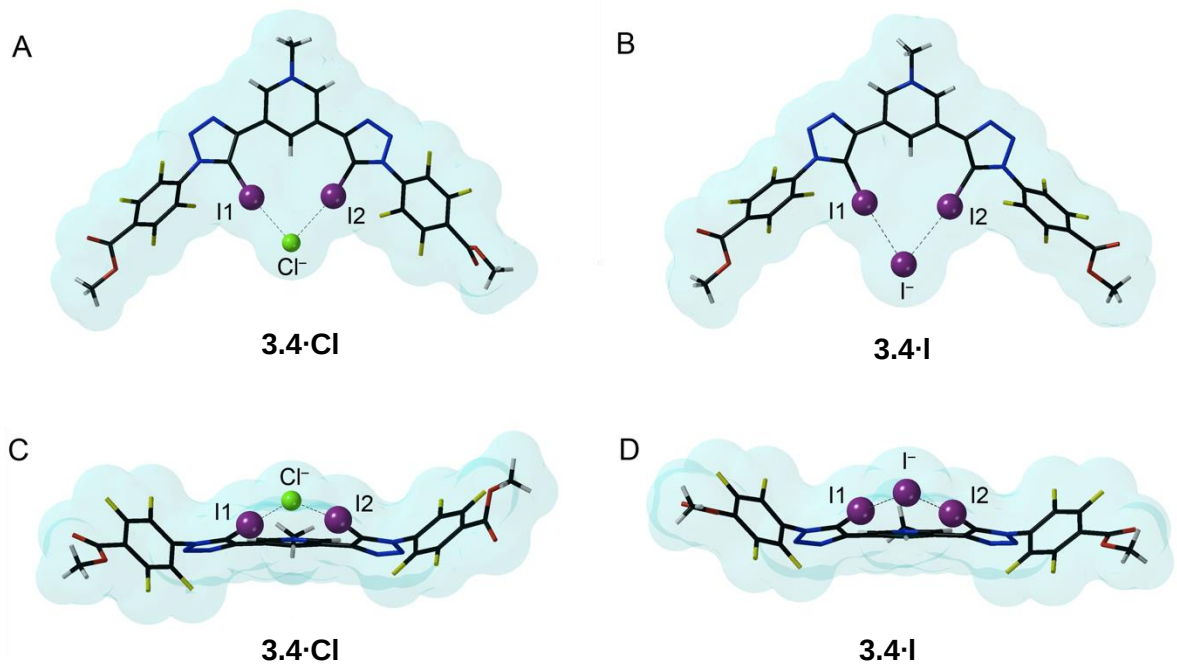

Figure 3.12 Molecular structures of **3.4·Cl** and **3.4·I**: A, B) front view; B, C) side view. In **3.4·Cl**, two molecules of acetone of crystallization have been omitted for clarity. Triazole−I···Cl^{-} (3.1419(6), 3.0079(6) Å) and triazole–I···I^{-} (3.4010(3), 3.3522(3) Å) halogen bonds are indicated as dashed lines. The halide receptor framework is pictured as capped sticks with translucent space-filling van der Waals surfaces for a probe of 1 Å radius. Hydrogen atoms omitted for clarity.

Table 3.2. XB bond lengths and percentage shortening of the sum of the van der Waals radii (%VdW).[255]

guest anion	interatomic distances (I···X⁻/Å)	%vdW
Cl⁻	3.1419(6), 3.0079(6)	83, 79%
I⁻	3.4010(3), 3.3522(3)	81, 80%

[a] Calculated errors given in parenthesis.

The I···X⁻ halogen bonds in **3.4·Cl** are 21 and 17% shorter than the sum of standard van der Waals radii of the interacting atoms, whereas they are about 20% smaller in **3.4·I**. For **3.4·Cl**, these interactions are shorter than those found in a previously reported iodotriazole−I···Cl⁻ octyl derivative (3.121(2) and 3.195(2) Å, corresponding to 84 and 86% vdW).[254] In addition, the non-planar arrangement in the bis(iodotriazole)−pyridinium−halide motif in **3.4·Cl** and **3.4·I** contrasts with the planarity found in the aforementioned octyl derivative. The crystal packing of **3.4·Cl** reveals a complementary charge-assisted electrostatic network between hydrogen donor and X⁻ acceptor sites which influences the overall orientation of the molecules in the lattice. These are weak intermolecular Me···Cl⁻ interactions, including three independent receptor molecules *via* OMe···Cl⁻ contacts (range 3.01-3.45 Å), two through pyridinium-Me···Cl⁻ (2.90 and 3.45 Å) and one acetone, solvent of crystallisation, Me···Cl⁻ (2.83 Å). On the other hand, the larger I⁻ in **3.4·I** interacts with three neighbouring molecules through weak OMe···I⁻ electrostatic contacts (range 3.43-3.62 Å), one through long pyridinium-Me···I⁻ interaction (3.62 Å) and an additional receptor molecule *via* anion–π interactions with the pyridinium ring (pyridinium-centroid···I⁻, 3.56 Å).

3.6 Synthesis of XB [2]rotaxane host structures

The anion template directed methodology for synthesising a range of interlocked structures has been established;(Ref) however investigating the relationship between the effectiveness of interlocked structure formation and the strength of anion binding template motifs has yet to be reported. In this section, the novel XB donor bis-(iodotriazole)pyridinium structural motifs of the three acyclic receptors (Section 3.53) are integrated into a bis-permethylated β-cyclodextrin stoppered axle component for subsequent rotaxane formation using a chloride anion-templated amide condensation clipping rotaxanation reaction to afford a series of target [2]rotaxane host structures **3.12·PF$_6$** – **3.14·PF$_6$** (Figure 3.13).

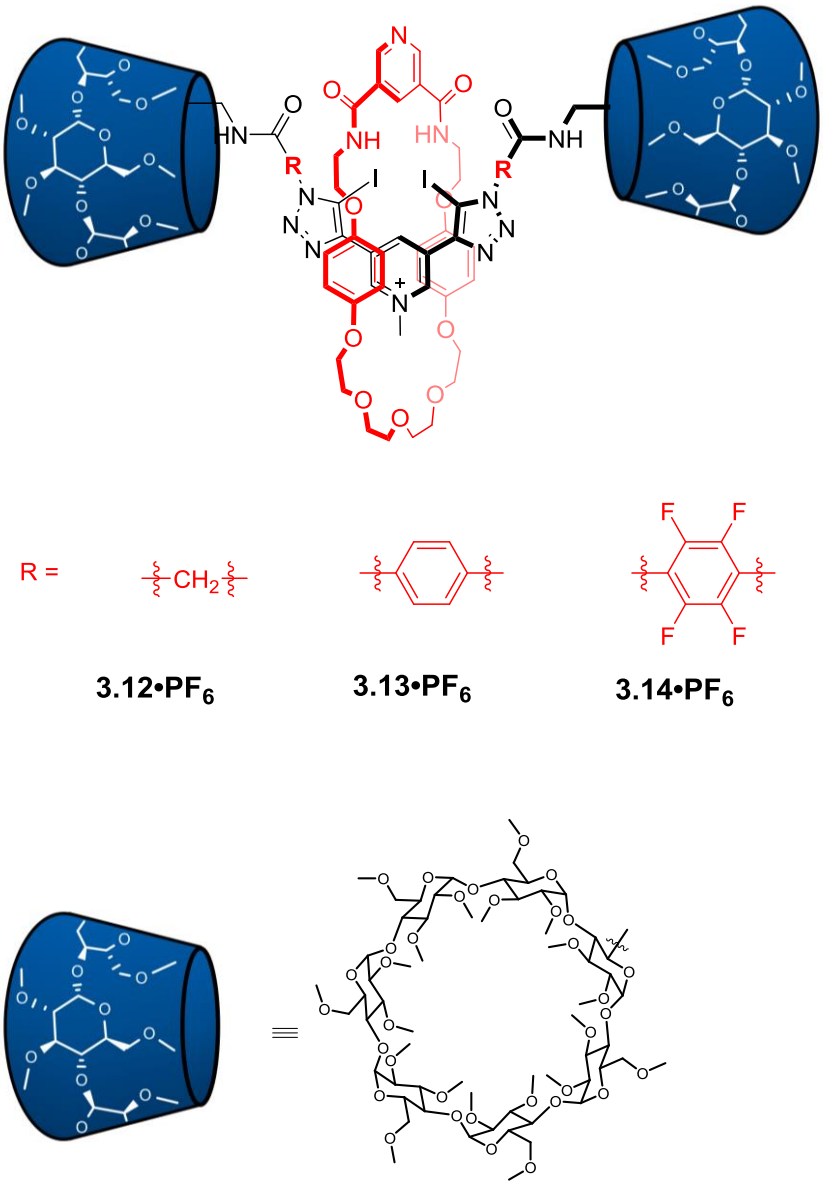

Figure 3.13 Target monocationic XB [2]rotaxane host molecules.

3.6.1 Synthesis of XB axle components

(a) Synthesis of mono-functionalised permethylated β-cyclodextrin amine stopper

The initial target amine mono-functionalised permethylated β-cyclodextrin **3.19** was synthesised using modified literature synthetic procedures (Scheme 3.4).[252, 256, 257] β-Cyclodextrin **3.15** was suspended in water in the presence of p-toluenesulfonyl chloride for 2 hours and subsequent addition of an aqueous NaOH solution afforded the monotosylate **3.16** in 23% yield after recrystallization in hot methanol/water. Methylation reaction of **3.16** using an excess of NaH and iodomethane, followed by chromatographic purification gave a white compound **3.17** in 70% yield. Interestingly, a monoiodo-substituted permethylated β-cyclodextrin was occasionally observed as a side product which can also be used without further purification in the next step. Nucleophilic substitution reaction of **3.17** with NaN_3 in DMF at 100°C afforded the monoazide **3.18** quantitatively. Finally, reduction of the monoazide **3.18** with hydrazine monohydrate in the presence of Pd/C in MeOH at 60°C gave amine **3.19** in quantitative yield without further purification.

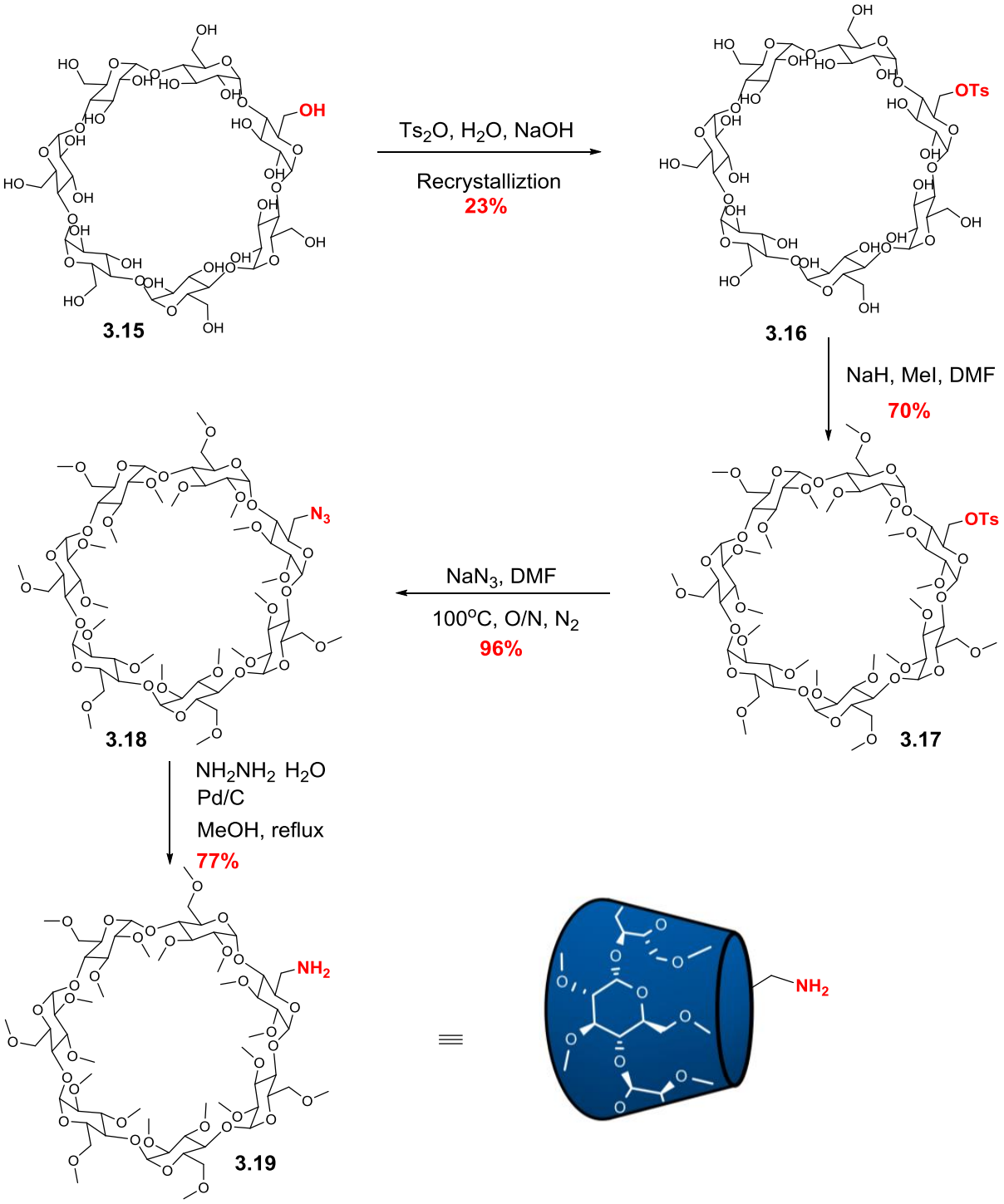

Scheme 3.4 Synthesis of permethylated β-cyclodextrin amine **3.19**.

(b) Synthesis of azide functionalised permethylated β-cyclodextrin stopper derivatives

A condensation reaction between bromoacetyl bromide and cyclodextrin amine **3.19** in anhydrous DCM was attempted. However, this procedure was found to be low yielding due to hydrolysis of the cyclodextrin moiety as evidenced by an increased complexity of cyclodextrin anomeric proton resonances in the ^{1}H NMR spectrum of the crude material. An alternative approach exploited a less reactive amide coupling reagent by preparing activated ester N-hydroxysuccinimidyl bromoacetate **3.20**. The dicyclohexylcarbodiimide (DCC) promoted esterification of commercially available bromoacetic acid in 1,4-dioxane gave **3.20** quantitatively (Scheme 3.5a). An amide condensation reaction between **3.20** and **3.19** in DCM with a catalytic amount of 4-dimethlyaminopyridinine (DMAP), followed by reaction with NaN_3 in DMSO afforded the methylene spacer cyclodextrin azide **3.21** in 90% yield over two successive steps (Scheme 3.5b).

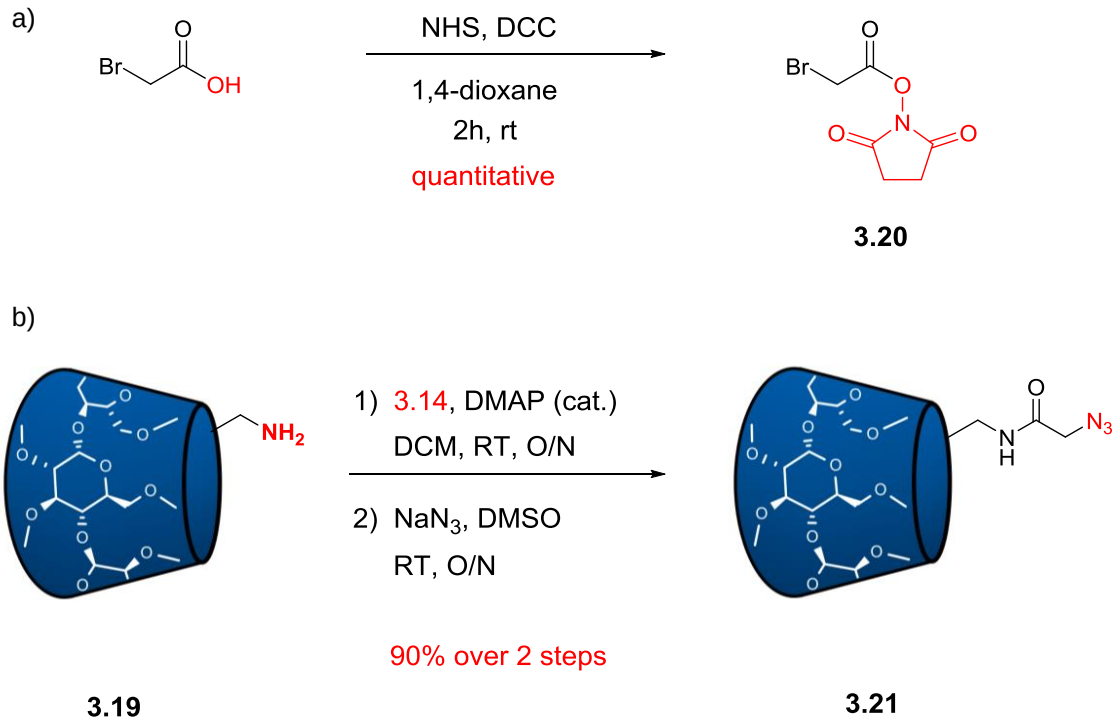

Scheme 3.5 Synthesis of the methylene azide **3.21**.

The corresponding aryl spaced azide derivatives **3.23** and **3.26** were prepared using similar synthetic procedures. Firstly, 4-azidobenzoic acid **3.6** was reacted with NHS in the presence of DCC affording **3.22** in 43% yield after purification by silica gel column chromatography. This relatively low yield was attributed to a partial hydrolysis of the activated ester group by acidic silanol moieties present in the silica gel. Alternatively, recrystallization of the crude product from DCM/petroleum ether provided pure **3.22** in an increase in yield to 90%. Reaction of **3.22** with permethylated β-cyclodextrin amine **3.19** in the presence of a catalytic amount of DMAP gave azide **3.23** in 78% yield (Figure 3.6b).

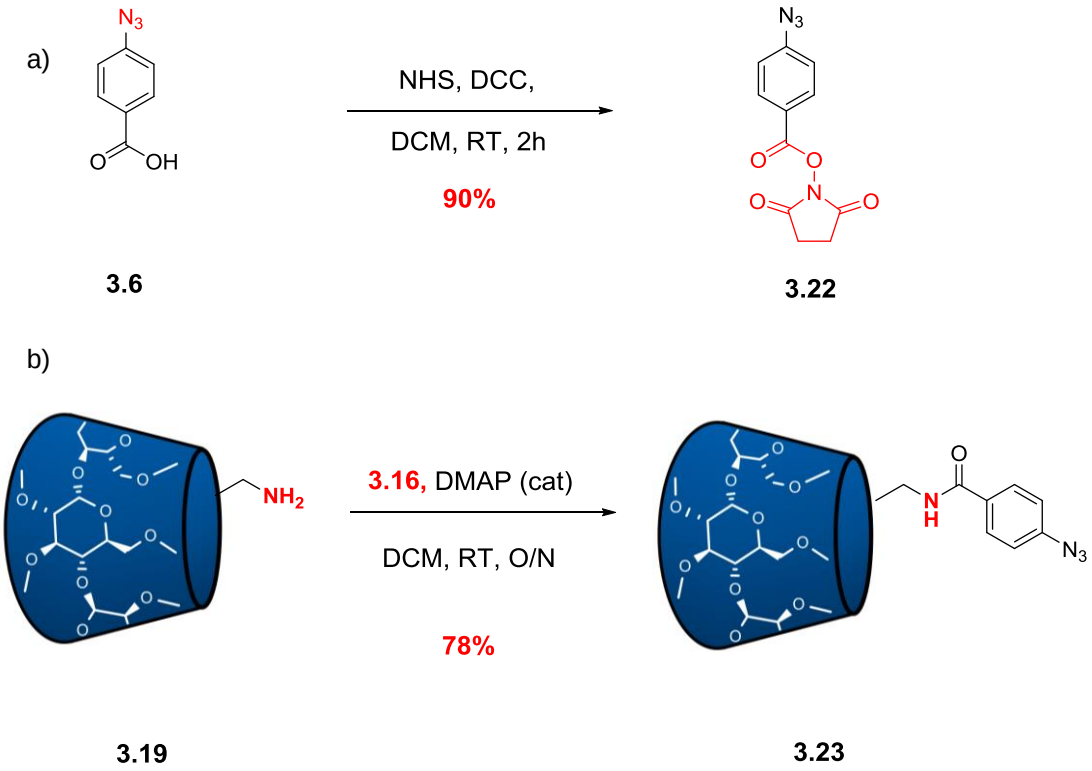

Scheme 3.6 Synthesis of the aryl azide **3.23**

Azide **3.8** described in Section 3.5.1, was hydrolysed under basic condition at room temperature, affording a quantitative yield of acid **3.24**. Esterification reaction of **3.24** with NHS using the DCC mediated coupling reaction provided activated ester **3.25** in 78% yield. An amide condensation reaction between **3.25** and permethylated β-cyclodextrin amine **3.19** in DCM afforded a perfluoroaryl azide **3.26** in 82% yield after chromatographic purification (Scheme 3.7)

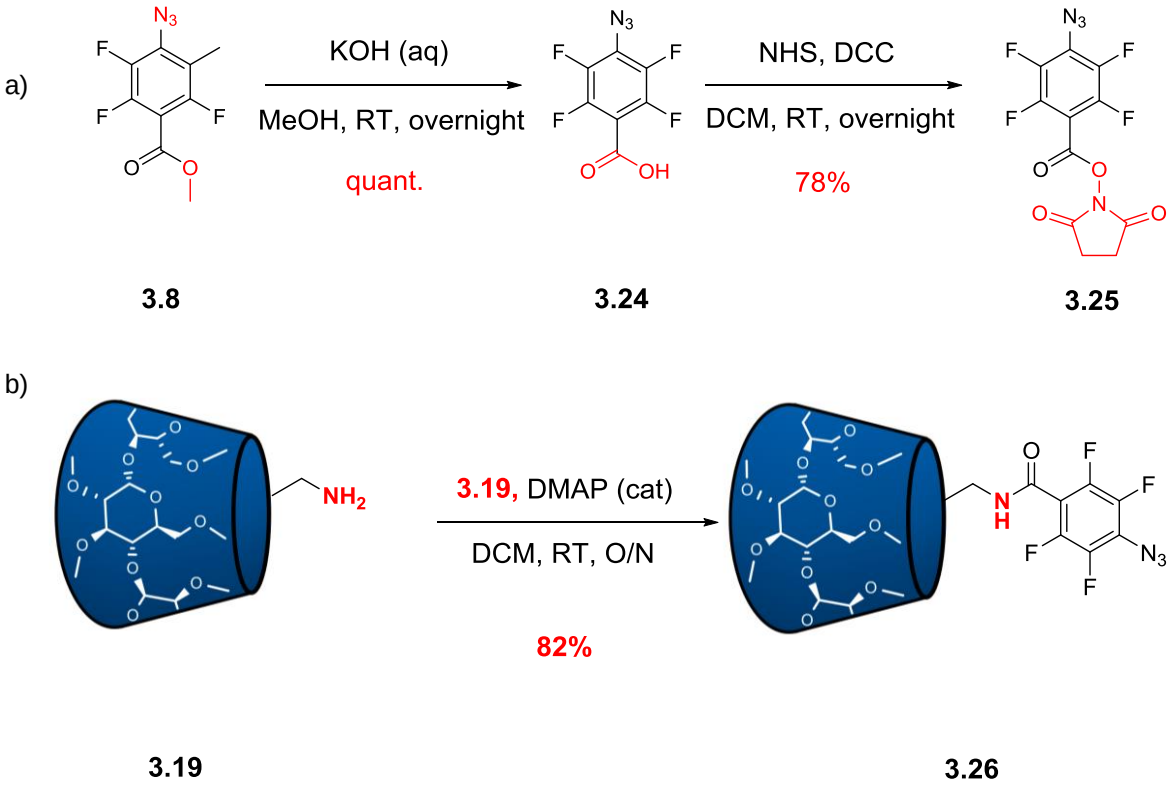

Scheme 3.7 Synthesis of the perfluoroaryl azide **3.26.**

(c) Synthesis of XB 3,5-bis-(iodotriazole)pyridinium chloride axles

The permethylated-β-cyclodextrin appended 3,5-bis-(iodotriazole)pyridine derivatives were synthesised *via* CuAAC reaction between 3,5-diiodoethynyl pyridine **2.3** and 2.2 equivalents of the respective cyclodextrin azide (Scheme 3.8). The reaction was conducted in the presence of a catalytic amount of $Cu(MeCN)PF_6$ and TBTA in dry THF to afford neutral axle components **3.27**, **3.28**, and **3.29** in 51, 78, and 82 % yields, respectively after purification by silica gel column chromatography.

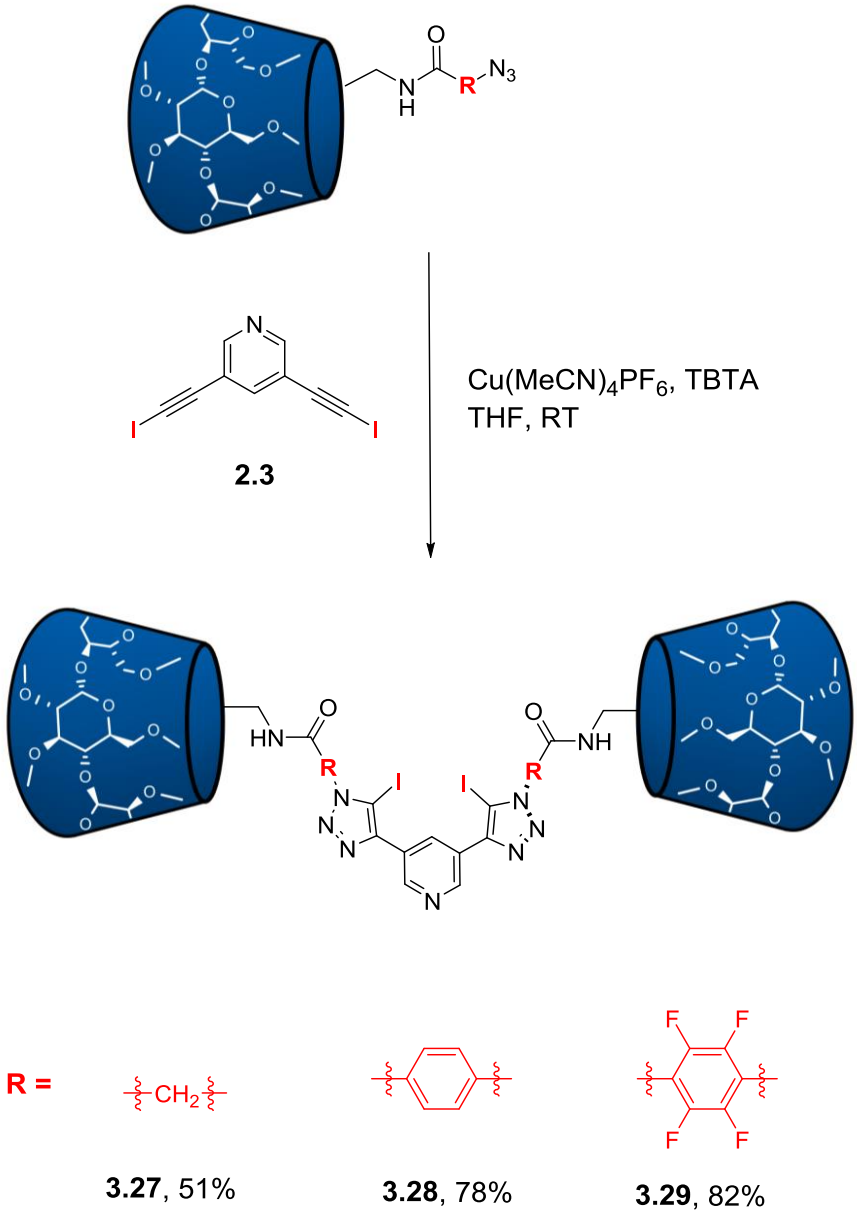

Scheme 3.8 Synthesis of XB 3,5-bis-iodotriazole pyridine axles.

Methylation reactions of **3.27**-**3.29** with an excess of iodomethane in $CHCl_3$ at 60 °C gave after anion exchange, the pyridinium chloride axles **3.30·Cl**-**3.32·Cl** (Scheme 3.9).

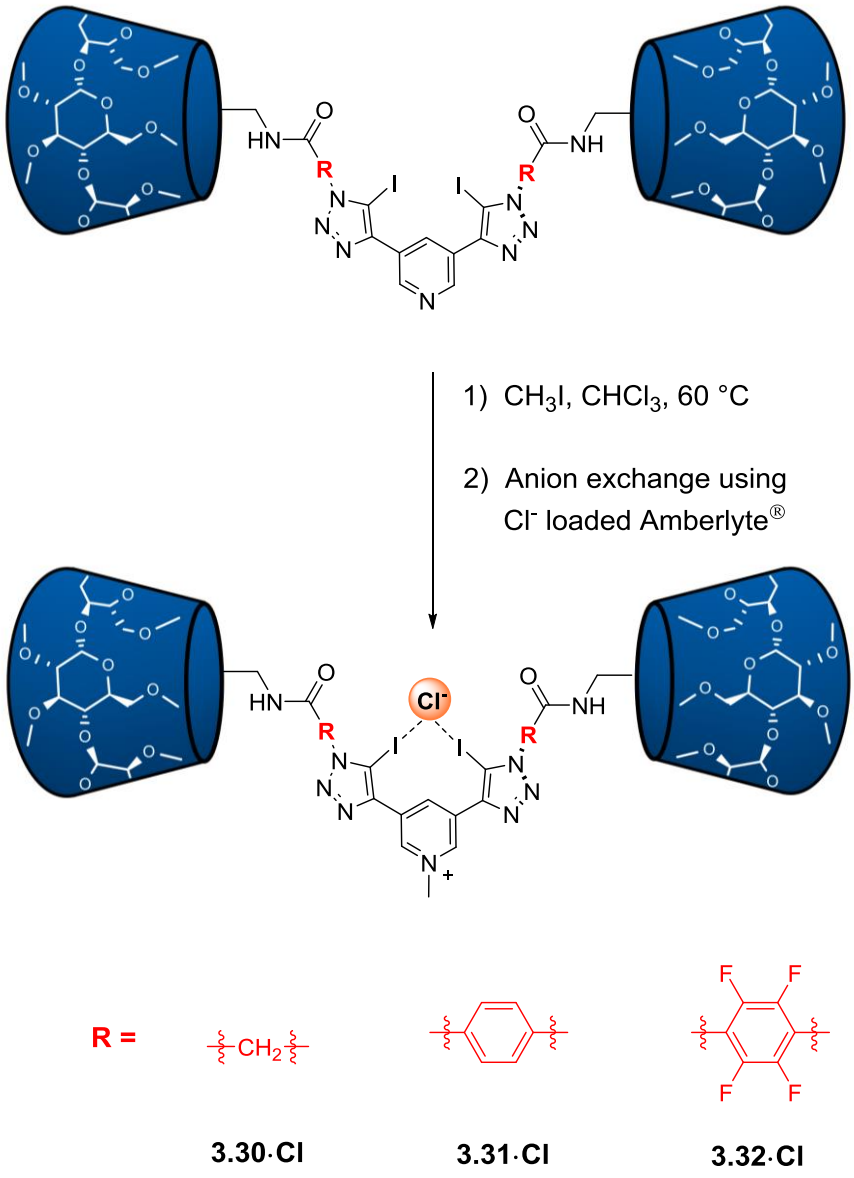

Scheme 3.9 Synthesis of XB 3,5-bis-(iodotriazole)pyridinium chloride axles**.**

3.6.2 Synthesis of macrocycle precursor

The synthesis of MIMs using the chloride anion-templated amide condensation method required the bis-aminepolyether macrocycle precursor **3.36**, prepared following synthetic routes shown in Scheme 3.10.[178] Commercially available hydroquinone was monoalkylated using bromoacetonitrile and NaOH in degassed 1:1 1,4-dioxane/water solution at room temperature to afford monofunctionalised hydroquinone **3.33** in 56% yield. Tosylation of tetraethylene glycol using *p*-toluenesulfonyl chloride and KOH in dichloromethane at 0°C gave the ditosylate **3.34** in quantitative yield. Alkylation reaction of **3.33** with **3.34** was carried out in refluxing MeCN with K_2CO_3 for 3 days to obtain bis-nitrile **3.35** in 79% yield after chromatographic purification. The bis-nitrile **3.35** was subsequently reduced to bis-amine **3.36** using a solution of borane in THF at 70°C affording the desired product in 70% yield (Scheme 3.10).

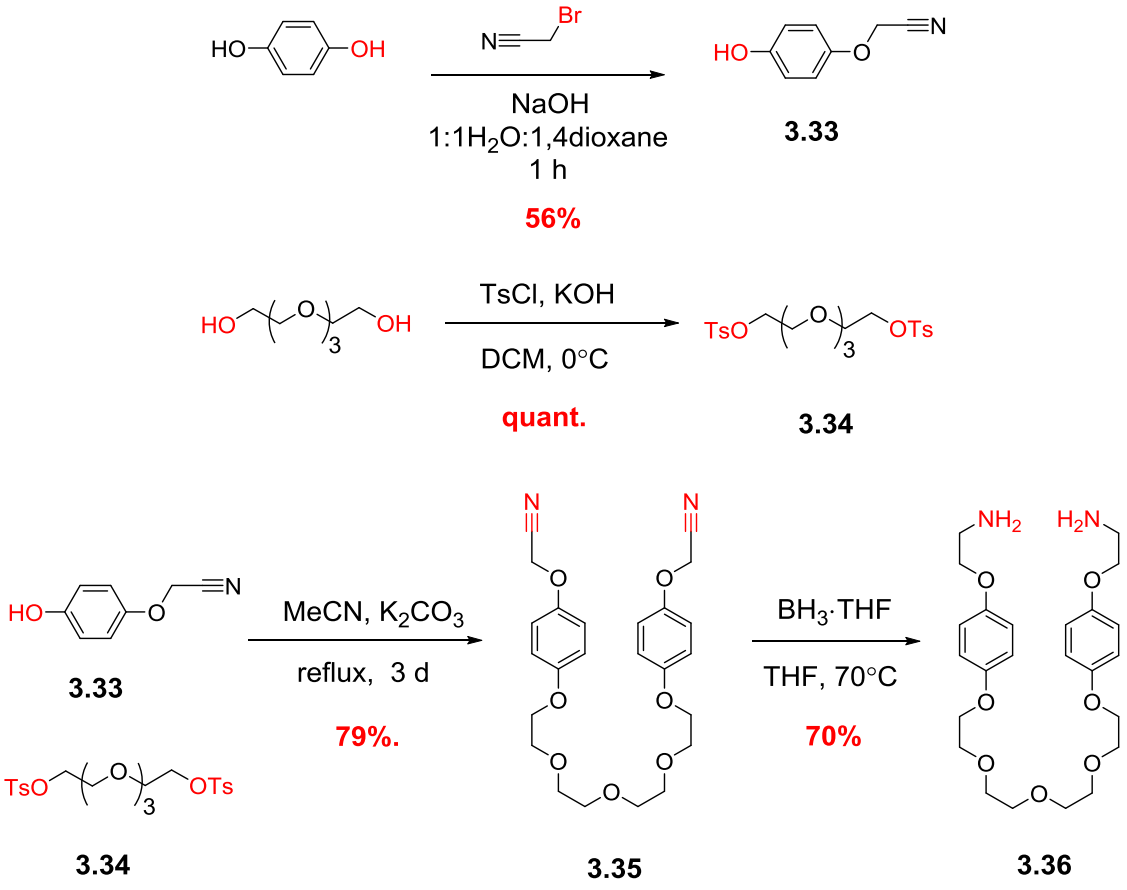

Scheme 3.10 Synthesis of bis-amine polyether macrocycle precursor.

3.6.3 Synthesis of XB [2]rotaxane

The axles **3.30·Cl**, **3.31·Cl**, **3.32·Cl** were each stirred with the bis-amine macrocycle precursor **3.36**[178] and NEt_3 in dry CH_2Cl_2 at 0°C, whereupon addition of 3,5-bis-chlorocarbonyl pyridine **3.37** afforded, after purification by preparative thin layer silica gel chromatography and anion exchange to their PF_6^- salts, the target XB [2]rotaxanes **3.12·PF$_6$**, **3.13·PF$_6$** and **3.14·PF$_6$** in respective isolated yields of 40%, 45% and 91% (Scheme 3.11)

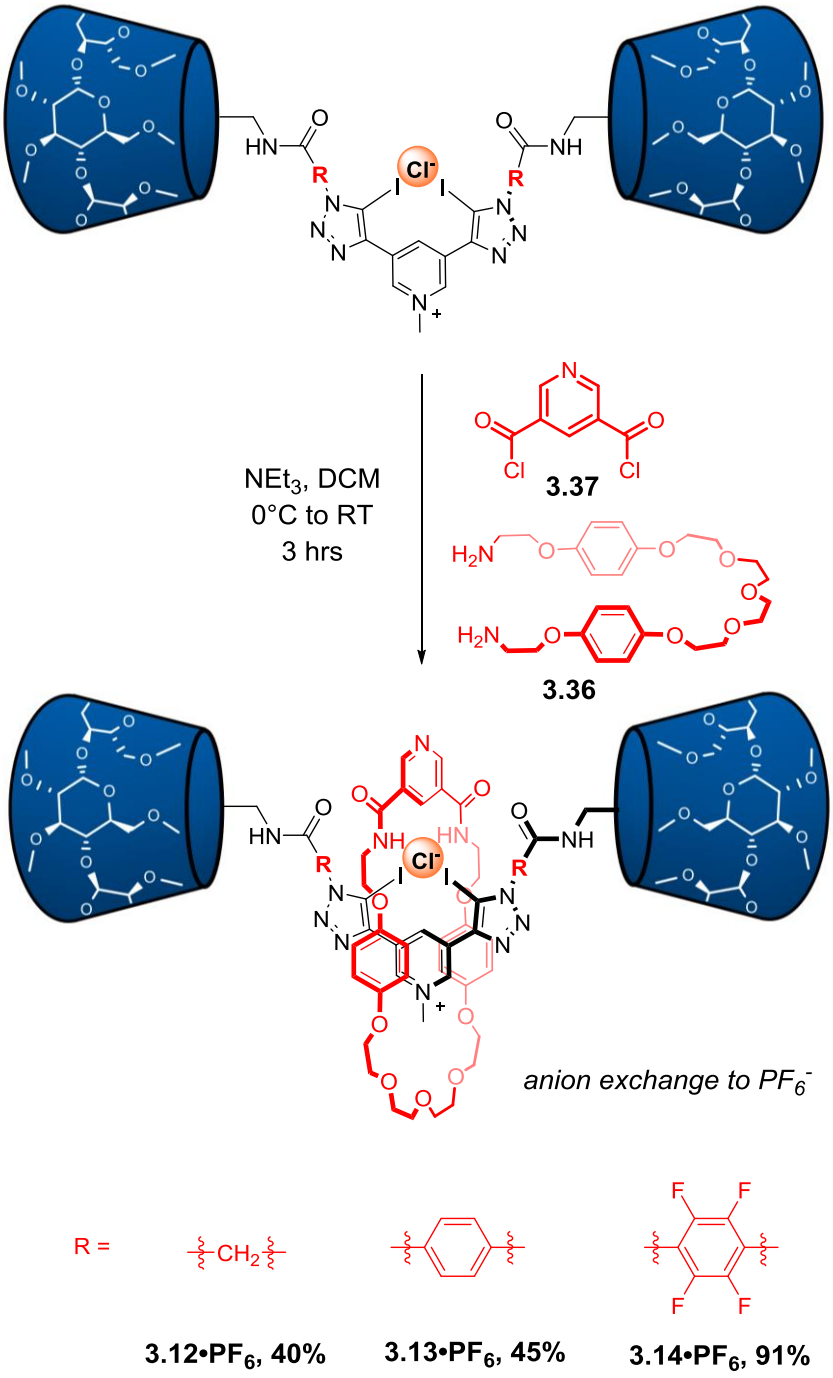

Scheme 3.11 Synthesis of XB [2]rotaxanes *via* anion template clipping methodology.

(a) ^{1}H-NMR spectroscopic characterisations

The [2]rotaxanes as chloride salts were characterized by ^{1}H and ^{13}C-NMR spectroscopy, and high resolution mass spectrometry (HRMS). In the case of **3.14·Cl**, the ^{1}H-NMR spectra of the axle **3.32·Cl**, the monocationic rotaxane **3.14·Cl**, and the neutral pyridine macrocycle **3.38** in 1:1 $CDCl_3$/d_4-methanol at 298 K are compared (Figure 3.14). The interlocked nature of the rotaxane results in the upfield perturbation and significant splitting of the hydroquinone protons (H_3 and H_4) of the macrocycle, likely arising from characteristic aromatic donor-acceptor interactions between the electron rich hydroquinones and the positively charged electron deficient pyridinium axle groups. The downfield perturbation of axle methyl pyridinium protons (H_c) in the [2]rotaxane is a result of the HB interactions of the N^+–Me group and the polyether's oxygens in the macrocycle. Moreover, a significant upfield shift of H_1 in the macrocycle and H_a in the axle components was also observed together with a downfield shift of H_2 and H_b. Similar spectroscopic observations were also noted in the ^{1}H-NMR spectra of **3.12·Cl** and **3.13·Cl** (Figure 3.15a and Figure 3.16a).

Unequivocal evidence for the interlocked nature of the rotaxanes was shown by two-dimensional ^{1}H-ROESY NMR spectra which revealed through space interactions between proton resonances of the mechanically bonded axle and macrocycle components of the [2]rotaxanes. ROESY spectrum of **3.14·Cl** revealed a correlation arising from the anomeric protons of the permethylated β-cyclodextrin stopper groups and an external pyridine proton (H_2) of the macrocycle (Figure 3.14b). In the case of **3.12·Cl**, a through space interaction between a pyridinium H_b proton from the axle and the hydroquinone protons of the contiguous macrocycle was observed (Figure 3.15b). For **3.13·Cl,** the pyridinium protons (H_a, H_b), and aryl spacer protons (H_{aryl}) from the axle components show a correlation with the hydroquinone protons (H_3,H_4) of the pyridine macrocycle (Figure 3.16b).

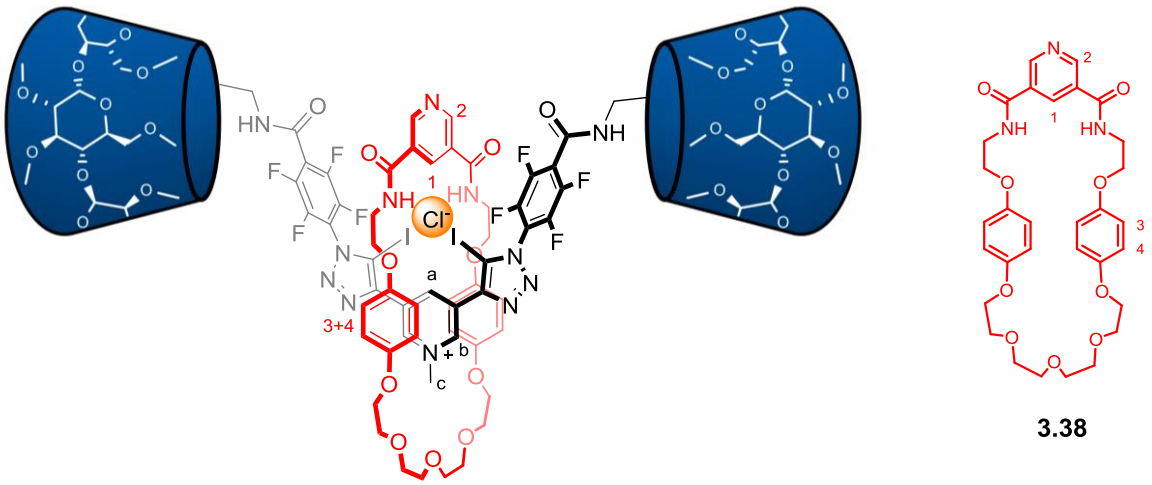

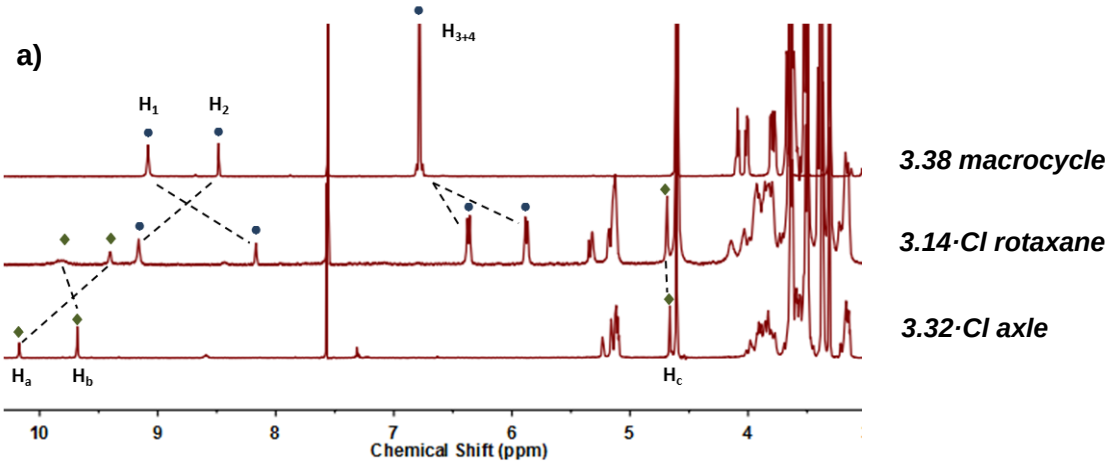

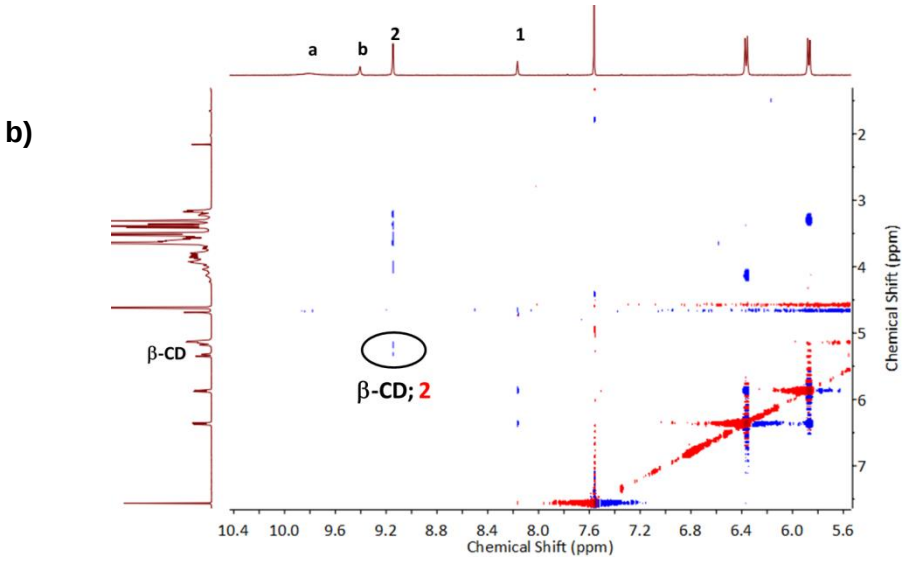

Figure 3.14 (a) Truncated ^{1}H-NMR spectra of the axle **3.32·Cl**, [2]rotaxane **3.14·Cl**, and pyridine macrocycle **3.38** in 1:1 $CDCl_3$/d_4-MeOD, 298 K, 500 MHz (b) 2D-ROESY spectrum of **3.14·Cl** in $CDCl_3$/d_4-MeOD at 298 K.

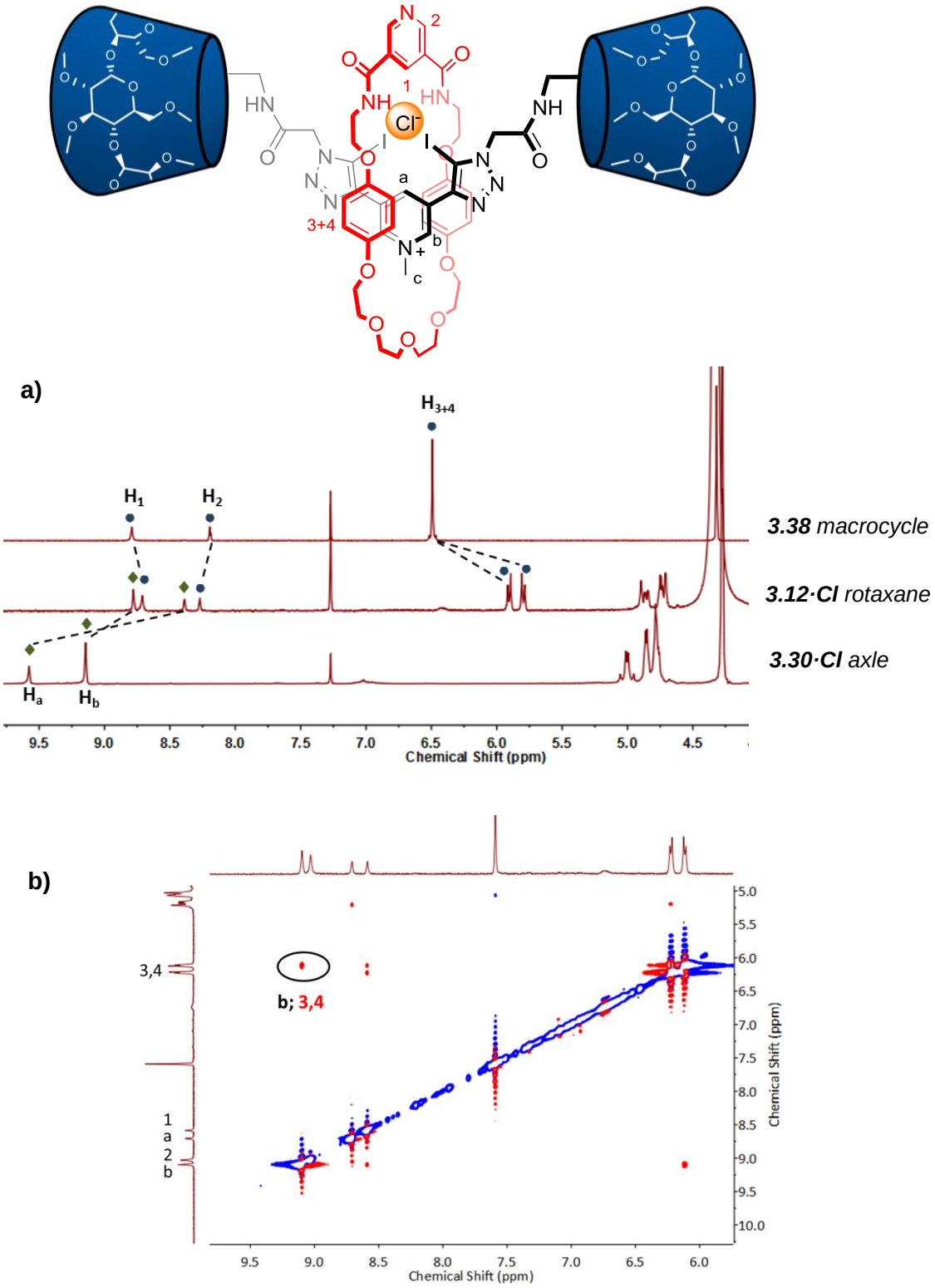

Figure 3.15 (a) Truncated ^{1}H-NMR spectra of the axle **3.30·Cl**, [2]rotaxane **3.12·Cl**, and pyridine macrocycle **3.38** in 1:1 $CDCl_3/d_4$-MeOD, 298 K, 500 MHz (b) 2D-ROESY spectrum of **3.12·Cl** in $CDCl_3/d_4$-MeOD at 298 K.

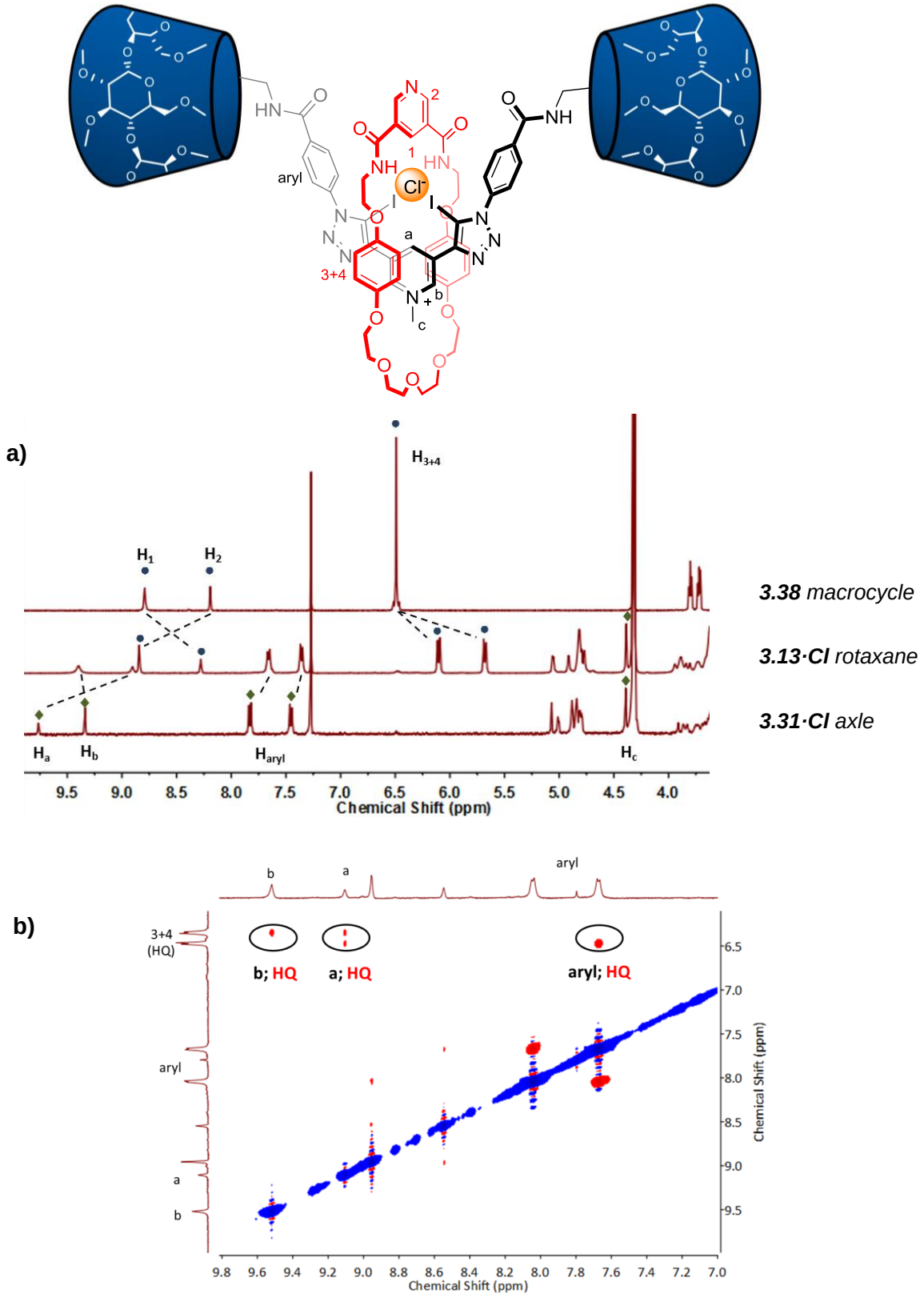

Figure 3.16 (a) Truncated ^{1}H-NMR spectra of the axle **3.31·Cl**, [2]rotaxane **3.13·Cl**, and pyridine macrocycle **3.38** in 1:1 $CDCl_3$/d_4-MeOD, 298 K, 500 MHz (b) 2D-ROESY spectrum of **3.13·Cl** in $CDCl_3$/d_4-MeOD at 298 K.

(b) Synthesis of HB perfluoroaryl [2]rotaxane

The HB rotaxane analogue of XB rotaxane **3.14·PF$_6$** was also prepared (Scheme 3.14). The HB axle **3.39·Cl** was synthesised *via* analogous routes undertaken for the XB axles (Section 3.6.1); CuAAC reaction between 3,5-diethynylpyridine, followed by alkylation reaction using iodomethane and subsequent anion exchange to the chloride salt (Scheme 3.12). The clipping methodology afforded the resulting HB [2]rotaxane with the perfluoroaryl spacer in the axle component **3.40·PF$_6$** after anion exchange in the isolated yield of 42%.

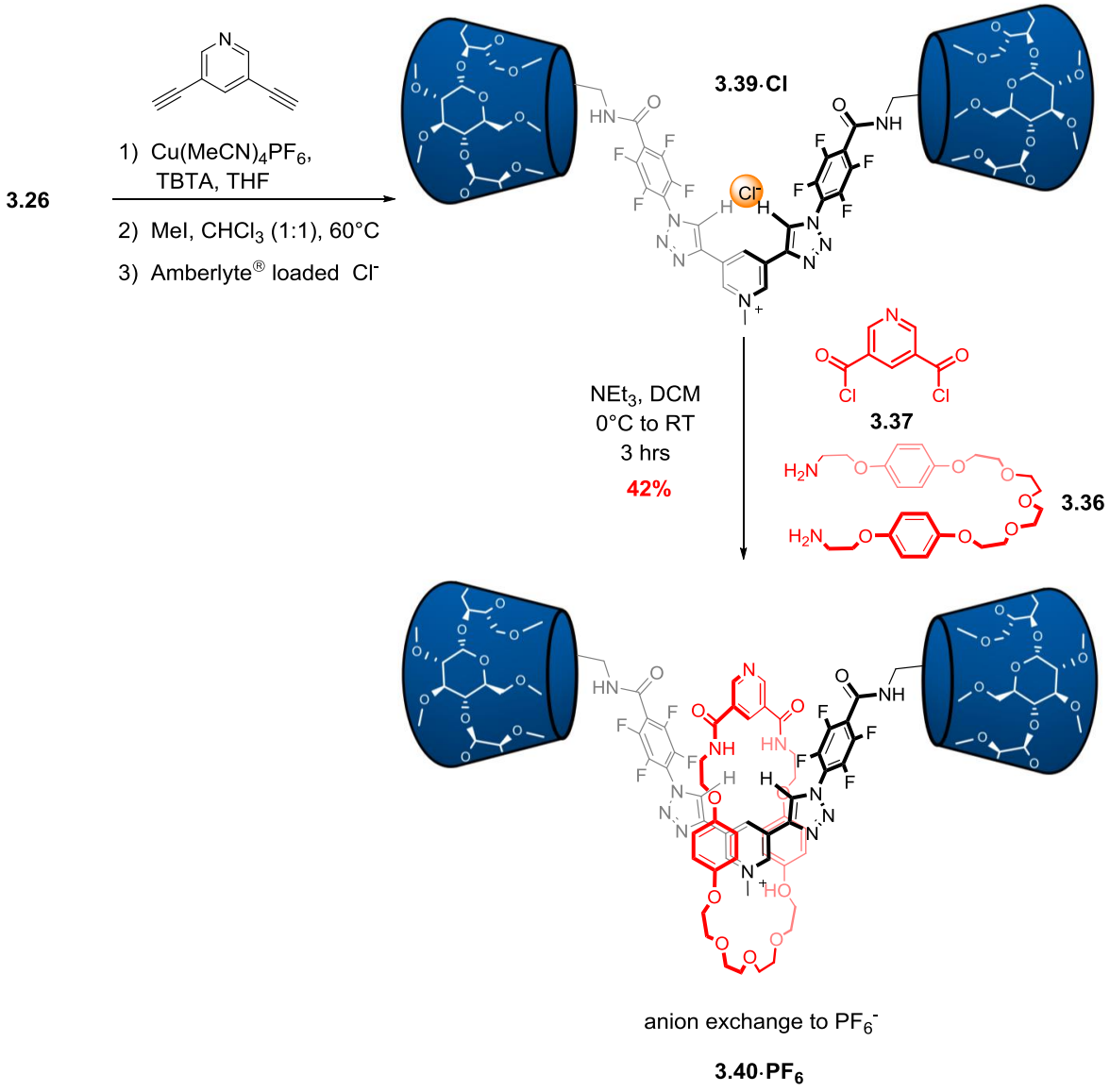

Scheme 3.12 Synthesis of HB perfluoroaryl [2]rotaxane **3.37·PF$_6$** *via* anion-templated clipping methodology.

Clearly the perfluorinated benzene functionalized XB axle **3.32·Cl** acted as the most efficient anion template for rotaxane synthesis as evidenced by the impressive 91% yield of XB [2]rotaxane **3.14·PF_6**, arising from a combination of the polarizability of 3,5-bis-(iodotriazole)pyridinium XB donors and strong electron withdrawing perfluoroaryl substituents.

(c) Correlation of acyclic anion binding template strength with rotaxane yield

The chloride binding affinities of acyclic receptors incorporating benzyl (**3.1·Cl**), methylene (**3.2·Cl**), aryl (**3.3·Cl**) and perfluoroaryl (**3.4·Cl**) substituents can be used to represent the anion template strength of their corresponding permethylated β-cyclodextrin stoppered XB axles. The axle containing the non-fluorinated aromatic and alkyl spacers resulted in [2]rotaxane formation (Table 3.3) corresponding to the typical yield range for the anion template method of 40-60%.[178, 249, 258] By taking into account the chloride anion association constant data shown in Table 3.1, there is an obvious correlation of chloride anion association strength with yield of rotaxane formation. Notably, the observed > 90% yield for the preparation of [2]rotaxane **3.14·PF_6** *via* this XB anion template clipping method matches the highest yields obtained for MIM formation using metal cation , π–π donor–acceptor and hydrogen bond templates. [157, 240-246]

Table 3.3 Anion association constants (M^{-1}) and isolated rotaxane yield.

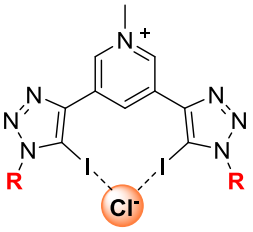

XB Acyclic template

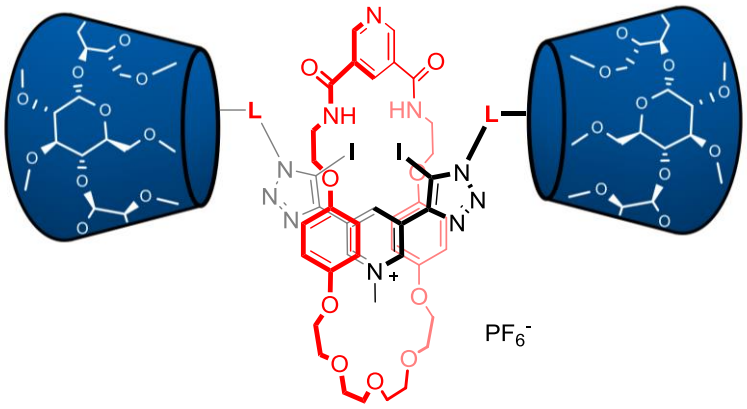

XB [2]rotaxane hosts

XB acyclic template	K_a for Cl^- in d_6-DMSO (M^{-1})	XB[2]rotaxane hosts	Isolated yield (%)
3.1·Cl 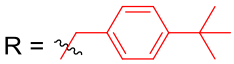	387	**3.41·PF_6** 	33[ref]
3.2·Cl 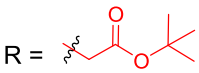	403	**3.12·PF_6** 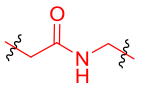	40
3.3·Cl 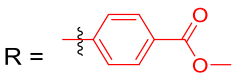	429	**3.13·PF_6** 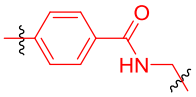	45
3.4·Cl 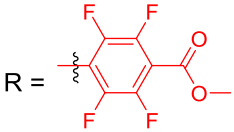	1395	**3.14·PF_6** 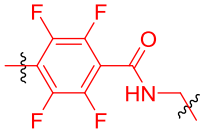	91

3.7 ^{1}H-NMR aqueous anion binding studies of monocationic [2]rotaxanes

The halide anion recognition properties of perfluorinated XB monocationic rotaxane **3.14·PF$_6$** together with the analogous HB rotaxane **3.40·PF$_6$** and axle **3.32·PF$_6$** were investigated using ^{1}H-NMR titration experiments in D_2O:d_6-acetone (1:1), in comparison to anion binding properties of non-fluorinated XB [2]rotaxane **3.41·PF$_6$** (Figure 3.17).[249] For the rotaxanes the addition of halide anion caused significant perturbations of interlocked cavity proton resonances (H_a and H_1) (Figure 3.18). The downfield shift of the axle component internal pyridinium proton (H_a) from the rotaxanes **3.14·PF$_6$** and the axle **3.32·PF$_6$** were monitored as a function of equivalents of anion added (Figure 3.19). WinEQNMR2[253] analysis of the titration data for XB interlocked and acyclic hosts revealed 1:1 stoichiometric association constants for halide anions (Table3.4).

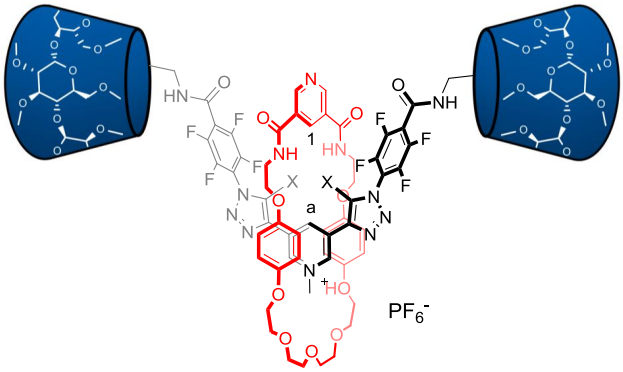

X = I (3.14·PF$_6$)
X = H (3.40·PF$_6$)

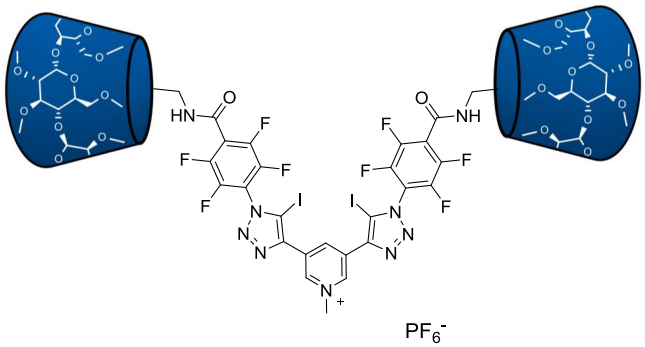

3.32·PF$_6$

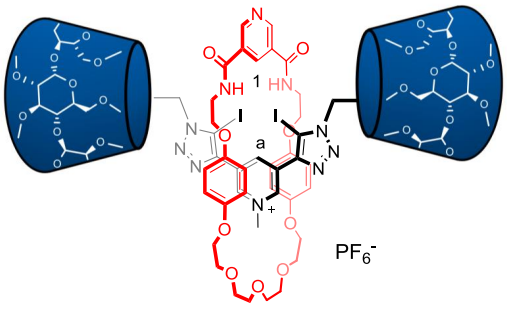

3.41·PF$_6$

Figure 3.17 Acyclic and Interlocked host structures.

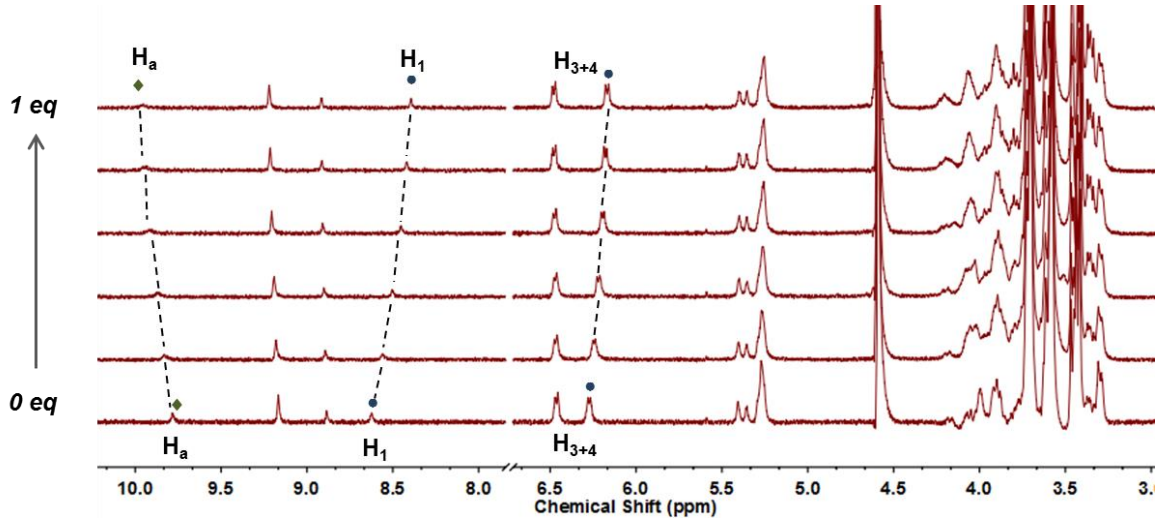

Figure 3.18 Truncated ^{1}H-NMR of **3.14·PF$_6$** in D_2O:d_6-Acetone (1:1) upon addition of iodide anion as its TBA salt (500 MHz, 298K).

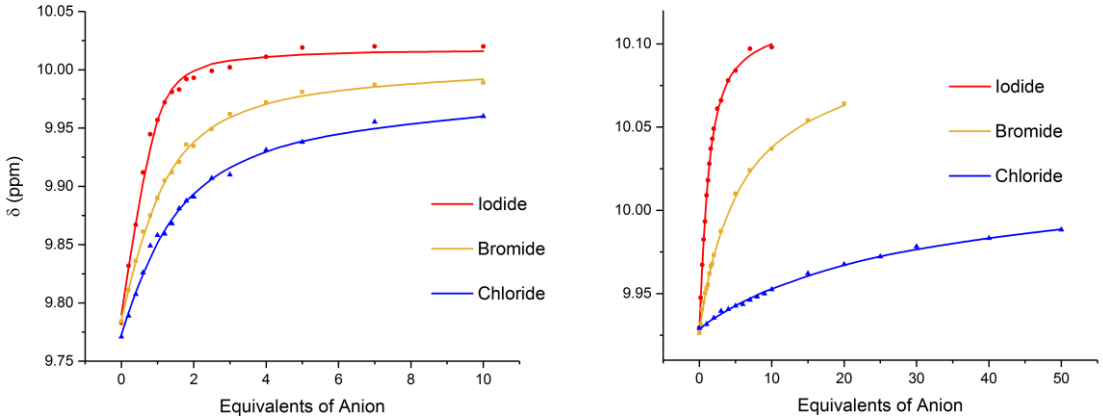

Figure 3.19 Anion binding isotherms of (a) **3.14·PF$_6$** and (b) **3.32·PF$_6$** , [host] = 1mM and [guest] = 50 mM (1:1 D_2O/ d_6-Acetone, 500MHz, 298K).

Table 3.4 Anion association constants (K_a/M^{-1}) for acyclic and [2]rotaxane hosts in D_2O:d_6-Acetone (1:1)[a]

Entry	Receptors	K_a (M^{-1}) in 1:1 D_2O/d_6-Acetone		
		Chloride	Bromide	Iodide
Perfluorinated Hosts				
1	Monocationic XB Perfluoroaryl Rotaxane **3.14·PF$_6$**	930	1727	$>10^4$
2	Monocationic HB Perfluoroaryl Rotaxane **3.40·PF$_6$**	NB[b]	NB[b]	63
3	Axle **3.32·PF$_6$**	24	181	1309
Non-fluorinated Hosts				
4	Monocationic XB Rotaxane **3.41·PF$_6$**	150	436	1036

[a] Anions added as TBA salts, errors (±) less than 10%, 1:1 association constants calculated using WinEqNMR2 software,35 monitoring the perturbation of the internal pyridinium proton Ha (500MHz, 298K). [b] NB =No binding.

In the highly competitive 1:1 D_2O/ d_6-acetone solvent mixture, the halogen bonding rotaxane **3.14·PF$_6$** displays remarkably strong binding for Cl^-, Br^-, and I^- anions. Indeed, the association constant for iodide binding is $>10^4$ M^{-1}, whilst those of bromide and chloride are 1727 M^{-1} and 930 M^{-1}, respectively (Table 3.4, Entry 1). This preferential binding to the larger and less highly hydrated halide anions is presumably governed by the Hofmeister series bias.[80, 259, 260] In contrast, the halide anion recognition strength of the hydrogen bonding rotaxane analogue **3.40·PF$_6$**, where iodotriazole groups are substituted with C–H prototriazole motifs is dramatically diminished, demonstrating only weak affinity to I^- and no binding for Cl^- and Br^- (Table 3.4, Entry 2). The remarkable enhancement of halide complexation by XB **3.14·PF$_6$** rotaxane by at the very least two orders of magnitude in comparison to HB rotaxane **3.40·PF$_6$** illustrates again the superiority of halogen bonding over hydrogen bonding in aqueous anion recognition.[92, 249, 258, 261-263]

The importance of the interlocked host cavity of **3.14·PF$_6$** for anion recognition is apparent when comparing anion affinities with the acyclic axle component **3.32·PF$_6$** where the augmented anion binding strength highlights the consequence of halide guest encapsulation by convergent XB and HB interactions in the unique three-dimensional cavity of the rotaxane. It is noteworthy that the acyclic XB axle component **3.32·PF$_6$** is a potent and superior host for halides in comparison to the HB rotaxane **3.40·PF$_6$**, being capable of even binding, albeit weakly, the most hydrated chloride anion (Table 3.4, Entry 1 and 3).

Finally, in an effort to elucidate the effect of incorporating the perfluoroaryl motif into the axle component of **3.14·PF_6,** the halide anion binding properties of monocationic XB rotaxane **3.41·PF_6** were determined (Table 3.4). As expected, **3.14·PF_6** demonstrates notable enhancement of halide binding, with the strength of iodide complexation at least an order of magnitude greater than the **3.41·PF_6** rotaxane (Table 3.4, Entry 1 and 4), which can be attributed to the rigid, electron deficient and hydrophobic nature of the perfluoroaryl substituents of the 3,5-bis-(iodotriazole)pyridinium axle component of **3.14·PF_6**, facilitating in particular the amplified potency of XB donor–halide anion interactions in highly competitive aqueous solvent media.

Part II: Thermodynamic Investigations of Novel Water Soluble XB Acyclic and Interlocked Anion Host Molecules

3.8 Water soluble XB acyclic and interlocked host structures

As discussed previously, anion binding investigations of the perfluorinated [2]rotaxanes were limited to being undertaken in a maximum of 50% water. In this section, novel water soluble XB acyclic and rotaxane anion host structures containing 3,5-bis-(iodotriazole) pyridine, pyridine-N-oxide, and pyridinium motifs are prepared, and their aqueous anion binding properties are investigated *via* ^{1}H-NMR spectroscopic titration and isothermal titration calorimetric (ITC) analysis.

3.8.1 Design and synthesis of XB acyclic hosts

XB anion receptors containing a central pyridinium motif substituted at the 3,5-positions with iodotriazole groups have been demonstrated to be effective bidentate XB donors for halide anions in highly competitive aqueous media (Section 3.7), while an analogous HB receptor failed to bind anions under the same solvent conditions. With the idea of incorporating an electron withdrawing aryl spacer group whilst maintaining water solubility, acyclic 3,5-bis-(iodotriazole) pyridine **3.42**, **3.43** and **3.44·NO$_3$** hosts containing four permethylated β-cyclodextrin groups covalently linked *via* isophthalamide motifs were synthesised (Figure 3.20).

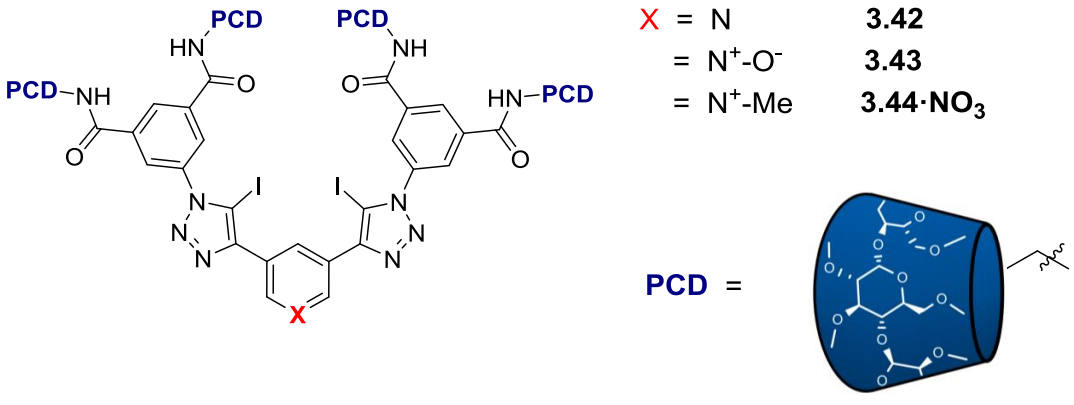

Figure 3.20 Water soluble XB acyclic receptors in this study.

I. Synthesis of Azide Precursor

The series of target XB anion receptors required the synthesis of a bis-(permethylated β-cyclodextrin) substituted 1,3-isophthalamide azide derivative **3.45** (Figure 3.21).

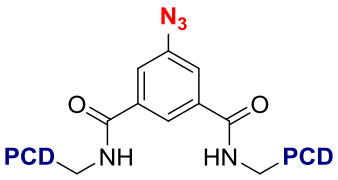

3.45

Figure 3.21 Target bis-(permethylated β-cyclodextrin) azide **3.45.**

The multi-stepped synthesis of azide **3.45** started with preparation of an aryl-azide containing bis-NHS ester **3.46** (Scheme 3.13). Diazotisation of commercially available 5-amino isophthalic acid under acidic conditions followed by reaction with NaN_3 afforded an off-white powder of 5-azido isophthalic acid **3.47** in 80% yield. Esterification of **3.47** with four equivalents of *N*-hydroxysuccinimide was carried out in the presence of EDC·HCl in DMF to obtain bis-NHS ester azide **3.46** in 67% yield.

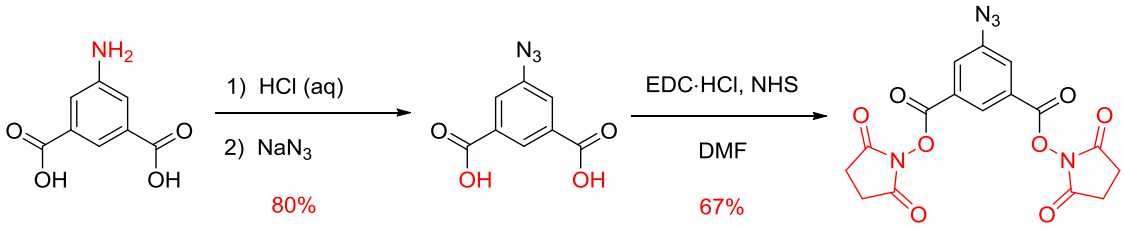

3.47 **3.46**

Scheme 3.13 Synthesis of bis-NHS ester **3.46**.

The reaction of bis-NHS ester **3.46** with two equivalents of permethylated β-cyclodextrin amine **3.19** in the presence of DMAP in DCM gave a crude product which was purified *via* silica gel column chromatography using 5% MeOH/DCM to afford azide **3.45** in 77% yield (Scheme 3.14). The ^{1}H-NMR spectrum of **3.45** is shown in Figure 3.22 indicating characteristic aryl proton resonances (H_a and H_b) as well as a complex multiplicity of C_1-anomeric proton resonances consistent with a loss of C_7 symmetry.

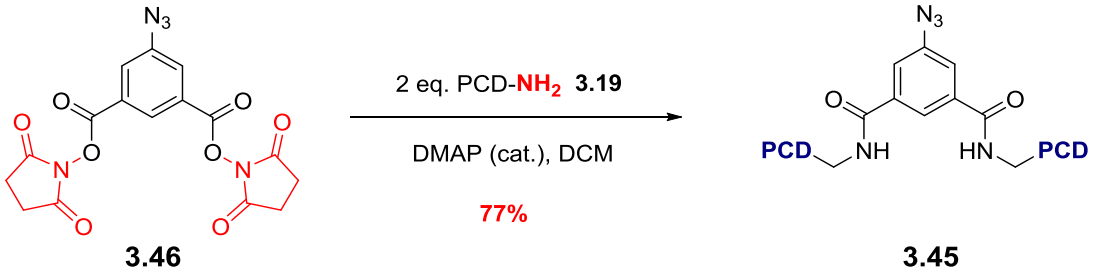

Scheme 3.14 Synthesis of bis-(permethylated β-cyclodextrin) azide **3.45**.

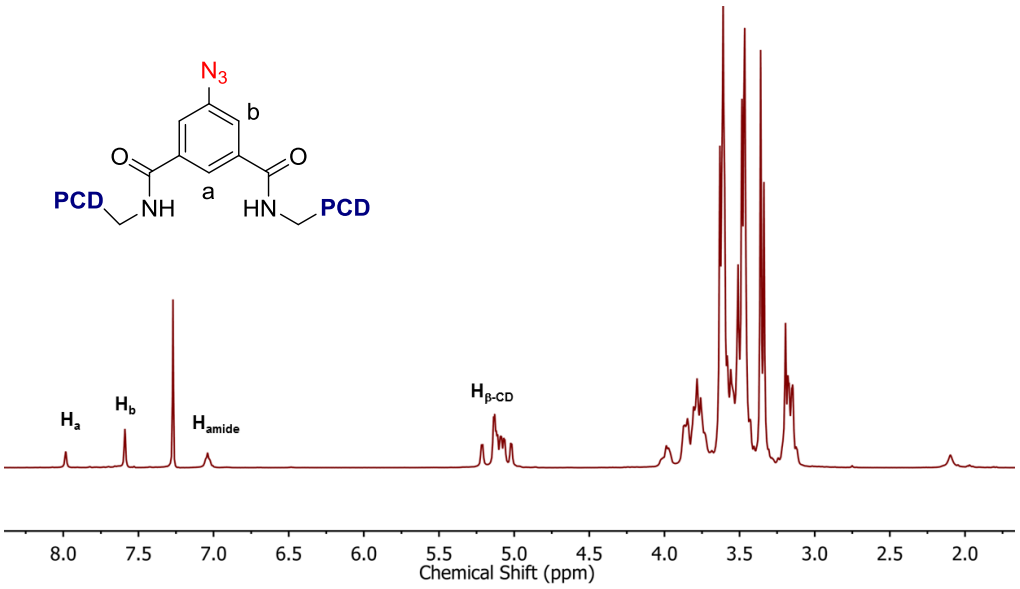

Figure 3.22 ^{1}H-NMR spectrum of azide **3.45** in $CDCl_3$ (500MHz, 298K).

II. *Synthesis of water soluble acyclic host structures*

The neutral XB receptor **3.42** was synthesised *via* analogous routes undertaken for XB neutral axles (Section 3.6.1 and Scheme 3.15); CuAAC reaction between 3,5-bis-(iodoethynyl)pyridine **2.3** and two equivalents of azide **3.45**, afforded a yellow solid product in 90% yield after chromatographic purification. The HB analogue was also prepared using the same protocol to give **3.48** in 72% yield. ^{1}H-NMR spectra of **3.42** and **3.48** are shown in Figure 3.23 and 3.24, respectively.

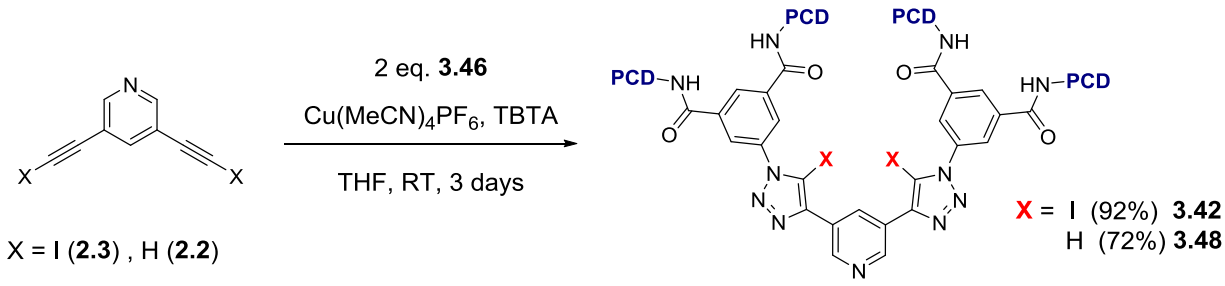

Scheme 3.15 Synthesis of neutral HB and XB pyridine Axle.

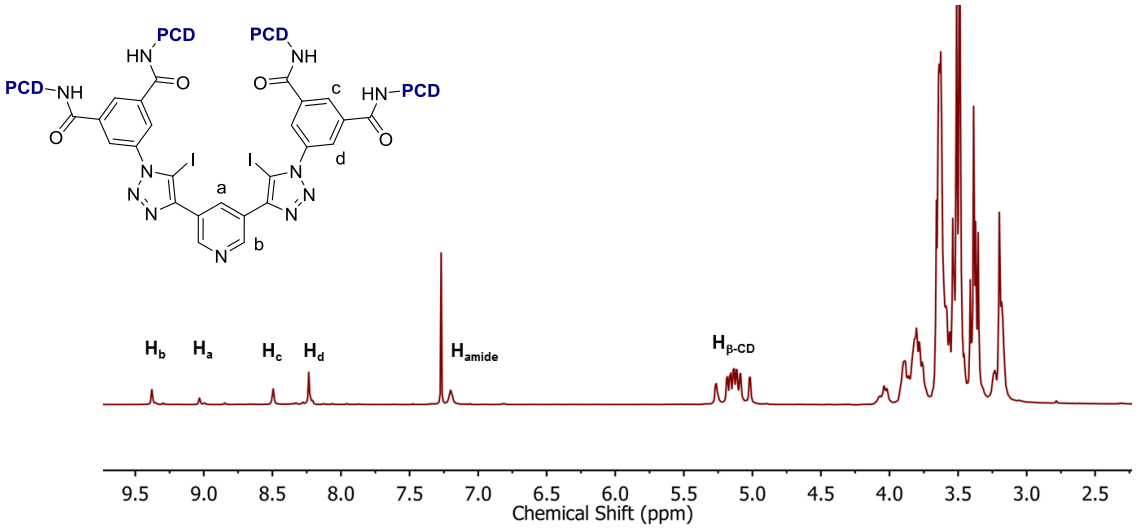

Figure 3.23 ^{1}H-NMR spectrum of neutral XB **3.42** in $CDCl_3$ (500MHz, 298K).

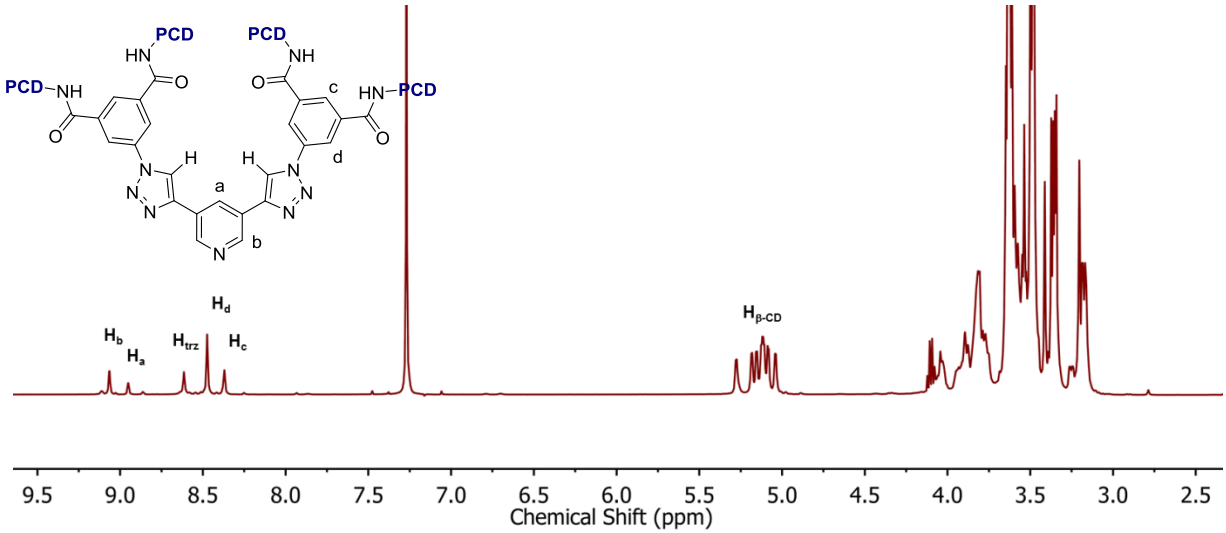

Figure 3.24 ^{1}H-NMR spectrum of neutral HB **3.48** in $CDCl_3$ (500MHz, 298K).

Oxidation of XB receptor **3.42** was initially attempted using Oxone®. However ESI-MS analysis of the crude reaction mixture showed a peak corresponding to the mono-prototriazole pyridine N-oxide decomposition product and the ^{1}H-NMR spectrum also displayed complex proton resonances showing a triazole proton signal. The desired product was obtained when XB **3.42** was reacted with an excess of m-CPBA in DCM to give receptor **3.43** isolated in 68 % yield by preparative TLC chromatography (Scheme 3.16). The ^{1}H-NMR spectrum of **3.43** is shown in Figure 3.25.

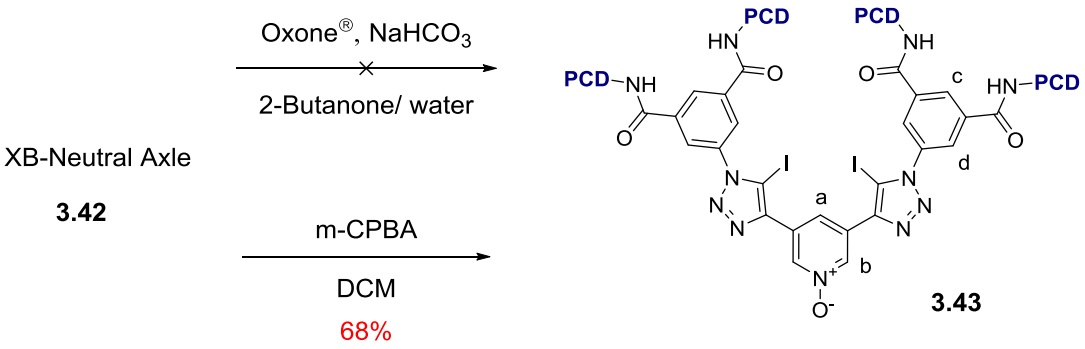

Scheme 3.16 Synthesis of XB pyridine N-oxide axle.

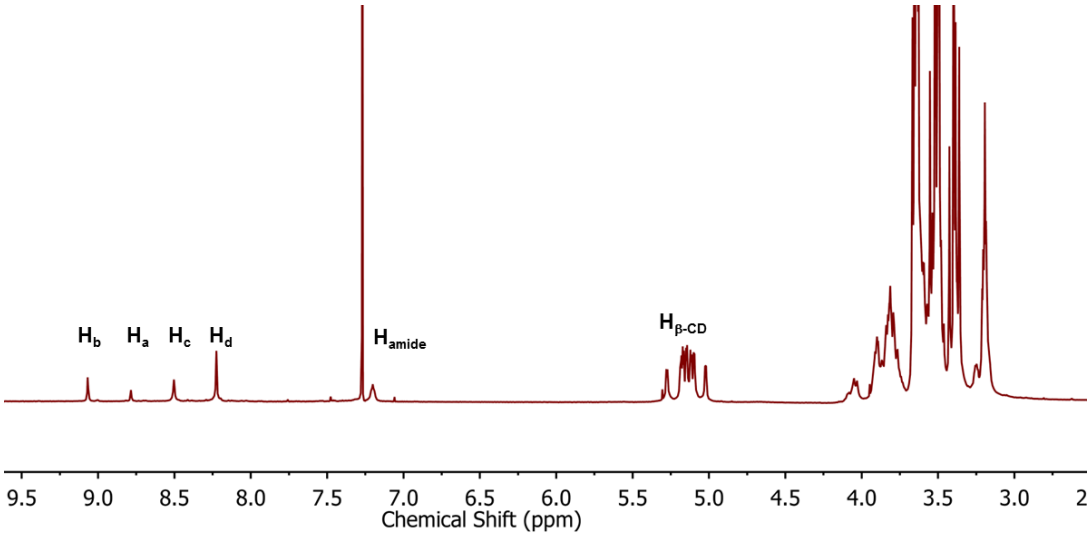

Figure 3.25 ^{1}H-NMR spectrum of pyridine N-oxide XB **3.43** in $CDCl_3$ (500MHz, 298K).

Heating a solution of **3.42** in a mixture of $CHCl_3$/CH_3I (1:1) in a sealed tube overnight afforded the pyridinium receptor, isolated as the nitrate salt, **3.44·NO_3** quantitatively**,** after anion exchange (Scheme 3.17). The analogous HB pyridinium receptor was prepared in an identical fashion to obtain **3.49·NO_3** in 85% yield. The ^{1}H-NMR spectra of both the XB and HB receptors are shown in Figure 3.26 and 3.27.

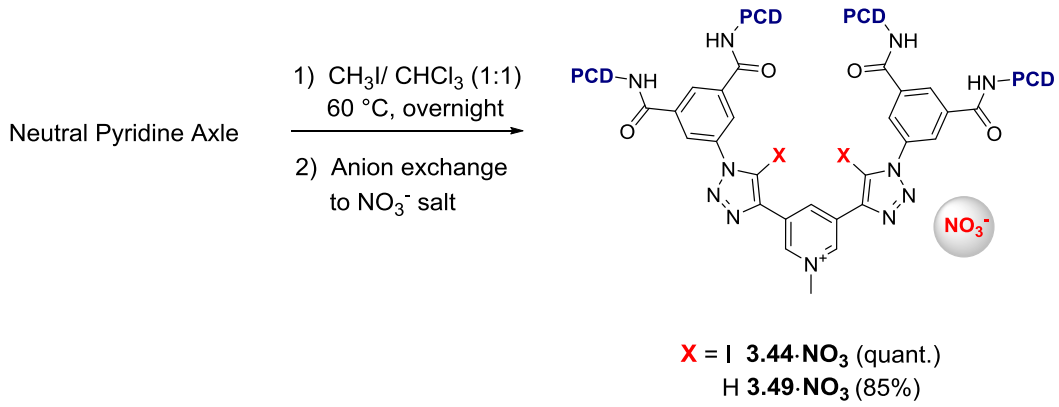

Scheme 3.17 Synthesis of XB and HB pyridinium nitrate axles.

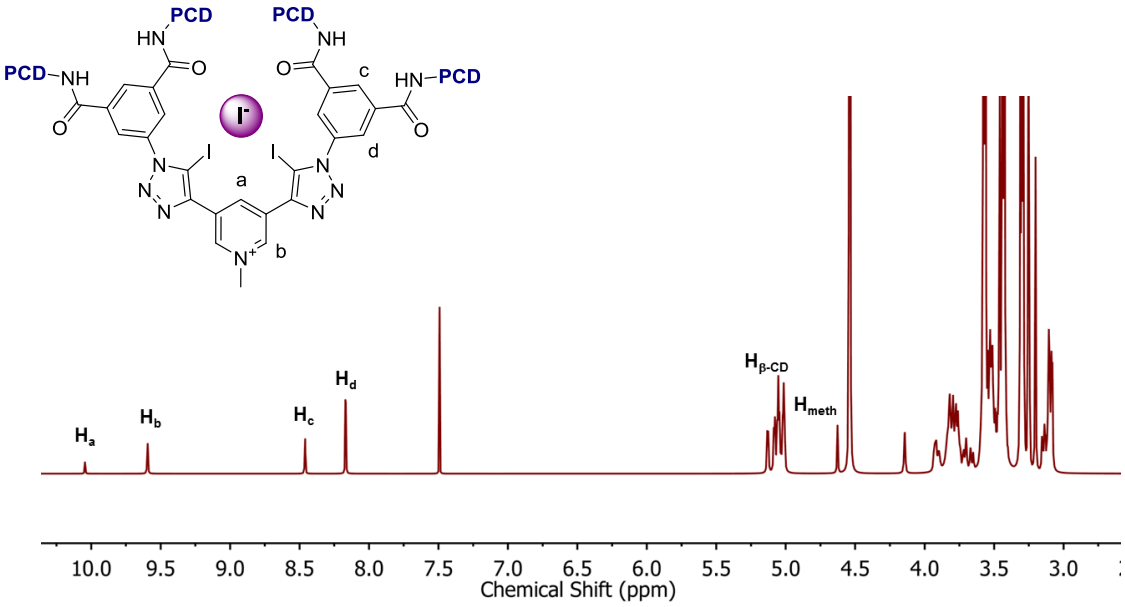

Figure 3.26 ^{1}H-NMR spectrum of pyridinium XB axle **3.44·I** in 1:1 $CDCl_3$/ d_4-MeOD (500MHz, 298K).

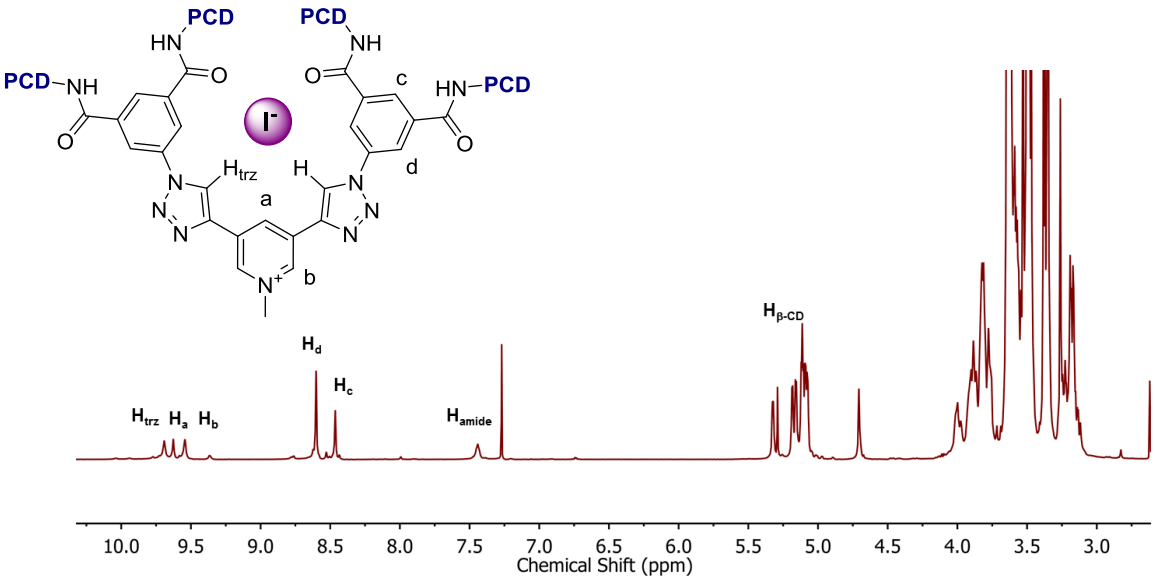

Figure 3.27 ^{1}H-NMR spectrum of pyridinium HB axle **3.49·I** in $CDCl_3$ (500MHz, 298K).

3.8.2 Synthesis of water soluble XB [2]rotaxane

The axle **3.44·Cl** was prepared *via* anion exchange of **3.44·I** using the same protocol in Section 3.6.3. Stirring **3.44·Cl** with polyether bis-amine **3.36** and NEt_3 in dry DCM, and addition of **3.37** gave [2]rotaxane **3.50·Cl** in 72% yield after preparative TLC purification (Scheme 3.18). High resolution ESI-MS ^{1}H-NMR and ROESY spectra of **3.50·Cl** confirmed the interlocked nature of the rotaxane, in particular showing through space interactions between proton signals of the mechanically bonded axle and macrocycle components of the [2]rotaxane; the hydroquinone protons and H_b, H_d, H_e (Figure 3.28 and 3.29).

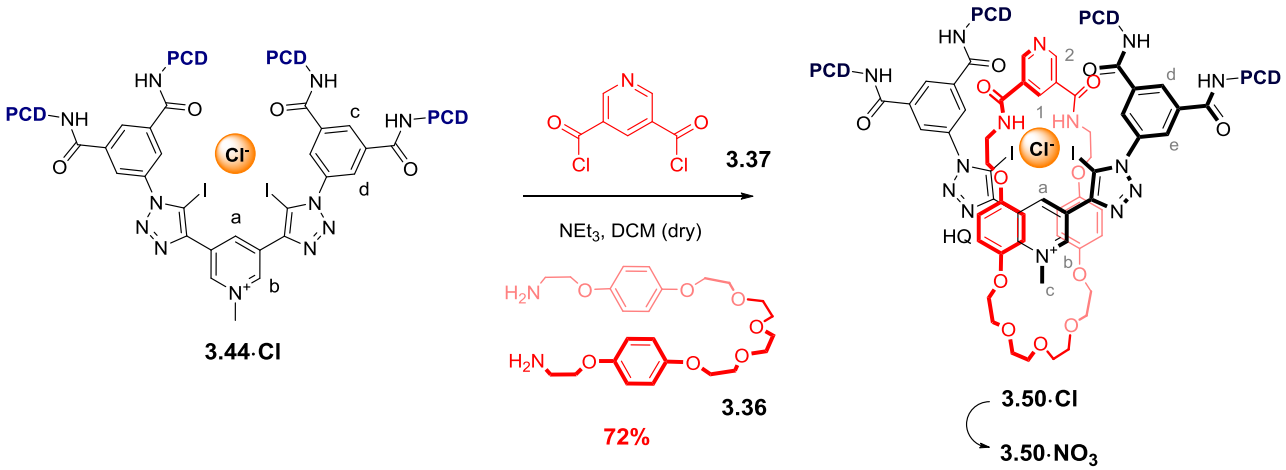

Scheme 3.18 Synthesis of XB [2]rotaxane **3.50·NO_3**.

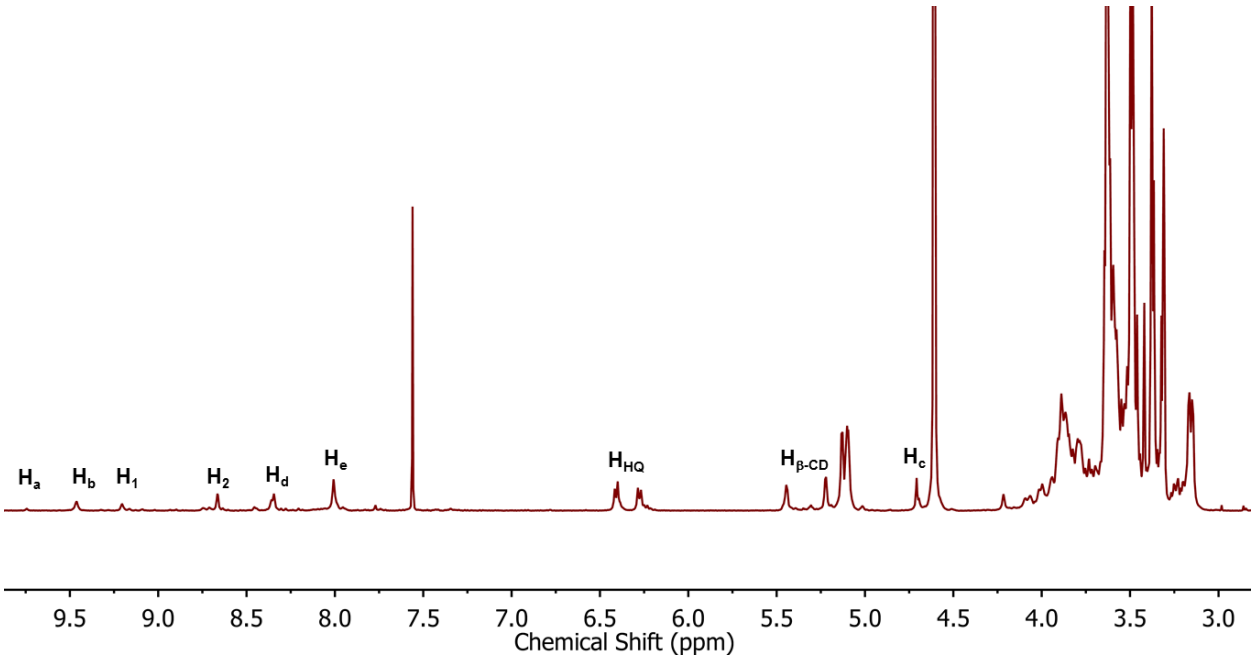

Figure 3.28 ^{1}H-NMR spectrum of [2]rotaxane **3.50·Cl** in 1:1 d_4-MeOD/ $CDCl_3$ (500MHz, 298K).

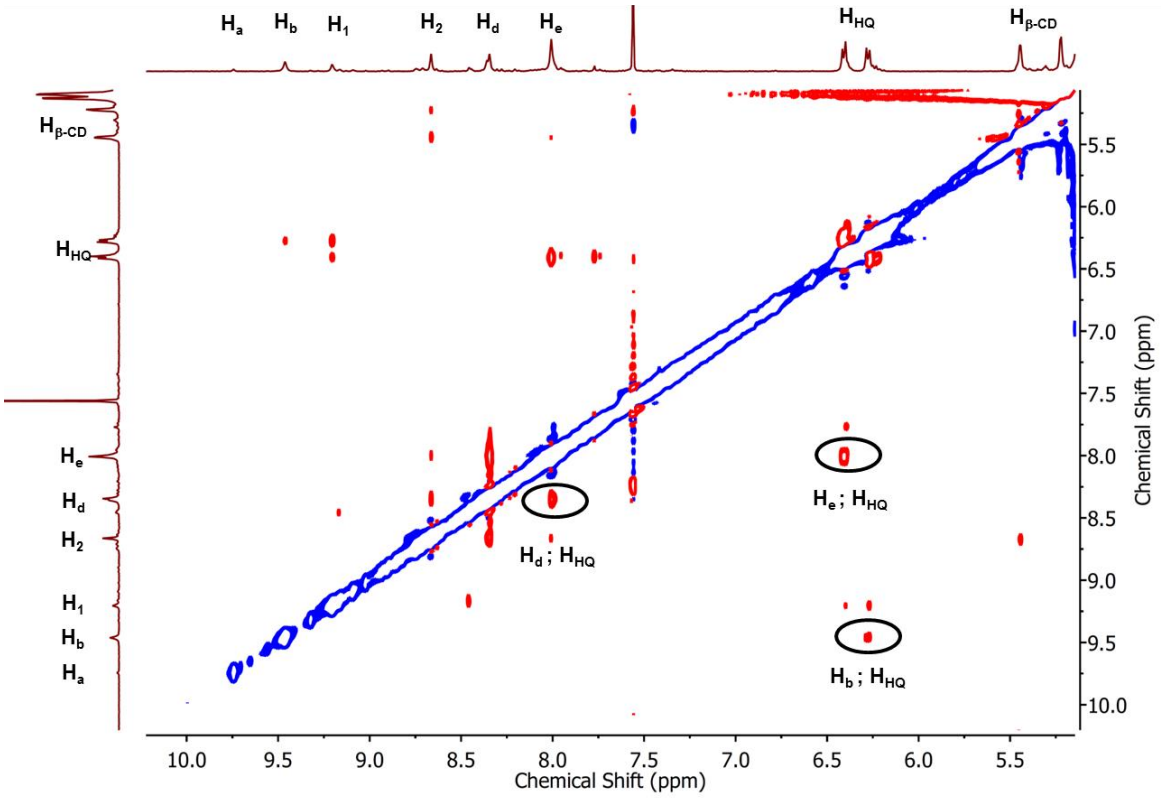

Figure 3.29 2D-ROESY spectrum of **3.50·Cl** in 1:1 d_4-MeOD/ $CDCl_3$ (500MHz, 298K).

3.9 ^{1}H-NMR spectroscopic anion recognition studies

Quantitative anion binding properties of XB **3.44·NO$_3$** were initially investigated *via* ^{1}H-NMR spectroscopic titration experiments and compared with the results of its HB analogue **3.49·NO$_3$** and the prototypical non-aromatic XB **3.51·NO$_3$** (Figure 3.30).[261, 264, 265]

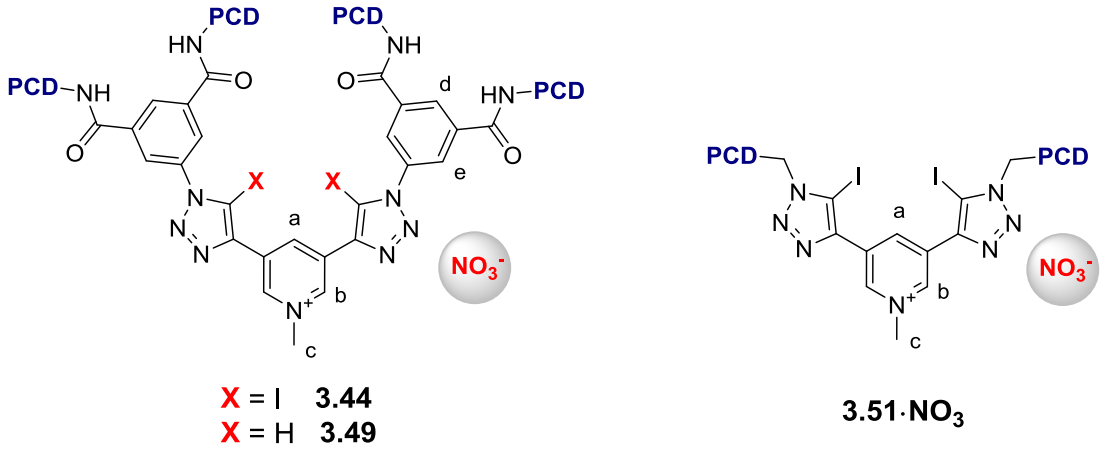

Figure 3.30 Water soluble anion acyclic host molecules.

In a typical titration procedure, a solution of anion as their sodium salt was added to a separate 1.0 mM solution of each acyclic host in D_2O, the chemical shifts of proton signals within the anion binding site (H_a) of each receptor were monitored as a function of anion concentration. In the case of **3.44·NO$_3$**, addition of NaI resulted in significant downfield shifts ($\Delta\delta$ > 0.1 ppm over 10 equivalents of anion) of the proton signals arising from the internal pyridyl proton (H_a), while the internal proton resonance (H_d) of the isophthalamide spacer showed negligible downfield shifts (Figure 3.31).

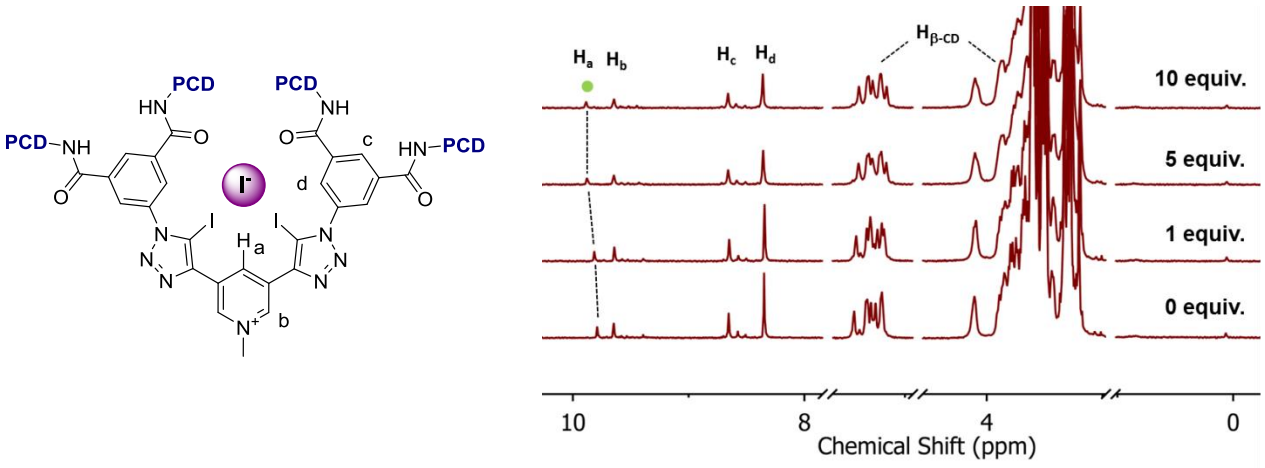

Figure 3.31 Truncated ^{1}H-NMR spectra of **3.44·NO$_3$** upon addition of NaI in D_2O (500MHz, 298K).

This indicated the iodide anion is bound preferentially to the bis-iodotriazole XB cleft with no interaction to the polarised NH bis-amide binding sites. Similar changes were observed in the case of HB analogue **3.49·NO$_3$** in which iodide binding occurred in the charge assisted CH triazole binding cleft as evidenced by significant downfield shifts of the internal pyridyl proton (H_a) and concomitant shifts of with the triazole proton (H_{trz}).

Table 3.5 Anion association constants (M^{-1}) of **3.44·NO$_3$**, **3.49·NO$_3$**, **3.51·NO$_3$** in D_2O.[a]

Anions	Anion Association Constants (M^{-1})		
	3.44•NO$_3$	**3.49•NO$_3$**	**3.51•NO$_3$**
Cl$^-$	13	9	-
Br$^-$	37	17	15
I$^-$	679	46	40

[a] Anions added as sodium salts, errors (±) are less than 10%, 1:1 stoichiometric association constants determined by WinEQNMR2 software, monitoring an internal pyridyl proton (H_a) for all receptors (T = 298K, 500 MHz).

WinEQNMR2[253] analysis of the downfield perturbations of the internal pyridyl proton (H_a) revealed 1:1 stoichiometric association constants (Table 3.5). XB axle **3.44·NO$_3$** displayed modest binding affinity for Cl^- (K_a = 13 M^{-1}) and Br^- (K_a = 37 M^{-1}), but exhibited remarkably strong binding for iodide (K_a = 679 M^{-1}). This halide binding selectivity follows anion hydrophobicity or Hofmeister bias where the least hydrated halide anion is bound more strongly. By simply replacing two iodine atoms of the 3,5-bis-(iodotriazole)pyridinium motif with two hydrogen atoms, HB axle **3.49·NO$_3$** exhibited an attenuated iodide association constant (K_a = 46 M^{-1}), an order of magnitude smaller than that of **3.44·NO$_3$**. Notably, **3.44·NO$_3$** displayed highly selective iodide binding in water and demonstrated the ability to discriminate amongst the halides ($K_{iodide}/K_{bromide}$ = 18 and $K_{iodide}/K_{chloride}$ = 52), whereas the prototypical XB axle **3.51·NO$_3$** and HB axle **3.49·NO$_3$** showed only modest anion discrimination.

Table 3.6 Iodide association constants (M^{-1}) of **3.44·NO_3** in different solvents[a].

Solvent	Anion Association Constants (M^{-1})
D_2O	679
1:3 D_2O/ d_4-MeOD	-[b]
1:1 D_2O/ d_4-MeOD	597
3:1 D_2O/ d_4-MeOD	911
d_4-MeOD	1134

[a] Iodide added as sodium salt, errors (±) are less than 10%, 1:1 stoichiometric association constants determined by WinEQNMR2 software, monitoring an internal pyridyl proton (H_a) for all receptors (T = 298K, 500 MHz). [b] Host was not soluble in this solvent mixture.

The solubility properties of **3.44·NO_3** allowed for iodide anion binding studies to be undertaken in *d_4*-MeOD as well as in mixtures of D_2O and *d_4*-MeOD. The solubility of the sodium halides however restricted investigations to NaI only. As expected based on the solvent's polarity, **3.44·NO_3** forms stronger association with iodide in *d_4*-MeOD compared to D_2O. Increasing the percentage of D_2O in MeOD resulted in decreasing K_a values (Table 3.6). Surprisingly, the 1:1 D_2O/ d_4-MeOD mixture appears to be more competitive than D_2O which is difficult to rationalize. However this oberservation is consistent Hunter's previous findings of enhanced solvation abilities of mixed hydrogen bonding solvent systems and reconciled by the augmented solvent-solute interactions.[266]

3.10 Thermodynamics of anion binding in water

The thermodynamic parameters of host-guest interactions between anions and the acyclic neutral pyridine **3.42,** pyridine *N*-oxide **3.43** and pyridinium **3.44·NO_3** hosts were determined by isothermal titration calorimetric (ITC) analysis (Table 3.7).

Table 3.7 Association constants (K_a) and thermodynamic parameters (ΔH, TΔS, and ΔG) of neutral **3.42**, N-oxide **3.43**, and axle **3.44·NO_3** hosts to various anions in water.

	K_a [a] [M^{-1}]	ΔH [kJ mol^{-1}]	TΔS [kJ mol^{-1}]	ΔG [kJ mol^{-1}]
I^-				
3.42	268	-13.1	+0.7	-13.8
3.43	309	-11.2	+3.0	-14.2
3.44·NO_3	806	-11.7	+5.0	-16.7
ClO_4^-				
3.42	197	-18.7	-5.6	-13.1
3.43	93	-36.3	-25.0	-11.3
3.44·NO_3	121	-40.0	-28.1	-11.9
ReO_4^-				
3.42	312	-44.1	-29.9	-14.2
3.43	262	-42.5	-28.7	-13.8
3.44·NO_3	769	-37.4	-20.9	-16.5
IO_4^-				
3.42	1060	-10.2	+7.1	-17.3
3.43	1630	-8.1	+10.3	-18.4
3.44·NO_3	1730	-17.5	+1.1	-18.6
SCN^-				
3.42	131	-18.8	-6.7	-12.1
3.43	202	-18.1	-4.9	-13.2
3.44·NO_3	288	-17.3	-3.2	-14.1

[a] values obtained by repeats at least in duplicate and standard deviation less than 10%.

With the exception of ClO_4^- the 3,5-bis-iodotriazole pyridinium receptor **3.44·NO_3** bound anions with the strongest affinities in comparison to the neutral pyridine and pyridine N-oxide analogues, as predicted for more favourable charge assisted XB-anion interactions.

For all XB receptors anion binding is driven by a significant favourable enthalpic contribution which is consistent with strong XB-anion interactions. It is noteworthy that for all three XB systems I^- and IO_4^- binding are also entropically driven; in contrast however, binding of ClO_4^-, ReO_4^- and SCN^- are all entropically disfavoured. All three hosts also demonstrate effective discrimination between tetrahedral anions with increasing affinity in the order; ClO_4^- < ReO_4^- < IO_4^-, with an impressively high association constant of K_a = 1730 M^{-1} observed between IO_4^- and **3.44·NO_3**.

Interestingly, the pyridine **3.42** receptor exhibited a larger affinity for ClO_4^- in comparison to the pyridinium **3.44·NO_3** and pyridine N-oxide **3.43** hosts. The superior binding of ClO_4^- to this neutral host is tentatively postulated to be due to the likelihood that the XB binding cleft of **3.42** is the least hydrated amongst the three hosts. The poorer host solvation resulting in an enhancement of affinity for highly hydrophobic anions, such as ClO_4^-, is supported by previously reported systems such as Bubusuril by Sindelar,[68] and Gibb's octacarboxylate cavitand.[80]

Table 3.8 Association constants (K_a) and thermodynamic parameters (ΔH, TΔS, and ΔG) of axle **3.44·NO_3** and rotaxane **3.51·NO_3** to various anions in water.[a]

	K_a [M^{-1}]	ΔH [kJ mol^{-1}]	TΔS [kJ mol^{-1}]	ΔG [kJ mol^{-1}]
I^-				
3.44·NO_3	806	-11.7	+5.0	-16.7
3.51·NO_3	1250	-13.0	+4.7	-17.7
ClO_4^-				
3.44·NO_3	121	-40.0	-28.1	-11.9
3.51·NO_3	478	-10.7	+4.6	-15.3
ReO_4^-				
3.44·NO_3	769	-37.4	-20.9	-16.5
3.51·NO_3	1240	-19.3	-1.6	-17.7
IO_4^-				
3.44·NO_3	1730	-17.5	+1.1	-18.6
3.51·NO_3	505	-17.7	-2.2	-15.5
SCN^-				
3.44·NO_3	288	-17.3	-3.2	-14.1
3.51·NO_3	222	-20.2	-6.8	-13.4

[a] values obtained by repeats at least in duplicate and standard deviation less than 10%.

ITC investigations were also carried out with rotaxane **3.51·NO_3**, which revealed the enhancement of I^-, ClO_4^-, and ReO_4^- binding affinity compared to its free axle host **3.44·NO_3** (Table 3.8). The stronger iodide association by the rotaxane relative to the acyclic receptor is accompanied by an increased exothermic term, highlighting the more favourable anion complexation by virtue of the three dimensional interlocked binding cavity. Interestingly the opposite was observed for ClO_4^-, and ReO_4^- in which binding to the rotaxane host resulted in a significantly reduced exothermic contribution. Hence the greater affinities observed for ClO_4^-, and ReO_4^- are mainly driven by entropy. Larger oxoanions such as IO_4^- and linear SCN^- bound to rotaxane **3.51·NO_3** less strongly than the free axle **3.44·NO_3**, suggesting poor size and shape complementarity between host-guest complex. The reasons for the contrasting anion selectivity trends of the rotaxane **3.51·NO_3** ($I^- \approx ReO_4^- > IO_4^- > ClO_4^- > SCN^-$) versus the acyclic axle component **3.44·NO_3** ($IO_4^- > I^- > ReO_4^- > SCN^- > ClO_4^-$) are difficult to elucidate and may be tentatively attributed to binding cavity geometric constraints in combination with receptor solvation.

Part III: Water Soluble Osmium (II) Anion Host Systems

XB acyclic and interlocked systems have been shown to be potent hosts for anion recognition in water, as demonstrated in Section 3.9 and 3.10. Attention now turned to the incorporation of reporter groups to allow such hosts to function as water soluble anion sensors. Of particular importance, are reporter groups exploiting photo and redox-active transition metal probes such as Re(I),[267] Ru(II),[268] and Os(II), Ir(III).[70, 269, 270]

In 2016, Beer and co-workers reported the first XB interlocked host structure capable of anion sensing in water by integrating the ruthernium(II)bipyridyl moiety into the macrocyclic component of an XB [2]rotaxane (Figure 3.32). Strong and selective iodide binding (K = 6300 M^{-1}) and a modest switching-on of the Ru(II)-MLCT emission intensity (6% enhancement) was observed with the XB host.[258]

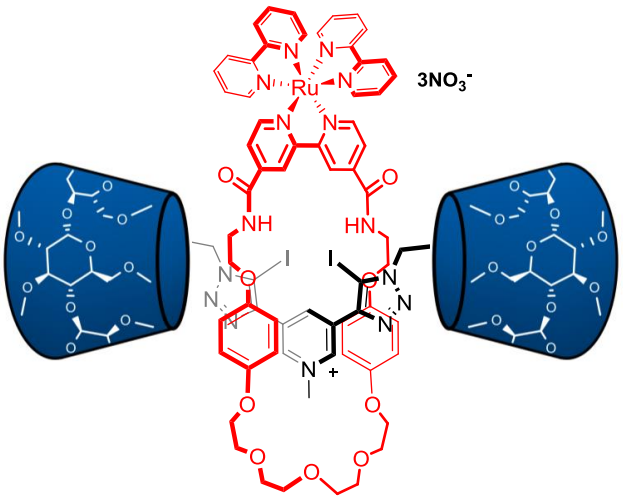

Figure 3.32 Ruthenium(II) XB [2]rotaxane.

The anion recognition and sensing properties of third row d^6-transition metal based anion receptors such as osmium(II) complexes is underexplored and have been mainly restricted to operating in organic solvent media. Baitalik and co-workers combined the bis-terpyridyl osmium(II) reporter group with a variety of acidic imidazole and benzimidazole motifs (Figure 3.33 and 3.34).[271-273] In the presence of basic anions such as F^- and CN^- in acetonitrile, deprotonation of the acidic imidazole/ benzimidazole N–H protons resulted in perturbations of the MLCT absorption spectra and quenching of luminescence intensities. Lahiri and co-workers exploited the bis-bipyridyl osmium(II) luminophore containing imidazole and pyrazole organic scaffolds for selective sensing of fluoride anion in acetonitrile.[274, 275]

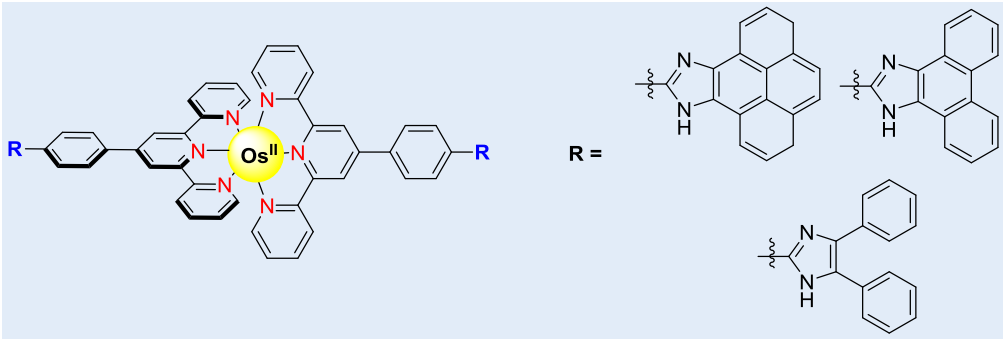

Figure 3.33 Bis-terpyridyl osmium(II) anion sensors.

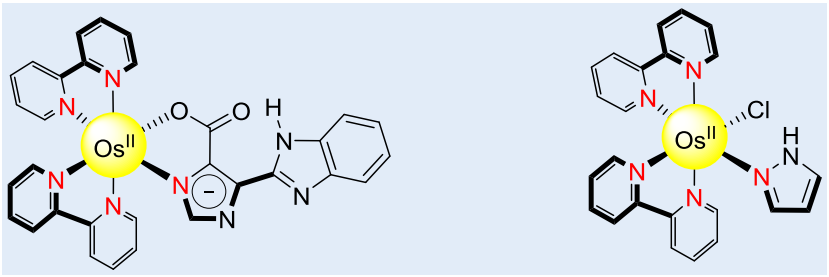

Figure 3.34 Bis-bipyridyl osmium(II) anion sensors.

Building on the promising results of XB ruthenium(II) rotaxane, a water soluble XB osmium(II) bipyridyl rotaxane and HB acyclic analogues were prepared and their anion recognition and sensing properties investigated (Figure 3.35).

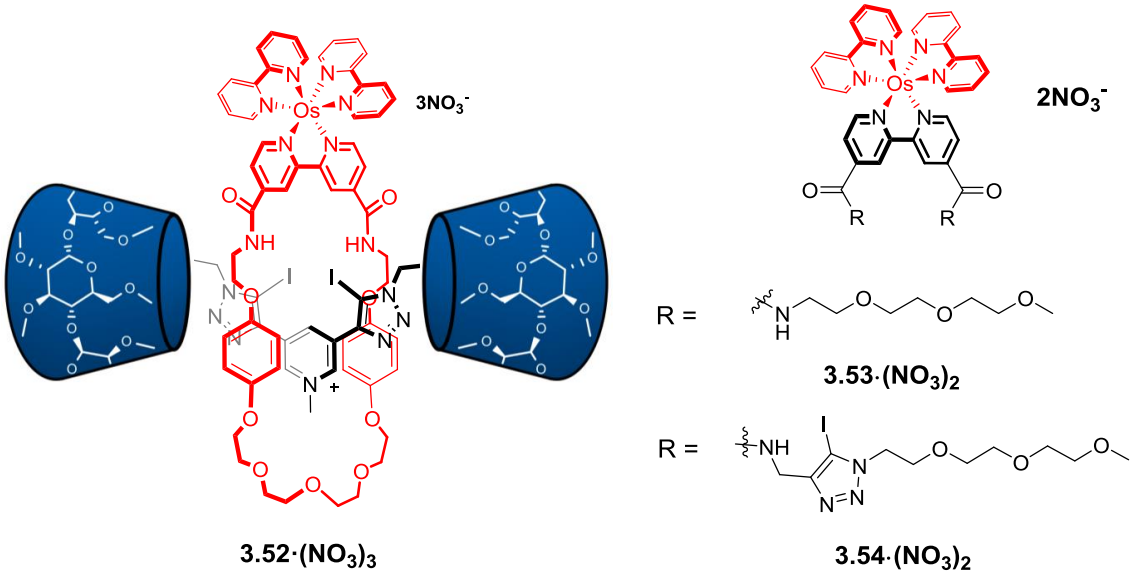

Figure 3.35 Target osmium(II)bipyridyl anion host molecules.

3.11 Synthesis and characterisations

3.11.1 Synthesis of osmium(II)bipyridyl rotaxane

The target osmium(II) bipyridyl rotaxane **3.51·$(NO_3)_3$** was prepared in two steps: *via* chloride anion template amide condensation clipping methodology, followed by coordination of the macrocyclic component with an osmium(II) bipyridyl complex. 4,4'-bischlorocarbonyl-2,2'-bipyridine **3.55** was synthesised by refluxing a suspension of the acid in dry DCM with oxalyl chloride to afford **3.55** as a pink solid in quantitative yield (Scheme 3.19).

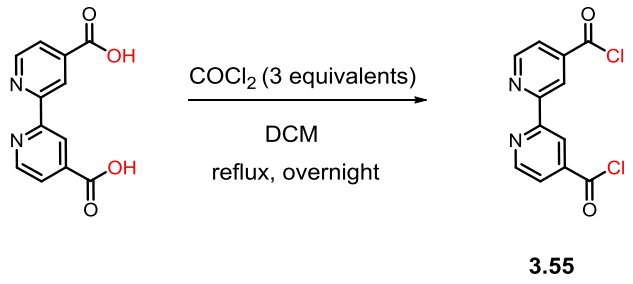

Scheme 3.19 Preparation of 4,4'-dichlorocarbonyl-2,2'-bipyridine **3.55**.

Using a modified literature procedure,[179, 258] the 3,5-bis-iodotriazole pyridinium axle **3.51·Cl** was stirred with a 10-fold excess of bis-amine macrocycle precursor **3.36** and NEt_3 in dry DCM at 0ºC. Gradual addition of acid chloride **3.55** to the reaction mixture followed by stirring for 2 hours at room temperature afforded the target XB bipyridyl [2]rotaxane **3.56·Cl** in 42% yield, after purification by preparative silica gel thin-layer chromatography and size-exclusion chromatography (Scheme 3.20).

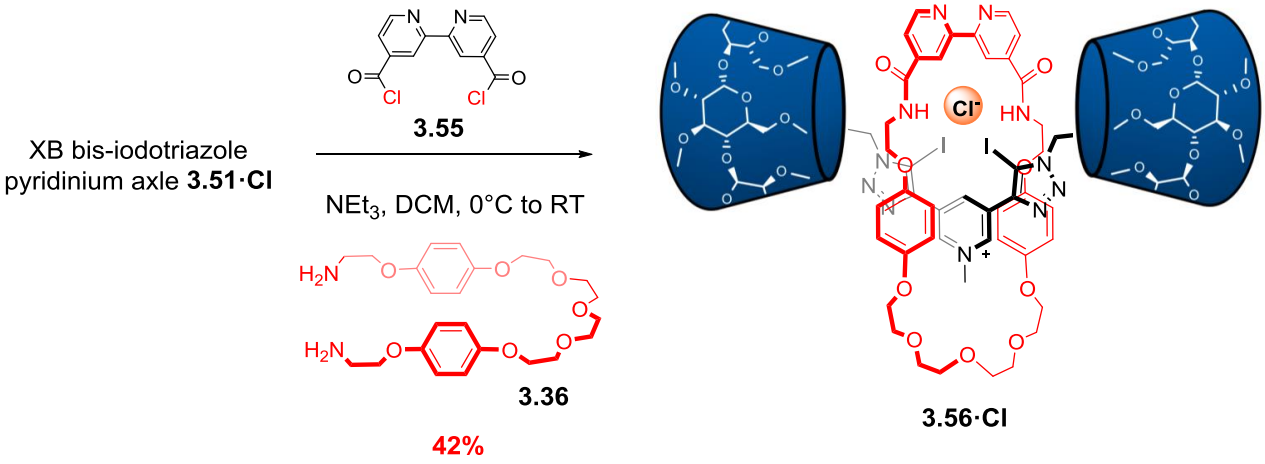

Scheme 3.20 Synthesis of XB bipyridyl [2]rotaxane **3.56·Cl**.

Stirring a solution of **3.56·Cl** with two equivalents of $Os(bipy)_2Cl_2$ in a 9:1 mixture of ethanol/H_2O gave a crude product which was purified *via* size-exclusion chromatography, and following subsequent anion exchange to the NO_3^- salt gave the target water soluble XB

Os(II)bipyridyl [2]rotaxane **3.52·$(NO_3)_3$** which was isolated in 90% yield (Scheme 3.21) and characterised by ^1H, ^{13}C-NMR spectroscopy and high resolution ESI-MS.

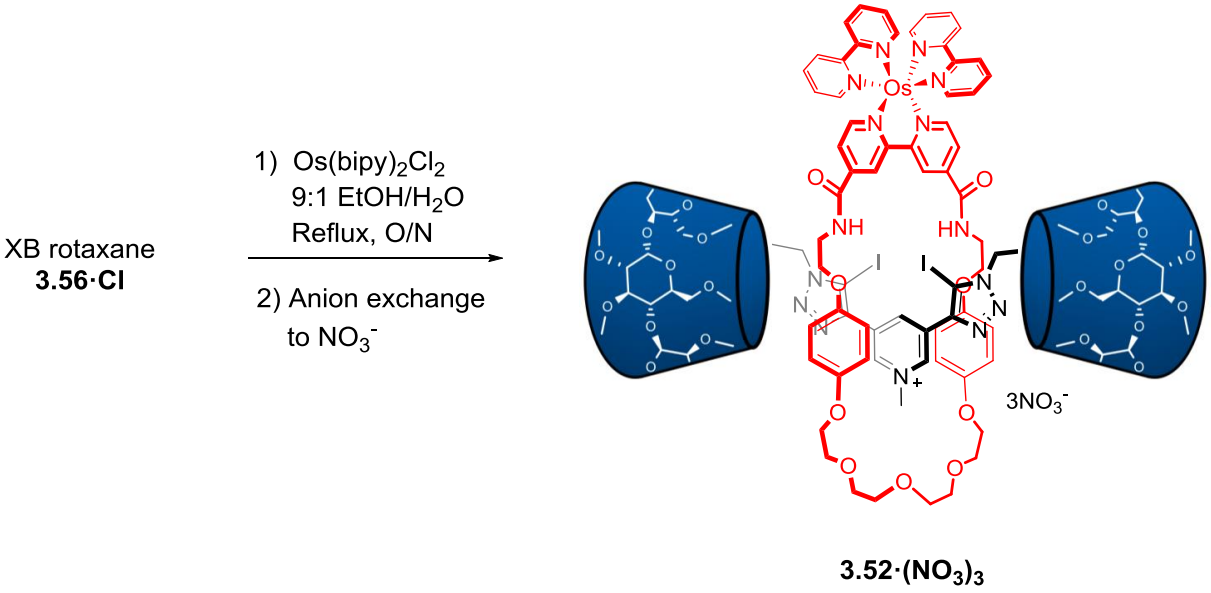

3.52·$(NO_3)_3$

Scheme 3.21 Synthesis of Os(II)bipyridyl [2]rotaxane **3.52·$(NO_3)_3$**.

The ^1H-NMR spectrum of [2]rotaxane **3.52·$(NO_3)_3$** shows similar proton resonance patterns to the analogous Ru(II)bipyridyl [2]rotaxane.[258] The interpenetration of the pyridinium bis-iodotriazole axle into the cavity of the bipyridyl macrocycle results in π–π donor and acceptor interactions, indicated by the splitting of hydroquinone protons (H_3 and H_4) for the interlocked structure (Figure 3.36 a). ^1H—^1H ROESY NMR spectroscopy also confirmed through space interactions between proton signals arising from the pyridinium motif of the axle component (H_a and H_b) and hydroquinone group in the macrocycle component (H_3 and H_4) (Figure 3.36 b).

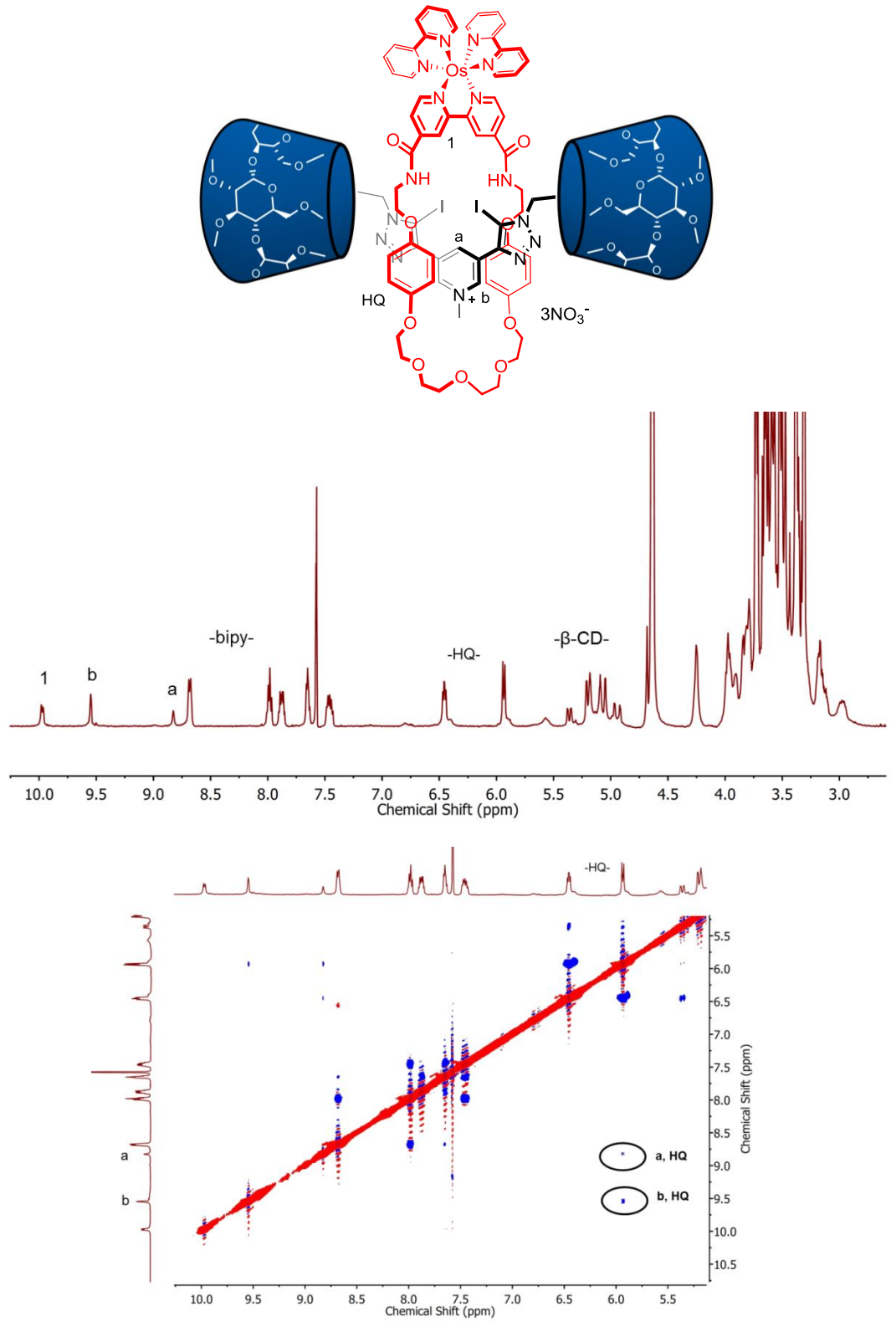

Figure 3.36 (a) ^{1}H-NMR and (b) ^{1}H—^{1}H ROESY spectrum of **3.52·$(NO_3)_3$** (1:1 $CDCl_3$/d_4-CD_3OD, 298K, 500MHz).

3.11.2 Synthesis of Osmium(II)Bipyridyl Acyclic Receptors

New water soluble osmium(II) acyclic receptors (Figure 3.37) were also synthesised.

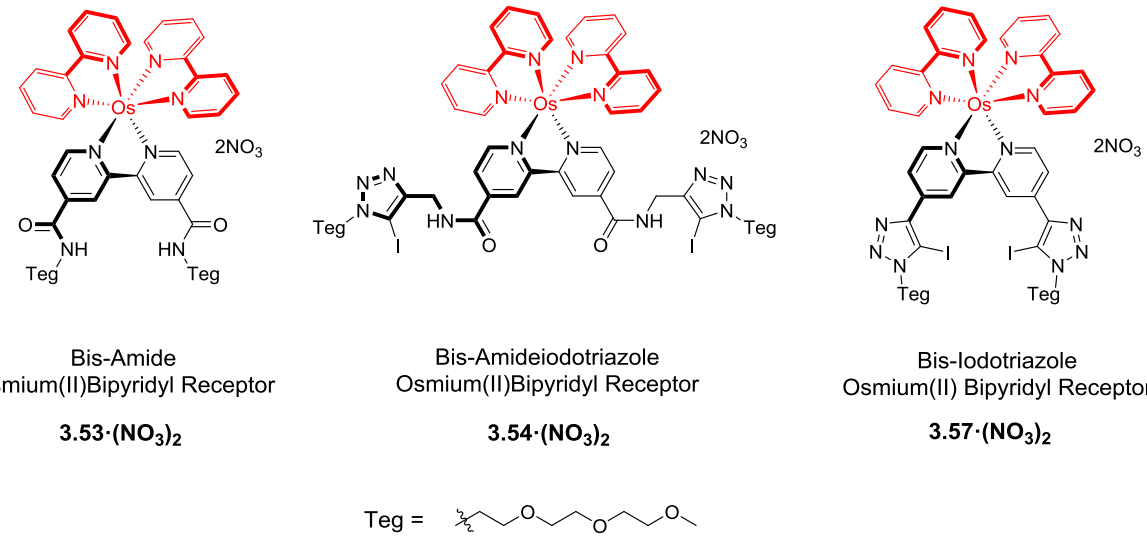

Bis-Amide Osmium(II)Bipyridyl Receptor **3.53·$(NO_3)_2$**

Bis-Amideiodotriazole Osmium(II)Bipyridyl Receptor **3.54·$(NO_3)_2$**

Bis-Iodotriazole Osmium(II) Bipyridyl Receptor **3.57·$(NO_3)_2$**

Teg =

Figure 3.37 Target osmium(II)bipyridyl based-anion receptors.

A. Synthesis of Triethyleneglycol Amine Precursor

Triethylene glycol monomethyl ether was reacted with methanesulfonyl chloride (MsCl) in DCM in the presence of diisopropyl ethylamine (DIPEA) at room temperature to afford triethylene glycol mesylate **3.58** in quantitative yield. The nucleophilic substitution (S_N2) reaction of mesylate **3.58** with NaN_3 in a mixture of methanol and water gave triethyleneglycol azide **3.59** as a colourless oil in quantitative yield. Reduction of the azide **3.59** using $LiAlH_4$ in Et_2O at 0°C provided the target amine **3.60** in 72 % yield (Scheme 3.22).

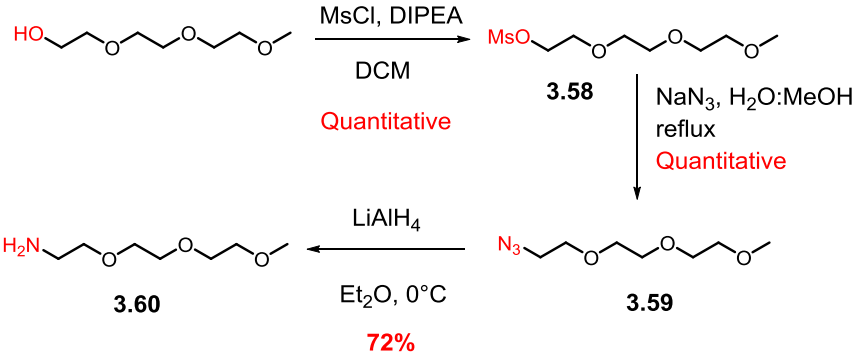

Scheme 3.22 Synthesis of triethyleneglycol amine **3.60**.

B. Synthesis of Bis-Amide Osmium(II) Bipyridyl Receptor

The bis-amide osmium(II) bipyridyl receptor **3.53·$(NO_3)_2$** was prepared as an HB receptor analogue. Condensation of dichloride **3.55** with two equivalents of triethyleneglycol amine **3.60** and NEt_3 in DCM at room temperature gave the 4,4'-bis-amide bipyridine **3.61** in 70 % yield after chromatographic purification. Metal complexation and anion exchange to the nitrate salt produced the bis-amide osmium(II) bipyridyl receptor **3.53·$(NO_3)_2$** in 89 % yield (Scheme 3.23). The ^{1}H-NMR spectra of **3.53·$(NO_3)_2$** is shown in Figure 3.38 and the receptor was also characterised by ^{13}C-NMR and ESI-MS.

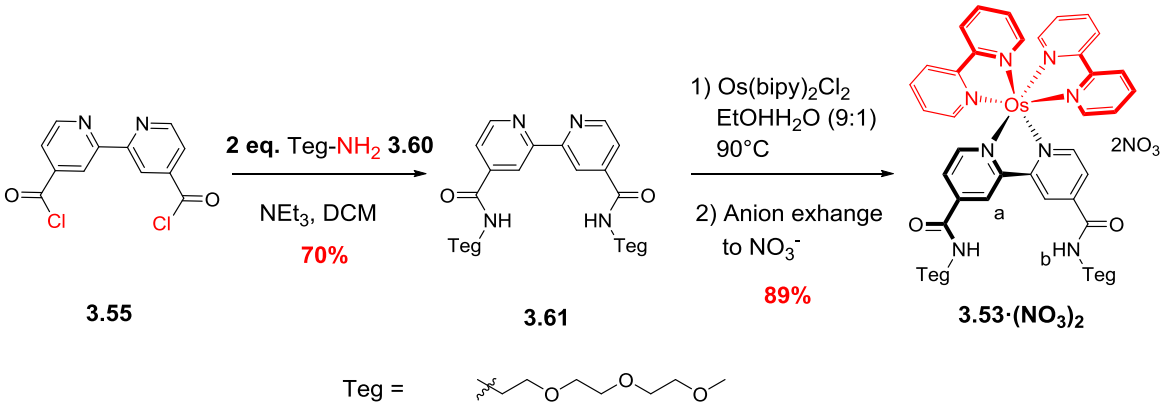

Scheme 3.23 Synthesis of bis-amide osmium(II) bipyridyl receptor **3.53·$(NO_3)_2$**.

D. Attempts Towards Synthesis of Bis-Iodotriazole Osmium(II) Bipyridyl Receptor

Attention turned to covalently linking the iodotriazole moiety directly to the bipyridyl metal chelating motif. To this end a Sonogashira cross coupling reaction of 4,4'-dibromo-2,2'-bipyridine with TMS-acetylene in the presence of $Pd(PPh_3)_2Cl_2$, CuI, and NEt_3 in THF afforded the bis-TMS protected alkyne **3.68** in 72% yield. Iodination of **3.68** with *N*-iodosuccinimide in the presence of $AgNO_3$ was carried out in acetone/water to give 4,4'-bis(iodoethynyl)-2,2'-bipyridine **3.69** as a yellow solid in 30% yield (Scheme 3.26).

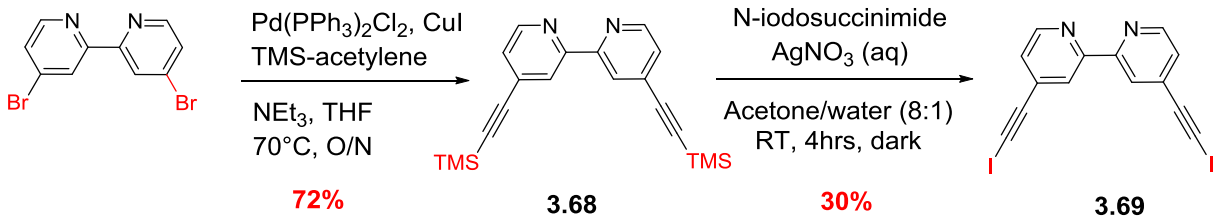

Scheme 3.26 Synthesis of 4,4'-bis(iodoethynyl)-2,2'-bipyridine **3.69**.

The compound **3.69** was found to be poorly soluble in a range of organic solvents To circumvent this, the subsequent CuAAC reaction between 4,4'-bis(iodoethynyl)-2,2'-bipyridine **3.69** and triethyleneglycol azide **3.59** was achieved using an excess of CuI (1.4 equivalents) and TBTA in DMF at room temperature. The crude product was washed with a basic aqueous solution of EDTA to afford the bis-iodotriazole-bipyridine **3.70** in 50% yield (Scheme 3.27).

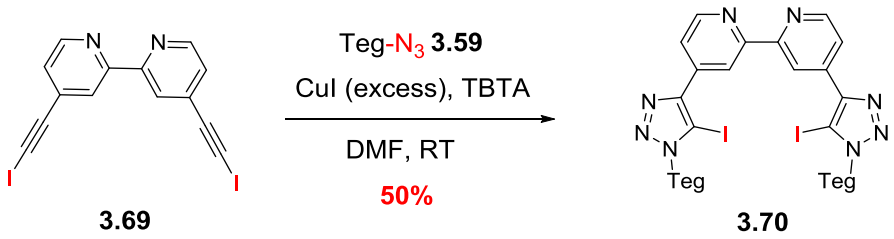

Scheme 3.27 Synthesis of 4,4'-bis-iodotriazole-2,2'-bipyridine **3.70**.

The metal complexation of **3.70** with an excess of $Os(bipy)_2Cl_2$ employing the reaction conditions described in Scheme 3.28 proved to be challenging and did not afford the desired product. The more labile $Os(bipy)_2(NO_3)_2$, prepared *via* a salt metathesis reaction between $Os(bipy)_2Cl_2$ and $AgNO_3$, was used instead (Scheme 3.28); however, only decomposition of starting materials was observed. The poor coordinating power of the bipyridyl ligand in **3.70**

due to the highly electron withdrawing nature of the iodotriazole substituents may be responsible for the failed metal complexation reactions.

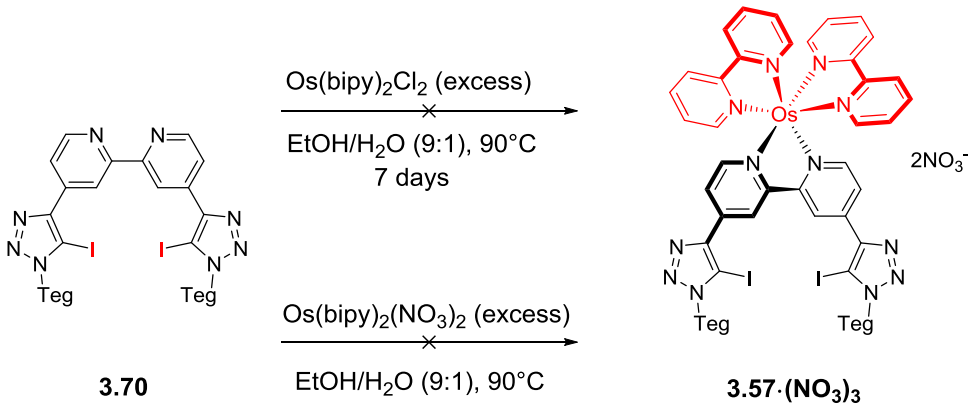

Scheme 3.28 Attempted syntheses of **3.57·$(NO_3)_2$**.

3.12 ^{1}H-NMR anion recognition experiments in water

The quantitative anion binding properties of rotaxane **3.52·$(NO_3)_3$** were initially investigated using ^{1}H-NMR spectroscopic titration experiments. Increasing quantities of halide anions as their sodium salts were added to a solution of XB [2]rotaxane **3.52·$(NO_3)_3$** (1.0 mM) in D_2O and perturbations of proton resonances (H_1, H_a, H_b) within the interlocked anion binding cavity were monitored (Figure 3.39). Using iodide as an example, addition of the halide anion to a solution of rotaxane host **3.52·$(NO_3)_3$** caused notable downfield shifts of the external axle pyridinium proton (H_b) concomitant with upfield shifts of the internal axle pyridinium proton (H_a) and the internal macrocycle bipyridyl proton (H_1). This is indicative of the halide being encapsulated within the interlocked host binding cavity formed between the axle and macrocycle components, *via* chelating XB interactions from the bidentate 3,5-bis-iodotriazole pyridinium unit and HB interactions from the bis-amide bipyridyl macrocyclic component. Additionally, further splitting of hydroquinone protons suggested conformation changes in the rotaxane in order to accommodate the iodide guest during the anion binding event.

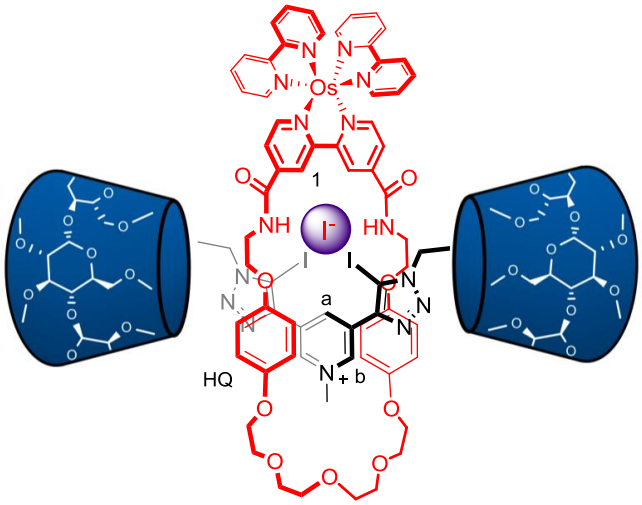

3.52·I(X)$_2$

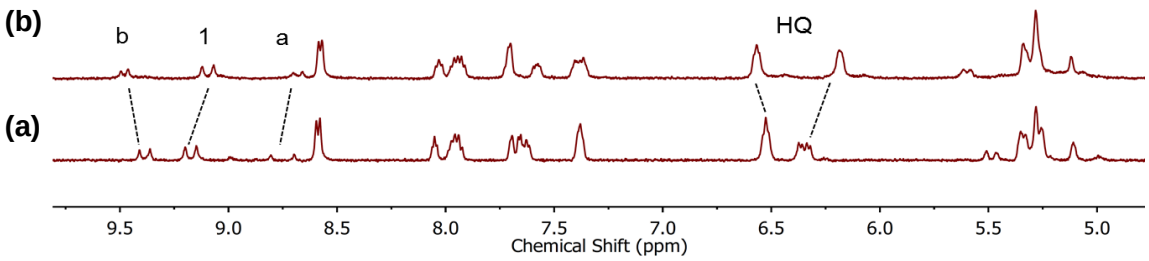

Figure 3.39 Partial ^{1}H-NMR spectrum of (a) **3.52·$(NO_3)_2$** and (b) **3.52·$(NO_3)_2$** in the presence of 10 equivalents of NaI (D_2O, 298K, 500 MHz).

By monitoring the external axle pyridinium proton (H_b), anion binding titration isotherms of **3.52·$(NO_3)_3$** revealed the largest chemical shift perturbations upon addition of NaI and the smallest change observed for the titration with NaCl (Figure 3.40). WinEQNMR2 analysis[253] of the titration data determined 1:1 stoichiometric host-guest association constants summarised in Table 3.9, together with quantitative data for the Ru(bipy)$_2$ rotaxane analogue.

Table 3.9 Association constants (M^{-1}) in D_2O at 298 K.

Anion	K_a (M^{-1}) in D_2O	
	Os(II) rotaxane 3.52·$(NO_3)_3$	Ru(II) rotaxane·$(NO_3)_3$
Cl^-	163	190
Br^-	1468	1020
I^-	$>10^4$	6300

[a] Calculated using WinEQNMR2 monitoring the chemical shift data of external pyridine proton (H_b) ; estimated standard errors are less than 10% (298 K).

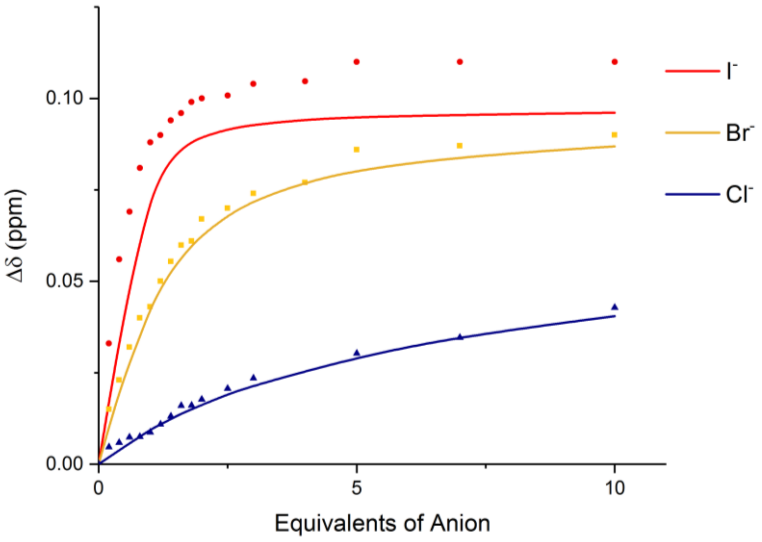

Figure 3.40 Chemical shift changes of H_b within rotaxane **3.52·$(NO_3)_3$** as a function of anion equivalents.

The Os(II)bipyridyl [2]rotaxane **3.52·$(NO_3)_3$** displayed high affinity for iodide ($K_a > 10^4$ M^{-1}) with remarkable selectivity over bromide (K_a = 6300 M^{-1}), and chloride (K_a = 163 M^{-1}) in pure D_2O.[79, 260, 276] Notably, the Os(II)bipyridyl [2]rotaxane **3.52·$(NO_3)_3$** exhibited superior iodide and bromide binding relative to the previously reported Ru(II) bipyridyl [2]rotaxane analogue (Figure 3.32) by Beer and co-workers. This observation is consistent with previous reports by Beer and co-workers demonstrating the enhancement of dihydrogen phosphate binding in d_6-DMSO using a bimetallic Os(II) complex.[277] Furthermore in comparison to the acyclic osmium(II) bipyridyl bis-amide **3.53·$(NO_3)_2$** and did not bind any halides studied under these conditions, highlighting the necessity of XB interactions in the recognition of anionic species in aqueous media.

3.13 Isothermal Titration Calorimetric (ITC) Analysis

The anion binding affinity of Os(II)bipyridyl [2]rotaxane **3.52·$(NO_3)_3$** in water for bromide and iodide was also quantified by using isothermal titration calorimetry (ITC) (Figure 3.41).

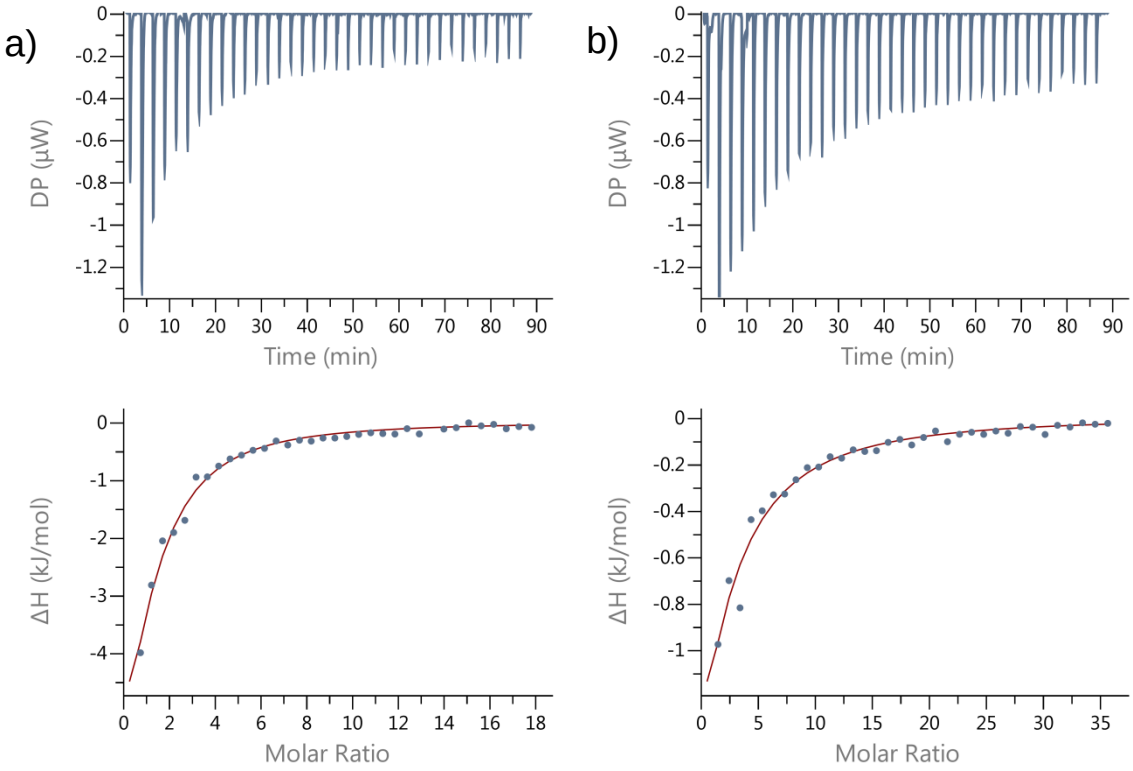

Figure 3.41 Anion binding isotherm from ITC analysis of **3.52·$(NO_3)_3$** titrated with a) iodide and b) bromide ([host] = 0.5×10^{-3} M, [guest] = $5.0\ 10^{-2}$ M).

Table 3.10 Association constants and thermodynamic parameters determined for **3.52·(NO$_3$)$_3$** with NaBr and NaI in H_2O at 298 K.

Anion	Rotaxane 3.52·(NO$_3$)$_3$	
	Br$^-$	**I$^-$**
K_a (M^{-1})	1739	13495
ΔG (kJ/mol)	-18.5	-23.6
ΔH (kJ/mol)	-8.36	-11.9
TΔS (kJ/mol)	10.2	11.7

Importantly, the thermodynamic anion binding parameters shown in Table 3.13 reveal, in agreement with the ^{1}H NMR anion binding data (Table 3.10), that the rotaxane **3.52·(NO$_3$)$_3$** binds both halides and that binding is driven enthalpically with a favourable entropic contribution. The enthalpic term is attributed to the formation of favourable XB-anion interactions whilst the entropic term is throught to derive from the release of water from the highly hydrated tricationic binding site.

3.14 Preliminary Luminescence anion-sensing investigations

Characteristic MLCT absorption bands for the tris(bipyridyl)osmium(II)chromophore were observed in the UV-visible spectrum of [2]rotaxane **3.52·$(NO_3)_3$** at 452 nm in water and 443 nm in MeCN (Figure 3.43). In deoxygenated water, excitation of the Os-centred MLCT absorption wavelength gave no characteristic MLCT emission in the range of 500-800 nm, presumably due to luminescence emission quenching in the presence of water. This assumption was corroborated by observing 75% MLCT emission quenching, over addition of 50 equivalents of water in to a solution of [2]rotaxane **3.52·$(NO_3)_3$** in MeCN (Figure 3.42). Similar quenching behaviour was also observed in both acyclic receptor **3.53·$(NO_3)_2$** and **3.54·$(NO_3)_2$** under the same conditions. These observations are consistent with the experimental results reported by Beer and co-workers, in which the emission spectrum of osmium(II)based anion receptors in acetonitrile/water (97:3) revealed the decreased emission intensities concomitant with the bathochromic shift of the Os-centred MLCT emission into the near infrared region.[278] As a result, anion sensing properties of osmium(II)bipyridyl anion hosts were alternatively carried out in acetonitrile solution.

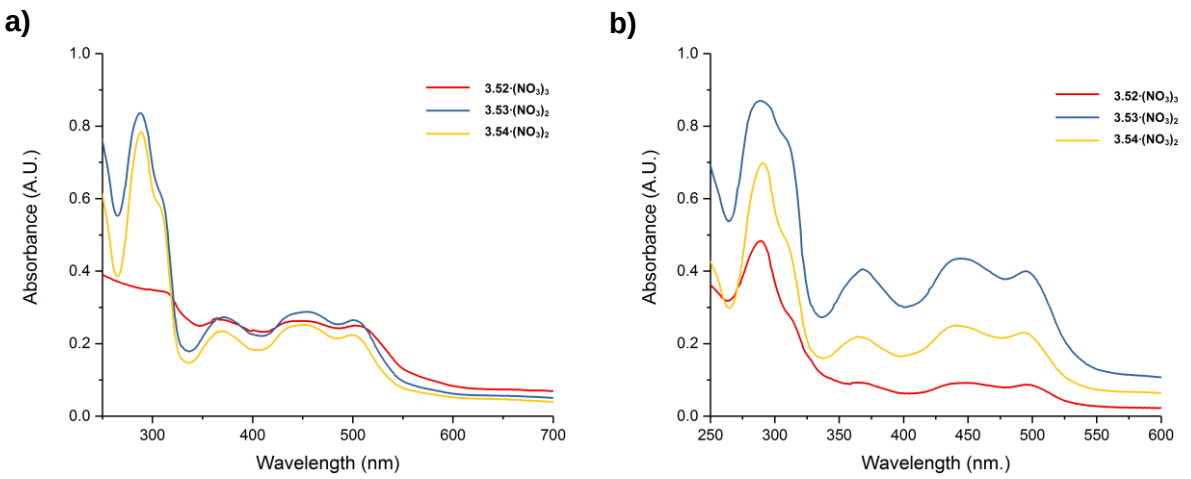

Figure 3.42 UV-visible spectra of **3.52·$(NO_3)_3$** (red), **3.53·$(NO_3)_2$** (yellow) and **3.54·$(NO_3)_2$** (blue) in a) water and b) MeCN ([host] = 1.0 ×10^{-4} M, T= 298 K).

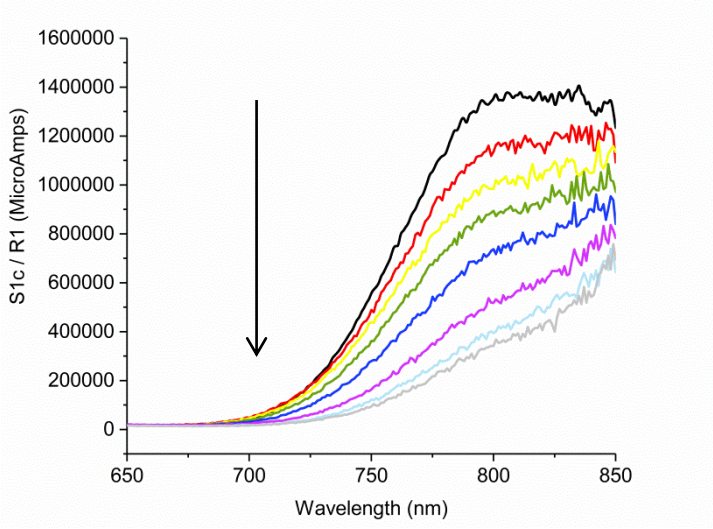

Figure 3.43 Fluorescence emission spectra of **3.52·$(NO_3)_3$** in MeCN upon gradual additions of water at an excitation wavelength = 443 nm ([host] = 0.5 ×10^{-4} M, T= 298 K).

Excitation of **3.52·$(NO_3)_3$** at wavelength = 443 nm produced an emission band in the range of 700-850 nm. Addition of halide anions as their tetrabutylammonium salts to a 0.5 ×10^{-4} M solution of rotaxane **3.52·$(NO_3)_3$** in acetonitrile resulted in a quenching of the MLCT emission intensities. Integration of the luminsecent spectra revealed a 12%, 13% (Figure 3.44), and 9% decrease in the emission intensity in the presence of excess (3mM) chloride, bromide, and iodide salt, respectively.

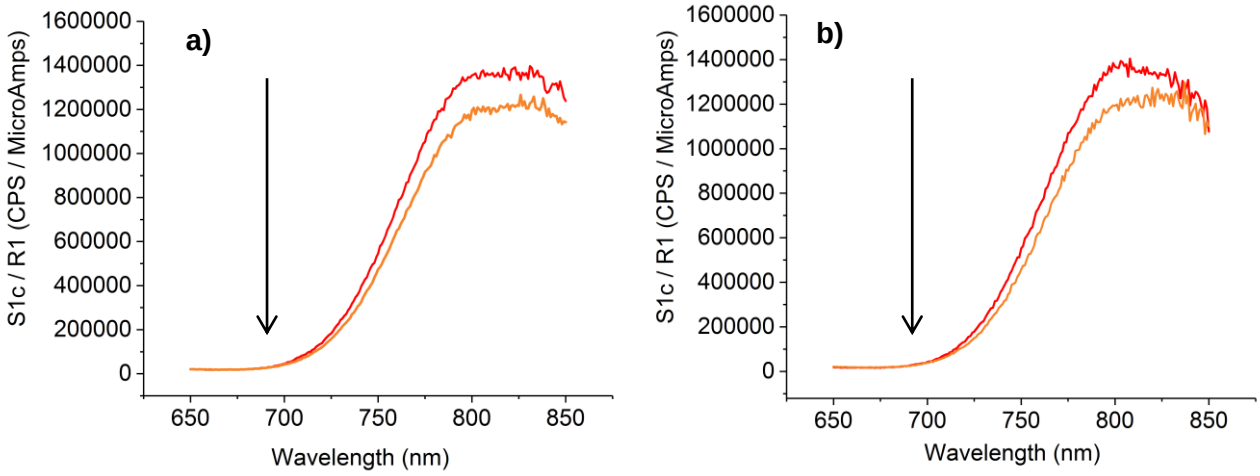

Figure 3.45 Fluorescence emission spectra of **3.52·$(NO_3)_3$** upon additions of a) TBACl and b) TBABr in MeCN at an excitation wavelength = 443 nm ([host] = 0.5 ×10^{-4} M, T= 298 K).

Table 3.11 Characteristic energy of the absorption and emission wavelength of **3.53·$(NO_3)_2$** and **3.54·$(NO_3)_2$** in the absence and presence of anions in CH_3CN.

Receptor	Enhanced Intensity (ΔI, %)
3.53·$(NO_3)_2$	
Cl^-	45
Br^-	13
I^-	1
SO_4^{2-}	152
3.54·$(NO_3)_2$	
Cl^-	82
Br^-	33
I^-	3
SO_4^{2-}	213

Analogous luminescent halide anion titration experiments with acyclic receptors **3.53·$(NO_3)_2$** and **3.54·$(NO_3)_2$** resulted a 5nm hypsochromic shift in the emission wavelength with significant enhancement of the Os-centred MLCT emission in the presence of Cl^- (Figure 3.46) and Br^-.

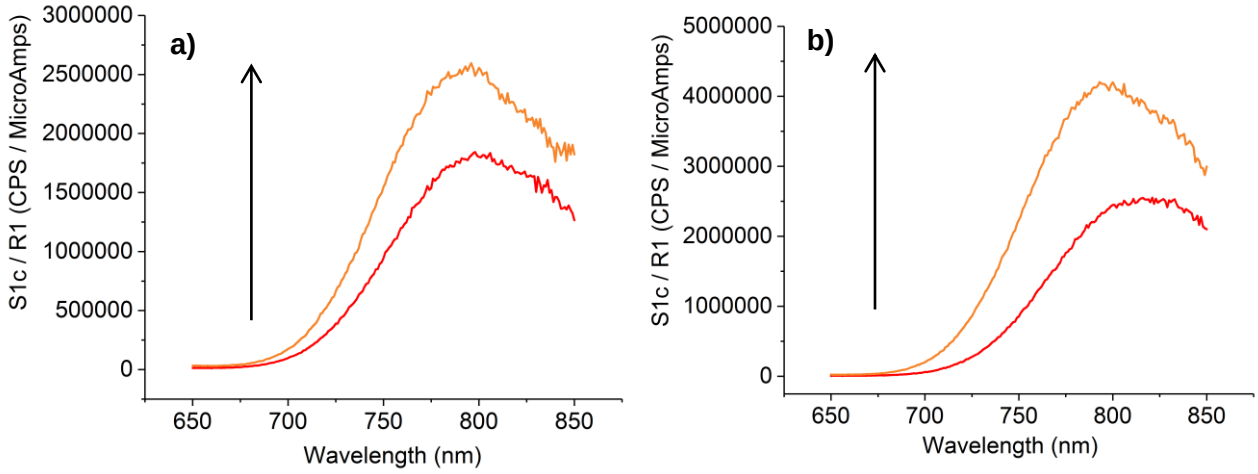

Figure 3.46 Fluorescence emission spectra of a) **3.53·$(NO_3)_2$** and b) **3.54·$(NO_3)_2$** upon additions of TBACl in MeCN at excitation wavelength = 443 nm ([host] = 0.5 ×10^{-4} M).

Addition of dianionic sulfate to **3.53·(NO$_3$)$_2$** caused a notable enhancement (152%) of the emission intensities to reach its maximum value in the presence of 2 mM sulfate, pleasingly the bis-amideiodotriazole **3.54·(NO$_3$)$_2$** even further increased the emission intensity to reach 213 % enhancement (Table 3.11, Figure 3.47).

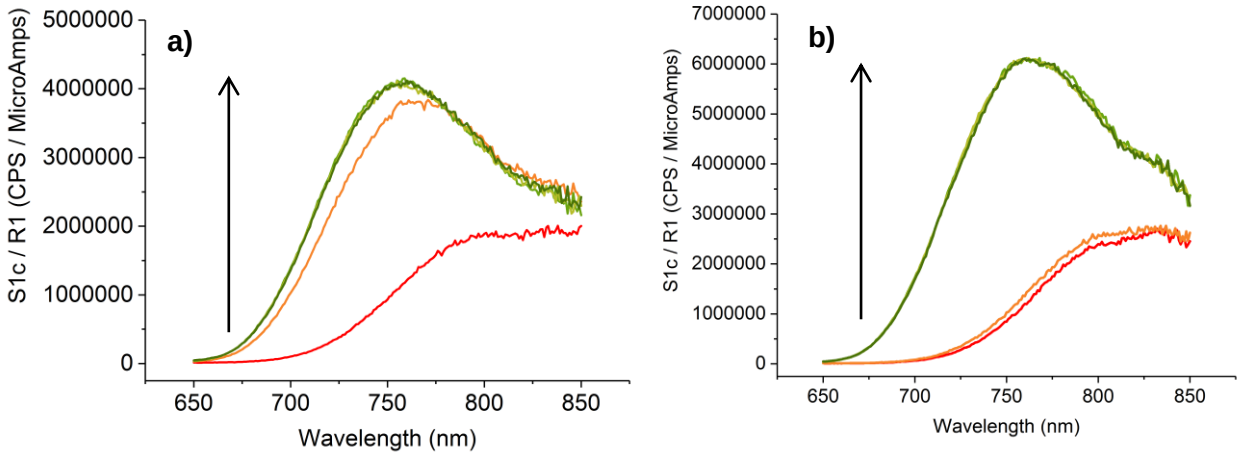

Figure 3.47 Fluorescence emission spectra of a) **3.53·(NO$_3$)$_2$** and b) **3.54·(NO$_3$)$_2$** upon additions of TBA_2SO_4 in MeCN at excitation wavelength = 443 nm ([host] = 0.5 $\times 10^{-4}$ M).

The luminescence anion sensing properties of [2]rotaxane **3.52·(NO$_3$)$_3$** and acyclic hosts **3.53·(NO$_3$)$_2$** and **3.54·(NO$_3$)$_2$** revealed a few noteworthy points to discuss. Firstly, different changes of the emission spectral profile were observed during anion binding by the rotaxane and acyclic hosts. The quenching of the MLCT emission upon halide binding by **3.52·(NO$_3$)$_3$** spectra supported the anion induced photoinduced electron transfer (PET) quenching mechanism. In contrast, anion binding by the osmium(II) acyclic receptors **3.53·(NO$_3$)$_2$** and **3.54·(NO$_3$)$_2$** exhibited notable enhancements of fluorescence emission intensities. This is postulated to be caused by the increased rigidity of the halide bound **3.53·(NO$_3$)$_2$** and **3.54·(NO$_3$)$_2$** complex in comparison to the free receptors, which decreases non-radiative vibrational relaxation pathways. Presumably, this process is more favourable than the anion-induced quenching, resulting in the observed enhancement of emission intensities. Secondly, osmium(II)based acyclic receptors displayed higher sensitivity for anion sensing compared to the [2]rotaxane host under the same conditions, despite stronger anion binding affinity observed for the rotaxane **3.52·(NO$_3$)$_3$**.

3.15 Preliminary electrochemical anion sensing

Electrochemical anion sensing studies were carried out by Robert Hein, a joint D.Phil student between the Beer group and Davis group.

Initially, the electrochemical properties of acyclic osmium(II) **3.53·$(NO_3)_2$** and **3.54·$(NO_3)_2$** were investigated in three different polar solvents including MeCN, MeOH, and H_2O. In all solvents, a well-defined one-electron oxidation at high potential characteristic of the metal-centered $Os^{2+/3+}$ redox couple was observed. Only in MeCN were three redox couples associated with the reduction of the bipyridyl ligand resolved (Figure 3.47). Moreover, the half-wave potential of the $Os^{2+/3+}$ redox couple observed in **3.54·$(NO_3)_2$** is slightly higher than that of **3.53·$(NO_3)_2$**, presumably due the electron withdrawing nature of the iodotriazole moiety.

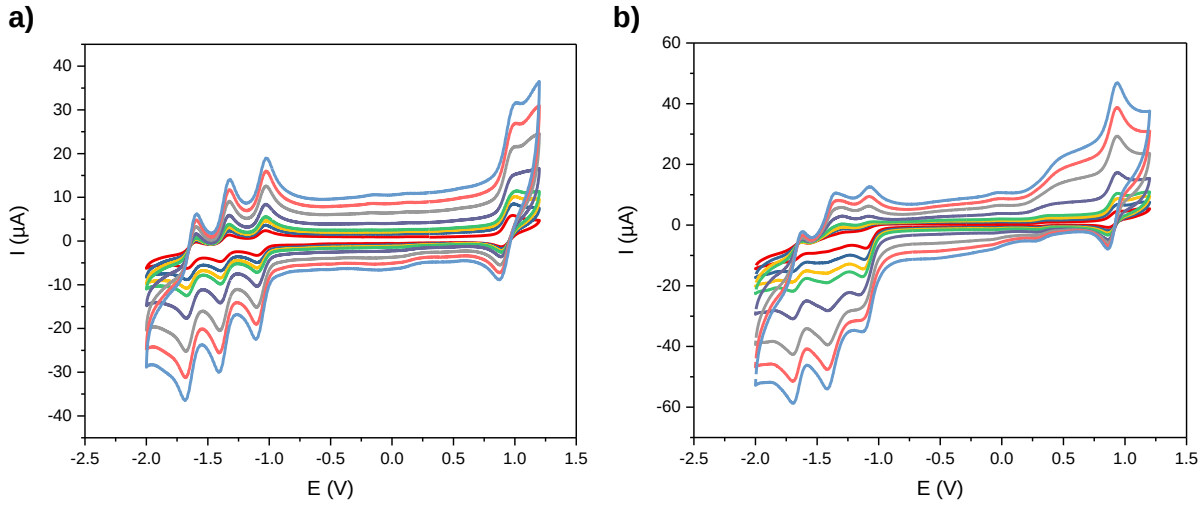

Figure 3.47 Cyclic voltammograms of 0.3 mM a) **3.52·$(NO_3)_2$** and b) **3.53·$(NO_3)_2$** in degassed MeCN containing 100 mM $TBAPF_6$ at varying scan rates.

The electrochemical reversibility of both receptors, revealing quasi-reversible one-electron redox couples with the ratio of anodic and cathodic peak currents I_{pa}/I_{pc} close to unity, allowed the exploitation of the $Os^{2+/3+}$ redox couple as an efficient transducer for anion binding. Electrochemical anion titrations of the receptors with monovalent anions (chloride and perrhenate) undertaken in a mixture of 9:1 MeCN/H_2O showed negligible cathodic shifts, while addition of the divalent anions induced larger voltammetric shifts of up to -100 mV for sulfate (Figure 3.48).

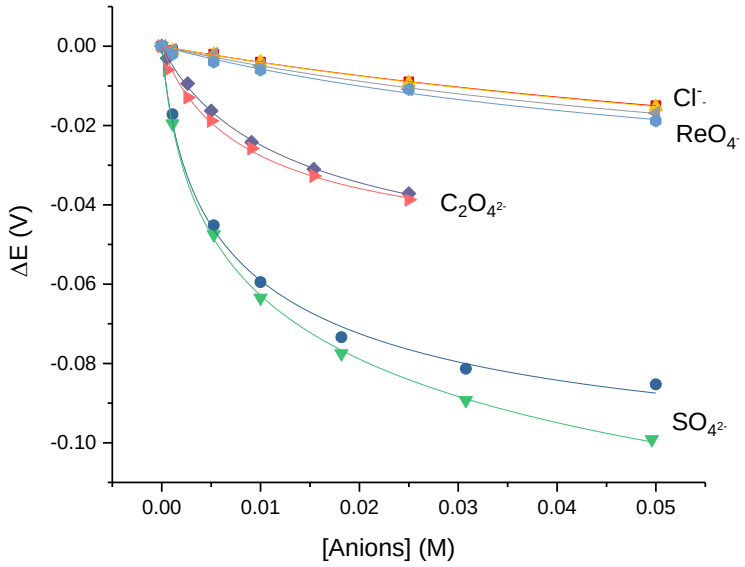

Figure 3.48 Shift of half-wave potential of $Os^{2+/3+}$ redox couple of **3.53·$(NO_3)_2$** and **3.54·$(NO_3)_2$** in the presence of various anions in 9:1 MeCN/H_2O (containing 100 mM $TBAPF_6$, [host] = 0.1 mM).

Quantitative analysis of anion titration isotherms according to equation 1 revealed that anion association constants of the oxidised receptor (K_{Ox}) with all anions are, as expected, larger than the reduced form ($K_{OX} > K_{Red}$) (Table 3.12).

$$\Delta E = -\frac{RT}{nF} * \ln\left(\frac{1+K_{Ox}*[G]}{1+K_{Red}*[G]}\right) \qquad \text{(Eq. 1)}$$

Table 3.12 Anion Association constants K_{ox}/K_{red} (M^{-1}) of **3.53·$(NO_3)_2$** and **3.54·$(NO_3)_2$** in 9:1 MeCN/H_2O.

	Cl^-	ReO_4^-	$C_2O_4^{2-}$	SO_4^{2-}
3.53·$(NO_3)_2$	19/2	19/2	216/19	1058/15
3.54·$(NO_3)_2$	25/3	31/5	303/37	1089/4

Both **3.53·$(NO_3)_2$** and **3.54·$(NO_3)_2$** exhibited a selective binding of sulfate over an equally charged oxalate ($C_2O_4^{2-}$) anion and monovalent anions. Importantly, **3.54·$(NO_3)_2$** demonstrated a more pronounced switching on (K_{Ox}/K_{Red}) of sulfate binding, compared to **3.53·$(NO_3)_2$**. An enhancement of sulfate binding of **3.54·$(NO_3)_2$** can be attributed to a

combination of an additional XB donor group and electrostatic stabilisation of the Os-bipyridyl motif from anions; further studies are currently under investigation.

The anion sensing properties of **3.54·(NO$_3$)$_2$** with sulfate were further investigated in highly competitive aqueous media with increasing percentages of water. Upon addition of sulfate, the cathodic shifts of the $Os^{2+/3+}$ redox couple were still observed in the mixture of 8:2 and 7:3 MeCN/H_2O (Figure 3.49); with decreasing anion association affinities (Table 3.13). No such changes were observed in pure aqueous media.

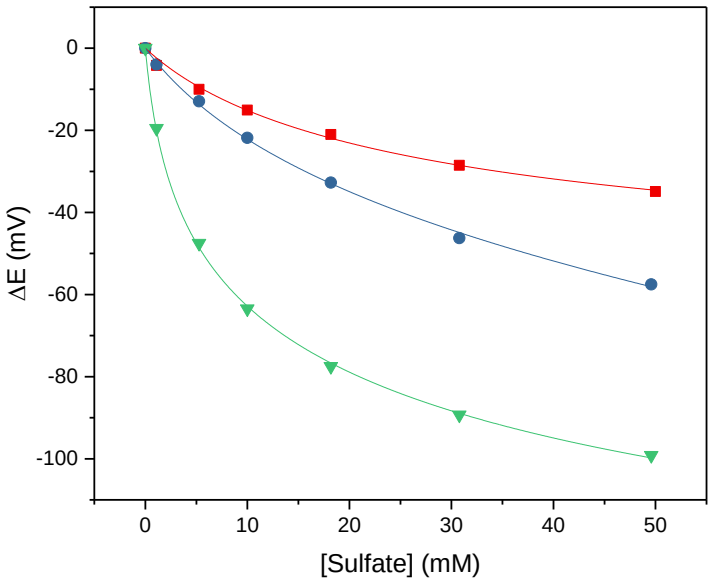

Figure 3.49 Shift of half-wave potential of $Os^{2+/3+}$ redox couple of **3.54·(NO$_3$)$_2$** in the presence of sulfate in 9:1 MeCN/H_2O (green triangles), 8:2 MeCN/H_2O (blue circles) and 7:3 MeCN/H_2O (red squares; all solvent mixtures contain 100 mM $TBAPF_6$, [host] = 0.1 mM).

Table 3.13 Sulfate binding constants K_{ox}/K_{red} (M^{-1}) of **3.54·(NO$_3$)$_2$** in various solvent mixtures (containing 100 mM $TBAPF_6$, [host] = 0.1mM).

	9:1 MeCN/H_2O	8:2 MeCN/H_2O	7:3 MeCN/H_2O
3.54·(NO$_3$)$_2$	1089/4	126/-5	101/11

3.16 Conclusion and Future Directions

To summarise, a series of permethylated β-cyclodextrin stoppered [2]rotaxanes containing various XB axles were synthesised *via* a chloride anion templated amide condensation method. The integration of an electron withdrawing perfluoroaryl group into the 3,5-(bisiodotriazole)pyridinium axle enabled a strong chloride binding affinity, allowing for the unprecedented near quantitative yield preparation of a [2]rotaxane *via* discrete anion templation. In such, a [2]rotaxane containing the perfluoroaryl spacer covalently linked XB axle exhibited strong and selective anion binding in 50% water (1:1 D_2O/ d_6-acetone), while its HB analogue failed to recognise halides under the same aqueous solvent conditions.

A novel isophthalamide azide appended bis-permethylated β-cyclodextrin synthon was exploited as a water soluble electron withdrawing aryl spacer group for the preparation of neutral water soluble XB acyclic pyridine, pyridine N-oxide and cationic pyridinium receptors. All acyclic XB receptors exhibited superior halide and oxoanion recognition in water over a prototype water soluble XB axle reported by Beer. Importantly, the thermodynamic parameters of anion binding by these hosts were elucidated *via* ITC analysis. Moreover, a monocationic [2]rotaxane containing the pyridhium axle was also synthesised for anion binding studies.

The integration of the luminescence and redox active osmium(II)bipyridyl moiety into the macrocyclic component of a [2]rotaxane was undertaken. This strategy produced an XB rotaxane capable of iodide recognition pure water, exhibiting superior anion binding affinity over its ruthernium(II) analogue. In addition simple acyclic bis-amide osmium(II) complexes have shown to be effective anion sensors capable of electrochemical sulfate sensing in aqueous media.

The work in this chapter could be expanded by increasing the rigidity and number of XB donors incorporated into the framework. Having reactive functional groups within the macrocyclic hosts allows for further post-synthetic modifications in the construction of complex water soluble anion hosts (Figure 3.50).

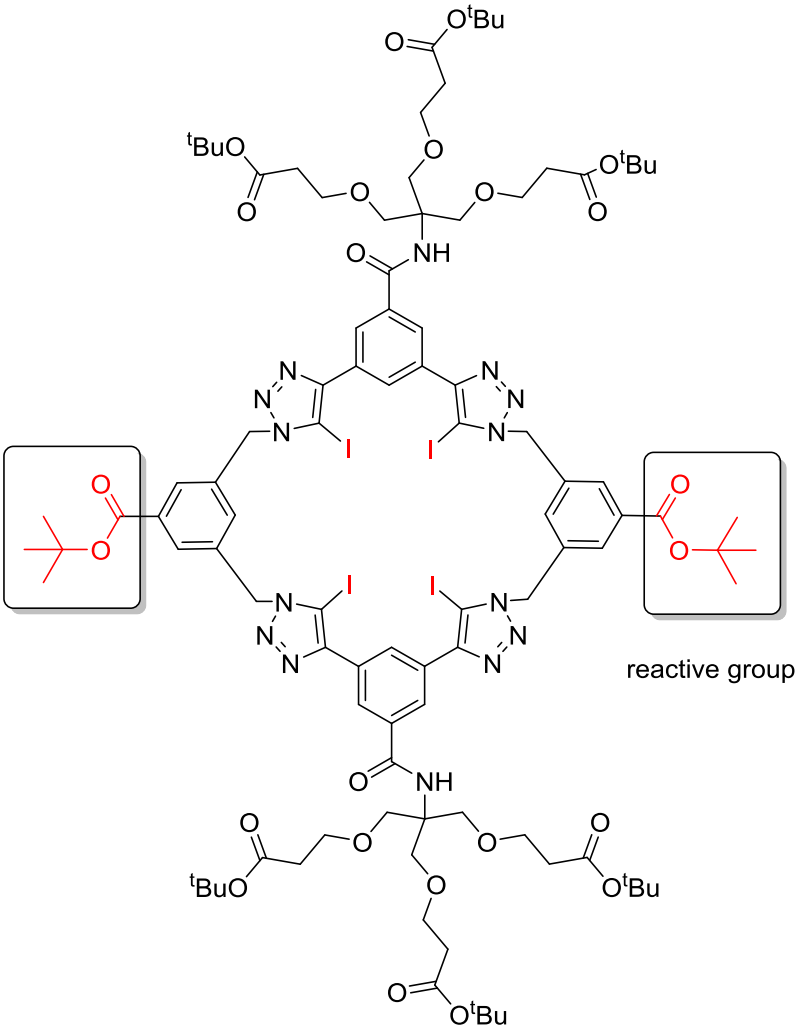

Figure 3.50 A tetradentate iodotriazole macrocycle.

Chapter 4

Acyclic, Macrocyclic, and Interlocked 1,2-(Iodotriazolium) benzene XB Hosts for Anion Recognition

Chapter 4: Acyclic, Macrocyclic, and Interlocked 1,2-(Iodotriazolium) benzene XB Hosts for Anion Recognition

4.1 Introduction

4.1.1 Charge-Assisted Bidentate Halogen Bond Receptors

The designs of XB anion receptors to date have relied on the incorporation of neutral or cationic XB donor motifs into various organic scaffolds as discussed in Section 1.3. The extensive studies on their anion binding properties have provided a better understanding of XB–anion interactions and rational designs of XB host molecules. Amongst the XB anion receptors reported to date, the charge-assisted bidentate XB systems have been shown to be potent chelating motifs for anion complexation.[18, 81] This section summarises a few examples of cationic XB cleft-type receptors, with brief discussions on their anion coordination properties.

In 2012 Huber and co-workers reported a dicationic *meta*-bis(iodoimidazolium) benzene anion receptor (Figure 4.1a), exhibiting 1:1 stoichiometric host-guest association with halide anions in MeCN. Single crystal X-ray structural analysis of the bromide complex displayed convergent XB donor groups binding the anion, in which the iodoimidazolium rings twist out of the plane of the central phenyl ring (Figure 4.1a).[279] A similar feature has been observed in the bis-iodotriazolium analogues reported by Schubert and co-workers binding anions including sulfate (Figure 4.1b).[280]

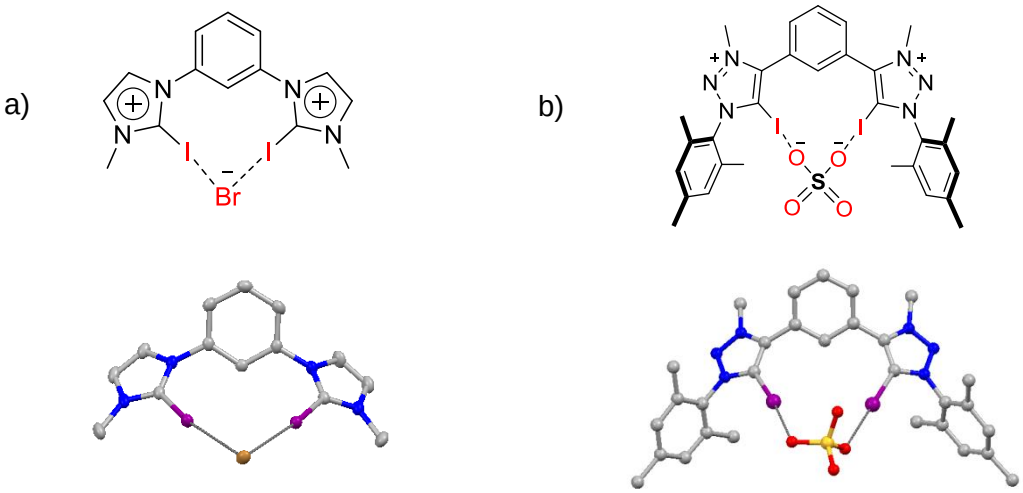

Figure 4.1 XB anion receptors based (a) bis-iodoimidazolium and (b) bis-iodotriazolium motifs. XB interactions shown as dashed lines.

Beer and co-workers introduced the novel 3,5-bis-iodotriazole pyridinium motif capable of anion recognition in d_6-DMSO (Figure 4.2).[210] X-ray crystallographic analysis of the chloride salt revealed convergent iodotriazole—chloride XB interactions and planarity across the pyridinium-iodotriazole motif, in contrast to **3.4·Cl** (Section 3.5.4),

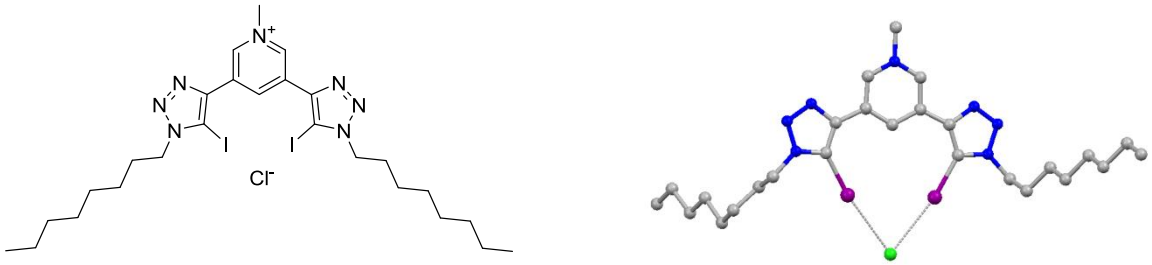

Figure 4.2 3,5-Bis-iodotriazole pyridinium XB receptor and X-ray crystal structure.

Bidentate bis-iodotriazolium motifs have also been integrated into organic scaffolds containing carbazole[281] and naphthalene[282] serving as axle components in XB interlocked host architectures (Figure 4.3).[283]

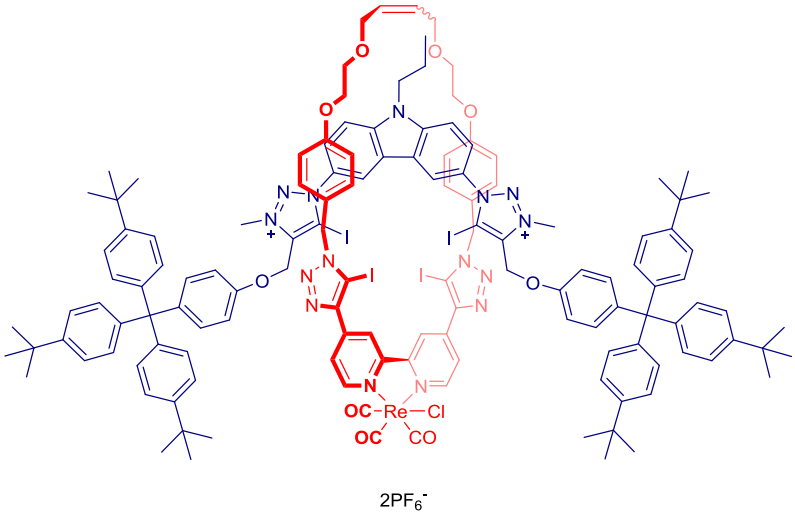

Figure 4.3 An all XB bis-iodotriazolium carbazole [2]rotaxane.

4.1.2 Active metal template synthesis of all XB [2]rotaxanes

In 2015 Beer and co-workers exploited active metal template (AMT) methodology to prepare an all-XB [2]rotaxane through the design of a macrocycle containing the flexible bidentate bis-iodotriazole motif. Endotopic coordination of the Cu(I) active species facilitated a CuAAC reaction between an azide and terminal iodoalkyne axle precursors, forming a neutral all-XB [2]rotaxane. After the removal of the copper template, complexation of rhenium(I) to the bis-iodotriazole motif in the macrocycle component enforced the formation of an exotopic metal complex due to its steric bulk. This enhanced preorganisation of the XB donors, produced a neutral interlocked 3D-binding cavity for anion recognition (Figure 4.4 a).[284] This AMT methodology was subsequently applied to afford a tetradentate iodotriazole XB [2]rotaxane (Figure 4.4 b) capable of halide recognition in the competitive 9:1 d_6-acetone/D_2O solvent mixture.[285]

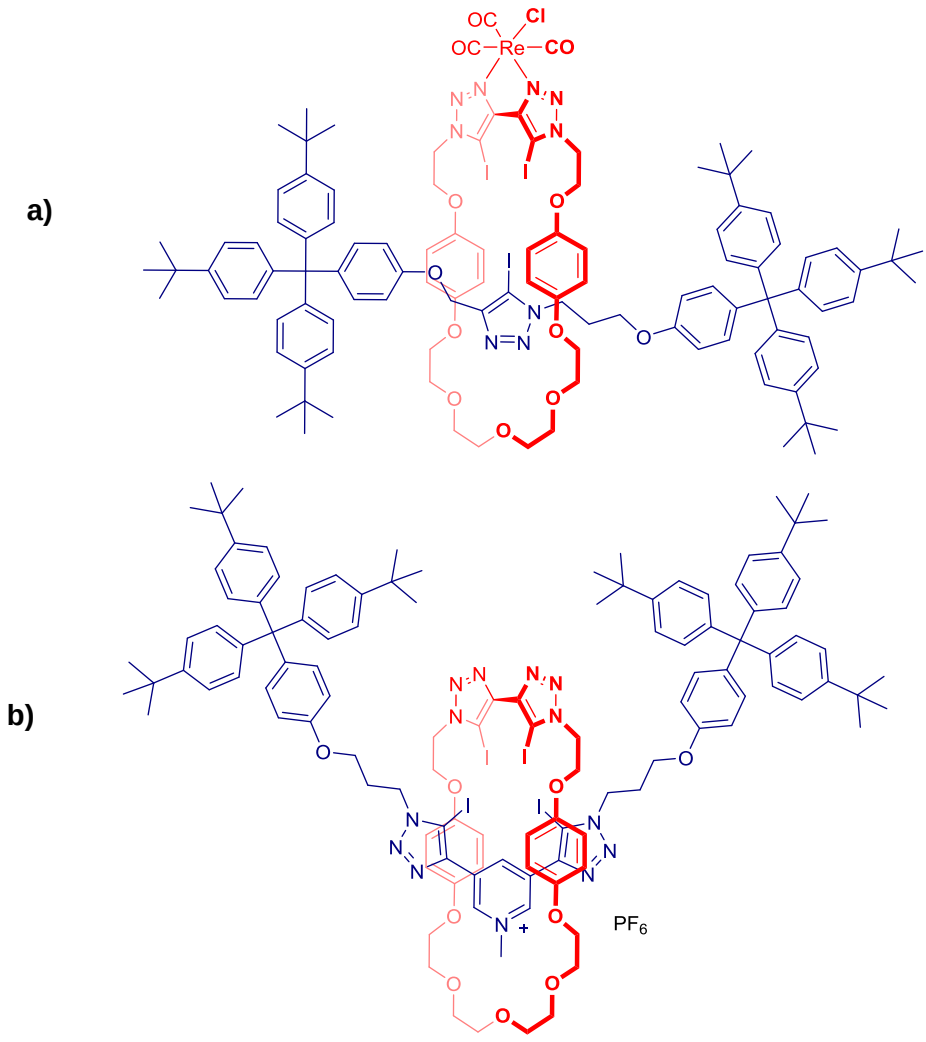

Figure 4.4 All-XB [2]rotaxanes prepared using the CuAAC active metal template reaction.

4.2 Chapter Aims

Inspired by the aforementioned examples of convergent XB–anion interactions of bis-iodotriazole XB donor motifs, this chapter investigates the anion coordination properties of 1,2-bis-iodotriazolium benzene based receptors (Figure 4.5) using quantitative ^{1}H-NMR titration experiments and single crystal X-ray structural analysis. Moreover, a 1,2-bis-iodotriazole benzene macrocycle is prepared for the construction of a novel [2]rotaxane *via* AMT synthetic methodology and its anion binding properties are determined.

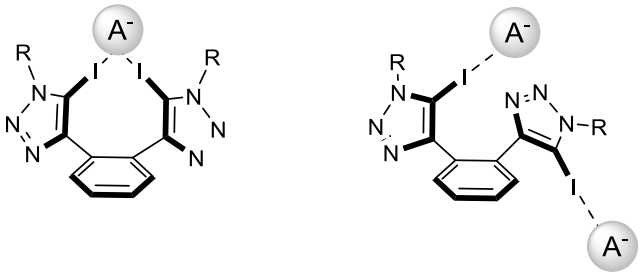

Syn-conformation *Anti-conformation*

Figure 4.5 Plausible anion binding geometry of 1,2-bis-iodotriazolium benzene based receptors.

4.3 Acyclic Receptors

4.3.1 Synthesis of 1,2-diethynylbenzene

1,2-Diethynylbenzene was used as a precursor to prepare the target acyclic 1,2-iodotriazolium benzene receptors and their HB analogues. Sonogashira cross coupling reaction of 1,2-dibromobenzene with an excess of TMS-acetylene catalysed by $Pd(PPh_3)Cl_2$ and CuI in NEt_3 was carried out at room temperature. After 5 days there was no evidence of the bis-TMS alkyne **4.1** formed in the reaction (Scheme 4.1a). Another approach was undertaken using microwave irradiation at 130°C for 1.5 hours, and again only low conversion to the mono-alkyne **4.2** was observed (Scheme 4.1b).

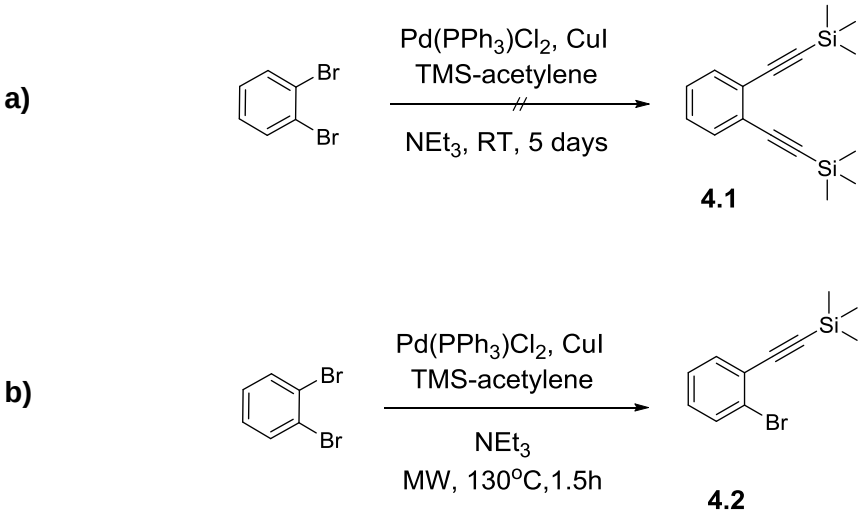

Scheme 4.1 Attempts to prepare 1,2-bis((trimethylsilyl)ethynyl)benzene **4.1**.

Changing the base to diethylamine ($NHEt_2$) gave the target product **4.1** whereupon removal of the TMS groups using K_2CO_3 in MeOH afforded 1,2-diethynylbenzene **4.3** in 88% yield over two steps, after purification by silica gel column chromatography (Scheme 4.2).

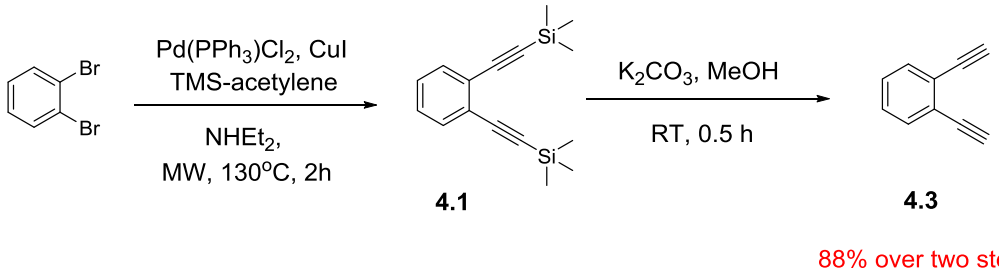

Scheme 4.2 Synthesis of 1,2-diethynylbenzene **4.3**.

4.3.2 Synthesis of organic azides

Organic azide precursors were prepared using literature procedures.[210, 286] Benzyl azide **4.4** was synthesised *via* nucleophilic substitution of the parent benzyl bromide with sodium azide (Figure 4.3a). In the case of aryl azides, *in situ* generation of their respective diazonium salts with $NaNO_2$ under acidic conditions and subsequent addition of NaN_3 afforded mesityl azide **4.5** and perfluoroaryl azide **4.6** in excellent yield (Scheme 4.3 b and c).

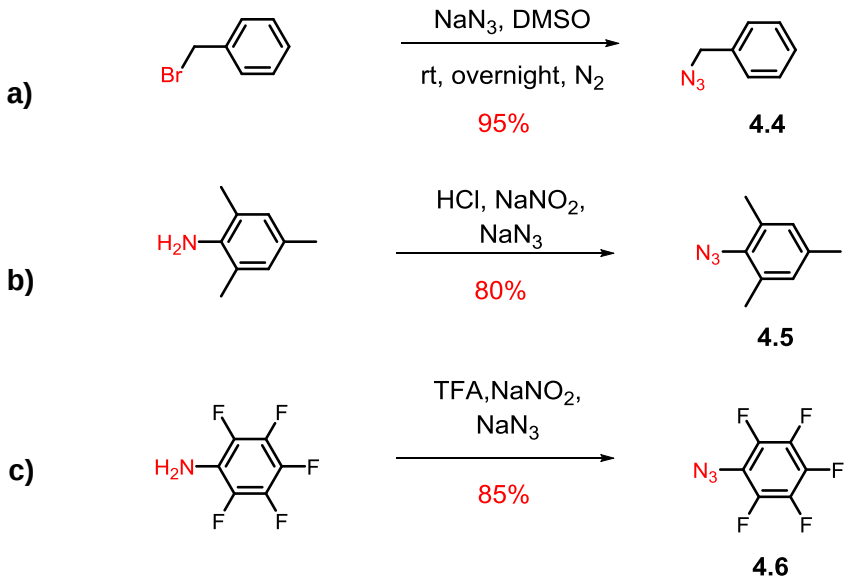

Scheme 4.3 Synthesis of organic azides.

4.3.3 Synthesis of 1,2- bis-iodotriazolium benzene based XB anion receptors

The cationic 1,2-iodotriazolium benzene receptors were synthesised *via* CuAAC reaction followed by iodotriazole alkylation and anion exchange to the BF_4^- non-coordinating counter anion. The bis-iodoalkyne precursor **4.7** was prepared from bis-alkyne **4.3** by an iodination reaction using *N*-iodosuccinimide with a catalytic amount of $AgNO_3$. CuAAC reaction between **4.7** and two equivalents of the appropriate azide, in the presence of $[Cu(MeCN)_4]PF_6$ and TBTA in 1:1 MeCN/THF gave 1,2-bisiodotrizole derivatives **4.8**, **4.9**, and **4.10** in yields of 70%, 56%, and 71%, respectively (Scheme 4.4).

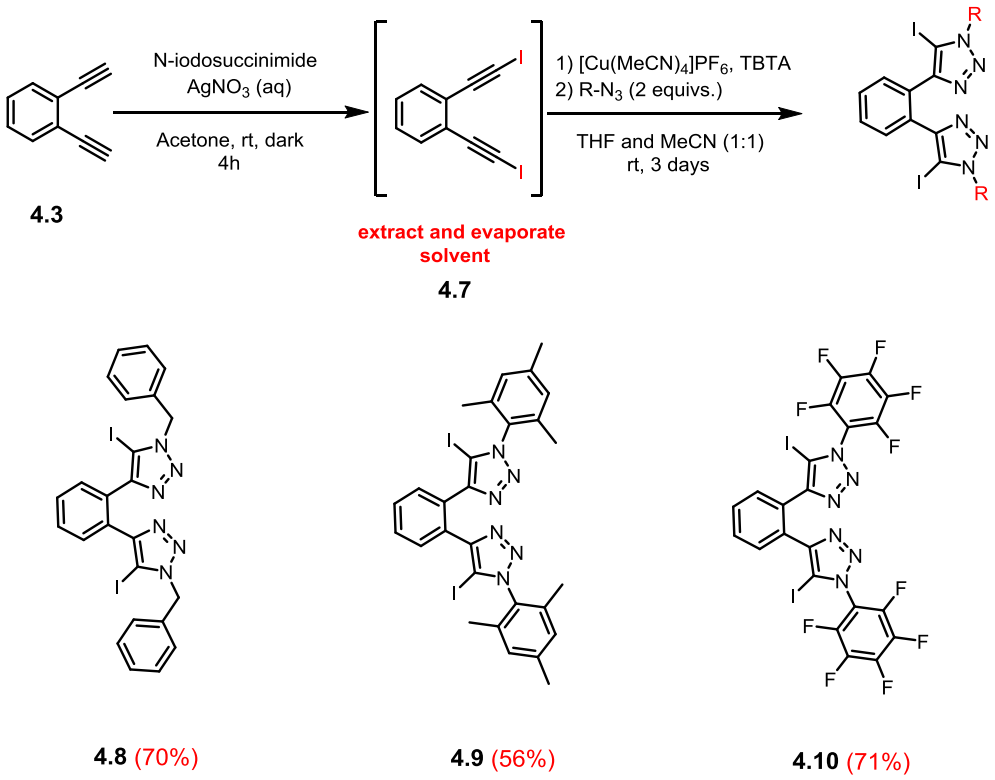

Scheme 4.4 Synthesis of the 1,2-bis-iodotriazole derivatives.

Slow evaporation of a saturated solution of **4.9** in MeCN at low temperature (~ 5 °C) gave suitable crystals for characterisation by synchrotron X-ray crystallography. The solid state structural data was collected and refined by Dr. Sean Robinson and Dr. Nicholas White. The structure of **4.9** (Figure 4.6) shows that both iodotriazoles are twisted out of plane with the central benzene ring, facing opposite directions, presumably this is a consequence of the intrinsic steric clashes between the bulky iodine atoms. This results in one dimensional polymeric chains formed by intermolecular N–$I_{iodotriazole}$ XB interactions (Figure 4.6). The halogen bonds are short (80% of the sum of the van der Waals radii[1] of N and I, Table 4.1) and relatively linear (171–172°).

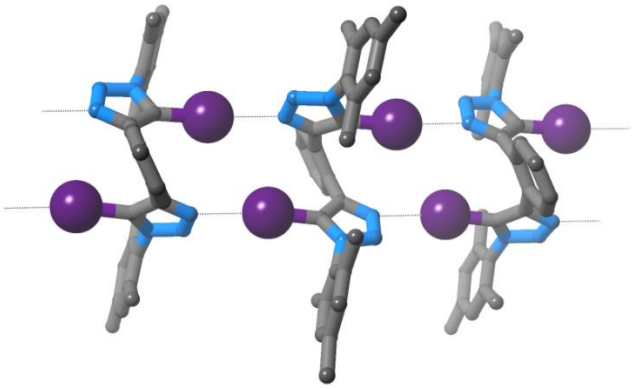

Figure 4.6 X-ray crystallographic structure of **4.9**. XB interactions are shown in dashed lines.

Table 4.1 Details of halogen bonds in the solid state structure of **4.9** (estimated standard deviations are given in parentheses).

Halogen bond	C–I distance (Å)	I···N distance (Å)	I···N distance (% VdW)[a]	C–I···N angle (°)
Iodotriazole···N, I(1)···N(23)	2.06(2)	2.97(14)	80	172.4(6)
Iodotriazole···N I(2)···N(9)	2.06(2)	2.96(16)	80	171.5(7)

[a] %VdW = the distance as a % of the sum of the van der Waals radii[1] of iodine and nitrogen.

Alkylation of **4.8**, **4.9** and **4.10** with four equivalents of trimethyloxonium tetrafluoroborate $[Me_3O]BF_4$ in dry DCM at room temperature gave only the mono-iodotriazolium product (Scheme 4.5). Neither the addition of a large excess of $[Me_3O]BF_4$ or applying heat to the reaction could afford the 1,2-diiodotriazolium products, in contrast to the analogous reaction with the corresponding meta-substituted bis-iodotriazole derivatives reported by Schubert and Beer.[92, 280] This could stem from the electron-withdrawing nature of the resulting iodotriazolium group in the *ortho*-position which decreases the nucleophilicity of the N atoms on the adjacent iodotriazole, thus deactivating the alkylation reaction. The mono-iodotriazolium compounds **4.11·BF$_4$** - **4.13·BF$_4$** and characterised by ^{1}H, ^{13}C-NMR spectroscopy and high resolution ESI-MS.

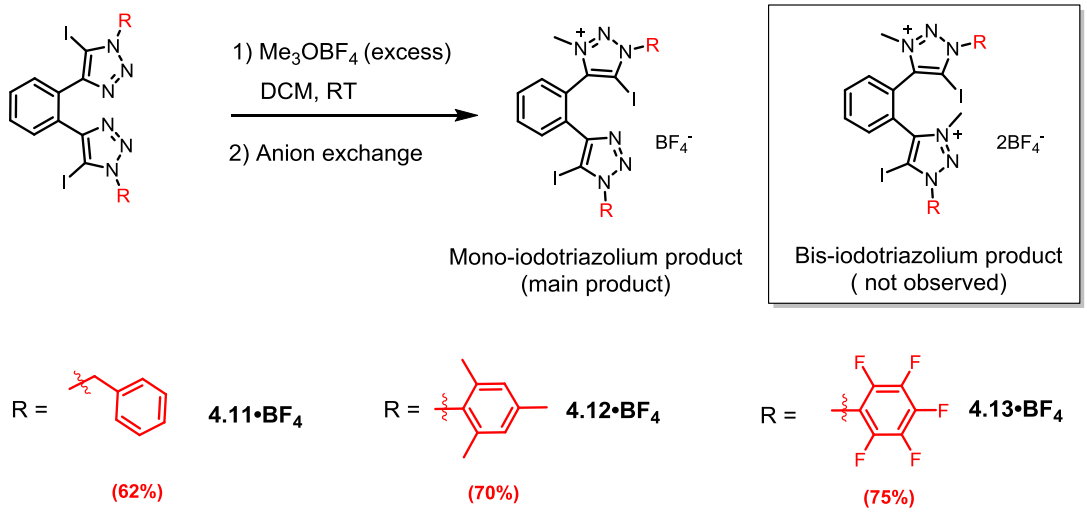

Scheme 4.5 Attempts to synthesise the 1,2-bis-iodotriazolium products.

4.3.4 Synthesis of 1,2-bis-triazolium benzene based HB anion receptors

The HB 1,2-bis-triazoliumbenzene analogues were prepared *via* a similar synthetic route to the XB receptors. Reaction of **4.3** with two equivalents of organic azide in the presence of $[Cu(MeCN)_4]PF_6$, TBTA, and DIPEA in DCM at room temperature overnight (Scheme 4.6). The bis-triazole products were purified by silica gel column chromatography to afford **4.14** - **4.16** in 49, 48, and 36 % yield, respectively (Scheme 4.6).

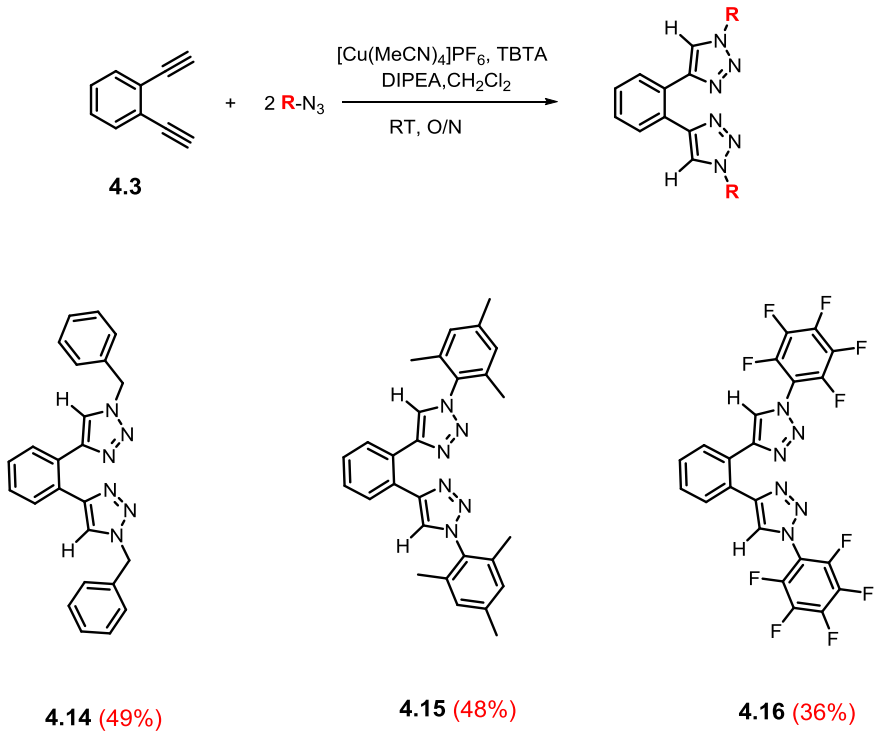

Scheme 4.6 Synthesis of the HB 1,2-bis-triazole benzene derivatives.

Alkylation using three equivalents of Me_3OBF_4 in dry DCM afforded the dicationic 1,2-derivative **4.17·$(BF_4)_2$** - **4.19·$(BF_4)_2$** in near quantitative yield. Interestingly, no evidence of the monotriazolium intermediates was observed.

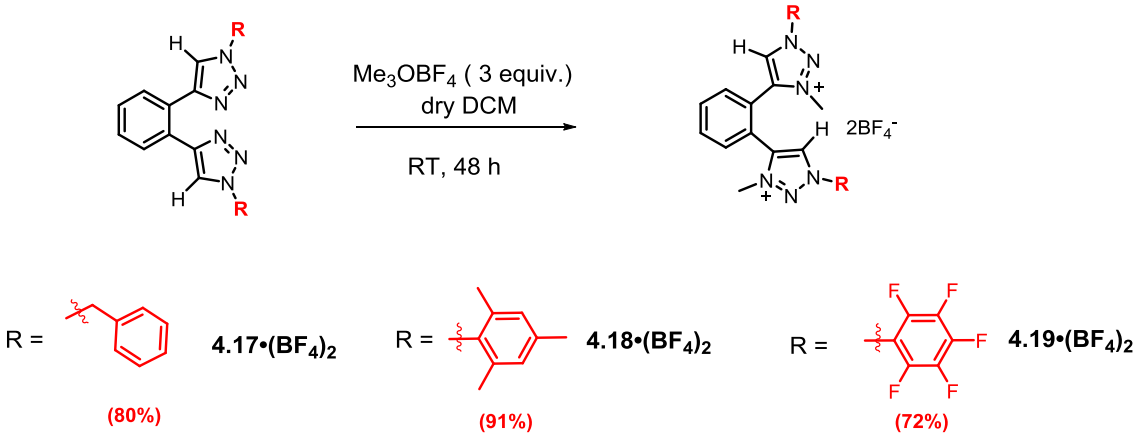

Scheme 4.7 Synthesis of 1,2-ditriazolium benzene anion receptor.

A 1:1 $CDCl_3$:CD_3CN solution of **4.18·$(BF_4)_2$** in the presence of ten equivalents of tetrabutylammonium iodide gave crystals suitable for X-ray structural analysis determined by Dr. Nicholas White. Like that of **4.9** (Figure 4.7), both prototriazolium groups are twisted out of the plane. The structure consists of a 1D polymeric chain where two receptors are bridged by an iodide anion through a triazolium···I^-···triazolium HB–anion interactions (Figure 4.7, Table 2.2).

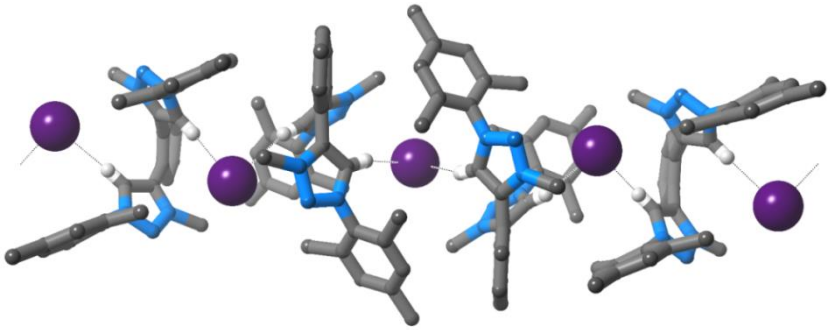

Figure 4.7 Solid state structure of **4.18^{2+}** as a mixture of I^- and BF_4^- salts.

Table 4.2 Details of hydrogen bond[a] in the solid state structure of **4.18^{2+}** as iodide salt.

Hydrogen bond	C–H distance (Å)	H···I distance (Å)	H···I distance (% $VdW_{H,I}$)[b]	C–H···I angle (°)
Triazolium···I	0.93	2.83	87	161

[a] As hydrogen atom positions cannot be determined precisely by conventional X-ray diffraction techniques, these values are approximate only, and hence are given only to a small number of significant figures. [b] %VdW = the distance as a % of the sum of the van der Waals radii[1] of iodine and nitrogen.

4.3.5 Anion Binding Studies

4.3.5.1 Acyclic perfluoroaryl XB receptor

Spectroscopic characteristics of the perfluoroaryl XB receptors are described in this section. ^{19}F-NMR spectrum of the neutral perfluoroaryl host **4.10** in 1:1 $CDCl_3/CD_3CN$ at 298K showed three distinct signals, arising from three different fluorine environments; one doublet (δ_{Fa} = -142.93 ppm), and two triplets (δ_{Fc} = -148.51 ppm and δ_{Fb} = -160.25 ppm) (Figure 4.8). This is indicative of magnetically equivalent ^{19}F resonances of two perfluoroaryl substituents.

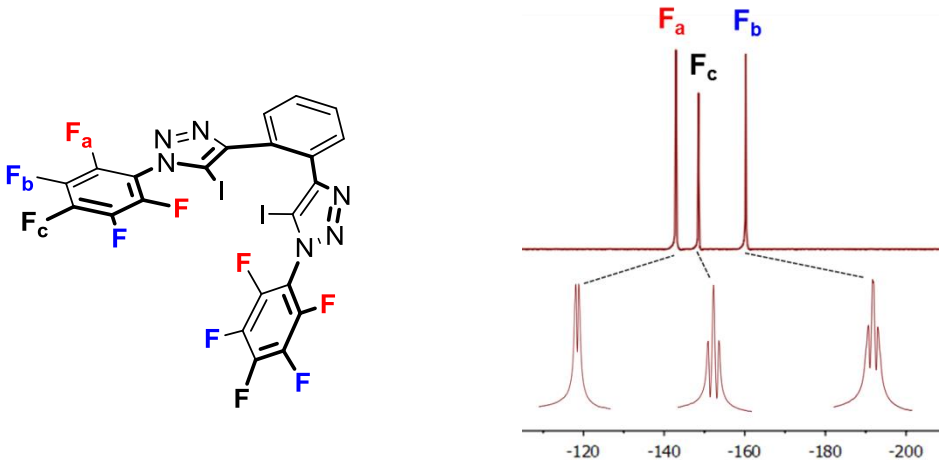

Figure 4.8 ^{19}F-NMR spectra of the neutral **4.10** in 1:1 $CDCl_3/CD_3CN$ at 298K.

Due to the asymmetry of the monocationic **4.13·BF_4** receptor, desymmetrisation of two perfluoroaryl substituents is expected to result in six unique fluorine environments shown in ^{19}F-NMR spectrum, however a set of ten ^{19}F resonances with complex multiplicity was observed (Figure 4.9). A ^{19}F-^{19}F COSY spectroscopic experiment which revealed long-range through-bond coupling between ^{19}F nuclei of the same perfluoroaryl group, allowing the assignment of all fluorine signals (Figure 4.9 and Table 4.3). Interestingly a highly unusual form of coupling between F_e –F_5 was also observed (ε in Figure 4.9 and Table 4.3), despite being separated by 13 bonds. The resulting coupling pattern can only feasibly be a result of a through-space mechanism by virtue of the close proximity of the fluorine atoms.[287-290] The restricted rotation of the perfluoroaryl units, as a result of the sterically encumbering methyl group on the iodotriazolium ring, led to the resulting difference in all ^{19}F signals.

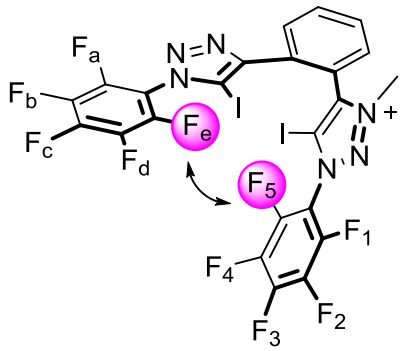

Table 4.3 Through-space and through-bond coupling of **4.13·BF$_4$** observed by ^{19}F-^{19}F COSY spectroscopy.

Iodotriazole	Iodotriazolium ring
α (F_c to F_b, F_d)	γ (F_3 to F_2, F_4)
β (F_a, F_e to F_b, F_d)	δ (F_2, F_4 to F_1, F_5)
ε (F_e to F_5)	

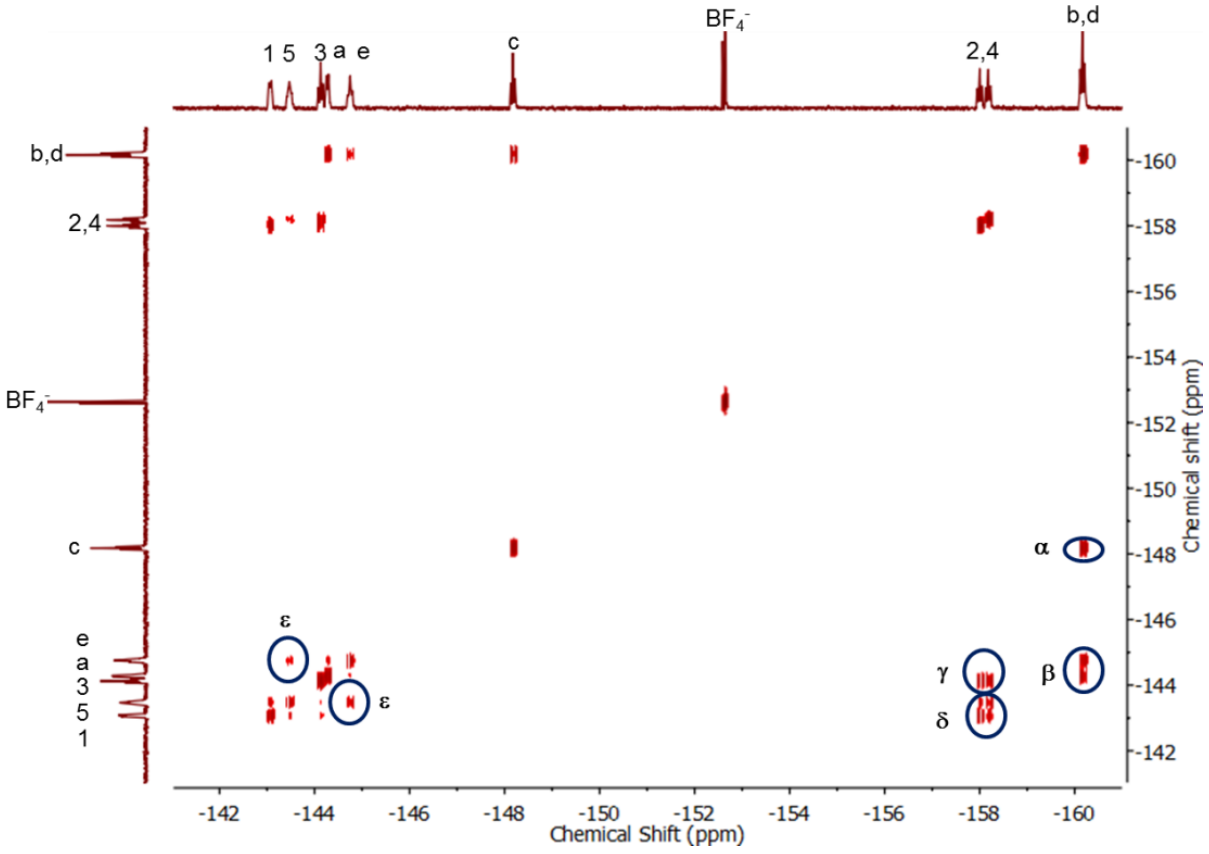

Figure 4.9 ^{19}F-^{19}F COSY 2D spectrum of **4.13·BF$_4$**.

Due to the lack of proton signals around the binding cavity of **4.13·BF$_4$**, anion binding studies of **4.13·BF$_4$** were undertaken using ^{19}F-NMR titration experiments in 1:1 $CDCl_3/CD_3CN$ in the presence of trifluorotoluene as an internal standard. The addition of TBACl revealed remarkable changes in ^{19}F signals (Figure 4.10). A significant downfield perturbation of F_e ($\Delta\delta$ = +0.43 ppm over 10 equivalents of Cl^-) was observed, while ^{19}F signals arising from fluorine atoms in the *ortho* position of the perfluoroaryl substituent linked to a triazolium ring (F_1 and F_5), were shifted upfield. Attempts to determine quantitative binding data using WinEQNMR2[253] and Bindfitv.05[291] analysis failed to give a reliable association constants with Cl^- and other halides. Analogous titrations in competitive solvents including both 9:1 and 1:1 $CDCl_3/CD_3OD$ also failed to produce any reliable data suggesting complex equilibria were involved in the anion binding process.

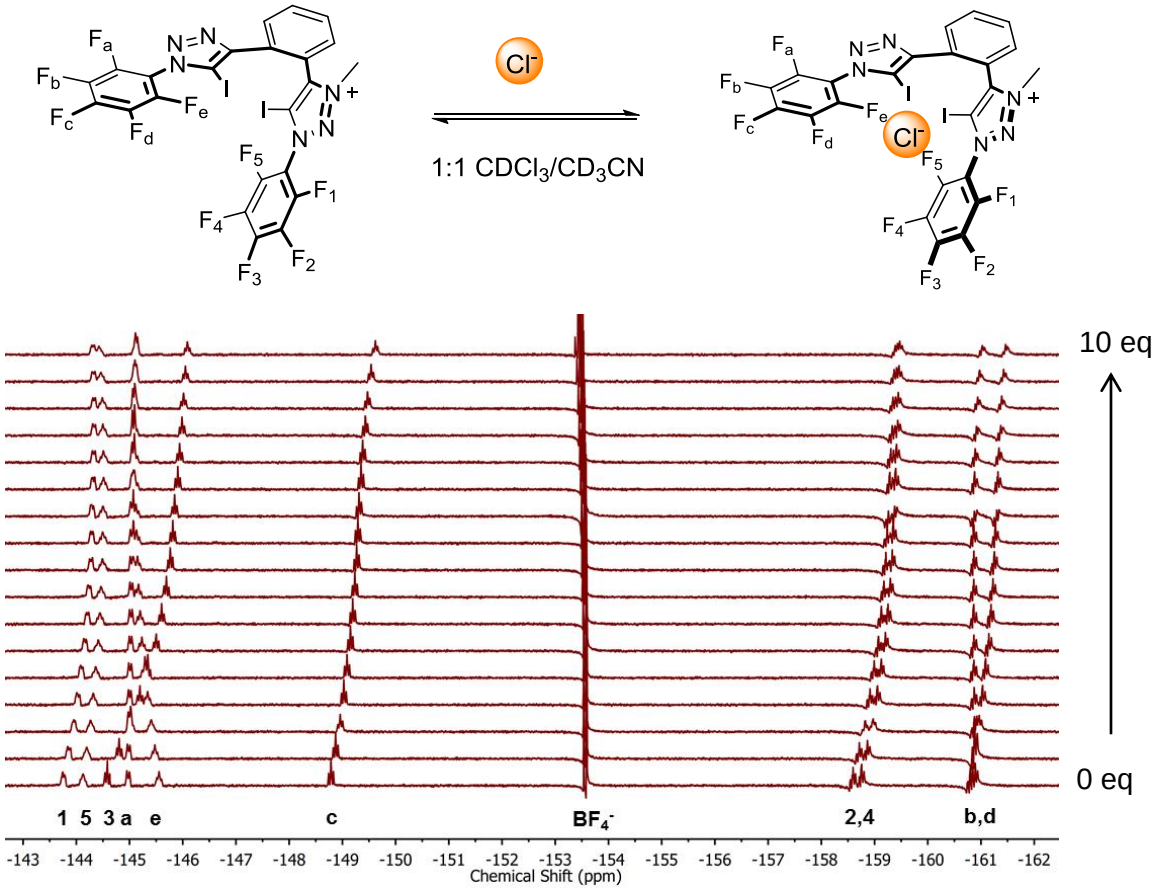

Figure 4.10 ^{19}F-NMR spectra of **4.13·BF$_4$** in the presence of increasing quantities of Cl^- ([**4.13·BF$_4$**] = 1.0 mM, 1:1 $CDCl_3/CD_3CN$, T=298K).

4.3.5.2 Acyclic perfluoroaryl XB halide solid state structures

Investigations of XB–halide anion coordination in the solid-state were carried out. Crystals were grown by vapour diffusion of diisopropyl ether into a solution of **4.13·BF_4** with ten equivalents of the tetrabutylammonium halide salts in 1:1 $CDCl_3$/CD_3CN. The solid state structures were determined by single crystal X-ray diffraction using synchrotron radiation. The data was collected by Dr. Asha Brown and refined by Dr. Jason Lim and Dr. Nicholas White. All the solid state structures of **4.13$^+$** with halide anions are very similar: a one dimensional polymeric structure is formed where XB–halide anion interactions bridge iodotriazolium and iodotriazole units of different molecules. The structures revealed the non-convergent nature of receptor's iodotriazole and iodotriazolium XB donors for anion binding (Figure 4.11-4.13). This contrasts the solid state structures of XB–anion interactions observed in the *ortho*- and *meta*- substituted bis-iodotriazolium receptors.[292, 293] The *ortho*-substituted iodotriazolium benzene receptor **4.13·BF_4** possesses a smaller chelating bite angle than that of the meta-substituted isomeric analogues (see Section 4.1), hence cooperative anion binding *via* bidentate XB–anion coordination was not observed with all the halides studied. Table 4.4 shows all the halogen bonds are short (76–83% of the sum of the van der Waals radii[1] of the atoms involved) and linear (C–I···halide angles > 175°). As expected, the charge assisted halogen bonds involving the iodotriazolium group are slightly shorter than those involving the neutral iodotriazole group. Importantly, there is no evidence of anion—π interactions to the perfluoroaryl groups in the solid state, highlighting anion coordination is driven exclusively by XB—anion interactions.

Table 4.4 Details of halogen bonds in the solid state structures of **4.13·Cl**, **4.13·Br** and **4.13·I** (estimated standard deviations are given in parentheses).

Halogen bond	C–I distance (Å)	I···halide distance (Å)	I···halide distance (% VdW)[a]	C–I···halide angle (°)
4.13·*Cl*				
Iodotriazolium···Cl^-	2.086(2)	2.944(1)	76	175.59(7)
Iodotriazole···Cl^-	2.083(2)	3.038(1)	79	176.36(7)
4.13·*Br*				
Iodotriazolium···Br^-	2.087(4)	3.072(1)	79	176.26(12)
Iodotriazole···Br^-	2.088(4)	3.169(1)	81	176.87(12)
4.13·*I*				
Iodotriazolium···I^-	2.093(4)	3.265(1)	80	177.49(10)
Iodotriazole···I^-	2.091(3)	3.367(1)	83	178.17(10)

[a] %VdW = the distance as a % of the sum of the van der Waals radii[1] of iodine and halides.

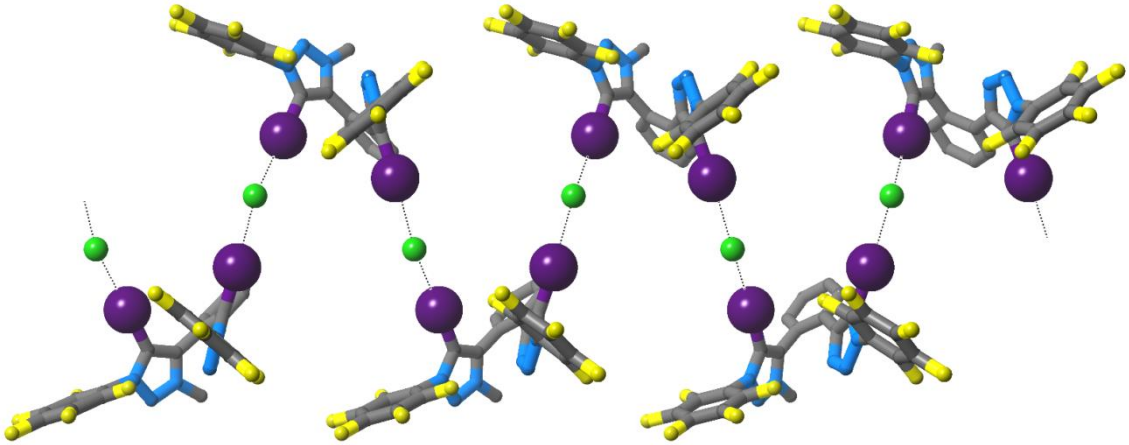

Figure 4.11 Solid state structure of **4.13·Cl**.

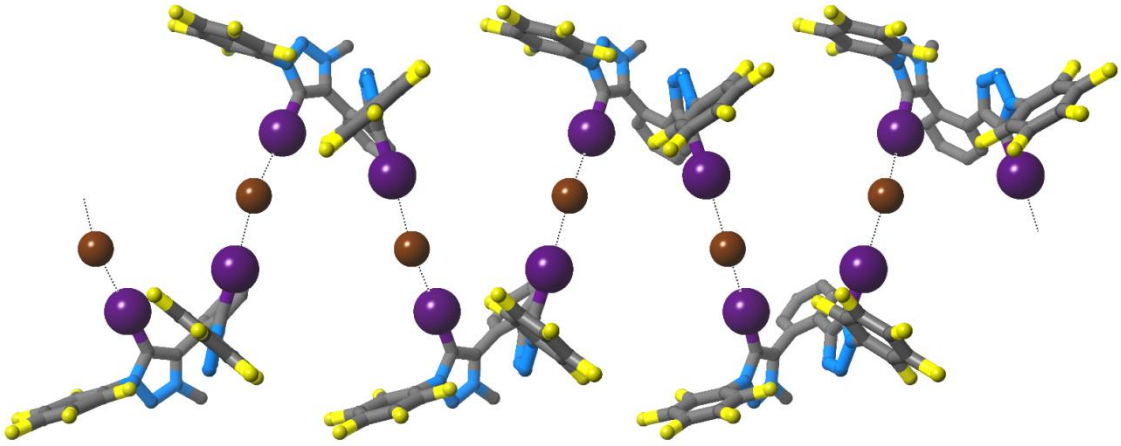

Figure 4.12 Solid state structure of **4.13·Br**.

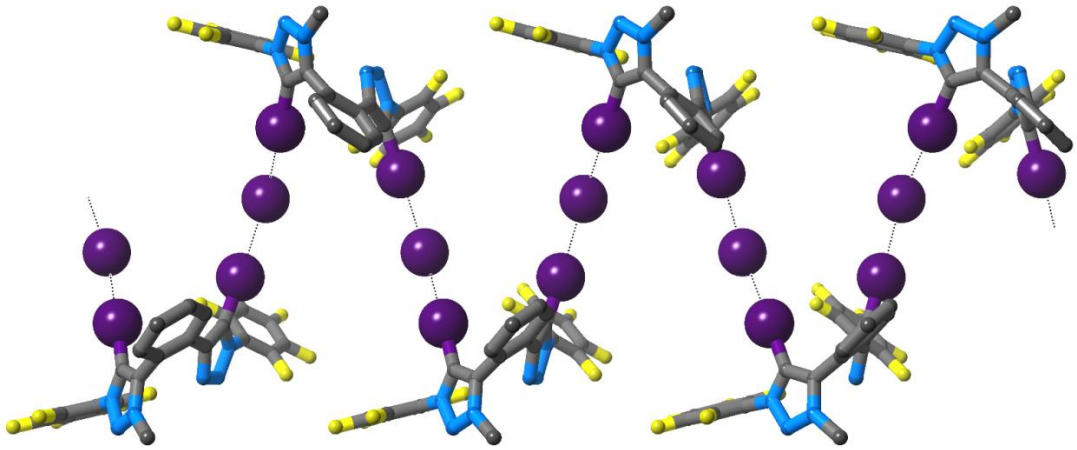

Figure 4.13 Solid state structure of **4.13·I.**

4.3.5.3 Benzyl substituted XB anion receptor

The ^{1}H-NMR spectrum of **4.11·BF$_4$** receptor in a mixture of 1:1 $CD_3CN/CDCl_3$ was initially obtained, showing a complex splitting pattern of methylene proton signals due to germinal couplings of each proton pair ($H_{a'}$–H_a and $H_{b'}$–H_b) (Figure 4.14). This highlights the restricted conformation of the monocationic XB receptor in a similar fashion to that of **4.13·BF$_4$**. This was not observed in the ^{1}H NMR spectra of HB analogues **4.17·BF$_4$** and **4.17·(BF$_4$)$_2$** (Figure 4.14).

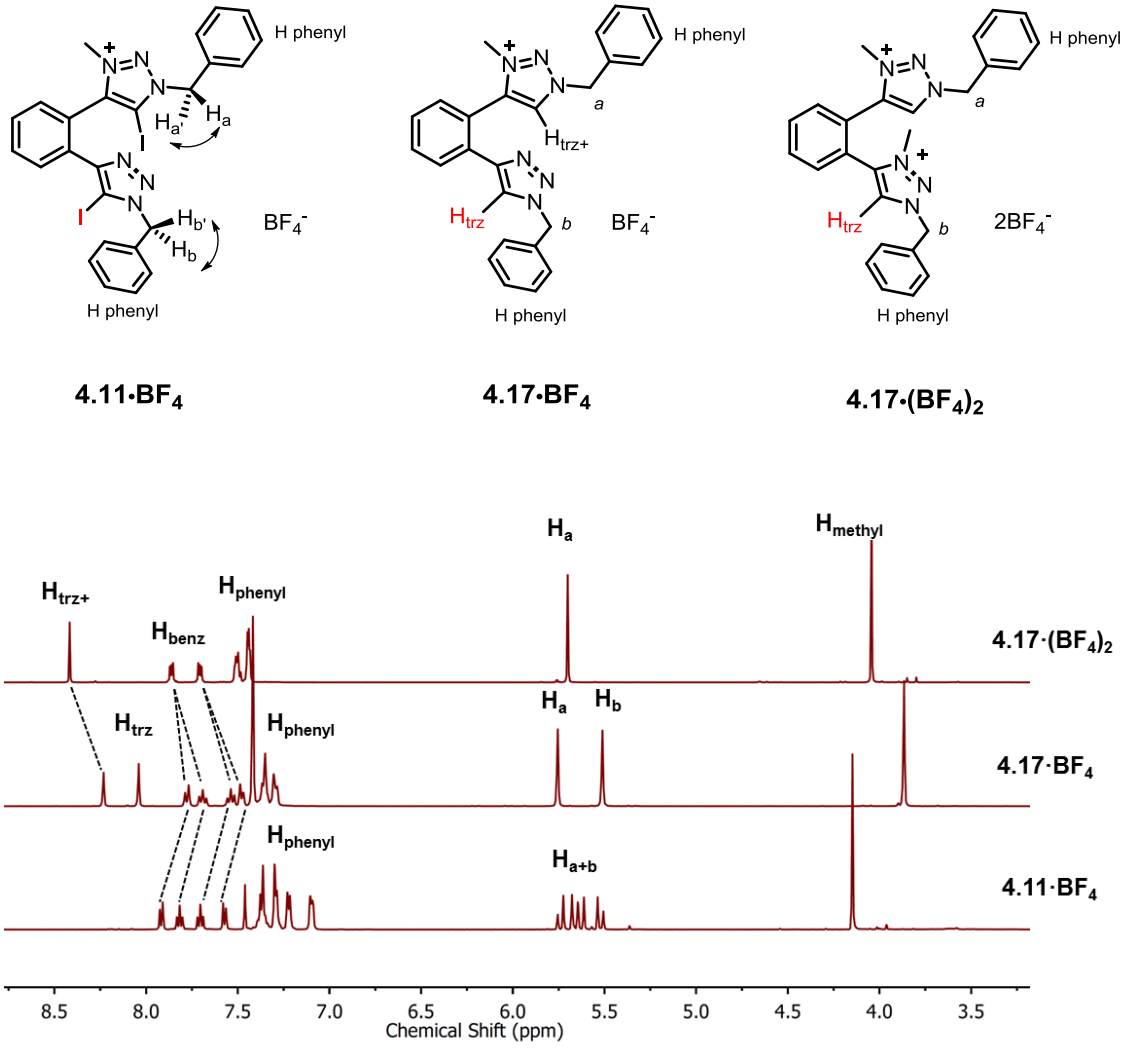

Figure 4.14 Truncated ^{1}H-NMR spectra of **4.11·BF$_4$**, **4.17·BF$_4$** and **4.17·(BF$_4$)$_2$** in 1:1 $CD_3CN/CDCl_3$ (T=298K, 500 MHz).

Quantitative ^{1}H-NMR titration experiments of **4.11·BF$_4$** were undertaken in a mixture of 1:1 $CD_3CN/CDCl_3$ with tetrabutylammonium halide salts. Upon addition of Cl^-, methylene (H_a and H_b) and phenyl (H_{phenyl}) proton signals displayed significant changes in their splitting patterns. Complex proton resonances of H_a and H_b coalesce into two broad signals, attributed to an anion binding induced conformational change of the receptor (Figure 4.15). Halide addition to HB receptors **4.17·BF$_4$** and **4.17·(BF$_4$)$_2$** resulted in remarkable downfield shifts of the triazolium proton (H_{trz+}) signal, with significantly smaller perturbation of triazole proton (H_{trz}) of the monocationic analogue **4.17·BF$_4$** (Figure 4.16). Also the methylene (H_a of **4.17·(BF$_4$)$_2$** and H_a,H_b of **4.17·BF$_4$**) and phenyl proton (H_{phenyl}) signals underwent downfield shifts with concomitant much smaller upfield perturbations of the benzene proton resonances ($H_{benzene}$) upon chloride binding.

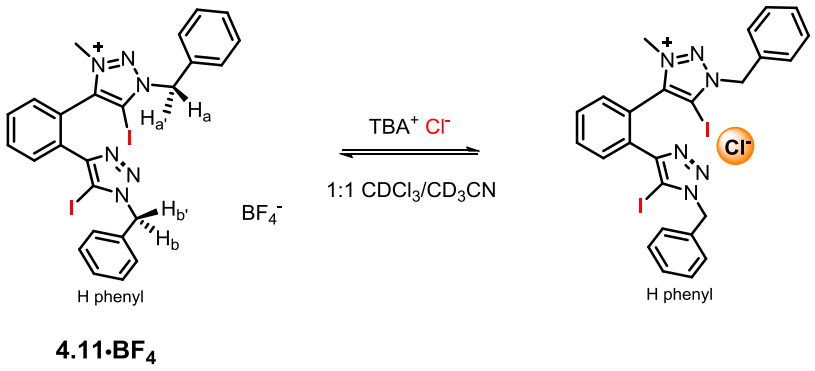

4.11·BF$_4$

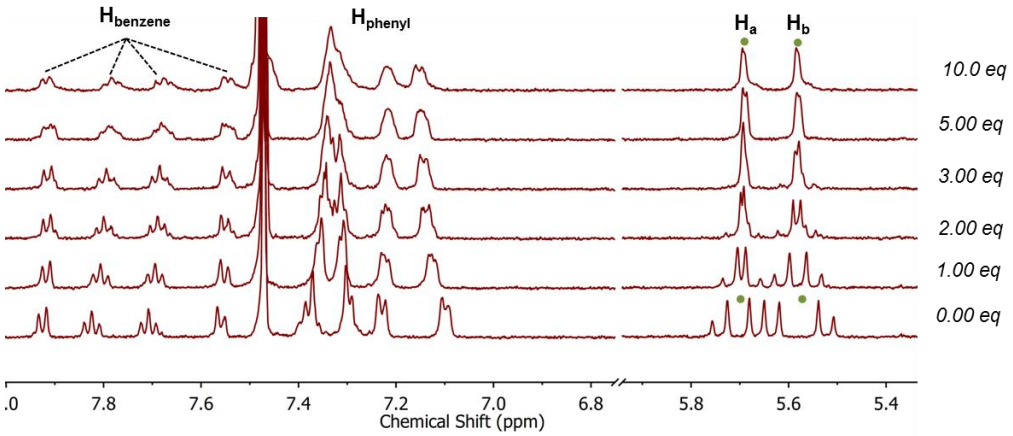

Figure 4.15 Truncated ^{1}H-NMR spectra of **4.11·BF$_4$** in 1:1 $CD_3CN/CDCl_3$ upon addition of TBACl (T=298K, 500 MHz).

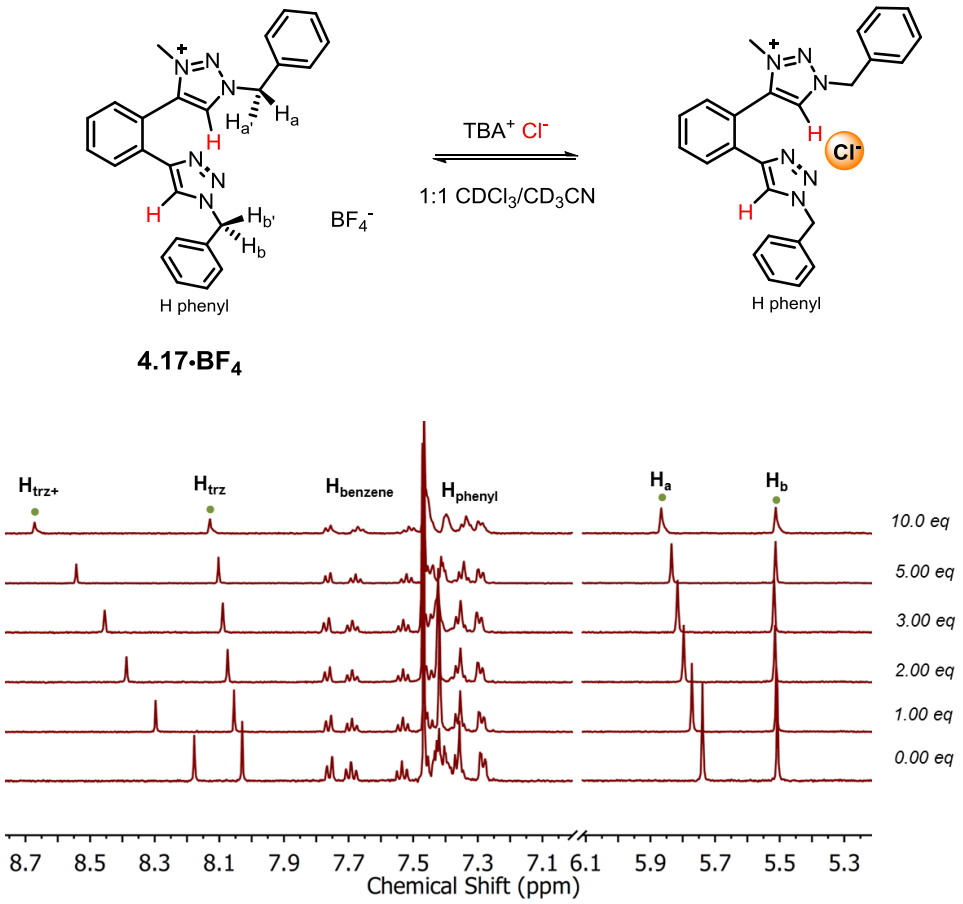

Figure 4.16 Truncated ^{1}H-NMR spectra of **4.17·BF$_4$** in 1:1 $CD_3CN/CDCl_3$ upon addition of TBACl (T=298K, 500 MHz).

Table 4.5 Anion association constants K_a (M^{-1}) for **4.11·BF$_4$**, **4.17·BF$_4$** and **4.17·(BF$_4$)$_2$** in 1:1 $CD_3CN/CDCl_3$.[a]

Anion	K_a(M^{-1}) in 1:1 $CDCl_3/CD_3CN$ at 298 K		
	4.11·BF$_4$ XB	**4.17·BF$_4$ HB**	**4.17·(BF$_4$)$_2$ HB**
Cl$^-$	1758 (155)	43 (3)	376 (27)
Br$^-$	597 (5)	35 (3)	220 (11)
I$^-$	802 (63)	27 (2)	105 (3)

[a] Methylene proton H_a monitored for all receptors. Values of K_a are determined by the WinEQNMR2 software using a 1:1 host-guest binding model, Errors (±) are less than 10% ([host]=2.0mm, 500 MHz, T=298 K)

WinEQNMR2[253] analysis of the titration determined 1:1 stoichiometric host guest halide association constants (Table 4.5), monitoring the methylene proton H_a of the respective receptor. The monocationic XB receptor **4.11·BF$_4$** displayed superior halide recognition properties over both mono- and dicationic HB analogues (**4.17·BF$_4$** and **4.17·(BF$_4$)$_2$**) for all anions studied (Table 4.5).This is especially remarkable despite the enhanced electrostatic attractions between the halides and dicationic **4.17·(BF$_4$)$_2$**. Moreover, the XB receptor exhibited selectivity for Cl^- >I^- >Br whereas the HB analogues show the anion binding trend which follows anion basicity (Cl^- > Br^- > I^-). The greater anion binding strength of dicationic HB receptor **4.17·(BF$_4$)$_2$** in comparison to the monocationic analogue **4.17·BF$_4$** is attributed to a combination of more favourable electrostatic interactions and a greater polarisation of the C-H HB donors.

4.4 Attempted synthesis of [2]rotaxane *via* anion templation

Given the strong chloride anion binding properties of the monocationic 1,2-bis-iodotriazolium benzene motif, the synthesis of a [2]rotaxane containing this motif in the axle component, was attempted using chloride anion template methodology with two different clipping reactions.

4.4.1 Synthesis of axle component

The synthesis of the target axle component containing the 1,2-iodotriazolium benzene motif required the preparation of an azide functionalised bulky terphenyl stopper group **4.20**, made by Dr.Simon Picot. The CuAAC reaction between **4.7** and two equivalents of stopper azide **4.20** in THF, gave axle precursor **4.21** in 55% yield (Scheme 4.8). Subsequent mono-alkylation using an excess of $[Me_3O]BF_4$ in dry DCM at room temperature gave the monocationic iodotriazolium axle **4.22·BF$_4$** which was anion exchanged to its chloride salt **4.22·Cl** in 84% yield (Scheme 4.8).

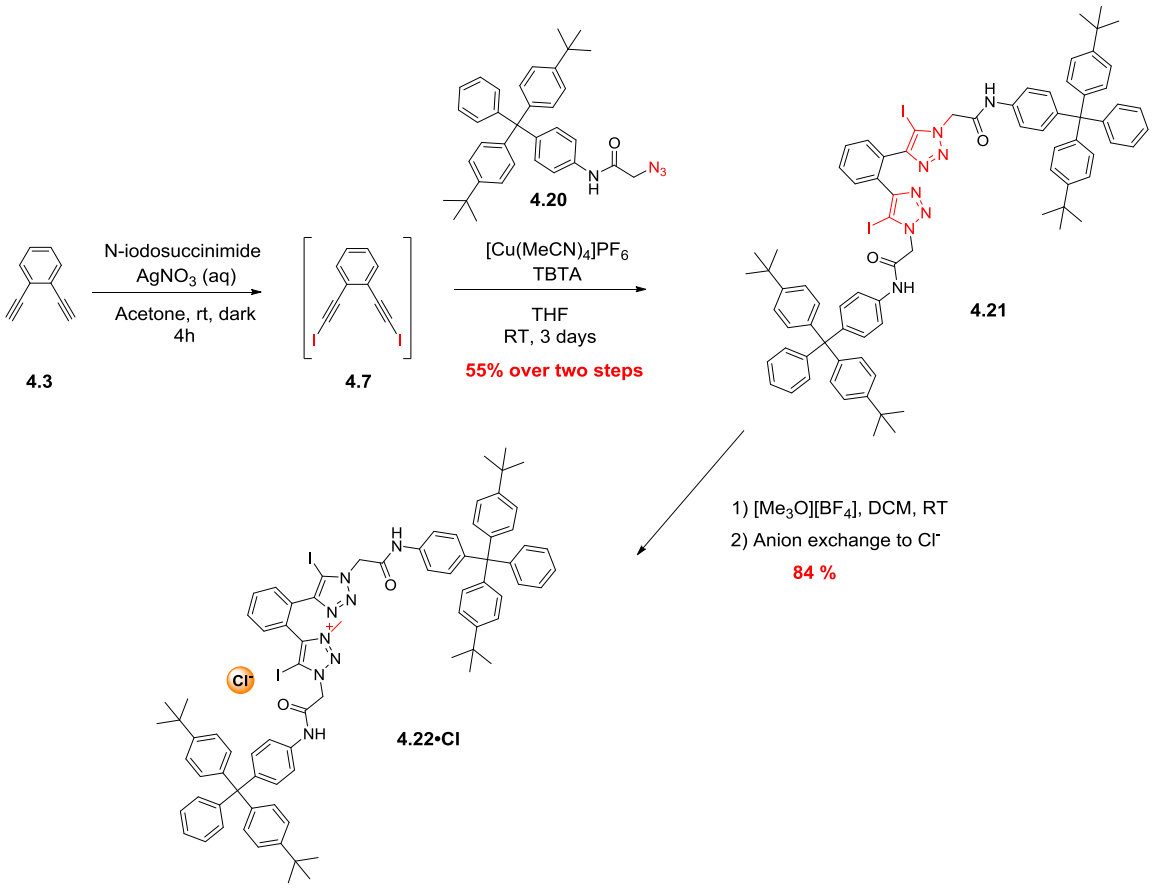

Scheme 4.8 Synthesis of the axle **4.22·Cl**.

4.4.2 Attempted synthesis of [2]rotaxane *via* ring closing metathesis

Synthesis of target monocationic [2]rotaxane **4.24·Cl** was first attempted by a chloride anion template ring closing metathesis (RCM) clipping methodology (Scheme 4.9). A catalytic amount of the 2nd generation Grubbs' catalyst was added to a mixture of axle **4.22.Cl** and bis-vinyl-functionalised macrocycle precursor **4.23**. ESI-MS of the crude reaction mixture showed m/z = 2075 and 1453, corresponding to the molecular mass of the target cationic [2]rotaxane **4.24**$^{+}$ and an unreacted iodotirazolium axle **4.21**$^{+}$, respectively. However, attempts to isolate the interlocked product failed, suggesting if present was in very low yield.

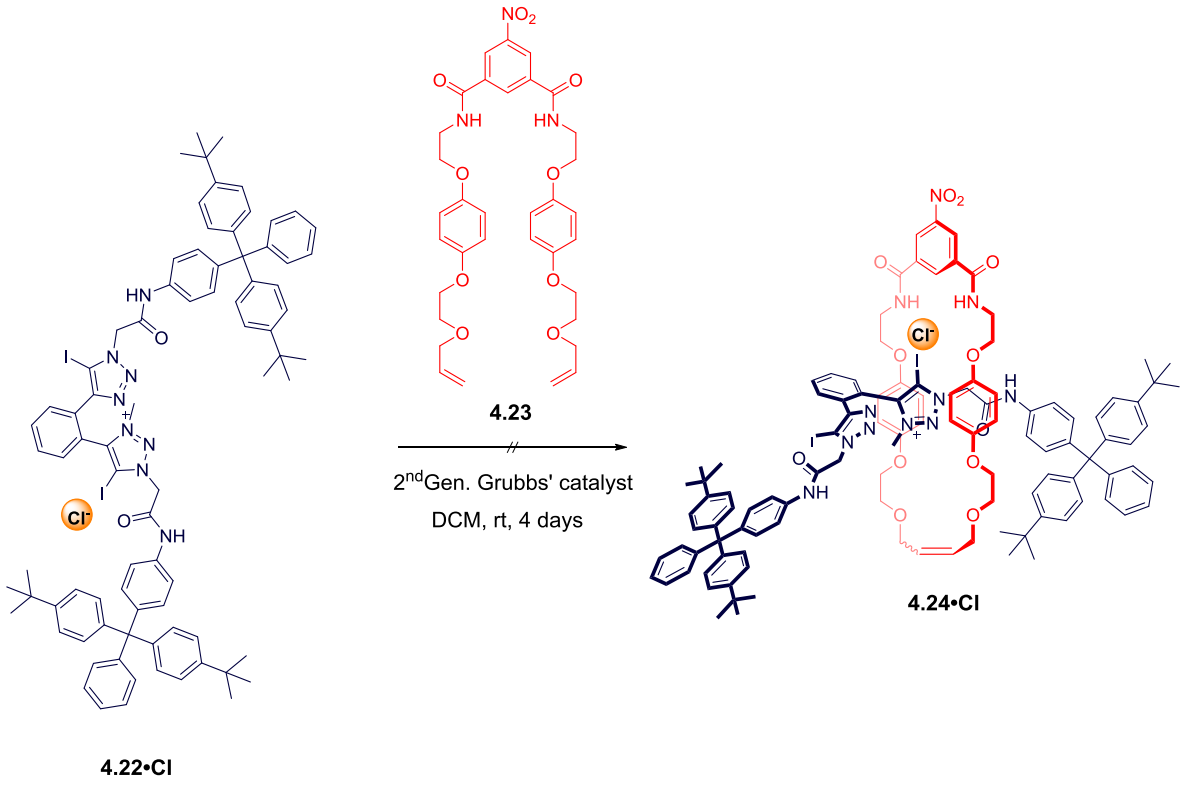

Scheme 4.9 Attempt to synthesise [2]rotaxane **4.24·Cl** *via* RCM.

4.4.3 Attempted synthesis of [2]rotaxane *via* amide macrocyclisation reaction

A chloride anion template acid chloride amine condensation clipping reaction was also undertaken (Scheme 4.10). The axle component **4.22·Cl** was stirred with an excess of bis-amine macrocycle precursor **3.36** and NEt_3 in dry DCM at 0°C. Addition of 3,5-dichlorocarbonyl pyridine **3.37** solution to the reaction mixture gave a crude product by which ESI-MS analysis indicated the presence of m/z = 2050, corresponding to the target monocationic [2]rotaxane **4.25**$^+$. Again, attempts to isolate the interlocked product *via* chromatography failed.

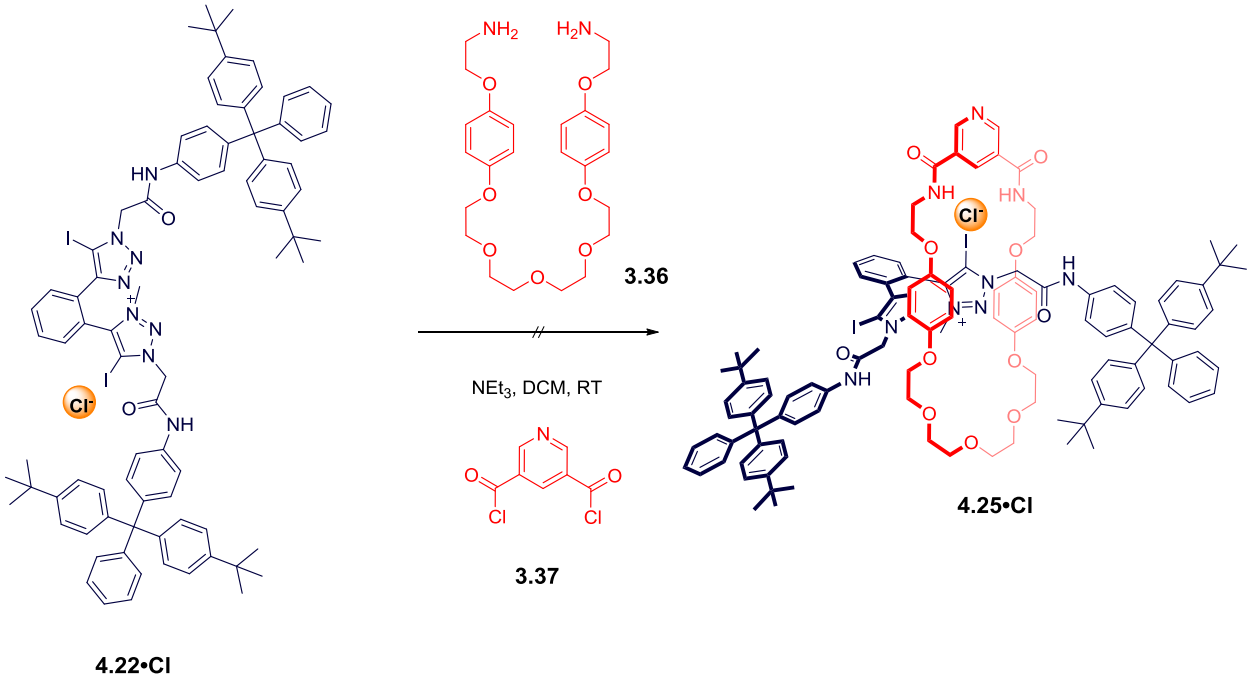

Scheme 4.10 Attempt to synthesise [2]rotaxane **4.25·Cl** *via* amide macrocyclisation reaction.

4.5 Synthesis of an XB [2]rotaxane *via* active metal template methodology

4.5.1 Synthesis of 1,2-bis-iodotrizole benzene macrocycle

As demonstrated in the previous section, the integration of the 1,2-bis-iodotriazolium benzene axle component into [2]rotaxane host structures *via* anion templation proved challenging. Steric hindrance of proximal XB donor groups presumably inhibited the formation of a chloride template intermolecular assembly between the axle and the pre-macrocyclic component to form the [2]rotaxane.

Attention turned to using an active metal template approach for preparing the target [2]rotaxane. This required the synthesis of macrocycle ***ortho*-4.26** (Figure 4.17) as a potential ligand for Cu(I) to catalyse the a CuAAC-AMT. This work was undertaken in collaboration with Dr. Jason Lim who prepared the 1,3-bis-iodotriazole benzene macrocycle ***meta*-4.26** for investigations into the AMT synthesis of XB rotaxanes.

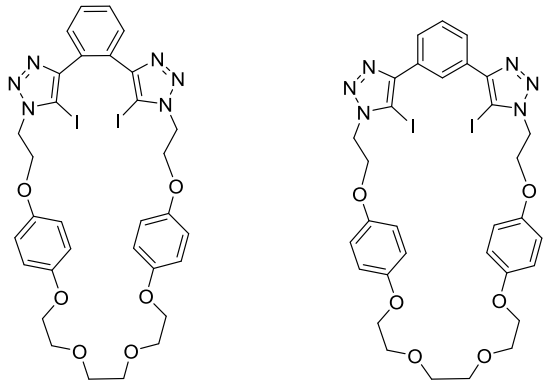

***ortho*-4.26** ***meta*-4.26**

Figure 4.17 Target isomeric XB bis-iodotriazole benzene macrocycles **4.26**.

The ***ortho*-4.26** macrocycle was prepared according to Schemes 4.11 and 4.12. A mono-alkylation reaction between hydroquinone **4.27** and an excess of 1,2-dibromoethane in the presence of K_2CO_3 afforded **4.28** which was used in the next step without purification. A nucleophilic substitution reaction of **4.28** with NaN_3 in DMF gave monoazide phenol **4.29** as a colourless oil in 32% yield over two steps, after silica gel chromatographic purification. Reaction of **4.29** with chloromethyl methyl ether in the presence of DIPEA afforded **4.30** in 72% yield (Scheme 4.11).

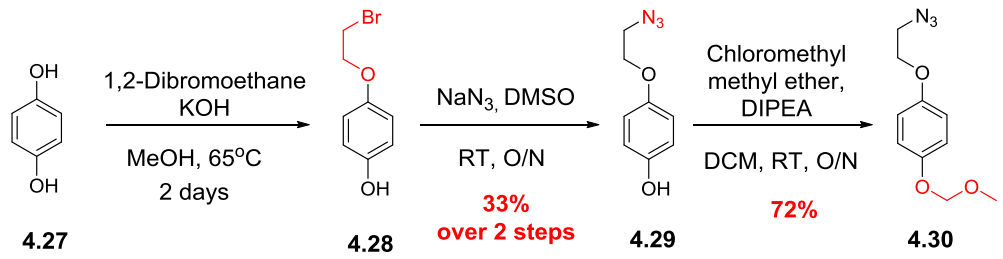

Scheme 4.11 Synthesis of azide precursor **4.30**.

The CuAAC reaction of 1,2-diiodoethynyl benzene **4.7** and two equivalents of azide precursor **4.30**, in the presence of $Cu(MeCN)_4PF_6$ and TBTA in dry THF afforded a bis-iodotriazole derivative **4.31** in 56% yield over two steps. Acidic deprotection of **4.31** produced diphenol **4.32** as an off-white solid in quantitative yield. High dilution macrocyclisation of **4.32** and triethylene glycol ditosylate was accomplished under basic conditions of Cs_2CO_3 in dry DMF. After purification by preparative thin layer chromatography and re-crystallization from ethanol gave macrocycle ***ortho*-4.26** (Scheme 4.12), which was characterised by ^{1}H (Figure 4.18) and ^{13}C-NMR spectroscopy, and HRMS.

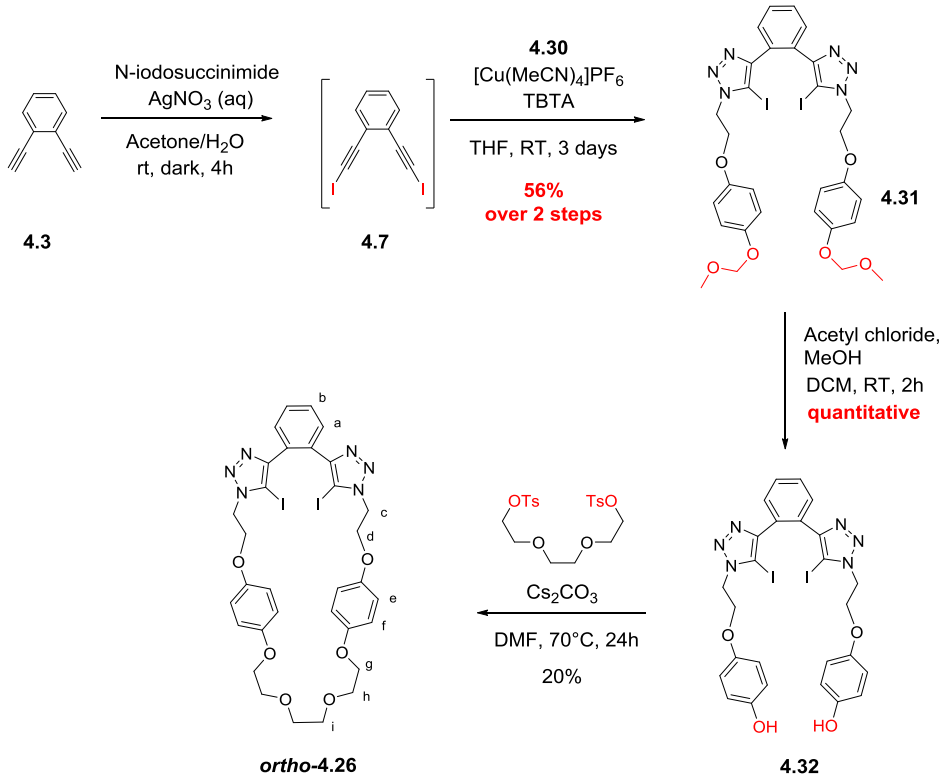

Scheme 4.12 Synthesis of macrocycle ***ortho*-4.26**.

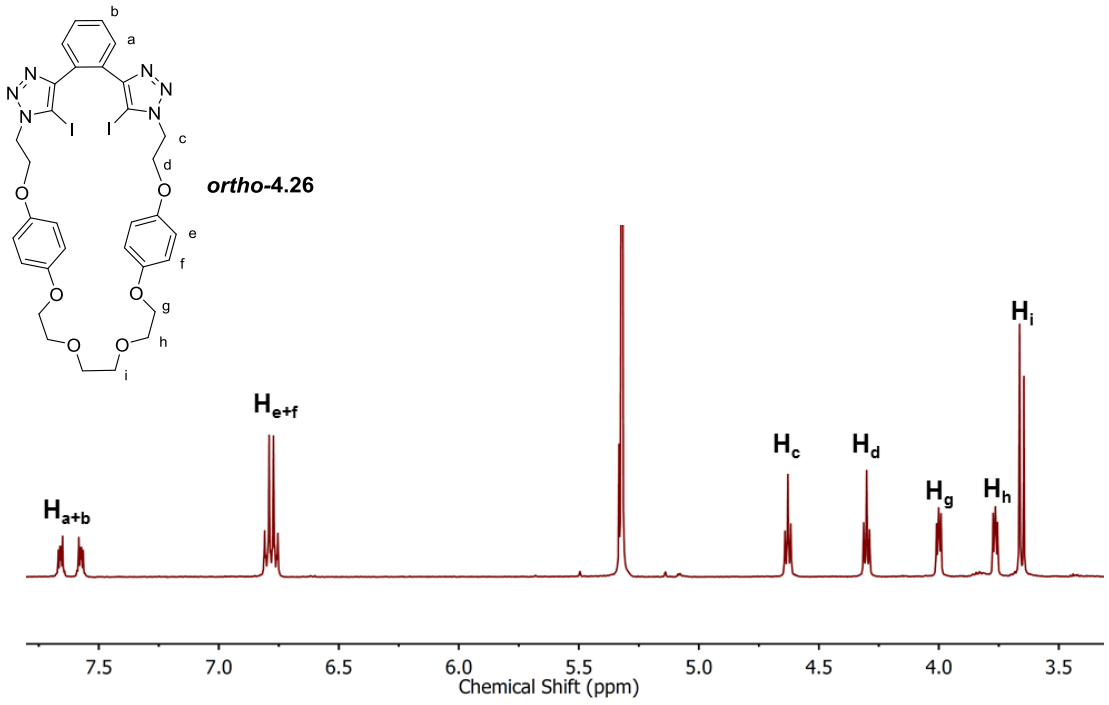

Figure 4.18 Truncated ^{1}H-NMR of ***ortho*-4.26** in d_2-dichloromethane.

4.5.2 Copper(I) binding

An effective preparation of a XB [2]rotaxane by CuAAC-AMT synthesis crucially relies on formation of a thermodynamically favoured endotopic coordination of the copper(I) catalyst to the XB macrocycle. Therefore, the Cu(I) binding properties of an XB 1,2-bisiodotriazole benzene macrocycle ***ortho*-4.26** were studied by qualitative ^{1}H-NMR titration experiments.

The addition of a solution of $Cu(MeCN)_4PF_6$ in CD_2Cl_2, to macrocycle ***ortho*-4.26** caused slight broadening of spectrum (Figure 4.19). The ^{1}H NMR resonances arising from the central benzene protons (H_a and H_b) displayed initial upfield perturbations up until to 0.5 equivalents of Cu(I), and then moved downfield in the opposite direction upon further Cu(I) addition. These observations suggested the formation of a 2:1 host-guest complex followed by a 1:1 binding mode at higher Cu(I) concentration (Figure 4.19). By monitoring the benzene spacer protons (H_a and H_b), WinEQNMR2 analysis of the titration data determined an association constant for Cu(I) binding $K_{2:1} > 10^4$ M^{-1}. In stark contrast, the isomeric macrocycle ***meta*-4.26**, prepared by Dr. Jason Lim, showed more complex ^{1}H-resonances upon addition of Cu(I) from 0.25-0.75 equivalents, indicating that the Cu(I) binding process was slow on the NMR time scale with multiple equilibria in the same deuterated solvent. Notably, no perturbation of signals from the polyether regions of both ***ortho*-4.26** and ***meta*-4.26** macrocycles was seen during the titration experiments, indicating that Cu(I) was bound exclusively by the N-donor atoms of the iodotriazole groups.

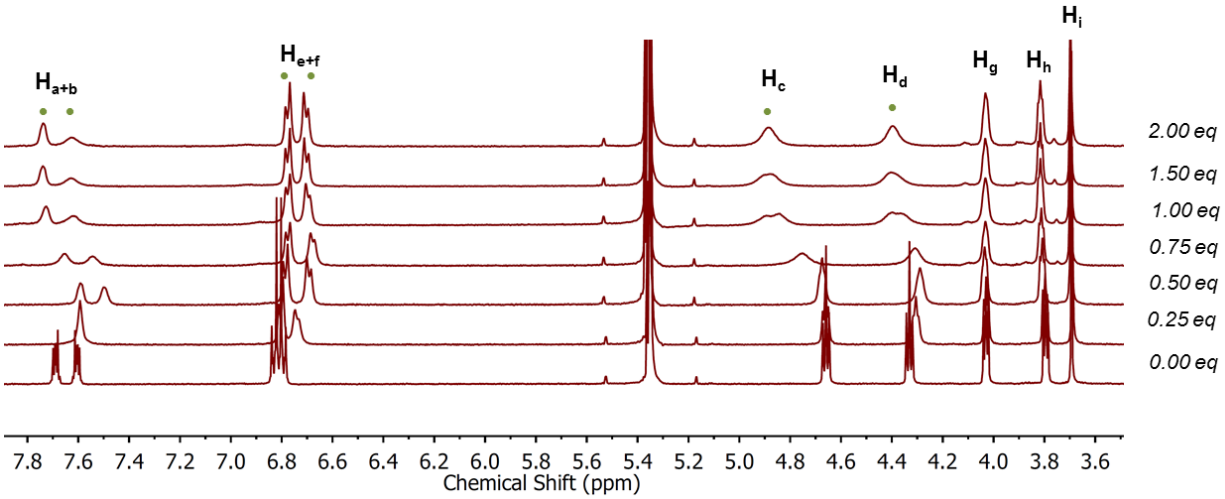

Figure 4.19 Truncated ^{1}H-NMR spectra of ***ortho*-4.26** macrocycle in d_2-dichloromethane upon addition of Cu(I).

4.5.3 Rotaxane synthesis *via* active metal template methodology

The apparent strong binding of Cu(I) by macrocycle ***ortho*-4.26** observed by ^{1}H NMR led to the CuAAC-AMT synthesis of the rotaxane being undertaken. A 1:1 THF/DCM solution containing an equimolar of macrocycle ***ortho*-4.26** and $Cu(MeCN)_4PF_6$ with a five-fold excess of stopper alkyne **4.33** and azide **4.34** was stirred at room temperature. After 72 hours, complete consumption of the alkyne and azide reactants, was observed with ESI-MS analysis suggesting evidence of XB [2]rotaxane ***ortho*-4.35** formation (m/z = 1981 for $[M+H]^+$). The removal of copper with an aqueous solution of EDTA followed by a chromatographic purification afforded pure [2]rotaxane ***ortho*-4.35** in 30%yield (Scheme 4.13), while the 1,3-isomer ***meta*-4.35** was isolated in 41% yield. This successful preparation of both regioisomeric [2]rotaxanes suggested that conformational flexibility of both macrocycles facilitated effective endo-coordination of the Cu(I) catalyst. The [2]rotaxane ***ortho*-4.35** was characterised by ^{1}H (Figure 4.20) and ^{13}C-NMR spectroscopy and HRMS.

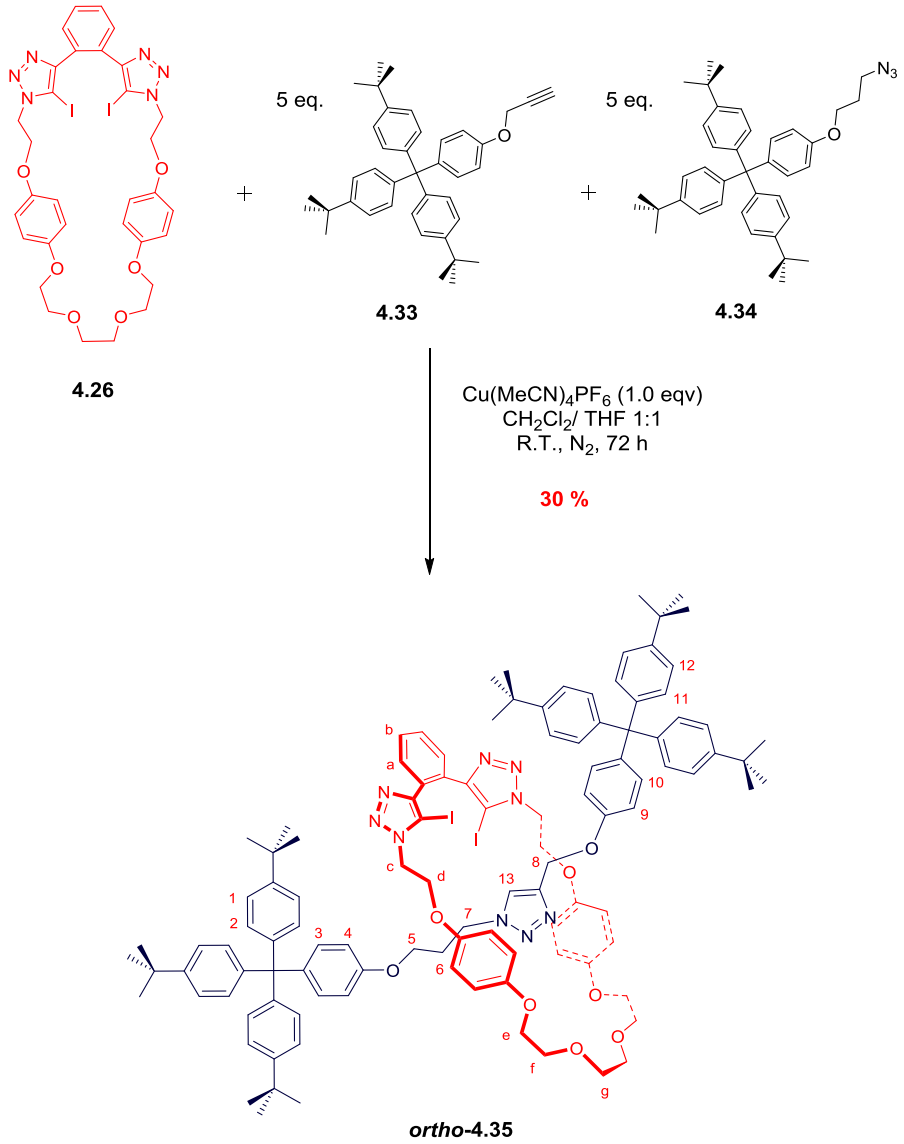

Scheme 4.13 Synthesis of [2]rotaxane ***ortho*-4.35**.

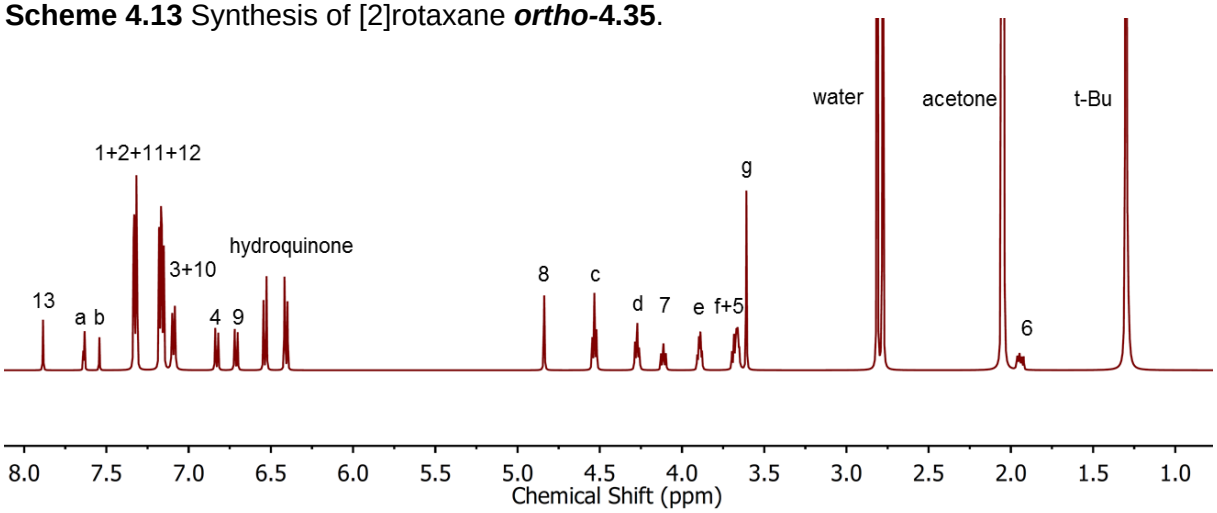

Figure 4.20 ^{1}H-NMR of [2]rotaxane ***ortho*-4.35** in d_6-acetone.

The interlocked nature of the rotaxane ***ortho*-4.35** was confirmed by $^{1}H—^{1}H$ two-dimensional ROESY spectroscopy (Figure 4.21). A range of inter-component through space couplings were observed including triazole proton (H_{13}) and polyether protons ($H_{f,g,e}$) as well as hydroquinone protons and propyl protons ($H_{7,8}$) from the axle component.

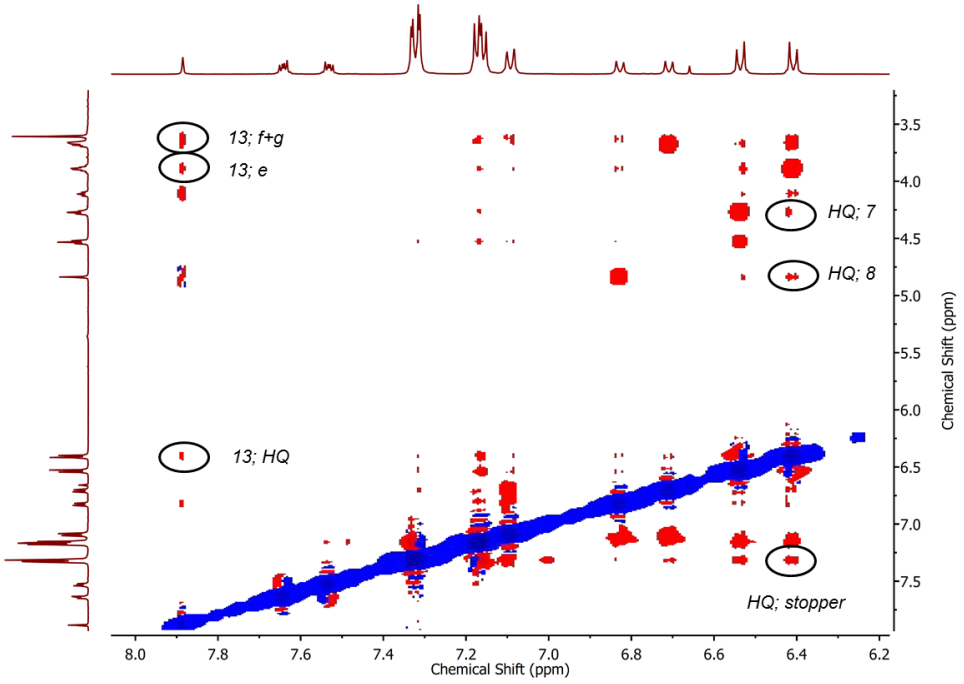

Figure 4.21 ^{1}H- ROESY NMR of a [2]rotaxane ***ortho*-4.35**.

4.5.4 Anion Binding Studies

The anion binding studies of XB rotaxane ***ortho*-4.35** were investigated by ^{1}H-NMR spectroscopic titration experiments in d_6-acetone. The addition of TBACl led to significant downfield perturbations ($\Delta\delta$ > 0.2 ppm) of the axle triazole proton (H_{13}), indicating the halide anion being bound close to the rotaxane binding cavity (Figure 4.22). ^{1}H-NMR titration of Br^-, I^-, and SO_4^{2-} resulted in similar chemical shift changes to the rotaxane's protons were observed with Br^-, I^-, and SO_4^{2-}.

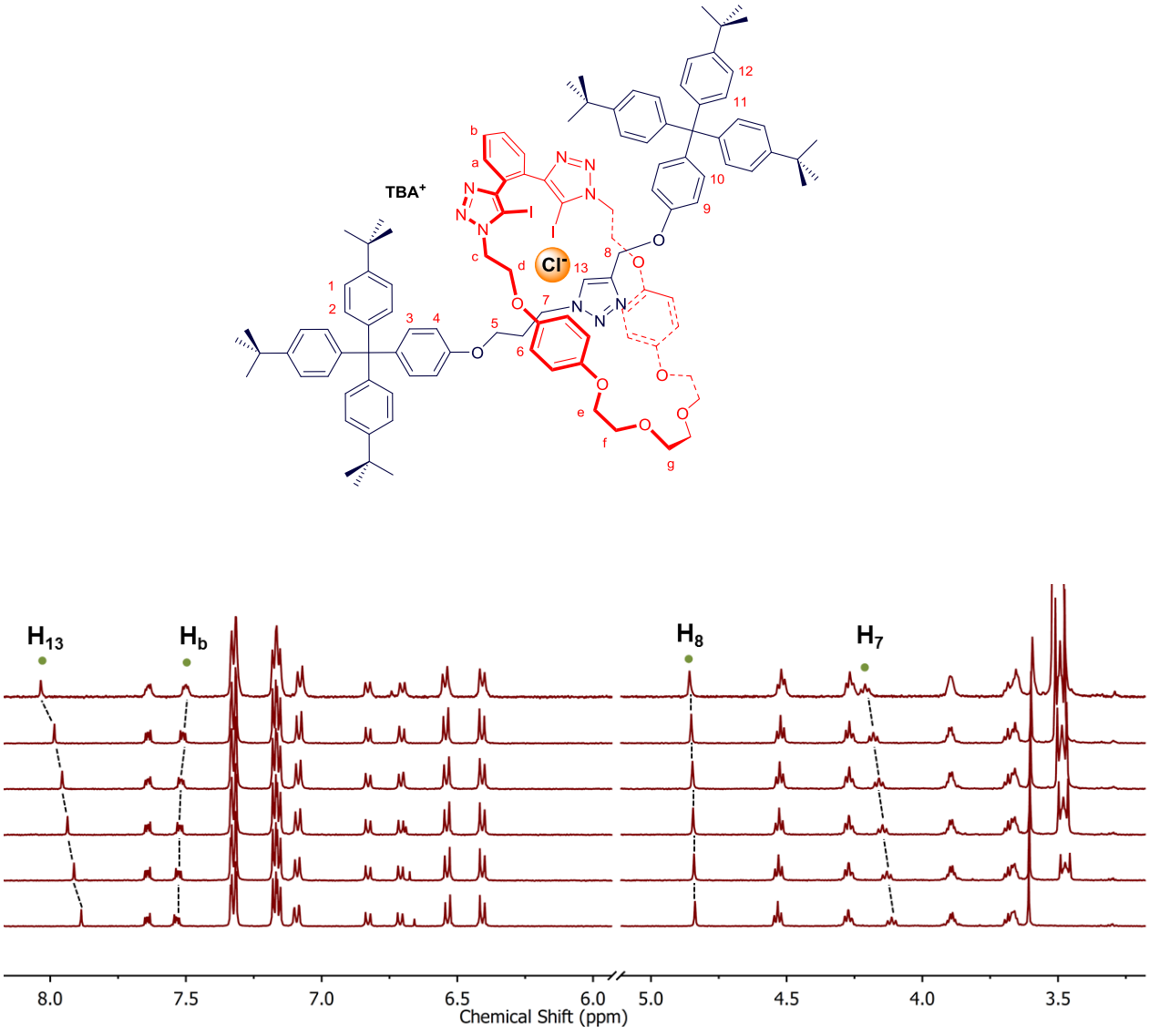

Figure 4.22 Truncated ^{1}H-NMR of ***ortho*-4.35** in the presence of an increasing amount of chloride anion added as the tetrabutylammonium salt.

Table 4.6 Anion association constants K_a (M^{-1}) for ***ortho-*** and ***meta*-4.35** in d_6-Acetone. [a]

Anion	$K_a(M^{-1})$ in d_6-Acetone at 298 K	
	***ortho*-4.35**	***meta*-4.35**
Cl^-	89	4384
Br^-	64	2139
I^-	34	902
SO_4^{2-}	$K_{2:1} = 211$[b] $K_{1:1} = 425$[b]	$>10^4$

[a] Axle triazole proton H_{13} monitored for both rotaxanes. Values of Ka are determined by the WinEQNMR2 software using a 1:1 host-guest binding model unless otherwise stated. Errors (±) are less than 10%, [b] Values of K_a calculated using BindFit following a host–guest 2:1 binding model. ([rotaxanes]=1.0 mm, 500 MHz, T=298 K)

WinEQNMR2 analysis of the titration data obtained by monitoring chemical shift changes in the triazole axle proton H_{13} (Figure 4.23) determined modest association constants summarised in Table 4.6 Anion constants obtained from rotaxane ***ortho*-4.35** and ***meta*-4.35** displayed anion binding selectivity preference SO_4^{2-} > Cl^- > Br^- > I^-, in order of increasing anion charge density and basicity. Despite the 1,2-bis-iodotriazole benzene motif being competent for CuAAC-AMT reaction the anion recognition capabilities of ***ortho*-4.35** are modest in comparision to ***meta*-4.35**, this stark constrast in halide and oxoanion affinity is rationalised by the non-convergent nature of the XB donors of ***ortho*-4.35.**

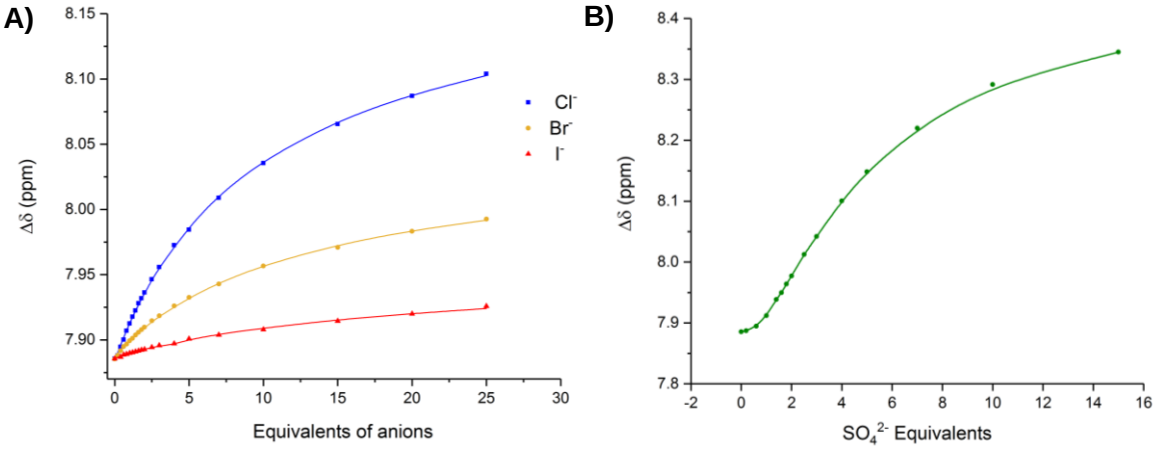

Figure 4.23 Binding isotherms showing the changes in the chemical shift of axle prototriazole aromatic proton H_{13} with increasing equivalents of anions added (A) halides binding and (B) sulfate binding ([***ortho*-4.35**] = 1.0 mM, 500 MHz, T = 298 K).

4.6 Conclusion and Future Directions

The work described in this chapter aimed to study the anion coordination chemistry of 1,2-bis-iodotriazolium benzene as a novel XB motif for anion recognition by its incorporation in acyclic receptors and an interlocked host.

Whilst demonstrating strong halide affinity and enhanced anion recognition in comparison to their HB analogues, the 1,2-bis-iodotriazolium motif is somewhat limited in its application due to the steric and electronic consequences of two ortho substituted iodotriazoles. Hence, attempts to prepare interlocked host structures *via* anion templation using this motif also proved challenging. Despite its successful employment as a Cu(I) binding motif in the CuAAC-AMT assembly of an interlocked host, the resultant rotaxane displayed modest anion recognition capabilities in comparison to its regioisomeric analogue.

Interestingly the solid state evidence for divergent XB–anion interactions observed suggests that the 1,2-bis-iodotriazolium benzene motif could be a potent molecular building block for anion induced assembly of 1D-supramolecular polymers in solution, further investigation could produce a series of XB-anion mediated responsive materials.

Chapter 5

Experiments and Synthetic Procedures

Chapter 5: Experiments and Synthetic Procedures

5.1 General considerations

5.1.1 Chemicals and solvents

All solvents and reagents used in this thesis were purchased from commercial suppliers. Dry solvents were obtained by purging with nitrogen and then passing through an MBraun MPSP-800 column. Deionised water was collected from a Milli-Q$_r$ Millipore machine. TBA salts, Grubbs' I catalyst, Grubbs' II catalyst, $[Cu(MeCN)_4][PF_6]$ were stored in a vacuum desiccator containing phosphorus pentoxide prior to use. TBTA was synthesised and kept in the freezer after used. Triethylamine was distilled from a commercial package and stored over potassium hydroxide. Brine refers to a saturated aqueous solution of NaCl, $NH_4OH_{(aq.)}$ refers to a 28–30% solution of NH_3 in water. Column chromatography was carried out on Merck$_r$ silica gel 60 under a positive pressure of nitrogen, preparative TLC was performed on 20×20 cm plates, with a silica layer of thickness 1 mm. Amberlite® was "loaded" by washing the resin with $NaOH_{(aq.)}$ (10%), water, and either $NH_4Cl_{(aq.)}$ (1M), $NaNO_{3\ (aq.)}$ (1 M) or $NH_4PF_{6(aq.)}$ (0.1 M), followed by further water, and the solvent to be used in the anion exchange.

5.1.2 Instrumentations

Routine NMR spectra were recorded on either a Varian Mercury 300, a Bruker AVIII 400 or a Bruker AVIII 500 spectrometer with 1H NMR titrations recorded on a Bruker AVIII 500 spectrometer. Chemical shifts are quoted in parts per million relative to the residual solvent peak with signal splittings denoted as singlet (s), doublet (d), triplet (t), quartet (quart.), quintet (quint.), septet (sep.) and multiplet (m). Mass spectra were carried out on Waters Micromass LCT and Bruker microTOF spectrometers. Fluorescence, UV-Vis and circular dichroism spectra were recorded on a Horiba Fluorolog 3, T60U (PG Instruments Ltd) spectrophotometer and Applied Photophysics Chirascan instrument respectively using a quartz cuvette with path length of 1 cm. Isothermal titration calorimetry experiments were performed on a Microcal PEAQ-ITC automated system and an iTC MicroCalorimeter.

5.2 ^{1}H-NMR titration protocols

5.2.1 Anion binding in organic and aqueous-organic mixture

Spectra for ^{1}H NMR titrations were recorded at 293 K on a Varian Unity Plus 500 spectrometer with ^{1}H operating at 500 MHz. Initial sample volumes were 0.50 mL and concentrations were 2.0 mM of host in all cases. Anion solution (100 mM) as the tetrabutylammonium salts were added in aliquots, the samples thoroughly shaken and spectra recorded. Spectra were recorded at 0, 0.2, 0.4, 0.6, 0.8, 1.0, 1.2, 1.4, 1.6, 1.8, 2.0, 2.5, 3.0, 4.0, 5.0, 7.0 and 10 equivalents of anion. In all cases where association constants were calculated, bound and unbound species were found to be in fast exchange on the NMR timescale. In all cases where association constants were calculated, bound and unbound species were found to be in fast exchange on the NMR timescale. Stability constants were obtained by analysis of the resulting data using the WinEQNMR2328 computer**.**

5.2.2 Anion binding in water

For the permethylated β-cyclodextrin-appended acyclic hosts and osmium(II)rotaxane in Chapter 3, aliquots of the anion guest as the sodium salt, (100-200 mM in D_2O) were added to 0.5 mL of a 1.0 mM solution of the host in D_2O at 298 K. A trace amount of acetone was added as an internal reference, such that it made up less than 0.05% of the total volume, and all spectra referenced to its resonance at 2.20 ppm. Spectra were recorded at 0, 1, 2, 3, 5, 7, 10, 15, 20, 25, 30, 40, 50, 60, 80, 100 and 120 equivalents of anion. In all cases where association constants were calculated, bound and unbound species were found to be in fast exchange on the NMR timescale. Stability constants were obtained by analysis of the resulting data using the WinEQNMR2328 program**.**

5.2.3 Anion titration of heteroditopic hosts

Spectra for ^{1}H NMR titrations were recorded at 293 K on a Varian Unity Plus 500 spectrometer with ^{1}H operating at 500 MHz. Initial sample volumes were 0.50 mL and concentrations were 2.0 mM of host in all cases.

Sodium ions bound receptor titrations, the solution of 4mM $NaPF_6$ in a selected solvent was used to dissolve solid host solution. Anion solution (100 mM) as the tetrabutylammonium salts were added in aliquots, the samples thoroughly shaken and spectra recorded. Spectra were recorded at 0, 0.2, 0.4, 0.6, 0.8, 1.0, 1.2, 1.4, 1.6, 1.8, 2.0, 2.5, 3.0, 4.0, 5.0, 7.0 and 10 equivalents.

In case of uncomplexed hosts titration, solid powder of host was dissolved in a selected solvent to obtain 2 mM of host. Anion solution (250 mM) as the the

tetrabutylammonium salts were added in aliquots, the samples thoroughly shaken and spectra recorded.

In all cases where association constants were calculated, bound and unbound species were found to be in fast exchange on the NMR timescale. Stability constants were obtained by analysis of the resulting data using the WinEQNMR2328 program**.**

5.3 Luminescence anion binding titration protocols

Titrations were typically carried out by starting with 1.5 mL of a 5×10^{-5} M solution of the host and adding aliquots of a solution containing the same concentration of the host together with a known concentration of the anion under study.

5.4 Isothermal titration calorimetry anion binding titration protocols

The isothermal titration calorimetry experiments were performed on a Microcal PEAQ-ITC automated system for receptor **3.42, 3.43, 3.44·NO_3** in unbuffered distilled water at 298 K. An initial concentration of the host was 0.2 mM, with a 20 mM solution of NaI and $NaReO_4$, and 50 mM solution of $NaClO_4$, $NaIO_4$, NaSCN added in 35 aliquots. The data from the first addition of 0.5 µL was discarded, with data collected for the subsequent 34 additions of 1 µL. Heats of dilution were measured by a titration of anion solution as their sodium salts into water. The MicroCal PEAQ-ITC Analysis Software determined values of K_a and ΔH *via* a non-linear least squares regression fit of the experimental data to the one-set of sites model. These values were then used to determine the ΔG and ΔS values.

5.5 Isothermal titration calorimetry anion binding titration protocols

All electrochemical experiments were performed with an Autolab Potentiostat using a three-electrode setup: A glassy carbon disk working electrode (3 mM diameter, BASi), a platinum wire counter electrode and a Ag|AgCl (3.4 M KCl) leak-free reference electrode (Innovative Instruments). In order to circumvent the development of junction potentials of this electrode in the presence of various ions a Ag|AgCl reference electrode with a Pt wire frit was utilized for titration experiments. Cyclic voltammetry was performed at a scan rate of 0.1 V/s, unless otherwise noted. Reversibility studies were performed at the following scan rates: 0.025, 0.05, 0.075, 0.1, 0.2, 0.4, 0.6 and 0.8 V/s. Square wave voltammetry was performed utilizing a frequency of 25 Hz, an amplitude of 20 mV and a step potential of 2 mV (titrations) or 5 mV (all other experiments). During titration experiments the host concentration as well as the overall anion concentration was kept constant, at 0.1 mM and 100 mM, respectively.

5.6 Solid-liquid extraction experiments

To conduct a solid-liquid extraction experiment, 2mM solution of receptor (0.5 ml) in a selected solvent was added to a clean and sealed *via*l containing an excess of respective solid Na^+ salt (5 equivalents with respect to a receptor). The solid salt remains insoluble in a solvent. The mixture was allowed to sonicate for an hour at room temperature. After that, the remaining solid was filtered-off to get a clear post-extraction solution. The post-extraction solution of each samples was monitored their chemical shift changes *via* ^{1}H-NMR spectroscopy in comparison to a pre-extraction solution. Aliquots of a post-extraction solution were taken to analyse ESI-MS spectra of ion-pair complex.

5.7 Synthetic Procedures and Characterisations of Compounds in Chapter 2

3,5-Diethynylpyridine (2.2)

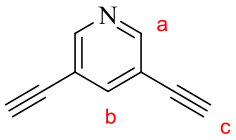

3,5-Dibromopyridine (1.426 g, 6mmol), CuI (68 mg, 0.35mmol), PPh3 (0.268 g, 1mmol), and Pd2(dba)3 (95 mg, 0.1mmol) were added to round bottom flask. Triethylamine (30 ml) was added to the mixture, and then deoxygenated by bubbling N_2 to the reaction mixture. Trimethysilylacetylene (1.529 g or2.2 ml, 15.6 mmol) was added through septum. The reaction container was sealed and heated to 75°C for 18 hours. After that, the mixture was allowed to cool to room temperature, and filtered through a cotton wool plug. To collect organic yellow solution, Diethylether (5x40 ml) was poured to wash solid residue. The organic phase was dried under vacuum to get TMS-protected product. In the deprotection step, the residual yellow oil was dissolved in MeOH, followed by a 5.0M KOH (4 ml). The mixture was stired under ambient reaction temperature for 30 min, or until the disappearance of starting material. The product was extracted by pentane (7x40 ml). The combined organic phase was filtered through a cotton wool plug, and evaporated at standard temperature and pressure to get yellow solid. The yellow solid as sublimed to get the feathery white crystal (0.59 g, 75%).

^{1}**H-NMR** (400MHz, $CDCl_3$) δ = 8.66 (2H, d, J = 2.0 Hz, H_a), 7.86 (1H, s, H_b), 3.25 (2H, s, H_c).

3,5-bis(iodoethynyl)pyridine (2.3)

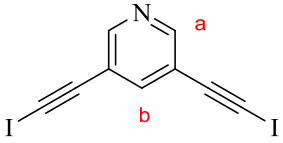

3,5-Dethynylpyridine (0.127 g, 1mmol) was dissolved in dry THF (10 ml), followed by CuI (29 mg, 0.15 mmol) and N-iodomorpholine (0.75 g, 2.2mmol). The reaction was stirred at room temperature for 2 hours, after which white precipitation had formed. The suspension was poured onto an alumina pad saturated with dichloromethane to collect the filtration. The solid phase was washed with dichloromethane (4x10 ml). The combined organic fractions was washed with a solution of $Na_2S_2O_3$, and dried over $MgSO_4$. The solvent was removed in *vacuo*. The residue was taken up in 10% EtOAc/Hexane, and run through a short silica plug.

The solvent was removed to afford the solid precipitation which can be purified by recrystallization from hexane (0.223 g, 59%). The pure product should be use immediately and kept in dark

^{1}H-NMR (400MHz, $CDCl_3$) δ = 8.58 (2H, d, J = 2.0 Hz, H_a), 7.74 (1H, t, J = 2.0 Hz, H_b).

NO_2-Benzo[15]crown-5 (2.5)

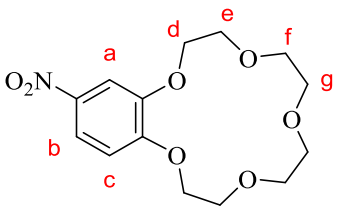

Benzo[15]crown-5 (1 g, 3.75 mmol) was dissolved in the mixture of $CHCl_3$ (22 ml) and acetic acid (17 ml) in round bottom flask, and cooled the mixture in an ice bath. Then, a cool solution of 70% HNO_3 (6.4 ml) in acetic acid (5ml) was slowly dropped to the mixture. The reaction was stirred overnight at room temperature. The organic phase was diluted with $CHCl_3$ and washed with water (50 ml), followed by 5% aqueous solution of Na_2CO_3 (50 ml). The organic residue was dried over $MgSO_4$ and removed under vacuum to get yellowish solid (95%). At this stage, compound is pure by ^{1}H-NMR. To obtain white solid of 4-nitro-benzo[15]crown-5, recrystallization of product from hot ethanol can be used to obtain purer product.

^{1}H-NMR (400MHz, $CDCl_3$) δ = 7.90 (1H, dd, J = 8.9 Hz, J = 2.6 Hz, H_b), 7.73 (1H, d, J = 2.6 Hz, H_a), 6.88 (1H, d, J = 8.9 Hz, H_c), 4.18 - 4.26 (4H, m, H_d), 3.91 - 3.98 (4H, m, H_e), 3.77 (8H, dquin, J = 3.4 Hz, J = 1.9 Hz, $H_{f\text{-}g}$)

NH_2-Benzo[15]crown-5 (2.6)

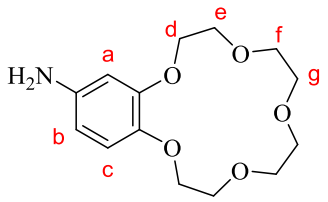

The mixture of Pd/C (10%loading) (123 mg) and hydrazine monohydrate (10 ml) were prepared in ethanol (22 ml), then NO_2-Benzo[15]crown-5 **2.5** (1 g, 3.5 mmol) was added subsequently. The reaction was refluxed for 5h, and then solid residue was removed by filtering through Celite plug. The solvent was removed *in vacuo* obtaining emulsion oil. The crude product was redissolved in DCM and dried over $MgSO_4$. Solvent was removed *in vacuo* to get colourless oil in quantitative yield. The compound was used in the next step without further purification.

^{1}H-NMR (400MHz, $CDCl_3$) δ = 6.74 (1H, d, J = 8.4 Hz, H_c), 6.28 (1H, d, J = 2.6 Hz, H_a), 6.22 (1H, dd, J = 8.4 Hz, J = 2.6 Hz, H_b), 4.05 - 4.11 (4H, m, H_d), 3.85 - 3.92 (4H, m, H_e), 3.73 - 3.78 (8H, m, $H_{f\text{-}g}$)

N_3-Benzo[15]crown-5 (2.7)

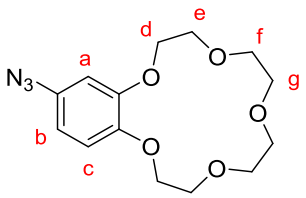

NH_2-Benzo[15]crown-5 (0.5 g, 1.76 mmol) was added to a solution of 37% HCl in water (1:1, 10 ml), followed by ethanol (5 ml). The reaction mixture was cooled to 0°C. $NaNO_2$ (0.18g, 2.5 mmol) was subsequently added portionwise with stirring further 15 minutes, then NaN_3 (0.16 g, 2.5 mmol) added while stirring at 0°C. The reaction mixture was allowed to room temperature and stirred overnight. The mixture was diluted with water and extracted with diethyl ether (3x30 ml). The combined organic phase was washed with $NaHCO_3$ (50 ml), brine (30 ml), dried over $MgSO_4$, and concentrated to dryness *in vacuo* to give the desired product as brown solid in 90% yield without further purification.

^{1}H-NMR (400MHz, $CDCl_3$) δ = 6.86 (1H, d, J = 8.4 Hz, H_c), 6.59 (1H, dd, J = 8.6 Hz, J = 2.6 Hz, H_b), 6.53 (1H, d, J = 2.6 Hz, H_a), 4.10 - 4.15 (4H, m, H_d), 3.91 (4H, dt, J = 5.5 Hz, J = 3.5 Hz, H_e), 3.74 - 3.79 (8H, m, H_f and H_g)

XB heteroditopic receptor (2.1·XB)

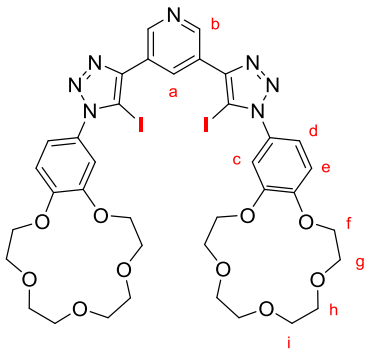

A solution of $[Cu(MeCN)_4]PF_6$ (34 mg, 0.09 mmol) and TBTA (48 mg, 0.09) in a mixture of 1:1 THF/DCM (3 ml) was added 3,5-diiodoethylnylpyridine **2.3** (114 mg, 0.3 mmol) and N_3-Benzo[15]crown-5 (204 mg, 0.66 mmol). The mixture was stirred under atmosphere of N_2 at room temperature for 3 days. Dichloromethane (10 mL) was added, and then the organic layer was washed with 35% aqueous ammonia solution (2 x 30 mL). The aqueous layer was extracted with dichloromethane (2 x20 mL) and the combined organics were wash with H_2O (3 x 30 ml). Solvent was removed *in vacuo* to obtain dark brown solid. The solid was washed with Et_2O (3 x30 ml); after which MeOH was added to the mixture, sonicated and decanted. The MeOH washing process was repeated for 3 times to get brown shiny solid (0.27 g, 90%)

^{1}H-NMR (400 MHz, $CDCl_3$) δ = 9.27 (d, *J* = 2.2 Hz, 1H), 7.07 – 7.00 (m, 1H), 6.99 – 6.91 (m, 2H), 4.15 (dt, *J* = 15.8, 4.3 Hz, 4H), 3.88 (dt, *J* = 9.0, 4.2 Hz, 4H), 3.76 – 3.70 (m, 3H), 3.71 (s, 4H).

^{13}C-NMR(126 MHz, $CDCl_3$) δ = 150.82, 149.47, 148.44, 147.36, 133.38, 129.93, 126.39, 119.59, 113.18, 112.21, 71.28, 70.50, 69.47, 69.38, 69.27, 69.20.

HRMS (ESI+ve) m/z: 998.10339 ($[M+H]^+$, $C_{37}H_{41}O_{10}N_7I_2$ requires 998.10770)

HB heteroditopic receptor (2.1·HB)

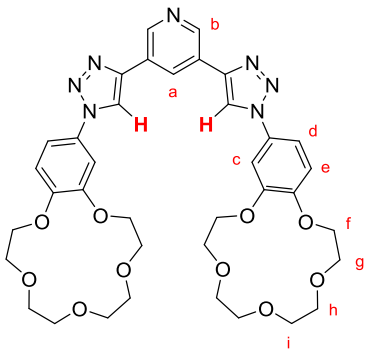

A solution of $[Cu(MeCN)_4]PF_6$ (16 mg, 0.045 mmol) and TBTA (23 mg, 0.045) in DCM (1 ml) was added 3,5-diethylnylpyridine (18.7 mg, 0.15 mmol), N_3-Benzo-15-crown-5 (100 mg, 0.323 mmol), and DIPEA (194 µl, 0.4 mmol). The reaction was stirred at room temperature for 2 days; after which the reaction was found to turn green. The product was purified with the same method for XB analogous. The obtaining product is off white solid (109 mg, 72%)

^{1}H-NMR (400 MHz, $CDCl_3$) δ = 9.14 (s, 2H, H_b), 8.77 (s, 1H, H_a), 8.32 (s, 2H, H_{trz}), 7.42 (s, 2H, H_c), 7.28 (s, 2H, H_e), 7.01 (d, *J* = 8.6 Hz, 2H, H_d), 4.25 (dt, *J* = 17.5, 4.4 Hz, 8H, H_f), 3.97 (dt, *J* = 6.8, 2.5 Hz, 8H, H_g), 3.79 (p, *J* = 2.7, 2.1 Hz, 16H, H_{h+i}).

^{13}C-NMR (126 MHz, $CDCl_3$) δ = 149.93, 149.72, 146.52, 144.86, 130.58, 129.87, 126.63, 118.71, 113.80, 112.95, 106.96, 71.09, 71.07, 70.40, 70.36, 69.38, 69.27, 69.20, 69.13.

HRMS (ESI+ve) m/z: 746.31421 ($[M+H]^+$, $C_{37}H_{44}O_{10}N_7$ requires 746.31442)

Fluorotriazole receptor (2.8)

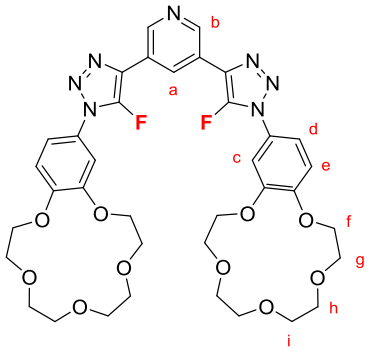

2.1·XB (200 mg, 0.200 mmol) was suspended in CH_3CN (5 ml) in a microwave vial, to which was added a solution of KF (120 mg, 2.07 mmol) in H_2O (5 ml), the vial was then sealed and heated by microwave irradiation to 175^0C for 10 minutes to obtain a brown solution. The reaction mixture was diluted with H_2O (50 ml) and $CHCl_3$ (50 ml) and organic and aqueous layers separated, the aqueous was then extracted by $CHCl_3$ (50 ml). The combined organics were then concentrated *in vacuo* to afford a brown residue, which was subjected to purification by preparatory thin layer chromatography using 7% MeOH/$CHCl_3$ as an eluent to afford **2.8** as an orange solid (31 mg, 20 %).

^{1}H-NMR (400 MHz, $CDCl_3$) δ = 9.15 (d, *J* = 2.0 Hz, 2H, H_b), 8.74 (s, 1H, H_a), 7.32 – 7.17 (m, 4H, under solvent peak, H_{c+d}), 7.03 (d, *J* = 8.6 Hz, 2H, H_d), 4.23 (dt, *J* = 6.8, 2.4 Hz, 8H, H_f), 3.96 (dq, *J* = 4.4, 1.9 Hz, 8H, H_g), 3.79 (dq, *J* = 3.8, 2.2 Hz, 16H, H_{h+i}).

^{13}C-NMR (101 MHz, $CDCl_3$) δ = 150.86, 150.36, 149.95, 148.01, 146.13, 146.09, 128.93, 127.19, 125.17, 125.12, 124.83, 124.75, 114.98, 114.94, 113.71, 108.39, 71.23, 70.50, 69.44, 69.35, 69.28, 69.25.

^{19}F-NMR (376 MHz, $CDCl_3$) δ = -148.01.

HRMS (ESI+ve) m/z: 782.29547 ($[M+H]^+$, $C_{37}H_{42}O_{10}N_7F_2$ requires 782.29557)

ChB heteroditopic receptor (2.1·ChB)

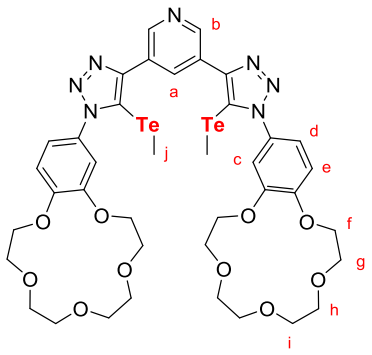

Tellurim powder (65 mg, 0.509 mmol) suspended in a minimum of dry THF and the sealed vial cooled to 0^0C, to which was added a solution of a 1.6M solution of MeLi in diethyl ether (0.27 ml, 0.432 mmol). After the suspension had warmed to room temperature the mixture was sonicated until the formation of a brown suspension was evident and left to stir for 1 hour. Separately a suspension of **2.8** (59 mg, 0.0755 mmol) in a minimum of THF was made and added dropwise to the brown suspension, the mixture was then heated in the dark at 80^0C for 4 hours. The mixture was then allowed to warm to room temperature and MeI (18.3 µl, 0.294 mmol) added and left to stir for 30 minutes. After which time the mixture was diluted with H_2O (50 ml) and extracted into $CHCl_3$ (50 ml), collected organic phase was dried over MgSO4 and subjected to purification by preparatory thin layer chromatography (eluent: 7 % MeOH/$CHCl_3$) to afford the **2.1·ChB** as an orange-brown solid (11.7 mg, 0.0113 mmol, 15 %).

^{1}H-NMR (500 MHz, $CDCl_3$) δ = 9.27 (s, 2H), 8.92 (d, *J* = 2.1 Hz, 1H), 7.13 (dd, *J* = 8.4, 2.4 Hz, 2H), 7.11 (d, *J* = 2.4 Hz, 2H), 7.01 (d, *J* = 8.4 Hz, 2H), 4.23 (dt, *J* = 17.6, 4.1 Hz, 8H), 3.97 (dt, *J* = 11.2, 4.4 Hz, 8H), 3.80 (th, *J* = 6.2, 3.3 Hz, 16H), 1.85 (s, 6H).

^{13}C-NMR (126 MHz, $CDCl_3$) δ = 150.66, 150.45, 149.39, 148.80, 134.80, 131.09, 127.44, 119.17, 113.12, 112.02, 101.21, 71.24, 70.48, 69.48, 69.38, 69.21, 69.15, -12.88.

^{125}Te-NMR (158 MHz, $CDCl_3$) δ = 166.77.

HRMS (ESI+ve) m/z: 1030.15585 ($[M+H]^+$, $C_{39}H_{48}N_7O_{10}Te_2$ requires 1032.15460)

NO_2-Dibenzo[24]crown-8 (2.21)

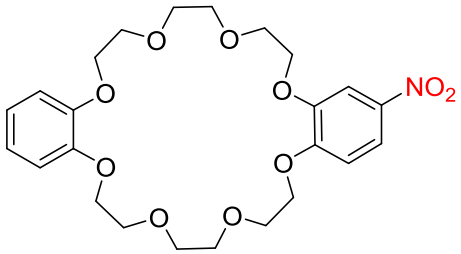

Ditosylate **2.20** (2.87g, 4.2 mmol), 2-nitrocatechol (653 mg, 4.2 mmol), and KPF_6 (928 mg, 5.04 mmol) were mixed in MeCN (140 ml), and then degassed throughout a solution. K_2CO_3 (2.32g, 16.8 mmol) was added to a reaction mixture which was refluxed in the absence of light for 72 hours. After cool down to room temperature and removing solid residues, the reaction was dried and re-dissolved in DCM. The organic residue was washed with pyridine hydrochloride solution (3 times) and water (3 times), and subsequently dried over $MgSO_4$. Solvent was removed to obtain a yellow solid product of **2.21** in 90% yield.

^{1}H-NMR (400 MHz, $CDCl_3$) δ = 7.87 (dd, *J* = 8.9, 2.6 Hz, 1H), 7.72 (d, *J* = 2.6 Hz, 1H), 6.88 (q, *J* = 5.2, 4.6 Hz, 5H), 4.23 (dt, *J* = 7.6, 4.0 Hz, 4H), 4.15 (t, *J* = 4.3 Hz, 4H), 3.99 – 3.88 (m, 9H), 3.83 (d, *J* = 2.8 Hz, 8H).

^{13}C-NMR (101 MHz, $CDCl_3$) δ = 154.46, 148.93, 148.85, 148.47, 141.57, 121.64, 121.57, 118.18, 114.17, 114.06, 111.47, 108.54, 71.47, 71.28, 69.95, 69.88, 69.73, 69.55, 69.49, 69.43, 69.30.

HRMS (ESI+ve) m/z: 511.22855 ($[M+NH_4]^+$, $C_{24}H_{35}N_2O_{10}$ requires 511.22862)

NH_2-Dibenzo[24]crown-8 (2.22)

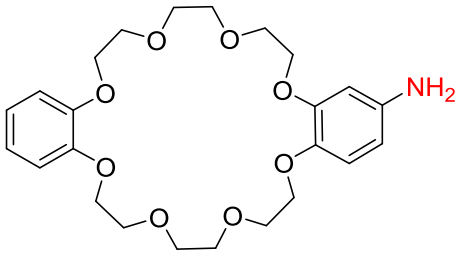

To a solution of NO_2-dibenzo[24]crown 8 **2.21** (1.07g, 2.03 mmol) in EtOH (10 ml) was added a suspension of 10%(w/w) Pd/C (100 mg) in water (0.5ml) and hydrazine monohydrate (5.5ml). The mixture was refluxed at 80°C for 5 hrs, followed by filtered through Celite® and removed solvent to afford a white solid in quantitative yield. Product can be used in the next step without further purification.

^{1}H-NMR (400 MHz, $CDCl_3$) δ = 6.88 (d, *J* = 2.4 Hz, 4H), 6.70 (d, *J* = 8.4 Hz, 1H), 6.25 (d, *J* = 2.6 Hz, 1H), 6.18 (dd, *J* = 8.4, 2.6 Hz, 1H), 4.14 (t, *J* = 4.3 Hz, 4H), 4.06 (q, *J* = 5.0 Hz, 4H), 3.96 – 3.71 (m, 16H).

^{13}C-NMR (101 MHz, $CDCl_3$) δ = 150.22, 148.98, 148.95, 141.70, 141.55, 121.49, 121.46, 117.32, 114.25, 114.18, 107.20, 102.55, 71.19, 70.98, 70.65, 70.18, 69.91, 69.89, 69.86, 69.44, 69.33, 69.03.

HRMS (ESI+ve) m/z: 464.22760 ($[M+H]^+$, $C_{24}H_{34}NO_8$ requires 464.22789)

N_3-Dibenzo[24]crown-8 (2.23)

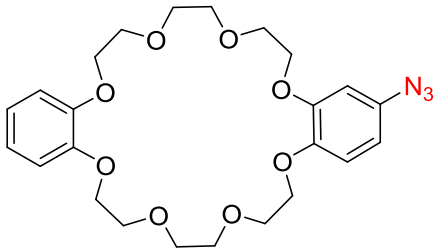

A solution of NH_2-Dibenzo[24]crown-8 **2.22** (139 mg, 0.3 mmol) in EtOH (5ml) was cooled down and added 1:1 HCl (37%)/H_2O. $NaNO_2$ (62 mg, 0.9 mmol) was subsequently added to a reaction mixture, then stirring at 0°C for 1 hour. After addition of NaN_3 (59 mg, 0.9 mmol), the reaction was left stirring overnight, followed by dilute with water. An aqueous solution was extracted using Et_2O, the organic layer was dry over $MgSO_4$ and removed solvent to obtain the target product **2.23** as a brown solid in 90% yield.

^{1}H-NMR (400 MHz, $CDCl_3$) δ = 6.94 – 6.80 (m, 5H), 6.58 (dd, *J* = 8.5, 2.6 Hz, 1H), 6.52 (d, *J* = 2.6 Hz, 1H), 4.14 (dt, *J* = 8.6, 4.0 Hz, 8H), 3.90 (q, *J* = 6.2, 5.3 Hz, 8H), 3.82 (s, 8H).

^{13}C-NMR (101 MHz, $CDCl_3$) δ = 150.09, 148.99, 148.96, 146.34, 133.45, 121.61, 115.45, 114.32, 114.26, 111.27, 105.57, 71.19, 70.00, 69.90, 69.70, 69.47, 69.45, 69.39.

HRMS (ESI+ve) m/z: 512.20007 ($[M+Na]^+$, $C_{24}H_{31}N_3O_8$ requires 512.20034)

Azido-catenane (2.25·PF_6)

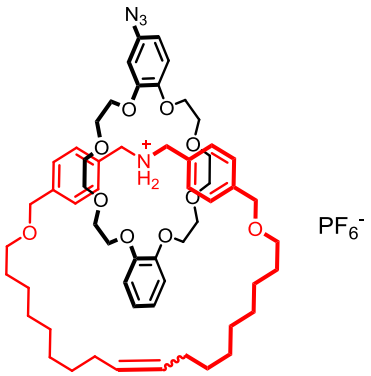

A solution of N_3-Dibenzo[24]crown-8 (100mg, 0.204 mmol) in dry and degassed DCM (100 ml) was added the bis-vinyl thread (139 mg, 0.204 mmol). After stirring at room temperature for 30 minutes, the first generation Grubbs' catalyst (35 mg, 0.043 mmol) was added to a reaction mixture and refluxed at 40°C for 48 hours. The crude mixture was stirred with activated charcoal (1 g) then filtered through Celite® to collect an organic residue. The mixture was purified by silica gel column chromatography (5% MeOH/DCM) and size exclusion chromatography to obtain the desire product in 16% yield.

^{1}H-NMR (500 MHz, 1:1 $CDCl_3$/MeOD) δ = 7.30 (dd, *J* = 8.2, 2.0 Hz, 4H), 7.19 (dd, *J* = 8.0, 3.1 Hz, 4H), 6.91 – 6.87 (m, 2H), 6.86 – 6.75 (m, 3H), 6.60 (ddd, *J* = 8.7, 4.0, 2.5 Hz, 1H), 6.44 (dd, *J* = 4.1, 2.5 Hz, 1H), 5.33 – 5.22 (m, 2H), 4.41 (d, *J* = 3.6 Hz, 4H), 4.18 – 4.03 (m, 8H), 3.84 – 3.70 (m, 8H), 3.54 – 3.35 (m, 12H), 1.90 (dq, *J* = 16.8, 6.3 Hz, 4H), 1.58 (hept, *J* = 7.4 Hz, 5H), 1.38 – 1.32 (m, 4H), 1.31 – 1.18 (m, 18H).

^{13}C-NMR (126 MHz, 1:1 $CDCl_3$/MeOD) δ = 149.20, 149.19, 147.98, 147.95, 147.93, 145.68, 145.66, 140.78, 140.75, 134.39, 134.35, 131.52, 130.92, 130.31, 130.03, 129.94, 128.47, 128.39, 122.45, 122.42, 122.40, 114.30, 113.36, 113.34, 113.31, 113.29, 111.83, 111.80, 105.10, 105.07, 72.64, 72.59, 71.29, 71.23, 71.19, 70.92, 70.89, 70.83, 70.77, 70.71, 70.68, 69.30, 69.24, 68.97, 68.93, 68.91, 68.86, 68.81, 52.79, 32.97, 30.39, 30.24, 30.20, 30.16, 30.06, 29.88, 29.71, 29.67, 29.25, 27.71, 26.97, 26.88.

HRMS (ESI+ve) m/z: 995.60962 ($[M\text{-}PF_6]^+$, $C_{58}H_{83}N_4O_{10}$ requires 995.61037)

Ammonium catenane functionalised XB Receptor (2.26·(PF$_6$)$_2$)

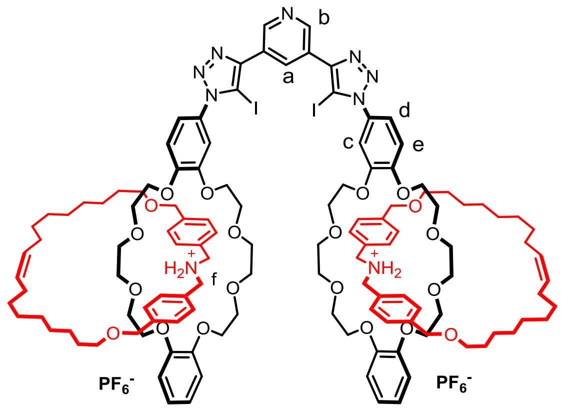

A mixture of Cu(MeCN)$_4$PF$_6$ (2.3 mg, 0.006 mmol) and TBTA (2.4 mg, 0.005 mmol) was stirred in dry and degassed DCM (0.5 ml) at room temperature for 15 minutes. 3,5-Diiodoethynylpyridine (5.7 mg, 0.015 mmol) was added to a solution mixture , followed by azido-catenane **2.25·PF$_6$** (36 mg, 0.036 mg). The reaction was stirred at room temperature for 72 hours prior to purify by preparative plate chromatography in 3% MeOH/DCM to afford a pure product in 85% yield after anion exchange to PF$_6^-$ salt.

^{1}H-NMR (500 MHz, 1:1 CDCl$_3$/MeOD) δ = 7.30 (dd, *J* = 8.2, 2.0 Hz, 4H), 7.19 (dd, *J* = 8.0, 3.1 Hz, 4H), 6.91 – 6.87 (m, 2H), 6.86 – 6.75 (m, 3H), 6.60 (ddd, *J* = 8.7, 4.0, 2.5 Hz, 1H), 6.44 (dd, *J* = 4.1, 2.5 Hz, 1H), 5.33 – 5.22 (m, 2H), 4.41 (d, *J* = 3.6 Hz, 4H), 4.18 – 4.03 (m, 8H), 3.84 – 3.70 (m, 8H), 3.54 – 3.35 (m, 12H), 1.90 (dq, *J* = 16.8, 6.3 Hz, 4H), 1.58 (hept, *J* = 7.4 Hz, 5H), 1.38 – 1.32 (m, 4H), 1.31 – 1.18 (m, 18H).

^{13}C-NMR (126 MHz, 1:1 CDCl$_3$/MeOD) δ = 149.20, 149.19, 147.98, 147.95, 147.93, 145.68, 145.66, 140.78, 140.75, 134.39, 134.35, 131.52, 130.92, 130.31, 130.03, 129.94, 128.47, 128.39, 122.45, 122.42, 122.40, 114.30, 113.36, 113.34, 113.31, 113.29, 111.83, 111.80, 105.10, 105.07, 72.64, 72.59, 71.29, 71.23, 71.19, 70.92, 70.89, 70.83, 70.77, 70.71, 70.68, 69.30, 69.24, 68.97, 68.93, 68.91, 68.86, 68.81, 52.79, 32.97, 30.39, 30.24, 30.20, 30.16, 30.06, 29.88, 29.71, 29.67, 29.25, 27.71, 26.97, 26.88.

HRMS (ESI+ve) m/z: 1185.02466 ([M-2PF$_6$]$^{2+}$, $C_{125}H_{169}N_9O_{20}I_2$ requires 1185.02811)

5.8 Synthetic Procedures and Characterisations of Compounds in Chapter 3

Part I: Near Quantitative Chloride Anion Template Synthesis of an XB[2]Rotaxane Capable of Selective Anion Recognition in Aqueous Media

General synthetic method A: *CuAAC reaction for neutral acyclic receptors*

CuI (0.03 mmol) and TBTA (0.03 mmol) was dissolved in dry and degassed THF (3 ml) and stirred under N_2 atmosphere for 5 min to obtain yellow suspension. 3,5-diiodoethynyl pyridine (0.3 mmol) and the corresponding azides (0.66 mmol) were added to a solution of copper complex. The reaction was stirred at room temperature and monitored until full conversion of 3,5-diiodoethynyl pyridine and mono-iodotriazole intermediate to the bis-iodotriazole product. After completion, the reaction mixture was concentrated and redissolved in DCM (10 ml). The organic layer was stirred with 0.1 M EDTA solution in NH_4OH, then washed with water and brine. The organic residue was dried over $MgSO_4$ and concentrated to obtain the crude mixture which was isolated the product by silica gel chromatographic purification.

XB bis-(iodotriazole) pyridine acyclic receptor (3.9)

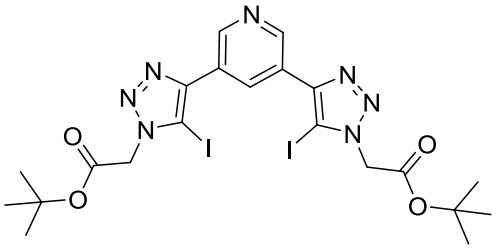

See general procedure A, quantities used: 3,5-bis-(iodoethynyl)pyridine **2.3** (114 mg, 0.3 mmol), *tert*-butyl-2-azidoacetate **3.5** (104 mg, 0.66 mmol), CuI (6 mg, 0.03 mmol), TBTA (16 mg, 0.03 mmol), and THF (3 ml). The crude product was purified by silica gel column chromatography using gradient from DCM to 30% EtOAC/DCM to yield a pure product as white powder (51%).

^{1}H-NMR (400 MHz, d_6-DMSO) δ = 9.19 (d, *J* = 2.1 Hz, 2H), 8.86 (t, *J* = 2.1 Hz, 1H), 5.43 (s, 4H), 1.47 (s, 18H).

^{13}C-NMR (101 MHz, d_6-DMSO) δ = 165.37, 146.89, 145.87, 131.23, 126.39, 84.21, 82.92, 52.26, 27.61.

HRMS (ESI+ve) m/z: 694.01184 ($[M+H]^+$, $C_{21}H_{26}I_2N_7O_4$ requires 694.01301).

XB bis-(iodotriazole) pyridine acyclic receptor (3.10)

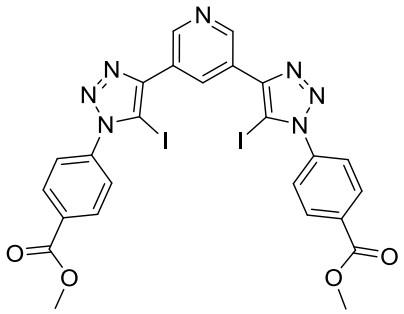

See synthetic procedure A, quantities used: 3,5-bis-(iodoethynyl)pyridine **2.3** (114 mg, 0.30 mmol), methyl-4-azidobenzoate **3.6** (145 mg, 0.66 mmol), CuI (6 mg, 0.03 mmol), TBTA (16 mg, 0.03 mmol), and THF (3 ml). The crude product was purified by silica gel column chromatography using gradient from DCM to 3% MeOH/DCM to yield pure product as a white powder (57%).

^{1}H-NMR (500 MHz, d_6-DMSO) δ = 9.28 (d, *J* = 2.2 Hz, 2H), 8.99 (t, *J* = 2.1 Hz, 1H), 8.27 – 8.21 (m, 4H), 7.93 – 7.85 (m, 4H), 3.93 (s, 7H).

^{13}C-NMR (126 MHz, d_6-DMSO) δ = 165.32, 147.57, 146.70, 140.17, 132.39, 131.28, 130.48, 127.05, 126.30, 84.51, 52.65.

HRMS (ESI+ve) m/z: 733.94977 ($[M+H]^+$, $C_{25}H_{18}I_2N_7O_4$ requires 733.95041)

XB bis-(iodotriazole) pyridine acyclic receptor (3.11)

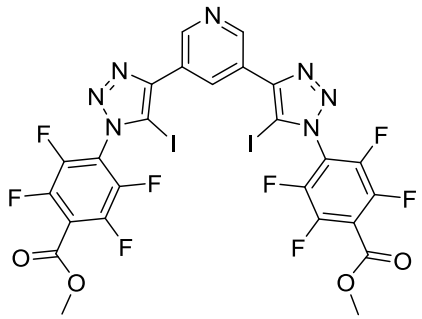

See synthetic procedure A, quantities used: 3,5-bis-(iodoethynyl)pyridine **2.3** (114 mg, 0.3 mmol), methyl-4-azidoperfluorobenzoate **3.8** (164 mg, 0.66 mmol), CuI (6 mg, 0.03 mmol), TBTA (6 mg, 0.03 mmol), and THF (3 ml). The crude product was purified by silica gel column chromatography using 5% EtOAc/DCM to yield pure product as an off-white powder (93%).

^{1}H-NMR (500 MHz, $CDCl_3$) δ = 9.43 (d, *J* = 2.2 Hz, 2H), 9.08 (t, *J* = 2.2 Hz, 1H), 4.09 (s, 6H).

^{13}C-NMR (126 MHz, $CDCl_3$) δ = 159.08, 148.61, 147.89, 144.84, 143.09, 133.11, 125.58, 118.44, 116.08, 80.69, 54.13.

^{19}F-NMR (471 MHz, $CDCl_3$) δ = -136.04 – -137.19 (m), -141.04 – -142.23 (m).

HRMS (ESI+ve) m/z: 877.87439 ($[M+H]^+$, $C_{25}H_{10}F_8I_2N_7O_4$requires 878.1956)

General synthetic method B: *Selective methylation*

The neutral XB receptor (50 mg) was dissolved in a solution of iodomethane/chloroform (1:1, v/v) 1 mL . The reaction vessel was sealed and refluxed 63^{o}C overnight to obtain a suspension. The liquid residue was removed *in vacuo,* yielding the solid product as its iodide salt. The iodide salt of the receptor was then exchanged to the hexafluorophosphate (PF_6^-) counter anion.

XB bis-(iodotriazole) pyridinium acyclic receptor (3.2·PF_6)

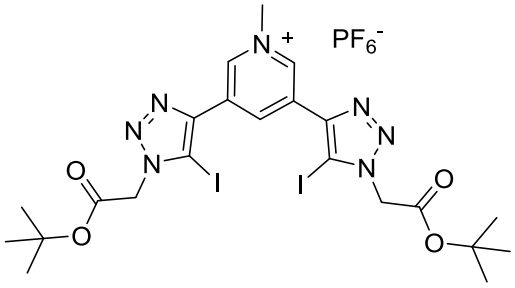

See general procedure B, the product was obtained as a pale yellow powder (quantitative)

^{1}H-NMR (500 MHz, $CDCl_3$) δ = 9.68 (t, *J* = 1.5 Hz, 1H), 9.27 (d, *J* = 1.6 Hz, 2H), 5.18 (s, 4H), 4.54 (s, 3H), 1.48 (s, 18H).

^{13}C-NMR (126 MHz, $CDCl_3$) δ = 164.42, 143.03, 141.42, 136.43, 131.96, 84.84, 82.63, 52.64, 50.11, 31.08, 28.10.

HRMS (ESI+ve) m/z: 708.02740 ($[M-PF_6^-]^+$, $C_{22}H_{28}I_2N_7O_4$ requires 708.02866).

XB bis-(iodotriazole) pyridinium acyclic receptor (3.3·PF_6)

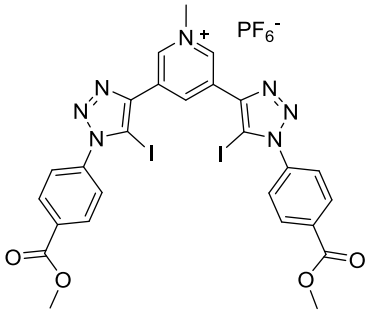

See synthetic procedure B, the product was obtained as a white powder (82%)

^{1}H-NMR (500 MHz, d_6-DMSO) δ = 9.74 (d, *J* = 1.7 Hz, 1H), 9.69 (d, *J* = 1.7 Hz, 2H), 8.30 – 8.23 (m, 4H), 7.93 – 7.85 (m, 4H), 5.75 (s, 6H), 4.62 (s, 3H).

^{13}C-NMR (126 MHz, d_6-DMSO) δ = 165.26, 143.86, 142.99, 139.80, 137.14, 131.58, 130.62, 130.25, 127.06, 87.57, 54.93, 52.70, 48.95, 48.61.

HRMS (ESI+ve) m/z: 747.96594 ($[M\text{-}PF_6^-]^+$, $C_{26}H_{20}I_2N_7O_4$ requires 747.96606)

XB bis-(iodotriazole) pyridinium acyclic receptor (3.4·PF_6)

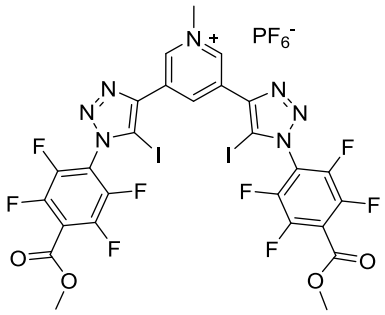

See synthetic procedure B, the product was obtained as a pale yellow powder (90%).

^{1}H-NMR (500 MHz, d_6-DMSO) δ = 9.80 (t, *J* = 1.6 Hz, 1H), 9.75 (d, *J* = 1.6 Hz, 2H), 4.61 (s, 3H), 4.03 (s, 6H).

^{13}C-NMR (126 MHz, d_6-DMSO) δ = 158.58, 144.72, 144.52, 143.55, 142.33, 129.38, 117.54, 115.17, 54.08, 48.87.

^{19}F-NMR (471 MHz, d_6-DMSO) δ = -69.39, -70.90 (hexafluorophosphate moieties), -136.78, -143.43 (perfluoroaryl moieties).

HRMS (ESI+ve) m/z: 891.89069 ($[M\text{-}PF_6^-]^+$, $C_{26}H_{12}F_8I_2N_7O_4$ requires 891.89069)

_N_-hydroxysuccinimidyl bromoacetate (3.20) [256]

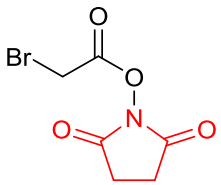

The solids bromoacetic acid (278 mg, 2.00 mmol), *N*-hydroxysuccinimide (276 mg, 2.40 mmol) and dicyclohexylcarbodiimide (DCC) (454 mg, 2.20 mmol) were suspended in 1,4-dioxane (16 mL) and allowed to stir at room temperature for 2 hours. The suspension was filtered and the filtrate concentrated to dryness, the resultant crude product was recrystallised from DCM and petroleum ether to yield a white solid of **3.20** (472 mg, 2.00 mmol, quantitative).

^{1}H-NMR (400 MHz, $CDCl_3$) δ = 4.11 (s, 2 H, CH_2), 2.81 - 2.95 ppm (s, 4 H, CH_2).

Methylene azide (3.21)

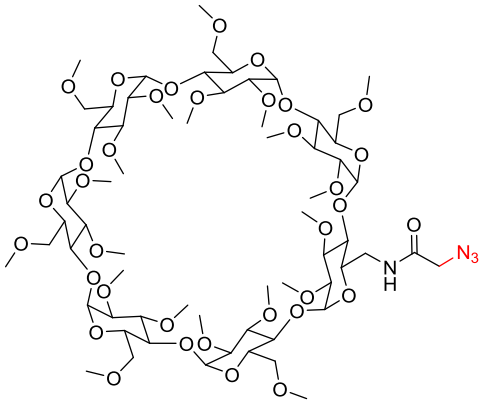

N-hydroxysuccinimidyl bromoacetate **3.20** (38 mg, 0.161 mmol) and permethylated β-cyclodextrin amine **3.19** (187 mg, 0.132 mmol) were dissolved in dry DCM (2 mL), DMAP (2 mg, 0.02 mmol) was added and the mixture was left to stir at room temperature. After 2 hours the reaction showed no evidence of permethylated β-cyclodextrin amine **3.19** by TLC or ESI-MS. The solvent was removed *in vacuo* and the crude product was purified by silica gel column chromatography (2% MeOH/$CHCl_3$) to yield a white solid (172 mg, 0.11 mmol, 90%). The pure product (149 mg, 0.097 mmol) and NaN_3 (16 mg, 0.24 mmol) were dissolved in DMSO (0.5 mL) and left to stir at room temperature overnight. The resulting mixture was

then diluted with H_2O (5 mL) and extracted with EtOAc (2 x 20 mL), the combined organics were then dried over $MgSO_4$, and the solvent removed *in vacuo*, to yield a white solid (145 mg, 0.097 mmol, quant.)

^{1}H-NMR (400 MHz, $CDCl_3$) δ = 6.67 (br. s., 1 H), 5.01 - 5.30 (7 H, β-CD H_1), 3.07 - 3.98 ppm (β-CD $H_{2\text{-}6}$ and CH_2).

^{13}C-NMR (101 MHz, $CDCl_3$) δ = 166.6, Cyclodextrin signals consistent with loss of C_7 symmetry; 99.0 (β-CD C_1), 81.4, 71.1, 61.4, 58.8, 52.7, 40.7 ppm.

HRMS (ESI+ve) m/z: 1497.7140 ($[M+H]^+$, $C_{64}H_{113}O_{35}N_4$ requires 1497.7180).

N-hydroxysuccinimidyl 4-azidobenzoate (3.22)[257]

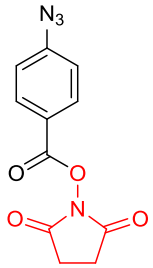

The solids 4-azidobenzoic acid (489 mg, 3.00 mmol), *N*-hydroxysuccinimide (348 mg, 3.11 mmol) and DCC (630 mg, 3.06 mmol) were suspended in dry DCM (20 mL) and allowed to stir at room temperature for 2 hours. The suspension was filtered and filtrate collected and concentrated to dryness, the resultant crude product was recrystallised from DCM and petroleum ether to yield and orange solid of **3.22** (681 mg, 2.62 mmol, 90%).

^{1}H-NMR (400MHz, $CDCl_3$) δ = 8.00 - 8.25 (m, 2 H, *Ar*H), 7.01 - 7.22 (m, 2 H, *Ar*H), 3.05 ppm (s, 4 H, CH_2).

Aryl azide (3.23)

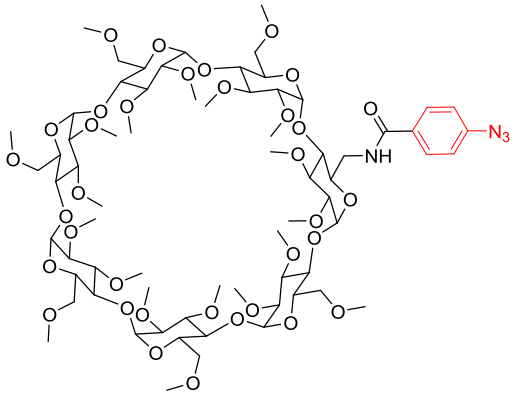

N-hydroxysuccinimidyl 4-azidobenzoate **3.22** (65 mg, 0.25 mmol) and permethylated β-cyclodextrin amine **3.19** (295 mg, 0.208 mmol), were dissolved in dry DCM (2 mL). To this mixture was added DMAP (2 mg, 0.02 mmol), the reaction was left to stir at room temperature monitoring by TLC. After 2 hours permethylated β-cyclodextrin amine **3.19** was completely consumed and the solvent was removed *in vacuo*. The resultant crude was purified by silica gel column chromatography (1% MeOH/$CHCl_3$), to yield a white solid (255 mg, 0.163 mmol, 78%).

^{1}H-NMR (400MHz, $CDCl_3$) δ = 7.81 (d, *J*=8.4 Hz, 2 H, benzoic *Ar*H), 7.07 (d, *J*=8.4 Hz, 2 H, benzoic *Ar*H), 6.88 (br. s., 1 H, amide *N*H), 4.92 - 5.35 (7 H, β-CD H_1), 3.03 - 4.28 ppm (β-CD $H_{2\text{-}6}$ and *C*H_2).

^{13}C-NMR (101MHz, $CDCl_3$) δ = 166.3, 143.2, 130.9, 128.8, 118.8, Cyclodextrin signals consistent with loss of C_7 symmetry; 99.5 - 98.8 (β-CD C_1), 81.8, 80.3, 71.2, 69.9, 61.3, 58.7 ppm.

HRMS (ESI+ve) m/z: 1559.7285 ($[M+H]^+$, $C_{69}H_{115}O_{35}N_4$ requires 1559.7336).

N-hydroxysuccinimidyl 4-azidoperfluorobenzoate (3.25)[252]

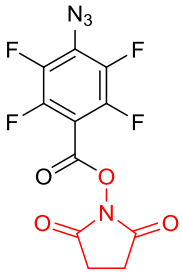

The solids 4-azidobperfluoroenzoic acid **3.24** (489 mg, 3.00 mmol), *N*-hydroxysuccinimide (348 mg, 3.11 mmol) and DCC (630 mg, 3.06 mmol) were suspended in dry DCM (20 mL) and allowed to stir at room temperature overnight. The suspension was filtered and the solid collected, the resultant crude product was recrystallised from DCM and petroleum ether to yield a white powder.

^{1}H-NMR (400MHz, $CDCl_3$) δ = 2.919 (s)

Perfluoroaryl azide (3.26)

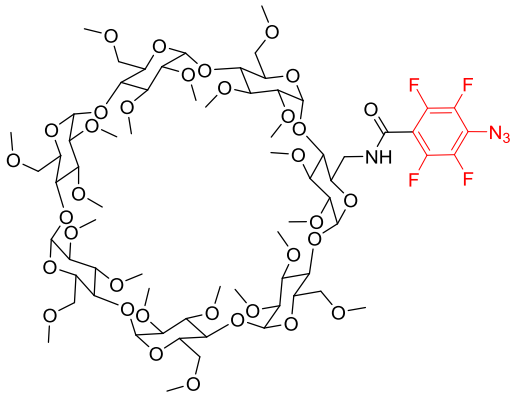

N-hydroxysuccinimidyl-4-azidoperfluorobenzoate **3.25** (288 mg, 0.87 mmol) and permethylated β-cyclodextrin amine **3.19** (942 mg, 0.67 mmol), were dissolved in dry DCM (2 mL) in the presence of a few crystals of DMAP (cat). The reaction was left to stir at room temperature monitoring by TLC. After overnight, permethylated β-cyclodextrin amine **3.19** was completely consumed and the solvent was removed *in vacuo*. The resultant crude was purified by silica gel column chromatography (3% MeOH/DCM), to yield a yellow dry solid (82%).

^{1}H NMR (500MHz, $CDCl_3$) δ = 6.76 (t, *J* = 5.6 Hz,1 H, amide *N*H), 5.15-5.01 (7 H, β-CD H_1), 3.69 – 3.08 (β-CD $H_{2\text{-}6}$ and *C*H_2)

^{19}F NMR (470 MHz, $CDCl_3$) δ -140.90 to -140.97, -150.61 to -150.68.

^{13}C NMR (125MHz, $CDCl_3$) δ = Perfluoroaryl moiety 157.73, 144.97 and 142.97, 141.49 - 141.36 and 139.49-139.35, 121.66, 112.09. β-Cyclodextrin signals consistent with loss of C_7 symmetry 99.38 – 98.73 (β-CD C_1), 82.20-81.00, 80-71-79.66, 71.68-70.87, 61.65-61.22, 59.32-58.30 ppm.

HRMS (ESI+ve) m/z: 1653.67259 ($[M+Na]^+$, $C_{69}H_{110}F_4N_4O_{35}Na$ requires 1653.67289).

General synthetic method C: *CuAAC reaction for neutral cyclodextrin axles*

$[Cu(MeCN)_4PF_6]$ (0.8 equiv.) was dissolved in dry THF to which was added TBTA (0.4 equiv.) and the mixture left to stir for 10 minutes. Bis-alkyne or bis-iodoalkyne (1 equiv.) was then added to the mixture followed by the corresponding cyclodextrin azide derivative (2.2 equiv.) and left stirring at room temperature excluding from light. The reaction was monitored by TLC and ESI-MS, following the presence of the bis-iodotriazole pyridine product. After 3 days the reaction mixture showed no evidence of 3,5-di(iodo)ethynylpyridine, after which the solvent was removed *in vacuo* and washed with NH4OH, brine, and dried over MgSO4. The crude product was then purified by silica gel column chromatography.

Methylene spacer substituted 3,5-bis(iodotriazole)pyridine (3.27)

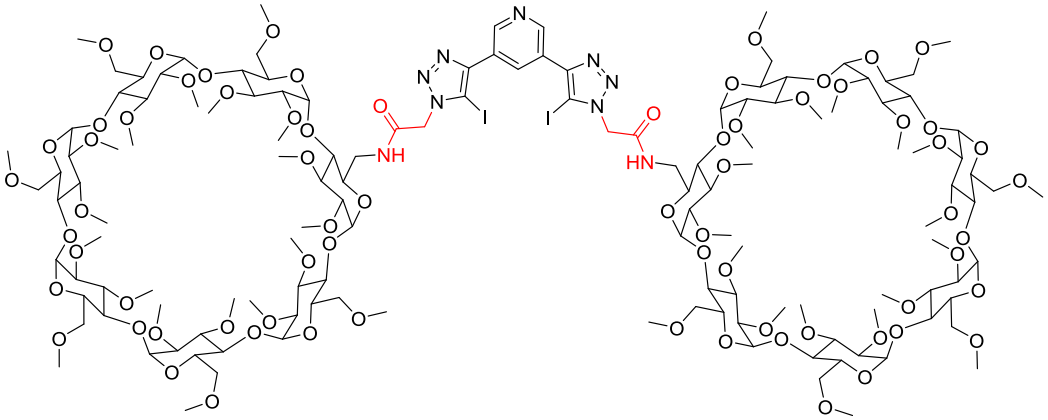

See general synthetic procedure C. Quantities used: azide **3.21** (205 mg, 0.137 mmol), 3, 5-bis-(iodoethynyl)pyridine **2.3** (24.3 mg, 0.0641 mmol), $[Cu(MeCN)_4PF_6]$ (22 mg, 0.059 mmol), TBTA (15 mg, 0.028 mmol), dry and degassed THF (5 ml). The crude product was purified by silica gel column chromatography using 5% MeOH/$CHCl_3$ as the eluent. The product was isolated as a white solid (51%).

^{1}H-NMR (400MHz, $CDCl_3$) δ = 9.24 (s, 2 H, pyridine *Ar*H), 8.87 (s, 1 H, pyridine *Ar*H), 6.48 (br. s., 2 H, amide *N*H), 4.92 - 5.25 (14 H, β-CD H_1), 3.04 - 3.97 ppm (β-CD $H_{2\text{-}6}$ and CH_2).

^{13}C-NMR (101MHz, $CDCl_3$) δ = 164.2, 147.6, 132.7, 126.0, Cyclodextrin signals consistent with loss of C_7 symmetry; 98.7 (β-CD C_1), 81.0, 71.0, 61.2, 58.6, 53.2, 40.3 ppm.

HRMS (ESI) m/z: 1709.1102 ($[M+2Na]^{2+}$, $C_{137}H_{227}O_{70}N_9{}^{127}I_2{}^{23}Na_2$ requires 1709.1178).

Aryl spacer substituted 3,5-bis(iodotriazole)pyridine (3.28)

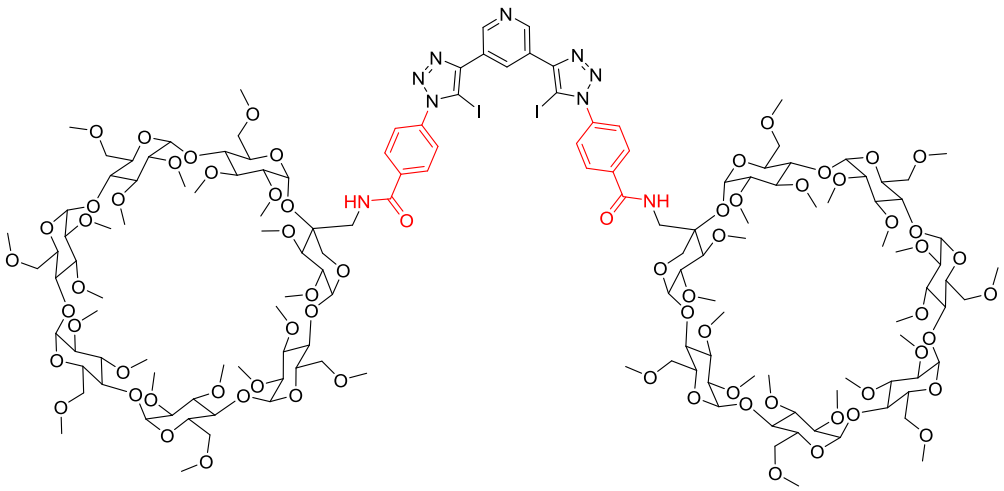

See general synthetic procedure C Quantities used: azide **3.23** (217 mg, 0.139 mmol), 3, 5-bis-(iodoethynyl)pyridine **2.3** (24.3 mg, 0.0641 mmol), $[Cu(MeCN)_4PF_6]$ (22 mg, 0.059 mmol), TBTA (15 mg, 0.028 mmol), dry and degassed THF (5 ml). Crude product was purified by silica gel column chromatography using 5% MeOH/ $CHCl_3$ as the eluent. The product was isolated as a white solid (78%).

^{1}H-NMR (400 MHz, $CDCl_3$) δ = 9.35 (s, 2 H, pyridine *Ar*H), 8.98 (s, 1 H, pyridine *Ar*H), 8.06 (d, *J*=8.3 Hz, 4 H, benzoic *Ar*H), 7.69 (d, *J*=8.3 Hz, 4 H, benzoic *Ar*H), 7.13 (br. s., 2 H, amide *N*H), 4.96 - 5.30 (14 H, β-CD H_1), 3.12 - 4.26 ppm (β-CD $H_{2\text{-}6}$ and CH_2).

^{13}C-NMR (101 MHz, $CDCl_3$): δ = 165.3, 147.2, 143.0, 130.9, 128.8, 126.3, 118.8, Cyclodextrin signals consistent with loss of C_7 symmetry; 99.5 - 98.8 (β-CD C_1), 81.8, 80.3, 71.2, 69.9, 61.3, 58.7 ppm.

HRMS (ESI) m/z: 1771.1317 ($[M+2Na]^{2+}$, $C_{147}H_{231}O_{70}N_9{}^{127}I_2{}^{23}Na_2$ requires 1771.1333).

Perfluoroaryl spacer substituted 3,5-bis(iodotriazole)pyridine (3.29)

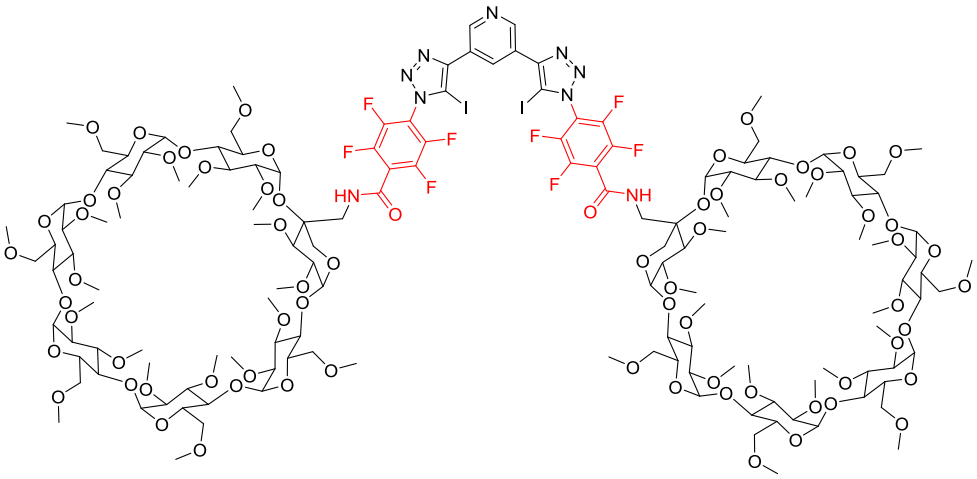

See general synthetic method C. Quantities used: azide **3.26** (200 mg, 0.123 mmol), 3, 5-bis-(iodoethynyl)pyridine **2.3** (21 mg, 0.056 mmol), $[Cu(MeCN)_4PF_6]$ (10 mg, 0.027 mmol), TBTA (9 mg, 0.028 mmol), dry and degassed THF (5 ml). Crude product was purified by silica gel column chromatography using 5% MeOH/DCM as the eluent. The product was isolated as a yellow solid (82%).

^{1}H-NMR (500 MHz, $CDCl_3$) δ = 9.42 (d, *J* = 2.2 Hz, 2H, pyridine *Ar*H), 9.06 (t, *J* = 2.1 Hz, 1H, pyridine *Ar*H), 7.17 (t, *J* = 5.7 Hz, 2H, amide *N*H), 5.22 – 5.03 (m, 14H, β-CD H_1), 4.29-3.19 (β-CD $H_{2\text{-}6}$ and CH_2).

^{19}F-NMR (376 MHz, $CDCl_3$) δ = -138.32 to -138.42, -138.52 to -138.62, -141.37 to-141.47, -141.59, -to -141.70.

^{13}C-NMR (126 MHz, $CDCl_3$) δ 156.97, 148.52, 147.83, 143.75, 143.70, 142.99, 133.08, 125.58, 120.38, 117.11, Cyclodextrin signals consistent with loss of C_7 symmetry; 99.41 - 98.81 (β-CD C_1), 82.36-79.69, 71.91-70.01, 61.77- 61.27, 59.56-58.30.

HRMS (ESI) m/z: 3663.20605 ($[M+Na]^+$, $C_{147}H_{223}O_{70}N_9F_8I_2Na$ requires 3663.20205).

Perfluoroaryl spacer substituted 3,5-bis(triazole)pyridine (3.39)

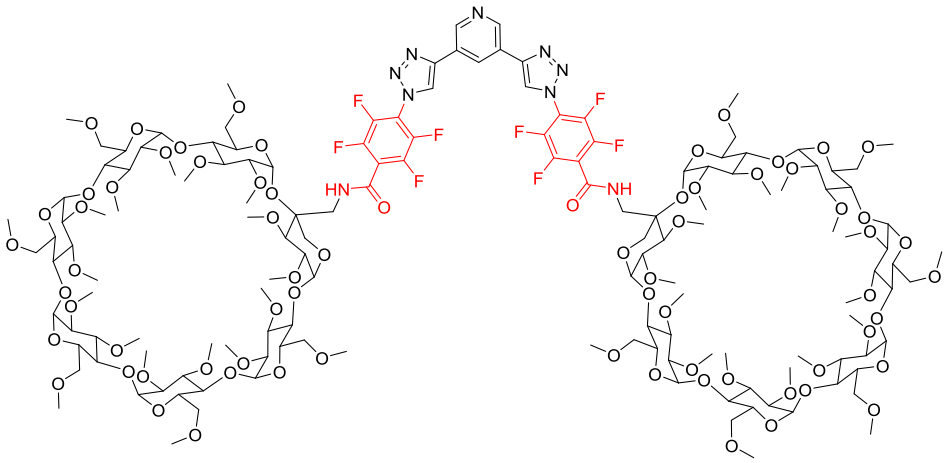

See general synthetic method C. Quantities used: azide **3.26** (290 mg, 0.178 mmol), 3,5-diethynylpyridine **2.2** (9.4 mg, 0.074 mmol), $[Cu(MeCN)_4PF_6]$ (13.2 mg, 0.035 mmol), TBTA (11.7 mg, 0.022 mmol), dry and degassed DCM (7 ml). Crude product purified was purified by silica gel column chromatography using 5% MeOH/ DCM as the eluent. The product was isolated as a white solid (72%)

^{1}H-NMR (500MHz, $CDCl_3$) δ = 9.18 (br., 2H, external Pyridine), 8.81 (s, 1H), 8.30 (s, 2H), 7.08 (t, *J*=5.8 Hz, 2H, NH amide), 5.19-5.05 (m, 14H, β-CD anomeric H), 4.22-3.18 (m, β-CD moieties)**.**

^{19}F-NMR (470 MHz, $CDCl_3$) δ = -138.3892 to -138.4670, -144.6769 to -144.7560**.**

^{13}C-NMR (126 MHz, $CDCl_3$) δ= 167.45, 157.02, 147.42 and 145.01, 144.02, 143.46 and141.40, 141.57, 130.57, 122.64, 118.71, 117.60, Cyclodextrin signals consistent with loss of C_7 symmetry; 99.47 and 98.85, 82.31-79.75, 71.92-70.99, 69.95, 68.10, 61.78-61.30, 59.48- 58.35 ppm**.**

HRMS (ESI) m/z: 3390.43043 ($[M+H]^+$, $C_{147}H_{226}O_{70}N_9F_8$ requires 3390.43019).

General synthetic method D: *Selective N-Alkylation and Anion exchange*

The solid compound of the neutral pyridine axle was dissolved in 1: 1 iodomethane/$CHCl_3$ (1 ml) in the sealed vessel. The reaction vessel was heated at 60^{o}C overnight. The reaction was allowed to cool to the ambient temperature. The residual solvent was removed *in vacuo* to obtain a solid product as an iodide salt. The product was subsequently anion exchanged to its chloride salt by passing a solution of product in 10% H_2O in acetone through a column of loaded Amberlyte® with chloride salts three times. Anion exchange process was monitored by ^{1}H-NMR spectrum to compare the successful anion exchange process.

Methylene spacer substituted 3,5-bis(iodotriazole)pyridinium chloride (3.30·Cl)

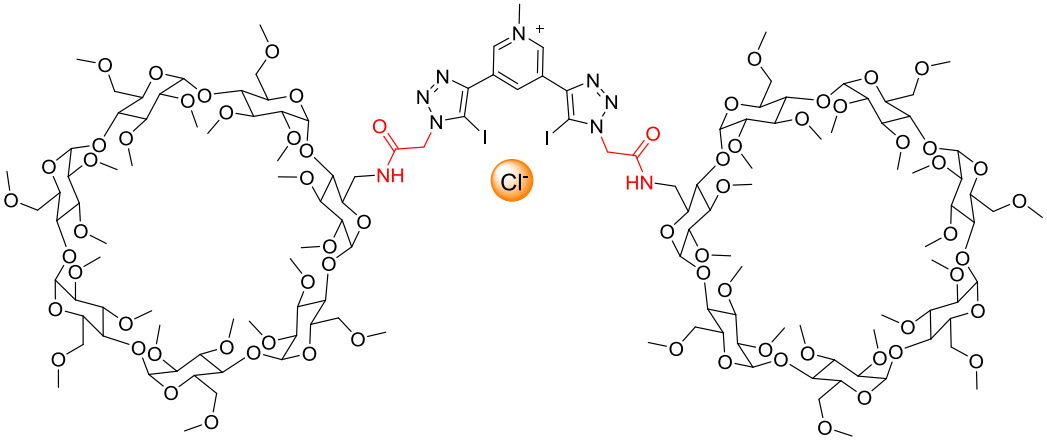

See general synthetic method D. **^{1}H-NMR** (400MHz, $CDCl_3$/d_4-MeOD (1:1)) δ = 9.57 (s, 1 H, pyridinium *Ar*H), 9.13 (s, 2 H, pyridinium *Ar*H), 4.68 - 5.08 (14 H, β-CD H_1), 2.75 - 3.63 ppm (β-CD $H_{2\text{-}6}$ and CH_2).

^{13}C-NMR (101MHz, $CDCl_3$/d_4-MeOD (1:1)) δ = 165.9, 143.5, 133.0, Cyclodextrin signals consistent with loss of C_7 symmetry; 99.3 (β-CD C_1), 82.6, 80.6, 71.6, 61.9, 59.4, 53.3, 41.1, 30.3 ppm.

HRMS (ESI) m/z: 1705.1267 ($[M\text{-}Cl+Na+H]^{2+}$, $C_{138}H_{230}O_{70}N_9{}^{127}I_2{}^{23}Na$ requires 1705.1345).

Aryl spacer substituted 3,5-bis(iodotriazole)pyridinium chloride (3.31·Cl)

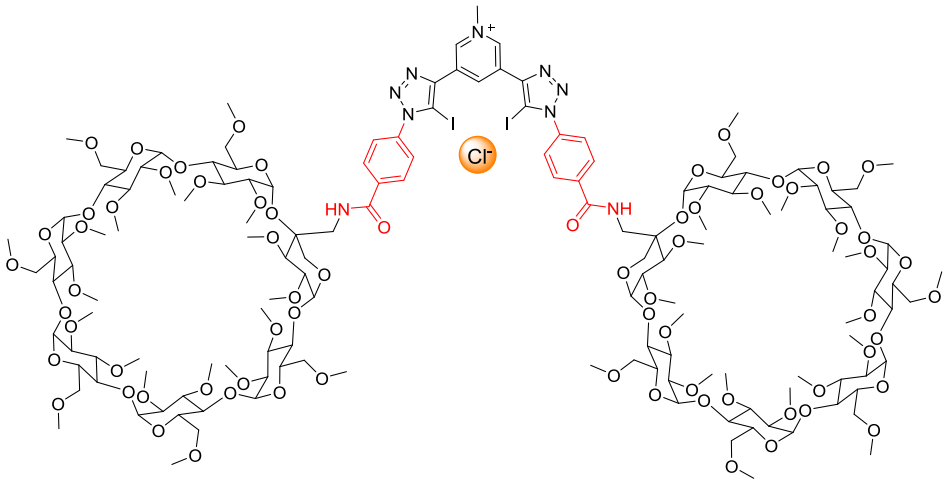

See general synthetic method D. **^{1}H-NMR** (400MHz, $CDCl_3$/d_4-MeOD (1:1)) δ = 10.32 (s, 1 H, pyridinium *Ar*H), 9.88 (s, 2 H, pyridinium *Ar*H), 8.37 (d, *J*=8.4 Hz, 4 H, benzoic *Ar*H), 8.00 (d, *J*=8.4 Hz, 4 H, benzoic *Ar*H), 5.29 - 5.58 (14 H, β-CD H_1), 4.94 (s, 3 H, *N*-Methyl CH_3), 3.35 - 4.44 ppm (β-CD $H_{2\text{-}6}$ and CH_2).

^{13}C-NMR (101MHz, $CDCl_3$/d_4-MeOD (1:1)) δ = 163.1, 146.1, 143.9, 131.9, 128.8, 126.3, 118.8, Cyclodextrin signals consistent with loss of C_7 symmetry; 99.5 - 98.8 (β-CD C_1), 81.8, 80.3, 71.2, 69.9, 61.3, 58.7, 50.1 ppm.

HRMS (ESI) m/z: 1767.1455 ($[M\text{-}Cl+Na]^{2+}$, $C_{148}H_{234}O_{70}N_9{}^{127}I_2{}^{23}Na$ requires 1767.1502).

Perfluoroaryl spacer substituted 3,5-bis(iodotriazole)pyridinium chloride (3.32·Cl)

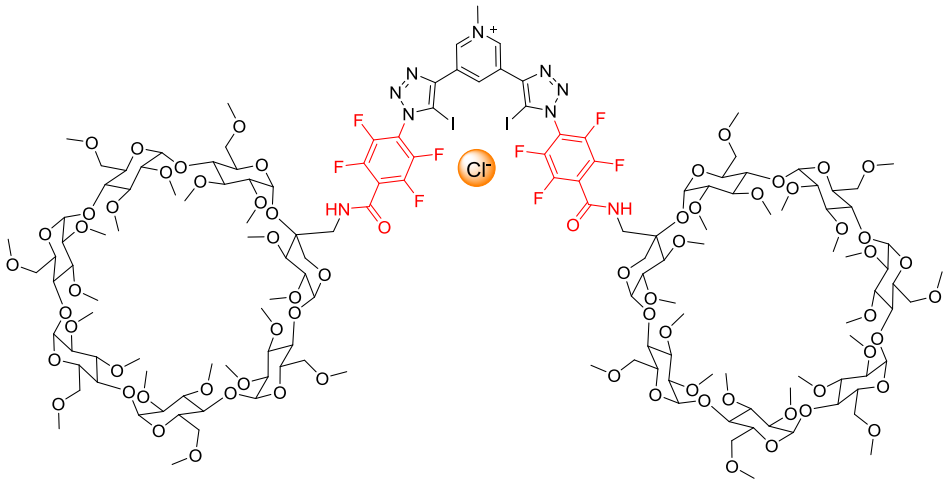

See general synthetic method D.^{1}**H-NMR** (500 MHz, $CDCl_3$) δ 10.43 (s, 1H), 9.52 (s, 2H), 7.08 (s, 2H), 5.27 – 5.06 (m, 14H β-CD H_1), 4.71 (d, *J* = 4.7 Hz, 3H), 4.11-3.18 (β-CD $H_{2\text{-}6}$ and CH_2) ^{19}**F-NMR** (376 MHz, $CDCl_3$) δ -138.26 to -138.44, -141.78 to -142.24.

^{13}**C-NMR** (126 MHz, $CDCl_3$) δ 155.98, 143.54 and 142.80, 141.57 and 140.64, 141.24, 139.75, 133.20, 131.84, 127.30, 119.30 and 119.13, 115.86. Cyclodextrin signals consistent with loss of C_7 symmetry; 98.03-97.56, 81.16-78.50, 70.80-69.81, 60.60-60.16, 58.61, 58.12-57.21.

HRMS (ESI) m/z: 1839.61438 ($[M\text{-}Cl+Na]^{2+}$, $C_{148}H_{227}O_{70}N_9F_8{}^{127}I_2{}^{23}Na$ requires 1839.61640).

Perfluoroaryl spacer substituted 3,5-bis(triazole)pyridinium chloride (3.39·Cl)

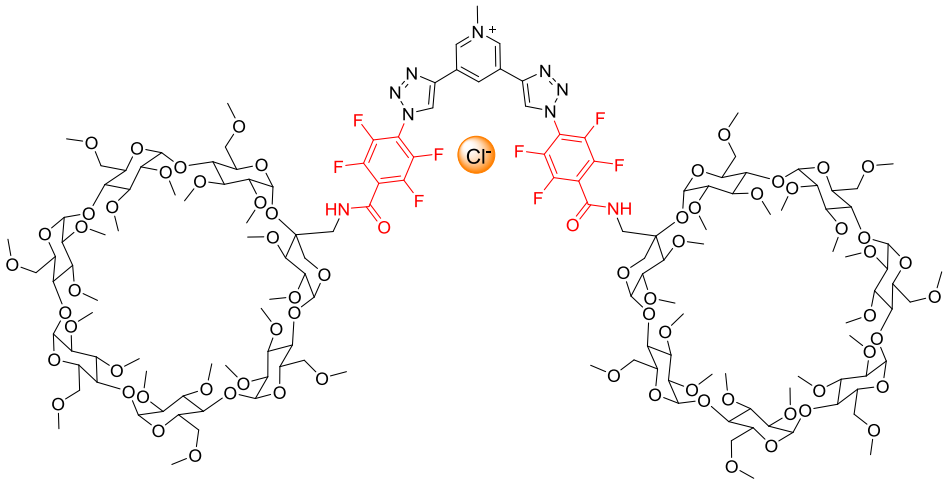

See general synthetic method D. **^{1}H-NMR** (500 MHz, $CDCl_3$) δ = 10.25 (s, 1H), 9.99 (s, 2H), 9.79 (s, 2H), 6.99 (d, *J* = 5.9 Hz, 2H), 5.24 – 5.03 (m, 14H), 4.75 (s, 3H), 4.13-3.19 (β-CD $H_{2\text{-}6}$ and C*H*$_2$)

^{19}F-NMR (471 MHz, $CDCl_3$) δ = -138.18 to -138.21, -144.23 to -144.26.

^{13}C-NMR (126 MHz, $CDCl_3$) δ = 179.33, 157.87, 156.99, 144.00, 141.80, 140.75, 132.45, 128.90, 119.25, 117.15 Cyclodextrin signals consistent with loss of C_7 symmetry; 99.27 – 98.82, 82.34-79.90, 71.87-71.01, 61.76-61.37, 59.53-58.42.

HRMS(ESI) m/z: 1713.21130 ($[M\text{-}Cl+Na]^{2+}$, $C_{148}H_{228}O_{70}N_9F_8Na$ requires 1713.21585).

General synthetic method E: *Rotaxane synthesis*

Step 1: Synthesis of 3,5-dichlorocarbonyl pyridine **3.37**

Solid 3,5-pyridine dicarboxylic acid (1 equiv.) was suspended in dry DCM, then oxalyl chloride (4 equiv.) was added to the reaction mixture. A drop of DMF was added to a reaction, immediately generating white fumes. The reaction was refluxed at 40^{o}C for 3 hours to obtain a homogeneous yellow solution. Solvent was removed *in vacuo* to dryness, affording a yellow solid of 3,5-dichlorocarbonyl pyridine which will be used in the next step immediately without any purification.

Step 2: Rotaxane synthesis *via* amide condensation

A solution of polyether bis-amine **3.36** (10 equiv.) and pyridinium axle component (1 equiv.) as a chloride salt was stirred in dry DCM at 0^{o}C under N_2 for 20 min, then NEt_3 (5 equiv.) added. A solution of 3,5-dichlorocarbonyl pyridine (10 equiv.) in dry DCM (2ml) was added dropwise over 20-30 minutes. The reaction was stirred at room temperature for 3 hours and monitored the formation of [2]rotaxane product by ESI-MS and TLC. Solvent was removed *in vacuo* to afford crude product which was purified by preparative thin layer chromatography and anion exchanged to its PF_6^- salt.

XB [2]rotaxane (3.12·PF_6)

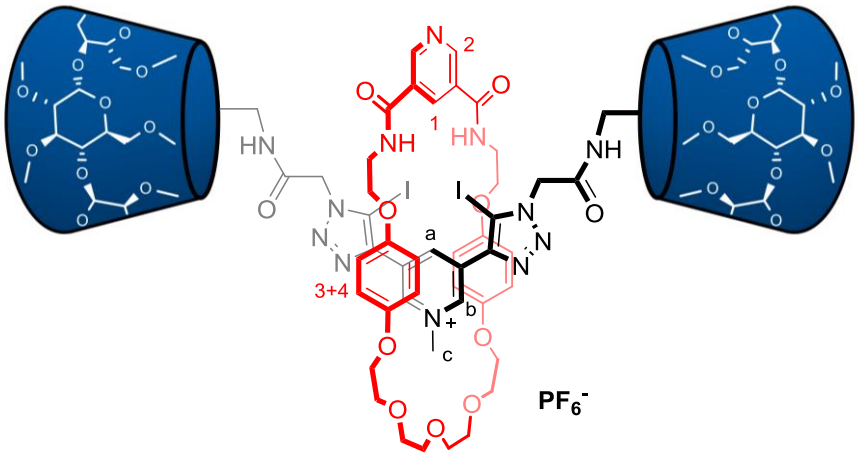

See general synthetic procedure E, Quantities used: **3.30·Cl** (31mg, 0.0082 mmol), bis-amine **3.36** (38 mg, 0.082 mmol), 3,5-pyridinedicarboxylic acid (13mg, 0.082 mmol), NEt_3 (28 µl, 0.2 mmol), DCM (23ml).

^{1}H-NMR (500MHz, $CDCl_3$/d_4-MeOD (1:1)): δ 9.61 - 9.72 (s, 2 H, pyridinium *Ar*H, H_b), 9.45 (s, 3 H, pyridinium/pyridine *Ar*H, H_{a+2}), 8.52 - 8.62 (s, 1 H, pyridine *Ar*H, H_1), 6.65 (d, *J*= 9.0 Hz, 4 H, hydroquinone *Ar*H), 6.20 - 6.31 (d, *J*= 9.0 Hz, 4 H, hydroquinone *Ar*H), 5.31 - 5.57 (14 H, β-CD H_1), 3.29 - 4.39 ppm (β-CD $H_{2\text{-}6}$ macrocycle CH_2, axle CH_2).

^{13}C-NMR (126MHz, $CDCl_3$/d_4-MeOD (1:1)): δ 166.9, 165.6, 153.7, 152.4, 143.2, 131.2, 115.5, Cyclodextrin signals consistent with loss of C7 symmetry; 99.3 (β-CD C_1), 82.7, 80.4, 72.0, 70.7, 68.5, 66.7, 61.9, 60.1, 59.4, 40.6, 30.3 ppm.

HRMS (ESI) m/z: 2002.7557 ($[M\text{-}Cl+Na]^{2+}$, $C_{169}H_{267}O_{79}N_{12}{}^{127}I_2{}^{23}Na$ requires 2002.7610).

XB [2]rotaxane (3.13·PF_6)

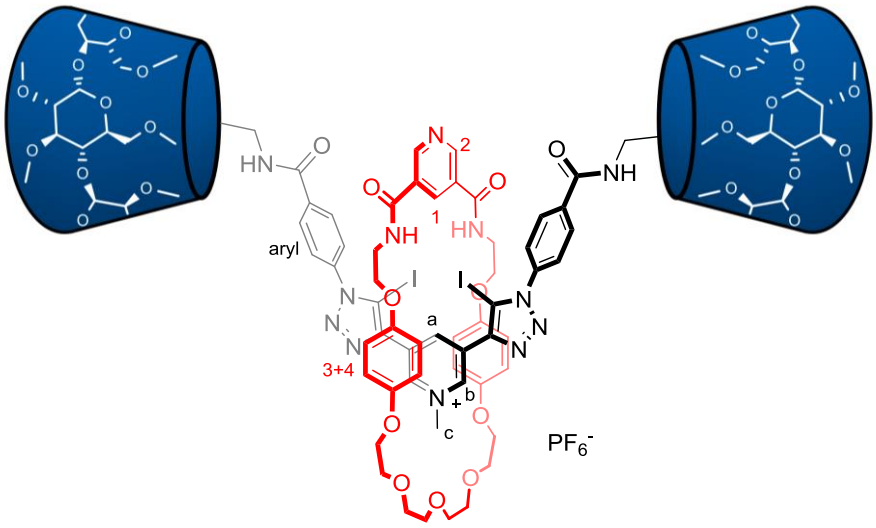

See general synthetic procedure E, Quantities used: **3.31·Cl** (31mg, 0.0082 mmol), bis-amine **3.36** (38 mg, 0.082 mmol), 3,5-pyridinedicarboxylic acid (13mg, 0.082 mmol), NEt_3 (28 µl, 0.2 mmol), DCM (23ml)

^{1}H-NMR (500MHz, $CDCl_3$/d_4-MeOD (1:1)) δ = 9.72 (s, 2 H, pyridinium *Ar*H), 9.22 (s, 1 H, pyridinium *Ar*H), 9.16 (s, 2 H, pyridine *Ar*H), 8.61(s, 1 H, pyridine *Ar*H), 7.98 (d, *J*=8.0 Hz, 4 H, benzoic *Ar*H), 7.68 (d, *J*=8.0 Hz, 4 H, benzoic *Ar*H), 6.44 (d, *J*=8.9 Hz, 4 H, hydroquinone *Ar*H), 6.01 (d, *J*=8.9 Hz, 4 H, hydroquinone *Ar*H), 5.38 – 5.09 (14 H, β-CD H_1), 4.71 (s, 3 H, *N*-Methyl *C*H_3), 3.27 - 4.55 ppm (β-CD $H_{2\text{-}6}$ macrocycle *C*H_2, axle *C*H_2).

^{13}C-NMR (126 MHz, $CDCl_3$/d_4-MeOD (1:1)) δ = 166.9, 153.6, 144.3, 139.8, 137.1, 130.8, 129.5, 127.0, 115.5, Cyclodextrin signals consistent with loss of C_7 symmetry; 99.5 (β-CD C_1), 82.7, 80.8, 72.0, 68.6, 62.0, 59.4, 41.3 ppm.

HRMS (ESI) m/z: 2064.7725 ($[M\text{-}Cl+Na]^{2+}$, $C_{179}H_{271}O_{79}N_{12}{}^{127}I_2{}^{23}Na$ requires 2064.7767).

XB [2]rotaxane (3.14·PF_6)

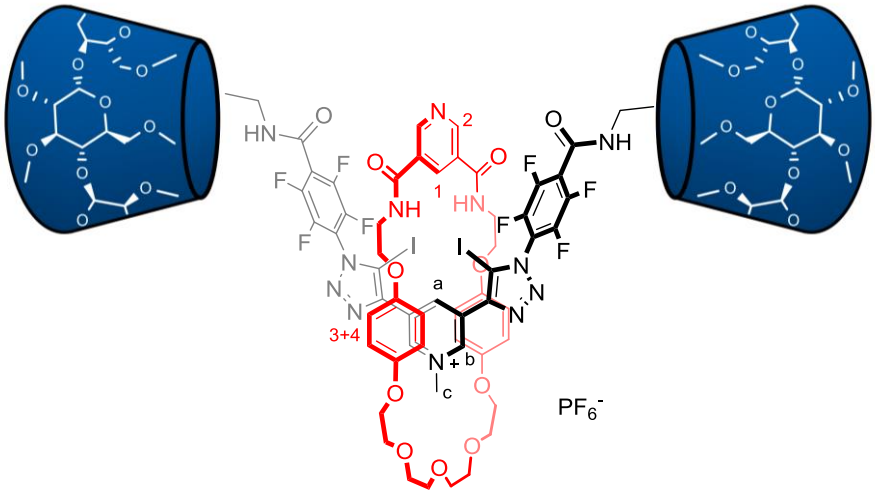

See general synthetic procedure E, Quantities used: **3.32·Cl** (31mg, 0.0082 mmol), bis-amine **3.36** (38 mg, 0.082 mmol), 3,5-pyridinedicarboxylic acid (13mg, 0.082 mmol), NEt_3 (28 µl, 0.2 mmol), DCM (23ml).

^{1}H-NMR (500 MHz, $CDCl_3$/d_4-MeOD (1:1)) δ 9.83 (s, 2H), 9.41 (s, 1H), 9.15 (d, *J* = 2.1 Hz, 2H), 8.17 (s, 1H), 6.36 (d, *J* = 8.8 Hz, 4H), 5.87 (d, *J* = 8.7 Hz, 4H), 5.32 – 5.06 (14 H, β-CD H_1), 4.69 (s, 3H), 4.2-3.15 (β-CD $H_{2\text{-}6}$ macrocycle CH_2, axle CH_2).

^{19}F-NMR (471 MHz, $CDCl_3$) δ = -139.1783 to -139.2310, -143.4942 to -143.6410.

^{13}C-NMR (126 MHz, $CDCl_3$/d_4-MeOD (1:1)) δ = 165.35, 158.28, 153.52, 152.35, 151.71, 144.08, 133.97, 133.56, 130.22, 129.67, 121.42, 115.75, 114.72, 99.44-99.12, 82.62-80.28, 72.04- 70.48, 68.31, 65.98, 61.89- 61.76, 61.69, 59.57-59.07, 58.97-58.82.

HRMS (ESI) m/z: 2126.75113 ($[M\text{-}PF_6+H]^{2+}$, $C_{179}H_{264}F_8I_2N_{12}O_{79}$ requires 2126.75134).

XB [2]rotaxane (3.40·PF_6)

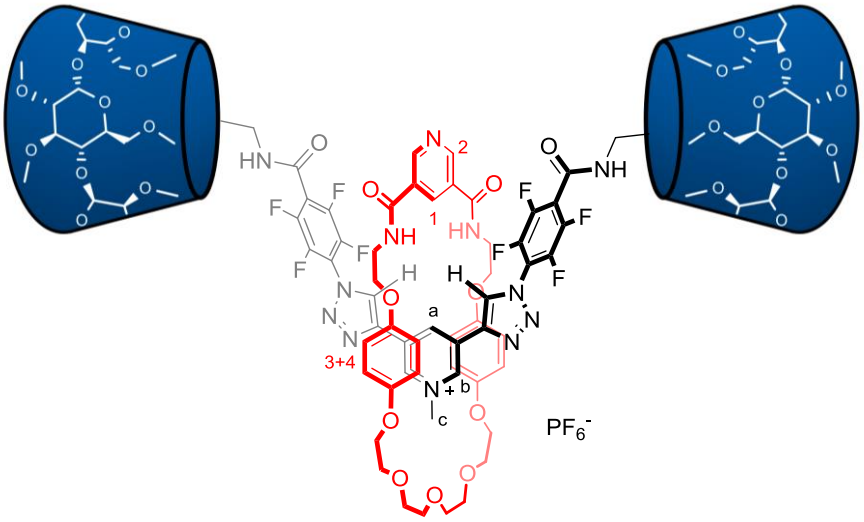

See general synthetic procedure E, Chemical used: **3.39·Cl** (28mg, 0.0082 mmol), bis-amine **3.36** (38 mg, 0.082 mmol), 3,5-pyridinedicarboxylic acid (13mg, 0.082 mmol), NEt_3 (28 µl, 0.2 mmol), DCM (23ml).

^{1}H-NMR (500 MHz, $CDCl_3$/d_4-MeOD (1:1)) δ = 9.40 (s, 2H), 9.32 (s, 1H), 9.20 (d, *J* = 2.1 Hz, 2H), 9.13 (d, *J* = 1.5 Hz, 2H), 8.79 (s, 1H), 6.30 – 6.21 (m, 4H), 6.16 – 6.11 (m, 4H), 5.32 (d, *J* = 3.8 Hz, 2H), 5.22 (d, *J* = 3.5 Hz, 2H), 5.16 – 5.10 (m, 10H), 4.28 (s, 2H), 4.03-3.14 (β-CD $H_{2\text{-}6}$ macrocycle CH_2, axle CH_2).

^{19}F-NMR (471 MHz, $CDCl_3$/d_4-MeOD (1:1)) δ = -135.64, -135.66, -141.87, -141.90.

^{13}C-NMR (126 MHz, $CDCl_3$/d_4-MeOD (1:1)) δ = 166.41, 158.30, 153.79, 153.23, 144.19, 142.31, 142.27, 131.01, 129.10, 119.99, 117.58, 115.46, 115.17, 99.46, 99.32, 99.18, 82.67, 82.58, 82.31, 82.21, 81.71, 80.86, 80.71, 80.59, 80.45, 80.20, 72.01, 71.90, 71.75, 71.69, 71.48, 71.35, 70.72, 70.61, 68.80, 66.49, 61.92, 61.90, 61.88, 61.86, 61.82, 59.60, 59.43, 59.37, 59.05, 59.03, 58.98, 58.94, 58.87, 41.34, 30.24.

HRMS (ESI) m/z: 2010.84600 ($[M\text{-}PF_6+Na]^{2+}$, $C_{179}H_{265}F_8N_{12}O_{79}$ requires 2010.84234).

Part II: Thermodynamic Investigations of Novel Water Soluble XB Acyclic and Interlocked Anion Host Molecules

Water soluble azide (3.46)

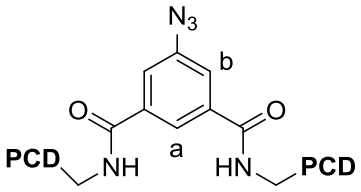

Amine **3.19**(292 mg, 0.21 mmol) and bis-NHS ester 3.47 (40 mg, 0.1 mmol) were mixed in DCM (5 ml) in the presence of catalytic amount of DMAP. The reaction was stirred at room temperature for 24 hours. Crude product was purified by silica gel column chromatography using 5% MeOH/DCM as an eluent to afford a pure product **3.46** in 77% yield.

^{1}H-NMR (400 MHz, $CDCl_3$) δ = 7.98 (s, 1H, H_a), 7.59 (s, 2H, H_b), 7.04 (s, 2H, H_{amide}), 5.25 – 4.98 (m, 14H, H_1 of β-CD), 4.05-3.94 (m, 4H), 3.69-3.11 (m, 200H).

^{13}C-NMR (101 MHz, $CDCl_3$) δ = (165.85; amide C), (141.22, 136.64, 122.09, 120.59; isophthalamide C), *β*-CD signals consistent with loss of C7 symmetry 99.42- 98.72 (*β*-CD C_1), 82.35, 82.23, 82.16, 82.06, 81.86, 81.78, 81.65, 81.45, 80.88, 80.75, 80.63, 80.46, 80.24, 80.09, 71.78, 71.67, 71.52, 71.31, 71.21, 71.12, 71.08, 70.98, 70.95, 69.88, 61.66, 61.60, 61.54, 61.48, 61.42, 61.33, 61.25, 59.34, 59.31, 59.09, 59.05, 58.99, 58.95, 58.74, 58.71, 58.56, 58.36, 40.67.

Water soluble bis-(iodotriazole)pyridine (3.42)

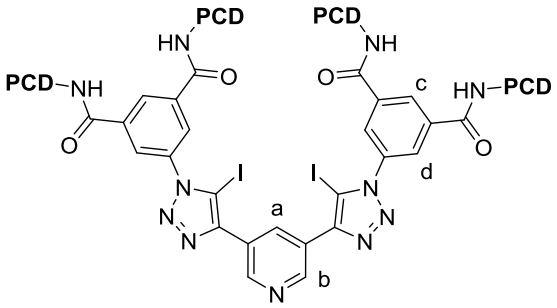

A mixture of $Cu(MeCN)_4PF_6$ (7.5 mg, 0.02 mmol) and TBTA (6.5 mg, 0.012 mmol) was stirred in dry and degassed THF (8.5 ml) under N_2. 3,5-Diiodoethylnylpyiridine **2.3** (15.6 mg, 0.04 mmol) and azide **3.46** (260 mg, 0.09 mmol) were subsequently added to a solution in a sequential order. The reaction was left to stir at room temperature for 48 hours, followed by removing THF residue. The mixture was re-dissolved in DCM and washed with an aqueous solution of NH_4OH (conc.). An aqueous layer was extracted with DCM and dried over $MgSO_4$. The pure product **3.42** was obtained in 90% yield after purification by silica gel column chromatography using 15% MeOH in EtOAC as an eluent.

^{1}H-NMR (500 MHz, $CDCl_3$) δ = 9.38 (s, 2H, H_b), 9.03 (s, 1H, H_a), 8.49 (s, 2H, H_c), 8.23 (s, 4H, H_d), 7.20 (s, 4H, H_{amide}), 5.27- 5.02 (m, 28H, H_1 of β-CD), 4.08-3.18 (m, 408H).

^{13}C-NMR (126 MHz, $CDCl_3$) δ = (165.4; amide C), (148.53, 147.93, 137.17; pyridine C), (136.63, 133.73, 127.83, 127.74; isophthalamide C), (127.58, 126.35; iodotriazole C), *β*-CD signals consistent with loss of C7 symmetry 99.25-98.76(*β*-CD C_1),82.37, 82.28, 82.22, 82.13, 82.10, 81.95, 81.93, 81.90, 81.84, 81.56, 81.21, 80.79, 80.46, 80.37, 80.13, 80.05, 78.81, 72.01, 71.76, 71.58, 71.43, 71.32, 71.27, 71.20, 71.03, 69.80, 61.78, 61.64, 61.61, 61.52, 61.45, 61.38, 59.45, 59.18, 59.16, 59.14, 59.07, 59.03, 58.81, 58.61, 58.45, 58.38.

Water soluble bis-(triazole)pyridine (3.48)

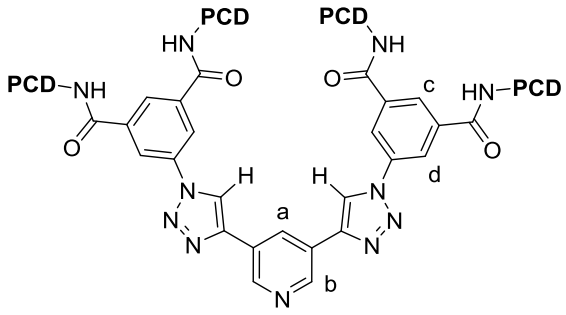

A mixture of $Cu(MeCN)_4PF_6$ (2.6 mg, 0.007 mmol) and TBTA (cat.) was stirred in dry and degassed DCM (5ml) under N_2. 3,5-Diethylnylpyiridine **2.2** (3 mg, 0.024 mmol) and azide **3.46** (150 mg, 0.05 mmol) were subsequently added to a solution in a sequential order. The reaction was left to stir at room temperature for 72 hours, then additional $Cu(MeCN)_4PF_6$ (1mg) was added. After 24 hours, the reaction was removed copper residue by stirring with an aqueous solution of NH_4OH (conc.) and extracted the crude product with DCM. The pure product **3.48** was obtained in 72% yield after purification by silica gel column chromatography using 15% MeOH in EtOAC as an eluent.

^{1}H-NMR (500 MHz, $CDCl_3$) δ = 9.06 (d, *J* = 2.1 Hz, 2H, H_b), 8.95 (d, *J* = 2.3 Hz, 1H, H_a), 8.61 (s, 2H, H_{trz}), 8.47 (s, 4H, H_d), 8.37 (s, 2H, H_c), 5.39 – 4.96 (m, 28H), 4.04-3.16 (m, 408H)

^{13}C-NMR (126 MHz, $CDCl_3$) δ = 171.20, 165.36, 146.99, 145.46, 137.25, 136.83, 130.12, 126.68, 125.95, 121.83, 118.63, 99.32, 99.16, 99.03, 98.92, 98.83, 98.79, 82.39, 82.26, 82.19, 82.08, 81.93, 81.89, 81.81, 81.51, 81.20, 80.77, 80.74, 80.47, 80.43, 80.39, 80.11, 79.99, 72.03, 71.74, 71.57, 71.44, 71.33, 71.24, 71.19, 71.17, 71.01, 70.99, 69.86, 61.73, 61.61, 61.56, 61.49, 61.41, 61.32, 61.30, 60.46, 59.41, 59.37, 59.13, 59.09, 59.07, 59.03, 58.94, 58.78, 58.74, 58.56, 58.41, 58.35, 21.13, 14.29.

Water soluble bis-(iodotriazole)pyridinium nitrate (3.44·NO_3)

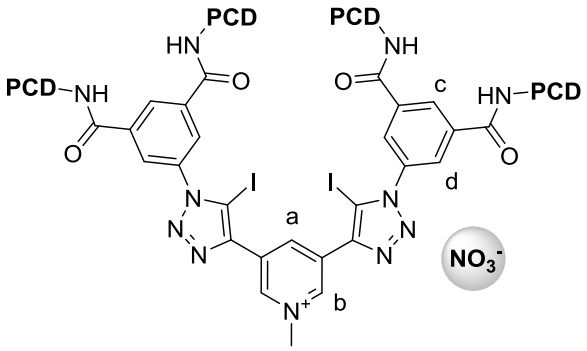

A solution of **3.42** (85 mg, mmol) in a mixture of 1:1 $CHCl_3$/CH_3I was heated in a seal tube at 60 °C overnight. The reaction mixture was dried *in vacuo* to obtain a yellow solid of **3.44·I** in a quantitative yiled. The iodide salt of **3.44**$^+$ was exchanged to a nitrate salt by passing its solution in 95:5 acetone/water through a nitrate loaded Amberlyte® anion exchange resin for three times. A solution was dried to obtain **3.44·NO_3** in quantitative yield.

^{1}H-NMR (500 MHz, 1:1 $CDCl_3$/ MeOD) δ =10.37 (t, *J* = 1.7 Hz, 1H, H_a), 9.92 (d, *J* = 1.6 Hz, 2H, H_b), 8.79 (t, *J* = 1.6 Hz, 2H, H_c), 8.50 (d, *J* = 1.6 Hz, 4H, H_d), 5.74 – 5.31 (m, 28H), 4.54 – 4.44 (m, 3H, H_{methyl}), 4.25-3.41 (m, 408H).

^{13}C-NMR (126 MHz, 1:1 $CDCl_3$/ MeOD) δ = 216.64, 214.71, 171.51, 148.82, 147.49, 142.54, 142.24, 137.87, 133.89, 133.53, 104.37, 104.29, 104.25, 104.21, 104.13, 87.66, 87.59, 87.50, 87.44, 87.33, 87.26, 87.01, 85.99, 85.77, 85.66, 85.43, 85.26, 85.01, 77.15, 77.03, 76.90, 76.70, 76.60, 76.53, 75.51, 75.20, 66.98, 66.84, 66.82, 66.80, 66.72, 66.66, 64.78, 64.44, 64.40, 64.37, 64.34, 64.04, 63.98, 63.86, 63.72, 60.23, 37.07, 35.94, 34.30.

Water soluble bis-(iodotriazole)pyridinium nitrate (3.49·NO_3)

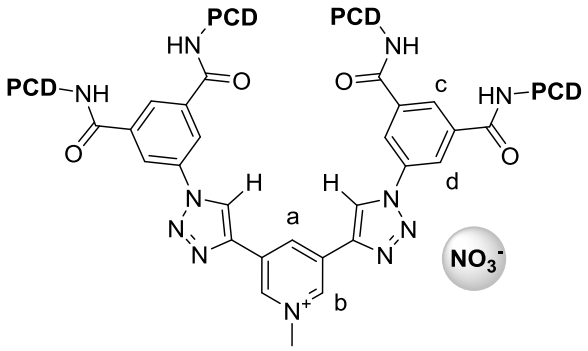

A solution of **3.48** (50 mg, 0.008 mmol) in a mixture of 1:1 $CHCl_3$/CH_3I was heated in a seal tube at 60 °C overnight. The reaction mixture was dried *in vacuo* to obtain a yellow solid of **3.49·I** in a quantitative yiled. The iodide salt of **3.49$^+$** was exchanged to a nitrate salt by passing a solution in 95:5 acetone/water through a nitrate loaded Amberlyte® anion exchange resin for three times. A solution was dried to obtain **3.49·NO_3** in 85% yield.

^{1}H-NMR (500 MHz, $CDCl_3$) δ = 9.69 (s, 2H, H_{trz}), 9.63 (s, 1H, H_a), 9.54 (s, 2H, H_b), 8.60 (s, 4H, H_d), 8.46 (s, 2H, H_c), 7.44 (s, 2H), 5.36 – 5.03 (m, 28H), 4.71 (s, 3H), 4.00-3.12 (m, 408).

^{13}C-NMR (126 MHz, $CDCl_3$) δ = 210.94, 165.34, 165.27, 141.00, 140.60, 136.85, 136.75, 136.10, 133.00, 126.98, 122.87, 122.31, 99.15, 99.07, 98.99, 98.84, 98.81, 82.26, 82.18, 82.07, 82.05, 81.97, 81.94, 81.88, 81.82, 81.74, 81.44, 80.53, 80.47, 80.23, 80.00, 79.83, 71.66, 71.60, 71.39, 71.24, 71.13, 71.10, 71.01, 70.96, 69.98, 69.62, 61.68, 61.56, 61.55, 61.53, 61.43, 61.41, 61.30, 59.40, 59.23, 59.12, 59.06, 59.03, 58.75, 58.71, 58.64, 58.48, 58.46, 58.44.

Water soluble bis-(iodotriazole)pyridine *N*-oxide (3.43)

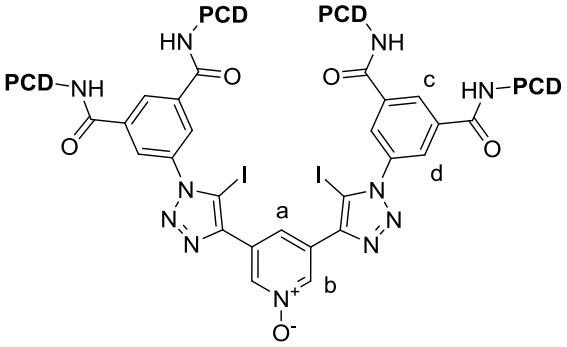

A solution of **3.42** (59 mg, 0.009 mmol) in DCM (0.5 ml) and m-CPBA (purity 67%, 26 mg, 0.09 mmol) was stirred at room temperature overnight. A reaction mixture was diluted with DCM (10 ml) and washed with water. The crude product was purified by preparative thin layered chromatography using a mixture of 85: 10: 5 MeCN/ H_2O/ KNO_3 (sat.) as an eluent. The product was extracted from silica with 25% MeOH/ DCM to obtain **3.43** in 68% yield.

^{1}H-NMR (500 MHz, $CDCl_3$) δ = 9.07 (d, *J* = 1.5 Hz, 2H, H_b), 8.78 (t, *J* = 1.6 Hz, 1H, H_a), 8.50 (s, 2H, H_c), 8.23 (d, *J* = 1.5 Hz, 4H, H_d), 7.20 (s, 2H), 5.30 – 5.01 (m, 28H), 4.09-3.16 (m, 408).

^{13}C-NMR (126 MHz, $CDCl_3$) δ = (165.37; amide C), (145.45, 136.90; pyridine C), (136.74, 129.99, 127.82; isophthalamide C), *β*-CD signals consistent with loss of C7 symmetry 99.29-98.8 (*β*-CD C_1), 82.44, 82.30, 82.23, 82.13, 81.94, 81.86, 81.58, 81.17, 80.85, 80.54, 80.40, 80.18, 72.05, 71.79, 71.61, 71.45, 71.32, 71.22, 71.05, 69.77, 61.81, 61.68, 61.65, 61.53, 61.49, 61.40, 59.53, 59.45, 59.20, 59.18, 59.16, 59.09, 59.03, 58.84, 58.62, 58.45, 58.42, 58.40.

Rotaxane 3.50·NO_3

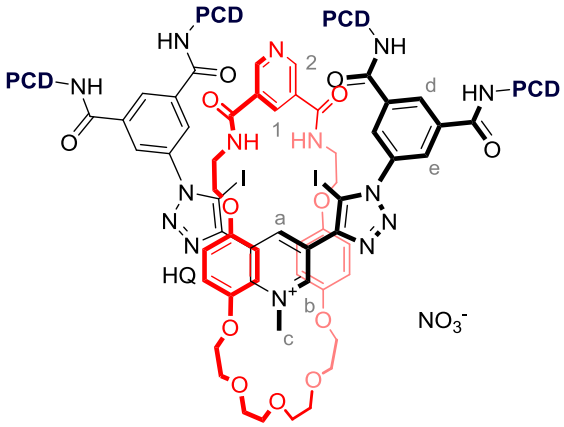

A solution of bis-amine **3.36** (29 mg, 0.062 mmol) and axle (40 mg, 0.0062 mmol) as a chloride salt was stirred in dry DCM (20 ml) at 0°C under N_2 for 20 min, then NEt_3 (26 µL, 0.31 mmol) added. A solution of 3,5-dichlorocarbonyl pyridine (prepared from 3,5-pyridinedicarboxylic acid 10 mg, 0.062 mmol) in dry DCM (3 ml) was added dropwise over 20-30 minutes. The reaction was stirred at room temperature for 3 hours and monitored the formation of [2]rotaxane product by ESI-MS and TLC. After removing solvent, the crude product was purified *via* preparative thin layer chromatography using 14% MeOH/DCM as an eluent followed by anion exchanged to NO_3^- salt using a nitrate loaded Amberlyte® to afford rotaxane **3.50·NO_3** in 72% yield.

^{1}H-NMR (500 MHz, 1:1 $CDCl_3$/d_4-MeOD) δ = 9.74 (s, 1H), 9.46 (s, 2H), 9.20 (s, 1H), 8.66 (d, *J* = 2.1 Hz, 2H), 8.35 (d, *J* = 7.2 Hz, 2H), 8.01 (s, 4H), 6.41 (d, *J* = 8.6 Hz, 4H), 6.28 (d, *J* = 8.5 Hz, 4H), 5.52 – 5.05 (m, 28H), 4.71 (s, 3H), 4.26-3.12 (m, 408H)

^{13}C-NMR (126 MHz, 1:1 $CDCl_3$/d_4-MeOD) δ = 211.59, 167.08, 166.84, 153.77, 152.85, 142.84, 137.29, 130.14, 129.05, 128.64, 115.79, 115.43, 99.45, 99.34, 99.28, 99.22, 82.76, 82.59, 82.53, 82.46, 82.40, 82.33, 82.25, 81.26, 80.93, 80.85, 80.75, 80.51, 80.37, 79.83, 72.04, 72.00, 71.85, 71.74, 71.64, 71.43, 70.60, 70.21, 69.20, 67.10, 61.96, 61.87, 61.85, 61.80, 61.78, 59.79, 59.44, 59.42, 59.37, 59.29, 59.07, 59.01, 58.96, 58.93, 58.89, 58.76, 55.29, 41.14, 40.68, 32.47, 32.07, 30.93, 30.20, 29.89, 29.32.

Part III: Water Soluble Osmium (II) Anion Host Systems

4,4'-Bis-amide bipyridine (3.61)

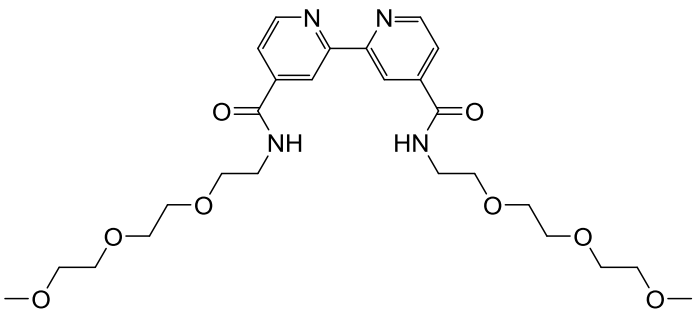

A solid compound of 2,2'-bipyridine-4,4'-dicarboxylic acid (55.6 mg, 0.228 mmol) was suspended in DCM (3 ml) with oxalyl chloride (4 equivalents) in the presence of catalytic amount of DMF, stirred overnight at 40°C to give a dark purple solution of 2,2'-bipyridine-4,4'-dicarbonyl dichloride **3.55**. To a solution of the polyether amine **3.60** (95 mg, 0.5 mmol) in dry dichloromethane (5 ml) with NEt_3 (5 equivalents) was added a solution of the acid chloride **3.55** dropwise and stirred the mixture for 3 hours. The crude product was purified by silica gel column chromatography (3%-5% MeOH/DCM) to afford 4,4'-bis-amide bipyridine **3.61** in 70% yield

^{1}H-NMR (500 MHz, $CDCl_3$) δ = 8.81 (d, *J* = 5.0 Hz, 2H), 8.74 (t, *J* = 1.2 Hz, 2H), 7.80 (dd, *J* = 5.0, 1.7 Hz, 2H), 7.24 (s, 2H), 3.74 – 3.63 (m, 20H), 3.53 – 3.44 (m, 4H), 3.28 (s, 6H).

^{13}C-NMR (126 MHz, $CDCl_3$) δ = 165.74, 150.18, 143.12, 122.30, 118.19, 72.02, 70.71, 70.63, 70.45, 69.77, 59.06, 40.17.

HRMS (ESI) m/z: 557.25897 ($[M+Na]^+$, $C_{26}H_{38}N_4O_8Na$ requires 557.25819).

4,4'-Bis-amideiodotriazole bipyridine (3.67)

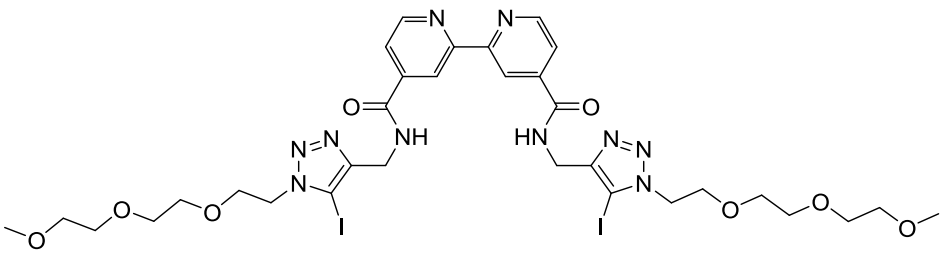

A solid compound of 2,2'-bipyridine-4,4'-dicarboxylic acid (61 mg, 0.25 mmol) was suspended in DCM (3ml) with oxalyl chloride (127 mg, 1 mmol) in the presence of catalytic amount of DMF, stirred overnight at 40°C to give a dark purple solution which was dried *in vacuo* to afford the 2,2'-bipyridine-4,4'-dicarbonyl dichloride **3.55** without purification. A solution of the iodotriazole ammonium trifluoroacetate **3.66·HTFA** (242 mg, 0.5 mmol) in DCM (10 mL) was cooled down to 0°C and added NEt_3 (209 µL), then stirring for 15 min before addition of acid chloride **3.55** solution in DCM (2 mL). After 3 hours, the crude mixture was purified by silica gel column chromatography (3%-5% MeOH/DCM) to afford 4,4'-bis-amideiodotriazole bipyridine **3.67** in 73% yield.

^{1}H-NMR (500 MHz, $CDCl_3$) δ = 8.80 (d, *J* = 5.0 Hz, 2H), 8.72 (s, 2H), 7.81 (d, *J* = 4.9 Hz, 2H), 4.76 (d, *J* = 5.1 Hz, 3H), 4.59 (t, *J* = 5.8 Hz, 4H), 3.97 (t, *J* = 5.8 Hz, 4H), 3.73 – 3.46 (m, 16H), 3.35 (s, 6H).

^{13}C-NMR (101 MHz, $CDCl_3$) δ = 165.31, 156.09, 150.15, 147.56, 142.29, 122.14, 117.86, 79.81, 71.87, 70.78, 70.55, 70.51, 69.23, 59.03, 50.34, 36.19.

HRMS (ESI) m/z: 949.13550 ($[M+H]^+$, $C_{32}H_{43}N_{10}O_8I_2$ requires 949.13492).

Bis-amide osmium(II) bipyridyl receptor ($3.53\cdot(NO_3)_2$)

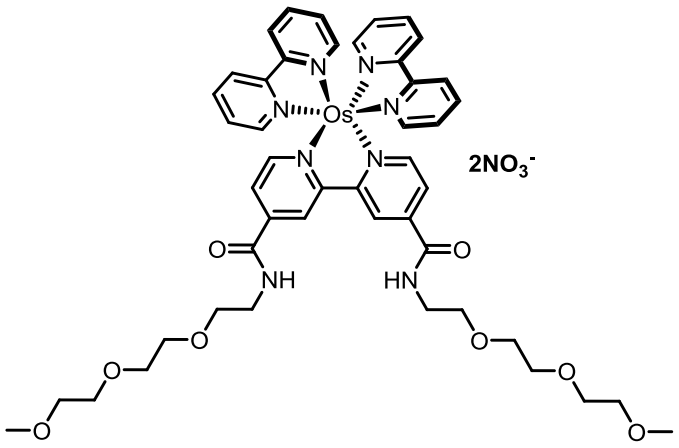

A mixture of the bipyridine bisamide **3.61** (19.6 mg, 0.0367 mmol) and $Os(bipy)_2Cl_2$ (29 mg, 0.0514 mmol) in 9:1 EtOH/H_2O (2ml) was refluxed under N_2 atmosphere in a sealed tube overnight. The resulting solution was poured into a solution of 85: 15: 5 MeCN: H_2O: $KNO_{3(aq)}$ (sat) and stirred for 2 hours. The mixture was dried and redissolved in $CHCl_3$. The organic residue was passed through Celite® and purified by size exclusion chromatography using $CHCl_3$ as an eluent to obtain black solid product of bis-amide osmium(II) bipyridyl receptor **$3.53\cdot(NO_3)_2$** (90%).

^{1}H-NMR (500 MHz, Acetone-d_6) δ = 10.11 (s, 2H), 9.48 (s, 2H), 8.87 (dd, *J* = 14.0, 8.1 Hz, 4H), 8.09 (d, *J* = 5.9 Hz, 2H), 8.07 – 8.00 (m, 6H), 7.98 (d, *J* = 5.5 Hz, 2H), 7.81 (d, *J* = 6.1 Hz, 2H), 7.50 (dt, *J* = 31.9, 6.6 Hz, 4H), 3.74 (t, *J* = 6.2 Hz, 4H), 3.63 (dd, *J* = 6.4, 4.3 Hz, 8H), 3.61 – 3.54 (m, 8H), 3.44 (d, *J* = 3.6 Hz, 4H), 3.23 (s, 6H).

^{13}C-NMR(126 MHz, Acetone-d_6) δ = 162.95, 162.87, 161.00, 159.86, 159.79, 152.36, 152.10, 151.79, 142.32, 142.28, 138.61, 129.35, 129.25, 127.74, 125.67, 125.65, 123.13, 72.65, 71.20, 71.16, 71.08, 70.89, 69.67, 58.77, 40.52, 40.40.

Bis-amideiodotriazole osmium(II) bipyridyl receptor (3.54·$(NO_3)_2$)

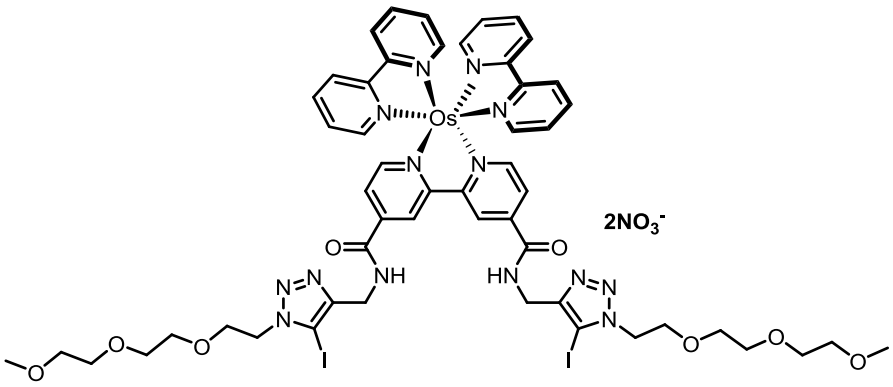

A mixture of the **3.67** (10 mg, 0.012 mmol) and $Os(bipy)_2Cl_2$ (10.3 mg, 0.018 mmol) in 9:1 EtOH/H_2O (2 ml) was refluxed under N_2 atmosphere in a sealed tube overnight. The resulting solution was poured into a solution of 85: 15: 5 MeCN: H_2O: $KNO_{3(aq)}$ (sat) and stirred for 2 hours. The mixture was dried and re-dissolved in $CHCl_3$. The organic residue was passed through Celite® and purified by size exclusion chromatography using $CHCl_3$ as an eluent to obtain black solid product of **3.54·$(NO_3)_2$** in 80% yield.

^{1}H-NMR (500 MHz, 1:1 $CDCl_3$/d_4-MeOD) δ = 9.11 (d, *J* = 1.9 Hz, 2H), 8.61 (t, *J* = 8.3 Hz, 4H), 7.93 (tt, *J* = 7.9, 1.5 Hz, 4H), 7.81 (d, *J* = 6.1 Hz, 2H), 7.75 (dd, *J* = 6.0, 1.8 Hz, 2H), 7.62 (d, *J* = 5.7 Hz, 4H), 7.40 (dddd, *J* = 19.0, 7.4, 5.8, 1.3 Hz, 5H), 4.67 – 4.66 (m, 4H), 4.56 (t, *J* = 5.6 Hz, 4H), 3.92 (t, *J* = 5.6 Hz, 4H), 3.58 (qd, *J* = 5.0, 2.8 Hz, 12H), 3.53 – 3.45 (m, 4H), 3.33 (s, 6H).

^{13}C-NMR (126 MHz, 1:1 $CDCl_3$/d_4-MeOD) δ = 164.29, 160.31, 159.25, 159.04, 151.59, 151.28, 150.88, 148.08, 142.33, 138.73, 129.23, 129.17, 127.20, 125.43, 123.26, 72.36, 71.11, 70.97, 70.92, 69.64, 59.14.

HRMS (ESI) m/z: 726.11270 ($[M-2NO_3^-]^{2+}$, $C_{52}H_{58}N_{14}O_8I_2$ requires 726.1126).

Osmium(II) bipyridyl [2]rotaxane ($3.52\cdot(NO_3)_3$)

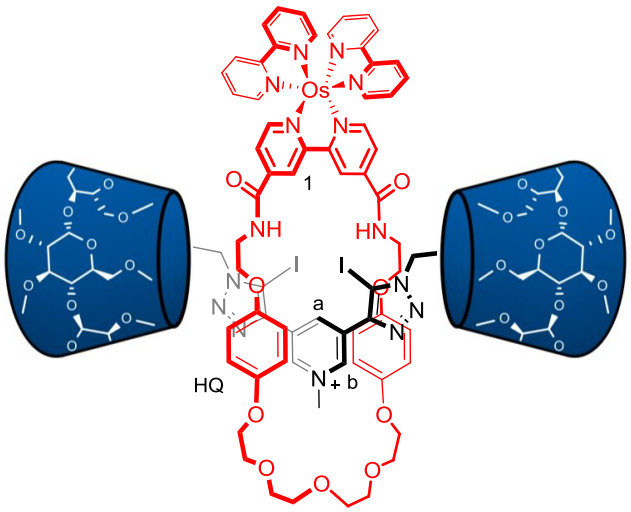

$3.52\cdot(NO_3)_3$

A solution of bis-amine **3.36** (27 mg, 0.060 mmol) and 3.51·Cl (19 mg, 0.006 mmol) as a chloride salt was stirred in dry DCM (17 ml) at 0°C under N_2 for 20 min, then triethylamine (20 µL) added. A solution of 3,5-dichlorocarbonyl pyridine (prepared from 17 mg of 2,2'-bipyridine-4,4'-dicarboxylic acid, 0.060 mmol) in dry DCM (3 ml) was added dropwise over 20-30 minutes. The reaction was stirred at room temperature for 3 hours and monitored the formation of [2]rotaxane product by ESI-MS and TLC. After removing solvent, the crude product was purified *via* preparative thin layer chromatography using 8% MeOH/$CHCl_3$ as an eluent to afford rotaxane **3.56·Cl** in 42% yield. A solution of **3.56·Cl** (14 mg, 0.0036 mmol) in 9:1 EtOH/H_2O (5 ml) was added $Os(bipy)_2Cl_2$ (9 mg, 0.016 mmol), and refluxed at 90 °C overnight. The resulting solution was poured into a solution of 85: 15: 5 MeCN: H_2O: $KNO_{3(aq)}$ (sat) and stirred for 2 hours. The mixture was dried and re-dissolved in $CHCl_3$. The organic residue was passed through Celite® and purified by size exclusion chromatography using $CHCl_3$ as an eluent to obtain black solid product of **$3.52\cdot(NO_3)$** in 90% yield.

^{1}H-NMR (500 MHz, 1:1 $CDCl_3$/d_4-MeOD) δ = 9.96 (m, 2H, H_b), 9.55 (s, 2H, H_1), 8.83 (s, 1H, H_a), 8.68 (dd, *J* = 8.1, 4.9 Hz, 4H, H_{bpy}), 7.99 (q, *J* = 7.4 Hz, 4H, H_{bpy}), 7.88 (dtd, *J* = 13.3, 6.0, 3.0 Hz, 4H, H_{bpy}), 7.65 (t, *J* = 4.8 Hz, 4H, H_{bpy}), 7.54 – 7.39 (m, 4H, H_{bpy}), 6.46 (dd, *J* = 8.8, 5.5 Hz, 4H, H_{HQ}), 5.94 (d, *J* = 8.5 Hz, 4H, H_{HQ}), 5.67 – 4.88 (m, 14H, β-CD H_1), 4.68 (s, 6H), 4.29-2.96 (β-CD $H_{2\text{-}6}$ and CH_2)

^{13}C-NMR (126 MHz, 1:1 $CDCl_3$/d_4-MeOD) δ = 163.46, 160.46, 159.47, 159.00, 153.60, 152.78, 151.69, 150.93, 142.65, 141.71, 138.95, 131.59, 129.28, 128.19, 125.63, 123.15,

115.96, 114.97, 99.42, 98.80, 98.70, 98.14, 72.29, 72.16, 71.83, 71.63, 71.41, 70.58, 62.40, 62.20, 62.09, 62.02, 61.68, 61.66, 61.58, 61.21, 60.24, 59.78, 59.47, 59.44, 59.41, 59.35, 59.27, 59.24, 58.77, 58.67, 58.57, 40.67, 32.48, 30.20, 29.90, 23.20, 14.32.

HRMS (ESI) m/z: 1480.53528 ($[M-3NO_3^-]^{3+}$, $C_{190}H_{280}N_{15}O_{77}Os$ requires 1480.53511).

5.9 Synthetic Procedures and Characterisations of Compounds in Chapter 4

1,2-Diethynylbenzene (4.3)

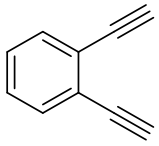

1,2-Diethynylbenzene was prepared by a modification of literature procedures. A 20ml-microwave vial was loaded with 1,2-dibromobenzene (1g, 4.24 mmol), triphenylphosphine (48 mg, 0.296). $Pd(PPh_3)_2Cl_2$ (32 mg, 0.044 mmol), CuI (3.2 mg, 0.016 mmol), and diethylamine (12 ml). A mixture was de-oxygenated with nitrogen bubbling through the solution for 10 minutes. Then, TMS-acetylene (1.8 ml, 13.4 mmol) was added, the vial sealed and heated under microwave irradiation at 130°C for 2 hours. The resulting brown solution was filtered through cotton wool, with the solid residue being washed with hexane until getting colourless solution. The solution was concentrated *in vacuo* to get brown oil which was taken up in MeOH (40 ml). The solution of KOH (1 g) in water (20 ml) was added, and the solution stirred for 30 minutes. Then solvents were removed *in vacuo*, the residue being extracted with hexane (5x20 ml), brine, and dried over $MgSO_4$. The product was isolated by silica gel column chromatography using 5% DCM/hexane to afford **4.3** in 88% yield.

^{1}H-NMR (400MHz, $CDCl_3$) δ = 7.50 - 7.56 (2H, m), 7.30 - 7.35 (2H, m), 3.35 (2H, s).

General synthetic method F: CuAAC reaction for XB receptors

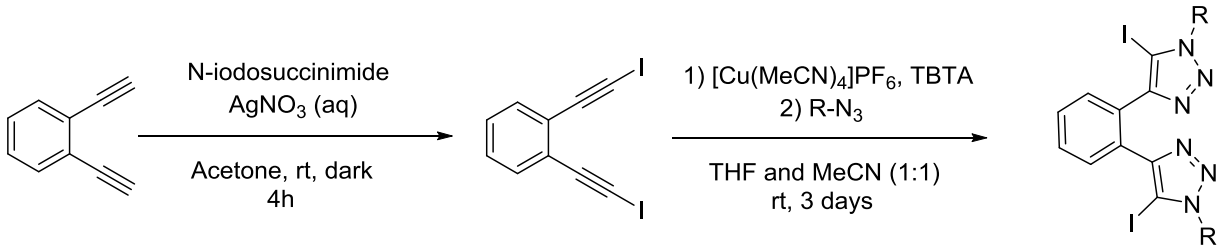

To a solution of 1,2-diethynylbenzene in acetone was added N-iodosuccinimide. An aqueous solution of $AgNO_3$ was added dropwise. The reaction vessel was covered with foil and stirred in the dark for 4h at room temperature, then diluted with DCM (50 ml), washed with water (50 ml) and brine (50 ml), dried over $MgSO_4$, filtered to remove solid residue. The solvent was removed *in vacuo* to get yellow oily mixture. Then, the green suspension of $[Cu(MeCN)_4]PF_6$ and TBTA in dry and degassed THF was added to the resulting oily residue, followed by MeCN. The mixture was stirred for 5 min, after that the solution of azide in THF was added, the reaction vessel covered with foil and stirred under the atmosphere of N_2 in the dark for 3 days. The crude was extracted with DCM. The organic fraction was washed with a solution of EDTA (0.02M) in NH_4OH (1M), water, and brine. Then, the residue was dried over $MgSO_4$ and removed solvent *in vacuo*. The pure compound can be obtained by silica gel column chromatography.

XB benzyl acyclic (4.4)

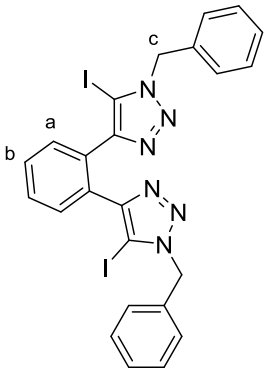

See general synthetic method F: 1,2-diethynylbenzene **4.3** (64 mg, 0.5 mmol), acetone (8 ml), *N*-iodosuccinimide (240 mg, 1.13 mmol), a solution of $AgNO_3$ (17 mg in 1 ml H_2O), $[Cu(MeCN)_4]PF_6$ (56 mg, 0.015 mmol), TBTA (26.5 mg, 0.05 mmol),dry and degassed THF (1.5 ml), dry and degassed MeCN (1.5 ml), benzyl azide **4.4** (147 mg, 1.1 mmol). The resulting crude mixture was purified by silica gel column chromatography using the gradient of 3% to 10% EtOAC/Hexane to afford the product as off-white powder in 70% yield.

^{1}H-NMR (400 MHz, $CDCl_3$) δ = 7.63 (dd, *J* = 5.7, 3.4 Hz, 2H, H_b), 7.52 (dt, *J* = 5.8, 3.8 Hz, 2H, H_a), 7.37 – 7.27 (m, 6H, H_{phenyl}), 7.22 – 7.15 (m, 4H, H_{phenyl}), 5.52 (s, 4H, H_c).
^{13}C-NMR (101 MHz, $CDCl_3$) δ = 151.49, 134.48, 131.38, 129.96, 129.17, 128.92, 128.43, 127.89, 80.28, 54.44.
HRMS (ESI) m/z: 644.97528 ($[M+H]^+$, $C_{24}H_{19}N_6I_2$ requires 644.97551).

XB mesityl acyclic (4.5)

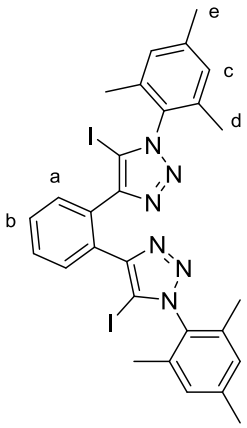

See general synthetic method F: 1,2-diethynylbenzene **4.3** (64 mg, 0.5 mmol), acetone (8 ml), N-iodosuccinimide (240 mg, 1.13 mmol), a solution of $AgNO_3$ (17 mg in 1 ml H_2O), $[Cu(MeCN)_4]PF_6$ (56 mg, 0.015 mmol), TBTA (26.5 mg, 0.05 mmol),dry and degassed THF (1.5 ml), dry and degassed MeCN (1.5 ml), mesityl azide **4.5** (177 mg, 1.1 mmol). The resulting crude mixture was purified by silica gel column chromatography using the gradient of 3% to 10% EtOAC/Hexane to afford the product as off-white powder in 56% yield.
^{1}H-NMR (500 MHz, d_6-DMSO) δ = 7.87 – 7.52 (m, 4H, H_{a+b}), 7.11 (s, 4H, H_c), 2.34 (s, 6H, H_e), 1.83 (s, 12H, H_d).
^{13}C-NMR(126 MHz, d_6-DMSO) δ = 150.42, 140.08, 135.34, 132.98, 131.17, 130.30, 128.92, 128.86, 87.19, 20.71, 17.23.
HRMS (ESI) m/z: 701.03760 ($[M+H]^+$, $C_{28}H_{27}N_6I_2$ requires 701.03811).

XB perfluoroaryl acyclic (4.6)

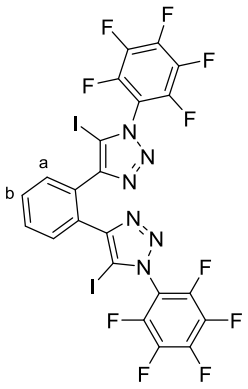

See general synthetic method F: 1,2-diethynylbenzene **4.3** (64 mg, 0.5 mmol), acetone (8 ml), *N*-iodosuccinimide (240 mg, 1.13 mmol), a solution of $AgNO_3$ (17 mg in 1 ml H_2O), $[Cu(MeCN)_4]PF_6$ (56 mg, 0.015 mmol), TBTA (26.5 mg, 0.05 mmol),dry and degassed THF (1.5 ml), dry and degassed MeCN (1.5 ml), perfluoroaryl azide **4.6** (229 mg, 1.1 mmol). The resulting crude mixture was purified by silica gel column chromatography using the gradient of 0.05% to 0.3% MeOH/DCM to afford the product as off-white powder. (71%)

^{1}H-NMR (500 MHz, CD_2Cl_2) δ = 7.80 (dd, *J* = 5.8, 3.3 Hz, 2H, H_a), 7.70 (dt, *J* = 5.7, 3.5 Hz, 2H, H_b).

^{19}F-NMR (470 MHz, CD_2Cl_2) δ = -142.95, -148.51, -160.21.

^{13}C-NMR (126 MHz, CD_2Cl_2) δ = 152.13, 145.27, 143.23, 139.62, 137.58, 131.87, 130.38, 129.53, 84.94.

HRMS (ESI) m/z: 796.84930 ($[M+H]^+$, $C_{22}H_5N_6I_2F_{10}$ requires 796.84999).

General synthetic method G: CuAAC reaction for HB receptors

To a solution of azide in dry and degassed DCM in a round bottom flask covered with aluminum foil, a solution of alkyne in DCM was added to the reaction mixture. $[Cu(MeCN)_4]PF_6$, TBTA, diisopropylethylamine were sequentially added. The reaction mixture was stirred under an atmosphere of N_2 in dark. The progress of the reaction was monitored by ESI-MS to follow the absence of starting materials and the mono-triazole product. To work up the reaction, a solution of EDTA (0.02M) in NH_4OH (1M) was added, and then keep stirring the mixture for 30 min. DCM was used for the extraction of organic compounds. The obtaining organic layer was dried over $MgSO_4$. The crude product was purified by silica gel column chromatography.

HB benzyl acyclic (4.14)

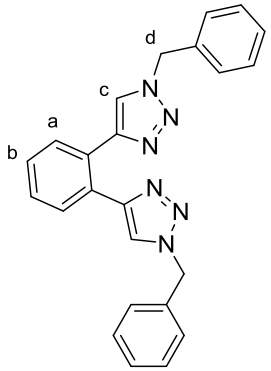

See general synthetic method G. benzyl azide **4.4** (198 mg, 1.5 mmol), dry and degassed DCM (12 ml), 1,2-diethynylbenzene **4.3** (63 mg, 0.5mmol), $[Cu(MeCN)_4]PF_6$ (51.6 mg, 0.138 mmol), TBTA (80.8 mg, 0.152mmol), DIPEA (0.24 ml, 1.384 mmol). The reaction mixture was stirred under an atmosphere of N_2 in dark at room temperature. The crude product was purified *via* silica gel column chromatography using gradient of 20% to 40% to afford the desire product in 49% yield.

^{1}H-NMR (400 MHz, $CDCl_3$) δ = 7.71 (dd, *J* = 5.8, 3.4 Hz, 2H, H_a), 7.42 (dd, *J* = 5.8, 3.4 Hz, 2H, H_b), 7.39 – 7.30 (m, 6H, H_{phenyl}), 7.24 – 7.15 (m, 6H, H_{phenyl}, H_c), 5.39 (s, 4H).

^{13}C-NMR (101 MHz, $CDCl_3$) δ = 147.06, 134.84, 130.24, 129.62, 129.23, 128.85, 128.68, 128.08, 122.59, 54.15.

HRMS (ESI) m/z: 393.18225 ($[M+H]^+$, $C_{24}H_{21}N_6$ requires 393.18222).

HB perfluoroaryl acyclic (4.16)

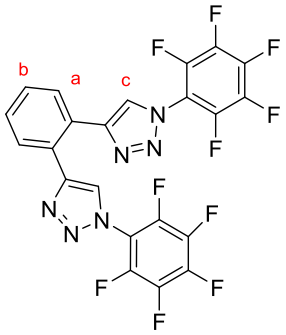

See general synthetic method G. perfluoroaryl azide **4.6** (229 mg, 1.1 mmol), dry and degassed CH_2Cl_2 (12 ml), 1,2-diethynylbenzene **4.3** (63 mg, 0.5mmol), $[Cu(MeCN)_4]PF_6$ (51.6 mg, 0.138 mmol), TBTA (80.8 mg, 0.152mmol), DIPEA (0.24 ml, 1.384 mmol). The reaction mixture was stirred under an atmosphere of N_2 in dark at room temperature. The crude product was purified by silica gel column chromatography using DCM to give the product in 36% yield.

^{1}H-NMR (500 MHz, $CDCl_3$) δ = 7.88 (dd, *J* = 5.7, 3.4 Hz, 2H, H_a), 7.79 (s, 2H, H_c), 7.60 (dd, *J* = 5.8, 3.3 Hz, 2H, H_b).

^{13}C-NMR (126 MHz, $CDCl_3$) δ =146.88, 142.54, 142.52, 138.23, 130.78, 129.61, 128.67, 125.26, 112.88.

HRMS (ESI) m/z: 545.05658 ($[M+H]^+$, $C_{22}H_7N_6F_{10}$ requires 545.05670).

General synthetic method H: Alkylation reaction

A solution of bis-triazole or iodotriazole in dry DCM was added $[Me_3O]BF_4$, and stirred at ambient temperature for 3 days. The reaction was quenched with methanol and stirred for 30 minutes. The solvent was removed *in vacuo* to obtain a crude mixture which was purified *via* preparative thin layered chromatography using the mixture of 5: 10: 85 ethanol, acetonitrile, and dichloromethane as an eluent.

XB benzyl substituted iodotriazolium acyclic receptor (4.11·BF_4)

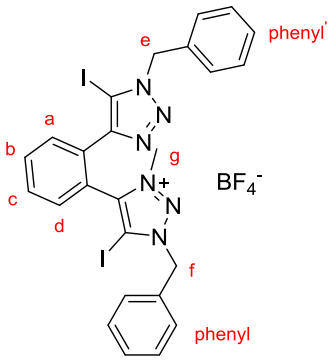

See general synthetic method H. **4.8** (56 mg, 0.075 mmol), $[Me_3O]BF_4$ (28 mg, 0.19 mmol)**,** DCM (2 ml)

^{1}H-NMR (500 MHz, 1:1 CD_3CN/CD_3Cl) δ = 7.92 (dd, *J* = 8.0, 1.3 Hz, 1H, H_d), 7.82 (td, *J* = 7.7, 1.4 Hz, 1H, H_b), 7.70 (td, *J* = 7.7, 1.4 Hz, 1H, H_c), 7.57 (dd, *J* = 7.8, 1.4 Hz, 1H, H_a), 7.41 – 7.33 (m, 3H, H_{phenyl}), 7.29 (dd, *J* = 5.4, 1.7 Hz, 3H, $H_{phenyl'}$), 7.22 (dd, *J* = 7.3, 1.9 Hz, 2H, H_{phenyl}), 7.14 – 7.06 (m, 2H, H_f), 5.78 – 5.46 (m, 2H, H_e), 4.15 (d, *J* = 1.5 Hz, 3H, H_g).
^{13}C-NMR (126 MHz, 1:1 CD_3CN/CD_3Cl) δ = 148.55, 148.43, 134.73, 133.10, 131.81, 131.74, 131.73, 130.90, 130.39, 129.86, 129.70, 129.30, 128.83, 128.31, 128.01, 121.73, 91.37, 81.88, 58.08, 54.84, 39.75
HRMS (ESI) m/z: 658.99023 ($[M-BF_4]^+$, $C_{25}H_{21}N_6{}^{127}I_2$ requires 658.99116).

XB perfluoroaryl substituted iodotriazolium acyclic receptor (4.13·BF_4)

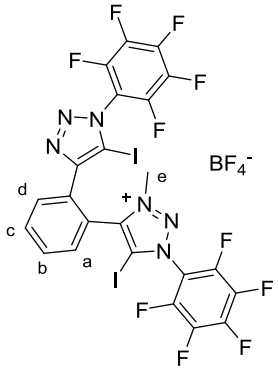

See general synthetic method H. **4.10** (50 mg, 0.063 mmol), $[Me_3O]BF_4$ (23 mg, 0.016 mmol)**,** DCM (6 ml)**.**

^{1}H-NMR (500 MHz, 1:1 $CDCl_3$, CD_3CN) δ = 8.12 (m, 1H), 7.95 (td, *J* = 7.5, 1.9 Hz, 1H), 7.89 – 7.75 (m, 2H), 4.37 (s, 3H).

^{19}F-NMR (470 MHz, 1:1 $CDCl_3$, CD_3CN) δ = -142.61, -143.25, -143.70, -144.02, -144.63, -147.89, -152.65, -157.69, -157.93, -159.94.

^{13}C-NMR (126 MHz, 1:1 $CDCl_3$, CD_3CN) δ = 149.37, 149.08, 146.76, 144.60, 142.48, 139.74, 137.82, 133.87, 132.01, 131.26, 131.16, 130.86, 120.97, 96.61, 40.94.

HRMS (ESI) m/z: 810.86414 ($[M-BF_4]^+$, $C_{23}H_7N_6F_{10}{}^{127}I_2$ requires 810.86564).

HB benzyl substituted bis-triazolium acyclic receptor (4.17·BF_4)

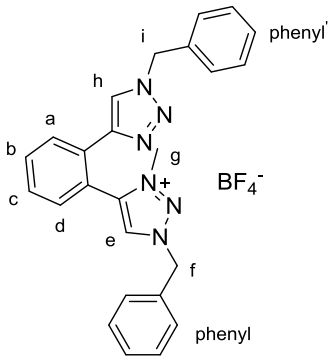

See general synthetic method H. **4.14** (18 mg, 0.044 mmol), $[Me_3O]BF_4$ (8 mg, 0.05 mmol)**,** DCM (2 ml)**.**

^{1}H-NMR (400 MHz, 1:1 CD_3CN/CD_3Cl) δ = 8.23 (s, 1H, H_d), 8.04 (d, *J* = 2.1 Hz, 1H, H_b), 7.78 (d, *J* = 7.9 Hz, 1H, H_c), 7.69 (td, *J* = 7.6, 1.5 Hz, 1H, H_a), 7.57 – 7.50 (m, 1H, H), 7.50 – 7.45 (m, 2H), 7.42 (same position with $CHCl_3$ in solvent, 4H), 7.35 (q, *J* = 5.0 Hz, 3H), 7.29 (dd, *J* = 7.3, 2.2 Hz, 3H), 5.75 (s, 2H, H_g), 5.51 (s, 2H, H_e), 3.87 (s, 3H, H_g).

^{13}C-NMR (101 MHz, 1:1 CD_3CN/CD_3Cl) δ = 145.72, 144.03, 135.49, 133.04, 132.39, 131.60, 130.09, 129.78, 129.45, 129.36, 129.34, 129.19, 129.15, 129.06, 128.59, 123.46, 119.17, 57.60, 54.35, 38.47.

HRMS (ESI) m/z: 407.19727 ($[M-BF_4]^+$, $C_{25}H_{23}N_6$ requires 407.19787).

HB benzyl substituted bis-triazolium acyclic receptor (4.17·$(BF_4)_2$)

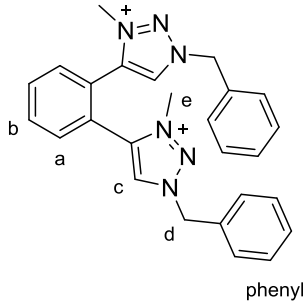

See general synthetic method H. **4.14** (18 mg, 0.044 mmol), $[Me_3O]BF_4$ (15 mg, 0.1mmol)**,** DCM (2 ml)**.**

^{1}H-NMR (500 MHz, 1:1 CD_3CN/CD_3Cl) δ = 8.42 (s, 2H, H_c), 7.86 (dd, J = 5.8, 3.4 Hz, 2H, H_a), 7.71 (dd, J = 5.8, 3.4 Hz, 2H, H_b), 7.56 – 7.50 (m, 4H, H_{phenyl}), 7.46 – 7.41 (m, 6H, H_{phenyl}), 5.70 (s, 4H, H_d), 4.04 (s, 6H, H_e).

^{13}C-NMR (101 MHz, 1:1 CD_3CN/CD_3Cl) δ = 256.53, 250.25, 249.63, 249.05, 247.16, 246.96, 246.64, 240.15, 234.38, 174.84, 155.97.

HB mesityl substituted bis-triazolium acyclic receptor (4.18·$(BF_4)_2$)

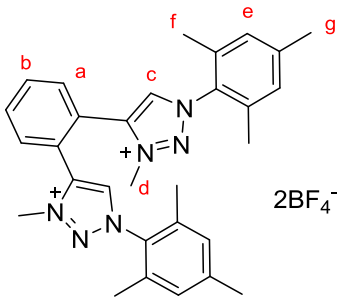

See general synthetic method H. **4.15** (17 mg, 0.038 mmol), $[Me_3O]BF_4$ (16 mg, 0.11 mmol)**,** DCM (4 ml)

^{1}H-NMR (500 MHz, *d*$_3$-MeCN) δ = 8.54 (s, 2H, H_c), 8.01 (ddt, *J* = 23.7, 6.0, 3.4 Hz, 4H, H_{a+b}), 7.16 (s, 4H, H_e), 4.29 (s, 6H, H_d), 2.37 (s, 6H, H_g), 2.02 (s, 12H, H_f).

^{13}C-NMR (126 MHz, CD_3CN) δ = 143.99, 140.89, 135.30, 134.10, 133.71, 132.80, 131.93, 130.92, 123.45, 40.49, 21.21, 17.80.

MOM protected XB macrocycle precursor (4.31)

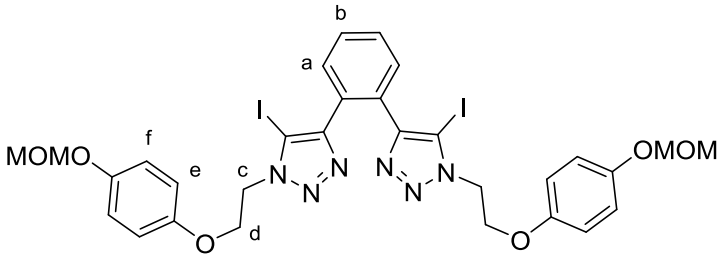

Intermediate **4.31** was synthesised *via* CuAAC reaction between 1,2-diiodoethynylbenzene **4.3** and azide **4.30**. In order to prepare bis-iodoalkyne, 1,2-diethynylbenzene[294](66 mg, 0.5 mmol) was dissolved in acetone (8 mL) in a round bottom flask wrapped with aluminum foil. *N*-iodosuccinimide (240 mg, 1.13 mmol) and an aqueous solution of $AgNO_3$ (17 mg, 0.103 mmol in H_2O 1 mL) were added. The reaction was stirred at room temperature for 4 hrs. Brine (20 mL) was added to the mixture. The aqueous layer was extracted with dichloromethane (3x20 mL), and then dried over $MgSO_4$. Solvent was removed *in vacuo* to get yellow oil residue. ^{1}H-NMR of crude product shows the disappearance of ethynyl protons which corresponds to the reported spectrum. The crude product can be used without further purification in the next step.

To a solution of $Cu(MeCN)_4PF_6$ (56 mg, 0.15 mmol) and TBTA (15 mg, 0.03 mmol) in dry and degassed THF (2 ml) was added a solution of bis-iodoalkyne from the previous step in THF (0.5 ml) and azide **4.30** (246 mg, 1.1 mmol) in THF (0.5 ml). The reaction was stirred at room temperature for 3 days, after which the reaction mixture was found to turn green. Dichloromethane (10 mL) was added, and then the organic layer was washed with 35% aqueous ammonia solution (2 x 30 mL). The aqueous layer was extracted with dichloromethane (2 x20 mL) and the combined organics were dried with brine (50 mL) and $MgSO_4$. Solvent was removed *in vacuo* to obtain black solid which was purified by column chromatography (eluent: 2 % *v/v* MeOH in DCM) to afford the solid pure product (232 mg, 56% over 2 steps).

^{1}H-NMR (400 MHz, $CDCl_3$) δ = 7.64 (2H, dd, *J* = 5.7, 3.4 Hz, H_a), 7.54 (2H, dd, *J* = 5.8, 3.4 Hz, H_b), 7.09 – 6.87 (4H, m, H_e), 6.86 – 6.62 (4H, m, H_f), 5.09 (4H,s), 4.64 (4H, t, ^3J =5.7 Hz, H_c), 4.31 (4H, t, ^3J =5.7 Hz, H_d), 3.46 (6H,s)

^{13}C-NMR (101 MHz, $CDCl_3$) δ = 153.13, 152.03, 151.04, 131.52, 129.88, 129.20, 117.77, 115.72, 95.33, 81.28, 77.16, 66.91, 56.03, 49.97.

HRMS (ESI) *m/z* 825.0382 ($[M + H]^+$, $C_{32}H_{33}O_6N_6I_2$ requires 825.0389).

XB macrocycle precursor (4.32)

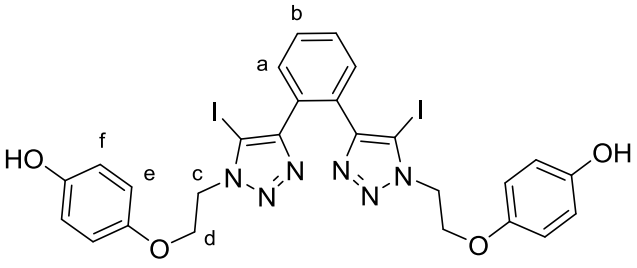

Acetyl chloride (0.6 mL, 8.5 mmol) was added to methanol (3 mL) at 0 ^{o}C and stirred for 5 minutes, before being warmed to ambient temperature and stirred for a further 15 minutes. Intermediate **4.31** (233 mg, 0.28 mmol) was dissolved in dichloromethane (3 mL) and added portionwise to the vigorous acidic methanol solution and stirred for 2 hours. After the reaction was complete (checked using TLC with 5 % methanol in DCM as eluent), the solvent was evaporated and the product dried on the high vacuum for a day to yield the product as a grey solid in excellent purity (206 mg, quantitative). The product was used without further purification.

^{1}H-NMR (500 MHz, Acetone-d_6) δ = 8.09 (2H, dd, J = 5.8, 3.3 Hz, H_a), 8.02 (2H, dd, J = 5.7, 3.3 Hz, H_b), 7.28 – 7.15 (8H, m, hydroquinone-ArH), 5.16 (4H, t, ^{3}J =5.5 Hz, H_c), 4.81 (4H, t, ^{3}J =5.5 Hz, H_d);

^{13}C-NMR (126 MHz, Acetone) δ 152.73, 152.49, 151.34, 132.25, 131.50, 129.62, 116.87, 116.70, 83.37, 68.00, 50.94.

XB macrocycle (*ortho*-4.26)

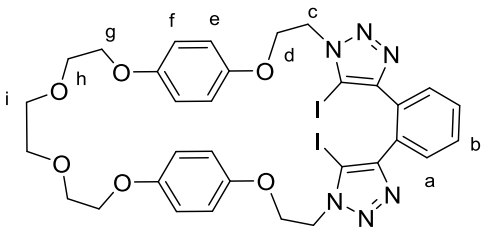

To a mixture of **4.32** (150 mg, 0.204 mmol) and triethylene glycol bis-tosylate (94 mg, 0.204 mmol) was added to anhydrous degassed DMF (27 mL) and the mixture stirred under N_2 till both solids dissolved. Subsequently, cesium carbonate (534 mg, 1.64 mmol) was added and the vigorously-stirred suspension was allowed to stir at 70 °C under N_2 for 24 hours until starting material **10** could not be observed by ESI-MS. After which, the DMF was removed on the rotary evaporator and the resulting solid stirred in a mixture of chloroform (50 mL) and water (50 mL). The aqueous and organic layers were separated and the aqueous layer extracted thoroughly with chloroform (4 x 30 mL). The combined organics were then dried with brine (3 x 20 mL) and $MgSO_4$. After solvent removal, the crude reaction mixture was purified by preparatory thin layer chromatography (2.5 % methanol in DCM) and recrystallisation in EtOH to afford macrocycle ***ortho*-4.26** as a white solid (34 mg, 20 %).

^{1}H-NMR (500MHz, *d_2*-dichloromethane) δ 7.66 (2H, dd, *J*=5.6, 3.5 Hz, H_a), 7.57 (2H, dd, J=5.8, 3.4 Hz, H_b), 6.74 - 6.82 (8H, m, hydroquinone-Ar*H*), 4.63 (4H, t, ^3J =6.0 Hz, H_c), 4.30 (4H, t, ^3J =6.0 Hz, H_d), 3.96 - 4.04 (4H, m, H_g), 3.73 - 3.80 (4H, m, H_h), 3.66 ppm (4H, s, H_i).

^{13}C-NMR (126MHz, *d_2*-dichloromethane) δ 154.1, 152.6, 151.7, 131.8, 130.4, 129.6, 116.3, 116.2, 81.6, 71.2, 70.1, 68.7, 67.2, 50.0.

HRMS (ESI +ve) *m/z* 851.0542 ($[M + H]^+$, $C_{32}H_{33}O_6N_6I_2$, calc. 851.0546).

XB Rotaxane *ortho*-4.35

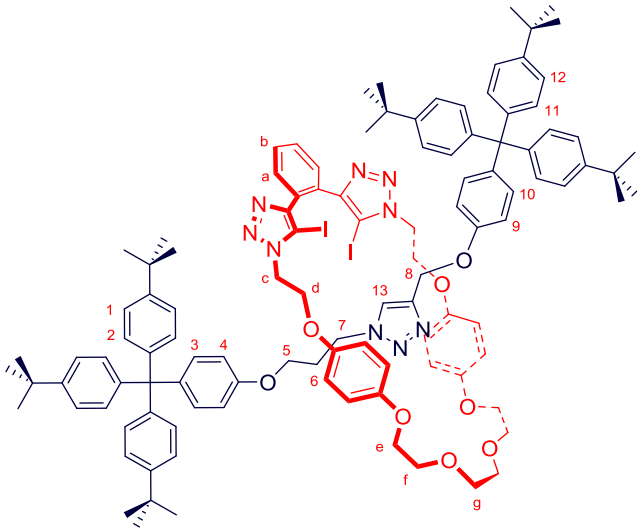

Macrocycle ***ortho*-4.26** (15 mg, 0.018 mmol) was suspended in the mixture of 1:1 dry degassed dichloromethane and tetrahydrofuran (3 mL). $[Cu(CH_3CN)_4]PF_6$ (6.6 mg, 0.018 mmol) was added to obtain a clear solution which was stirred for 15 minutes under N_2. To the colourless solution was added proto-alkyne **4.33** (47.7 mg, 0.088 mmol) and azide **4.32** (51.7 mg, 0.088 mmol) portionwise successively obtaining a green solution. The reaction was stirred under N_2 for 72 hours. After which, the reaction was diluted with chloroform (20 mL) and washed with 0.02 M EDTA in 1M aqueous ammonia (2 x 20 mL), followed by water (3 x 20 mL). The organic layer was dried with $MgSO_4$ and the solvent removed to give a white solid. Purification by preparatory thin layer chromatography (2.5 % methanol in DCM) afforded the rotaxane as a white solid (10.17 mg, 30 %).

^{1}H-NMR (500MHz, Acetone): δ = 8.33 (1H, s, H_{13}), 8.09 (2H, dd, *J* = 5.8, 3.4 Hz, H_a), 7.98 (2H, dd, *J* = 5.7, 3.4 Hz, H_b), 7.84 – 7.70 (12H, m, stopper-phenyl), 7.66 – 7.57 (12H, m, stopper-phenyl), 7.54 (4H, d, *J* = 8.7 Hz, H_3+ H_{10}), 7.28 (2H, d, *J* = 8.9 Hz, H_9), 7.16 (2H, d, *J* = 8.8 Hz, H_4), 7.03 – 6.75 (4H ,m, hydroquinone-Ar*H*), 6.87-6.84 (4H ,m, hydroquinone-Ar*H*), 5.29 (4H, s, H_8), 4.98 (4H, t, ^3J = 6.4 Hz, H_c), 4.72 (4H, t, ^3J = 6.1 Hz, H_d), 4.56 (2H, t, ^3J = 7.3 Hz, H_7), 4.34 (4H, q, *J* = 4.0 Hz, H_e), 4.17 – 4.08 (m, 4H, H_f+ H_5), 4.06 (4H, s, H_g), 2.43 – 2.32 (2H, m, H_6), 1.75 (54H, s, stopper-^{t}Bu).

^{13}C-NMR (126MHz, Acetone)): δ = 156.6, 156.4, 153.3, 151.4, 150.4, 148.2, 144.5, 143.0, 139.4, 139.3, 131.8, 131.4, 130.5, 128.6, 124.3, 116.3, 115.1, 113.6, 113.5, 82.3, 70.6, 69.5, 67.6, 66.5, 64.5, 63.1, 61.3, 49.0, 46.7, 34.0, 30.8.

HRMS (ESI +ve) *m/z* 1980.7929 ($[M+H]^+$, $C_{112}H_{128}O_8N_9I_2$, calc. 1980.7969).

References

References

1. J. W. Steed and J. L. Atwood, *Supramolecular Chemistry*, Wiley, Chichester, UK, 2nd edn., 2009.
2. F. Emil, *Ber. Dtsch. Chem. Ges*, 1894, **27**, 2985-2993.
3. F. Emil, *Ber. Dtsch. Chem. Ges*, 1890, **23**, 2611-2624.
4. K. D. E., *Angew. Chem. Int. Ed*, 1995, **33**, 2375-2378.
5. C. J. Pedersen, *J. Am. Chem. Soc.*, 1967, **89**, 7017-7036.
6. C. H. Park and H. E. Simmons, *J. Am. Chem. Soc.*, 1968, **90**, 2431-2432.
7. S. Jean-Pierre, *Angew. Chem. Int. Ed*, 2017, **56**, 11080-11093.
8. S. J. Fraser, *Angew. Chem. Int. Ed*, 2017, **56**, 11094-11125.
9. F. B. L., *Angew. Chem. Int. Ed*, 2017, **56**, 11060-11078.
10. M. Szwarc, *Acc. Chem. Res.*, 1969, **2**, 87-96.
11. H. Umeyama and K. Morokuma, *J. Am. Chem. Soc.*, 1977, **99**, 1316-1332.
12. J. P. L. Cox, I. A. Nicholls and D. H. Williams, *J. Chem. Soc., Chem. Commun.*, 1991, 1295-1297.
13. R. Desiraju Gautam, P. S. Ho, L. Kloo, C. Legon Anthony, R. Marquardt, P. Metrangolo, P. Politzer, G. Resnati and K. Rissanen, *Pure Appl. Chem.*, 2013, **85**, 1711.
14. P. Metrangolo, F. Meyer, T. Pilati, G. Resnati and G. Terraneo, *Angew. Chem. Int. Ed*, 2008, **47**, 6114-6127.
15. L. C. Gilday, S. W. Robinson, T. A. Barendt, M. J. Langton, B. R. Mullaney and P. D. Beer, *Chem. Rev.*, 2015, **115**, 7118-7195.
16. J. S. Murray, P. Lane and P. Politzer, *J. Mol. Model.*, 2009, **15**, 723-729.
17. P. Politzer, J. S. Murray and T. Clark, *Phys. Chem. Chem. Phys.*, 2013, **15**, 11178-11189.
18. J. Y. C. Lim and P. D. Beer, *Chem*, 2018, **4**, 731-783.
19. E. Lanzarotti, R. R. Biekofsky, D. A. Estrin, M. A. Marti and A. G. Turjanski, *J. Chem. Inf. Model.*, 2011, **51**, 1623-1633.
20. M. O. Sinnokrot, E. F. Valeev and C. D. Sherrill, *J. Am. Chem. Soc.*, 2002, **124**, 10887-10893.
21. S. E. Wheeler and K. N. Houk, *J. Am. Chem. Soc.*, 2008, **130**, 10854-10855.
22. M. R. Battaglia, A. D. Buckingham and J. H. Williams, *Chem. Phys. Lett.*, 1981, **78**, 421-423.
23. J. C. Ma and D. A. Dougherty, *Chem. Rev.*, 1997, **97**, 1303-1324.
24. D. A. Dougherty, *Acc. Chem. Res.*, 2013, **46**, 885-893.
25. W. Zhong, J. P. Gallivan, Y. Zhang, L. Li, H. A. Lester and D. A. Dougherty, *Proc. Natl. Acad. Sci*, 1998, **95**, 12088-12093.
26. P. Gamez, *Inorg, Chem. Front.*, 2014, **1**, 35-43.
27. M. Mascal, A. Armstrong and M. D. Bartberger, *J. Am. Chem. Soc.*, 2002, **124**, 6274-6276.
28. D. Chandler, *Nature*, 2005, **437**, 640.
29. B. Wilfried and E. J. B. F. N., *Angew. Chem. Int. Ed*, 1993, **32**, 1545-1579.
30. J. M. Sturtevant, *Proc. Natl. Acad. Sci*, 1977, **74**, 2236-2240.
31. N. Muller, *Acc. Chem. Res.*, 1990, **23**, 23-28.
32. F. Biedermann, W. M. Nau and H.-J. Schneider, *Angew. Chem. Int. Ed*, 2014, **53**, 11158-11171.
33. H. Zhao, L. A. Leamer and F. P. Gabbai, *Dalton Trans.*, 2013, **42**, 8164-8178.
34. M. J. Kelly, A. E. J. Broomsgrove, I. R. Morgan, I. Siewert, P. Fitzpatrick, J. Smart, D. Vidovic and S. Aldridge, *Organometallics*, 2013, **32**, 2674-2684.
35. J. S. Jones and F. P. Gabbaï, *Acc. Chem. Res.*, 2016, **49**, 857-867.
36. H. T. Ngo, X. Liu and K. A. Jolliffe, *Chem. Soc. Rev.*, 2012, **41**, 4928-4965.

37. T. Zhang, N. Y. Edwards, M. Bonizzoni and E. V. Anslyn, *J. Am. Chem. Soc.*, 2009, **131**, 11976-11984.
38. E. Parravicini, C. Fontana, G. L. Paterlini, P. Tagliabue, F. Rovelli, K. Leung and R. I. Stark, *Pediatrics*, 1996, **98**, 730-734.
39. G. F. McIsaac, M. B. David, G. Z. Gertner and D. A. Goolsby, *Nature*, 2001, **414**, 166-167.
40. V. H. Smith and D. W. Schindler, *Trends. Ecol. Evol.*, 2009, **24**, 201-207.
41. M. Sadeq, C. L. Moe, B. Attarassi, I. Cherkaoui, R. ElAouad and L. Idrissi, *Int. J. Hyg. Environ. Health.*, 2008, **211**, 546-554.
42. A. M. Richard, J. H. Diaz and A. D. Kaye, *Ochsner J*, 2014, **14**, 392-398.
43. G. E. Likens and F. H. Bormann, *Science*, 1974, **184**, 1176-1179.
44. P. D. Beer and P. A. Gale, *Angew. Chem. Int. Ed*, 2001, **40**, 486-516.
45. H. Luecke and F. A. Quiocho, *Nature*, 1990, **347**, 402.
46. J. W. Pflugrath and F. A. Quiocho, *Nature*, 1985, **314**, 257.
47. Philip A. Gale, Ethan N. W. Howe and X. Wu, *Chem*, 2016, **1**, 351-422.
48. N. H. Evans and P. D. Beer, *Angew. Chem. Int. Ed*, 2014, **53**, 11716-11754.
49. E. Graf and J. M. Lehn, *J. Am. Chem. Soc.*, 1976, **98**, 6403-6405.
50. B. Dietrich, T. M. Fyles, J.-M. Lehn, L. G. Pease and D. L. Fyles, *J. Chem. Soc., Chem. Commun.*, 1978, 934-936.
51. K. H. Y. and S. Carsten, *Chem. Eur. J*, 2011, **17**, 5311-5318.
52. N. Ahmed, B. Shirinfar, I. Geronimo and K. S. Kim, *Org. Lett.*, 2011, **13**, 5476-5479.
53. N. G. White and P. D. Beer, *Chem. Commun.*, 2012, **48**, 8499-8501.
54. H. Zhou, Y. Zhao, G. Gao, S. Li, J. Lan and J. You, *J. Am. Chem. Soc.*, 2013, **135**, 14908-14911.
55. Y. Hua and A. H. Flood, *Chem. Soc. Rev.*, 2010, **39**, 1262-1271.
56. J. Cai, B. P. Hay, N. J. Young, X. Yang and J. L. Sessler, *Chem. Sci.*, 2013, **4**, 1560-1567.
57. R. A. Pascal, J. Spergel and D. Van Engen, *Tetrahedron Lett.*, 1986, **27**, 4099-4102.
58. K. Kavallieratos, S. R. de Gala, D. J. Austin and R. H. Crabtree, *J. Am. Chem. Soc.*, 1997, **119**, 2325-2326.
59. K. Kavallieratos, C. M. Bertao and R. H. Crabtree, *J. Org. Chem*, 1999, **64**, 1675-1683.
60. P. A. Gale, J. L. Sessler, V. Král and V. Lynch, *J. Am. Chem. Soc.*, 1996, **118**, 5140-5141.
61. P. Anzenbacher, K. Jursíková and J. L. Sessler, *J. Am. Chem. Soc.*, 2000, **122**, 9350-9351.
62. P. Anzenbacher, A. C. Try, H. Miyaji, K. Jursíková, V. M. Lynch, M. Marquez and J. L. Sessler, *J. Am. Chem. Soc.*, 2000, **122**, 10268-10272.
63. K. P. McDonald, R. O. Ramabhadran, S. Lee, K. Raghavachari and A. H. Flood, *Org. Lett.*, 2011, **13**, 6260-6263.
64. S. Lee, Y. Hua, H. Park and A. H. Flood, *Org. Lett.*, 2010, **12**, 2100-2102.
65. S. Kubik, R. Kirchner, D. Nolting and J. Seidel, *J. Am. Chem. Soc.*, 2002, **124**, 12752-12760.
66. F. Sommer and S. Kubik, *Org. Biomol. Chem.*, 2014, **12**, 8851-8860.
67. Y. Hua, Y. Liu, C.-H. Chen and A. H. Flood, *J. Am. Chem. Soc.*, 2013, **135**, 14401-14412.
68. M. A. Yawer, V. Havel and V. Sindelar, *Angew. Chem. Int. Ed*, 2015, **54**, 276-279.
69. P. A. Gale, *Coord. Chem. Rev.*, 2003, **240**, 191-221.
70. P. D. Beer and E. J. Hayes, *Coord. Chem. Rev.*, 2003, **240**, 167-189.
71. J. Comarmond, P. Plumere, J. M. Lehn, Y. Agnus, R. Louis, R. Weiss, O. Kahn and I. Morgenstern-Badarau, *J. Am. Chem. Soc.*, 1982, **104**, 6330-6340.

72. A. Brugnara, F. Topic, K. Rissanen, A. d. l. Lande, B. Colasson and O. Reinaud, *Chem. Sci.*, 2014, **5**, 3897-3904.
73. K. K. Y. Yuen and K. A. Jolliffe, *Chem. Commun.*, 2013, **49**, 4824-4826.
74. S. Scheiner, *Molecules*, 2018, **23**, 1147.
75. H. Masato and G. F. P., *Angew. Chem. Int. Ed*, 2015, **54**, 1205-1209.
76. S. J. Butler and D. Parker, *Chem. Soc. Rev.*, 2013, **42**, 1652-1666.
77. B. S. J., M. B. K., P. Robert, P. David and W. J. W., *Chem. Eur. J*, 2013, **19**, 9511-9517.
78. C. L. D. Gibb and B. C. Gibb, *J. Am. Chem. Soc.*, 2011, **133**, 7344-7347.
79. R. S. Carnegie, C. L. D. Gibb and B. C. Gibb, *Angew. Chem. Int. Ed*, 2014, **53**, 11498-11500.
80. P. Sokkalingam, J. Shraberg, S. W. Rick and B. C. Gibb, *J. Am. Chem. Soc.*, 2016, **138**, 48-51.
81. A. Brown and P. D. Beer, *Chem. Commun.*, 2016, **52**, 8645-8658.
82. A. Mele, P. Metrangolo, H. Neukirch, T. Pilati and G. Resnati, *J. Am. Chem. Soc.*, 2005, **127**, 14972-14973.
83. M. G. Sarwar, B. Dragisic, S. Sagoo and M. S. Taylor, *Angew. Chem. Int. Ed*, 2010, **49**, 1674-1677.
84. E. Dimitrijevic, O. Kvak and M. S. Taylor, *Chem. Commun.*, 2010, **46**, 9025-9027.
85. S. M. G., D. Bojan, D. Elena and T. M. S., *Chem. Eur. J*, 2013, **19**, 2050-2058.
86. M. Cametti, K. Raatikainen, P. Metrangolo, T. Pilati, G. Terraneo and G. Resnati, *Org. Biomol. Chem.*, 2012, **10**, 1329-1333.
87. A. Caballero, N. G. White and P. D. Beer, *CrystEngComm*, 2014, **16**, 3694-3698.
88. F. Zapata, A. Caballero, N. G. White, T. D. W. Claridge, P. J. Costa, V. Félix and P. D. Beer, *J. Am. Chem. Soc.*, 2012, **134**, 11533-11541.
89. C. Antonio, W. N. G. and B. P. D., *Angew. Chem. Int. Ed*, 2011, **50**, 1845-1848.
90. R. Tepper, B. Schulze, H. Görls, P. Bellstedt, M. Jäger and U. S. Schubert, *Org. Lett.*, 2015, **17**, 5740-5743.
91. T. K. Mole, W. E. Arter, I. Marques, V. Félix and P. D. Beer, *J. Organomet. Chem.*, 2015, **792**, 206-210.
92. J. Y. C. Lim and P. D. Beer, *Chem. Commun.*, 2015, **51**, 3686-3688.
93. F. Zapata, A. Caballero, P. Molina, I. Alkorta and J. Elguero, *J. Org. Chem*, 2014, **79**, 6959-6969.
94. G. E. Garrett, G. L. Gibson, R. N. Straus, D. S. Seferos and M. S. Taylor, *J. Am. Chem. Soc.*, 2015, **137**, 4126-4133.
95. J. Y. C. Lim, I. Marques, A. L. Thompson, K. E. Christensen, V. Félix and P. D. Beer, *J. Am. Chem. Soc.*, 2017, **139**, 3122-3133.
96. M. Hidekazu, S. Wataru and S. J. L., *Angew. Chem. Int. Ed*, 2000, **39**, 1777-1780.
97. B.-x. Shen, Y. Qian, Z.-q. Qi, C.-g. Lu, Q. Sun, X. Xia and Y. Cui, *J. Mater. Chem. B*, 2017, **5**, 5854-5861.
98. N. K. A., B. Steffen and J. J. O., *Chem. Eur. J*, 2011, **17**, 11001-11007.
99. A. J. McConnell and P. D. Beer, *Angew. Chem. Int. Ed*, 2012, **51**, 5052-5061.
100. S. K. Kim and J. L. Sessler, *Chem. Soc. Rev.*, 2010, **39**, 3784-3809.
101. Y. Agnus, R. Louis, J. P. Gisselbrecht and R. Weiss, *J. Am. Chem. Soc.*, 1984, **106**, 93-102.
102. S. O. Kang, J. M. Llinares, V. W. Day and K. Bowman-James, *Chem. Soc. Rev.*, 2010, **39**, 3980-4003.
103. D. Chen and A. E. Martell, *Tetrahedron*, 1991, **47**, 6895-6902.
104. S. Jurgen, v. D. J. P. M., E. J. F. J. and R. D. N., *Angew. Chem. Int. Ed*, 1996, **35**, 1090-1093.
105. B. Akhuli and P. Ghosh, *Chem. Commun.*, 2015, **51**, 16514-16517.

106. K. Maity, D. K. Panda, R. J. Gallup, C. K. Choudhury and S. Saha, *Org. Lett.*, 2018, **20**, 962-965.
107. A. Arduini, E. Brindani, G. Giorgi, A. Pochini and A. Secchi, *J. Org. Chem*, 2002, **67**, 6188-6194.
108. A. Arduini, G. Giorgi, A. Pochini, A. Secchi and F. Ugozzoli, *J. Org. Chem*, 2001, **66**, 8302-8308.
109. A. Lledó and A. Soler, *Org. Chem. Front*, 2017, **4**, 1244-1249.
110. M. J. Deetz, M. Shang and B. D. Smith, *J. Am. Chem. Soc.*, 2000, **122**, 6201-6207.
111. J. M. Mahoney, A. M. Beatty and B. D. Smith, *J. Am. Chem. Soc.*, 2001, **123**, 5847-5848.
112. C. Suksai, P. Leeladee, D. Jainuknan, T. Tuntulani, N. Muangsin, O. Chailapakul, P. Kongsaeree and C. Pakavatchai, *Tetrahedron Lett.*, 2005, **46**, 2765-2769.
113. M. D. Lankshear, A. R. Cowley and P. D. Beer, *Chem. Commun.*, 2006, 612-614.
114. L. M. D., D. I. M., C. Kar-Man, C. A. R., S. S. M., F. Vitor and B. P. D., *Chem. Eur. J*, 2008, **14**, 2248-2263.
115. M. D. Lankshear, I. M. Dudley, K.-M. Chan and P. D. Beer, *New J. Chem.*, 2007, **31**, 684-690.
116. A. J. McConnell, C. J. Serpell and P. D. Beer, *New J. Chem.*, 2012, **36**, 102-112.
117. R. S. Kumar, H. Alexandre, V. Mahesh, B. Céline and L. Jérôme, *Chem. Eur. J*, 2018, **24**, 2944-2951.
118. J. Hu, L. Chen, J. Shen, J. Luo, P. Deng, Y. Ren, H. Zeng, W. Feng and L. Yuan, *Chem. Commun.*, 2014, **50**, 8024-8027.
119. S. Shi, Y. Zhu, X. Li, X. Yuan, T. Ma, W.-L. Yuan, G.-H. Tao, W. Feng and L. Yuan, *RSC. Adv.*, 2016, **6**, 39839-39845.
120. A. Galan, D. Andreu, A. M. Echavarren, P. Prados and J. De Mendoza, *J. Am. Chem. Soc.*, 1992, **114**, 1511-1512.
121. S. Moerkerke, J. Wouters and I. Jabin, *J. Org. Chem*, 2015, **80**, 8720-8726.
122. E. Brunetti, S. Moerkerke, J. Wouters, K. Bartik and I. Jabin, *Org. Biomol. Chem.*, 2016, **14**, 10201-10207.
123. D. J. White, N. Laing, H. Miller, S. Parsons, P. A. Tasker and S. Coles, *Chem. Commun.*, 1999, 2077-2078.
124. I. Carreira-Barral, M. Mato-Iglesias, A. de Blas, C. Platas-Iglesias, P. A. Tasker and D. Esteban-Gómez, *Dalton Trans.*, 2017, **46**, 3192-3206.
125. H. Qing, P. G. Marie, L. V. M. and S. J. L., *Angew. Chem. Int. Ed*, 2017, **56**, 13396-13400.
126. H. Qing, W. N. J., O. J. Hyun, L. V. M., K. S. Kuk, M. B. A. and S. J. L., *Angew. Chem. Int. Ed*, **57**, 11924-11928.
127. J. M. Mahoney, G. U. Nawaratna, A. M. Beatty, P. J. Duggan and B. D. Smith, *Inorg. Chem.*, 2004, **43**, 5902-5907.
128. M. G. Fisher, P. A. Gale, J. R. Hiscock, M. B. Hursthouse, M. E. Light, F. P. Schmidtchen and C. C. Tong, *Chem. Commun.*, 2009, 3017-3019.
129. J. H. Lee, J. H. Lee, Y. R. Choi, P. Kang, M.-G. Choi and K.-S. Jeong, *J. Org. Chem*, 2014, **79**, 6403-6409.
130. J. F. S. Carson J. Bruns, *The Nature of the Mechanical Bond: From Molecules to Machines*, John Wiley & Sons, Hoboken, NJ, 2017.
131. J. F. Nierengarten, C. O. Dietrich-Buchecker and J. P. Sauvage, *J. Am. Chem. Soc.*, 1994, **116**, 375-376.
132. K. S. Chichak, S. J. Cantrill, A. R. Pease, S.-H. Chiu, G. W. V. Cave, J. L. Atwood and J. F. Stoddart, *Science*, 2004, **304**, 1308-1312.
133. J. S. Siegel, *Science*, 2004, **304**, 1256-1258.

134. C. D. Pentecost, K. S. Chichak, A. J. Peters, G. W. V. Cave, S. J. Cantrill and J. F. Stoddart, *Angew. Chem. Int. Ed*, 2007, **46**, 218-222.
135. I. T. Harrison and S. Harrison, *J. Am. Chem. Soc.*, 1967, **89**, 5723-5724.
136. C.-W. Chiu, C.-C. Lai and S.-H. Chiu, *J. Am. Chem. Soc.*, 2007, **129**, 3500-3501.
137. K. Jia-Ling, U. Shau-Hua, C. Ching-Wei, L. Chien-Chen, L. Yi-Hung, P. Shie-Ming and C. Sheng-Hsien, *Chem. Eur. J*, 2010, **16**, 6950-6960.
138. I. Yoon, M. Narita, T. Shimizu and M. Asakawa, *J. Am. Chem. Soc.*, 2004, **126**, 16740-16741.
139. I. T. Harrison, *J. Chem. Soc., Chem. Commun.*, 1972, 231-232.
140. B. E. Fletcher, M. J. G. Peach and N. H. Evans, *Org. Biomol. Chem.*, 2017, **15**, 2797-2803.
141. E. Wasserman, *J. Am. Chem. Soc.*, 1960, **82**, 4433-4434.
142. C. O. Dietrich-Buchecker, J. P. Sauvage and J. P. Kintzinger, *Tetrahedron Lett.*, 1983, **24**, 5095-5098.
143. J. P. Sauvage and M. Ward, *Inorg. Chem.*, 1991, **30**, 3869-3874.
144. S. M. Goldup, D. A. Leigh, P. J. Lusby, R. T. McBurney and A. M. Z. Slawin, *Angew. Chem. Int. Ed*, 2008, **47**, 6999-7003.
145. A. J. Blake, C. O. Dietrich-Buchecker, T. I. Hyde, J.-P. Sauvage and M. Schroder, *J. Chem. Soc., Chem. Commun.*, 1989, 1663-1665.
146. C. Hamann, J. M. Kern and J. P. Sauvage, *Dalton Trans.*, 2003, 3770-3775.
147. C. Hamann, J.-M. Kern and J.-P. Sauvage, *Inorg. Chem.*, 2003, **42**, 1877-1883.
148. T. Shun-Te, L. Chien-Chen, L. Yi-Hung, P. Shie-Ming and C. Sheng-Hsien, *Angew. Chem. Int. Ed*, 2013, **52**, 13269-13272.
149. Y.-W. Wu, P.-N. Chen, C.-F. Chang, C.-C. Lai and S.-H. Chiu, *Org. Lett.*, 2015, **17**, 2158-2161.
150. F. Zapata, O. A. Blackburn, M. J. Langton, S. Faulkner and P. D. Beer, *Chem. Commun.*, 2013, **49**, 8157-8159.
151. V. Aucagne, J. Berná, J. D. Crowley, S. M. Goldup, K. D. Hänni, D. A. Leigh, P. J. Lusby, V. E. Ronaldson, A. M. Z. Slawin, A. Viterisi and D. B. Walker, *J. Am. Chem. Soc.*, 2007, **129**, 11950-11963.
152. L. Hicham, J. Kajally, W. Michael and G. S. M., *Angew. Chem. Int. Ed*, 2011, **50**, 4151-4155.
153. Q.-F. Luo, L. Zhu, S.-J. Rao, H. Li, Q. Miao and D.-H. Qu, *J. Org. Chem*, 2015, **80**, 4704-4709.
154. S. J. Loeb and J. A. Wisner, *Chem. Commun.*, 1998, 2757-2758.
155. S. J. Loeb and J. A. Wisner, *Chem. Commun.*, 2000, 845-846.
156. J. Tiburcio, G. J. E. Davidson and S. J. Loeb, *Chem. Commun.*, 2002, 1282-1283.
157. K. Zhu, V. N. Vukotic, N. Noujeim and S. J. Loeb, *Chem. Sci.*, 2012, **3**, 3265-3271.
158. D. B. Amabilino, P. R. Ashton, A. S. Reder, N. Spencer and J. F. Stoddart, *Angew. Chem. Int. Ed*, 1994, **33**, 1286-1290.
159. C. A. Hunter, *J. Am. Chem. Soc.*, 1992, **114**, 5303-5311.
160. F. Vögtle, S. Meier and R. Hoss, *Angew. Chem. Int. Ed*, 1992, **31**, 1619-1622.
161. A. G. Johnston, D. A. Leigh, R. J. Pritchard and M. D. Deegan, *Angew. Chem. Int. Ed*, 1995, **34**, 1209-1212.
162. A. G. Johnston, D. A. Leigh, L. Nezhat, J. P. Smart and M. D. Deegan, *Angew. Chem. Int. Ed*, 1995, **34**, 1212-1216.
163. A. G. Johnston, D. A. Leigh, A. Murphy, J. P. Smart and M. D. Deegan, *J. Am. Chem. Soc.*, 1996, **118**, 10662-10663.
164. J.-J. Lee, A. G. White, J. M. Baumes and B. D. Smith, *Chem. Commun.*, 2010, **46**, 1068-1069.

165. T. S. Jarvis, C. G. Collins, J. M. Dempsey, A. G. Oliver and B. D. Smith, *J. Org. Chem*, 2017, **82**, 5819-5825.
166. E. Arunkumar, C. C. Forbes, B. C. Noll and B. D. Smith, *J. Am. Chem. Soc.*, 2005, **127**, 3288-3289.
167. D. G. Hamilton, J. K. M. Sanders, J. E. Davies, W. Clegg and S. J. Teat, *Chem. Commun.*, 1997, 897-898.
168. H. Ogino, *J. Am. Chem. Soc.*, 1981, **103**, 1303-1304.
169. F. M. J. and A. H. L., *Angew. Chem. Int. Ed*, 2007, **46**, 1028-1064.
170. H. G. M., G. Jens, S. Christian and V. Fritz, *Angew. Chem. Int. Ed*, 1999, **38**, 383-386.
171. S. Lee, C.-H. Chen and A. H. Flood, *Nat.Chem.*, 2013, **5**, 704.
172. W. J. A., B. P. D. and D. M. G. B., *Angew. Chem. Int. Ed*, 2001, **40**, 3606-3609.
173. J. A. Wisner, P. D. Beer, N. G. Berry and B. Tomapatanaget, *Proc. Natl. Acad. Sci*, 2002, **99**, 4983-4986.
174. J. A. Wisner, P. D. Beer, M. G. B. Drew and M. R. Sambrook, *J. Am. Chem. Soc.*, 2002, **124**, 12469-12476.
175. N. H. Evans, C. J. Serpell and P. D. Beer, *Angew. Chem. Int. Ed*, 2011, **50**, 2507-2510.
176. N. H. Evans and P. D. Beer, *Chem. Eur. J*, 2011, **17**, 10542-10546.
177. T. A. Barendt, A. Docker, I. Marques, V. Félix and P. D. Beer, *Angew. Chem. Int. Ed*, 2016, **55**, 11069-11076.
178. L. M. Hancock, L. C. Gilday, S. Carvalho, P. J. Costa, V. Félix, C. J. Serpell, N. L. Kilah and P. D. Beer, *Chem. Eur. J*, 2010, **16**, 13082-13094.
179. L. M. Hancock, E. Marchi, P. Ceroni and P. D. Beer, *Chem. Eur. J*, 2012, **18**, 11277-11283.
180. M. J. Langton and P. D. Beer, *Chem. Commun.*, 2014, **50**, 8124-8127.
181. B. Huang, S. M. Santos, V. Felix and P. D. Beer, *Chem. Commun.*, 2008, 4610-4612.
182. Y. Li, K. M. Mullen, T. D. W. Claridge, P. J. Costa, V. Felix and P. D. Beer, *Chem. Commun.*, 2009, 7134-7136.
183. N. Weber, C. Hamann, J.-M. Kern and J.-P. Sauvage, *Inorg. Chem.*, 2003, **42**, 6780-6792.
184. J. D. Badjić, V. Balzani, A. Credi, S. Silvi and J. F. Stoddart, *Science*, 2004, **303**, 1845-1849.
185. S. S. Zhu, P. J. Carroll and T. M. Swager, *J. Am. Chem. Soc.*, 1996, **118**, 8713-8714.
186. M. J. MacLachlan, A. Rose and T. M. Swager, *J. Am. Chem. Soc.*, 2001, **123**, 9180-9181.
187. V. Balzani, M. Clemente-León, A. Credi, J. N. Lowe, J. D. Badjić, J. F. Stoddart and D. J. Williams, *Chem. Eur. J*, 2003, **9**, 5348-5360.
188. J. Lehr, T. Lang, O. A. Blackburn, T. A. Barendt, S. Faulkner, J. J. Davis and P. D. Beer, *Chem. Eur. J*, 2013, **19**, 15898-15906.
189. V. Blanco, D. A. Leigh, V. Marcos, J. A. Morales-Serna and A. L. Nussbaumer, *J. Am. Chem. Soc.*, 2014, **136**, 4905-4908.
190. G. Marzia, L. J. E. M. and G. S. M., *Angew. Chem. Int. Ed*, 2015, **54**, 13545-13549.
191. X. Bao, I. Isaacsohn, A. F. Drew and D. B. Smithrud, *J. Am. Chem. Soc.*, 2006, **128**, 12229-12238.
192. X. Bao, I. Isaacsohn, A. F. Drew and D. B. Smithrud, *J. Org. Chem*, 2007, **72**, 3988-4000.
193. F. Anthony, V. Aurélien, C. Frédéric, P. Stéphanie, L. D. A., A. Vincent and P. Sébastien, *Angew. Chem. Int. Ed*, 2009, **48**, 6443-6447.
194. A. Fernandes, A. Viterisi, V. Aucagne, D. A. Leigh and S. Papot, *Chem. Commun.*, 2012, **48**, 2083-2085.
195. R. Shukla, T. Kida and B. D. Smith, *Org. Lett.*, 2000, **2**, 3099-3102.
196. H. C. A. and A. H. L., *Angew. Chem. Int. Ed*, 2009, **48**, 7488-7499.

197. B. Qiao, A. Sengupta, Y. Liu, K. P. McDonald, M. Pink, J. R. Anderson, K. Raghavachari and A. H. Flood, *J. Am. Chem. Soc.*, 2015, **137**, 9746-9757.
198. A. J. Evans and P. D. Beer, *Dalton Trans.*, 2003, DOI: 10.1039/B308541D, 4451-4456.
199. E. N. W. Howe, M. Bhadbhade and P. Thordarson, *J. Am. Chem. Soc.*, 2014, **136**, 7505-7516.
200. S. S. Flack, J.-L. Chaumette, J. D. Kilburn, G. J. Langley and M. Webster, *J. Chem. Soc., Chem. Commun.*, 1993, 399-401.
201. L. H. Uppadine, J. E. Redman, S. W. Dent, M. G. B. Drew and P. D. Beer, *Inorg. Chem.*, 2001, **40**, 2860-2869.
202. G. Tumcharern, T. Tuntulani, S. J. Coles, M. B. Hursthouse and J. D. Kilburn, *Org. Lett.*, 2003, **5**, 4971-4974.
203. D. M. Rudkevich, J. D. Mercer-Chalmers, W. Verboom, R. Ungaro, F. de Jong and D. N. Reinhoudt, *J. Am. Chem. Soc.*, 1995, **117**, 6124-6125.
204. L. A. J. Chrisstoffels, F. de Jong, D. N. Reinhoudt, S. Sivelli, L. Gazzola, A. Casnati and R. Ungaro, *J. Am. Chem. Soc.*, 1999, **121**, 10142-10151.
205. C. Gargiulli, G. Gattuso, C. Liotta, A. Notti, M. F. Parisi, I. Pisagatti and S. Pappalardo, *J. Org. Chem*, 2009, **74**, 4350-4353.
206. T. Tozawa, Y. Misawa, S. Tokita and Y. Kubo, *Tetrahedron Lett.*, 2000, **41**, 5219-5223.
207. M. P. Wintergerst, T. G. Levitskaia, B. A. Moyer, J. L. Sessler and L. H. Delmau, *J. Am. Chem. Soc.*, 2008, **130**, 4129-4139.
208. J. L. Sessler, S. K. Kim, D. E. Gross, C.-H. Lee, J. S. Kim and V. M. Lynch, *J. Am. Chem. Soc.*, 2008, **130**, 13162-13166.
209. R. Tepper, B. Schulze, P. Bellstedt, J. Heidler, H. Gorls, M. Jager and U. S. Schubert, *Chem. Commun.*, 2017, **53**, 2260-2263.
210. S. W. Robinson, C. L. Mustoe, N. G. White, A. Brown, A. L. Thompson, P. Kennepohl and P. D. Beer, *J. Am. Chem. Soc.*, 2014.
211. J.-S. Yang, C.-Y. Hwang and M.-Y. Chen, *Tetrahedron Lett.*, 2007, **48**, 3097-3102.
212. J. C. Tripp, L. B. Krasnova, K. B. Sharpless and V. V. Fokin, *Angew. Chem. Int. Ed*, 2009, **48**, 8018-8021.
213. B. T. Worrell, J. E. Hein and V. V. Fokin, *Angew. Chem. Int. Ed*, 2012, **51**, 11791-11794.
214. N. A. Semenov, A. V. Lonchakov, N. A. Pushkarevsky, E. A. Suturina, V. V. Korolev, E. Lork, V. G. Vasiliev, S. N. Konchenko, J. Beckmann, N. P. Gritsan and A. V. Zibarev, *Organometallics*, 2014, **33**, 4302-4314.
215. P. D. Beer, P. K. Hopkins and J. D. McKinney, *Chem. Commun.*, 1999, 1253-1254.
216. K. P. McDonald, B. Qiao, E. B. Twum, S. Lee, P. J. Gamache, C.-H. Chen, Y. Yi and A. H. Flood, *Chem. Commun.*, 2014, **50**, 13285-13288.
217. S.-J. Rao, Q. Zhang, J. Mei, X.-H. Ye, C. Gao, Q.-C. Wang, D.-H. Qu and H. Tian, *Chem. Sci.*, 2017, **8**, 6777-6783.
218. H. V. Schroder, S. Sobottka, H. Hupatz, M. Gaedke, B. Sarkar and C. A. Schalley, *Chem. Sci.*, 2017, **8**, 6300-6306.
219. G. Gholami, K. Zhu, G. Baggi, E. Schott, X. Zarate and S. J. Loeb, *Chem. Sci.*, 2017, **8**, 7718-7723.
220. K. M. Tomczyk, M. Wozny, S. Domagala, A. Wickowska, J. Pawlowska, K. Wozniak and B. Korybut-Daszkiewicz, *New J. Chem.*, 2017, **41**, 6004-6013.
221. H. Iwamoto, W. Takizawa, K. Itoh, T. Hagiwara, E. Tayama, E. Hasegawa and T. Haino, *J. Org. Chem*, 2013, **78**, 5205-5217.
222. H. Iwamoto, S. Tafuku, Y. Sato, W. Takizawa, W. Katagiri, E. Tayama, E. Hasegawa, Y. Fukazawa and T. Haino, *Chem. Commun.*, 2016, **52**, 319-322.
223. P. R. Aston, P. T. Glink, J. F. Stoddart, P. A. Tasker, A. J. P. White and D. J. Williams, *Chem. Eur. J*, 1996, **2**, 729-736.

224. X. Wang, V. Ervithayasuporn, Y. Zhang and Y. Kawakami, *Chem. Commun.*, 2011, **47**, 1282-1284.
225. H. R. Wessels and H. W. Gibson, *Tetrahedron*, 2016, **72**, 396-399.
226. G. C. Vougioukalakis and R. H. Grubbs, *Chem. Rev.*, 2010, **110**, 1746-1787.
227. S. H. Hong, A. G. Wenzel, T. T. Salguero, M. W. Day and R. H. Grubbs, *J. Am. Chem. Soc.*, 2007, **129**, 7961-7968.
228. S. T. Nguyen, L. K. Johnson, R. H. Grubbs and J. W. Ziller, *J. Am. Chem. Soc.*, 1992, **114**, 3974-3975.
229. J. E. M. Lewis, M. Galli and S. M. Goldup, *Chem. Commun.*, 2017, **53**, 298-312.
230. M. J. Langton and P. D. Beer, *Acc. Chem. Res.*, 2014, **47**, 1935-1949.
231. M. C. Jimenez-Molero, C. Dietrich-Buchecker and J.-P. Sauvage, *Chem. Commun.*, 2003, 1613-1616.
232. M. C. Jiménez, C. Dietrich-Buchecker and J. P. Sauvage, *Angew. Chem. Int. Ed*, 2000, **39**, 3284-3287.
233. J. A. Bravo, F. M. Raymo, J. F. Stoddart, A. J. P. White and D. J. Williams, *Eur. J. Org. Chem.*, 1998, **11**, 2565-2571.
234. P. T. Glink, A. I. Oliva, J. F. Stoddart, A. J. P. White and D. J. Williams, *Angew. Chem. Int. Ed*, 2001, **40**, 1870-1875.
235. W. Clegg, C. Gimenez-Saiz, D. A. Leigh, A. Murphy, A. M. Z. Slawin and S. J. Teat, *J. Am. Chem. Soc.*, 1999, **121**, 4124-4129.
236. D. G. Hamilton, L. Prodi, N. Feeder and J. K. M. Sanders, *J. Chem. Soc., Perkin Trans. 1*, 1999, **8**, 1057-1066.
237. D. G. Hamilton, N. Feeder, L. Prodi, S. J. Teat, W. Clegg and J. K. M. Sanders, *J. Am. Chem. Soc.*, 1998, **120**, 1096-1097.
238. M. R. Sambrook, P. D. Beer, J. A. Wisner, R. L. Paul and A. R. Cowley, *J. Am. Chem. Soc.*, 2004, **126**, 15364-15365.
239. G. T. Spence and P. D. Beer, *Acc. Chem. Res.*, 2013, **46**, 571-586.
240. B. Mohr, J. P. Sauvage, R. H. Grubbs and M. Weck, *Angew. Chem. Int. Ed*, 1997, **36**, 1308-1310.
241. M. Weck, B. Mohr, J.-P. Sauvage and R. H. Grubbs, *J. Org. Chem*, 1999, **64**, 5463-5471.
242. J. E. M. Lewis, J. Winn, L. Cera and S. M. Goldup, *J. Am. Chem. Soc.*, 2016, **138**, 16329-16336.
243. J. E. M. Lewis, F. Modicom and S. M. Goldup, *J. Am. Chem. Soc.*, 2018, **140**, 4787-4791.
244. O. Š. Miljanić and J. F. Stoddart, *Proc. Natl. Acad. Sci*, 2007, **104**, 12966-12970.
245. S. Li, M. Liu, J. Zhang, B. Zheng, C. Zhang, X. Wen, N. Li and F. Huang, *Org. Biomol. Chem.*, 2008, **6**, 2103-2107.
246. F. G. Gatti, D. A. Leigh, S. A. Nepogodiev, A. M. Z. Slawin, S. J. Teat and J. K. Y. Wong, *J. Am. Chem. Soc.*, 2001, **123**, 5983-5989.
247. G. Cavallo, P. Metrangolo, R. Milani, T. Pilati, A. Priimagi, G. Resnati and G. Terraneo, *Chem. Rev.*, 2016, **116**, 2478-2601.
248. N. L. Kilah, M. D. Wise, C. J. Serpell, A. L. Thompson, N. G. White, K. E. Christensen and P. D. Beer, *J. Am. Chem. Soc.*, 2010, **132**, 11893-11895.
249. M. J. Langton, S. W. Robinson, I. Marques, V. Félix and P. D. Beer, *Nat.Chem.*, 2014, **6**, 1039-1043.
250. D. Dou, G. He, Y. Li, Z. Lai, L. Wei, K. R. Alliston, G. H. Lushington, D. M. Eichhorn and W. C. Groutas, *Bioorg. Med. Chem.*, 2010, **18**, 1093-1102.
251. Z. H. Mohamed, N. A. El-Koussi, N. M. Mahfouz, A. F. Youssef, G. A. Abdel Jaleel and S. A. Shouman, *Eur. J. Med. Chem.*, 2015, **97**, 75-82.
252. J. F. W. Keana and S. X. Cai, *J. Org. Chem*, 1990, **55**, 3640-3647.
253. M. J. Hynes, *J. Chem. Soc., Dalton Trans.*, 1993, 311-312.

254. S. W. Robinson, C. L. Mustoe, N. G. White, A. Brown, A. L. Thompson, P. Kennepohl and P. D. Beer, *J. Am. Chem. Soc.*, 2015, **137**, 499-507.
255. A. Bondi, *J. Phys. Chem.*, 1964, **68**, 441-451.
256. A. M. Reeve and C. A. Townsend, *Tetrahedron*, 1998, **54**, 15959-15974.
257. A. B. Smith, K. Sugasawa, O. Atasoylu, C.-P. H. Yang and S. B. Horwitz, *J. Med. Chem.*, 2011, **54**, 6319-6327.
258. M. J. Langton, I. Marques, S. W. Robinson, V. Félix and P. D. Beer, *Chem. Eur. J*, 2016, **22**, 185-192.
259. C. L. D. Gibb, E. E. Oertling, S. Velaga and B. C. Gibb, *J. Phys. Chem. B*, 2015, **119**, 5624-5638.
260. F. Hofmeister, *Arch. Exp. Pathol. Pharmacol*, 1888, **24**, 247-260.
261. S. W. Robinson and P. D. Beer, *Org. Biomol. Chem.*, 2017, **15**, 153-159.
262. S. P. Cornes, M. R. Sambrook and P. D. Beer, *Chem. Commun.*, 2017, **53**, 3866-3869.
263. J. Y. C. Lim, T. Bunchuay and P. D. Beer, *Chem. Eur. J*, 2017, **23**, 4700-4707.
264. M. J. Langton, S. W. Robinson, I. Marques, V. Félix and P. D. Beer, *Nature Chemistry*, 2014, **6**, 1039.
265. M. J. Langton, I. Marques, S. W. Robinson, V. Félix and P. D. Beer, 2016, **22**, 185-192.
266. J. L. Cook, C. A. Hunter, C. M. R. Low, A. Perez-Velasco and J. G. Vinter, 2008, **47**, 6275-6277.
267. D. J. Stufkens and A. Vlček, *Coord. Chem. Rev.*, 1998, **177**, 127-179.
268. A. Juris, V. Balzani, F. Barigelletti, S. Campagna, P. Belser and A. von Zelewsky, *Coord. Chem. Rev.*, 1988, **84**, 85-277.
269. V. Fernández-Moreira, F. L. Thorp-Greenwood and M. P. Coogan, *Chem. Commun.*, 2010, **46**, 186-202.
270. K. K.-W. Lo, W.-K. Hui, C.-K. Chung, K. H.-K. Tsang, D. C.-M. Ng, N. Zhu and K.-K. Cheung, *Coord. Chem. Rev.*, 2005, **249**, 1434-1450.
271. S. Mardanya, S. Karmakar, D. Mondal and S. Baitalik, *Inorg. Chem.*, 2016, **55**, 3475-3489.
272. C. Bhaumik, S. Das, D. Maity and S. Baitalik, *Dalton Trans.*, 2012, **41**, 2427-2438.
273. C. Bhaumik, D. Maity, S. Das and S. Baitalik, *Polyhedron*, 2013, **52**, 890-899.
274. A. Das, H. Agarwala, T. Kundu, P. Ghosh, S. Mondal, S. M. Mobin and G. K. Lahiri, *Dalton Trans.*, 2014, **43**, 13932-13947.
275. A. Das, P. Mondal, M. Dasgupta, N. Kishore and G. K. Lahiri, *Dalton Trans.*, 2016, **45**, 2605-2617.
276. A. M. Hyde, S. L. Zultanski, J. H. Waldman, Y.-L. Zhong, M. Shevlin and F. Peng, *Org. Process Res. Dev.*, 2017, **21**, 1355-1370.
277. P. D. Beer, S. W. Dent, G. S. Hobbs and T. J. Wear, *Chem. Commun.*, 1997, 99-100.
278. J. Lehr, T. Lang, O. A. Blackburn, T. A. Barendt, S. Faulkner, J. J. Davis and P. D. Beer, 2013, **19**, 15898-15906.
279. S. M. Walter, F. Kniep, L. Rout, F. P. Schmidtchen, E. Herdtweck and S. M. Huber, *J. Am. Chem. Soc.*, 2012, **134**, 8507-8512.
280. R. Tepper, B. Schulze, M. Jäger, C. Friebe, D. H. Scharf, H. Görls and U. S. Schubert, *J. Org. Chem*, 2015, **80**, 3139-3150.
281. B. R. Mullaney, B. E. Partridge and P. D. Beer, *Chem. Eur. J*, 2015, **21**, 1660-1665.
282. M. J. Langton and P. D. Beer, *Chem. Eur. J*, 2012, **18**, 14406-14412.
283. B. R. Mullaney, A. L. Thompson and P. D. Beer, *Angew. Chem. Int. Ed*, 2014, **53**, 11458-11462.
284. M. J. Langton, Y. Xiong and P. D. Beer, *Chem. Eur. J*, 2015, **21**, 18910-18914.
285. X. Li, J. Y. C. Lim and P. D. Beer, *Faraday Discuss.*, 2017, **203**, 245-255.

286. F. Kloss, U. Köhn, B. O. Jahn, M. D. Hager, H. Görls and U. S. Schubert, *Chem. Asian. J.*, 2011, **6**, 2816-2824.
287. S. K. Rastogi, R. A. Rogers, J. Shi, C. T. Brown, C. Salinas, K. M. Martin, J. Armitage, C. Dorsey, G. Chun, P. Rinaldi and W. J. Brittain, *Magn. Reson. Chem.*, 2016, **54**, 126-131.
288. F. B. Mallory, C. W. Mallory, K. E. Butler, M. B. Lewis, A. Q. Xia, E. D. Luzik, L. E. Fredenburgh, M. M. Ramanjulu, Q. N. Van, M. M. Francl, D. A. Freed, C. C. Wray, C. Hann, M. Nerz-Stormes, P. J. Carroll and L. E. Chirlian, *J. Am. Chem. Soc.*, 2000, **122**, 4108-4116.
289. D. Burgess, M. Finn, D. Jordan, I. Rae and D. Walters, *Aust. J. Chem.*, 1984, **37**, 1769-1773.
290. R. Schwarz, J. Seelig and B. Künnecke, *Magn. Reson. Chem.*, 2004, **42**, 512-517.
291. P. Thordarson, *Chem. Soc. Rev.*, 2011, **40**, 1305-1323.
292. R. Tepper and U. S. Schubert, *Angew. Chem. Int. Ed*, **57**, 6004-6016.
293. M. Pierangelo, M. Franck, P. Tullio, R. Giuseppe and T. Giancarlo, *Angew. Chem. Int. Ed*, 2008, **47**, 6114-6127.
294. G. F. Manbeck, W. W. Brennessel, C. M. Evans and R. Eisenberg, *Inorg. Chem.*, 2010, **49**, 2834-2843.
295. O. V. Dolomanov, L. J. Bourhis, R. J. Gildea, J. A. K. Howard and H. Puschmann, *J. Appl. Cryst.*, 2009, **42**, 339-341.

Appendices

Appendices

A1. Single crystal X-ray diffraction experiments for Chapter 2

Single crystal X-ray diffraction experiments for this Chapter and data preparation were conducted by Dr. Asha Brown at University of Oxford.

Data collection

Diffraction data for the structures of the complexes 1•HB•2NaI and 1•XB•HCl were collected at 100 K using silicon double crystal monochromated synchrotron radiation (λ = 0.6889 Å) at Diamond Light Source, beamline I19,[1] using a custom-built Crystal Logic diffractometer. Unit cell parameter determination and refinement and raw frame data integration were carried out using the CrysAlisPro [2] package.

Structures were solved by charge-flipping methods using SUPERFLIP[3] and refined by full matrix least squares on F^2 using the CRYSTALS suite.[4] All non-hydrogen atoms were refined with anisotropic displacement parameters. A more detailed discussion of each individual structure is given below, including a description of hydrogen atom treatment for each structure.

Sodium iodide ion-pair complex of the hydrogen-bonding receptor, 2.1·HB·2NaI

Crystals of the complex **2.1·HB·2NaI** suitable for X-ray structural determination were grown by slow evaporation of a chloroform:acetonitrile 9:1 solution of the receptor **2.1·HB·2NaPF$_6$** containing two molar equivalents of tetrabutylammonium iodide. The crystals were small and weakly diffracting; despite the use of synchrotoron radiation, the data are of relatively low quality. Consequently, where necessary, geometric restraints to bond lengths and angles were applied to ensure a physically reasonable model and thermal and vibrational restraints were applied to maintain sensible anisotropic displacement parameters. Some positional disorder was identified within the molecular framework of the ditopic ligand **2.1·HB**. To account for this three of the four triazole groups were modelled over two positions using refined partial occupancies. Comparatively large anisotropic displacement ellipsoids for two of the four benzotriazole groups were also observed, which may indicate further positional disorder within these regions of the structure. Since the quality of the data is insufficient to permit sensible modelling of these regions using two discrete positions for each atom, tight thermal restraints were instead applied. The two iodide counteranions which are not bound within the 3,5-bis-triazole pyridine anion recognition units were modelled over five partially occupied positions. Several partially occupied water molecules are also present within the asymmetric unit. Hydrogen atoms were generally visible in the Fourier difference map. Those attached to carbon atoms were initially positioned geometrically and refined

against the data with restraints on bond lengths and angles, after which their positions were used as the basis for a riding model.[5] Most of the hydrogen atoms on the water molecules were not clearly visible in the difference maps and it was not possible to sensibly refine their positions. These hydrogen atoms were inserted at idealised hydrogen bonding positions with O—H distances of 0.9 Å and constrained to ride on the attached oxygen atoms.

Crystallographic data, including structure factors, for the structure **2.1·HB·2NaI** have been deposited with the Cambridge Crystallographic Data Centre. Full crystallographic data and refinement details are provided in cif format, and selected data are also summarised in Table A1 below.

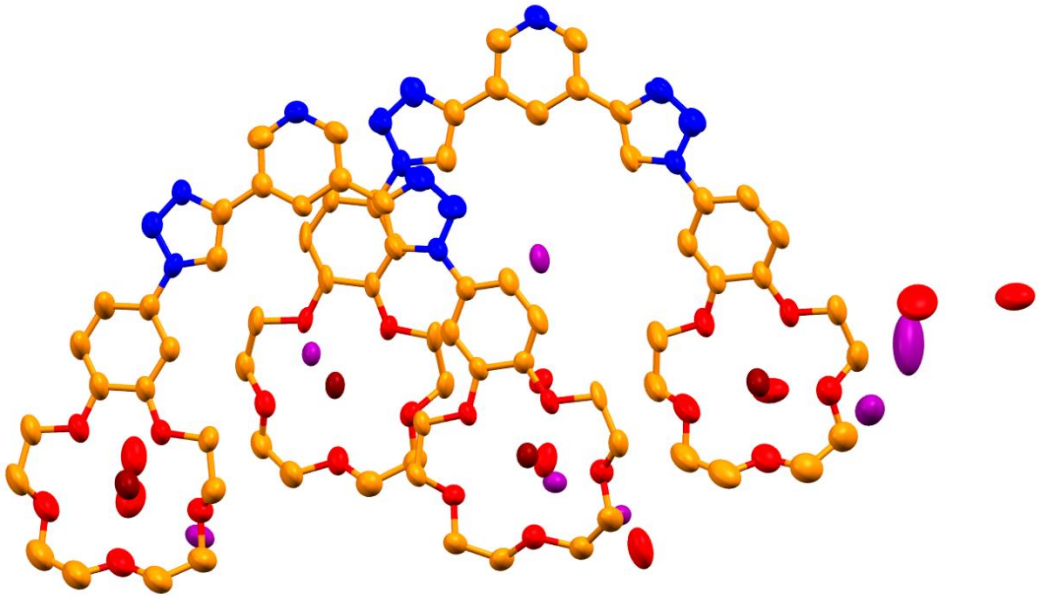

Figure A1. Thermal ellipsoid representation of the contents of the asymmetric unit for the solid state structure of the complex **2.1·HB·2NaI**. Ellipsoids are shown at the 50% probability level. For clarity, hydrogen atoms have been omitted.

Chloride complex of the protonated halogen-bonding receptor, 2.1·XB·HCl

X-ray quality crystals of the complex **2.1·XB·HCl** were obtained by slow evaporation of a dichloroethane/acetone solution of the receptor **2.1·XB**. The receptor crystallised as its hydrogen chloride salt **2.1·XB·HCl**, presumably owing to the presence of a low concentration of hydrogen chloride in the dichloroethane solvent. The crystals were small and weakly diffracting and the data were therefore collected using synchrotron radiation. However, the crystal suffered severe radiation damage during data collection. As a consequence it was only possible to obtain an incomplete set of low angle data from an initial phi scan. Despite several attempts, we were unable to obtain a more complete set of data. Nevertheless, it was possible to obtain a structure solution, which is presented here solely as a provisional guide to overall conformation and connectivity: while the overall structure is not in doubt, detailed inferences about bond lengths and angles cannot be drawn owing to the low quality of the data. Restraints to the geometries and ellipsoid parameters of all non-hydrogen atoms were applied in order to obtain a sensible refinement. Hydrogen atoms were inserted at calculated positions, refined against the data using soft restraints on bond lengths and angles and then included in the refinement using a riding model. Absent high angle data were removed after consulting the Wilson Plot.

The complex crystallised in the triclinic space group $P\bar{1}$. The asymmetric unit contains the protonated ditopic halogen-receptor **2.1·XB**, a chloride counteranion and a partially occupied dichloroethane solvent molecule. The chloride counteranion can be seen to interact with the receptor's *N*-protonated 5-bis-iodotriazole pyridinium cavity *via* bidentate C—I·····Cl^- halogen bonding interactions (Figure A2). The dichloroethane solvent molecule appears to be involved in four C—H·····O^- hydrogen bonding interactions with the oxygen atoms from a proximal crown ether group. The other crown ether group forms close contacts with the *N*-protonated pyridinium group from an adjacent molecule, which strongly implies the existence of intermolecular N—H·····O^- hydrogen bonding interactions. These interactions link the molecules in an infinite linear chain which is aligned with the crystallographic b axis (Figure A3 and A4). Although the electron density associated with the *N*-pyridinium proton could not be observed in the difference map its presence was inferred from the observation of this infinite linear chain, and from the presence of the chloride counteranion.

Selected crystallographic data for the **2.1·XB·HCl** structure are included in Table A1 below but, since the data are not of publication quality, this provisional structure has not been deposited with the Cambridge Crystallographic Data Centre, and full data in cif format are not included.

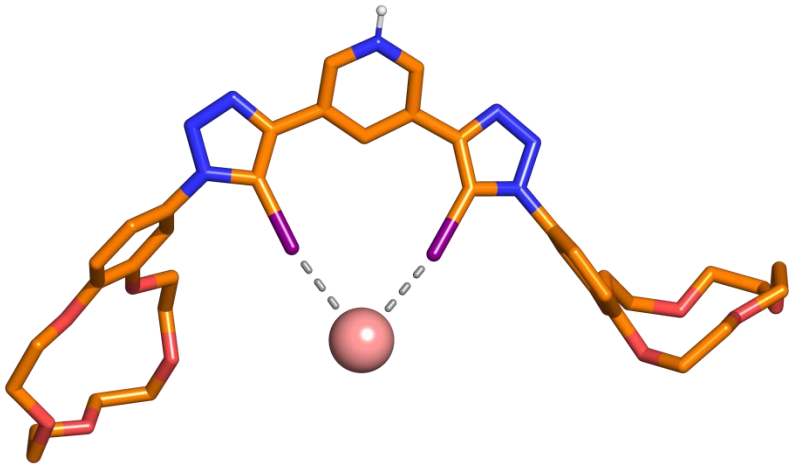

Figure A2. Content of the asymmetric unit for the solid state structure of the complex **2.1·XB·HCl**: the chloride counteranion can be seen to interact with the receptor's *N*-protonated bis-iodotriazole pyridinium cavity *via* bidentate C—I·····Cl^- halogen bonding interactions. For clarity, non-polar hydrogen atoms and a partially occupied dichloroethane solvent molecule have been omitted.

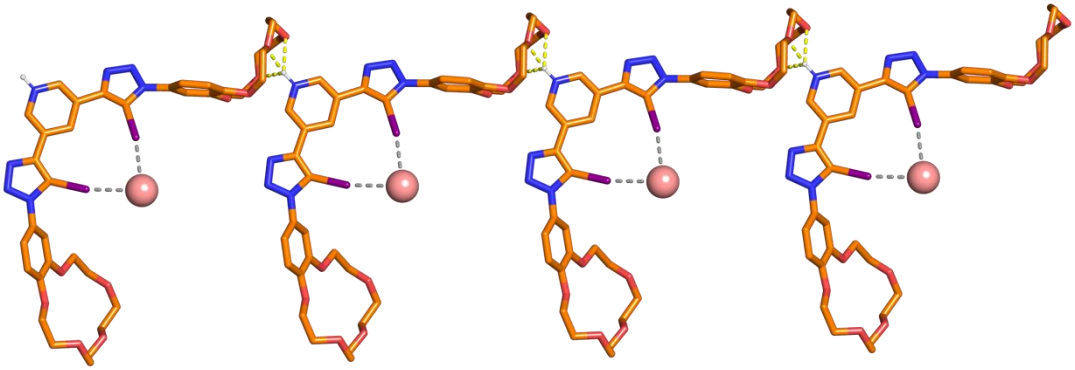

Figure A3. View of the solid state structure of the complex **2.1·XB·HCl**, showing the infinite linear chain which forms as a result of hydrogen-bonding interactions between *N*-protonated pyridinium and crown ether groups in adjacent molecules. For clarity, non-polar hydrogen atoms and a partially occupied dichloroethane solvent molecule have been omitted.

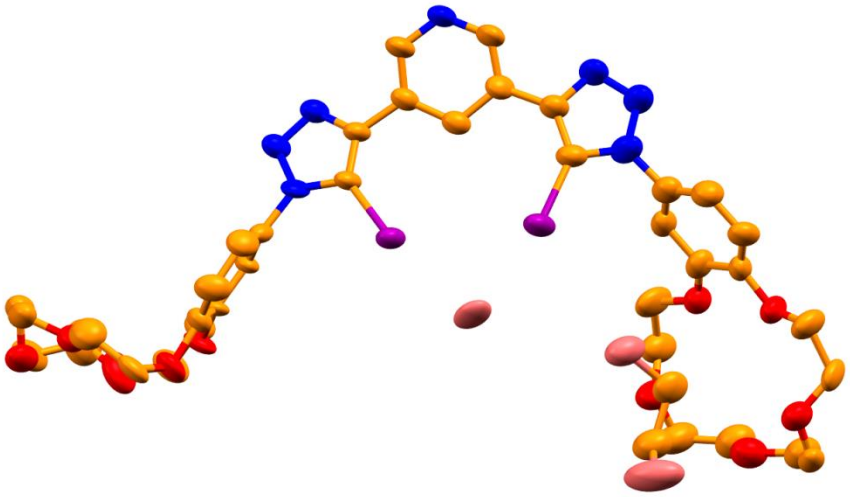

Figure A4. Thermal ellipsoid representation of the contents of the asymmetric unit for the solid state structure of the complex **2.1·XB·HCl**. Ellipsoids are shown at the 50% probability level. For clarity, hydrogen atoms have been omitted.

Table A1. Selected crystallographic data for the structures **2.1·HB·2NaI** and **2.1·XB·HCl**.

Compound	2.1·HB·2NaI	2.1·XB·HCl
CCDC number		—
Formula	$2(C_{37}H_{43}N_7Na_2O_{10})\cdot 5.39(H_2O)\cdot 4I$	$C_{37}H_{42}I_2N_7O_{10}\cdot 0.72(C_2H_4Cl_2)\cdot Cl$
Formula weight	2188.29	1105.31
a (Å)	8.2042(2)	9.2629(6)
b (Å)	23.9836(7)	14.0190(9)
c (Å)	24.5580(7)	18.8620(17)
α (°)	108.317(3)	71.859(7)
β (°)	96.490(2)	77.933(7)
γ (°)	90.532(2)	78.934(5)
Unit vell volume (Å^3)	4552.8(2)	2254.9(3)
Crystal system	Triclinic	Triclinic
Space group	$P\bar{1}$	$P\bar{1}$
Z	2	2
Temperature (K)	100	100
Radiation type	Synchrotron	Synchrotron
λ (Å)	0.6889	0.6889
Reflections (all)	34930	8786
Reflections (unique)	17680	5502
R_{int}	0.086	0.139
$R[I > 2\sigma(I)]$	0.076	0.141

wR(F^2) (all data)	0.221	0.369
S	0.99	1.04

References

[1] H. Nowell, S. A. Barnett, K. E. Christensen, S. J. Teat, D. R. Allan, *J. Synchrotron Radiat.* **2012**, *19*, 435–441.

[2] *CrysAlisPro*, Agilent Technologies, Yarnton, Oxfordshire, UK.

[3] L. Palatinus, G. Chapuis, *J. Appl. Crystallogr.* **2007**, *40*, 786–790.

[4] P. W. Betteridge, J. R. Carruthers, R. I. Cooper, K. Prout, D. J. Watkin, *J. Appl. Crystallogr.* **2003**, *36*, 1487.

[5] R. I. Cooper, A. L Thompson, D. J. Watkin, *J. Appl. Crystallogr*. **2010**, *43*, 1100–1107

A2. Single crystal X-ray diffraction experiments for Chapter 3

Single crystal X-ray diffraction experiments for this Chapter and data preparation were conducted by Dr. Antonio J. Martinez-Martinez at University of Oxford.

Crystal structure determinations

Single-crystal X-ray diffraction data for **3.4·Cl** and **3.4·I** were collected at 100 K on Oxford Diffraction/Agilent SuperNovae diffractometers with Cu-*Kα* (*λ* = 1.54184 Å) radiation equipped with nitrogen gas Oxford Cryosystems Cryostream unit.[6] Raw frame data were reduced using CrysAlisPro.[7] The structures were solved using SHELXT[8] and refined to convergence on F^2 and against all independent reflections by full-matrix least-squares using SHELXL[7] (version 2018/1) in combination with the GUI OLEX2[295] program. All non-hydrogen atoms were refined anisotropically and hydrogen atoms were geometrically placed and allowed to ride on their parent atoms. Distances and angles were calculated using the full covariance matrix. Selected crystallographic data are summarized in the text and full details are given in the supplementary deposited CIF files (CCDC 1825939-1825940). These data can be obtained free of charge from the Cambridge Crystallographic Data Centre *via* http://www.ccdc.cam.ac.uk/data_request/cif.

X-ray crystal structure of 5·Cl (CCDC 1825940)

Crystal data for **3.4·Cl**: $C_{32}H_{24}ClF_8I_2N_7O_6$, M = 1043.83 g/mol, triclinic, P-1, a = 10.8670(3), b = 12.9199(3), c = 13.3185(3) Å, α = 86.075(2), β = 80.433(2), γ = 87.387(2)°, V = 1838.48(8) Å^3, Z = 2, λ(Cu-*Kα*) = 1.54184 Å, T = 100.0(3) K, colorless needle, 41904 reflections collected, 7652 independent measured reflections (R_{int} = 0.0427), F^2 refinement, R_1(obs, $I > 2\sigma(I)$) = 0.0218, wR_2(all data) = 0.0541, 6931 independent observed reflections [$|F_o| > 4\sigma(|F_o|)$, 2θmax = 152.9°], 0 restrains, 512 parameters, GOF = 1.024 and residual electron density (e Å^{-3}) = 0.67/-0.81.

Additional details for **3.4·Cl**: This compound crystallised with two molecules of acetone (solvent of crystallization) within the crystal lattice.

X-ray crystal structure of 3.4·I (CCDC 1825939)

Crystal data for **3.4·I**: $C_{26}H_{12}F_8I_3N_7O_4$, M = 1019.13 g/mol, orthorhombic, *Pbcn*, a = 17.6930(2), b = 13.58401(13), c = 25.8324(2) Å, $\alpha = \beta = \gamma = 90°$, V = 6208.59(12) Å^3, Z = 8, λ(Cu-*Kα*) = 1.54184 Å, T = 100.0(4) K, colorless needle, 140707 reflections collected, 6482 independent measured reflections (R_{int} = 0.0767), F^2 refinement, R_1(obs, $I > 2\sigma(I)$) = 0.0323,

wR_2(all data) = 0.0908, 5848 independent observed reflections [$|F_o| > 4\sigma(|F_o|)$, 2θmax = 152.6°], 140 restrains, 450 parameters, GOF = 1.032 and residual electron density (e Å^{-3}) = 1.98/-0.70.

Additional details for **3.4·I**: One MeOC(O) group was modelled as disordered and freely refined over two domains, and restrained to maintain sensible metrics and displacement parameters.

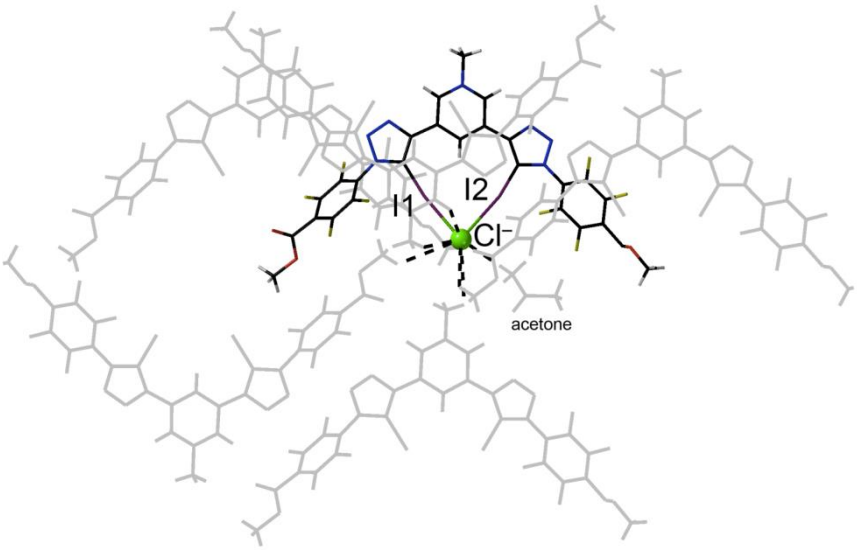

Figure A5 Packing diagram (front view) of **3.4·Cl** showing hydrogen donor/Cl^- acceptor interactions as dashed lines: OMe···Cl^- contacts (range 3.01-3.45 Å), pyridinium-Me···Cl^- (2.90 and 3.45 Å) and (acetone)Me···Cl^- (2.83 Å).

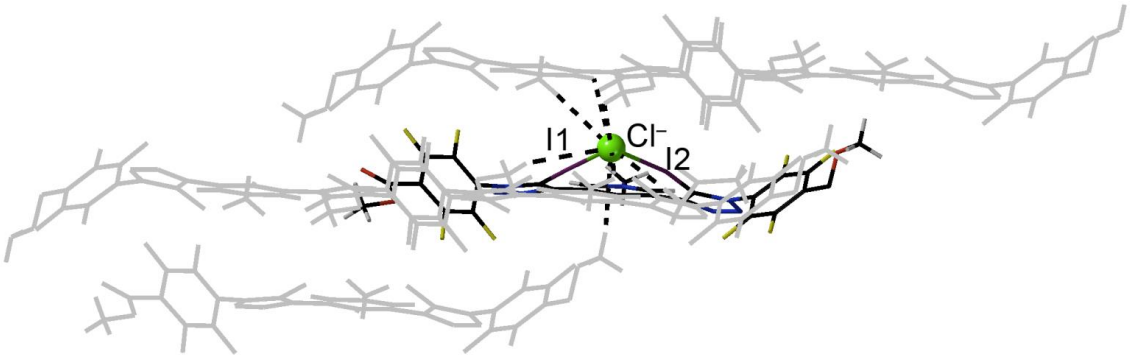

Figure A6 Packing diagram (side view) of **3.4·Cl** showing hydrogen donor/Cl^- acceptor interactions as dashed lines: OMe···Cl^- contacts (range 3.01-3.45 Å), pyridinium-Me···Cl^- (2.90 and 3.45 Å) and (acetone)Me···Cl^- (2.83 Å).

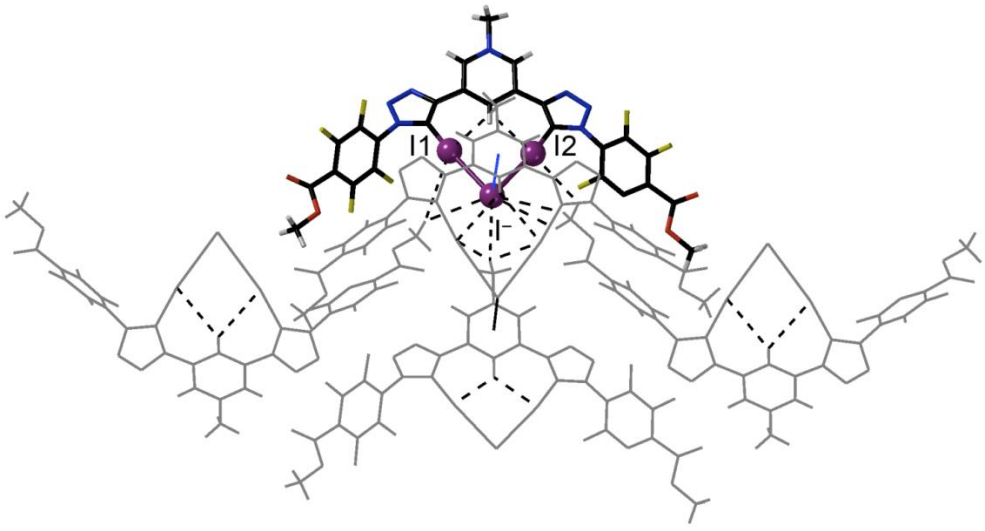

Figure A7 Packing diagram (front view) of **3.4·I** showing hydrogen and π-donor/I^- acceptor interactions as dashed lines: OMe···I^- (range 3.43-3.62 Å), pyridinium-Me···I^- (3.62 Å) and *via* anion-π-pyridinium ring (pyridinium-centroid···I^-, 3.56 Å).

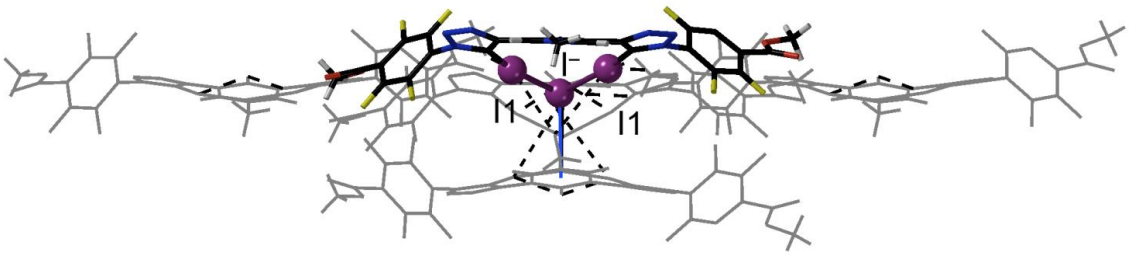

Figure A8 Packing diagram (side view) of **3.4·I** showing hydrogen and π-donor/I^- acceptor interactions as dashed lines: OMe···I^- (range 3.43-3.62 Å), pyridinium-Me···I^- (3.62 Å) and *via* anion-π-pyridinium ring (pyridinium-centroid···I^-, 3.56 Å).

References

[6] G. M. Sheldrick, *Acta Cryst. Sect. A*, 2015, **71**, 3-8.

[7] G. M. Sheldrick, *Acta Cryst. Sect. A*, 2008, **64**, 112-122

[8] O. V. Dolomanov, L. J. Bourhis, R. J. Gildea, J. A. K. Howard and H. Puschmann, *J. Appl. Cryst.*, 2009, **42**, 339-341

A3. Single crystal X-ray diffraction experiments for Chapter 4

Single crystal X-ray diffraction experiments for this Chapter and data preparation were conducted by Dr.Jason Lim at University of Oxford and Dr. Nicholas G. White at Australian National University.

Technical details

Crystal growth

Crystals were grown by vapour diffusion of diisopropyl ether into a solution of **4.13·BF_4** or **4.18·2BF_4** and ten equivalents of the appropriate tetrabutylammonium halide salt in 1:1 $CDCl_3$:CD_3CN. Crystals of **4.9** were grown by slow evaporation of a CH_3CN solution of the compound at low temperature (~ 5 °C).

Refinement details

Single crystal X-ray diffraction data were collected using synchrotron radiation on Beamline I19 at Diamond Lightsource.[2] Crystals were cooled to 100 K using a Cryostream N2 open-flow cooling device.[3] Cell parameters and intensity data (including inter-frame scaling) were processed using CrysAlis Pro.[4] Structures were solved by charge-flipping methods using SUPERFLIP[5] and refined within the CRYSTALS suite.[6] All non-hydrogen atoms were refined with anisotropic displacement parameters. Hydrogen atoms were visible in the difference map, and their positions refined using restraints, prior to their inclusion in the model using riding constraints.[7]

Table A2 Selected crystallographic data for the structures of **4.13·Cl**, **4.13·Br** and **4.13·I**.

Compound	**4.13·Cl**	**4.13·Br**	**4.14·I**	**4.13· BF_4**	**4.18·1.733I· 0.267BF_4**
Formula	$C_{23}H_7H_{10}I_2N_6$, Cl · *solvents*[a]	$C_{23}H_7H_{10}I_2N_6$, Br · *solvents*[a]	$C_{23}H_7H_{10}I_2N_6$, I· *solvents*[a]	$C_{28}H_{26}I_2N_6$	$C_{30}H_{34}N_6$, 1.733I, 0.267BF_4
Formula weight	846.59	891.04	938.04	700.36	721.75
a (Å)	16.6992(2)	16.9083(4)	17.1206(2)	16.6402(11)	19.4098(5)
b (Å)	12.9737(2)	12.9962(3)	13.0829(2)	14.3473(6)	19.4098(5)
c (Å)	27.5621(4)	27.5831(8)	27.6505(3)	22.1969(12)	21.6000(6)
α (º)	90	90	90	90	90
β (º)	90	90	90	90	90
γ (º)	90	90	90	90	120
Unit cell volume (Å^3)	5971.34(9)	6061.21(18)	6193.35(7)	5299.3(3)	7047.4(2)
Crystal system	orthorhombic	orthorhombic	orthorhombic	orthorhombic	trigonal
Space group	*Pbca*	*Pbca*	*Pbca*	*Pbca*	$R3_2$
Z	8	8	8	8	9
Reflections (all)	123664	119404	128080	61877	28966
Reflections (unique)	15310	15444	15587	5558	3246
R_{int}	0.110	0.118	0.121	0.257	0.069
R_1 [$I > 2\sigma(I)$]	0.033	0.048	0.046	0.098	0.094
$wR_2(F^2)$ (all data)	0.082	0.120	0.100	0.271	0.233

[a] PLATON-SQUEEZE[8] used

Disordered solvent in structures of ***4.13***$^{+}$

All three structures contained a region of diffuse electron density. In each case the residual electron density in this region looks very similar, and appears to correspond to positionally-disordered partial occupancy acetonitrile and chloroform molecules (Figure A9). Attempts were made to model this electron density as a mixture of partial occupancy solvent molecules for each structure: however despite the use of numerous restraints, it was not possible to achieve a stable refinement of this electron density and so PLATON-SQUEEZE[8] was used to include it in the refinement.

This revealed the presence of one void per asymmetric unit in each structure, with these voids having volumes of 118–125 Å^3 and containing 32–38 electrons (there is a small variation in void size and electron count between the three structures, see CIFs for specific details). One acetonitrile molecule has 22 electrons, while one chloroform molecule has 58 electrons, so these electron counts are consistent with the presence of a disordered mixture of these two solvents.

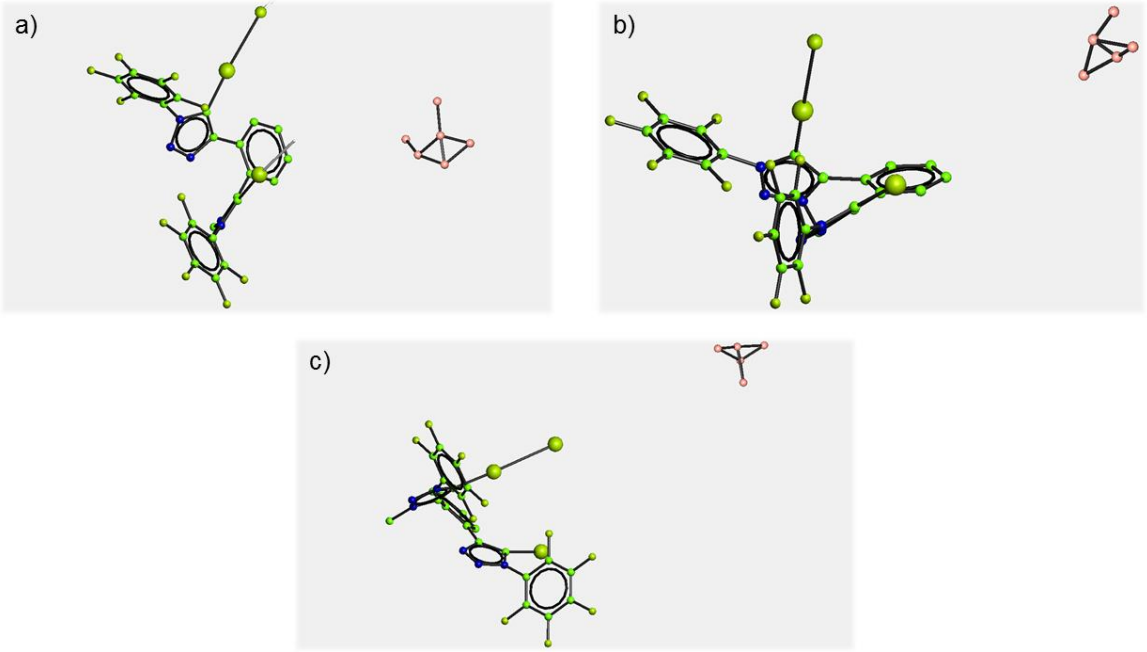

Figure A9. Image showing the largest peaks (pink dots) in the difference map after initial refinement of the structures of a) **4.13·Cl**, b) **4.13·Br** and c) **4.13·I**.

Structure of ***4.18·1.733I·0.267BF$_4$***

The structure crystallises in the trigonal space group $R3_2$. The asymmetric unit contains half a molecule of **4.18**$^{2+}$, as well as several anion positions (including on special positions). Overall, there is one full occupancy iodide anion, which is involved in hydrogen bonding to the triazolium groups (linking the compound into a 1D polymeric chain). The remaining anion per receptor is disordered over several positions – this was modelled as partial occupancy iodide and tetrafluoroborate anions, with a total of 1.733 iodide ions and 0.267 tetrafluoroborate ions per receptor. It was necessary to apply restraints to the BF_4^- bond lengths and angles, phenyl ring bond lengths, and thermal and vibrational ellipsoid parameters in order to achieve a sensible refinement.

Thermal Ellipsoid Plots

Thermal ellipsoid plots of the asymmetric unit cells of the complexes **4.13·Cl**, **4.13·Br**, **4.13·I**, **4.9** and **4.18·1.733I·0.267BF$_4$** are given in Figures A10 - A14.

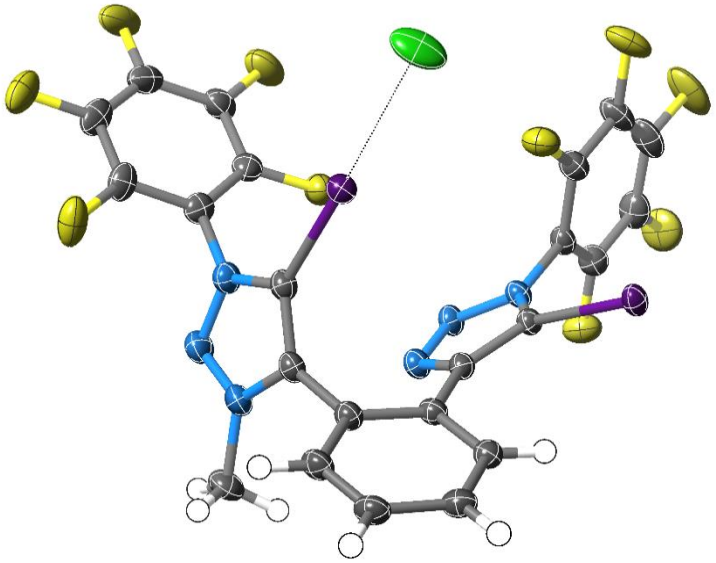

Figure A10 Thermal ellipsoid plot showing asymmetric unit cell of **4.13·Cl** (ellipsoids shown at 50% probability level).

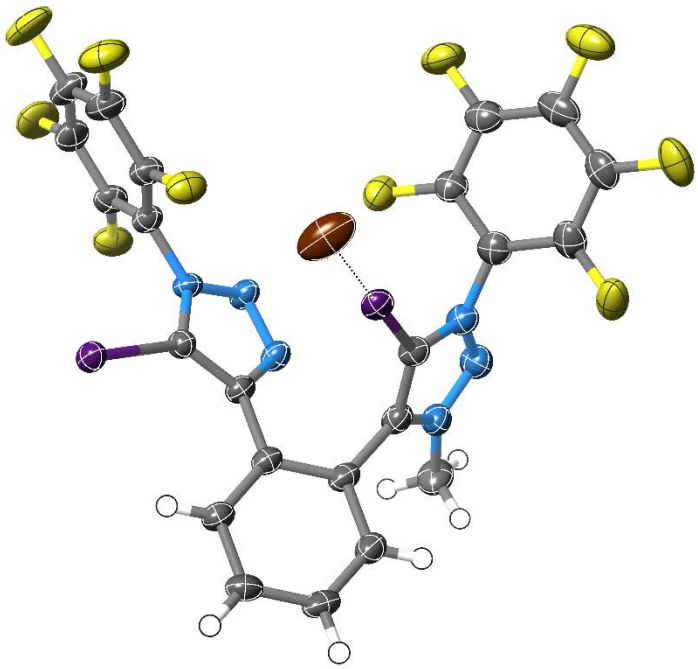

Figure A11 Thermal ellipsoid plot showing asymmetric unit cell of **4.13·Br** (ellipsoids shown at 50% probability level).

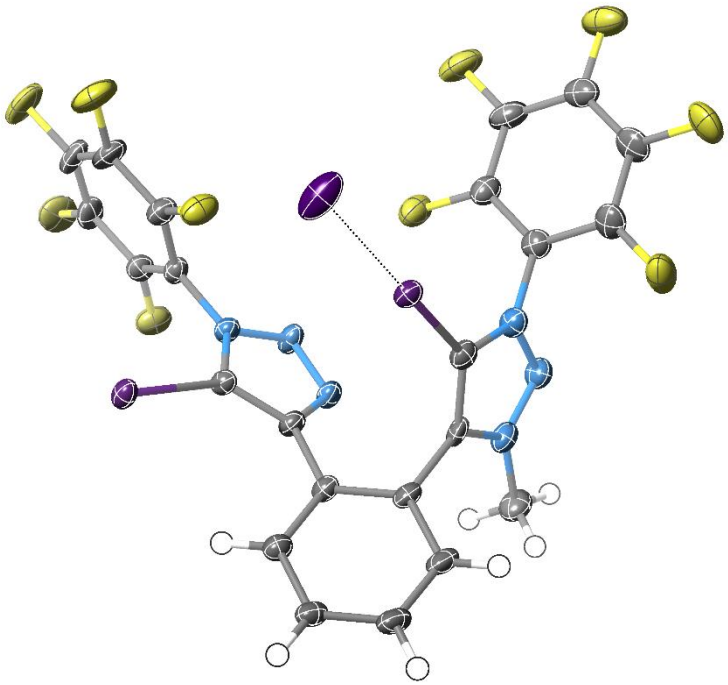

Figure A12 Thermal ellipsoid plot showing asymmetric unit cell of **4.13·I** (ellipsoids shown at 50% probability level).

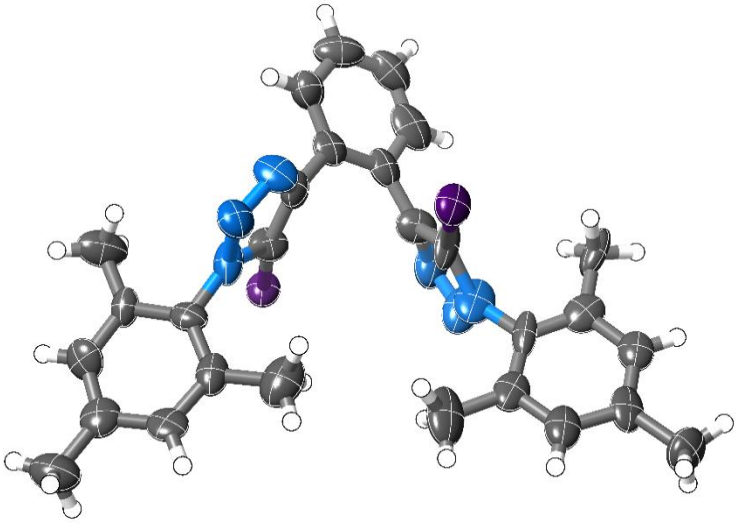

Figure A13 Thermal ellipsoid plot showing asymmetric unit cell of **4.9** (ellipsoids shown at 50% probability level).

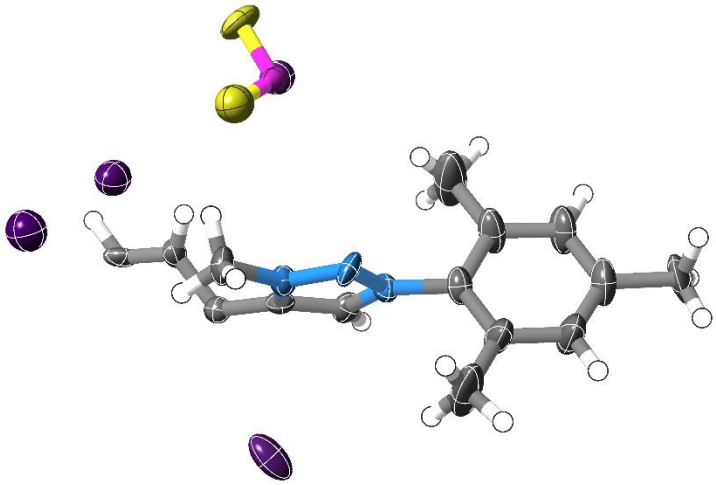

Figure A14 Thermal ellipsoid plot showing asymmetric unit cell of **4.18·1.733I·0.267BF$_4$** (ellipsoids shown at 50% probability level).

References

[1] S. Alvarez, A cartography of the van der Waals territories, *Dalton Trans.* **2013**, *42*, 8617–8636.

[2] H. Nowell, S. A. Barnett, K. E. Christensen, S. J. Teat, D. R. Allan, I19, the small-molecule single-crystal diffraction beamline at Diamond Light Source*, J. Synchrotron Radiat.* **2012**, *19*, 435–441.

[3] J. Cosier, A. M. Glazer, A nitrogen-gas-stream cryostat for general X-ray diffraction studies, *J. Appl. Crystallogr.* **1986**, *19*, 105–107.

[4] Agilent Technologies, *CrysAlisPro*, **2011**.

[5] L. Palatinus, G. Chapuis, *SUPERFLIP* – a computer program for the solution of crystal structures by charge flipping in arbitrary dimensions, *J. Appl. Crystallogr.* **2007**, *40*, 786–790.

[6] P. W. Betteridge, J. R. Carruthers, R. I. Cooper, K. Prout, D. J. Watkin, *CRYSTALS* version 12: software for guided crystal structure analysis, *J. Appl. Crystallogr.* **2003**, *36*, 1487.

[7] R. I. Cooper, A. L Thompson, D. J. Watkin, *CRYSTALS* enhancements: dealing with hydrogen atoms in refinement, *J. Appl. Crystallogr*. **2010**, *43*, 1100–1107.

[8] A. L. Spek, *PLATON* SQUEEZE: a tool for the calculation of the disordered solvent contribution to the calculated structure factors, *Acta Crystallogr.* **2015**, *C71*, 9–18.

A4. Isothermal Titration Calorimetric (ITC) Isotherms for Anion Titrations in Water

A4.1 Titration data for 3.44·NO_3

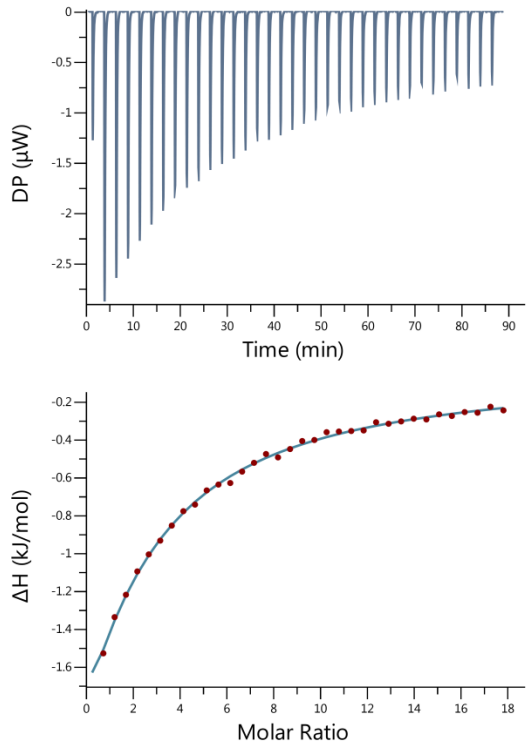

Figure A15 Raw ITC data for the sequential addition of NaI to **3.44·NO_3** in H_2O at 298K; integrated heat plot obtained from titration; [host] = 0.2 mM, [guest] = 20 mM

.

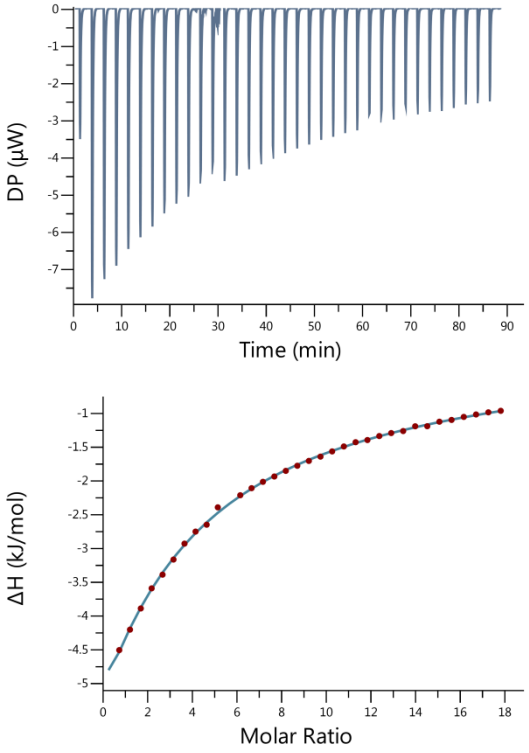

Figure A16 Raw ITC data for the sequential addition of $NaReO_4$ to **3.44·NO_3** in H_2O at 298K; integrated heat plot obtained from titration; [host] = 0.2 mM, [guest] = 20 mM

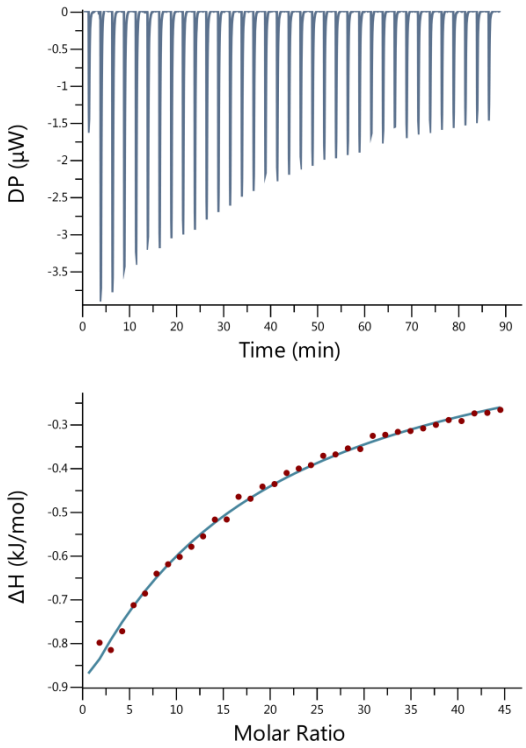

Figure A17 Raw ITC data for the sequential addition of $NaClO_4$ to **3.44·NO_3** in H_2O at 298K; integrated heat plot obtained from titration; [host] = 0.2 mM, [guest] = 50 mM

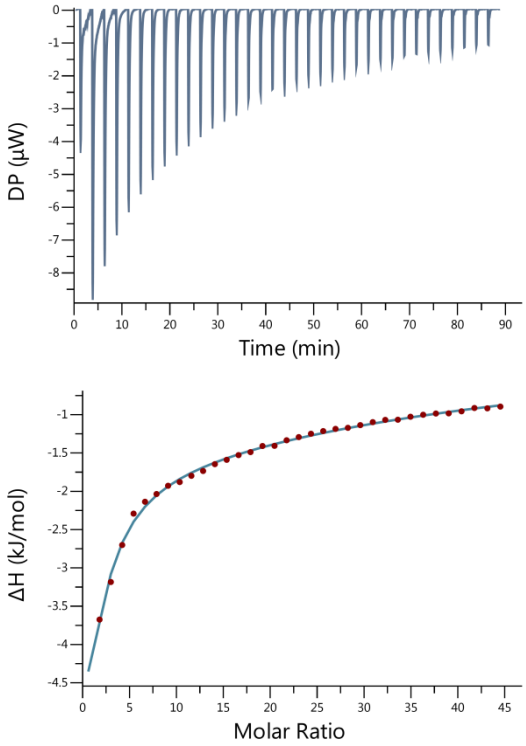

Figure A18 Raw ITC data for the sequential addition of $NaIO_4$ to **3.44·NO_3** in H_2O at 298K; integrated heat plot obtained from titration; [host] = 0.2 mM, [guest] = 50 mM

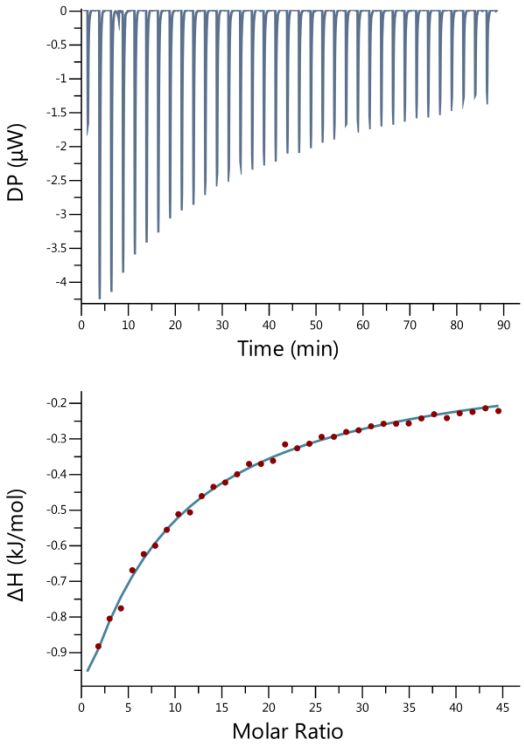

Figure A19 Raw ITC data for the sequential addition of NaSCN to **3.44·NO_3** in H_2O at 298K; integrated heat plot obtained from titration; [host] = 0.2 mM, [guest] = 50 mM

A4.2 Titration data for 3.42

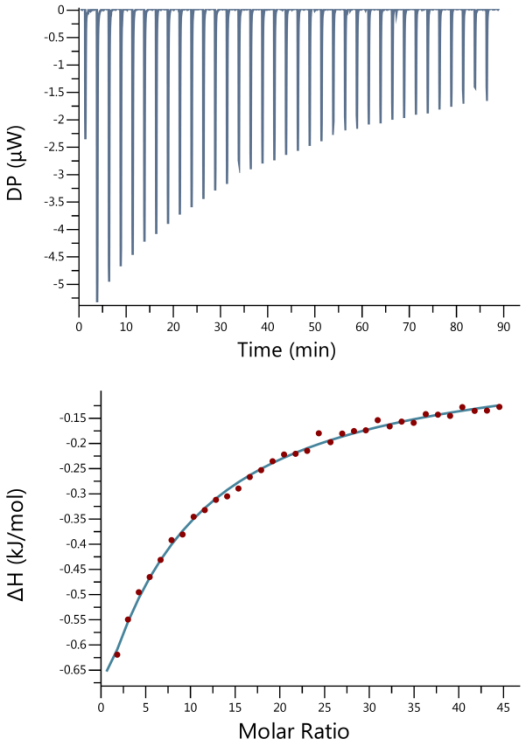

Figure A20 Raw ITC data for the sequential addition of NaI to **3.42** in H_2O at 298K; integrated heat plot obtained from titration; [host] = 0.2 mM, [guest] = 50 mM

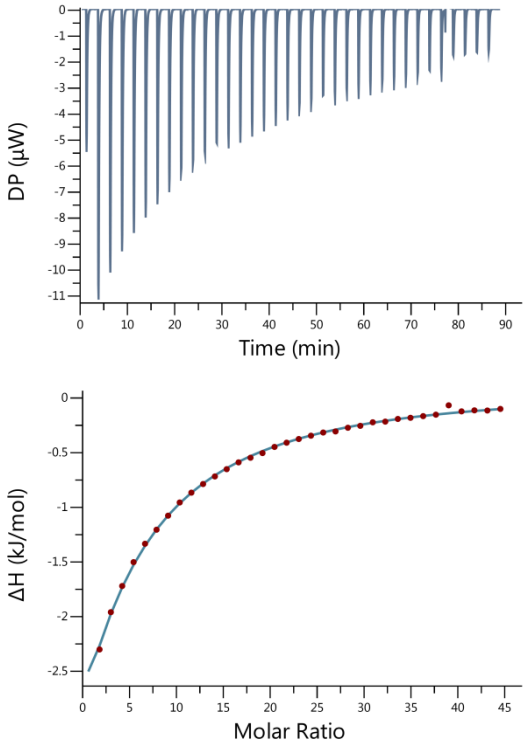

Figure A21 Raw ITC data for the sequential addition of $NaReO_4$ to **3.42** in H_2O at 298K; integrated heat plot obtained from titration; [host] = 0.2 mM, [guest] = 50 mM

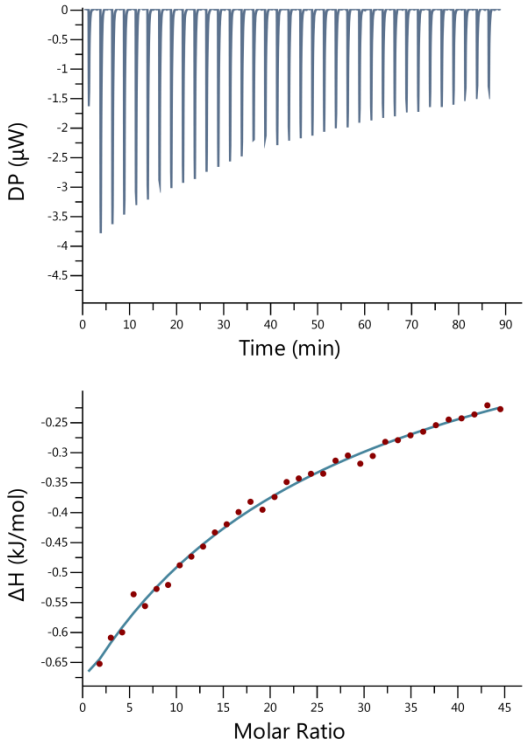

Figure A22 Raw ITC data for the sequential addition of $NaClO_4$ to **3.42** in H_2O at 298K; integrated heat plot obtained from titration; [host] = 0.2 mM, [guest] = 50 mM

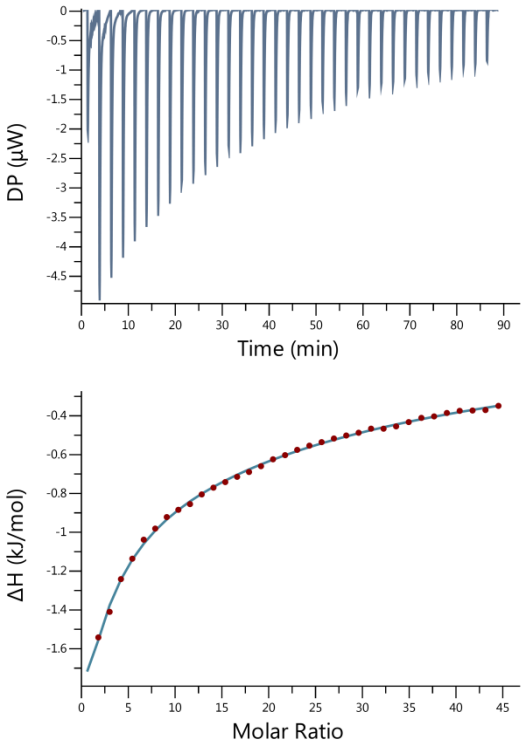

Figure A23 Raw ITC data for the sequential addition of $NaIO_4$ to **3.42** in H_2O at 298K; integrated heat plot obtained from titration; [host] = 0.2 mM, [guest] = 50 mM

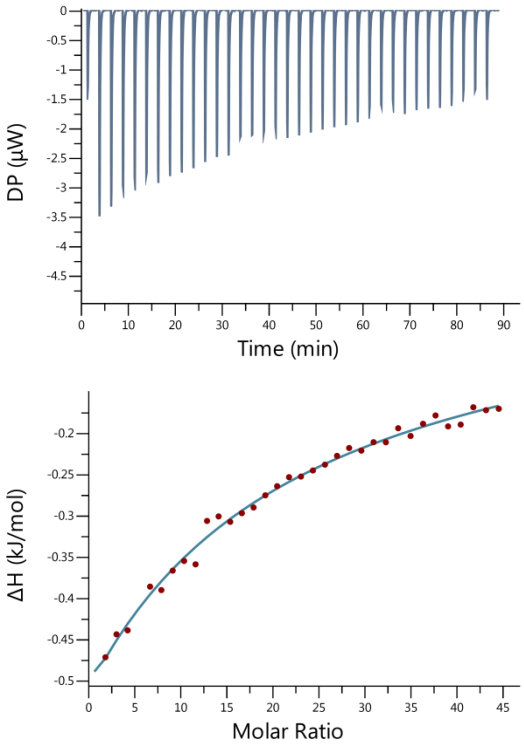

Figure A24 Raw ITC data for the sequential addition of NaSCN to **3.42** in H_2O at 298K; integrated heat plot obtained from titration; [host] = 0.2 mM, [guest] = 50 mM

A4.3 Titration data for 3.43

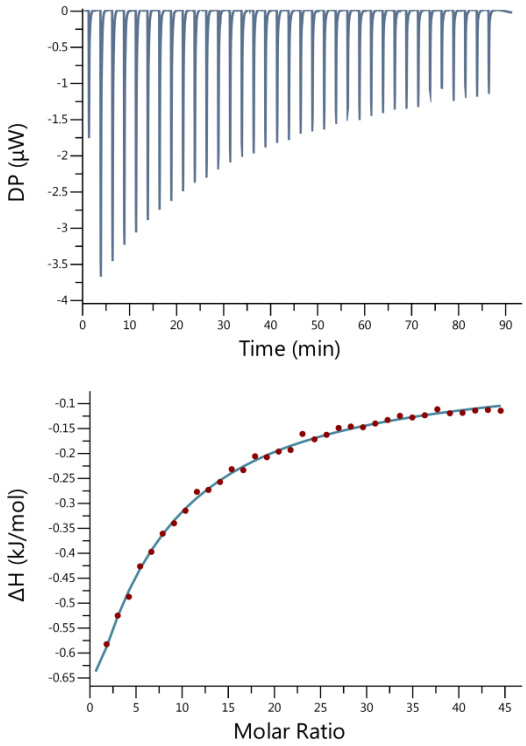

Figure A25 Raw ITC data for the sequential addition of NaI to **3.43** in H_2O at 298K; integrated heat plot obtained from titration; [host] = 0.2 mM, [guest] = 50 mM

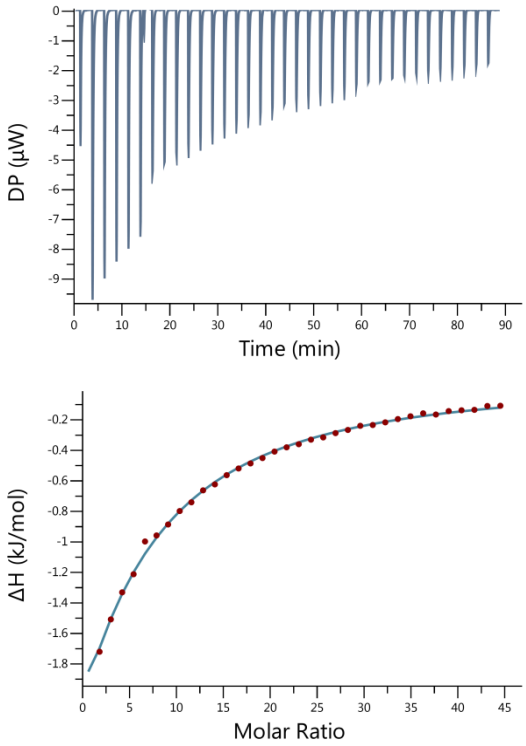

Figure A26 Raw ITC data for the sequential addition of $NaReO_4$ to **3.43** in H_2O at 298K; integrated heat plot obtained from titration; [host] = 0.2 mM, [guest] = 50 mM

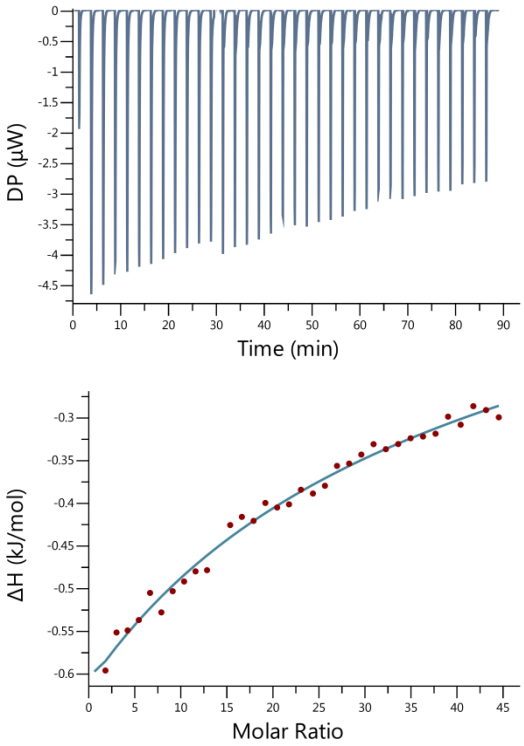

Figure A27 Raw ITC data for the sequential addition of $NaClO_4$ to **3.43** in H_2O at 298K; integrated heat plot obtained from titration; [host] = 0.2 mM, [guest] = 50 mM

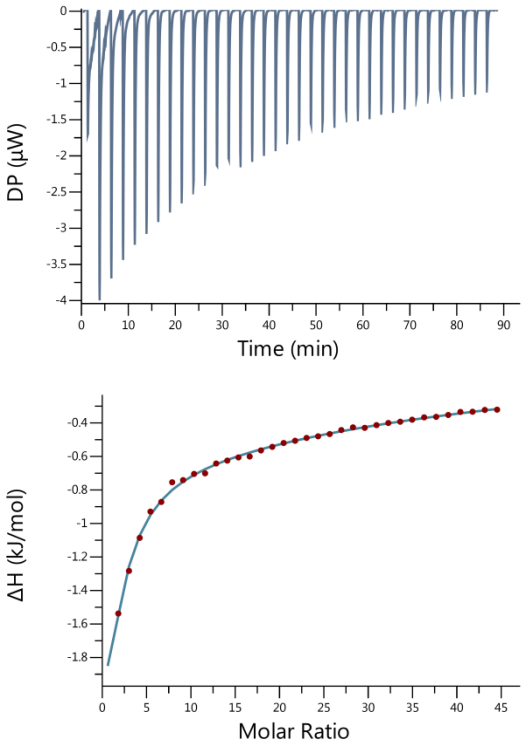

Figure A28 Raw ITC data for the sequential addition of $NaIO_4$ to **3.43** in H_2O at 298K; integrated heat plot obtained from titration; [host] = 0.2 mM, [guest] = 50 mM

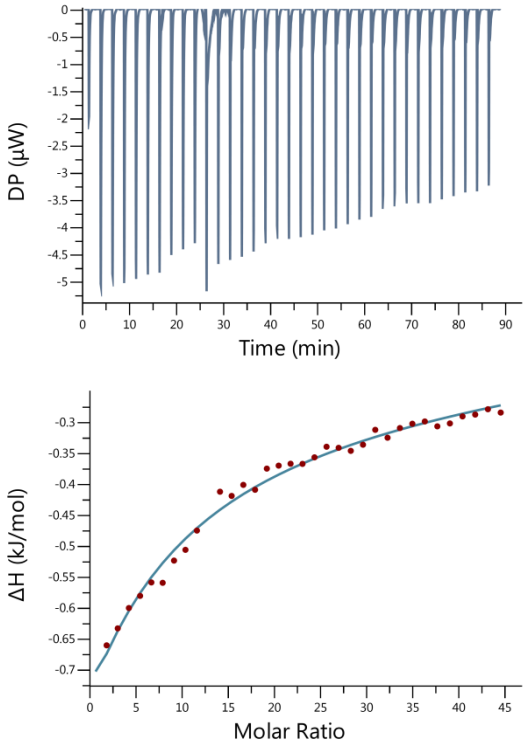

Figure A29 Raw ITC data for the sequential addition of NaSCN to **3.43** in H_2O at 298K; integrated heat plot obtained from titration; [host] = 0.2 mM, [guest] = 50 mM

A4.4 Titration data for 3.50

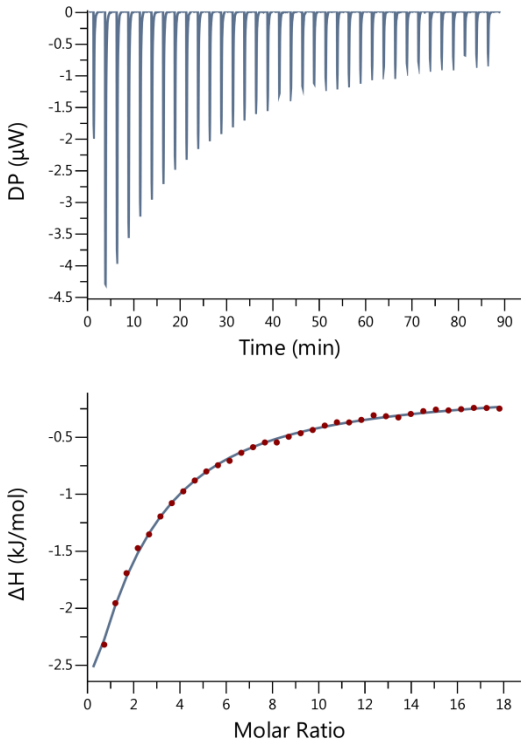

Figure A30 Raw ITC data for the sequential addition of NaI to **3.50·NO_3** in H_2O at 298K; integrated heat plot obtained from titration; [host] = 0.2 mM, [guest] = 20 mM

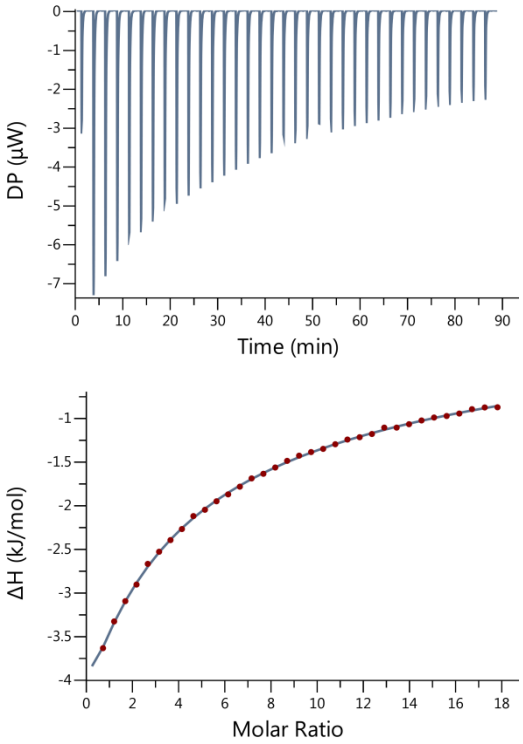

Figure A31 Raw ITC data for the sequential addition of $NaReO_4$ to **3.50·NO_3** in H_2O at 298K; integrated heat plot obtained from titration; [host] = 0.2 mM, [guest] = 20 mM

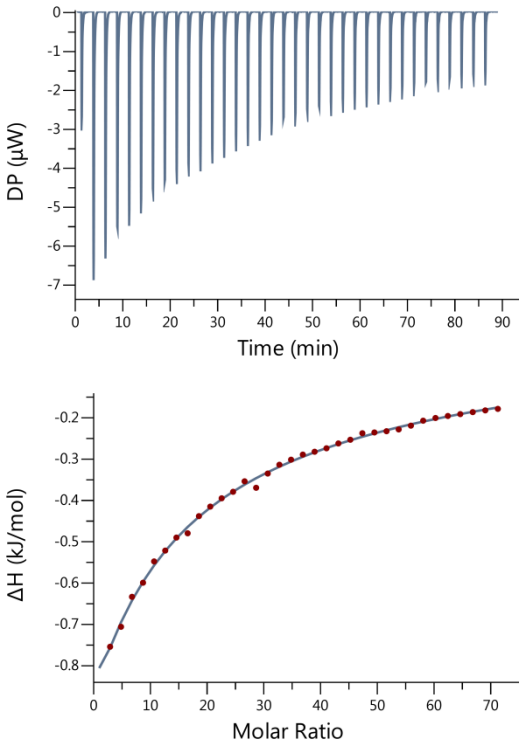

Figure A32 Raw ITC data for the sequential addition of $NaClO_4$ to **3.50·NO_3** in H_2O at 298K; integrated heat plot obtained from titration; [host] = 0.2 mM, [guest] = 80 mM

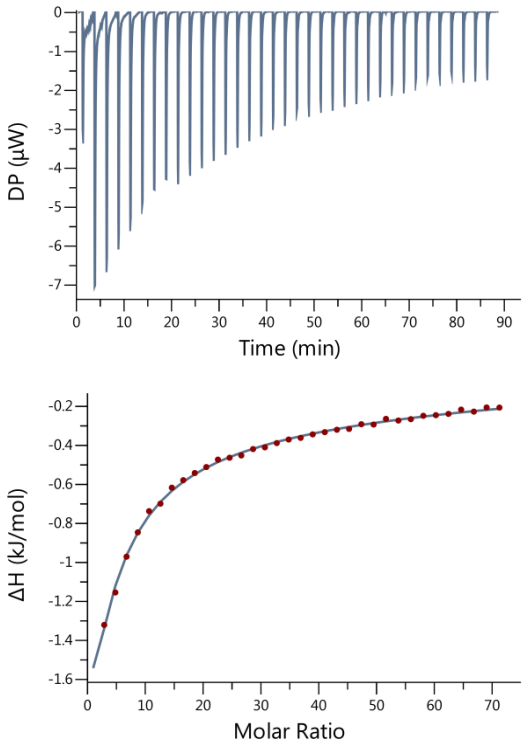

Figure A33 Raw ITC data for the sequential addition of $NaIO_4$ to **3.50·NO_3** in H_2O at 298K; integrated heat plot obtained from titration; [host] = 0.2 mM, [guest] = 80 mM

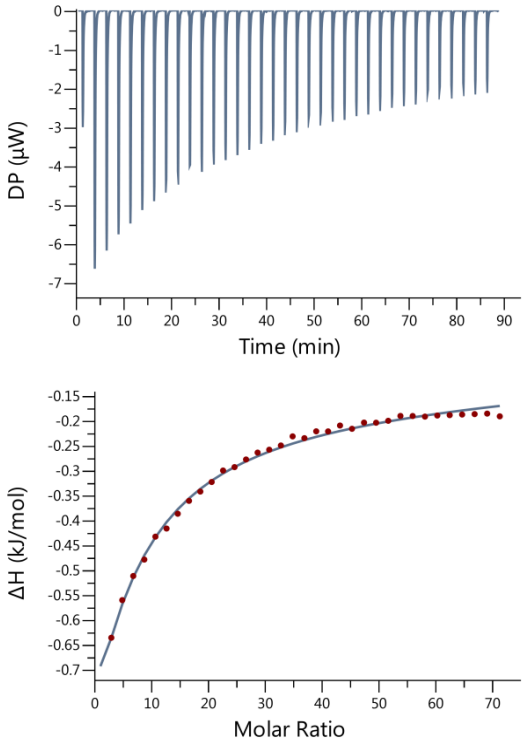

Figure A34 Raw ITC data for the sequential addition of NaSCN to **3.50·NO_3** in H_2O at 298K; integrated heat plot obtained from titration; [host] = 0.2 mM, [guest] = 80 mM